DECLASSIFIED-AUTHORITY-MEMO.US:
2313. TAINE TO SHARKANSKY
DATED JUNE 15, 1967

[redacted] X64 11941 <-> X64 11970

505

code 2

NASA TECHNICAL MEMORANDUM

NASA TM X-905

NASA TM X-905

Declassified by authority of NASA
Classification Change Notices No. 113
Dated ** 6/23/67

N67-31606 (ACCESSION NUMBER)
505 (PAGES)
TMX-905 (NASA CR OR TMX OR AD NUMBER)
FACILITY FORM
N67-31635 (THRU)
1 (CODE)
02 (CATEGORY)

PROCEEDINGS OF NASA CONFERENCE ON SUPERSONIC-TRANSPORT FEASIBILITY STUDIES AND SUPPORTING RESEARCH (U)

SEPTEMBER 17-19, 1963

Langley Research Center
Langley Station, Hampton, Va.

[redacted]

350

NATIONAL AERONAUTICS AND SPACE ADMINISTRATION • WASHINGTON, D. C. • DECEMBER 1963

[redacted]

[redacted]

Declassified by authority of NASA
Classification Change Notices No. 113
Dated ** 6/28/67

TECHNICAL MEMORANDUM X-905

PROCEEDINGS OF NASA CONFERENCE ON SUPERSONIC-TRANSPORT FEASIBILITY STUDIES AND SUPPORTING RESEARCH - SEPTEMBER 17-19, 1963

Langley Research Center
Langley Station, Hampton, Va.

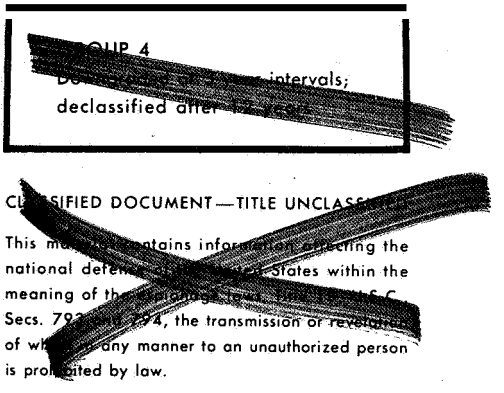

NATIONAL AERONAUTICS AND SPACE ADMINISTRATION

[redacted]

REPRODUCED

CONTENTS

INTRODUCTORY REMARKS v
By Dr. Floyd L. Thompson - Director,
NASA Langley Research Center

THE SUPERSONIC-TRANSPORT PROGRAM vii
By Mr. Charles H. Zimmerman - Director,
Aeronautical Research, NASA Headquarters

General Chairman - Laurence K. Loftin, Jr.

NASA FEASIBILITY STUDIES

1. OBJECTIVES AND GUIDELINES OF THE NASA SUPERSONIC-TRANSPORT FEASIBILITY STUDIES 1
By Laurence K. Loftin, Jr. (NASA Langley Research Center)

2. SUMMARY OF INITIAL NASA SCAT AIRFRAME AND PROPULSION CONCEPTS 5
By Donald D. Baals (NASA Langley Research Center)

3. SUMMARY OF LOCKHEED SCAT FEASIBILITY STUDIES 21
By R. Richard Heppe and Jim Hong (Lockheed California Company)

4. SUMMARY OF BOEING SCAT FEASIBILITY STUDIES 93
By Lloyd T. Goodmanson, William T. Hamilton, and Maynard L. Pennell (The Boeing Company)

5. NASA SUMMARY AND ASSESSMENT OF FEASIBILITY-STUDY RESULTS . . . 139
By John G. Lowry (NASA Langley Research Center)

TECHNICAL APPROACHES AND NASA SUPPORTING RESEARCH

PERFORMANCE AERODYNAMICS

Session Chairman - Donald D. Baals

6. ANALYSIS AND CORRELATION OF AIRCRAFT WAVE DRAG 153
By Roy V. Harris, Jr. (NASA Langley Research Center)

7. APPLICATION OF WING WARP AND AERODYNAMIC INTERFERENCE TO IMPROVE SUPERSONIC PERFORMANCE 165
By Francis E. McLean and Harry W. Carlson (NASA Langley Research Center)

8. STUDIES OF SKIN FRICTION AT SUPERSONIC SPEEDS 177
By K. R. Czarnecki, Mary W. Jackson, and William J. Monta (NASA Langley Research Center)

9. SOME FACTORS AFFECTING TURBULENT SKIN FRICTION AT SUPERSONIC SPEEDS 191
By Albert L. Braslow, John B. Peterson, Jr., and Donald I. McRee (NASA Langley Research Center)

CONFIGURATION AERODYNAMICS

Session Chairman - John G. Lowry

10. CONFIGURATION EFFECTS ON THE CHARACTERISTICS OF DELTA-WING SUPERSONIC TRANSPORTS 203
By Adrien E. Anderson (NASA Ames Research Center)

11. STABILITY AND HIGH-LIFT STUDIES APPLICABLE TO VARIABLE-SWEEP SUPERSONIC-TRANSPORT CONFIGURATIONS 223
By William J. Alford, Jr., Vernard E. Lockwood, Linwood W. McKinney (NASA Langley Research Center), and Richard K. Greif (NASA Ames Research Center)

12. NASA WING PLANFORM STUDIES 257
By Robert T. Taylor, William P. Henderson (NASA Langley Research Center), Raymond M. Hicks, and Edward J. Hopkins (NASA Ames Research Center)

13. LATERAL-DIRECTIONAL STABILITY STUDIES AT SUPERSONIC SPEEDS 267
By M. Leroy Spearman (NASA Langley Research Center)

14. ADDITIONAL CONFIGURATION APPROACHES 277
By A. Warner Robins and Richard T. Whitcomb (NASA Langley Research Center)

[redacted]

PROPULSION CONSIDERATIONS

Session Chairman - John G. Lowry

15. PROPULSION ASPECTS OF THE SUPERSONIC TRANSPORT 291
By James F. Dugan, Jr. (NASA Lewis Research Center), Arvid L. Keith, Jr., and Emanuel Boxer (NASA Langley Research Center)

16. STUDY OF AN AXISYMMETRIC SUPERSONIC-TRANSPORT INLET . . . . [redacted]
By Norman E. Sorensen (NASA Ames Research Center)

17. REVIEW OF NASA EXHAUST NOZZLE RESEARCH 315
By Jack F. Runckel (NASA Langley Research Center)

STRUCTURES AND MATERIALS

Session Chairman - Richard R. Heldenfels

18. STRUCTURAL CONCEPTS AND MATERIALS SELECTION IN THE FEASIBILITY STUDIES 333
By Richard A. Pride (NASA Langley Research Center)

19. NASA RESEARCH ON MATERIALS APPLICABLE TO SUPERSONIC TRANSPORTS 349
By Herbert F. Hardrath and George J. Heimerl (NASA Langley Research Center)

20. AEROELASTIC CONSIDERATIONS 365
By Robert W. Boswinkle, Jr., and E. Carson Yates, Jr. (NASA Langley Research Center)

NOISE AND SONIC BOOM

Session Chairman - Richard R. Heldenfels

21. CONFIGURATION EFFECTS ON SONIC BOOM 381
By Harry W. Carlson (NASA Langley Research Center)

[redacted]

22. FACTORS AFFECTING COMMUNITY ACCEPTANCE OF THE SONIC BOOM 399
By Harvey H. Hubbard and Domenic J. Maglieri (NASA Langley Research Center)

23. ENGINE AND BOUNDARY-LAYER NOISE CONSIDERATIONS 413
By Jimmy M. Cawthorn and Domenic J. Maglieri (NASA Langley Research Center)

OPERATING PROBLEMS AND AIRWORTHINESS

Session Chairman - Maurice D. White

24. OPERATIONAL FACTORS IN RELATION TO SUPERSONIC-TRANSPORT FUEL REQUIREMENTS 425
By Joseph W. Wetmore and Joseph W. Stickle (NASA Langley Research Center)

25. CONSIDERATION OF SOME AIRWORTHINESS REQUIREMENTS FOR SUPERSONIC TRANSPORTS 439
By Thomas L. Coleman (NASA Langley Research Center)

26. DEVELOPMENT OF SATISFACTORY HANDLING QUALITIES FOR A SUPERSONIC-TRANSPORT CONFIGURATION THROUGH SIMULATOR STUDIES 457
By Maurice D. White, Alan E. Fayk, Jr., and George E. Cooper (NASA Ames Research Center)

27. A SIMULATOR STUDY OF THE LATERAL DIRECTIONAL HANDLING QUALITIES OF TWO SCAT CONFIGURATIONS IN THE LANDING APPROACH 471
By Walter E. McNeill and Robert C. Innis (NASA Ames Research Center)

28. PILOTING PROBLEMS ASSOCIATED WITH THE SUPERSONIC-TRANSPORT MISSION PROFILE 485
By Glen W. Stinnett, Alan E. Fayé, Jr., and Emmett D. Fry (NASA Ames Research Center)

CONCLUSION

29. GENERAL SUMMARY AND ASSESSMENT 495
By Mark R. Nichols (NASA Langley Research Center)

[redacted]

INTRODUCTORY REMARKS

By Floyd L. Thompson, Director

NASA Langley Research Center

The Langley Research Center welcomes you to this meeting. The conferees assembled here represent an important assemblage of the aeronautical talent of the nation. We have with us personnel from the aerospace industry, the airlines, government agencies and laboratories, the Department of Defense, and members of various technical advisory committees to NASA. This meeting is similar in function to technical conferences on special subjects that are held from time to time here and elsewhere within NASA for the benefit of industry and government. The last such conference held at the Langley Research Center was in November 1960. That occasion was an NASA Conference on V/STOL Aircraft for the industry and the military services on the eve of the competition for the Tri-Service V/STOL airplane; the circumstances then were similar to those in which we find ourselves at present relative to the national program for a supersonic transport airplane.

The NASA has a responsibility for providing basic research and technical support for national aeronautical and space programs, whether of military or civil interest. In the aeronautical field, we are in fact continuing the function of the NACA which, from 1915 until the NACA became the nucleus of the NASA in 1958, was to "study the problems of flight with a view to their practical solution." In the discharge of its responsibilities NASA carries out extensive in-house research programs, augmented, on occasion, by contract research with industry, universities, and others. This combination of in-house research and contract studies has been utilized in directing our programs toward the achievement of efficient supersonic flight. During the course of NASA research relating to supersonic flight, several promising conceptual configurations for a supersonic transport have emerged. These conceptual designs, despite the attraction of their aerodynamic efficiency, raised many questions regarding their practical feasibility. Such questions were largely of an engineering nature and could only be answered by a diligent, comprehensive engineering design study - a type of activity outside the competence and scope of the NASA laboratories. Accordingly, NASA enlisted the aid of industry for the application of its engineering know-how to study, evaluate, and compare promising conceptual designs in all the areas of concern to a practical design. Such studies provide an important feedback to our research programs. They are particularly important at this time when the military aircraft procurement program no longer lays a groundwork of

[redacted]

technology and engineering experience for ready adaptation to commercial transports in the speed range of interest.

The purpose of this conference is to evaluate the present status of research by placing before you the results of our contractual feasibility studies of four conceptual supersonic transport designs, together with summaries of NASA in-house research pertinent to the supersonic transport. The material to be presented is intended to clarify and define the state of technology relative to those characteristics that can in fact be achieved. It is our intention to continue our research work, aided and guided by the knowledge gained from these studies.

N67-31602

THE SUPERSONIC-TRANSPORT PROGRAM

By Charles H. Zimmerman

Director, Aeronautical Research
NASA Headquarters

Gentlemen, the representatives of NASA Headquarters are pleased to add their welcome to that extended by the Langley Research Center. The NASA is gratified at the excellent response to the invitations to this conference. Indeed, we have been somewhat embarrassed by the number of requests from those who were not included in our invitation list and are sorry that space did not permit us to include everyone who might be considered to have some legitimate interest. Since such a plan was not practical, only those having a major interest have been included, and we trust that the selections made were wise and just.

It is *my* particular privilege at this time to introduce to you a representative of the Federal Aviation Agency, Mr. Gordon M. Bain, who has an especially vital interest in this conference and the information that it makes available. As you know, the President has given the Federal Aviation Agency the responsibility for directing the national Supersonic-Transport Program. Mr. Najeeb E. Halaby, Administrator of the FAA, has selected Mr. Bain to serve as his Deputy Administrator for Supersonic-Transport Development, and Mr. Bain will bear the heavy burden of directing that program. Will Mr. Bain please stand.

There has, I believe, been a certain amount of speculation about the role of NASA in the national Supersonic-Transport Program. I would like to say a few words on this point. The NASA Administrator, Mr. James E. Webb, has said that NASA will support the Supersonic-Transport Program to the full extent of its capabilities. NASA feels a heavy responsibility for insuring the success of the program and for making certain that available knowledge and technology is utilized to the fullest extent toward that end. The NACA traditionally fulfilled that function in support of military-aircraft development programs for many years, and the NASA expects to continue that role in collaborating with the FAA on this present program.

This conference was called at this time specifically to make the latest information available to those industrial firms planning to respond to the FAA's request for proposals, as well as to their major subcontractors, so that information can be fed into their proposal submissions. We appreciate the added effort that Boeing and Lockheed have devoted to their feasibility studies in order that this conference could be held at this time instead of at the later date originally planned.

I would now like to turn the meeting over to Mr. Laurence K. Loftin, Jr., of the Langley Research Center, who will serve as General Chairman of the Conference.

[redacted]

N67-31608

1. OBJECTIVES AND GUIDELINES OF THE NASA SUPERSONIC-TRANSPORT FEASIBILITY STUDIES

By Laurence K. Loftin, Jr.

NASA Langley Research Center

The purpose of this conference has been outlined in the "Opening Remarks" by Dr. Floyd L. Thompson. The material to be presented is divided into two parts. The first part is concerned with the configuration concepts employed in the feasibility studies and presents detailed results of those studies by the contractors. The second part presents summaries of the National Aeronautics and Space Administration research pertinent to supersonic-transport technical problems with particular emphasis given to research results dealing with those problems which were highlighted by the feasibility studies.

In order to provide a background for the papers presented in the first part of the conference, the objectives and guidelines of the feasibility studies are described. The objectives of the studies are as follows:

(1) To evaluate and compare promising design concepts relative to all facets of a successful commercial design

All facets include such factors as performance, weights, operating problems, airworthiness, and economics. Particular emphasis was placed on the achievement of accurate estimates of gross weight and range payload characteristics.

(2) To clarify the present state of the art for guidance of the national program

A definition of the state of the art relative to what characteristics can in fact be achieved in a supersonic transport is another way of expressing this objective.

(3) Definition of requirements for future NASA research

Both contractors were provided the same basic information as a starting point for their studies. The geometric shapes of 4 configuration concepts together with the aerodynamic characteristics throughout the entire speed range of interest were given in detail. The 4 concepts chosen for study were synthesized with the use of the most advanced and sophisticated aerodynamic ideas and represented the most promising

[redacted]

supersonic-transport configuration approaches to emerge from studies of some 20 different concepts. The characteristics of 4 conceptual engines were provided. The engine data were presented in such a way that engine size could be readily scaled up or down from a base point. The contractors were given freedom to select and size the engine type most suitable for each configuration. A set of desired design and performance objectives was provided.

The design and performance objectives utilized in the feasibility studies were formulated by the NASA more than a year ago as a means for obtaining realistic and comparable data for the 4 different configuration concepts. The payload was specified as 26,123 pounds which corresponds to 125 passengers plus their baggage. The maximum range for supersonic operation was specified as 3,200 nautical miles, with economic operation over ranges as low as 1,000 nautical miles at supersonic speeds being indicated as a desirable goal. Economic operations at subsonic speeds over stage lengths of 200 to 1,000 nautical miles were also indicated as being desirable. A design supersonic cruising Mach number of about 3 was specified for the studies of all 4 configuration concepts. The specification of a cruise speed of a Mach number of 3 is of course tantamount to specifying the use of either steel or titanium as a basic structural material. In accordance with a contract amendment made midway through the study, two of the configurations were also studied with aluminum used as the basic structural material. In this case, the contractors were asked to determine the maximum feasible value of the cruising Mach number. Primary emphasis was given to cruise at a Mach number of 3 because the flight efficiency factor tends to become a maximum in this speed range. The maximization of this factor in the vicinity of a Mach number of 3 is the reason why this Mach number has always been a desirable goal for flight at supersonic speeds. In the area of operations, a 9,500-foot take-off runway on a hot day at 1,000 feet above sea level and a landing runway of 7,000 feet were given as guidelines. Landing and take-off speeds comparable to those of present-day subsonic jets were thought desirable. The gross weight, size, and ground handling characteristics of the aircraft were to be such that operations could be carried out from present-day international airports without any basic change in facilities. Fuel reserves were to be determined on the basis of current Civil Air Regulations requirements.

The contractors were asked to give careful consideration to noise resulting from both sonic boom and engines. The sonic-boom noise requirement of 2 lb/sq ft during acceleration and $1\frac{1}{2}$ lb/sq ft during cruise was arrived at after the study was begun and the initially specified climb profile was found to result in intolerably high airplane gross weights. The variation of airplane gross weight with sonic-boom overpressure is discussed in detail in later papers. The values chosen

[redacted]

were the minimums that could be achieved, under the range payload guidelines of the present study, without incurring large increases in airplane gross weight. As is shown in paper no. 22 by Harvey H. Hubbard and Domenic J. Maglieri, the maximum sonic-boom overpressures utilized as a guideline in the study do not represent unique values which define a boundary between acceptable and unacceptable public reaction. Engine noise comparable to that of present subsonic jets was thought to be reasonable. An aircraft life of 15 years corresponding to a utilization of 30,000 to 50,000 hours was specified. Airworthiness criteria specified by the Civil Air Regulations were to be utilized in the studies. Applicable regulations were in some cases nonexistent, and, in these cases, the design rules to be used were agreed to mutually by the contractor and the NASA. It was, of course, desired that the economics of the supersonic transport be comparable with the present-day subsonic jets.

Very close liaison was maintained between the contractors and the NASA during the course of the studies. Changes in aerodynamic shape found necessary by the contractors in order to make possible more practical airplane designs were made only after consultation with and agreement by the NASA. Wind-tunnel data were supplied by the NASA during the course of the studies in order to insure that realistic aerodynamic characteristics were employed in evaluating configuration modifications.

The feasibility studies were carried out in great depth and resulted in a wealth of valuable information. Time at this conference does not permit the presentation of all this material; in fact, some aspects of the study - for example, economics, cost, and internal aircraft systems - are not discussed at this conference.

The first technical paper, paper no. 2 presented by Donald D. Baals of the Langley Research Center, introduces the 4 configuration concepts evolved by the NASA and utilized in the feasibility studies.

[redacted]

PRECEDING PAGE BLANK NOT FILMED.

N67-31609

2

SUMMARY OF INITIAL NASA SCAT AIRFRAME AND PROPULSION CONCEPTS

By Donald D. Baals

NASA, Langley Research Center

SUMMARY

In the course of the NASA research programs in support of the supersonic transport, four basic configuration concepts were evolved. These concepts were submitted to two airframe contractors for feasibility studies. The basic concepts are described herein and the supporting aerodynamic data are reviewed. In order to provide a basis for evaluation of the configuration concepts, estimated engine performance characteristics were provided to the feasibility-study contractors. These general engine characteristics are reviewed herein.

INTRODUCTION

Since 1958 the NASA has made a major research effort in support of the supersonic transport and has made substantial progress in several basic areas. It has established general mission capabilities and pinpointed the technical problems. Further, it has determined the general cycle characteristics of various propulsion systems relative to the complete mission. Substantial research advances have been made in such areas as airframe aerodynamics, flight simulation technology, configuration concepts, and sonic boom.

An analysis of the flight profile (fig. 1) will serve to highlight some of the technical problem areas. During take-off there are problems associated with engine noise, take-off velocity and distance, and lift-drag ratio in second-segment climb. The transonic acceleration phase results in critical problems associated with the sonic boom, transonic lift-drag ratio including trim effects, and augmentation characteristics of the engine. The problems of supersonic cruise are basically lift-drag ratio, sonic boom, and specific fuel consumption of the engine. During holding operations, the subsonic lift-drag ratio and partial-power engine characteristics are critical and affect reserve-fuel requirements. During landing, the basic problems are associated with approach velocity, landing distance, handling qualities, and approach engine noise.

A study of the fuel flow rate for a typical SCAT airframe-engine combination carrying the fuel reserves noted in figure 2 shows the following characteristics:

(a) The fuel required during take-off, climb, and transonic acceleration amounts to one-third the total fuel although the distance covered is only about 250 miles.

(b) Approximately 50 percent of the total fuel is consumed at supersonic cruise conditions.

(c) The weight of the fuel reserves is roughly the same order of magnitude as that of the payload.

This mission analysis established the fact that the supersonic transport requirements call for high efficiency in all speed regimes - subsonic, transonic, and supersonic. Some of the areas of aerodynamic advance - not only aerodynamic laws, but techniques of application - which have provided new levels of aerodynamic potential are as follows:

(a) Wing twist and camber

(b) Wave-drag computer technology

(c) Favorable aerodynamic interference

(d) Skin-friction validation

(e) Variable geometry - especially wing variable sweep

(f) Subsonic stability and high lift

(g) Sonic-boom configuration effects

In order to provide a focus for the NASA research programs in these areas and to establish a general level of supersonic transport efficiency, studies of various configuration concepts were initiated by NASA in early 1960. In these studies, an attempt was made to incorporate the aerodynamic advances into configurations which have the potential of accomplishing the supersonic transport mission.

SYMBOLS

A	aspect ratio
C_L	lift coefficient

DECLASSIFIED

$C_{m,o}$	pitching-moment coefficient at zero lift
F_n	net thrust, lb
h	altitude, ft
K_r	reflection factor
l	length of airplane, ft
L/D	lift-drag ratio
M	Mach nuniber
P	reference pressure, lb/sq ft
Δp	sonic-boom overpressure, lb/sq ft
q	dynamic pressure, lb/sq ft
W	weight, lb
W_e	weight of engine, lb
W_{TO}	take-off weight, lb
W_a	corrected weight airflow, lb/sec

$\beta = \sqrt{M^2 - 1}$

Subscript:

max	maximum

AIRFRAME AERODYNAMICS

Configuration Concepts

From the studies of various configuration concepts, the following four basic approaches (see fig. *3)* evolved:

Fixed-wing concepts:

(a) Highly swept arrow wing (SCAT 4)

(b) Delta wing - canard, or aft tail, or both (SCAT 17)

Variable-sweep concepts:

(a) Full-wing-panel sweep (SCAT 16)

(b) Overlapping winglets sweeping forward from the wing leading edge (SCAT 15)

In this section, the technical background of these configuration concepts is reviewed. It should be noted that the various areas of research upon which these configuration concepts were based, along with research advances made since the initiation of the feasibility studies, are discussed in greater detail in subsequent papers in this compilation.

SCAT 4.- Linear-theory analyses indicate that supersonic lift-drag ratios significantly greater than those for the delta-wing configuration might be obtained through the use of a warped arrow wing having a leading edge swept behind the Mach angle and having the trailing edge with substantial sweepback. Theory also indicates that the highly swept arrow wing should result in a relatively low sonic-boom overpressure. SCAT 4 (see fig. 4) is an idealized configuration employing these concepts. The engine nacelles are integrated into the rearward part of the wing to reduce the adverse thickness effects, and the fuselage, as well as the wing, is cambered to reduce the trim drag. The wing leading-edge sweep is only slightly greater than the Mach angle to maximize off-design performance.

The SCAT 4 configuration as submitted to the contractors was judged by NASA to have deficiencies in the following areas:

(a) Necessity for an elaborate flap system to eliminate low-speed pitch-up problems

(b) High structural-panel aspect ratio

(c) Complex inlet-wing integration

SCAT 17.- The SCAT 17 configuration (see fig. 5) was selected after consultation with various aircraft manufacturers. The design proposed was a delta-wing configuration having an aspect ratio of 2.17, leading-edge sweep at 59°, and hexagonal sections 2 percent thick. At cruise Mach number the wing leading edge is ahead of the Mach line. Such a configuration has the potential of simplicity of construction and low structural weight. A canard as well as an aft horizontal tail was employed to provide large subsonic pitching moments necessary to trim the effective flap system for landing.

A horizontal tail with variable dihedral programed with Mach number provided high directional stability at supersonic speeds and at the same time reduced the aerodynamic-center shift with Mach number.

Deficiencies in the following areas were noted:

(a) Low lift-drag ratio during subsonic cruise with marginal supersonic-cruise potential. (Reference here is to the delta planform which has little drag-due-to-lift potential at supersonic speeds beyond that of a flat delta wing.)

(b) Engine blast on the tail in the intermediate droop position

(c) Low usable C_L and low L/D in take-off and landing modes

SCAT 15.- The SCAT 15 configuration (see fig. 6) is designed for maximum supersonic efficiency with provision for variable-sweep auxiliary-wing panels which can be retracted to form a part of the basic swept wing for high-speed flight or can be swept forward to increase the aerodynamic efficiency for low-speed flight. The minimum drag of the configuration was reduced by careful application of the supersonic area rule and by wing-fuselage blending. The wetted area was minimized by the outboard location of the vertical tails and by the utilization of the flat-plate area of the engine nacelles to provide directional stability at high angles of attack. A twisted and cambered arrow wing carefully combined with a cambered fuselage provided favorable drag-due-to-lift characteristics at supersonic speeds, and positive pitching moments for minimizing the trim drag. The location of the outboard horizontal tails in an upwash field provided high control effectiveness and improved the listing efficiency of the wing. Improved drag-due-to-lift characteristics were also noted by virtue of the engine location underneath the wing and to the rear.

The major anticipated deficiencies of SCAT 15 were:

(a) Structural problems associated with the high panel aspect ratio of the variable-sweep wing

(b) Dynamic problems associated with wing overlap

(c) Pitch-up at subsonic speeds

SCAT 16.- SCAT 16 is a variable-sweep design (see fig. 7) aimed at combining the advantages of high supersonic aerodynamic efficiency with outstanding subsonic performance. High supersonic efficiency was obtained by the use of a highly swept twisted and cambered arrow wing designed for optimizing the drag due to lift. Wing-fuselage blending was incorporated to a degree to minimize the wave drag. Two of the engines were located under the wing to provide favorable interference for the lifting condition; the third engine was mounted on the vertical tail. A cambered fuselage along with appropriate twist to the wing

provided positive $C_{m,o}$ for minimizing trim drag at supersonic speeds. With the wing in the unswept position, outstanding subsonic lift-drag ratios as well as high lift coefficients during landing were obtained. During the course of the feasibility studies, data for a configuration having a lower aspect ratio were also supplied to the contractors to provide a basis for aerodynamic structural trades.

The anticipated problem areas of this configuration were:

(a) High structural-panel aspect ratio of wing

(b) Engine jet interference on the horizontal tail

(c) Pitch-up at subsonic speeds

(d) Marginal supersonic L/D

Lift-Drag-Ratio Characteristics

The levels of aerodynamic performance of these four basic SCAT configurations are shown in figure 8. These results are based on NASA wind-tunnel data supplied to the contractors. The following characteristics are noted:

(a) The highest supersonic lift-drag ratios for the fixed-wing SCAT 4 and variable-sweep-wing SCAT 15 are approximately 8.

(b) Large differences in L/D occur at subsonic speeds where the variable-sweep configurations have lift-drag ratios as much as twice those of the fixed-wing configurations.

(c) In the transonic regime, the lift-drag ratios for all four SCAT configurations are about the same. It is noted, however, that the fixed-wing SCAT configurations have significantly higher force break Mach numbers.

The basis for the continued interest in the potential of wing variable sweep, in view of its recognized structural complexity, is evident from the levels of lift-drag ratio for subsonic speeds. Further, the availability of increased span permits greater flexibility in high-lift system design and wing-area selection to provide the required take-off and landing performance.

This latter factor is illustrated in figure 9 where the general landing approach characteristics of two configurations having aspect ratios of 2 and 7 are presented. These aspect ratios 2 and 7 are char-

RESTRICTED

acteristic of fixed-wing and variable-sweep configurations, respectively. In figure 9 lift-drag ratio is plotted against lift coefficient for the subject configurations in the optimum landing-approach condition. Under approach conditions, the configuration having an aspect ratio of 7 has high values of L/D with $(L/D)_{max}$ occurring at a lift coefficient of approximately 1.0. The maximum lift-drag ratio of a configuration having an aspect ratio of 2 occurs at a lift coefficient of approximately 0.5.

The high usable C_L for the configuration having an aspect ratio of 7 permits low approach speeds at minimum drag. For the configuration having an aspect ratio of 2, approach at comparable values of C_L results in high drag (and therefore high engine thrust) and operation on the "back side" of the power-required curve. Alleviation of the latter condition necessitates substantial increases in wing area combined with effective high-lift and longitudinal control systems.

Sonic-Boom Characteristics

In another area of aerodynamic support, the NASA provided calculated data on the sonic-boom characteristics of the various initial SCAT configuration concepts. A summary of these results is shown in figure 10. In this figure, the "boom" parameter is plotted against the "lift" parameter for the four SCAT configurations. These parameters are explained in more detail in paper no. 21 by Harry W. Carlson. It is sufficient at this point to note only that the boom parameter is proportional to the overpressure on the ground, and that the SCAT configurations cruise at a lift parameter of about 0.01. There is a substantial configuration effect - as much as 10 percent - in the level of sonic boom for a given lift parameter. It should be pointed out that these boom parameters must be recomputed as each configuration changes its distribution of cross-sectional area or lift during the process of design.

PROPULSION SYSTEMS

Io order to afford a common basis for evaluation of the aerodynamic configurations, estimated engine performance, along with data on dimension and weight variation with airflow, was furnished initially to the contractors for the six classes of engines indicated in figure 11. The following engine characteristics are noted:

Engine A:
Mach 3 afterburning turbojet somewhat advanced beyond current technology with turbine-inlet temperature of 2,400° R
Engine B:
Mach 3 duct-burning turbofan with design bypass ratio of 1.5 and turbine-inlet temperature of 2,400° R
Engine C:
Mach 3 variable-geometry turbojet with turbine-inlet temperature of 2,700° R
Engine D:
Mach 3 variable-geometry duct-burning turbofan with design bypass ratio of 1.5 and turbine-inlet temperature of 2,700° R
Engine E:
Mach 2, 2,400° R turbojet
Engine F:
Mach 2, 2,400° R turbofan
Engines E and F were submitted relative to the design of the Mach 2 aluminum transport.

Later in the study, data on the variation of airflow schedule - specifically, low flowing of engine B at Mach 3 - were supplied to the contractors to permit reduction of transonic spillage drag. Also, data on a mixed-flow augmented version of engine D were supplied.

It is anticipated that the development of engines A and B, as well as E and F, could be initiated at the present time with a high degree of confidence. Engines C and D, on the other hand, are highly advanced and approach the limit of present developmental capability. The data presented are believed to be reasonably representative of future industry-developed engines of the several classes and, as such, should afford valid comparisons of airframe configurations and valid indications of the level of propulsion technology required.

The following table shows a comparison of the SCAT study engines:

Engine	Take-off			Specific fuel consumption			
	w_a, lb/sec	$\frac{F_{n,max}}{W_e}$	Noise increment[a], db	M = 1.2, h = 45,000 ft, W = 365,000 lb	M = 3.0, h = 65,000 ft, W = 300,000 lb	M = 0.9, h = 36,089 ft, W = 300,000 lb	M = 0.3, h = 1,500 ft, W = 200,000 lb
A	400	5.8	+10	2.02	1.54	1.27	1.45
B	560	4.9	+2	1.94	1.58	.92	1.18
C	390	6.0	+10	1.93	1.54	1.12	1.37
D	540	5.9	+1	1.82	1.56	.80	.99

For comparison, these engines were sized to provide 0.05g level acceleration at a Mach number of 1.2 and an altitude of 45,000 feet for an airplane having a take-off weight of 400,000 pounds. The following points are noted:

(a) Turbojet weight flows are about 400 pounds per second; turbofan weight flows are about 35 percent larger.

(b) There is a significant increase in engine thrust-weight ratio for the turbofan as the temperature is increased from 2,400° R to 2,700° R.

(c) Relative to the take-off noise of four suppressed J57 engines, the incremental take-off noise levels for the turbojets were about +10 decibels, but there was a negligible increase for the turbofans.

(d) For Mach 1.2 acceleration and Mach 3 cruise, all engine configurations had about the same specific fuel Consumption. One advantage of the turbofan not noted in the preceding table lies in its relatively "flat" curve of specific fuel consumption as a function of percent thrust; thus, engine-airframe match becomes less critical.

(e) As expected, at subsonic speeds the specific fuel consumption of turbofan engines is significantly less than that of turbojet engines.

An inspection of the preceding table clearly indicates that engine D has the greatest potential in terms of subsonic specific fuel consumption and take-off noise and has generally favorable characteristics in other areas of comparison.

DATA TRANSMITTAL

The results from the wind-tunnel studies and engine analyses were transmitted to all major aircraft companies, as well as to the Boeing Co. and Lockheed California Co., for feasibility studies. An estimated total of 7,000 sheets of information was eventually tranmitted to each contractor - about one-third of which was IBM tabular data. The transmitted data were not limited to one specific configuration in each family, but included the following data on alternate versions to assist in assessing aerodynamic trades:

(a) SCAT 4 data included a Mach 3.2 design, and a Mach 2.9 design with the wing trailing edge largely filled in.

(b) SCAT 15 data included a Mach 3, flat-wing configuration as well as a Mach 2.2 twisted- and cambered-wing design.

(c) SCAT 16 data, as noted previously, included results for a configuration with a lower aspect ratio and many detailed modifications.

(d) Scat 17 data included a range of data on engine location, canard surfaces, aft tail, and combinations thereof.

These aerodynamic and engine data were made available to the contractors with but one restraint. The resulting configuration finally proposed by the contractors should not depart from the basic concept so greatly as to render the basic NASA SCAT data inapplicable. On the basis of the mission guidelines enunciated by Laurence K. Loftin, Jr., in paper no. 1 and on the basis of the aerodynamic and propulsion data summarized herein, the SCAT feasibility studies were conducted.

DECLASSIFIED

SCAT FLIGHT PROFILE

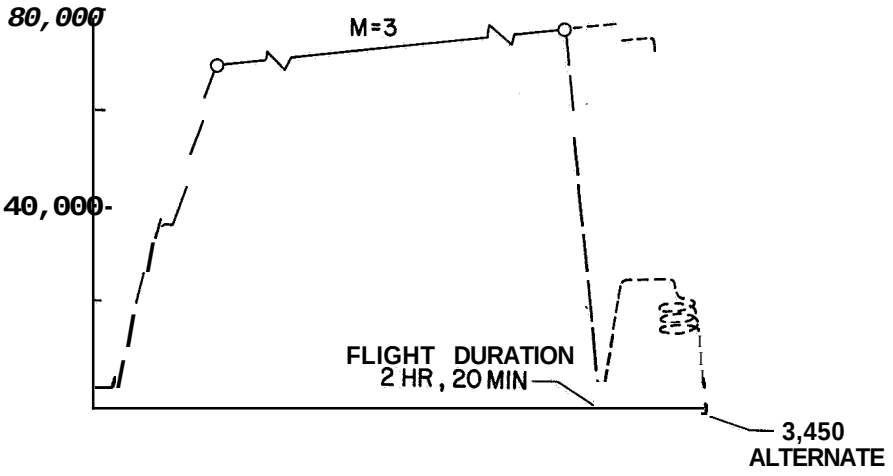

Figure 1

SUPERSONIC **TRANSPORT FUEL USAGE**

RANGE, *3200* N. MI.; TURBOFAN ENGINES

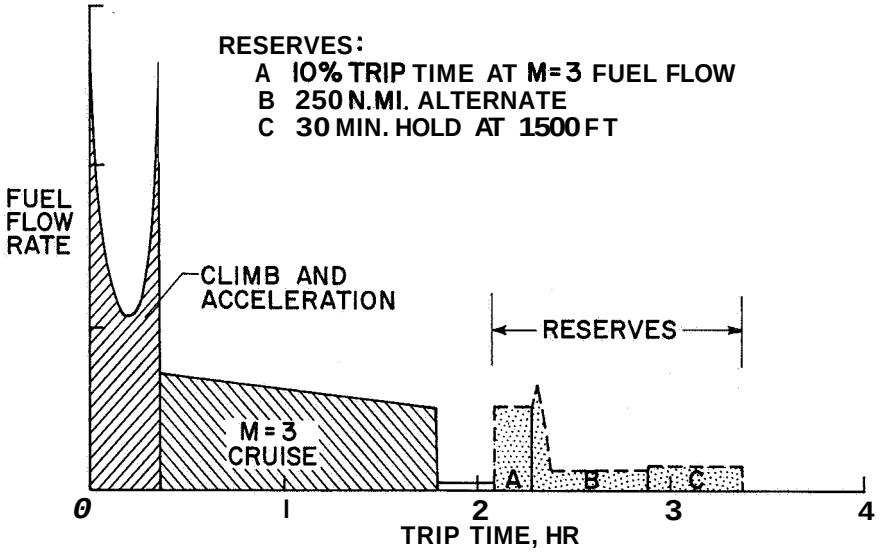

Figure *2*

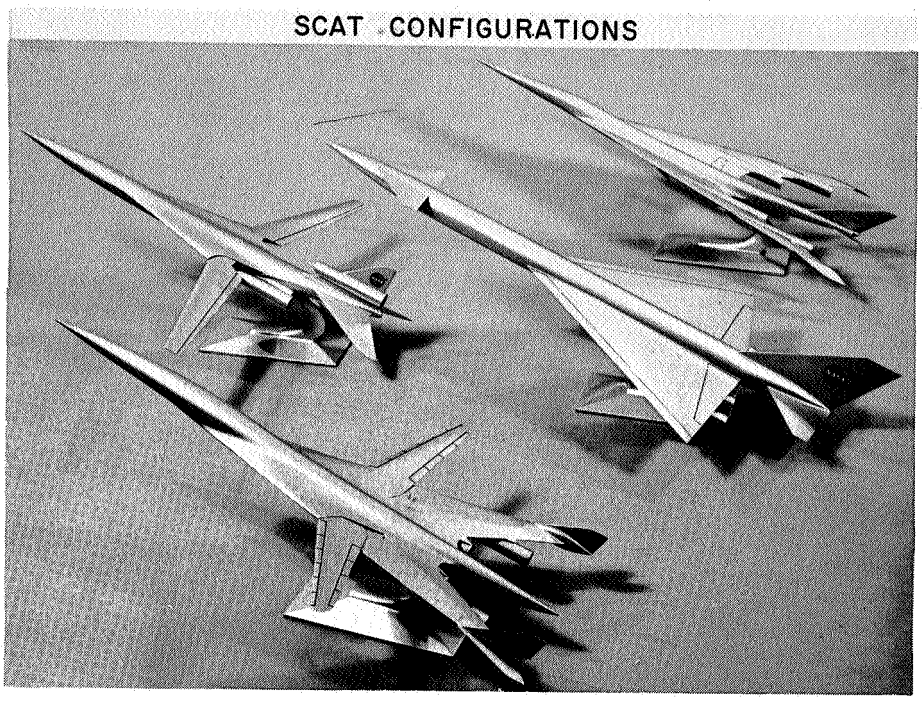

Figure 3

L-2095-15

SCAT 4

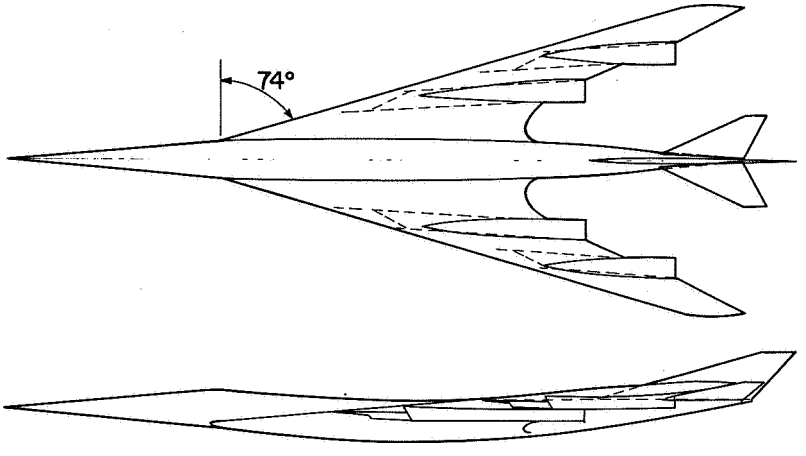

Figure 4

RELEASED

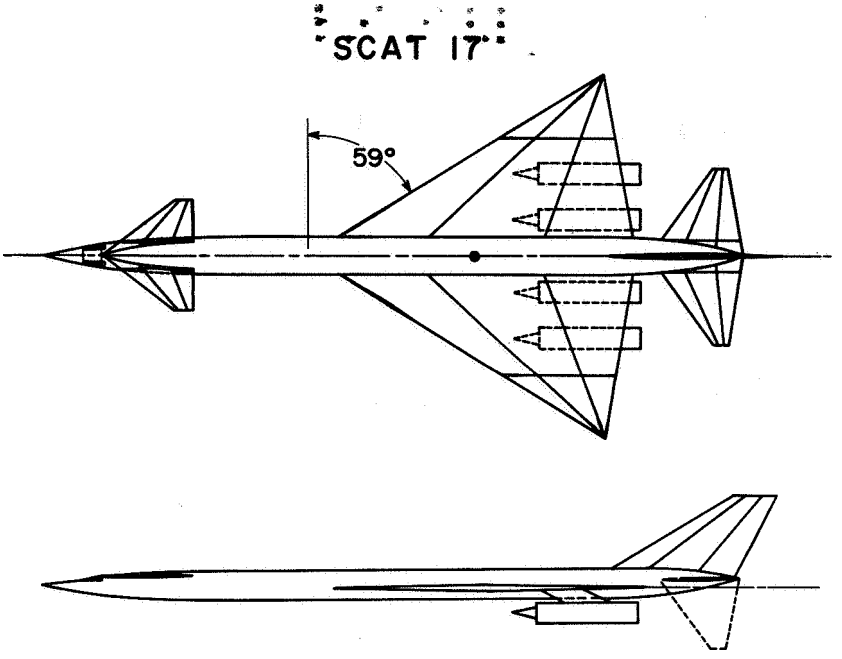

Figure 5

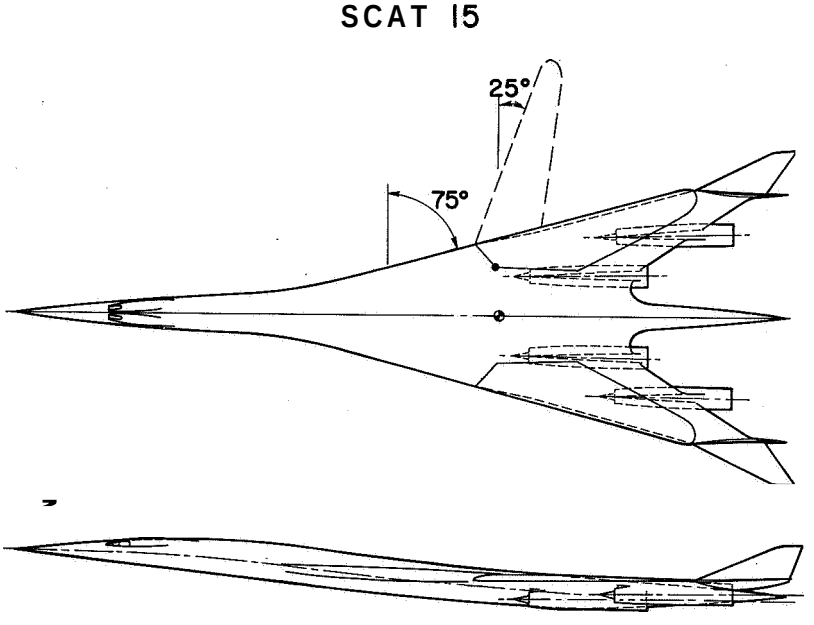

Figure 6

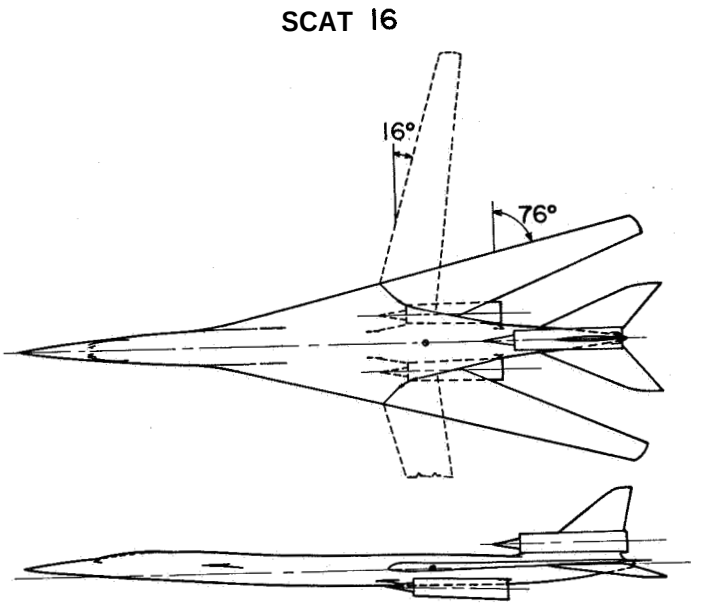

Figure 7

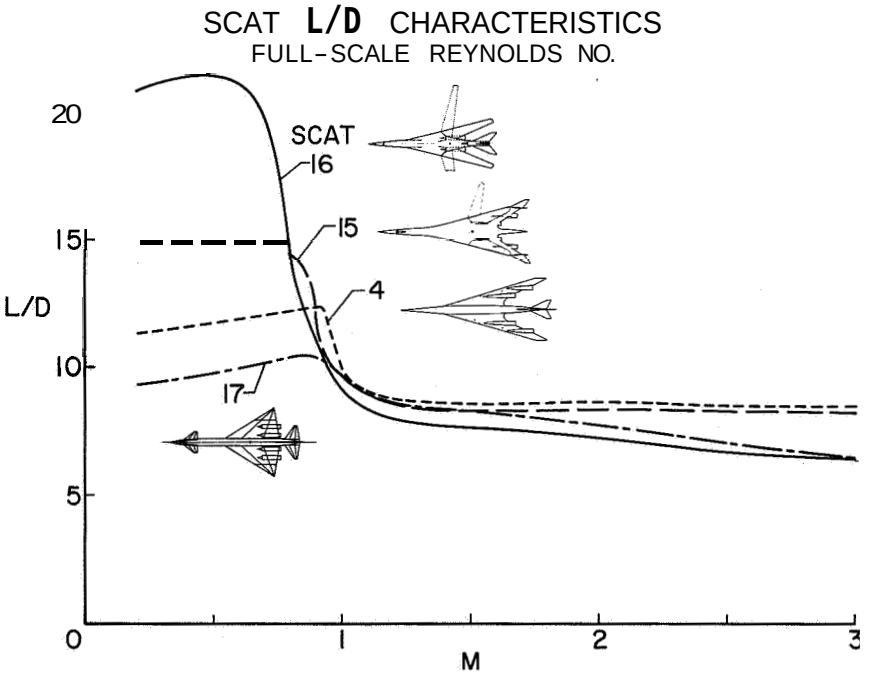

Figure 8

CONFIGURATION 'APPROACH CHARACTERISTICS

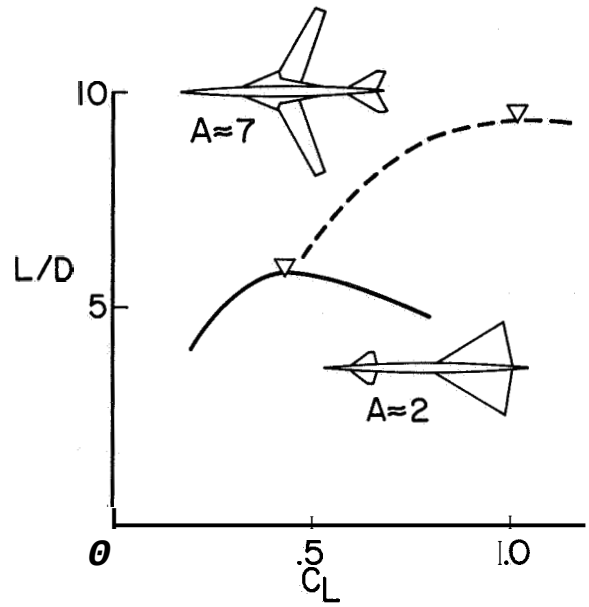

Figure 9

SONIC-BOOM CHARACTERISTICS

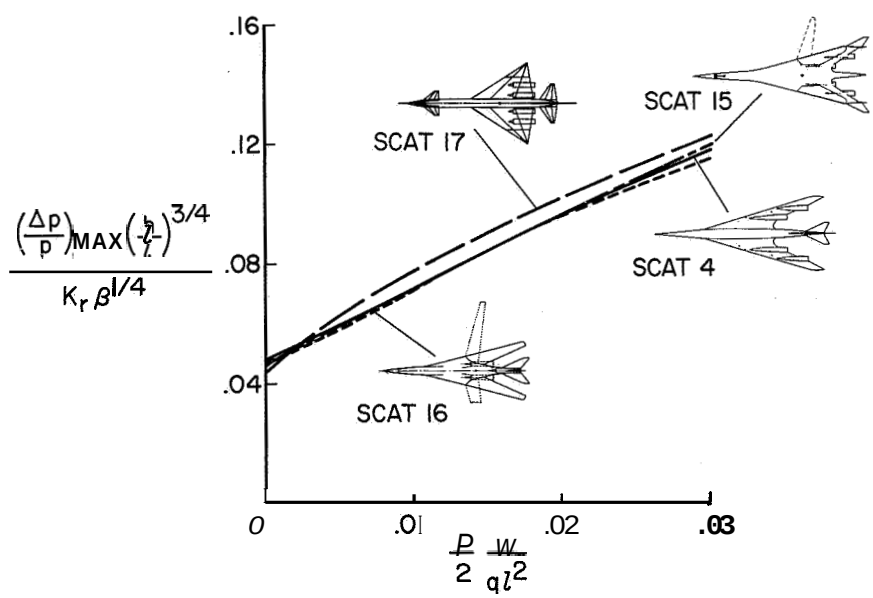

Figure 10

SCAT ENGINE TYPES

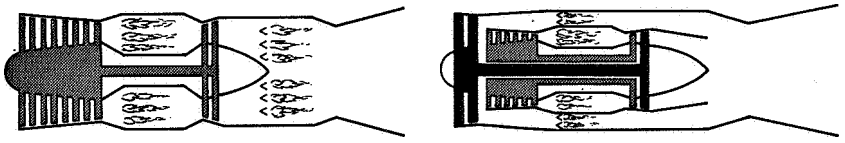

	TURBOJET			TURBOFAN		
	ENGINE			ENGINE		
DESIGN CONDITIONS	A	C	E	B	D	F
CRUISE M	3	3	2	3	3	2
TURBINE-INLET TEMP, °R	2,400	2,700	2,400	2,400	2,700	2,400
COMPRESSION RATIO:						
GENERATOR	8	8	12	10	12.5	14
FAN	—	—	—	2	2.5	2
BYPASS RATIO	—	—	—	1.5	1.5	1.5

Figure 11

[redacted] N67-31610

3. SUMMARY OF LOCKHEED SCAT FEASIBILITY STUDIES

By R. Richard Heppe and Jim Hong

Lockheed California Company, Burbank

Jim NASA
52403 04
11945
p. 21-92 only
conf.
AUTHOR

3

ABSTRACT

A review is presented of the results of a supersonic transport feasibility study made by the Lockheed California Company under contract to NASA. Several NASA research concepts were studied in depth with consideration to such details as passenger accommodations, airline requirements, structure and materials, and equipment and aircraft systems.

INTRODUCTION

The purpose of this paper is to review Lockheed's work in fulfilling the NASA Contract requirements for feasibility studies of several Mach 3.0 Supersonic Commercial Air Transport (SCAT) configuration concepts. This work was carried out to convert NASA research concepts into actual airline-type aircraft so that valid comparisons of the alternate approaches could be made. An important excursion in the basic study included the evaluation of an aluminum version of one of the concepts at a lower Mach number. The scope of the work and important findings are summarized.

STUDY APPROACH

Guidelines

The guidelines for the feasibility study and a description of the several NASA configuration concepts have been presented by NASA. The highlights of these guidelines are as follows:

Cruise Mach number	3.0
Range, nautical miles	3,200
Payload (number of passengers)	125
Sonic-boom overpressure:	
Climb, lb/sq ft	2
Cruise, lb/sq ft	1.5

[redacted]

Runway requirements:	
Take-off, ft	9,500
Landing, ft	7,000
Airport performance:	
Take-off speed, knots	165
Landing speed, knots	130
Airplane design use (target), hr	45,000

Many additional detailed guidelines were established through joint consultation between NASA and Lockheed. These included flight-station requirements, passenger cabin-space requirements, and detailed structural design criteria. The basic mission profile is illustrated in figure 1. Of special note are the reserve fuel requirements, consisting of allowances for a holding operation amounting to 10 percent of trip time, a 250-nautical-mile cruise to the alternate airport, and a 30-minute hold over the alternate at 1,500 feet.

Criteria and Analysis

The purpose of Lockheed's task as noted by the Work Statement provided by NASA was . . . to evaluate configuration concepts generated by NASA research in sufficient depth to assure confidence in gross weight and range payload characteristics and determine whether continued exploitation of the design approach would be of interest." Of particular importance are the key words, "confidence in gross weight and range payload characteristics," since these items dictate the resultant capability of any transport. To accomplish this result the designs must integrate considerations regarding detail design, passenger accommodations, airline requirements, structure and materials, equipment and aircraft systems, as well as compliance with regulations of the Federal Aviation Agency.

As noted by NASA, the SCAT configuration concepts each evolved from a long period of aerodynamic development. A large volume of wind-tunnel test data was generated in this work. It was Lockheed's task to examine these data, to select that which was applicable, and finally to generate a set of full-scale aerodynamic characteristics for each of the configurations. The most significant area, of course, is the establishment of full-scale drag. Here it was necessary to make the corrections for the items noted in figure 2. As the program proceeded, modifications to the configurations made it necessary to apply substantial corrections to the wind-tunnel data. These revisions were made with NASA's concurrence. The magnitude of these adjustments is noted in subsequent sections.

An integral part of the feasibility study consisted of evaluating the comparative merits of several basic engine cycles involving both

current and advanced state-of-the-art technology. The engines considered for the basic Mach 3 mission are shown in figure 3. NASA, supplied basic thrust and weight information on each of these engine types as well as scaling factors needed for the sizing studies on each aircraft configuration. As shown, engine performance ranges from a cruise specific fuel consumption of 1.51 for the advanced turbojet to 1.58 for a present-technology duct-burning turbofan. Thrust-weight ratios vary from 5.4 to 6.5. Very important differences appear in the off-design conditions, with specific fuel consumption, at low altitudes and partial power varying from 0.82 to 1.35. These differences exert a large influence on the airplane gross weight for the basic mission and its ability to perform various off-design operations such as subsonic cruise and hold.

Engine data for the Mach 3 aircraft were analyzed to determine the optimum engine type. Results were obtained in the form of take-off gross weight for various SCAT configurations to perform the mission. The summary shown in figure 4 for a typical SCAT shows a clear superiority for the NASA "D" advanced technology, duct-burning-turbofan type of engine. Later analysis showed that the advanced dry turbojet was actually a close competitor on the basic mission, but suffered in comparison to the fan for off-design conditions. Consequently, the advanced duct-burning fan type was used for all subsequent Mach 3 aircraft studies.

In order to assure realism in the feasibility studies, each airplane was subjected to a complete basic loads analysis in general accordance with the requirements of CAR 4b. Where the requirements were considered inappropriate or inadequate, because of marked differences from current transports in mission requirements and configuration characteristics, a criterion of safety equivalent to or better than current transport practice was used. Special studies were conducted to select overspeed margins. Gust power spectral and maneuver loads analyses were made, and landing and taxiing load analyses were carried out. Time histories of load and temperature were developed to ensure satisfactory material design, allowable strength, and adequate provision for thermally induced stresses.

The structural design speeds as a function of altitude are shown in figure 5. The values of maximum cruising speed and Mach number were selected so as to avoid restrictions on the desired optimum mission profile indicated by the dashed-arrow line. The speed margins between cruising speed and dive speed were selected on the basis of time-history studies In four degrees of freedom for the airplanes' response to various possible situations leading to overspeed.

Influence of structural material on the primary structure weight as a function of Mach number is shown in figure 6. The weight ratio

represents the factor by which the weight of the primary structure of a room-temperature aluminum airplane (2024-T81) of identical geometry must be multiplied to obtain the weight of the structure of an airplane of the material and at the cruise Mach number shown. In arriving at these weight estimates, the load factor and the percent reduction of allowables for fatigue are identical for all materials. Temperature effects on allowables are functions of cruise Mach number and the material selected. These data indicate that titanium alloy 8Al-1Mo-1V is the lightest structural material at all Mach numbers. Consequently, it was chosen as the basic structural material for all Mach 3 configuration studies.

Some additional material characteristics of interest in design and production are shown in figure 7. The basic material tear resistance and fatigue resistance of titanium are superior to the best aluminum alloy currently used. Exploitation of this superiority, however, is possible only by testing of specific designs to appropriate criteria reflecting the types of applications and the consequences of failures. For conservative reasons these characteristics were not fully exploited in weights estimated for this study. Sheet metal formability, expressed in terms of minimum allowable bend radius, represents a good index of the fabrication characteristics of a material for use as stringers, frames, clips, brackets, etc. Efficient sections require small bend radii; thus, it is apparent that hot-forming will be used extensively in titanium fabrication, as is current practice in 75 ST aluminum fabrication. For fittings and integrally stiffened or tapered-thickness skins, machinability is an important economic consideration in production. Compared with aluminum, which is one of the most easily machined materials, titanium is significantly slower to mill, the direct material removal rate being 1/30 that of aluminum. When set-up, knock-down, and inherently slow feed-tracing operations are included in the analysis, the comparison is considerably less severe. Titanium offers definite advantages over aluminum in the manufacture of built-up fittings, tube clusters, pressure vessels, etc., because of its good weldability. The corrosion resistance of titanium and its alloys in the presence of salt at high temperatures is not fully resolved, and development of protective coatings may be required. Overall, the choice of titanium as a basic structural material is well substantiated at this time, and continued research can be expected to further improve cost, machinability, and corrosion resistance.

To enhance the accuracy of the structural weight estimates, Lockheed performed, as part of its own research and development, structural research and tests. The results were used to check the predicted allowable stress levels for use in the structural analysis. Test specimens included integrally stiffened wing plank sections and various fuselage skin-stringer arrangements. Typical panels and results are

shown in figure 8. Crack propagation tests were also carried out on fuselage sections.

Particular attention was paid to the selection of suitable tension design allowables for the wing and fuselage structures, as shown in figure 9. Allowables were established at the same percentage of tensile ultimate strength as currently used in aluminum aircraft. This criterion is believed to be conservatively realistic.

Weights were established for all primary structural members by actual structural analysis. An indication of the extent of this work is shown in figure 10. Typical for each configuration was a complete preliminary stress analysis and member sizing for four fuselage cross sections, sixteen wing cross sections, six canard stations (where applicable), six landing-gear elements, and the wing pivots. Conditions investigated included subsonic and supersonic flight maneuvers and ground conditions of landing and taxi. Gust loads were found to be less critical than maneuver loads.

For the purpose of providing a substantial basis for structural analysis, a primary wing structural arrangement was designed for each configuration. Typical areas given consideration include those shown in figure 11. Basic wing structure consists of high efficiency, machined, integrally stiffened titanium skins stabilized by truss-type ribs and beams for minimization of thermal stresses. This basic construction provides integral fuel tanks similar to those in current use for storage of fuel burned off in the early part of flight. For fuel to be retained in the wing during cruise a system of thermally, isolated tanks are employed which function as self-contained, pressurized cells, acting in part as wing-shear-carrying material, with minimum, low-heat-conduction attachments to the surfaces. The lower surfaces and tanks are readily removable for inspection and maintenance of the wing structure.

A typical landing-gear arrangement is illustrated by the SCAT 17 main gear shown in figure 12. The gear retraction and stowage problem turned out to be an area of primary difficulty in all configurations. Large ground clearance angles required for take-off and landing, as well as large engines, contributed to the need for exceptionally long gears. No appreciable protuberance of the stowed gear was allowed. These factors demanded substantial detail development in the landing-gear studies. The large differences in configurations led to a different gear arrangement for each airplane. In every case retracting and door mechanisms were carefully worked out, the 80,000-pound equivalent single-wheel load requirement was met, and the gear stowage problem was solved. Cooling of tires and associated equipment was provided as required. Structural analyses of the landing gear included static

and dynamic load conditions encountered during take-off, landing, and taxiing, to establish reliable weight allowances for these installations.

For configurations with variable-sweep wings the detail design of fail-safe wing pivots was carried out (fig. 13). Also, design studies were made of actuator installations and routing of functional systems through the wing pivot area. These studies provided sufficient information to establish accurate weights in this critical area. The wing pivot illustrated is applicable to SCAT 16 and is adequate in all respects, although further development is required to ensure that the self-lubricating friction bearings have reasonable life in the elevated temperature environment. Detail system design problems were not completely resolved, and further development of the components is required for operation at the temperature under consideration.

Engine inlets received a substantial amount of attention during the feasibility studies, since the type and length of the inlet has a large influence on structural weight and airplane performance. Efforts were made to keep the inlets axisymmetric and short, located in an area of stable and undisturbed flow, so as to maintain a reasonable influence on the total longitudinal area distribution and to minimize mutual inlet interaction and instability. An engine inlet of a type employed on all of the final configurations is shown in figure 14. The inlets of all configurations involved the application of a movable spike, throat boundary-layer bleed, and suck-in doors; the latter for low-speed operation. The depth to which weight analyses were performed is indicated in figure 15. Primary structure was subjected to rigorous structural analysis, secondary structure was treated largely by comparison with existing aircraft, and equipment and functional-system items were sized by design analysis of requirements. The scope and selected emphasis of this work was adequate to provide a reliable, realistic weight basis for the study.

DESIGN DEVELOPMENT

The configuration history is illustrated in figure 16 where the number of configuration cycles is shown as a function of time for each concept. The four Mach 3 configurations underwent several cycles of design refinement during the program. For example, 10 versions of SCAT 16 were studied in perfecting the final design. Also shown is work on SCAT 4 and SCAT 15, which were tabled at midterm. This action took place after it was determined that each of these configurations had certain fundamental problems and was not competitive in its current form with SCAT 16 and SCAT 17. Also shown is the initiation of the Mach 2.2 aluminum study at the midterm of the contract.

At the outset, efforts were made to establish as many elements common to all four configurations as possible without departure from the basic concepts. Common fuselage cross-sectional geometry was established as shown in figure 17. Fuselage outside diameter is fixed at 125 inches with a standard wall thickness of 4 inches to the trim line. This gave the initial geometry as shown. Aisle width is 16 inches and seat width between the 2-inch arm rests is 17 inches. These accommodations are comparable with current economy class international coach service. Baggage, cargo, and systems areas were placed in pressurized compartments under the cabin floor. The cabin general arrangement, which is similar for all configurations, is shown in figure 18. The five abreast seating arrangement and 34-inch seat pitch evolved naturally for a 125-seat capacity from consideration of the effect of fuselage fineness ratio on the wave drag/wetted area drag trade-off and structural weight. A four abreast first-class section was provided in the forward part of the cabin.

Two entrances, servicing provisions, galleys, and three lavatories were provided. Emergency exits, life rafts, and other essentials were provided according to existing regulations for overwater service. One window per side, per passenger row, was provided. The windows are 8-inch diameter, clear vision, and consist of two structural panes designed to operate at boundary-layer temperatures, and additional panes arranged to minimize thermal stresses and provide a cool surface next to the passenger.

Configuration studies included establishment of a basic flight station for three crew members consisting of a pilot, copilot, and flight engineer, and an additional seat for an observer. No direct forward visibility was provided in the cruise mode because of the severe drag penalty involved. Take-off and landing visibility was obtained with a variable geometry nose. In this mode the fuselage forebody is rotated about a canted axis such that the upper forebody drops away, giving the pilot an unobstructed forward view with visibility superior to that of current subsonic jet transports.

The slender-fineness-ratio nose led to concern over the attainment of a practical flight station arrangement. Consequently, a complete flight station mockup, as shown in figure 19, was built outside of the provisions of the contract to examine these problems. Evolution of the flight station design and construction of the mockup have demonstrated the feasibility of this arrangement, which is believed to be acceptable, with suitable modifications, to airline operating personnel. Size limitations may result in some redistribution of duties among the pilot, copilot, and flight engineer.

SCAT 4 Analysis

The general arrangement of the original SCAT 4, as tested in the wind tunnel, included a high-aspect-ratio, arrow-type wing with a cambered fuselage, individual nacelles with two-dimensional inlets, and a carefully integrated engine air induction system and installation to obtain the maximum favorable interference effects. This arrangement is shown in figure 20. The empennage was conventionally arranged and fuselage mounted. Movable wing outer panels were employed for aerodynamic control. All elements of the configuration were precisely shaped and positioned through many hours of wind-tunnel development to provide exceptional aerodynamic efficiency in cruise.

Initial sizing studies indicated that the aerodynamic achievement was being overshadowed by a severe structural weight problem in the wing and nacelles. In preliminary studies, a take-off weight of 470,000 pounds produced a range of only 2,700 nautical miles. The high wing weight, over 92,000 pounds, represents 19.5 percent of the total gross weight. Studies of means of reducing this weight showed that the wing structural aspect ratio could be reduced to provide a weight saving that would more than offset the resulting drag-due-to-lift penalty. The modified wing planform is compared with the original planform in figure 21. The aspect ratio was reduced from 1.72 to 1.39, the wing trailing-edge notch was filled in as shown, and the wing thickness ratio was increased slightly. The increased primary structure area is evident from a comparison of the shaded areas in the figure.

The original engine arrangement utilized two-dimensional inlets located underneath the wing and ducts passing through the wing to a high trailing-edge location of the engines. This resulted in long, heavy engine inlets (fig. 22). In order to improve this situation, a variety of engine installations, including dual arrangements with both split and common inlets of various shapes, were investigated. Short, individual, axisymmetric inlets were finally incorporated as shown in figure 23. The low aspect ratio of the wing and critical ground clearance dictated close lateral spacing of the nacelles, as indicated, and necessitated the use of splitter plates between them to preclude adverse interference effects in the event of an inlet unstart during cruise. Compared with the original nacelles and inlets, the estimated overall weight saving was 19,000 pounds per airplane.

The original configuration incorporated a large number of individual Krueger type leading-edge flaps to improve maximum lift (fig. 24). A detailed design and weight analysis of such a leading-edge flap system was made, indicating an incremental weight of 8,000 pounds for the installation, Also, it was determined that the full effect of this flap system could not be utilized because of the

high angle of attack associated with its high lift coefficients. Superior range-payload characteristics resulted when the Krueger leading-edge flaps were eliminated and the wing area was increased slightly to compensate for their effect on maximum lift. Similarly, studies showed that replacement of the all-movable outer panels with conventional ailerons would result in a weight saving and would likewise improve the range-payload.

The major design modifications previously described, together with minor changes in detail design, resulted in the final SCAT 4 airplane shown in figure 25. It has a wing area of 5,150 square feet and an aspect ratio of approximately 1.39. Span is approximately 85 feet, and the length is 235 feet. All mission requirements are met at a gross weight of 384,000 pounds. With fuel distributed in the wing and fuselage as indicated by the shaded areas in figure 25, excellent balance characteristics are achieved.

As originally tested in the wind tunnel and corrected to full-scale values, the maximum subsonic lift-drag ratio of SCAT 4 was 14, whereas the final arrangement has an L/D of 11.5. This reduction results primarily from the reduced aspect ratio. The original wind-tunnel maximum lift-drag ratio corrected to full-scale Reynolds number at Mach 3 shows 8.2, whereas the final value is 7.5. This reduction is attributable to a number of geometric adjustments including tail size, a small increase in wing thickness ratio, and some degradation of the favorable interference of the original air induction systems and nacelles. These changes between initial and final lift-drag ratios are summarized in figure 26.

The final gross weight established for this airplane was 384,000 pounds. Distribution of this weight is shown in figure 27. It will be noted that the final wing weight has been reduced to less than 41,000 pounds, and is only 10.6 percent of the gross weight as compared with the original 19.5 percent.

A SCAT 4 size-optimization chart is shown in figure 28. The take-off gross weight (T.O.G.W.) and wing-area relation required to perform the mission are shown for several values of thrust-to-weight ratio T/W. Nominal thrust ratings here and throughout this study are uninstalled thrust ratings. This chart shows that if take-off field length and take-off lading-speed requirements were ignored, an airplane meeting design mission and sonic-boom requirements would have been achieved at a weight of approximately 350,000 pounds.

If the take-off and landing-speed requirements are to be met, a substantial wing-area increase is required, with a corresponding increase in airplane gross weight to 354,000 pounds. In order to meet

the 9,500-foot hot-day take-off field length requirement at an altitude of 1,000 feet, an increase in engine size, and a further increase in wing area is required, resulting in the final airplane weight of 384,000 pounds and wing area of 5,150 square feet. For SCAT 4, the take-off requirement was, in final analysis, the critical factor in girplane sizing. The second segment climb requirement is met or exceeded by the final airplane.

The final SCAT 4 characteristics summary is shown in figure 29. The gross weight is 384,000 pounds; and four NASA D type engines are used with an uninstalled thrust of 44,000 pounds of thrust per engine. Sonic-boom requirements are met. Take-off noise level under sea-level standard day conditions 3 miles from start of take-off is 107 PNdb after thrust is reduced to match the second segment climb requirement. Landing noise level under the same conditions is 110 PNdb 1 mile from the end of the runway on the 3° glide slope. Under hot-day conditions these levels will increase to 117 and 118 PNdb, respectively. Airport performance and speed requirements are met with the exception of landing distance. This latter can be met with minor design refinement.

Two low-speed aerodynamic problems exist on this airplane. These are illustrated in figure 30. The first is a low-speed pitch-up characteristic common to all arrow wing planforms, as indicated in the curve of pitching-moment coefficient C_m as a function of lift coefficient C_L. The longitudinal static stability is nonlinear through most of the lower ranges of lift coefficient C_L, with instability occurring in the final approach and landing flare regimes. The second major low-speed problem is that damping of the lateral-directional oscillation at approach speeds with dampers off is in the unsatisfactory range as shown in figure 30. (In this plot, $C_{1/2}$ is the number of cycles to damp to 1/2 amplitude, ϕ is the roll angle, and V_e is the equilibrium side velocity.) Improvement of this condition requires reduction of dihedral effects (C_{l_β}) and/or improvement in lateral control effectiveness in conjunction with a damping system. A damping system requiring spoiler operation to improve this condition was not considered practical because of the large drag penalty resulting from spoiler operation.

Because of the foregoing unresolved aerodynamic problems and because the final configuration was a sufficient departure from the original wind-tunnel arrangement to require additional wind-tunnel testing for further configuration development, contractor work on this concept was discontinued for the remainder of the program.

SCAT 15 Analysis

The NASA SCAT 15 concept, shown in figure 31, represents a highly advanced aerodynamic treatment of the requirements for efficient high- and low-speed flight. Both a fixed and a variable-sweep wing are employed, the two merging to form a single arrow wing for supersonic speeds. Vertical and horizontal tails are mounted on the tips of the fixed wing, the horizontal surfaces serving as longitudinal stabilizers and controllers, and lateral controllers. The fuselage is cambered, the power plants are carefully positioned for favorable interference effects, and the combination wing is precisely twisted and cambered for maximum supersonic aerodynamic efficiency.

Early in the development effort, it appeared that the wings would be a major weight problem. Definition of the loads in subsonic flight was difficult, and consequently wind-tunnel tests were conducted by NASA to obtain pressure distributions. Designs and analyses for strength based on these data, and analytically derived loads for taxiing and supersonic flight conditions, highlighted the basic wing weight problem of having essentially two high structural-aspect-ratio wings, each critical under different ground or flight conditions. A suggested modification to alleviate the weight problem is shown in figure 32. Filling in the trailing-edge notch reduced the structural aspect ratio and increased the physical thickness of the wing. The proposed modification was considered an unacceptable alteration of concept and was not adopted. The wing weight problem then was attacked by weight-drag trade-off studies to establish optimum thickness ratio. Only minor improvements in wing weight were possible by this means.

The wing-tip control and stabilizing surfaces provided exceptional aerodynamic qualities because of the local upwash field and the improvement of effective wing aspect ratio. However, in order to exploit these features, the fixed wing had to be made sufficiently stiff to maintain the required control-surface effectiveness at all speeds. This requirement compounded the basic wing weight to such an extent that it appeared advisable to mount the tail surfaces conventionally on the fuselage, as shown in figure 33. The proposed arrangement increased trim drag, substantially filled the arrow wing notch, and introduced sonic fatigue problems on the horizontal tail. Because of these factors, the arrangement was not adopted.

The final SCAT 15 configuration is shown in figure 34. Its basic geometric arrangement is essentially identical with the original NASA version. A "splitter" has been introduced between the inboard and outboard power plants to prevent inlet interaction in off-design and emergency situations including inlet unstart. Apart from this addition, the various components of the airplane have been adjusted in

relative size and shape only to the extent required to satisfy the payload and mission requirements in the most efficient manner that could be determined. The final wing area is 6,250 square feet, wing aspect ratio is 2.22, wing span is approximately 118 feet, and overall airplane length is 271 feet. Fuel is located in the wing and aft fuselage as shown in the shaded areas in figure 34. This arrangement provides satisfactory balance characteristics.

Since the final configuration is so similar to the original NASA wind tunnel (W.T.) model, the lift-drag ratios (L/D) for the airplane are virtually identical to the corrected values for the tunnel models. As shown in figure 35, subsonically the airplane L/D is 15.1 and the corrected tunnel model ratio is 15.0, while supersonically the airplane and model have identical L/D's of 8.0.

It should be noted that the SCAT 15 achieved the highest aerodynamic efficiencies of any of the SCAT configurations, and that these efficiencies were preserved during the development work as essential configuration concepts. The exceptional aerodynamic efficiency achievement previously noted for the SCAT 15 was overshadowed by the associated weight penalties. The weight breakdown and weight ratios are summarized in figure 36. The wing has a structural weight in excess of 119,000 pounds, representing about 22 percent of the airplane gross take-off weight. This weight fraction is roughly twice that of the other configurations and results in a high empty weight fraction of 51.3 percent. The resultant weight growth, coupled with sonic-boom restrictions in climb, leads to excessive engine-thrust requirements and high fuel consumption with resultant mismatch of the engine and airplane. Take-off gross weight was arbitrarily set at 550,000 pounds. The reasons for the high wing weight of this airplane deserve further explanation. Figure 37 summarizes the structural loading conditions that were investigated and identifies the critical conditions. It will be noted that the movable panel is designed by the 2.5g subsonic maneuver condition while the aft fixed wing is critical for taxiing. The lift on the movable wing supports most of the airplane weight subsonically without the benefit of appreciable inertia relief. Therefore, it experiences extremely high up-bending loads in this condition. Conversely, the aft fixed wing, which is loaded relatively lightly in flight, supports most of the major inertia items directly. These inertia items are responsible for dynamic down-bending loads of critical magnitude during taxi. Thus, the weight provided for strength in up-bending does not contribute materially to strength required in down-bending, and vice-versa. The result is virtually two independent wings and, consequently, twice the normal wing weight. The wing overlap problem compounds the weight problems of this configuration.

The SCAT 15 characteristics are summarized in figure 38. The take-off weight of 550,000 pounds yields a maxim range of only 2,650 nautical miles with a full payload of 26,125 pounds.

The airplane is powered by four NASA "D" engines, each having an uninstalled, sea-level, static thrust rating of 60,000 pounds. This high level of thrust, required primarily by sonic boom restrictions in climb and acceleration, provides exceptional take-off performance. The FAA take-off field length (hot-day), 1,000-foot altitude, is 7,000 feet, with a lift-off speed of 165 knots. The airplane follows the required 2-lb/sq ft sonic-boom overpressure profile in climb, using over half the total fuel for this portion of the mission because of the high gross weight. Even after this large fuel burnoff, and with the high thrust available, the airplane initial cruise-weight is sufficiently heavy to produce a sonic-boom overpressure of 1.67 lb/sq ft, which exceeds the specified value of 1.5 lb/sq ft.

At design landing weight, the touchdown speed is 130 knots and the FAA landing-field length is 7,260 feet, both within the operating levels of current subsonic jets. Ground noise is 80 PNdb during take-off at a point 3 miles down the runway from the start of take-off. This result is for standard-day conditions, with power cut back to that required by second-segment climb. A hot-day take-off adds 10 PNdb to the noise level. In landing approach, the standard-day ground noise level is 95 PNdb, 1 mile from the end of the runway. Hot-day conditions add 8 PNdb.

Because of the high gross weight, deficiency in range, and excessively high cruise sonic boom, the SCAT 15 configuration was tabled at the midterm point in the study.

SCAT 16 Analysis

The NASA SCAT 16 concept, shown in figure 39, originated as a three-engine variable-sweep configuration employing a high-aspect ratio twisted and cambered wing in combination with an aft, fuselage mounted empennage. Two of the three engine pods were strut mounted to the fuselage beneath the wing trailing edge, and the remaining pod was mounted in the root of the vertical tail. The fuselage was cambered to improve the trimmed L/D ratio in cruise. The subsonic aerodynamic efficiency of the high-aspect-ratio wing was excellent, while the supersonic characteristics compared reasonably well with the other configurations.

Initial studies indicated this airplane, in the wind-tunnel configuration, had a range of 1,890 nautical miles for a gross weight of 346,500 pounds. Wing weight was 19 percent of gross weight. Before

an effort was made at incorporating design modifications in other areas, the basic wing weight problem was attacked by trade-off studies of aspect ratio, thickness ratio, and weight to establish optimum wing geometry. The final arrangement is shown in figure 40.

An aspect ratio of 6 was derived, together with a root thickness ratio t/c of 12 percent and a tip thickness ratio of 7 percent, which yielded a reduction in wing weight of approximately 16,000 pounds and an increase in range from 1,890 miles to the required 3,200 miles. The aspect ratio A.R. was selected by using minimum design mission take-off weight as the optimizing criterion. Figure 40 also indicates reduction of wing sweep angle to alleviate the aerodynamic-center shift problem.

Studies up through the midterm of the analysis utilized the original three-engine arrangement; and it was found that satisfactory range-payload characteristics could be achieved. However, a three-engine arrangement does not appear to be entirely satisfactory because engine-out performance for extended range, over-water flights is marginal. In addition, this arrangement requires larger engine sizes which will make engine ground handling requirements more severe. Accessibility and engine removal of the power plant located in the vertical tail are poor. For these reasons, a four-engine arrangement was considered necessary. One possible four-engine arrangement that was studied briefly is shown in figure 41. Because of engine-out problems and design complexity, this arrangement was not acceptable.

The final four-engine arrangement adopted for the study employs individually podded engines, two below the wing and two above, as shown in figure 42. The underwing engines are strut mounted off the fixed wing root. Careful shaping of this root section and orientation of the pivot and movable wing within the root facilitate this installation and provide adequate structural continuity over the landing gear bay. The remaining two engines, strut mounted above the aft fuselage, are located so as to enhance airplane balance and to be accessible for service and replacement. A minimum spacing was selected to avoid inlet-shock-wave interference, to prevent jet impingement on the vertical tail, and to minimize stalled engine effects on airplane directional stability. The total installation helps to provide an arrangement with minimum landing-gear-length requirements and maximum latitude of gear-retraction motion; both of these items are of great importance in the design of a satisfactory, fuselage-mounted landing gear.

Incorporation of the proposed four-engine arrangement emphasizes the need for changes in the horizontal-tail position because of engine-exhaust impingement and sonic fatigue problems. The required change is shown in figure 43, where the horizontal tail is moved from the

original location low on the fuselage tail cone to a new position on top of the vertical stabilizer. To offset the high rolling moment due to sideslip of the high horizontal tail, negative wing dihedral has been incorporated.

The proposed arrangement has problems of the T tail, namely pitch-up in both high- and low-speed flight. For low-speed flight, the use of large chord, full-span slats on the low-aspect-ratio wing will provide adequate alleviation. Means for eliminating pitch-up tendencies in high-speed maneuvering flight are known, but will require further development for transport application.

The final arrangement of the SCAT 16, shown in figure 44, preserves the original twisted and cambered variable-sweep wing concept and the cambered fuselage, but departs significantly in wing aspect ratio, wing dihedral, horizontal-tail location, and number of engines. Detailed designs have been developed for the wing pivot, engine-support system and landing gear so that a reasonable level of confidence has been established in the feasibility and weights of these critical items. Fuel tanks are located in the wing and aft fuselage as shown by the shaded areas in figure 44. This arrangement provides acceptable balance characteristics. The design take-off gross weight of the airplane is 425,000 pounds, wing area is 3,000 square feet, wing aspect ratio is 6.0, span is 134 feet, and overall length is 241 feet.

A comparison of the original and final lift-drag ratios is shown in figure 45. The effects on L/D of the changes to tail and engine arrangements were determined analytically. Limited experimental verification of the final values is available from supplementary NASA and Lockheed wind-tunnel tests of similar configurations. The subsonic L/D was primarily affected by the aspect-ratio change, the final value of 15.2 being only 69 percent of the original 22. The change in supersonic L/D from 7.2 to 6.7 was caused primarily by the increase in nacelle wetted area.

The final weights and weight fractions for the SCAT 16 airplane are shown in figure 46. The wing weight fraction of 11.6 percent, although higher than those for the fixed-wing airplanes, is sufficiently low to permit an empty weight fraction of 43 percent. It should be noted that this is a substantial improvement over the original high-aspect-ratio configuration with a wing weight fraction of 19 percent. The final airplane weighs 425,000 pounds and performs the required mission.

By means of the same technique described for SCAT 4, size optimization of SCAT 16 was performed as shown in figure 47. With airport-performance requirements neglected, a take-off gross weight of

415,000 pounds, together with a thrust-weight ratio T/W of 0.37, would define the minimum size of airplane capable of achieving the desired range of 3,200 nautical miles while meeting all sonic-boom requirements. In order to satisfy airport speed requirements, wing loading W/S must be reduced by the addition of wing area beyond that required solely for range. With a trimmed usable lift coefficient of 1.4, the 165-knot take-off speed requirement is met with a wing loading of 142 pounds per square foot, so that the final wing area is 3,000* square feet and the take-off weight is 423,000 pounds. Critical field lengths, including hot-day take-off at 1,000-foot altitude, are satisfied by this combination of wing loading and thrust loading. The thrust-weight ratio of 0.37 is adequate for second-segment climb and transonic acceleration.

The final SCAT 16 characteristics are summarized in figure 48. The airplane performs the required 3,200-nautical-mile mission with a full payload of 26,125 pounds at a take-off gross weight of 425,000 pounds. The total fuel required, including reserves, is approximately 212,000 pounds.

The airplane is powered by four NASA "D" engines, each having an uninstalled sea-level static-thrust rating of 39,400 pounds. The engine size is determined primarily by transonic acceleration and take-off requirements. Take-off field length is 9,500 feet for hot-day, 1,000-foot-altitude operation, with a lift-off speed of 165 knots. Touchdown speed in landing is 128 knots, and an FAA field length of 7,100 feet is required at landing weight.

Noise levels are within requirements in all cases. The 2 lb/sq ft sonic-boom profile is flown in climb; and initial cruise overpressure is only 1.35 lb/sq ft. Critical standard-day ground noise levels in take-off and landing are 95 and 98 PNdb, respectively. These levels are increased to 105 and 106, respectively, for hot-day conditions.

SCAT 17 Analysis

The SCAT 17 concept, shown in figure 49, features a low-aspect-ratio fixed delta wing having thin airfoil sections. The concept achieves moderate supersonic lift-to-drag ratios in combination with a structurally efficient wing planform shape. The wing is a delta planform with a Supersonic leading edge incorporating a full-span flap. The fuselage is a straight, uncambered body mounting a conventional vertical tail, a canard, and an aft horizontal stabilizer, the latter folding down for aerodynamic-center control and improved directional stability in supersonic flight. The individually podded engines are strut mounted below the wing, well aft, and separated for avoidance of

*3,730 square feet in aft swept condition.

shock ingestion into the inlets. This installation also avoids exhaust impingement on the horizontal tail during take-off and climb.

Preliminary studies of this configuration indicated that a wing weight fraction of 11 percent could readily be achieved and that range payload would be in the desired area. Design effort on SCAT 17 was devoted to understanding and solving problems of stability and control and airport performance.

The original engine arrangement, well below the wing as shown in figure 50, dictated the need for an exceptionally long main landing gear. The final arrangement, shown in figure 50, minimizes landing gear length and improves drag characteristics by trading substantial reductions in wetted area (12 percent) and wave drag for lesser increases in interference drag. The outboard engine is moved up so the engine center line roughly coincides with the wing chord plane. The wing structure is carried over the top of the nacelle, leaving normal engine access doors for service and engine removal over the entire lower periphery of the nacelle.

The inboard engine is moved up so that the inlet is close to the lower surface of the wing. A bend is made in the aft portion of the induction system so that the engine itself penetrates the wing trailing edge and is inclined nose-down with respect to the wing chord plane for better alinement of the thrust axis with the cruise line of flight. The elimination of pylons and integration of wing and nacelle structures produced a net saving in propulsion-system weight.

An additional advantage of the modified engine arrangement is increased ground clearance, which permitted incorporation of negative wing dihedral to improve low-speed lateral-directional characteristics. This geometric negative dihedral also provided satisfactory dihedral effect at high speed without the folded down horizontal tail.

Wing thickness ratio has been increased from 2 percent to 3 percent to provide sufficient stiffness without structural weight penalty. This increased thickness, in combination with a slight decrease in wing sweep, provides a solution to wing flutter problems.

Studies related to drag, directional stability, lateral stability, and overall performance indicated the potential advantages of exploiting the inherent longitudinal control power of a canard mounted well forward on a long fuselage forebody. It was found that the wing tip fold-down action and the aft horizontal tail could be eliminated when vertical tail area was increased and a fully adjustable canard with folding tips and leading- and trailing-edge flaps was employed. This installation is shown in figure 51. The added complexity of the canard is

offset by the elimination of the folding wing tips and aft horizontal tail. The jet impingement and sonic fatigue problems disappear with the removal of the horizontal tail. The landing problem associated with failure of the folding-wing-tip actuation system is eliminated. The canard tips are folded during take-off and initial low-speed flight. Their slight destabilizing effect is compensated by a small increase in vertical-tail area. During cruise and for the remainder of the flight the tips are extended, and an increase of 0.0020 in the yawing moment due to sideslip C_{N_β} is realized.

The variable-area canard is a powerful device for controlling aerodynamic-center position and can be used to compensate effectively for large center-of-gravity movements and wing-aerodynamic-center shifts normally encountered between subsonic and supersonic flight. This is illustrated in figure 52, which shows the variation of the aerodynamic center in percent of the mean aerodynamic chord $\bar{c}$ with Mach number.

As used on the SCAT 17, the canard tips are folded down at take-off (T.O.) to position the airplane aerodynamic center at 20 percent of the wing mean aerodynamic chord. During transonic acceleration, the canard tips are extended; the added area offsets the aft movement of the wing aerodynamic center resulting from the increase in Mach number. During Mach 3 cruise, the aerodynamic center is at 25 percent chord. During landing, the canard tips remain extended and the airplane aerodynamic center moves forward to 15 percent chord. Because of fuel consumption during the flight, the center of gravity of the fully loaded airplane moves from 18 percent at take-off to 10 percent chord at landing.

Satisfactory stability margins are realized during all regimes of the mission profile. During cruise, the 11-percent static stability margin (rigid) is reduced by flexibility effects and does not impose large trim-drag penalties.

The final SCAT 17 general arrangement, shown in figure 53, preserves the straight fuselage, delta-planform wing, and conventional vertical tail of the original NASA concept. The aft tail and folding wing tips have been replaced by the incorporation of a more sophisticated canard than the original. The power-plant installation has been changed, the nacelles being raised well above their original positions so as to reduce landing-gear height and weight and to provide a fuselage floor height more suited to current terminal facilities. The wing-thickness-ratio increase from 2 percent to 3 percent provides additional fuel capacity close to the airplane center of gravity as shown in figure 53.

The final wing has an area of 5,500 square feet, an aspect ratio of 2.16, and a span of 109 feet. The airplane has a take-off weight of 380,000 pounds and is 253 feet long overall.

The final L/D characteristics are quite similar to the corrected wind-tunnel data as shown in figure 54. The subsonic ratio of 11.5, achieved with leading-edge-flap deflection, is slightly higher than the original value because of the reductions in wetted-area drag associated with the elimination of the horizontal tail and the revised power-plant installation. The final Mach 3.0 cruise L/D ratio of 7.0 is almost identical with the original tunnel model value. In this case, the wetted-area-drag reduction and the reduced wave drag of the higher-fineness-ratio fuselage forebody and afterbody is offset by the increased wave drag of the thicker wing.

The final weights and weight fractions for SCAT 17 are shown in figure 55. The wing weight fraction of 9.2 percent is the lowest of all the configurations. The compounding effect of low structural weight is demonstrated by the final take-off weight of 380,000 pounds at which the airplane meets all mission requirements.

The size optimization process for SCAT 17 is illustrated in figure 56. Neglecting airport performance requirements, an airplane with a take-off gross weight of 361,000 pounds and a thrust-to-weight ratio of 0.37 will meet the design mission and sonic-boom requirements. If the airport speed requirements are to be satisfied, an increase in wing area is required, so that the wing loading W/S is reduced and the take-off weight is increased to 370,000 pounds. This adjustment is based on wind-tunnel data and gives a usable trimmed lift coefficient of 0.70. The take-off field-length requirement demands an increase in thrust-weight ratio T/W, so that larger, heavier engines are needed and increased wing area is required to maintain the wing loading. The final take-off weight is 380,000 pounds, and the final thrust-weight ratio is 0.42.

The final SCAT 17 characteristics are summarized in figure 57. The airplane performs the 3,200 nautical mile design mission with full payload at a take-off weight of 380,000 pounds. The total fuel required, including reserves, is approximately 188,000 pounds. The airplane is powered by four **NASA** "D" engines, each having an uninstalled, sea level static thrust rating of 39,400 pounds. The engine size is determined by take-off requirements. Take-off field length is 9,500 feet for hot day, 1,000 feet altitude operation. Lift-off speed is 165 knots. Touchdown speed is 127 knots and landing field length is 7,200 feet.

Sonic-boom overpressures are limited to 2 lb/sq ft in climb and a maximum of 1.35 lb/sq ft at the start of cruise. Ground noise levels

for standard-day conditions are 107 PNdb in take-off at the 3-mile station with power cutback to second-segment climb requirement, and 105 PNdb in landing, 1 mile from the end of the runway. These will increase to 117 PNdb and 113 PNdb, respectively, for hot-day conditions.

Aluminum SCAT 17 Analysis

Following the midterm review, NASA authorized Lockheed to proceed with the study of an aluminum supersonic transport to evaluate engine and airframe technologies closer to the current state-of-the-art. NASA guidelines for this study are shown in figure 58. The basic SCAT 17 was to be modified and resized to meet all SCAT mission requirements. The cruise Mach number was to be appropriate to an aluminum structure, namely, in the Mach 1.9 to 2.4 range. Data on NASA's turbojet "E" and turbofan "F" were supplied for this study.

The influence of cruising speed on structural weight for several materials is shown in figure 59. As shown, the weight penalty for an aluminum structure becomes very severe at cruise Mach numbers substantially above Mach 2.0. Detailed performance trade-off studies led to selection of a cruise speed of Mach 2.2.

The characteristics of the afterburning turbojet (E) and duct burning turbofan (F) engines are shown in figure 60. Each is based on turbine inlet temperatures of 2,400° R. The thrust-to-weight ratio of the turbojet is superior to that of the turbofan. However, the specific fuel consumption (SFC) of the turbofan in both Mach 2.2 cruise and low-speed holding is superior. Studies of these combined effects have shown that the duct-burning turbofan yields a lighter take-off weight aircraft than the turbojet. For this reason the NASA "F" engine was selected for the aluminum airplane.

Studies of the Mach 2.2 airplane were initiated by re-engining the titanium Mach 3 SCAT 17 with unchanged gross weight and wing area. The engine thrust to meet the take-off requirement remains the same, as shown in figure 61. Resulting transonic thrust and acceleration capability remains essentially the same as with the "D" engine. It is of particular interest to note that cruise thrust available at Mach 2.2 is half the thrust available at Mach 3.0 for an altitude of 65,000 feet.

The reason for this reduction in thrust available is shown in figure 62, where the progressive change in thrust with Mach number for a specific engine type is illustrated. Note that the thrust available is

halved as Mach number is reduced from 3.0 to 2.2. This loss is a direct result of the reduction in density of the air p delivered at the engine face, due to the reduction in ram-pressure. At the 65,000-foot altitude this density decreases from 0.064 to 0.029 pounds per cubic foot as the airplane is slowed to Mach 2.2. This characteristic applies to all engines. Note that thrust available for engines "D" and "F" are the same at Mach 2.2 for equal values of take-off thrust.

This thrust reduction can be regained by throttle advance. For the Mach 2.2 design the engine must be operated at a very high duct-burning rate to regain the thrust, which increases the specific fuel consumption as shown in figure 63.

The need for throttle advance is illustrated in figure 64. This chart shows the altitudes which will be flown for various degrees of throttle advance. The altitudes shown for both the Mach 2.2 and Mach 3.0 airplanes are based on engines having the same sea-level static thrust. If the Mach 2.2 airplane were flown with the throttle set to give minimum specific fuel Consumption, the operating altitude would be only 40,000 feet. Maximum L/D, however, occurs at an altitude of 63,000 feet and can be realized only by much greater throttle advance and higher specific fuel consumption. Maximum range reflects the compromise between L/D and specific fuel consumption. It occurs at 59,000 feet and a resultant specific fuel consumption of 1.46. Opening the throttle further to achieve the altitude necessary to avoid excessive sonic boom further penalizes cruising specific fuel consumption, and results in an operating altitude of 65,000 feet and a specific fuel consumption of 1.63. Mismatch and conflicting requirements have in this case caused the initial cruising specific fuel consumption to be 25 percent higher than the minim theoretically obtainable.

A similar comparison is shown for the Mach 3.0 airplane at the top of figure 64. Note that the maximum range operating altitude is at 69,000 feet, and exceeds that required by sonic boom. The specific fuel consumption achieved in this case is 1.59, and is actually lower by 5 percent than that of the Mach 2.2 airplane at the start of cruise sonic-boom-limited altitude.

The effect of this fundamental mismatch between the engine and the airframe at Mach 2.2 can best be seen on the mission profile shown in figure 65. In the early portion of the flight when the airplane is heavy, it is necessary that the throttle be advanced to a high duct-burning rate with a consequent degradation in specific range. A 1.5-lb/sq ft sonic-boom profile is followed with duct-burning as required, until an altitude is reached where the remainder of the flight can be performed at maximum range conditions. Note that throughout the

flight the engine is operated far away from the altitude for its minimum specific fuel consumption.

With this understanding of the Mach 2.2 airplane characteristics, the effects on maximum range may be readily assessed, and are illustrated in figure 66. The engine-airframe mismatch and sonic-boom requirement result in an average specific fuel consumption at Mach 2.2 which is only slightly better than at Mach 3.0. As is well known, the lift-drag ratio is somewhat higher at Mach 2.2, in this case, L/D increases from 7 to 7.8, and an 11-percent range benefit is obtained. Airframe empty weight for equal take-off gross weight has increased approximately 5 percent as a result of the inefficiency of the aluminum structure in comparison with the titanium structure and the increase in engine specific weight. This weight increase results in a decrease in fuel-to-weight ratio, which leads to a 10-percent range loss. Cruise speed has been reduced from Mach 3 to 2.2, resulting directly in a 26.5-percent range loss. The net result of these four fundamental influences on range is that the Mach 2.2 airplane for equal gross weights inherently has approximately 21 percent less range potential.

Numerous studies such as installing larger engines, installing advanced technology engines with lighter weight, and decreasing cruise speed below Mach 2.2, were made to determine means of reversing this trend. Neither increased engine size nor decreased cruising speed offered any significant improvement. Improved engine technology over that represented by engine "E" and "F" gives small benefits. The final conclusion, however, is that the size of the aluminum airplane must be greater than that of the Mach 3 airplane to meet the range requirement.

Sizing studies are summarized in figure 67. It is shown that an airplane of approximately a 500,000-pound gross weight is required to meet the range requirement, provided that the sonic-boom restrictions can be ignored. When the 1.5-lb/sq ft sonic-boom overpressure ΔP is retained, the variation of gross weight with range becomes essentially vertical so that the 3,200 nautical mile range cannot be achieved regardless of weight. For this reason, the final version of aluminum SCAT 17 was arbitrarily established at a 440,000-pound gross weight with a range of approximately 2,750 nautical miles.

The aluminum SCAT 17 as it finally evolved is shown in figure 68. The configuration differs slightly from that of the Mach 3 SCAT 17. Wing loading and thrust loading remain the same, since they were determined by airport performance. With the resulting larger wing, all engines were installed in underwing nacelles similar to the inboard installations of the Mach 3.0 airplane. Inlet and spike geometries are optimized for Mach 2.2 cruising conditions. Wing area is 6,350 square feet with an aspect ratio of 2.17. Wing span is 118 feet, and the

overall length 255 feet. Balance is satisfactory with fuel distributed as shown.

A summary of the characteristics of two Mach 2.2 aluminum airplanes is presented in figure 69. The 440,000-pound take-off gross-weight airplane can meet the take-off and landing-field length and speed requirements and the sonic-boom requirements. It is, however, grossly deficient in range. The 500,000-pound take-off gross-weight airplane meets the range requirement, but exceeds cruise sonic boom requirements. These deficiencies are the result of an inherent mismatch between engine and airframe. The fundamental nature of this mismatch is such as to preclude intercontinental ranges unless very significant advancements in engine or airframe state of the art are made.

STABILITY AND CONTROL

Examination of the static longitudinal stability of all four SCAT versions shown on figure 70 shows that the center-of-gravity location and the horizontal-tail and/or canard size were established to provide minimum positive margins for the take-off configuration. These static margins were comparable to those of present-day transports.

In cruising flight at Mach 3, substantially larger static margins exist for all the configurations. Trim drag for SCAT's 4, 15, and 16 is alleviated by use of wing twist and camber and a highly cambered fuselage. The static margin on SCAT 17 is kept small at Mach 3 by incorporation of the folding type canard surface. SCAT 17 trim drag is also alleviated by the positive zero lift moment provided by the 1° of negative wing incidence.

Static margins are normal during approach conditions for all the designs except SCAT 16, where a substantial forward movement of the center of gravity attributable to fuel burnout results in a larger static margin. Sufficient control is available for trim. The effect of fuel burnout on SCAT 17 is similar to that on SCAT 16, but the static margin is held to a minimum by utilizing the larger unfolded canard for the approach and landing condition.

Figure 71 presents a curve of the flexible pitching-moment coefficient $C_{M_{c.g.}}$ as a function of angle of attack for the SCAT 16 and 17 airplanes at cruise Mach number. The substantial reduction in static

margin during cruise at maneuvering load factors for SCAT 16 results from a serious tendency toward pitch-up at angles of attack greater than 5°. The shape of the moment curve shows that neutral longitudinal stability occurs in 1.75g maneuvers. This maneuvering limitation on SCAT 16 implies that an automatic pitch control device will be necessary to prevent the pilot from overshooting structural limits. SCAT's 4 and 15, which have similar pitch-up tendencies at high speed, would also require this same type of automatic pitch control.

Wind-tunnel tests conducted on the SCAT 17 model at angles of attack up to 9° indicated no pitch-up tendencies at high Mach numbers. Figure 71 shows that an angle of attack of 8° is necessary to attain 2.5g maneuvering load factor, and thus no pitch-up problem is indicated.

The pitch-up problem on SCAT's 16, 4, and 15 clearly indicates the need for additional research in this connection.

Lateral-directional handling qualities as reflected by the Dutch roll characteristics are presented in figure 72 for SCAT's 16 and 17 in comparison with two widely different configurations, the F-104 and the Electra. The damping $(1/c_{1/2})$ and roll-to-yaw parameter (ϕ/v_e) are shown for the approach and cruise conditions, with the requirement of MIL-F-8785 as a reference. For the data shown, the aerodynamic data include flexibility effects and the same type of rate dampers on all configurations and conditions. It is seen that improved stability and damping can be attained by phasing and optimization of the roll and yaw dampers.

During the landing approach both SCAT's 16 and 17 exhibit satisfactory Dutch roll characteristics. Although both configurations are satisfactory with roll and yaw dampers off, significant improvement can be attained in terms of reducing roll-to-yaw ratio by using dampers. The approach Dutch roll characteristics of the SCAT's 16 and 17 can be made equivalent to or better than present-day jet transports with either dampers off or on.

The Dutch roll characteristics in cruise for SCAT's 16 and 17 are shown to be satisfactory with either dampers off or on in comparison with the appropriate requirement. It is believed that either SCAT 16 or 17 could be made equivalent or better than current jet transports during cruise from a Dutch roll criterion.

Calculations have shown that the sensitivity of the inertia properties, dihedral effect, and directional stability on all SCAT configurations demand close attention to geometric and aerodynamic parameters to attain satisfactory handling qualities. Spiral stability for SCAT's 16 and 17 appears acceptable during cruise. SCAT 17 is stable on

approach, and SCAT 16 is slightly divergent but satisfactory on approach. Spiral stability is not expected to be a problem in these SCAT configurations.

Longitudinal handling qualities as represented by the short period undamped natural frequency ω_n and damping ratio ζ are shown in figure 73 for SCAT's 16 and 17 with the boundaries from MIL-F-8785 as a reference. The approach and cruise results which are presented include flexibility effects and identical dampers for both SCAT's. Longitudinal characteristics of the F-104, which has a pitch damper, and the Electra, which does not utilize a damper, are shown for comparison.

All SCAT configurations studied have similar high damping and low natural frequency in the landing approach. The damper-off data show SCAT's 16 and 17 to be between a current subsonic jet and a prop-jet in both damping and natural frequency. It is concluded that the SCAT configurations will be satisfactory during landing approach with dampers off.

Recent stability research indicates that the longitudinal handling qualities can in some cases be improved by increasing the pitch frequency in conjunction with modified pitch damping. The effect of incorporating a phased damper which is dependent on both rate and attitude to increase the frequency on approach shows that the SCAT configurations are capable of a high degree of optimization. The effect of rate damping only for the approach is to increase both damping and frequency slightly as on the lower portion of the damper-on arrows. It is concluded that since a pitch damper has been found necessary for other flight regimes, it can be used to improve handling characteristics during normal landings.

All SCAT configurations will be characterized in cruise by low damping if no pitch augmentation is provided. The low damping resulting from high cruise altitudes will be satisfactory for emergency operation, but must be improved for normal cruise. The effect of the phased damper as used for the approach configuration is also shown for the cruise condition. The lower portion of the arrows reflect improvement similar to rate damping only. The upper portions indicate the-major effect of phase damping which is to increase the frequency as well as to improve damping. It can be concluded that a simple pitch damper will be required for cruise and the SCAT configurations are amenable to improvement of pitch handling qualities by pure rate damping and to further optimization by phased damping.

The phugoid modes for approach and cruise are stable and have periods greater than 40 seconds and 400 seconds, respectively. No serious problems are apparent in this area.

The most serious dynamic stability problem on the supersonic transport is the engine failure and inlet unstart during cruise. The major factors affecting the resulting transient response are engine location and thrust loss, duct drag, shock-wave interference from the inlet, basic airplane stability and control characteristics, and automatic damping. It has been assumed in the analysis that no pilot corrective action was taken before 3 seconds. The transient maneuver following an engine failure must be limited to prevent excessive airloads and any motion divergence. It can be seen in figure 74 that the major perturbations are pitch and roll for SCAT 16 and yaw in the case of SCAT 17.

The critical engine on SCAT 16 was found to be the upper inboard powerplant, which produces a large nose-up moment that results in a large change in angle of attack and causes more than 1/2g increase in load factor. This pitch change is critical since a pitch-up problem exists on SCAT 16 in the cruise configuration. The shock-wave interference on wing and horizontal tail is very complex, and the resulting dynamics are extremely sensitive to nacelle location. The yawing moment and shock interference on the wing result in a left roll, as indicated in figure 74. The peak sideslip and resulting side acceleration do not appear serious. The same engine failure, with rate dampers on 3 axes, indicates that the transient maneuver can be minimized and be made acceptable.

The critical failed engine on SCAT 17 is the outboard powerplant, which produces a large yawing moment with little pitch or roll moment. If no automatic control device or damping is provided, a large sideslip will develop, with attendant side acceleration greater than -1 g. The angle-of-attack change is small; and the small roll angle at 3 seconds results from the inertia characteristics and roll due to yaw. The roll angle will increase significantly after about 3 seconds when the sideslip has reached a maximum in the event of no pilot corrective action. The same engine failure was studied with a 3-axis rate damping, and an automatic inlet spike which extended after engine failure to reduce drag and interference. This configuration provided acceptable structural and aerodynamic transients,

It can be concluded from the engine-failure studies during cruise that both SCAT's 16 and 17 will require highly reliable automatic damping and possibly some form of inlet modification to avoid extreme structural weight, oversized tail surfaces, or aerodynamic divergence such as pitch-up.

Figure 75 shows the variation of thrust required to maintain a given approach flight path for SCAT's 16 and 17. The relatively higher-aspect-ratio wing of SCAT 16 allows approach at approximately neutral speed-thrust stability, whereas SCAT 17 is approaching with a slight speed instability.

Simulator studies to date have shown pilot ratings increasing about one rating number when $\frac{d(T/W)}{dV}$ changed from zero to -0.0014. Pilots generally felt that the airplane with neutral and negative speed-thrust stability could consistently be landed safely but required more concentrated attention than would be desirable for routine landings. Seriousness of this problem depends upon other dynamic characteristics of the vehicle but, if it is significant, changes in configuration must be sought to alleviate it. The development and use of an automatic throttle control is one practical solution. This device is inherently fail-safe, since a failure of the device was not considered to be of serious consequence by the pilots participating in the simulator studies.

SUMMARY

Supersonic and subsonic mission and reserve fuel requirements of SCAT's 16 and 17 are shown in figure 76. The block fuel required to perform the 3,200-nautical-mile design mission is substantially less for SCAT 17 than for SCAT 16, the difference being approximately 13 percent. For a subsonic short-range mission of 600 nautical miles, SCAT 16 consumes slightly less fuel, as expected from its superior subsonic lift-drag ratio. The difference is 2.7 percent. It is interesting that the reserve fuel required for the maximum-range supersonic flight is essentially identical for SCAT's 16 and 17, whereas SCAT 16 requires somewhat less fuel than SCAT 17 for the subsonic short-range flight.

Although it is not the purpose of this paper to present economic analyses, a brief look at the comparative direct operating costs of SCAT 16 and SCAT 17 gives a measure of their overall technical acceptability. Direct operating costs for each design have been computed for several ranges and are shown comparatively in figure 77. Costs have been calculated by the 1960 Air Transport Association method and are based on equal aircraft utilization. Airframe prices of $24.0 million for SCAT 16 and $21.3 million for SCAT 17 were assumed. These figures, whose absolute levels are by no means firm, are believed to be correct relative to each other. The higher price of SCAT 16 is due to its increased structural weight and complexity. For supersonic flight at ranges from 1,000 to 3,200 nautical miles, the direct operating cost of

SCAT 17 is approximately 10 percent less than that of SCAT 16, as would be expected from the block fuel and price data. Direct operating costs for subsonic flights at ranges of 200 and 600 miles show similar direct operating cost advantages for SCAT 17. These differences are attributable to the price difference and to the lower block speed of SCAT 16, which results from the lower critical Mach number of the thick wing in the forward position.

The effects of typical off-design situations on range are illustrated in figure 78. In each case, the range shown is achieved without using any reserve fuel. As noted, encountering a hot-day profile with temperatures 40° above standard for the entire trip will reduce the range of SCAT 16 from 3,200 to 2,670 nautical miles. The corresponding value for SCAT 17 is 2,760 nautical miles. The loss is somewhat greater for SCAT 16 because of its higher initial weight and slower transonic acceleration characteristics.

The effect of an emergency cabin decompression at midrange requires that the remainder of the flight be subsonic and at low altitude, in this case 8,000 feet. Substantial reductions in range are shown. SCAT 17 experiences somewhat greater range reduction (540 nautical miles) than SCAT 16 (400 nautical miles) for this condition because of the lower subsonic L/D of SCAT 17.

The result of a midpoint engine failure is essentially the same for either design, namely a reduction in range of about 330 nautical miles. This emergency condition is met by an increase in thrust of the remaining engines by duct burning at a higher level so that Mach 3.0 cruise is maintained with a small reduction in altitude.

In all of the cases shown, the full 3,200-nautical-mile range may be restored by use of the standard reserve fuel.

All SCAT airplanes produce excessive sonic boom in climb if the airplanes are allowed to follow the climb profile that minimizes climb fuel, inasmuch as this acceleration will be conducted at relatively low altitudes. When a practical limit, such as 2 pounds per square foot, is placed on sonic-boom overpressure, transonic acceleration must be made at a higher altitude, with a resultant increase in climb fuel. If the range is to be maintained while a 2-lb/sq ft overpressure profile is followed, it is seen that additional fuel is required, and therefore, the airplane *gross* weight is increased. Increased gross weight in turn increases the required transonic acceleration altitude. This process normally stabilizes at a *gross* weight which satisfies both range and sonic-boom requirements. This *gross* weight is dependent upon the boom requirement and will increase if the allowable overpressure is reduced.

A plot of this relationship for SCAT 17 is shown in figure 79, with the 380,000-pound airplane spotted on the curve at 2 pounds per square foot. The sensitivity of airplane take-off gross weight to the boom requirement is extreme: gross weight varies from 366,000 pounds to 428,000 pounds as the allowable overpressure varies from 2.2 to 1.8 pounds per square foot.

A severe penalty in take-off gross weight would result if sonic-boom overpressures of less than 2 pounds per square foot in climb were required. It is clear that the sonic boom is a new and vital factor affecting aircraft size, and that size and economic studies must give it full consideration. There are, however, some possibilities which offer potential for improvement. The most interesting of these are in areas of drag reduction or power augmentation. An increase of L/D of 0.5 in the transonic range will reduce the boom by 0.1 pound per square foot without increase in gross weight. An increase in cruising L/D of 0.5 will reduce the sonic boom by 0.2 pound per square foot at the same gross weight; and a transient augmentation of thrust during the acceleration will have an equal effect.

Throughout the SCAT study a number of assumptions have been made in calculating the sonic-boom effects. For example, a ground-reflectivity factor of 1.9 has been assumed, although this factor will actually vary with conditions of terrain and ground cover. Figure 79 shows a substantial reduction in boom if a reflectivity factor of 1.7 is used. Because of the importance of this and similar assumptions in sonic-boom predictions, it is evident that continuing research in understanding the sonic boom is required and that detail design attention must be given to its effects and interrelation with airplane size.

The SCAT evaluation effort disclosed numerous areas for research important to the development of a satisfactory Mach 3.0 transport. Several aerodynamic items are listed in figure 80. These cover both improvement and feasibility categories. For example, the pitch-up problem of highly swept wings with practical horizontal tail locations is an unresolved problem which could, if not solved satisfactorily, impair the feasibility of the concept. Subsonic aerodynamic improvements in maximum lift and lift-drag ratio for low-aspect-ratio wing configurations will permit substantial reductions in airplane gross weight. Methods for improving low-speed lateral control on low-aspect-ratio swept wings should be developed. Means for improving transonic lift-drag ratios should be examined in more detail, since transonic characteristics affect climb fuel, sonic boom, and sensitivity of the airplane to hot-day conditions. Wind-tunnel tests showing effects of camber and twist on low-aspect-ratio wings are needed to verify theoretical improvements in trimmed lift-drag ratio. Determination of

dynamic stability derivatives from wind-tunnel tests should be continued. In addition, use of flight simulators is recommended to assist in establishing stability criteria and provide guidance that will insure the achievement of satisfactory handling qualities for the supersonic transport.

Structural and propulsion research areas considered to be profitable are shown in figure 81. In structures the problems are concerned with loads, testing methods, and materials. As in the aerodynamic research area, these needs may be categorized as improvement, feasibility, and program facilitation items. Investigations of interference effects on aerodynamic heating are desirable to improve the definition of design temperatures in specific areas. Simulator studies to establish structural criteria are neededto facilitate and improve the accuracy of loads definitions. Methods for accelerating proof and fatigue tests, including temperature effects, would be of the utmost value in facilitating structural development and demonstrating structural adequacy prior to flight testing and operation. Investigations of the need for and development of corrosion protection for titanium are vital for full confidence in the use of this material for primary transport structure.

The propulsion field offers opportunities for improvement in many important areas. Higher propulsive efficiencies are potentially available through the development of high turbine temperature engines with commercially acceptable life, and by the improvement of high altitude combustion efficiencies in thrust augmentation systems. Improvements in inlet systems to decrease sensitivity to transient flow disturbances and distortions are desirable for better performance, safety, and reliability. The development of lightweight high-performance exhaust systems would contribute materially to improvement in the extremely important thrust-to-weight ratio.

The problems of take-off and landing noise rate extensive study, including investigation of suppression devices in both inlets and exhaust systems, propulsive-aerodynamic-weight compromises, and operating methods to minimize noise.

With the conclusion of the NASA SCAT feasibility studies, it appears that the original objective of identifying promising configuration approaches has been accomplished. A substantial amount of quantitative guidance and direction has been made available to NASA for use in orienting future aeronautical research. A number of overall conclusions can be added to the many detailed ones which are already apparent:

1. Simplicity and weight considerations have been shown to be equally as important as high aerodynamic efficiency. The challenge

RESTRICTED

lies in obtaining high aerodynamic efficiency with configurations incorporating design features and weight that are readily adaptable to airplane requirements.

2. Supersonic transport speed must be substantially greater than Mach 2.2 for intercontinental range unless very advanced state-of-the-art engines are utilized. Even when such engines are incorporated, a Mach 2.2 or slower transport will not achieve the capabilities of a higher speed transport.

3. Of the original four SCAT configurations suggested by NASA, at least two have been shown to make feasible supersonic transports. One of these has variable wing sweep and the other a fixed wing. Each has inherent, but different, advantages and disadvantages.

4. A configuration substantially improved over that offered by any of the initial SCAT arrangements is required for a fully successful United States supersonic transport. Definition has been given to the research necessary to achieve this result.

5. The final choice of configuration for an actual supersonic-transport airplane depends upon the quality, simplicity, and reliability of detail design achieved in advanced versions with the application of further research and development.

MISSION PROFILE

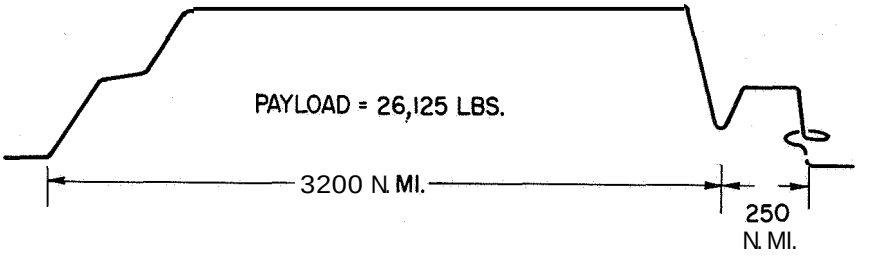

- CLIMB ALONG 2 PSF PROFILE
- CLIMB–CRUISE AT MACH 3 (BOOM LESS THAN 1.5 PSF)
- RESERVES
  - HOLD FOR 10 % TRIP TIME
  - *CRUISE 250 N. MI. TO ALTERNATE AIRPORT
  - *HOLD 30 MIN. AT 1500 FT.

Figure 1

AERODYNAMIC CORRECTIONS

WIND TUNNEL	AIRPLANE
$RN - 16 \times 10^6$	$RN \sim 400 \times 10^6$
STING MOUNTED - NO BASE DRAG	FUSELAGE AFTERBODY CLOSURE
SPECIFIC NACELLE SIZES, WING AND TAIL AREAS TESTED	COMPONENTS SIZED TO MEET MISSION & STABILITY REQUIREMENTS
MODELS TRIMMED ABOUT MOMENT REFERENCE CENTER	TRIM DRAG BASED ON ACTUAL CENTER OF GRAVITY POSITIONS
TOTAL PROPULSION DRAG NOT SIMULATED	SPILLAGE & BLEED DRAG INCREMENTS ADDED

Figure 2

[redacted]

NASA BASIC ENGINE COMPARISON

ENGINE TYPE	AFTER-BURNING TURBOJET	DUCT-BURNING TURBOFAN	DRY TURBOJET	AFTER-BURNING TURBOJET	DUCT-BURNING TURBOFAN
NASA DESIGNATION	A	B	C	C (A/B)	D
TURBINE INLET TEMP., °R	2,400	2,400	2,700	2,700	2,700
SLS THRUST	43,200	45,600	35,200	44,800	51,900
THRUST / WEIGHT	6.2	5.4	5.4	6.4	6.5
MIN SFC MACH 3.0	1.53	1.58	1.51	1.53	1.56
SFC -HOLDING AT 1500 FT.	1.35	1.01	1.23	1.13	.82

Figure 3

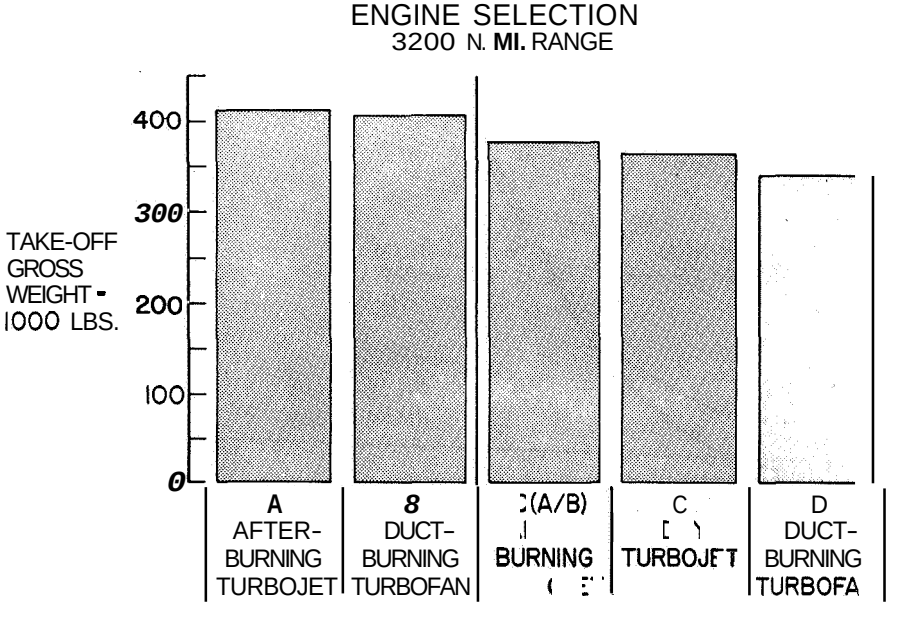

Figure 4

[redacted]

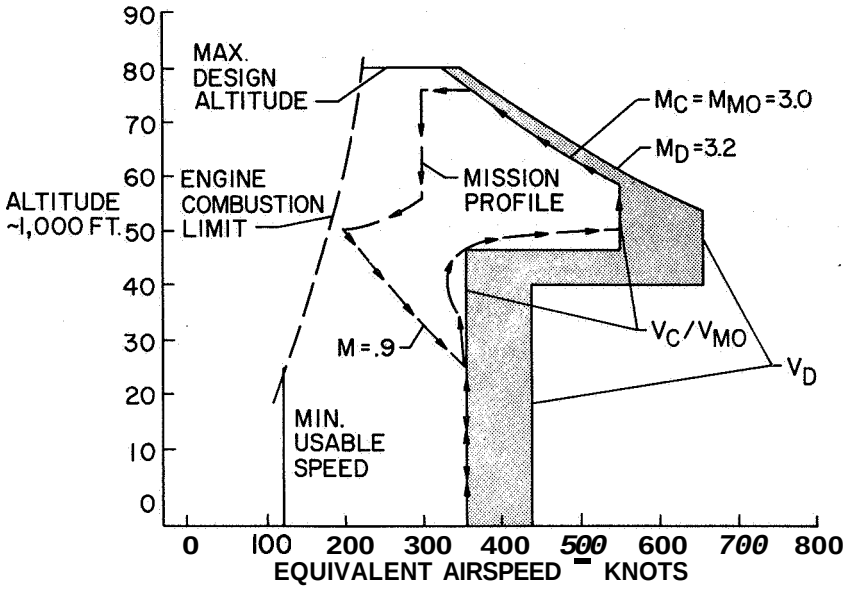

Figure 5

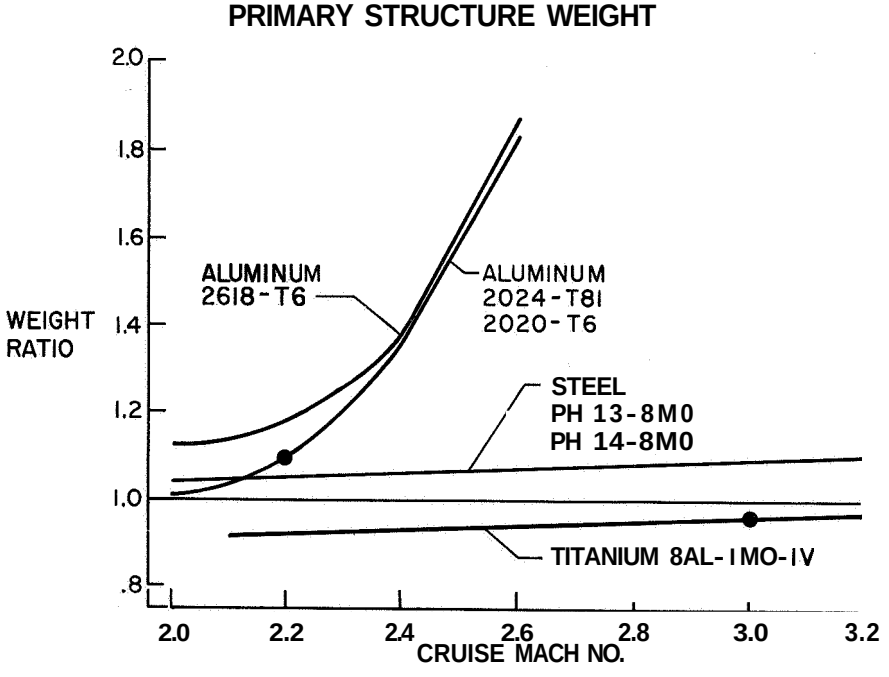

Figure 6

[redacted]

TITANIUM CHARACTERISTICS

TEAR RESISTANCE – RATIO $\frac{\text{TITAN. 8-1-1}}{\text{ALUM. 2024-T3}}$	1.56
FATIGUE RESISTANCE – RATIO $\frac{\text{TITAN. 8-1-1}}{\text{ALUM. 2024-T3}}$	1.50
FORMABILITY – BEND RADIUS – HOT	2T
– COLD	5T
MACHINABILITY – VOLUME REMOVAL (TITAN./ALUM.)	1/30
WELDABILITY – (TITAN./ALUM.)	YES/NO
CORROSION RESISTANCE – HOT SALT.	UNRESOLVED

Figure 7

STRUCTURAL WEIGHT SUBSTANTIATION

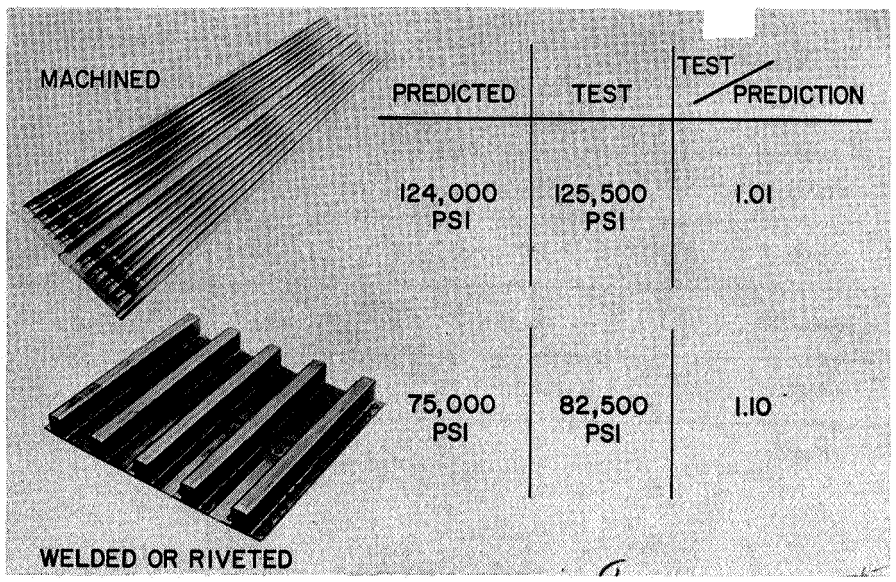

Figure 8

[redacted]

ALLOWABLE TENSION STRESSES

	TITANIUM		ALUMINUM	
	ALLOWABLE	% OF F_{tu}	ALLOWABLE	% OF F_{tu}
DESIGN ULTIMATE – LIFTING SURFACES & FUSELAGE BENDING	95,000	67%	50,000	67%
OPERATING STRESS – FUSELAGE HOOP TENSION	25,000	18%	11,000	18%

Figure 9

STRUCTURAL ANALYSIS SUMMARY

	STATIONS ANALYZED	CONDITION		
		SUPER-	SUB-SONIC	GROUND
FUSELAGE	4	✓	✓	✓
WING	16	✓	✓	✓
CANARD	6	✓	✓	✓
LANDING GEAR	6	–	✓	✓
PIVOTS	2	✓	✓	✓

Figure 10

PRIMARY WING STRUCTURE

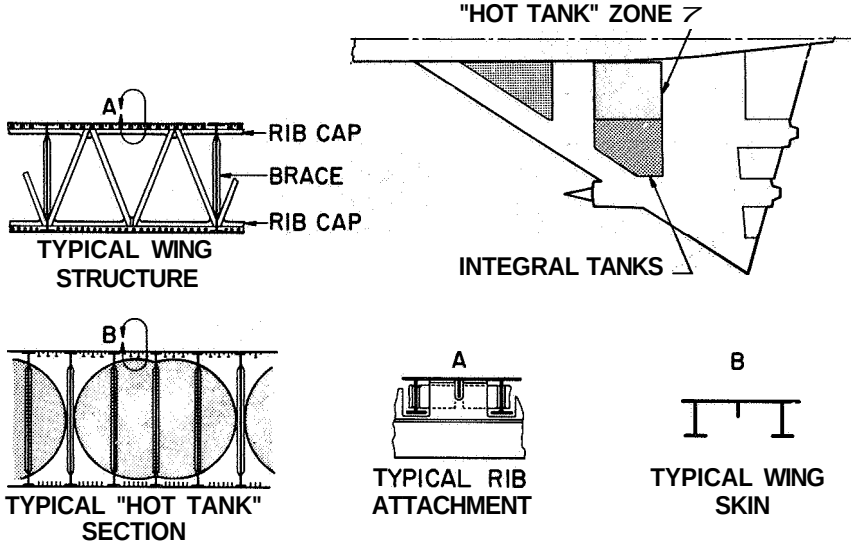

Figure 11

LANDING GEAR

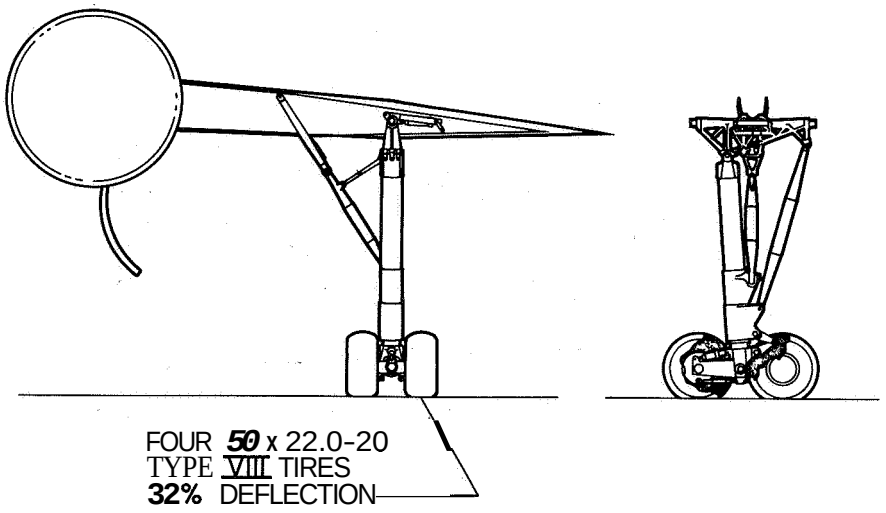

Figure 12

SCAT 16-WING PIVOT

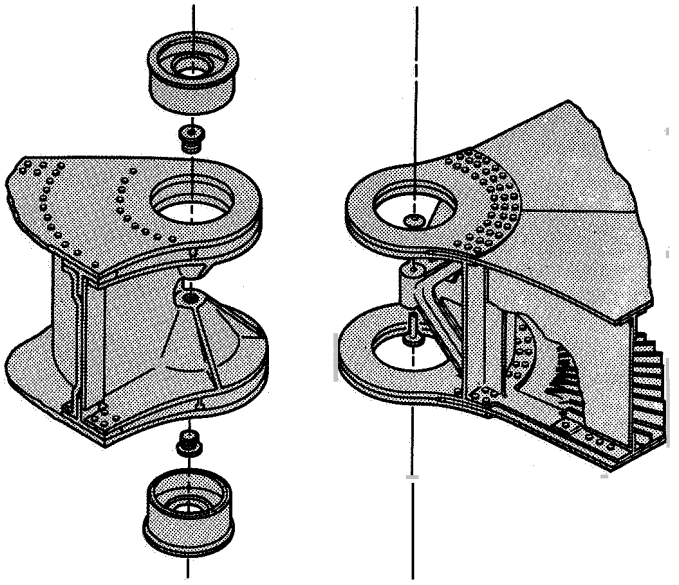

Figure 13

POWER PLANT INLET

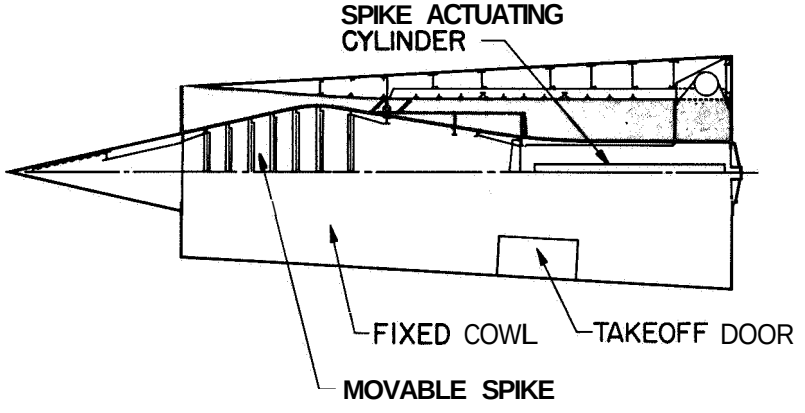

Figure 14

BASIS FOR WEIGHT PREDICTION

STRUCTURAL ANALYSIS	DESIGN ANALYSIS	COMPARISON WITH EXISTING AIRCRAFT
WING BOX BEAM	CABIN ENVIRONMENT	CONTROL SURFACES
FUSELAGE SHELL	PASSENGER FURNISHINGS	LEADING EDGE FLAPS
WING PIVOT	OPERATING EQUIPMENT	PROPULSION ACCESSORIES
LANDING GEAR	HYDRAULIC SYSTEM	AVIONICS
CANARD SURFACES	ELECTRICAL SYSTEM	SECONDARY STRUCTURE
AIR INDUCTION & NACELLE	CONTROL SYSTEM	TAIL SURFACES
TRAILING EDGE FLAP.		
KRUEGER FLAPS		

Figure 15

CONFIGURATION HISTORY

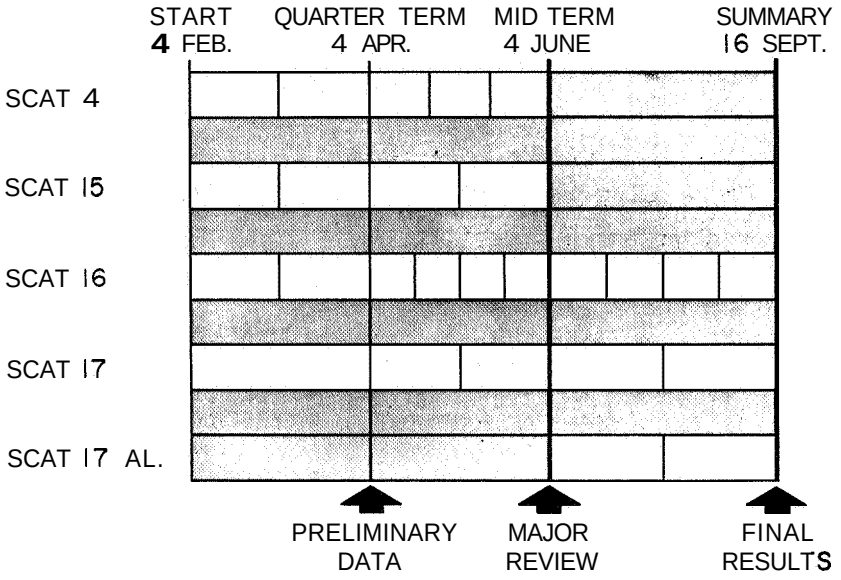

Figure 16

SCAT - TYPICAL CABIN CROSS SECTION

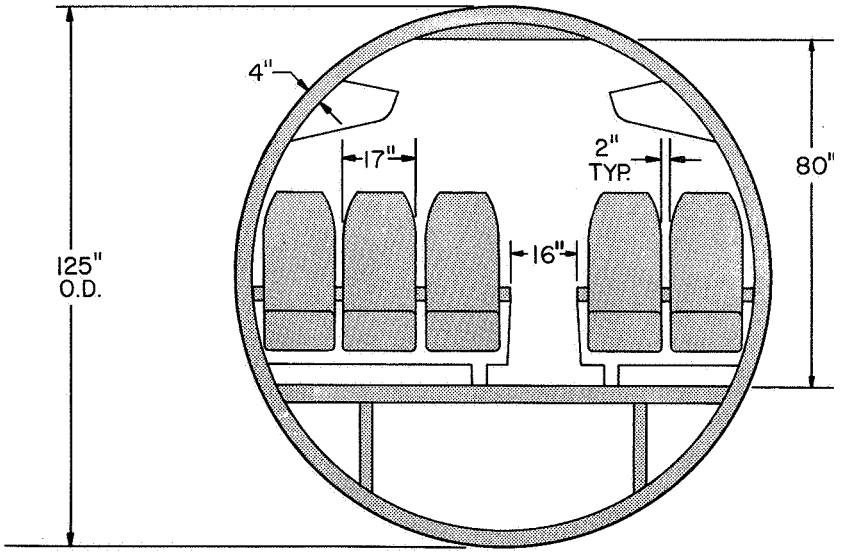

Figure 17

CABIN GENERAL ARRANGEMENT

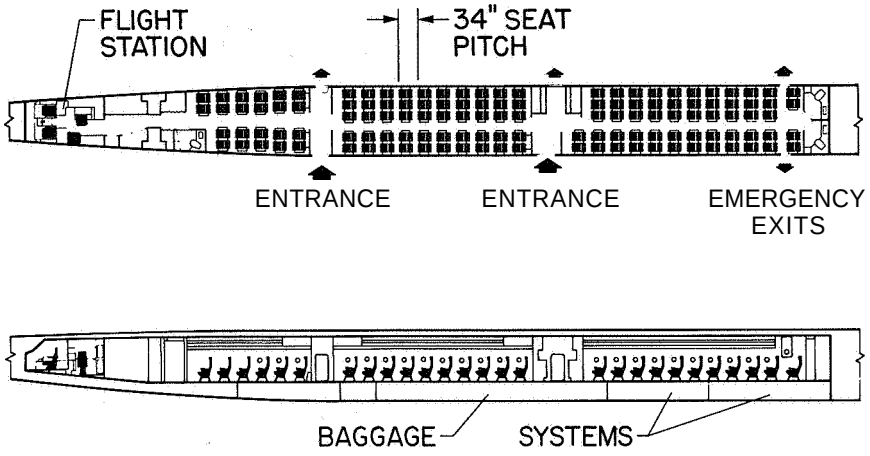

Figure 18

FLIGHT STATION
TAXI ATTITUDE

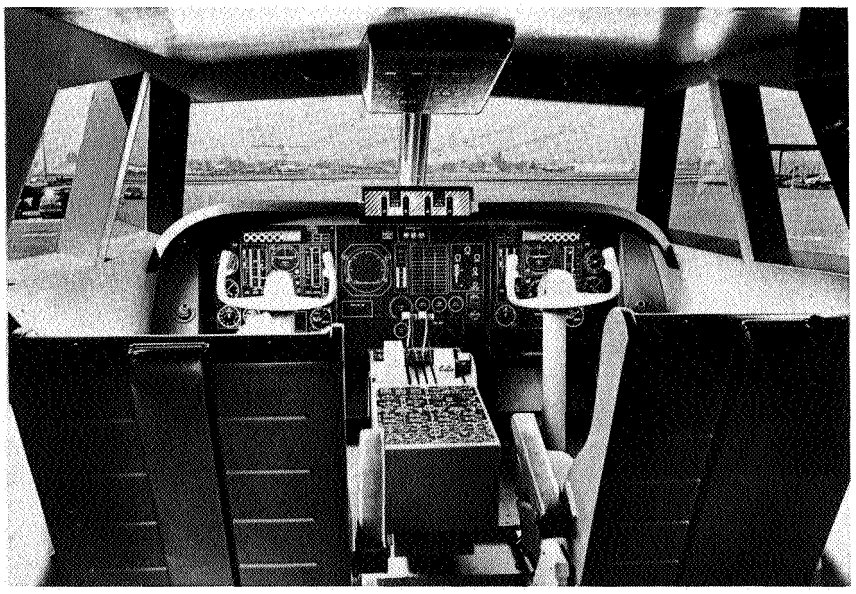

Figure 19

SCAT 4 -NASA CONFIGURATION GENERAL ARRANGEMENT

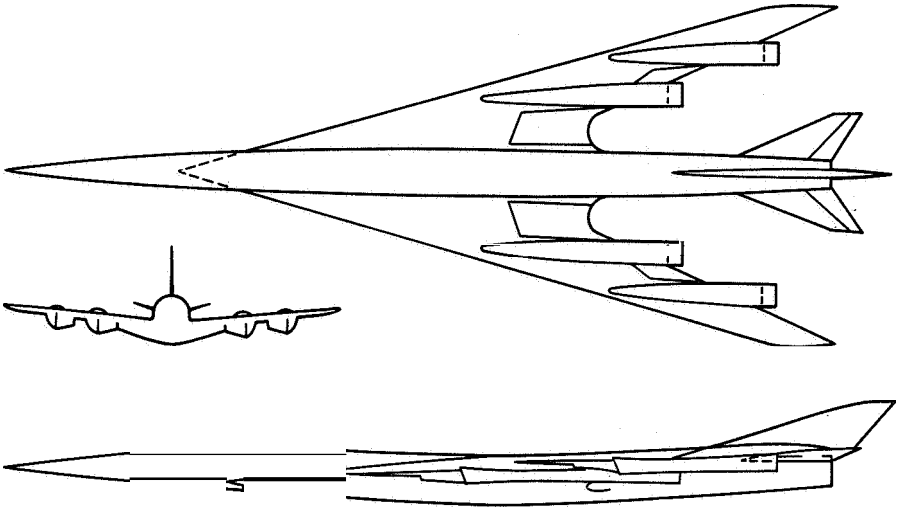

Figure *20*

SCAT 4–WING PLANFORM CHANGES

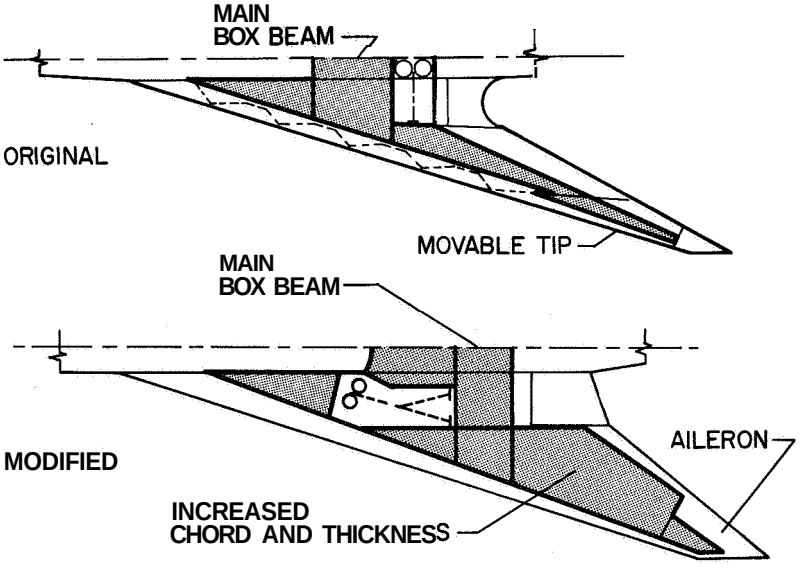

Figure 21

SCAT 4 - ORIGINAL ENGINE ARRANGEMENT

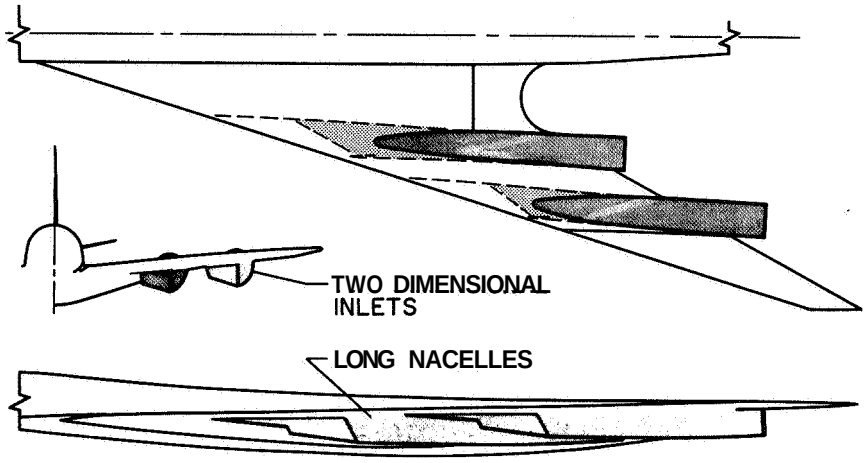

Figure 22

SCAT 4 - FINAL ENGINE ARRANGEMENT

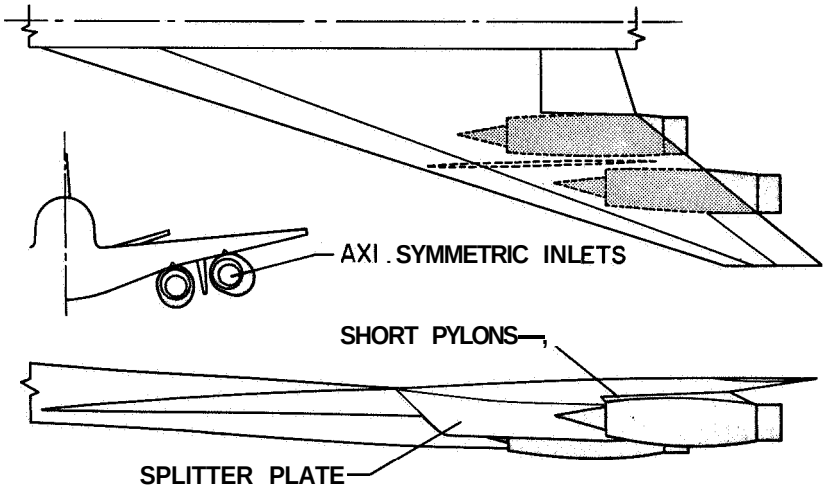

Figure 23

SCAT 4- WING LEADING EDGE FLAPS

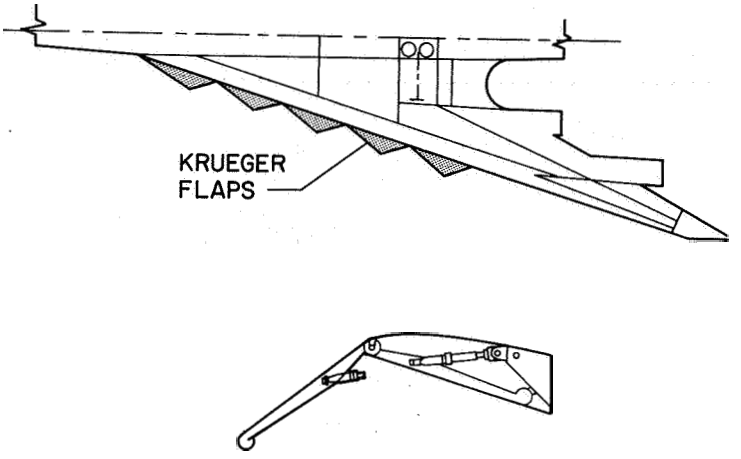

TYPICAL
SECTION

Figure 24

SCAT 4 - FINAL GENERAL ARRANGEMENT

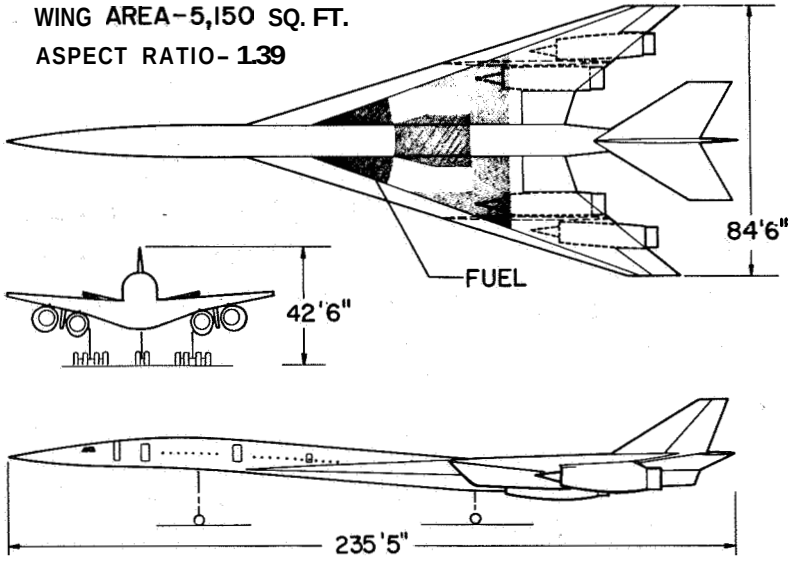

Figure 25

SCAT 4- L/D SUMMARY

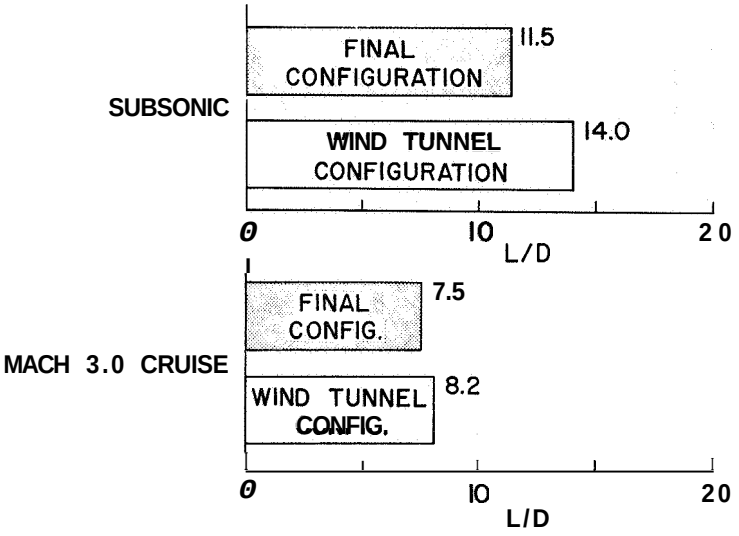

Figure 26

SCAT 4 -WEIGHT BREAKDOWN

	WEIGHT (LBS.)	% T.O.G.W.
WING	40,680	10.6
EMPENNAGE	8,000	2.1
FUSELAGE	25,904	6.7
LANDING GEAR	26,800	7.0
PROPULSION	46,050	12.0
FIXED EQUIPMENT	25,245	6.6
WEIGHT EMPTY	172,679	45.0
OPERATING EQUIPMENT	4,756	1.2
PAYLOAD	26,125	6.8
ZERO FUEL WEIGHT	203,560	53.0
FUEL/WATER	180,440	47.0
GROSS WEIGHT	384,000	100.0

Figure 27

SCAT 4 - SIZE OPTIMIZATION

3,200 N. MI. RANGE
2 PSF CLIMB

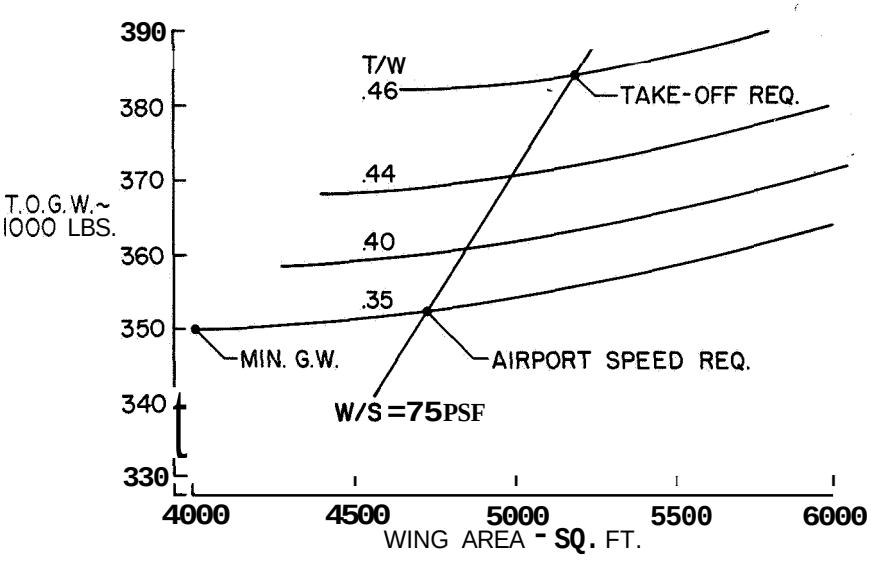

Figure 28

SCAT 4- CHARACTERISTICS SUMMARY

TAKE-OFF GROSS WEIGHT (LBS.)	384,000
FUEL (LBS.)	180,440
RANGE/PAYLOAD (N.MI./LBS.)	3200/26,125
ENGINE THRUST/AIRFLOW (LBS./LBS./SEC.)	44,000/508
SONIC BOOM, CLIMB/CRUISE (PSF.)	2.0/1.47
TAKE-OFF FIELD LENGTHISPEED (FT./KNOTS)	9500/165
AIRPORT NOISE- TAKE-OFF/LAND (PNDB)	107/110
LANDING FIELD LENGTH/SPEED (FT./ KNOTS)	7460/130

Figure 29

[redacted]

SCAT 4 STABILITY CHARACTERISTICS

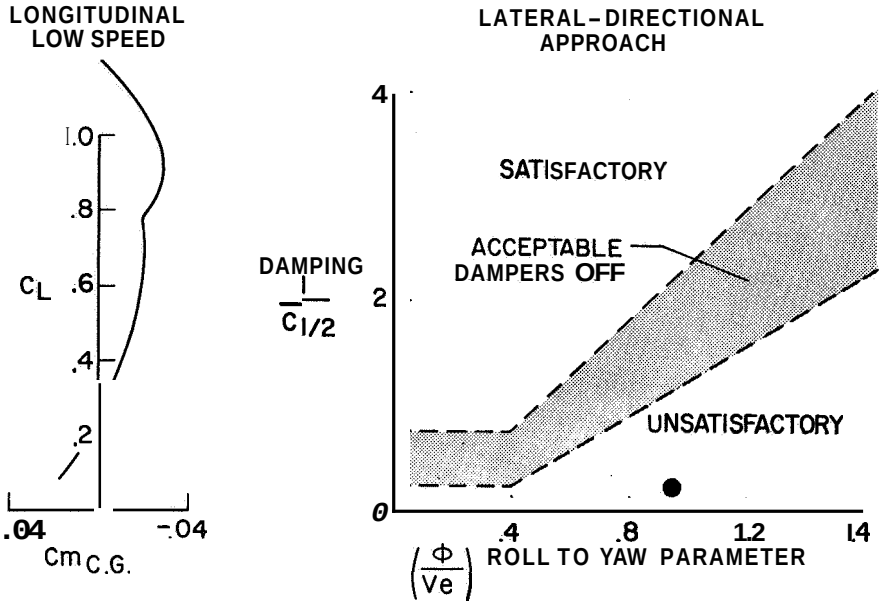

Figure 30

SCAT 15- NASA CONFIGURATION GENERAL ARRANGEMENT

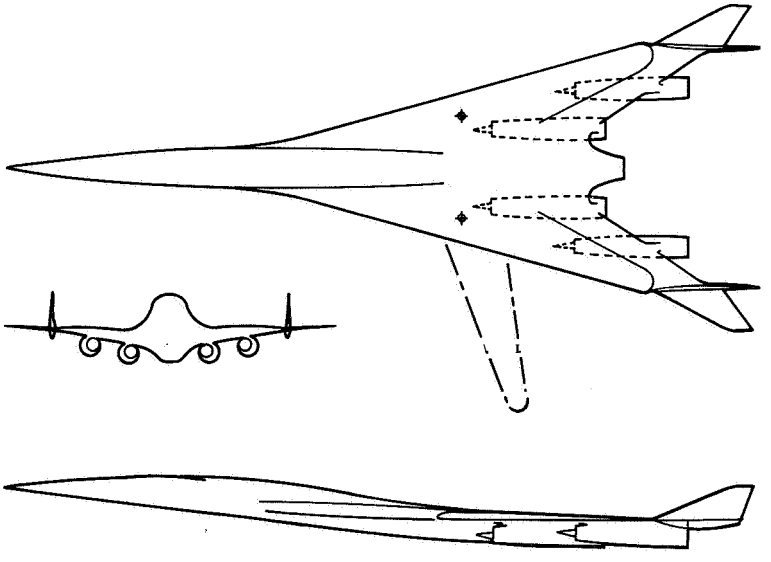

Figure 31

[redacted]

SCAT I5 – WING PLANFORM

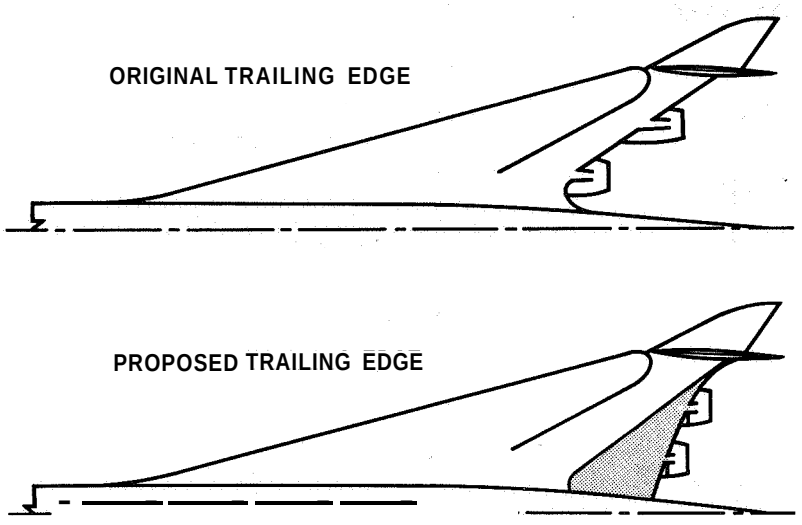

Figure 32

SCAT 15–TAIL POSITION

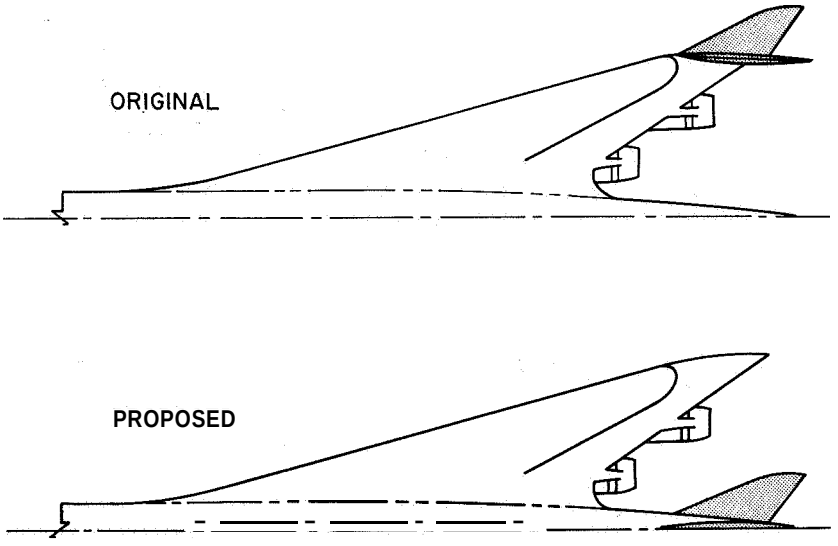

Figure 33

SCAT 15 - FINAL GENERAL ARRANGEMENT

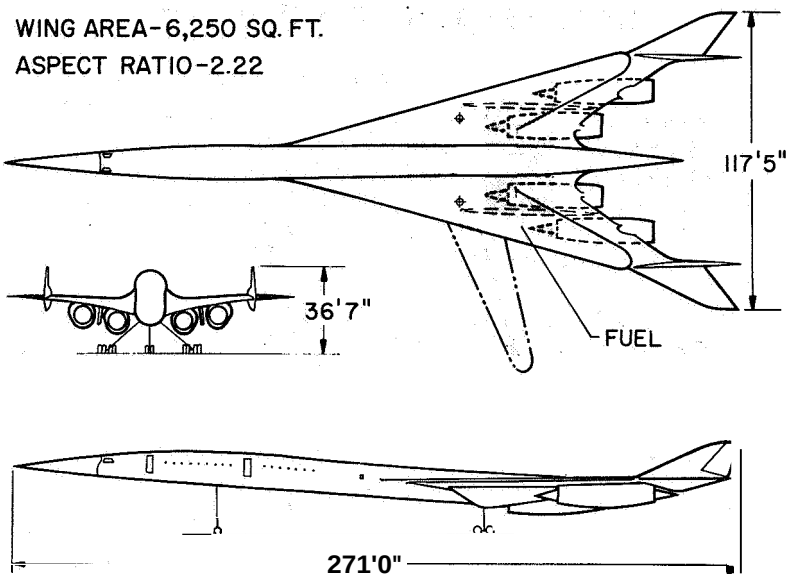

Figure 34

SCAT 15 - L/D SUMMARY

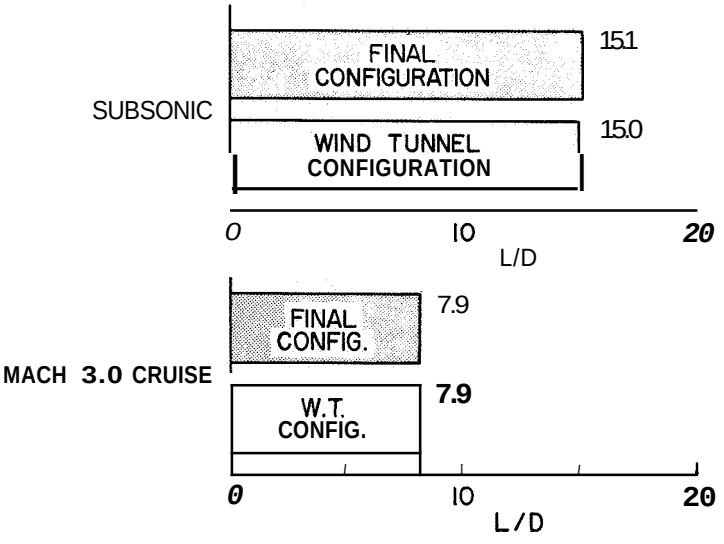

Figure 35

SCAT 15 - WEIGHT BREAKDOWN

	WEIGHT (LBS.)	% T O.G.W.
WING	119,375	21.7
EMPENNAGE	8,455	1.5
FUSELAGE	27,894	5.1
LANDING GEAR	38,000	6.9
PROPULSION	60,600	11.0
FIXED EQUIPMENT	27,955	5.1
WEIGHT EMPTY	282,279	51.3
OPERATING EQUIPMENT	4,756	0.9
PAYLOAD	26,125	4.7
ZERO FUEL WEIGHT	313,160	56.9
FUEL/WATER	236,840	43.1
GROSS WEIGHT	550,000	100.0

Figure 36

SCAT 15- WING DESIGN LOADS

	MOVABLE PANEL	FIXED AFT WING
SUBSONIC MANEUVER	CRITICAL	NOT CRITICAL
SUPERSONIC MANEUVER	NOT CRITICAL	"
LANDING	"	"
TAXI	"	CRITICAL

Figure 37

SCAT 15-CHARACTERISTICS SUMMARY

TAKE-OFF GROSS WEIGHT (LBS.)	550,000
FUEL (LBS.)	236,840
RANGE/PAYLOAD (N. MI./LBS.)	2650/26,125
ENGINE THRUST/AIRFLOW (LBS./LBS./SEC.)	60,000/693
SONIC BOOM, CLIMB/CRUISE (PSF.)	2.0/1.67
TAKE-OFF FIELD LENGTH/SPEED (FT./KNOTS)	7000/165
AIRPORT NOISE- T.O./LAND (PNDB)	90/95
LANDING FIELD LENGTH/SPEED (FT./KNOTS)	7260/130

Figure 38

SCAT 16-NASA CONFIGURATION GENERAL ARRANGEMENT

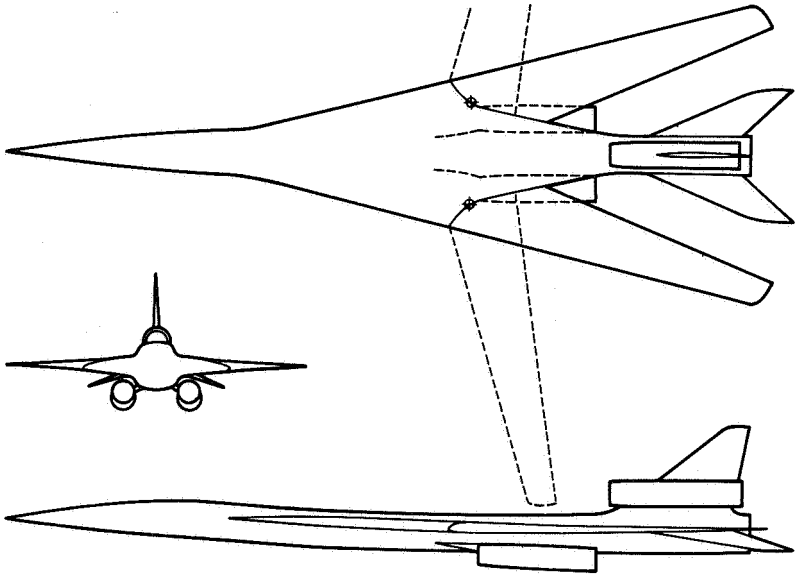

Figure 39

SCAT 16- WING CHANGES

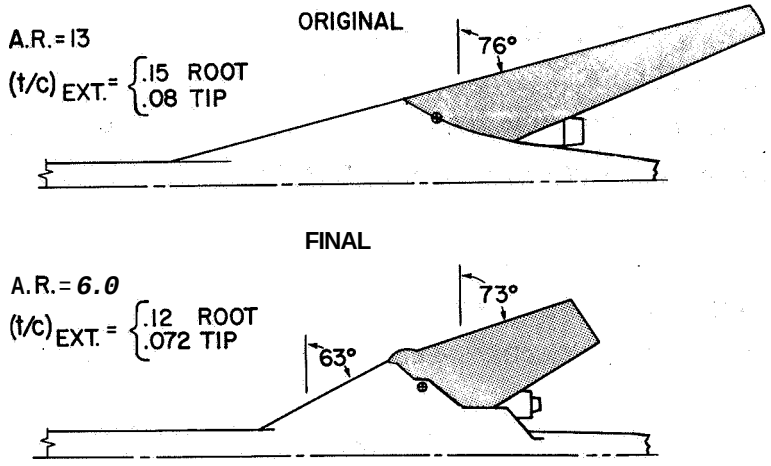

Figure 40

SCAT 16-ENGINE INSTALLATION
(PROPOSED)

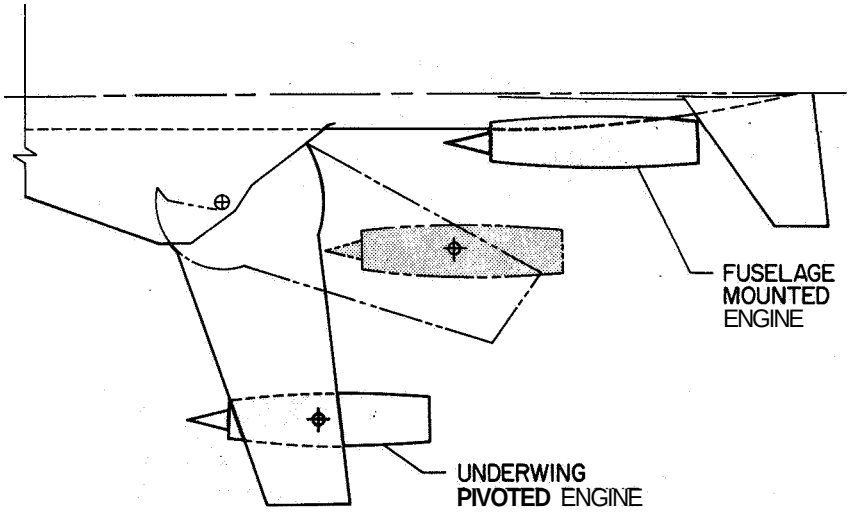

Figure 41

SCAT 16-FINAL ENGINE ARRANGEMENT

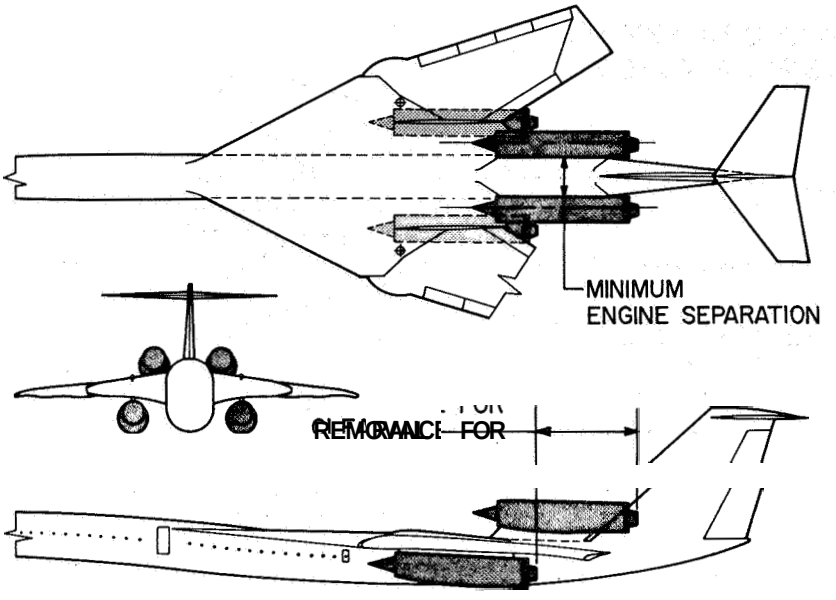

Figure 42

SCAT 16- HORIZONTAL TAIL LOCATION

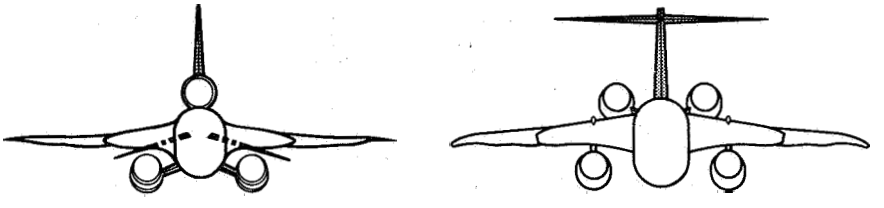

ORIGINAL

LOW TAIL
IN ENGINE WAKE

FINAL

T-TAIL & COMPENSATING
NEGATIVE WING DIHEDRAL

Figure 43

SCAT 16 -GENERAL ARRANGEMENT

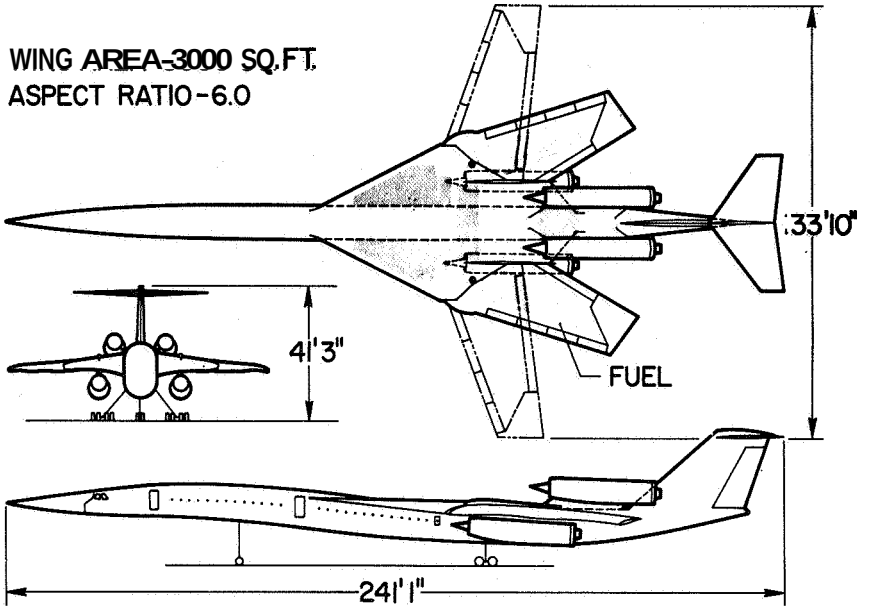

Figure 44

SCAT 16-L/D SUMMARY

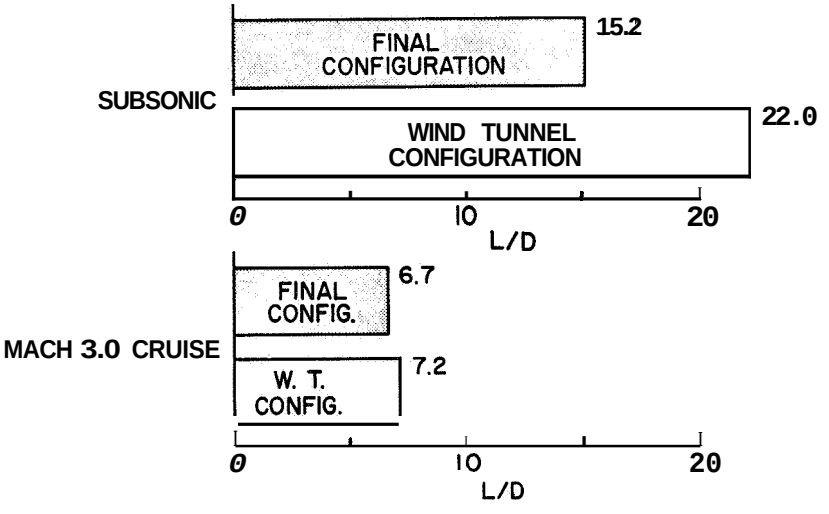

Figure 45

SCAT 16 -WEIGHT BREAKDOWN

	WEIGHT (LBS.)	% T.O.G.W.
WING	48,995	11.6
EMPENNAGE	8,000	1.9
FUSELAGE	28,950	6.8
LANDING GEAR	22,550	5.3
PROPULSION	43,395	10.2
FIXED EQUIPMENT	30,105	7.1
WEIGHT EMPTY	181,995	42.9
OPERATING EQUIPMENT	4,756	1.1
PAYLOAD	26,125	6.1
ZERO FUEL WEIGHT	212,876	50.1
FUEL/ WATER	212,124	49.9
GROSS WEIGHT	425,000	100.0

Figure 46

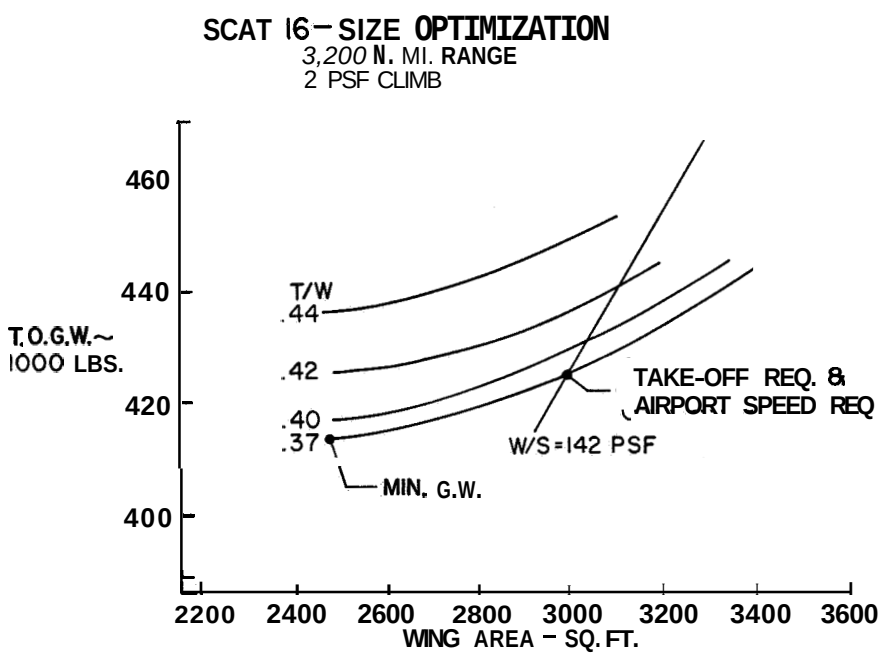

Figure 47

SCAT 16- CHARACTERISTICS SUMMARY

TAKE-OFF GROSS WEIGHT (LBS.)	425,000
FUEL (LBS.)	212,124
RANGE/PAYLOAD (N.MI./LBS.)	3200/26,125
ENGINE THRUST/AIRFLOW (LBS./LBS./SEC.)	39,4001455
SONIC BOOM, CLIMB/CRUISE (PSF.)	2.0/1.36
TAKE-OFF FIELD LENGTH/SPEED (FT./KNOTS)	9500/165
AIRPORT NOISE- T.O./LAND (PNDB)	95/90
LANDING FIELD LENGTHISPEED (FT./KNOTS)	7100/128

Figure 48

SCAT 17 - NASA CONFIGURATION GENERAL ARRANGEMENT

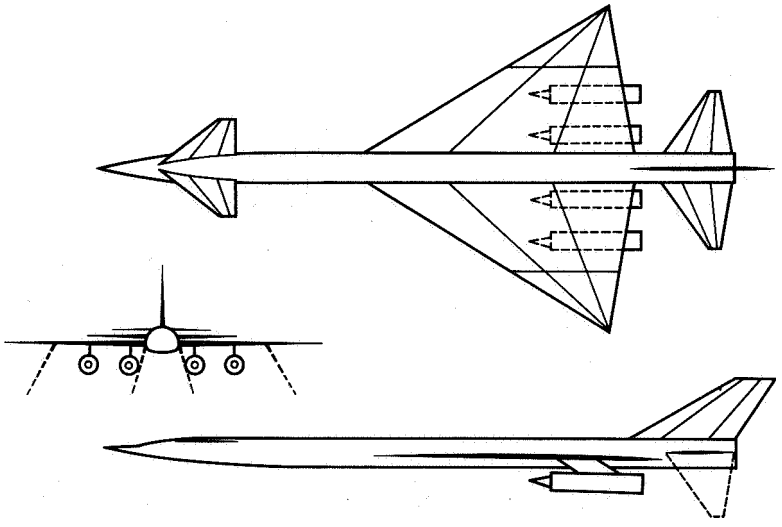

Figure 49

SCAT 17-WING & ENGINE ARRANGEMENT

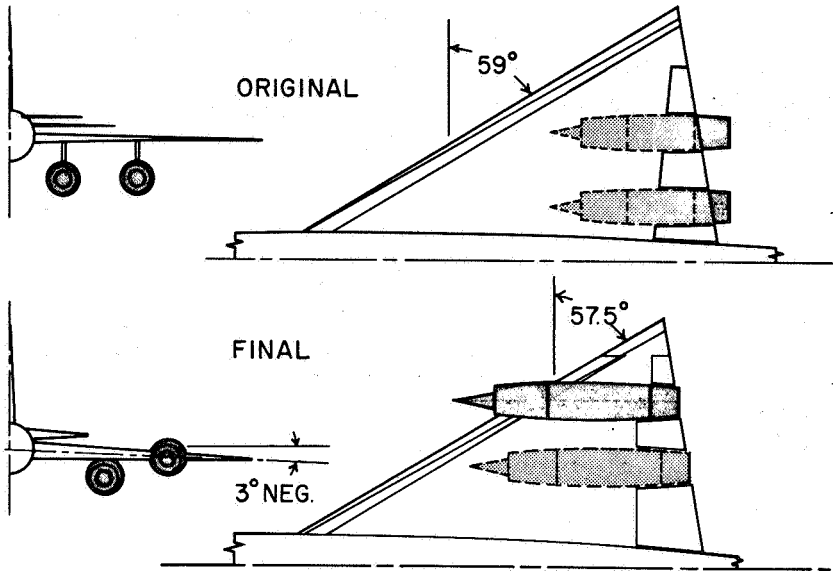

Figure 50

SCAT 17-FOLDING CANARD

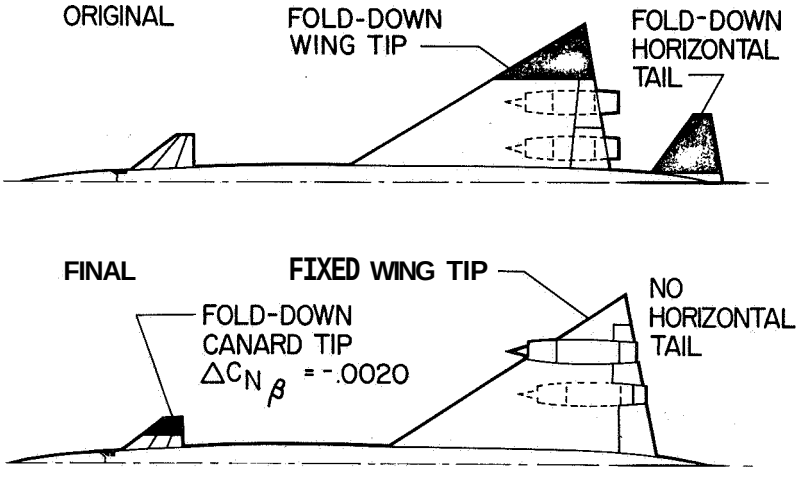

Figure 51

SCAT 17 AERODYNAMIC CENTER CONTROL

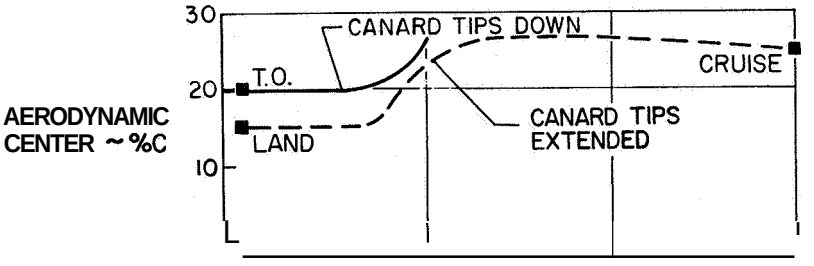

	T.O.	CRUISE	LAND
AERODYNAMIC CENTER	20	25	15
CENTER OF GRAVITY	18	14	10
STATIC MARGIN	2	11	5

Figure 52

SCAT 17- FINAL GENERAL ARRANGEMENT

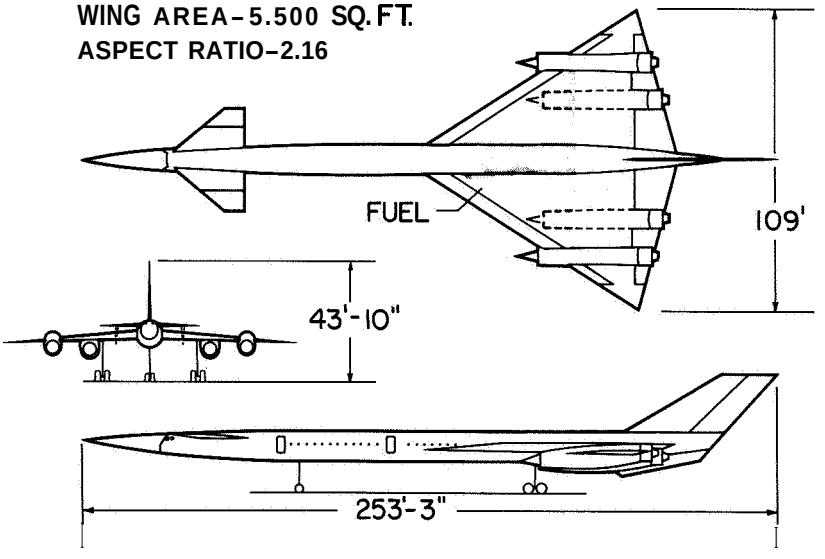

Figure 53

SCAT 17 - L/D SUMMARY

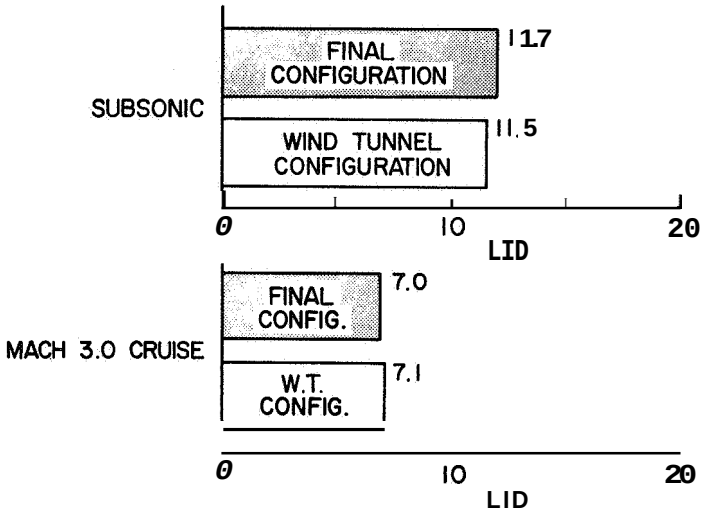

Figure 54

SCAT 17 - WEIGHT BREAKDOWN

	WEIGHT (LBS.)	% T.O.G.W.
WING	35,041	9.2
EMPENNAGE	9,595	2.5
FUSELAGE	26,600	7.0
LANDING GEAR	19,154	5.0
PROPULSION	41,365	10.9
FIXED EQUIPMENT	29,155	7.7
WEIGHT EMPTY	160,910	42.3
OPERATING EQUIPMENT	4,756	1.2
PAYLOAD	26,125	6.9
ZERO FUEL WEIGHT	191,791	50.4
FUEL/ WATER	188,209	49.6
GROSS WEIGHT	380,000	100.0

Figure 55

SCAT 17 - SIZE OPTIMIZATION
3,200 N. MI. RANGE
2 PSF CLIMB

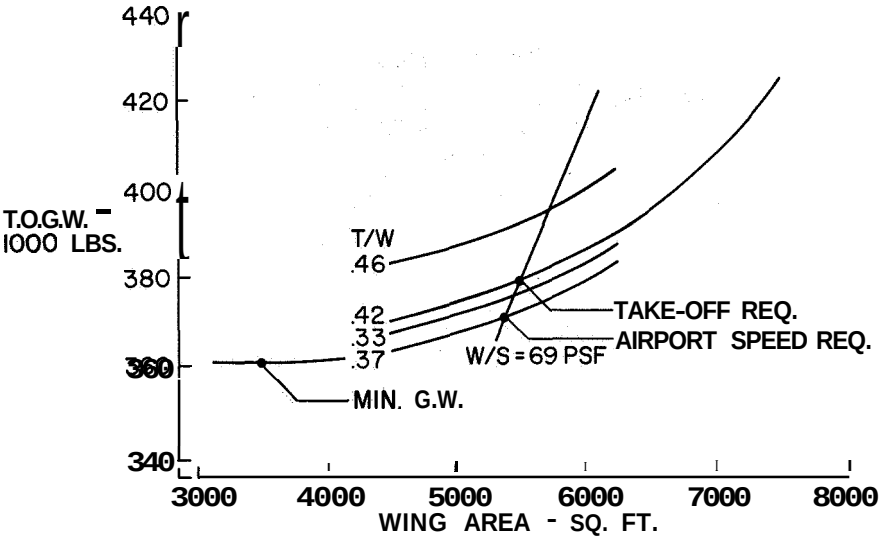

Figure 56

SCAT 17–CHARACTERISTICS SUMMARY

TAKE-OFF GROSS WEIGHT (LBS.)	380,000
FUEL (LBS.)	188,209
RANGE/PAY LOAD (N.MI./LBS.)	3200/26,125
ENGINE THRUST/AIRFLOW (LBS./LBS./SEC.)	39,4001455
SONIC BOOM, CLIMB/CRUISE (PSF)	2.0/1.35
TAKE–OFF FIELD LENGTH/SPEED (FT./KNOTS)	9500/165
AIRPORT NOISE–T.O./LAND (PNDB)	107/105
LANDING FIELD LENGTH/SPEED (FT./KNOTS)	7200/127

Figure 57

DECLASSIFIED

SCAT 17 - ALUMINUM

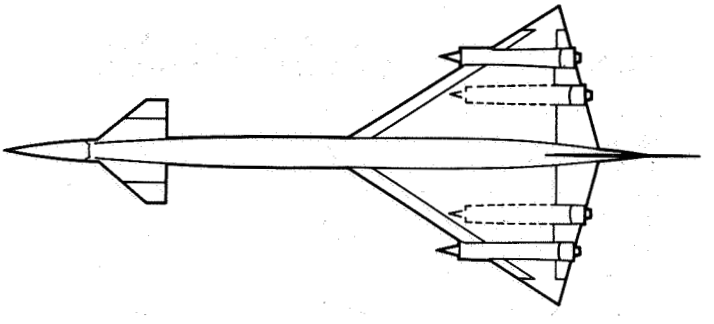

ALUMINUM ——— M = 1.9 - 2.4
"E" & "F"
ENGINE _____
ENGINE _____ 35,000-50.000 LBS. THRUST

Figure 58

SCAT 17 AL-SPEED SELECTION

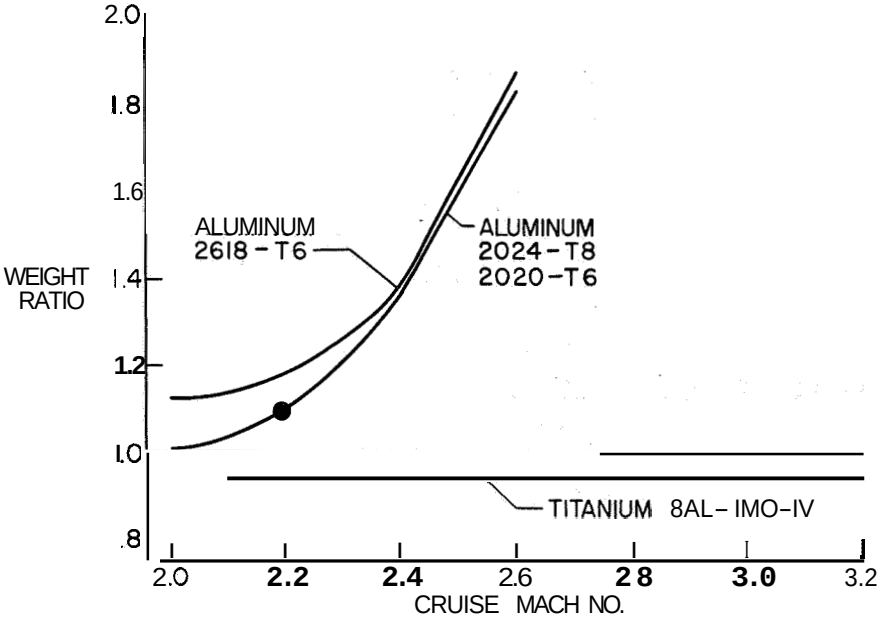

Figure 59

SCAT 17 AL - ENGINE SELECTION

ENGINE TYPE	AFTERBURNING TURBOJET	DUCT BURNING TURBOFAN
NASA DESIGNATION	E	F
TURBINE INLET TEMP. , °R	2,400	2,400
SLS THRUST	34,200	34,100
THRUST / WEIGHT	6.0	5.3
CRUISE SFC MACH 2.2	1.62	1.52
SFC HOLDING AT 1500 FT.	1.29	.87

Figure 60

SCAT 17 AL - ENGINE SIZING

T.O.G.W.= 380,000 LBS.

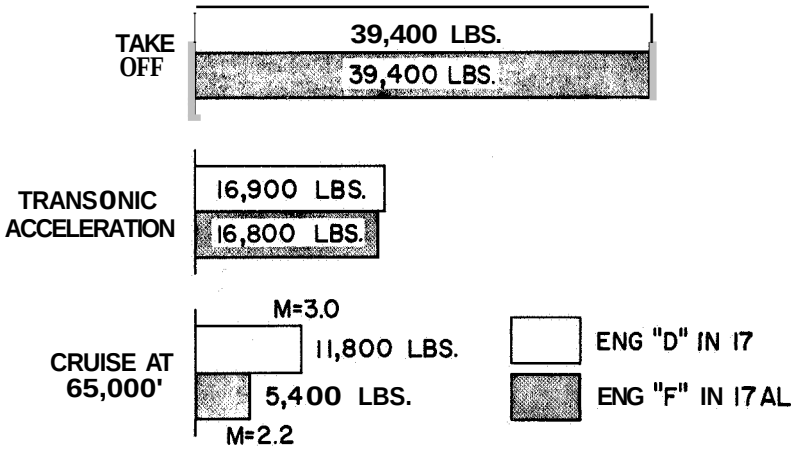

Figure 61

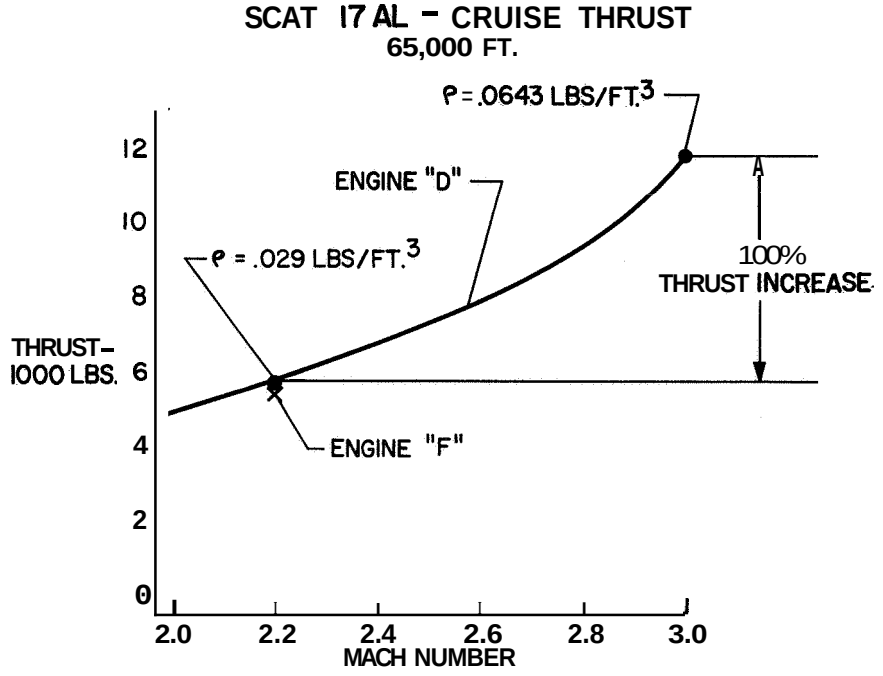

Figure 62

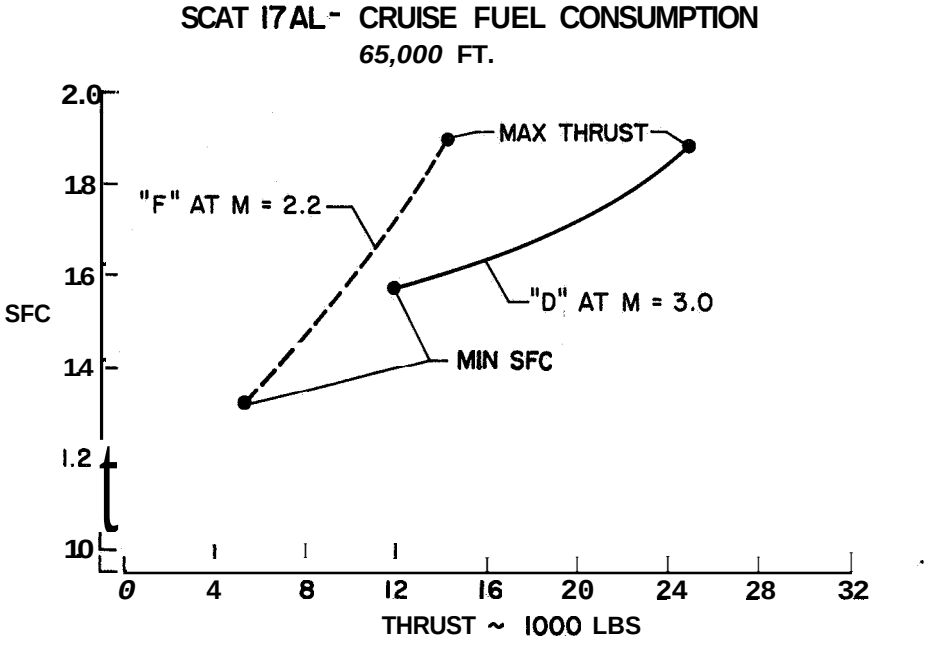

Figure 63

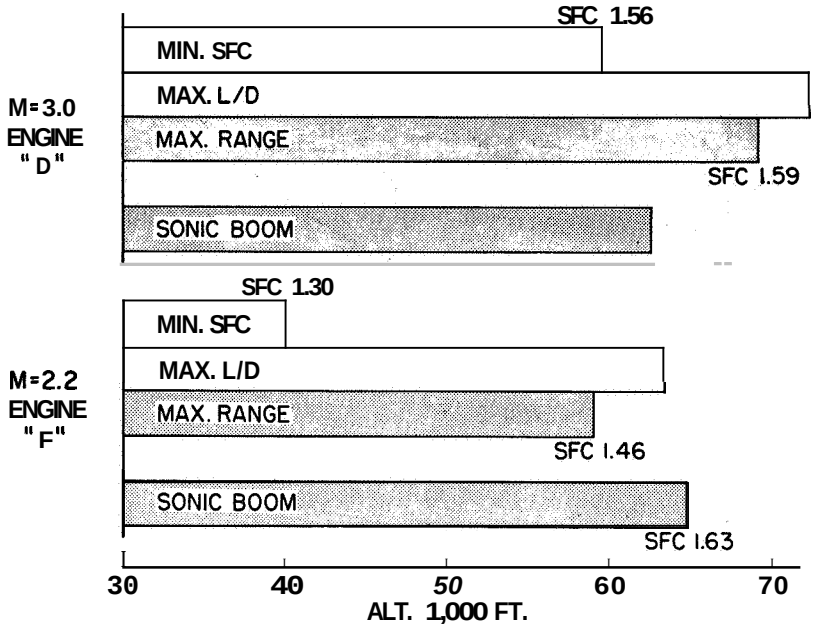

Figure 64

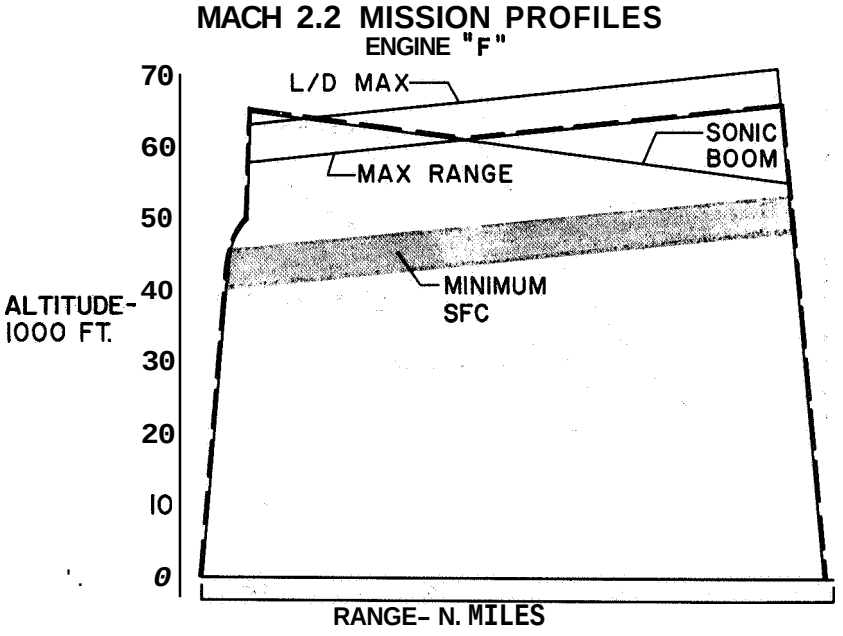

Figure 65

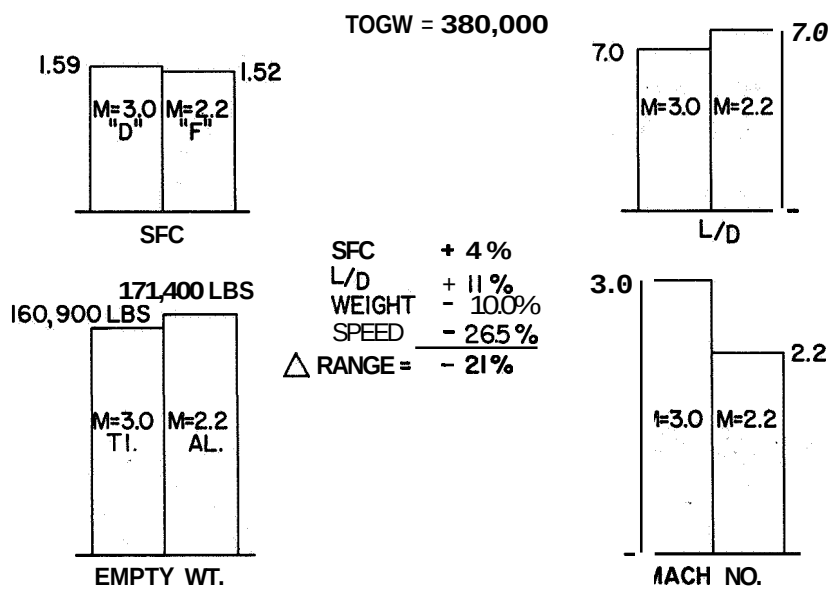

Figure 66

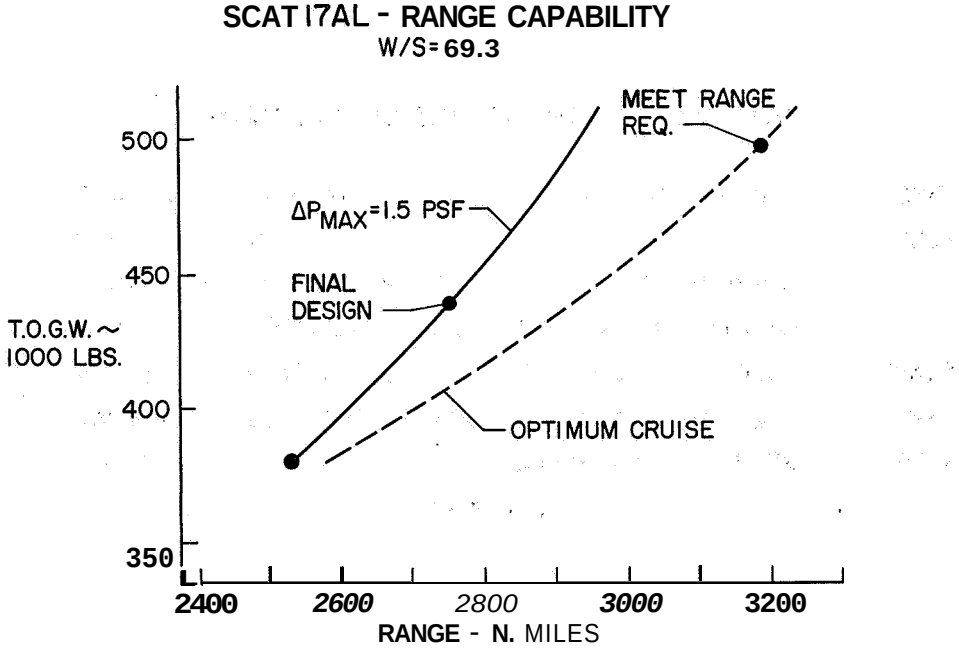

Figure 67

SCAT 17 AL – GENERAL ARRANGEMENT

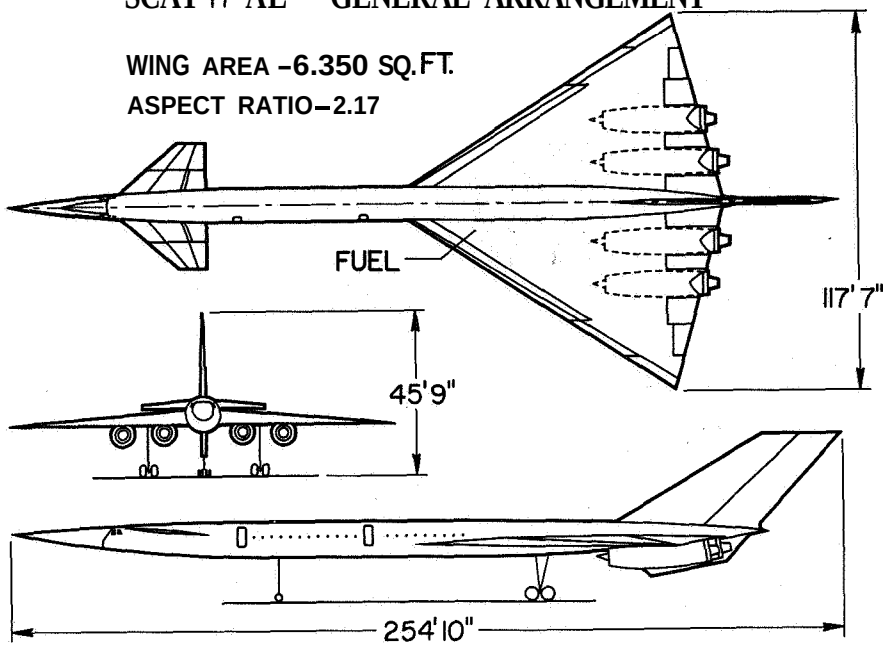

Figure *68*

SCAT 17AL – CHARACTERISTICS SUMMARY

TAKE-OFF GROSS WEIGHT (LBS.)	440,000	*500,000*
FUEL (LBS.)	217,690	257,000
RANGE/PAYLOAD (N.MI./LBS.)	2765/26,125	3200/26,125
ENGINE THRUST/AIRFLOW (LBS./LBS./SEC.)	45,600/600	51,800/680
SONIC BOOM, CLIMB/CRUISE (PSF.)	2.0/1.5	2.0/1.8
TAKE-OFF FIELD LENGTH/SPEED (FT./KNOTS)	9500/165	9500/165
AIRPORT NOISE- T.O./ LAND (PNDB)	107/105	107/105
LANDING FIELD LENGTHISPEED (FT./KNOTS)	7200/127	7200/127

Figure *69*

STATIC LONGITUDINAL STABILITY
1g - LEVEL FLIGHT

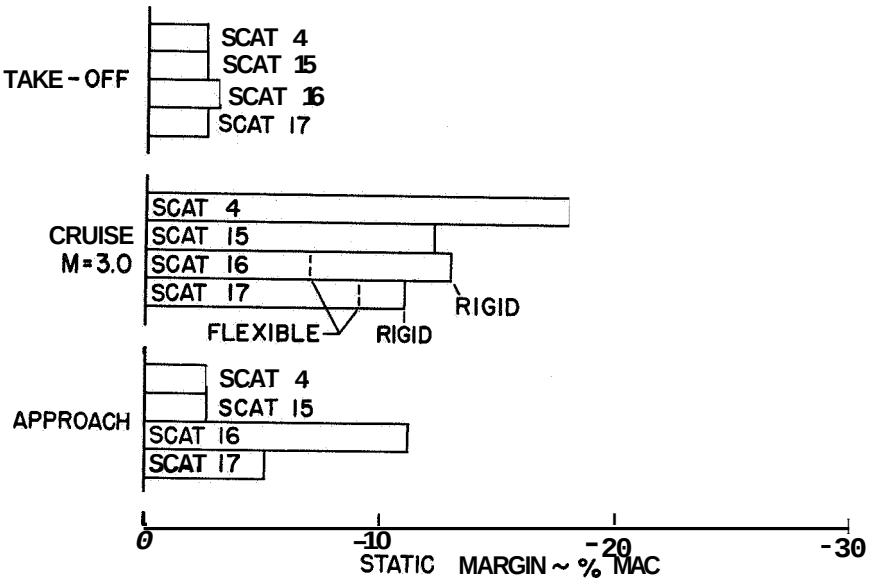

Figure 70

PITCH STABILITY IN CRUISE
M=3.0

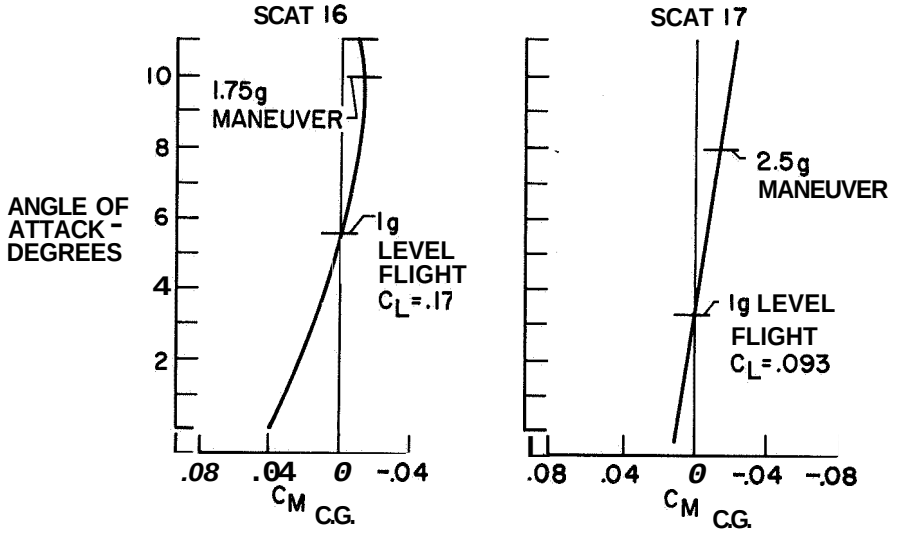

Figure 71

LATERAL - DIRECTIONAL HANDLING QUALITIES
MIL F-8785 (ASG) REQUIREMENTS

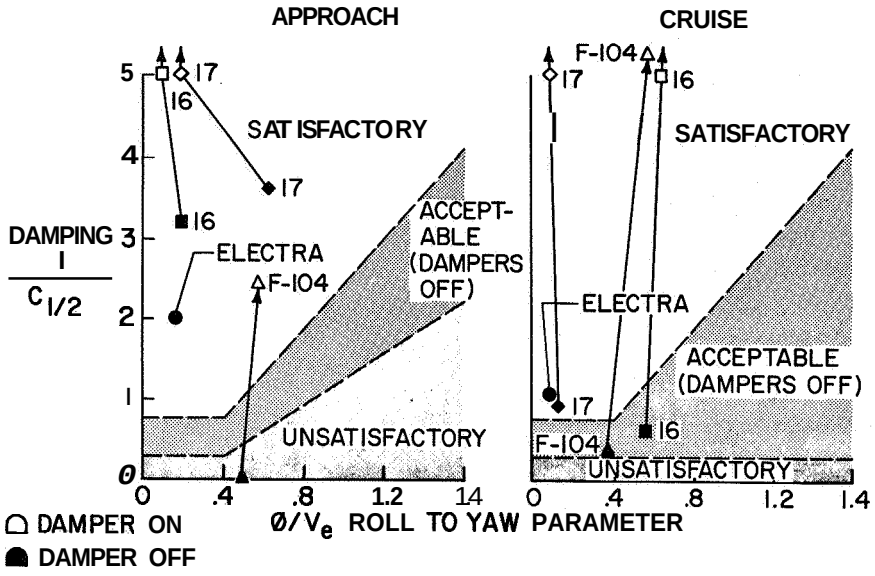

Figure 72

LONGITUDINAL HANDLING QUALITIES
MIL F-8785 (ASG) REQUIREMENTS

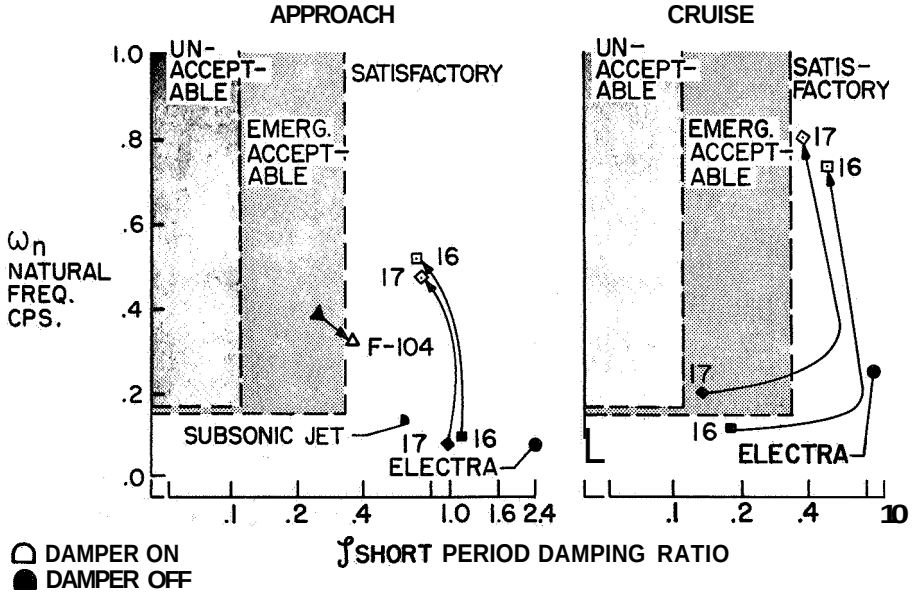

Figure 73

DECLASSIFIED

M = 3.0 CRUISE ENGINE FAILURE

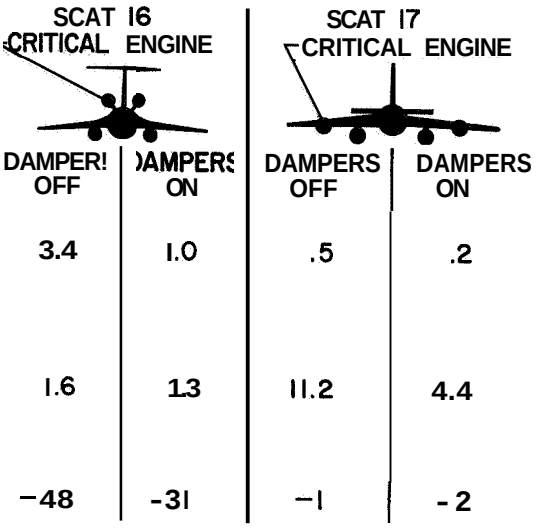

		SCAT 16 DAMPERS OFF	SCAT 16 DAMPERS ON	SCAT 17 DAMPERS OFF	SCAT 17 DAMPERS ON
$\Delta\alpha$	CHANGE IN ANGLE OF ATTACK AFTER 3 SEC. (DEG.)	3.4	1.0	.5	.2
β_{MAX}	SIDE SLIP ANGLE (DEG.)	1.6	1.3	11.2	4.4
ϕ	BANK ANGLE AFTER 3 SEC. (DEG.	−48	-31	−1	-2

Figure 74

SPEED STABILITY

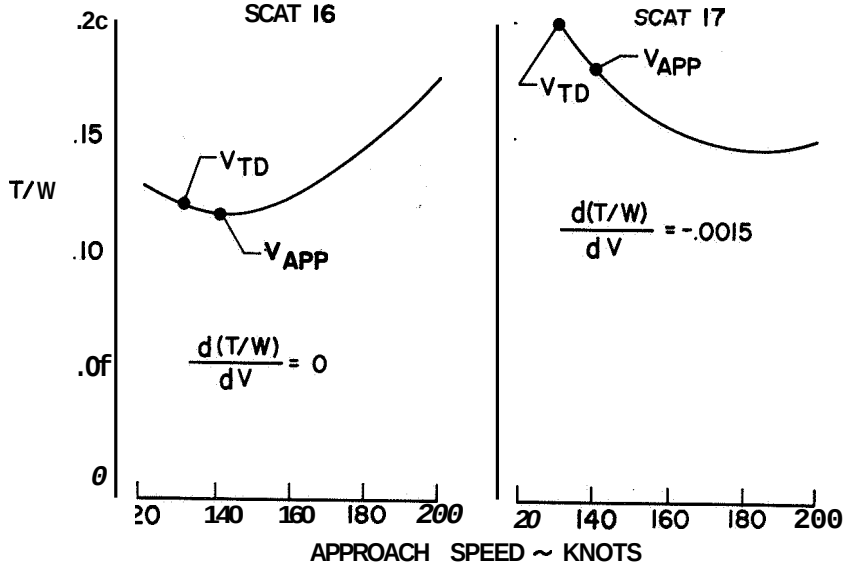

Figure 75

MISSION COMPARISON

3200 N. MI. @ M=3.0	SCAT 16 / SCAT 16	SCAT 17 / SCAT 17
BLOCK FUEL	182,550 / 182,550	158,900 / 158,900
RESERVE FUEL	29,600	29,300
BLOCK FUEL / MACH NO.	31,800/0.8	32,650/0.9
RESERVE FUEL	18,300	20,750

Figure 76

DIRECT OPERATING COST

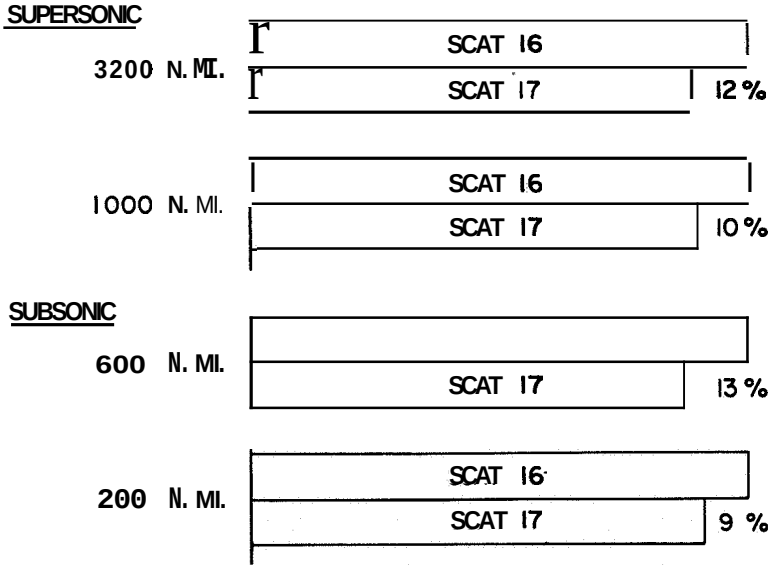

Figure 77

OFF-DESIGN OPERATION

3200 N. MI. MISSION LAND WITH FULL RESERVES

	SCAT 16	SCAT 17
HOT-DAY RANGE	2670	2760
RANGE TO ALTERNATE AFTER:		
MID POINT CABIN DECOMPRESSION	I200	1060
MID POINT ENGINE FAILURE	1280	I270

Figure 78

SONIC BOOM SENSITIVITY

3200 N.MI. RANGE

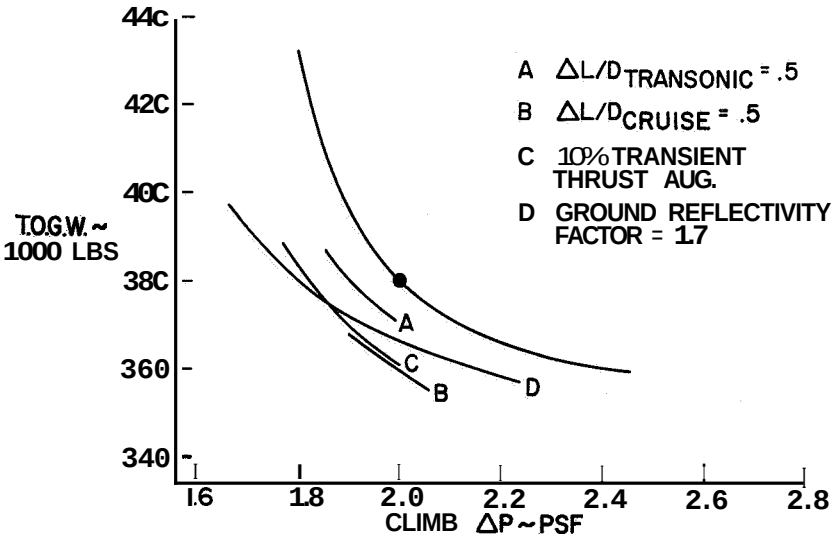

Figure 79

RESEARCH AREAS
AERODYNAMICS

- PITCH-UP OF SWEPT WING PLANFORMS
- SUBSONIC L/D, MAXIMUM LIFT, AND LATERAL CONTROL
- TRANSONIC L/D
- CAMBER AND TWIST ON LOW ASPECT RATIO WINGS
- DYNAMIC STABILITY DERIVATIVES
- HANDLING QUALITY CRITERIA BY SIMULATOR STUDIES

Figure 80

RESEARCH AREAS

STRUCTURES

- INTERFERENCE EFFECTS ON AERODYNAMIC HEATING
- SIMULATOR STUDIES TO ESTABLISH STRUCTURAL CRITERIA
- METHODS FOR ACCELERATED PROOF AND FATIGUE TEST
- CORROSION PROTECTION FOR TITANIUM

PROPULSION

- LONG LIFE HIGH TURBINE TEMPERATURE ENGINES
- TURBOFAN DUCT AND AFTERBURNER COMBUSTION
- HIGH STABILITY INLETS AND LIGHTWEIGHT EXHAUST
- TAKEOFF AND LANDING NOISE

Figure 81

N67-31611

4. SUMMARY OF BOEING SCAT FEASIBILITY STUDIES

By Lloyd T. Goodmanson, William T. Hamilton,
and Maynard L. Pennell

The Boeing Company, Airplane Division
Seattle, Wash.

In NASA - - - - -
3
12730021
11946
4

SUMMARY

A feasibility study of four configuration concepts for the supersonic commercial air transport (SCAT) has been conducted by The Boeing Company under contract to the Langley Research Center of the National Aeronautics and Space Administration. The four concepts, identified as SCAT's 4, 15, 16, and 17, were developed by the NASA.

The airplane configurations which have been developed to meet specific design objectives are described and comparative performance is presented. The technical aspects of the study in the areas of structural design, propulsion, and aerodynamics are briefly reviewed. The major conclusions are as follows:

The SCAT 16 and SCAT 17 concepts are feasible approaches to the design of a supersonic transport. The concept of variable-sweep wings, exemplified by SCAT 16, offers significant improvements in operational flexibility as compared with the conventional fixed-wing concept of SCAT 17.

SCAT's 4 and 15 exhibit superior aerodynamic efficiency. However, major deficiencies must be corrected through additional research in order to make these concepts feasible.

Titanium structure and advanced engine technology must be employed in the supersonic transport in order to achieve reasonable economic performance. Continued research in materials, structures, and propulsion, as well as in aerodynamics, is necessary in order to develop an airplane competitive with present subsonic jets. An aluminum airframe, designed to cruise at Mach numbers near 2.0 and according to the SCAT guidelines, has a gross weight too large to be economically feasible. In addition, it could not meet the sonic-boom overpressure limitations.

Allowable sonic-boom overpressures will have a major impact on the performance capability of the supersonic transport. Based on the technical state of the art employed in the SCAT study, an allowable overpressure arbitrarily selected too low could cause *any* configuration concept to be not feasible.

%
AUTHOR
p. 93-137
ref

INTRODUCTION

The Boeing Company under NASA Contract NAS1-2580 conducted a study of four airplane concepts developed by NASA aeronautical research to determine the feasibility of their use as supersonic commercial air transports. The contract initially required a cruise speed of Mach 3.0. Later it was amended to investigate one of these four configurations at a cruise speed in the Mach 2.0 range. The SCAT study began on February 4, 1963, and has continued for $7\frac{1}{2}$ months. This paper is divided into three parts to summarize the study findings.

Part I defines the changes and improvements made in the four primary SCAT configurations during the program. This part also summarizes the comparative performance of the SCAT models including the aluminum SCAT.

Part II summarizes the criteria which governed the SCAT program. This part includes a review of specific technologies as they were applied to the various SCAT models.

Part III summarizes the findings and various trade-offs developed from the SCAT program, including economic considerations, and provides general conclusions which are intended to help define future research in the field of supersonic transports.

GUIDELINES

The SCAT study guidelines on which all configurations were based are given in table I. All four of the principal SCAT configurations were designed for Mach 3.0 cruise. The aluminum SCAT (SCAT 16AL) was to be designed for cruise at or above Mach 2.0. A range of 3,200 nautical miles with a payload of 26,125 pounds was specified with take-off, landing, and approach characteristics comparable to those of present-day subsonic jets. Limits on sonic-boom overpressures were established at 2 pounds per square foot (psf) in climb and at 1.5 psf for cruise. Aircraft noise at the airport and in the neighboring community was to be equivalent to that of present-day jets.

Figure 1 indicates the design features that are common to all of the Boeing configurations. The design speed for the four original concepts was Mach 3.0. The cruise speed selection of Mach 2.0 for SCAT 16AL will be discussed later. All of the Mach 3.0 designs are based on titanium to minimize structural weight. Engine-cycle studies indicated

that engine **D,** an advanced technology turbofan, provided the best performance for all four Mach 3.0 SCAT's. Engine F, which was chosen for SCAT 16AL, is also a turbofan based on a slight increase beyond current engine technology. All four original SCAT concepts and the later aluminum SCAT are based on the SCAT guidelines.

SYMBOLS AND ABBREVIATIONS

C_L	lift coefficient
$C_{L,MAX}$	maximum lift coefficient
C_m	pitching-moment coefficient
C_{n_β}	directional-stability parameter
F_{cy}	compression yield strength
F_{tu}	ultimate tensile strength
L/D	lift-drag ratio
M	Mach number
M_C	cruise speed
M_D	dive speed
M_{MO}	maxim operating speed
ΔP	sonic-boom overpressure, psf
ΔP_{MAX}	maximum sonic-boom overpressure, psf
T	thrust, lb
t/c	thickness-chord ratio
V	airspeed, knots
W	airplane weight, lb

α	angle of attack, deg
A	change
Λ_{LE}	sweepback angle, deg
DOC	direct operating costs, cent/seat-mile
GW	gross weight
OWE	operating, weight empty
PL	payload
SFC	specific fuel consumption
TO	take-off

I. CONFIGURATION DEVELOPMENT AND PERFORMANCE

SCAT 4

SCAT 4 is a fixed arrow-wing concept based on the blending of the engine nacelles with the wing to achieve favorable aerodynamic interference and to minimize the structural weight through wing bending relief. (See figs. 2 and 3.)

The configuration at the end of 4 months of study differed from the original definition as a result of the following changes:

(1) To achieve lighter weight, it was decided to pass the full depth of the wing box below the floor rather than carry the wing bending moment through the fuselage frames. This made it possible to reduce the body diameter from 117 to 113 inches. Also, the body length was increased to shift the crew and passenger compartments forward relative to the wing, thereby improving the airplane balance.

(2) The wing planform experienced several changes. The sweepback angle was reduced from 75° to 72.8°, as recommended by the NASA early in the program, to provide a better compromise for Mach 3.0 cruise speeds. The wing trailing edge at the root was shifted aft with reduced sweep to allow the structural box to be moved aft. This change reduced the wing weight as a result of the shorter structural span.

(3) Wing-tip elevons were tested and recommended by the NASA when design studies revealed the difficulties involved in providing adequate strength and stiffness for an all-moving wing-tip control.

(4) The trapezoidal, two-dimensional engine inlets were replaced with lighter axisymmetric inlets.

(5) A delta planform was used for the horizontal tail instead of the higher aspect ratio, arrow configuration. This change provided more separation from the engine efflux and noise fields and increased the stiffness for a given weight.

SCAT 15

For SCAT 15 (figs. 4 and 5) a 75° arrow wing blends into the fuselage to achieve high aerodynamic efficiency. The engines are mounted as close as possible to the wing undersurface to develop favorable aerodynamic interference and to provide bending relief. Vertical fins are located on the wing tips in a good flow field throughout the flight envelope. The tail location also yields an improvement in the wing span loading by means of the end-plate effects. An auxiliary wing, pivoted from the main wing structure, produces higher subsonic lift-drag ratios and $C_{L,MAX}$ than can be obtained from the basic planform.

During the 4 months devoted to studying SCAT 15 many possible changes were investigated, but only a few were incorporated. The major changes were as follows:

(1) The fuselage was lengthened to provide volume for approximately 50 percent of the total required fuel load and to improve airplane balance.

(2) A body-mounted horizontal tail was added to improve stability and control. However, it was found in subsequent tests that the size chosen was inadequate to eliminate high-speed instabilities of the flexible airplane. The correct tail size was not incorporated because of termination of the SCAT 15 study.

After consideration of the data presented in the midterm report at the end of 4 months of study, SCAT's 4 and 15 were discontinued. The results presented therefore reflect 4 month's work only.

SCAT 16

The SCAT 16 concept (figs. 6 and 7) is based on a variable-sweep wing. The objective of this approach is to yield maximum off-design performance without sacrificing cruise capabilities. In contrast with SCAT's 4, 15, and 17, the SCAT 16 configuration was initially proposed with only three engines.

The SCAT 16 airframe definition changed in the following areas during the study:

(1) The midwing arrangement was changed to a low-wing design because of the weight penalties associated with carrying wing bending moments through the fuselage frames.

(2) The body cross section was increased because of the volumetric requirements of the main landing gear and fuselage fuel tanks.

(3) The wing pivot was shifted to the fuselage side because of expected savings in wing weight and the possibility for alleviating wings-forward pitch-up.

(4) The wing twist and camber were modified to improve the aerodynamic efficiency.

(5) The wings-forward aspect ratio was reduced from 13 to 7.5 to improve wing weight.

(6) Four engines were used instead of three to provide the same degree of multiengine capability as in the other configurations.

(7) The horizontal tail was changed from an arrow to a delta planform to obtain more stiffness for a given weight and to improve clearance for engine efflux and noise fields.

Figure 8 shows the general arrangement of the SCAT 16 fuel tanks, principal spars and bulkheads, pivot and landing-gear locations, and the flight control surfaces. Some of the fuel is carried below the main cabin floor. This is dictated by the limited volume available in the wings and the airplane balance requirements. Wing fuel is carried between the front and rear spars in the swinging section. The wing pivot is located well inboard at the side of the body to provide the maximum possible wing-span increase from the swep-tbackto the swept-forward position. The main landing gear is stowed in the lower lobe of the body. As the gear is extended, it swings forward and outboard to the down position. Both leading-edge and inboard trailing-edge flaps are employed, along with spoilers and outboard ailerons. The horizontal

stabilizer is a variable-incidence type with trailing-edge flaps. A two-segment split rudder and spoiler system provides the yaw control.

SCAT 17

The SCAT 17 configuration (figs. 9 and 10) incorporates a wing having 59° swept leading edge and zero-taper-ratio delta planform. Four axisymmetric power-plant installations are mounted from the lower wing surface. As initially conceived, SCAT 17 had a canard, fold-down wing tips, and a fold-down horizontal tail which was to provide reduced trim drag and increased directional stability during cruise.

During the study program the following changes were incorporated:

(1) The fuselage was shortened, and the cross section was reduced to accommodate four-abreast seating. This change resulted in reduced body wetted area and weight.

(2) The wing thickness-chord ratio was increased from 2 to $3\frac{1}{2}$ percent and the folding wing tips were eliminated.

(3) The canard and folding tail were replaced with a conventional high-aspect-ratio tail because of a longitudinal balance problem, inadequate canard control power, and excessive drag.

(4) The power plants were moved forward on the wing to improve overall balance and to increase the tail moment arm.

Figure 11 illustrates the general arrangement of the SCAT 17. Fuel is carried both in the exposed wing area between the front and rear spars and in the inboard center section. A dry bay is provided in the wing to accommodate the engine-driven aircraft accessories. The main gear is stowed in the wing adjacent to the body. It swings aft and outboard to the down position. The landing-gear strut lies below the wing fuel tank and is covered by an aerodynamic fairing when retracted. Full-span leading-edge flaps, inboard trailing-edge flaps, spoilers, and an outboard flaperon are employed on the main wing. The horizontal stabilizer is a variable-incidence type with trailing-edge flaps. A two-segment split rudder and spoiler system provides the yaw control.

SCAT 16AL

After the midterm contract review, the basic contract was amended to include the study of an aluminum variable-sweep-wing configuration (fig. 12). The aluminum SCAT 16 was based on the original SCAT 16,

with appropriate modifications in wing sweepback and thickness-chord ratio permitted by the lower cruise speed ($\Lambda_{LE} = 70°$, t/c = 4.75 percent at the pivot and 3 percent at the wing tip). The body cross section provides for four-abreast seating with a large lower lobe for containment of fuel and the landing gear.

The airplane has a much higher *gross* weight than its titanium counterpart because of the lower strength-weight ratio of aluminum. The SCAT 16AL received less detailed study than SCAT's 16 and 17 because of the shorter time available for refinement to optimize the configuration.

Comparative Performance

Data from the five SCAT configurations are compared in figure 13. SCAT's 4 and 15 are shown in the shaded area to indicate that studies on them were discontinued after the midterm review. Although SCAT 4 showed the lightest gross weight, stability and control problems, particularly at low speeds, led to termination of the study. SCAT 15 showed the highest weight at 490,000 pounds, and this high weight was its principal drawback. Although the SCAT 15 exhibited excellent aerodynamic characteristics, the weight of the dual overlapping wings led to discontinuance of the study. When built of titanium, SCAT's 16 and 17 have approximately the same weights. The aluminum SCAT, however, is about 90,000 pounds heavier.

The other factors presented in figure 13 - weight ratio, L/D, engine specific fuel consumption and sonic-boom overpressure - contribute significantly to the differences in *gross* weight for the five airplanes. The delta-wing SCAT 17 has the most favorable weight ratio. SCAT 16, on the other hand, has a somewhat higher lift-drag ratio, slightly better specific fuel consumption because of the engine match, and better fuel reserves. Both airplanes meet the sonic-boom overpressure limit of 2 psf in climb.

SCAT 16AL has a fairly high L/D primarily because of its lower cruise speed. SCAT 16AL also shows fairly good specific fuel consumption and its weight ratio benefits from its large size.

The weight breakdown for four airplanes is shown as total weights in figure 14 and as percentages of total weight in figure 15. In each chart, the weights of the three final airplanes are compared with the weight of the long-range Boeing 707 Intercontinental. As charted in figure 15, the supersonic transports show only about one-half of the payload—gross-weight ratio of present-day subsonic jets. Other significant facts shown in the weight breakdowns are as follows:

DECLASSIFIED

(1) Of the three final SCAT configurations, SCAT 17 has the lightest structural weight.

(2) SCAT 17 uses somewhat more fuel than either SCAT 16 or SCAT 16AL because of its lower range factor.

(3) All supersonic transports have a greater percentage of their gross weight in fuel than has the Boeing 707 Intercontinental.

Sonic-boom overpressure limitations have a fundamental effect on the sizing of large supersonic airplanes. Figure 16 relates airplane gross weight to maximum sonic-boom overpressure in climb for three of the SCAT configurations. Each curve on these figures represents a family of airplanes whose wing areas and power-plant sizes have been properly matched for minimum gross weight at the sonic-boom overpressures shown. Sizes of the final SCAT 16 and SCAT 17, chosen to meet the required climb sonic-boom overpressure of 2.0 psf, are indicated by the symbols. SCAT 16AL designed for a 3,200-nautical-mile range cannot meet the 2.0 psf requirement at any gross weight; therefore, the airplane was sized at the knee of the curve.

Climb schedules for SCAT's 16 and 17 sized for 2.0 psf overpressure are shown in figure 17. Note that SCAT 17 must accelerate through low supersonic speeds at a higher altitude than SCAT 16 to meet the overpressure limit. Both airplanes designed without regard to sonic-boom overpressure would use the lower altitude, maximum range-climb schedule. In this case, either would have a greater range for the same gross weight or could be smaller if matched to the same range. As is evident in figure 16, both SCAT's 16 and 17 are about 10 percent larger than would be necessary if a sonic-boom overpressure of 2.5 psf were acceptable.

The mission profiles for SCAT's 16 and 17 are plotted on the upper portion of figure 18. Resulting sonic-boom overpressures throughout the 3,200-nautical-mile mission are shown on the lower portion of the figure. Because of the higher required acceleration altitude and smaller excess thrust, SCAT 17 creates a 2.0 psf boom over a greater distance than does SCAT 16. The initial sonic-boom overpressure in cruise is 1.5 psf or below for both models. However, SCAT 17 must climb to an altitude above its optimum cruise altitude for maximum range before it can start cruise with a 1.5 psf boom. Consequently, SCAT 17 will fly at a constant altitude during the first portion of the cruise during which time the sonic-boom overpressure will gradually decrease as gross weight decreases with fuel burnoff. At the end of cruise, SCAT 17 has a sonic-boom overpressure of about 1.2 psf. Cruise boom overpressures for SCAT 16 start at about 1.5 psf and reduce to about 1.1 psf at the end of a climbing cruise. During the early portion of the deceleration and descent, the boom overpressure will increase slightly. Descent

overpressures are held below 1.5 psf as shown by decelerating to Mach 1.0 before the airplane has descended to 50,000 feet.

Sonic-boom overpressure restrictions have been shown in the SCAT study to have a major impact on the performance capability of the supersonic transport. Since presently available data do not indicate a significant difference in public reaction to sonic booms at overpressures near 2 psf, it is apparent that extreme caution should be used if arbitrary restrictions are imposed. It also should be recognized that the tolerable overpressures probably will be higher on over-water flights than on domestic routes. Therefore, flexibility in flight planning can result in significant decreases in operating costs.

Well-controlled flight tests to determine more accurately public reaction to sonic booms are necessary in order to resolve the conflicting requirements between performance and public acceptance of the supersonic transport. The United States possesses a unique capability to conduct sonic-boom flight tests, and it is urged that such a program be completed before the supersonic transport is committed to production.

11. CRITERIA AND TECHNOLOGY REVIEW

Structures

The operational speed-altitude envelope of SCAT vehicles is formed by a composite of boundaries representing aerodynamic, propulsion, and structural design limitations. This envelope varies somewhat with each SCAT configuration but the limits presented in figure 19 are generally representative of those for supersonic transports. The maximum operating speed M_{MO} is selected to give maximum performance and to meet sonic-boom requirements. Margin is provided for unintentional overspeeding to dive speed M_D as required in Civil Air Regulations (CAR) 4b.* The upper boundary is the thrust-limited airplane ceiling. Temperature usually restricts the maximum Mach number, although for the basic SCAT study the maxim speed was specified to be Mach 3.0. Other limitations may be imposed in varying degrees by buffet, flutter, gust, aerodynamic stability, and the engine. Sound structural design requires examination of the complete flight envelope for critical conditions. The structural design is affected by all flight regimes as well as landing and ground handling loads. Low-speed maneuvers and transonic gusts and maneuvers usually give the highest mechanical loadings. Certain supersonic cruise and overspeed maneuvers have the added effects

*Anon.: Airplane Airworthiness; Transport Categories. Civil Air Regulations Part 4b, FAA, Jan. 7, 1963.

of high temperature and thermal stresses which make these maneuvers slightly more critical in certain areas.

One of the first major decisions in developing a structural design is the selection of the material to be used. A group of seven of the most promising alloys including titanium, stainless steels, and superalloys were considered in the basic Mach 3.0 studies. Several heat-resistant aluminum alloys were also considered for the SCAT 16AL investigations. Figures 20 and 21 graphically compare the relative weight efficiency of the prime candidates AM 355 stainless steel, Ti-8AL-1Mo-1V titanium alloy, and 2024-T81 aluminum alloy at room and cruise temperatures. In this chart the longer the bar, the better the material is for the particular application. The titanium alloy is the most efficient material for components designed by static load requirements, as indicated by the tension and compression efficiencies (fig. 20). For the design of joints and components, such as the fuselage pressure cabin where fracture toughness and fatigue resistance are important, the titanium alloy again is superior for the Mach 3.0 application (fig. 21). Based on these considerations as well as corrosion resistance, ease of fabrication, and metallurgical stability, Ti-8AL-1Mo-1V was selected as the primary structural material for the basic Mach 3.0 SCAT studies. The heat-resistant 2024-T81 aluminum alloy was judged best for most primary applications on the SCAT 16AL.

After selection of the basic material, studies were made to determine the optimum cover-panel structural arrangements for the Mach 3.0 wing. Several arrangements that appeared feasible were evaluated on the basis of both weight and installed cost, with consideration given to joints and internal support structure. Since all wings studied during the contract contained fuel within the wing structural box, the insulating characteristics of each surface were considered in detail. Figure 22 shows four of the panel types studied for the wing surface covers. All four types meet the fuel insulation requirements. The single skin stringer cover panel with backing board and bladder fuel cell walls proved to be the least expensive on an installed cost basis. The titanium honeycomb sandwich panel was the most expensive and considerable fabrication development would be required to bring it to a production status. The weight comparison of these four panels is shown in figure 23 for the SCAT 16 wing structure. Based on a compromise between weight and installed cost, the double skin stringer with a nonstructural inner radiation shield was chosen for the upper surface and the double structural skin was selected for the lower surface of SCAT 16, as indicated by the shaded bars. For SCAT 17 the honeycomb structure results in the lightest upper surface because of the lower wing loads (fig. 24). However, the double skin stringer arrangements were again chosen for the final design because of the high costs and development required for the honeycomb cover panel. After the midterm review when the contract was amended to call for an evaluation of an

aluminum airplane, a structural weight study was conducted on an aluminum SCAT 16 sized to accomplish the SCAT payload-range mission at a Mach number of 2.0. Figure 25 shows the weight penalty associated with higher cruise Mach numbers. The structural weight penalty is due to the degradation of material properties by extended exposure to the higher design temperatures. The optimum cruise speed was not precisely determined because of the abbreviated contract period; however, it appears to be near a Mach number of 2.2 when both the combined weight and range factor effects are considered. Structural weight is influenced strongly by configuration and the basic design guidelines and, therefore, the optimum speed may be expected to vary somewhat as these factors change.

Propulsion

The operating conditions which significantly affect the engine-airplane matched performance are supersonic cruise, subsonic cruise, transonic acceleration, take-off, and holding, as indicated in figure 26. The optimum engine cycle characteristics and size, installed weight, and drag for any one of the operating conditions is generally not optimum for any other condition, nor for the airplane as a whole. Therefore, the relative merits of given engines or engine design variables cannot be assessed by a comparison of the propulsion-system data alone. Instead the total performance capability of particular airplane-engine configurations must be compared.

Both turbofan and turbojet engines were selected and data were supplied by the NASA for this study. Various degrees of augmentation were considered, from nonafterburning to full afterburning for the turbojets and from duct burning to mixed-flow burning for the turbofans (table 11). Low-flow versions of the turbofans also were studied because of the reduction in transonic spillage drag and the improved engine-airflow nozzle matching at cruise speed.

Two levels of engine design technology were included for the Mach 3.0 application. Engines A and B are representative of a small advancement over current military engine weight and turbine inlet temperature designs. Engines C and D represent a significant advance in these technology areas, particularly in the turbine inlet temperature. For the SCAT 16AL, engines E and F represent the same general design level as engines A and B.

The engine effects on overall airplane capability for SCAT's 16 and 17 are presented in figures 27 and 28, respectively. The take-off gross weight required to meet the design payload and range with a maximum sonic-boom overpressure of 2.0 psf is significantly less with the advanced turbofan engine D. Additional benefits are indicated in the

low-flow version of engine D. As used in this evaluation it has a reduced airflow schedule at Mach numbers between 2.5 and 3.0. Engine D (low flow) was the only engine providing the capability of meeting the sonic-boom overpressure objective of 2.0 psf for SCAT 17 (fig. 28). The superiority of engine D is basically due to the high turbine temperature and the accompanying higher cycle pressure ratio. These factors give this turbofan engine a thrust-weight ratio comparable to that of the high-temperature turbojet (engine C) with good cycle efficiencies at all Mach numbers. In particular, the specific fuel consumption at the required thrusts for subsonic cruise and holding are significantly less than those for the other engines and the reserve requirements are, therefore, lower. These advantages, together with lower fuel consumption during acceleration, more than offset the slight supersonic cruise SFC disadvantage of engine D as compared with engine C.

Airplane sizing studies call for the integration of a number of factors as detailed in figures 29 to 31. The performance trade in matching engine D to the SCAT 16 airframe is shown in figure 29 as contours of constant range capability at a gross weight of 430,000 pounds. These contours are plotted as a function of the total installed engine airflow (sea-level static rating) and airplane wing area. Performance analyses such as this one must be accomplished for a number of gross weights when actually sizing an airplane. In all cases, the airplanes are accelerated along a speed-altitude schedule to cruise which results in a maximum sonic-boom overpressure of 2.0 psf. The variations in range on this plot are caused by the trades between wing area and wing weight and between matched engine performance and engine weight. Increasing the wing area improves the lift-drag ratio but results in a greater weight empty, with less fuel available within the fixed gross weight. Similarly, larger engines provide greater acceleration capability during the critical transonic acceleration condition and match the airplane at a lower cruising specific fuel consumption. Such an engine offers improved fuel utilization but also increases the weight empty. The variation of these items causes the gradients in range capability shown. If range were the only consideration, a slightly smaller airplane would fulfill the SCAT requirements because the peak range capability is approximately 3,250 nautical miles.

Take-off limitations have been added to the range contours in figure 30. The CAR second-segment climb gradient of 0.03 fixes a lower limit to allowable engine thrust since the lift-drag ratio in the climb configuration is relatively insensitive to wing area. The requirement for a take-off velocity no greater than 165 knots fixes a lower limit to wing area. For a given airplane configuration, such as SCAT 16, these two limits are actually determined by the high-lift devices incorporated into the wing. The balance between take-off lift coefficient and climbout lift-drag ratio is achieved by optimizing the flap setting. The variable-sweep-wing geometry of SCAT 16 eliminates the

need for a penalizing compromise from the optimum combination of engine size and wing area for range to achieve good low-speed characteristics. The requirement for a take-off field length no greater than 9,500 feet is also shown, although the take-off speed limitation is more severe than the field-length requirement. Inasmuch as these values, 9,500 feet and 165 knots, typically occur simultaneously for long-range subsonic jets, the greater thrust-weight ratio available with maximum thrust augmentation on SCAT 16 provides the much shorter field length at comparable take-off speeds.

The landing requirements and the transonic thrust margin have been added to the data in figure 31. The requirement for a touchdown speed of 130 knots is more restrictive than the requirement for a 7,000-foot landing-field length. The sizing of SCAT 16 was determined by the somewhat arbitrary choice of a minimum transonic thrust margin equal to 0.3 of the drag on a standard day. This margin was selected as a reasonable compromise between standard-day and hot-day performance. A somewhat smaller airplane would result if less thrust margin were used (approximately 0.2 corresponds to the peak range); however, a greater range loss would occur on a hot day.

A similar sizing chart is shown for SCAT 17 in figure 32. The SCAT 17 characteristics which are fundamentally different from those of SCAT 16 result in more critical low-speed performance requirements. The take-off performance required a significant compromise in the airplane sizing. The lower lift-drag ratio in climbout, primarily due to the lower span and less effective flaps, sized the engines to meet second-segment climb requirements. The lower lift capability of the wing and flap geometry has caused the take-off speed requirement to increase the wing area considerably over the optimum area for range. A less conservative value of 0.22 for transonic thrust margin was accepted to meet the take-off requirements. The hot-day range loss is accordingly somewhat greater than that for SCAT 16. In figures 31 and 32 the shaded area represents the available combinations of wing area and engine airflow which meet the other limitations.

Engine noise at the airport and in the surrounding community represents another limit on propulsion-system selection. SCAT 16 alone meets the community noise goal of 112 PNdb maximum at take-off on a hot day. This low noise level is due primarily to the higher altitude achieved over the community and the lower power setting required to maintain the selected climb path after power cutback. The curves in figure 33 are for a hot day, since the bulk of comity noise complaints occur under these conditions. A point is also shown on the plot for SCAT 16 on a standard day, which indicates a reduction of about 6 PNdb. This reduction is typical for the other airplanes as well.

Take-off along the profiles plotted in figure 33 is made with full augmentation. For SCAT 17, full augmentation is required to meet the second-segment climb gradient with one engine out. For SCAT 16 and SCAT 16AL, the take-off and climbout requirements could be met with lower power settings but the community noise level would increase as a result of the flatter climb gradient.

Noise in the community under the flight path during landing, as shown in figure 34, ranges from 7 to 10 PNdb higher than the take-off noise shown in figure 33. The higher landing noise is due primarily to the low altitude over the community on the 3° glide slope. However, because of this low altitude, the high noise region does not spread to the side as much as in take-off. The take-off and landing noise levels would be equal at a lateral distance of 1,000 to 2,000 feet to either side of the flight path, and the landing noise would be less beyond this distance.

The fan whine contributes significantly to the landing noise. If the fan whine contribution could be deleted through compressor, duct burner liner, and/or inlet design and operation, the landing noise for SCAT 16 would be reduced about 6 PNdb, as shown by the point at the boundary of the comity. Reductions of the same magnitude would occur for the other airplanes as well. Any improvements in the airplane lift-drag ratio in the approach configuration would also reduce the landing noise by reducing the approach power requirements. A 10-percent reduction in approach power would reduce the noise level approximately 3 PNdb.

The continuing model noise test program at The Boeing Company began before the introduction of subsonic jets, and the data in figures 33 and 34 are based on the results obtained from this program. During this study, models duplicating the SCAT engine nozzle velocities, temperatures, and stream-tube area ratios were tested and these results were correlated with full-scale-engine test results, Among the models tested was a coannular design to simulate the duct burning fan exit nozzle.

Handling Qualities

The Boeing SCAT studies included extensive analyses of stability and handling qualities. The airplane configurations have been modified to ensure that all basic requirements have been met. Figures 35 to 39 have been included to illustrate the highlights of this work.

Investigations show that both SCAT's 16 and 17 possess satisfactory stability characteristics throughout the flight envelope., For each airplane tail sizing, wing planform selection, and center-of-gravity

location provide a configuration without pitch-up problems and with adequate static and maneuver margins at all flight conditions.

The effects of aeroelasticity on longitudinal stability dC_m/dC_L are larger for SCAT 16 than for SCAT 17 as shown in figure 35. The combined aerodynamic and elastic characteristics of the wing, fuselage, and tail cause the aerodynamic center to move 23 percent forward for SCAT 16 (total airplane) at supersonic M_D. As a result, tail sizing for minimum stability margins is as critical at the supersonic conditions (wings aft) as it is at the subsonic conditions (wings forward). For SCAT 17, the aeroelastic aerodynamic-center movement is only about one-fourth the magnitude of that for SCAT 16; consequently, the low-speed conditions dictate tail sizing and aerodynamic balance (a.c. relative to aft c.g. limit).

The degree of static directional stability required for the SCAT's 16 and 17 and the most critical flight condition which must be accounted for have not been completely resolved at this time. The typical deterioration in directional stability with angle of attack at supersonic Mach numbers between 2.0 and 3.0 requires that the uppermost boundary of the flight envelope (maximum α condition) be accurately determined and that the minimum stability level acceptable at these conditions be established. Once an upper flight boundary is defined, rigorous dynamics studies will be required to establish vertical-tail and ventral-area requirements to assure flight safety during *any* conceivable maneuver.

Figure 36 relates the deterioration in directional stability with angle of attack and structural aeroelasticity for SCAT's 16 and 17 at the Mach 3.0 cruise condition. For reference, the angle of attack at 2.5g is shown for each airplane at cruise conditions. Tails and ventrals were arbitrarily sized in this study to provide a minimum C_{n_β} level of 0.0005 at this condition. Since higher angles of attack may be encountered at off-design conditions, further study in this area appears necessary.

Analytical studies and flight simulator evaluations have shown that SCAT's 16 and 17 possess acceptable low-speed longitudinal dynamic characteristics without stability augmentation. Figure 37 indicates that, in the landing-approach condition, the longitudinal short-period oscillation is well damped and slightly longer in period than that of current jet transports. As a result, only a small amount of damping augmentation is required to optimize low-speed handling qualities. At supersonic cruise, however, the longitudinal short-period oscillation is very poorly damped for both configurations. Handling qualities for this flight condition appear to be unacceptable without damping augmentation. Further flight simulator research will be needed in this area.

The characteristic nature of the lateral-directional dynamic oscillation or Dutch roll is different for the SCAT 16 and SCAT 17 configurations, as shown graphically in figure 38, which includes the military requirements specified in MIL-F-8785.* At low speeds, the SCAT 16 Dutch roll oscillation is better damped with less rolling than that of SCAT 17. The better damping of SCAT 16 is due to the unsweeping of the wing. At supersonic cruise where the SCAT 16 wing is swept back 75°, the Dutch roll oscillation is less damped and with more rolling than for SCAT 17. The augmentation requirements appear to be moderate at Mach 3.0 cruise and small at low speed for either airplane. Present transports generally fall in the area near the SCAT 16 low-speed point. The final evaluation of handling qualities and augmentation for the supersonic transport will require inclusion of the pilot in the loop.

Positive speed stability during landing approach was specified as a desirable characteristic for the SCAT airplanes. The approach speeds which correspond to a touchdown speed of 130 knots at design landing weight are shown in figure 39. Scat 16 has satisfactory speed stability, which corresponds to that of present-day airplanes. SCAT 17 is slightly unstable but is well within the criterion of $\frac{d(T/W)}{dV} = -0.0012$ per knot which is considered acceptable by NASA pilots. Perhaps a more significant factor is approach attitude. For the conditions shown, SCAT 16 approaches at a body attitude of 4.3° with a speed of 135 knots and SCAT 17 approaches at an attitude of 10° with a speed of 136 knots. The relatively high attitude of SCAT 17 at touchdown probably would be considered more undesirable by pilots than the slight speed instability.

III. RESEARCH POTENTIAL AND CONCLUSIONS

The Boeing SCAT feasibility studies were very much like the usual preliminary design investigations in the early stages of the development of *any* new airplane. The process is roughly described in figure 40. So *many* complex variables are interrelated that both the initial choice of configuration and continued refinement require *many* repetitions of the design cycle. This design cycle approach has been typical of airplane development programs such as those for the Boeing B-47, B-52, 707, and 727. During the SCAT studies, the design cycle was repeated several times but without the benefit of adequate wind-tunnel testing of improvements each time through the cycle. The design

*Anon.: Flying Qualities of Piloted Airplanes. Military Specification MIL-F-8785(ASG), Sept. 1, 1954; Amendment-2, Oct. 17, 1955.

evolution does not stop once the original configuration is selected. The design cycle is repeated over and over to optimize the total program.

Operating Cost Comparisons

The effects of this continuing design refinement are clearly evident in the seat-mile economics of the Boeing 707, as shown in figure 41. The band of seat-mile costs for the 707 shows the improvement which has been achieved over a period of several years. The top of the band represents the direct operating costs (DOC) of the initial offerings to the airlines. The bottom of the band represents the better economies of the advanced 707 Intercontinental available today. As shown in figure 41 on a relative scale, the DOC of SCAT's 16 and 17 are not as good as those of the initial 707. However, neither of these SCAT designs has been optimized to the same extent as was the 707 at the time it was first offered to the airlines. The relative seat-mile costs of SCAT 16AL shown for Mach 2.0 cruise are even higher than those for SCAT's 16 and 17.

If additional effort had been applied and the design cycle repeated more often than the abbreviated period for the study of SCAT 16AL allowed, seat-mile costs could probably have been reduced somewhat. However, since the seat-mile costs of the SCAT 16AL are so much higher than those of SCAT's 16 and 17, it is doubtful if any significant improvement in seat-mile costs would be achieved. It is probable that the DOC of the aluminum airplane will never be competitive with those of the Mach 3.0 airplanes. The studies made to date indicate the need for substantial improvements in the supersonic transport if it is to be competitive from an economic standpoint with subsonic jets already available. There appears to be ample opportunity for improvement of the supersonic transport in the months and years ahead by repeating the design cycle. However, improved designs do not evolve simply as a result of the passage of time. Intensive effort is required and the research achievements in a number of technology areas must be integrated into an optimized configuration. Both basic research and the engineering application of many new ideas must be pursued vigorously if desired results are to be achieved.

Aerodynamic Trades

As a part of the SCAT studies, Boeing determined the impact of potential improvements in several important technology areas on the factors that affect operating costs. Figure 42 charts the influence of aerodynamic improvements on the *gross* weight of a supersonic transport

to perform a given job. For example, an improvement in cruise L/D for SCAT 16 from 6.6 to 7.0 would permit a reduction in gross weight of around 30,000 pounds or approximately 7 percent. This is a technology area where intensive effort is justified because of the impact of both gross weight and aerodynamic efficiency on operating costs. Improving aerodynamic efficiency will require both time and effort, but an L/D approaching 8 appears possible by 1970 to 1975. If the L/D for SCAT 16 could be improved to 8, the DOC would be reduced 15 to 20 percent from the level shown in figure 41.

Weight Trades

Another obvious area for continued research is in the reduction of the weight empty of the airplane. Applying effort to attaining minimum structural weight has been traditional in airplane design, but the job becomes more important as it becomes more difficult. Structural-weight minimization has been a difficult technical problem in the SCAT study, but the payoff in lower gross weights makes further progress very desirable (see fig. 43). For airplanes performing the same mission, 1,000 pounds saved in operating weight empty can reduce the take-off gross weight by 5,000 to 6,000 pounds. Alternatively, weight empty reductions can be converted directly into allowable payload with accompanying dramatic reductions in seat-mile costs.

Propulsion System Trades

The operating efficiency of an airplane is always very sensitive to the state of the art of the propulsion system. This critical relationship is particularly true for the supersonic transport. Figure 44 shows the effect of an improvement in engine design achieved principally through the use of higher turbine inlet temperature. Instead of a SCAT 16 with a gross weight of 430,000 pounds with engine D (turbine inlet temperature of 2700° R) the gross weight would have been about 490,000 pounds with engine B (turbine temperature of 2400° R). A similar effect is apparent for SCAT 17.

Figure 45 shows the effect on gross weight of small variations in three factors affecting propulsion-system installation efficiency. The relatively large effects point up the need to achieve an optimum installation as well as an optimum engine. Looking ahead, the guarantees which an airplane manufacturer must eventually make to the airline customer will permit only very minor tolerance variations in factors such as installation weight, nozzle efficiency, and inlet recovery. Compounding of a number of individual tolerances could have a tremendous effect on the final gross weight of the supersonic transport.

Other important factors related to the freedom of choice which the airframe designer will have in the eventual selection of the supersonic transport configuration were brought out by the SCAT studies. For example, aircraft designers have depended for many years on increasing payloads for improving the economics of new airplanes. If the same sonic-boom overpressures are assumed as those which were used in the SCAT studies, the amount of exploitation of size effects for obtaining improved economics will be severely limited. The left-hand chart in figure 46 indicates the effect of range and payload variations on DOC when the 2 psf sonic-boom-overpressure constraint is observed. If the sonic-boom overpressure were increased to 2.3 psf, reductions in seat-mile costs, such as those shown in the right-hand chart, are immediately available. Thus, if it were possible, for example, to operate at higher sonic-boom overpressures over ocean areas, improved economics on inter-continental routes should result. The reduced width of the shaded area on the right-hand chart is also significant. Direct operating costs show a substantially smaller increase with increasing design range at an overpressure of 2.5 psf than at 2 psf.

Conclusions

The practicability of a supersonic transport has been confirmed by the SCAT studies. This conclusion must, of course, be confirmed by construction and testing of full-scale hardware before the true answer is known. However, at present it appears that at least two of the five configurations studied are quite feasible when judged by the standards established for the SCAT studies. There is no clear-cut choice between these two configurations although the variable-sweep-wing airplane appears to have better "off-design point" characteristics than the delta-wing configuration. Furthermore, it is entirely possible that one of the other configurations can be made more attractive if sufficient inventiveness is applied. Certainly attempts to develop configurations which are basically superior to either SCAT 16 or SCAT 17 are to be encouraged.

The economic feasibility of the SCAT configurations is not as clear cut as the technical feasibility. The present configurations with airframe and engine costs generally considered probable for this type of airplane will not have as good DOC as the present-day highly refined subsonic jets. Further research and optimization of specific designs should do much to reduce the gap in direct operating costs which presently exists. During the initial operation of the supersonic transport, the higher unit costs would undoubtedly be more than offset by higher load factors and/or higher fares. However, in order to be economically sound for future operation, the ultimate product must be improved.

In view of the marginal acceptability of *any* of the configurations studied, an attempt must be made to select for further intensive work those types of configurations with the maximum improvement potential. For example, the extensive use of titanium in the structure of the airplane, although requiring additional development, appears to be necessary for this airplane whether it is to be operated at Mach 2 or at higher speeds.

Opportunities for further aerodynamic refinement and design optimization of SCAT 16 appear greater than for the other configurations studied and further investments in understanding and improving this configuration are particularly desirable.

Problems such as the sonic boom can likewise have a major influence on the ultimate usefulness of the supersonic transport. Although the sonic boom is a very real problem from the standpoint of public reaction, it is at least as great a problem from the standpoint of the designer. Careful study and research of this phenomenon is still very much in order.

Perhaps the most important thing to bear in mind is that September 1963 is literally only the threshold of the supersonic transport era. The research and development that has been expended toward the development of the supersonic transport must be continued and expanded. Aerodynamics, structures, and propulsion have always been important to the designer. They are even more important today. Industry must work on these fundamentals to the maximum extent that its resources will permit. Since these resources are limited and since substantial military developments in the supersonic airplane area are lacking, the supersonic transport requires direct government funding for continuing and intensified research. The supersonic transport is an important subject, one in which the stakes will be extremely large. Both the quality and the extent of the government research program must be consistent with the scope of the problem. These research efforts must be extended for many years if the kind of a program which the American public has come to expect of joint government-industry efforts is to be achieved. Boeing enters the supersonic era confident that a superior U.S. airliner can be achieved but fully cognizant of the extent of the effort which lies ahead.

TABLE I.- SCAT GUIDELINES

Cruise speed	Mach 3 (Mach 2 for 16AL)
Range	3,200 n.mi.
Payload	125 passengers (26,125 lb)
Take-off:	
Speed	165 knots
Distance	9,500 ft
Landing:	
Speed	130 knots
Distance	7,000 ft
Approach (speed stability desired)	145 knots
Sonic-boom overpressure:	
Climb	2 psf or less
Cruise	1.5 psf or less
Airport noise	Comparable to present-day jets

TABLE II.- ENGINE TYPES

Engine / Engine	Mach 3.0		Mach 2.0
	Turbine temperature, 2,400° R (a)	Turbine temperature, 2,700° R (b)	Turbine temperature, 2,400° R a
Turbojet	A Afterburning	C Nonafterburning N afterburning	E Afterburning
Turbofan	B Duct burning Low flow	D Duct burning Mixed burning Low flow	F Duct burning

[a]Present-day technology.

[b]Advanced technology.

DECLASSIFIED

BOEING CONFIGURATIONS

SCAT	4	15	17	16	16 AL
DESIGN SPEED	MACH 3				MACH 2
BASIC STRUCTURAL MATERIAL	TITANIUM (8AL-1MO-1V)				ALUMINUM (2024-T81)
POWER PLANT	ADVANCED TURBO-FAN (ENGINE D)				TURBO-FAN (ENGINE F)
ALL STUDIES BASED ON SCAT GUIDELINES					

Figure 1

SCAT 4
ORIGINAL CONCEPT

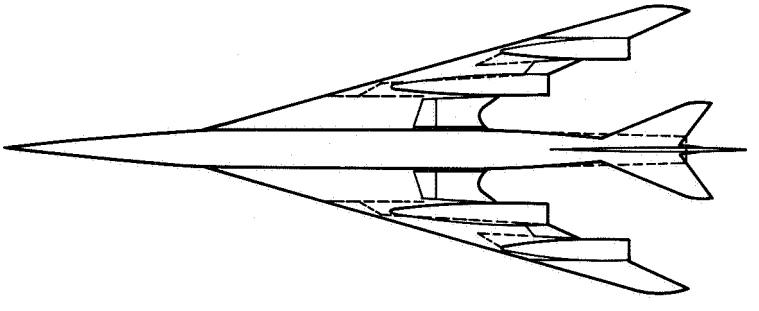

Figure 2

SCAT 4
FINAL CONFIGURATION–JUNE

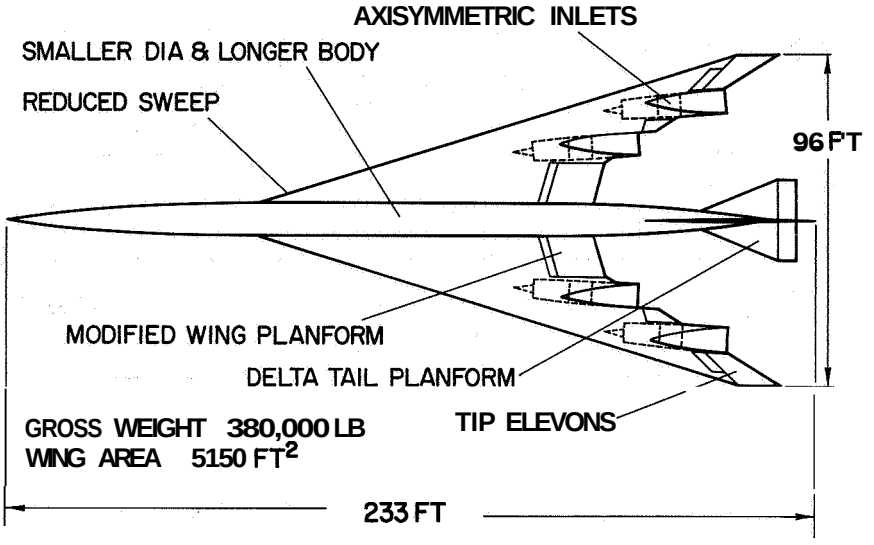

Figure 3

SCAT 15
ORIGINAL CONCEPT

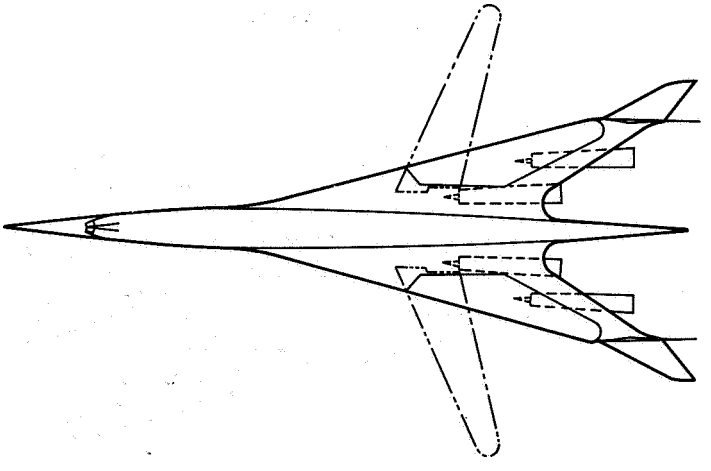

Figure 4

RELEASED

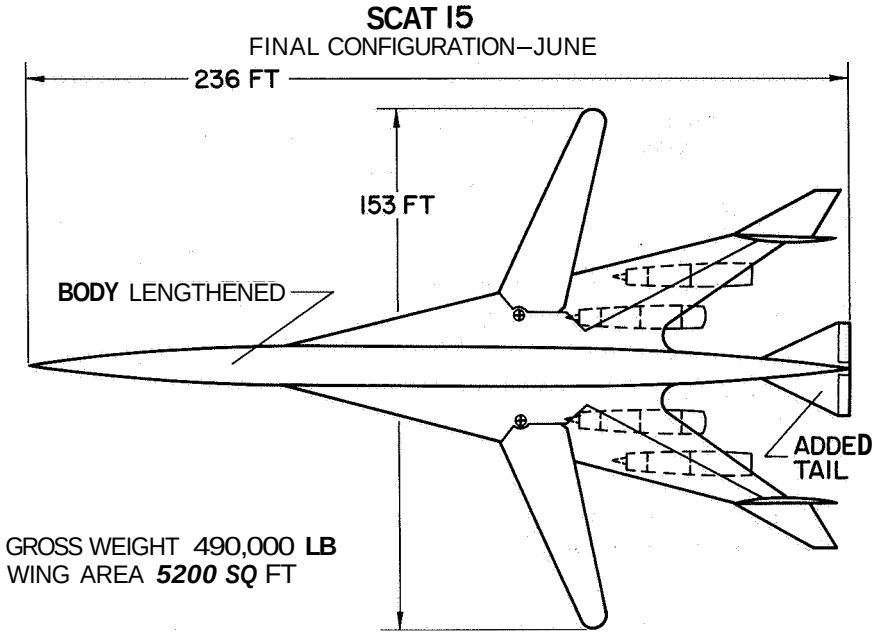

Figure 5

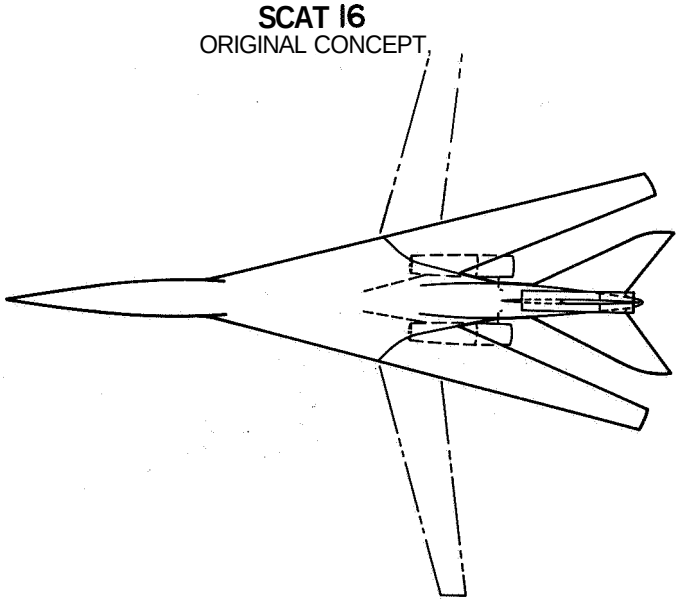

Figure 6

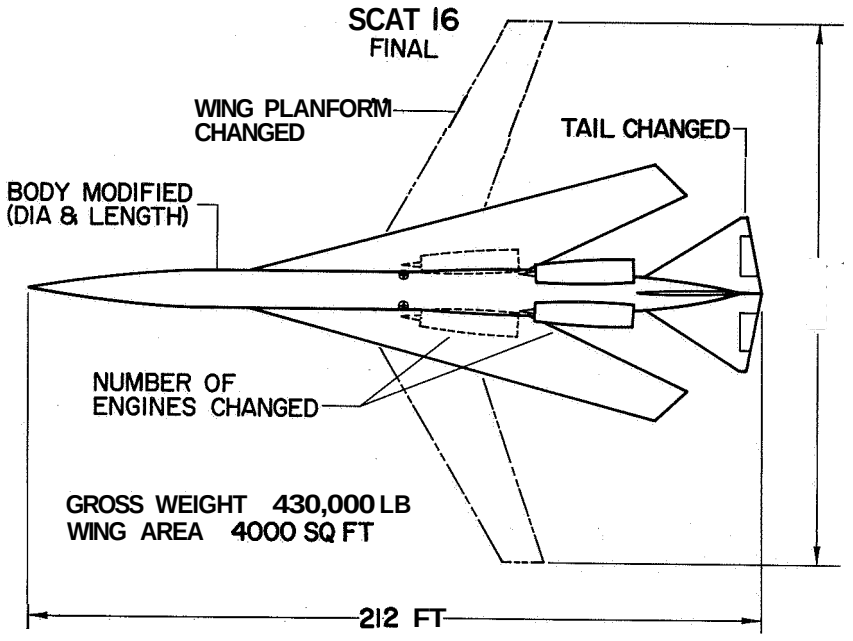

Figure 7

SCAT 16
FUEL AND PRIMARY STRUCTURE

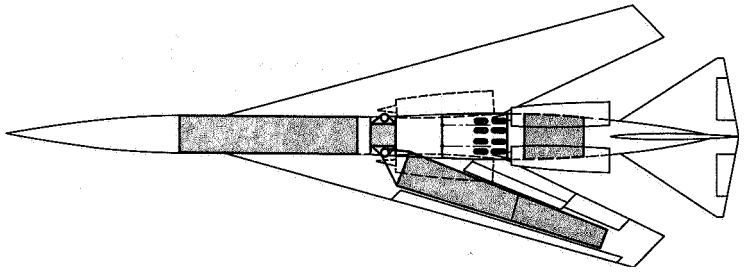

Figure 8

[redacted]

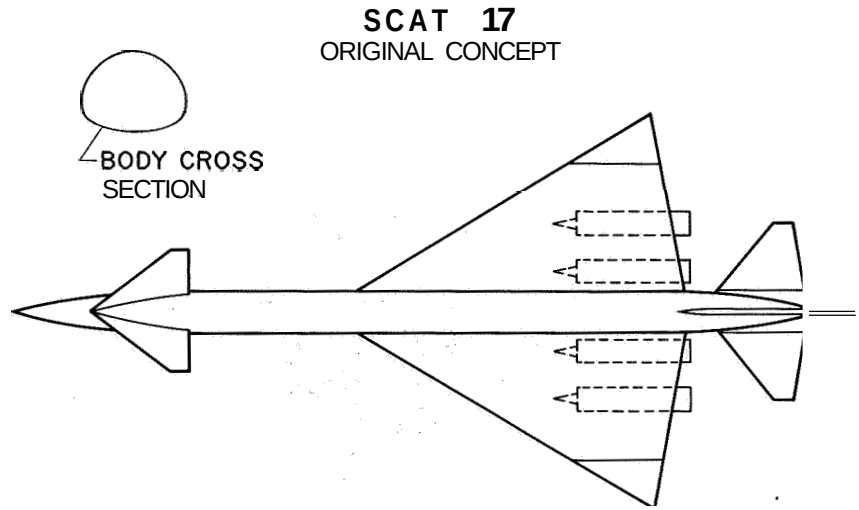

Figure 9

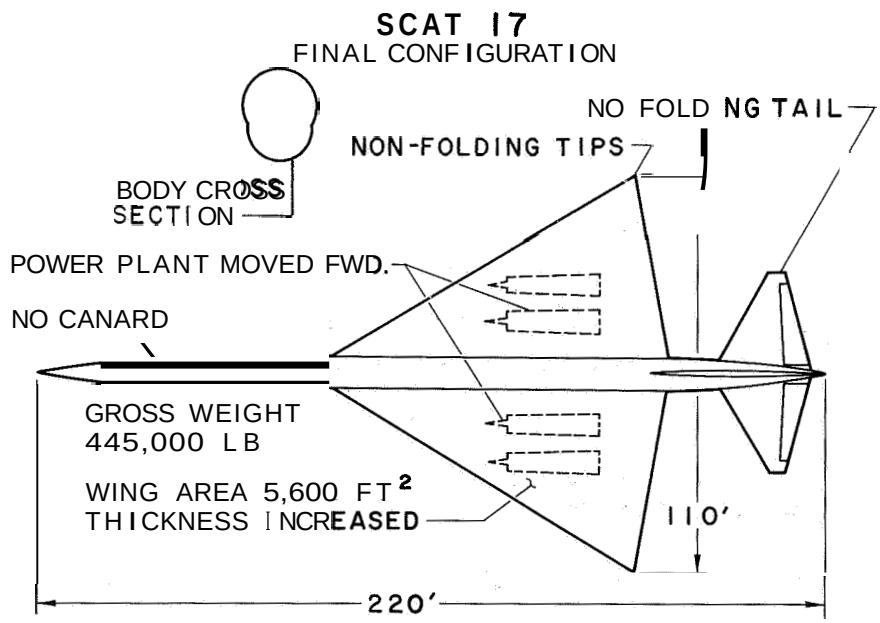

Figure 10

[redacted]

SCAT 17
FUEL AND PRIMARY STRUCTURE

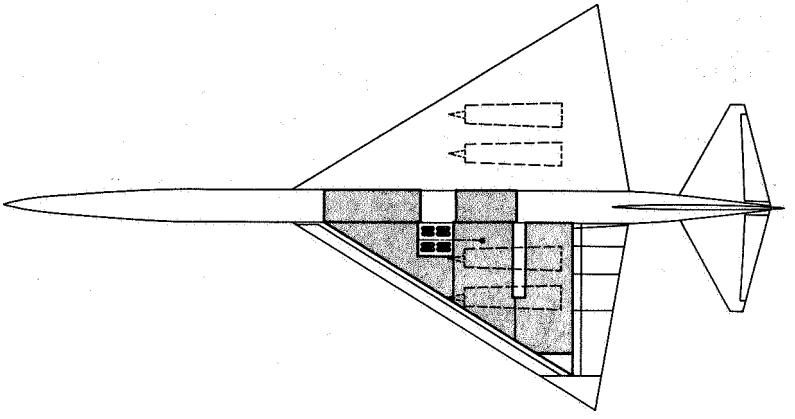

Figure 11

SCAT 16AL

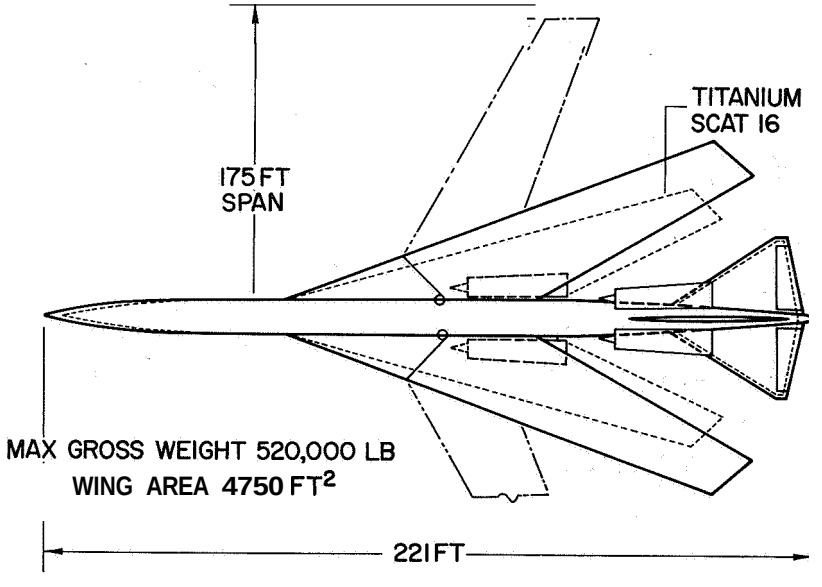

Figure 12

COMPARATIVE PERFORMANCE

RANGE - 3200 N.MI. PAYLOAD - 125 PASS.	SCAT 4	SCAT 15	SCAT 17	SCAT 16	SCAT 16 AL
CRUISE MACH NO.	TITANIUM 3	TITANIUM 3	TITANIUM 3	TITANIUM 3	AL. 2
GROSS WT. - 1000 LB	380	490	445	430	520
WEIGHT RATIO - GW/OWE	2.29	2.02	2.47	2.24	2.31
L/D - CRUISE	7.4	8.0	6.3	6.6	7.5
SFC - CRUISE - LB/LB/HR	1.59	1.57	1.67	1.63	1.40
RESERVE FUEL - % GW	9.6%	8.6%	8.2%	7.3%	7.0%
SONIC BOOM - CLIMB	2.0	2.4	2.0	2.0	2.2

Figure 13

WEIGHT BREAKDOWN

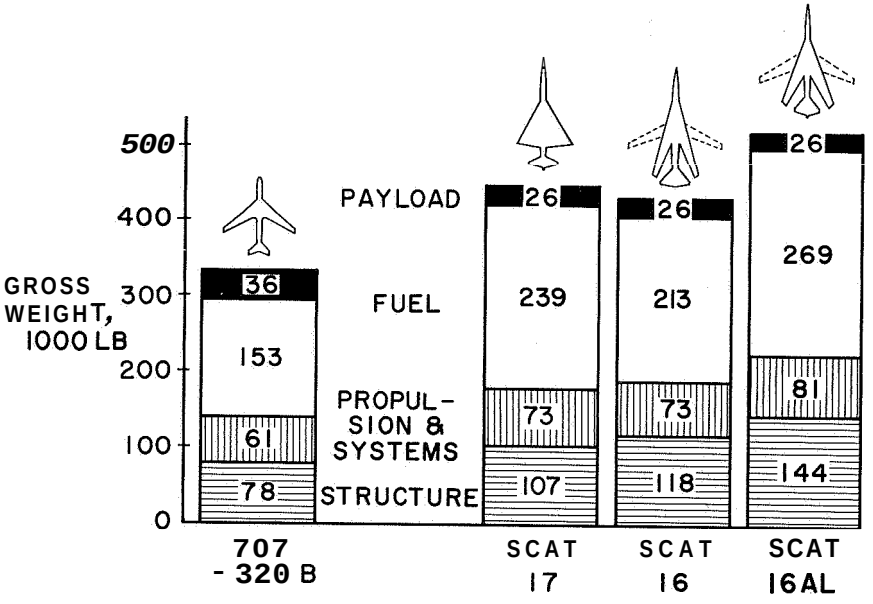

Figure 14

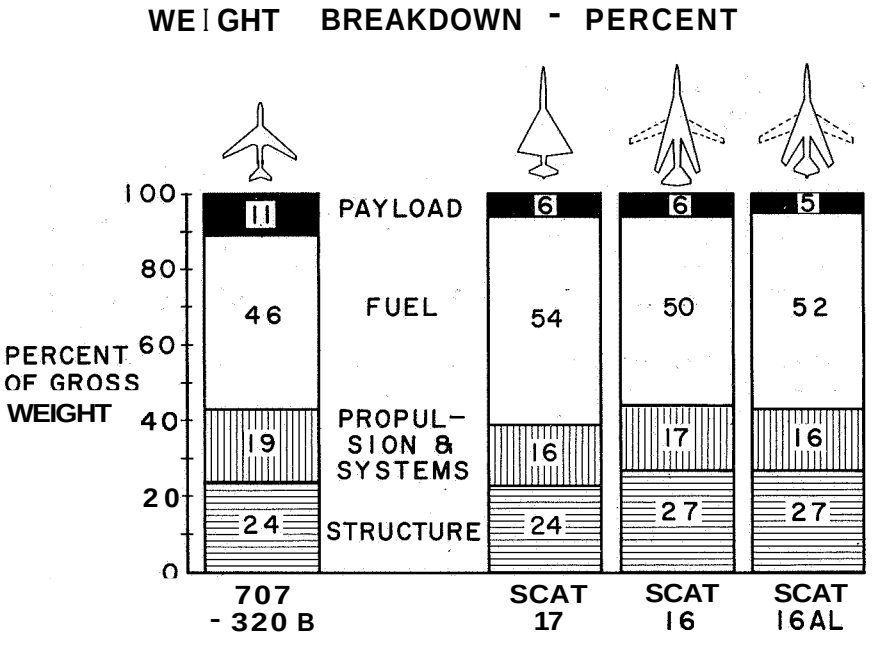

Figure 15

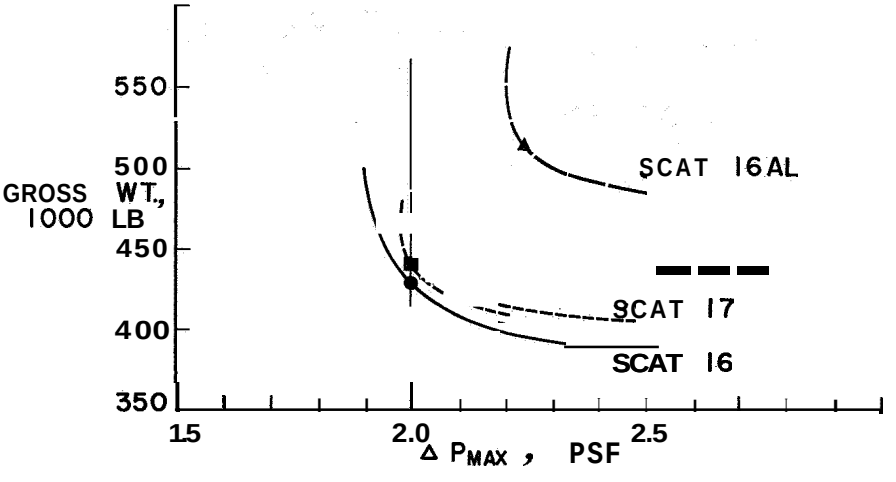

Figure 16

[redacted]

DECLASSIFIED

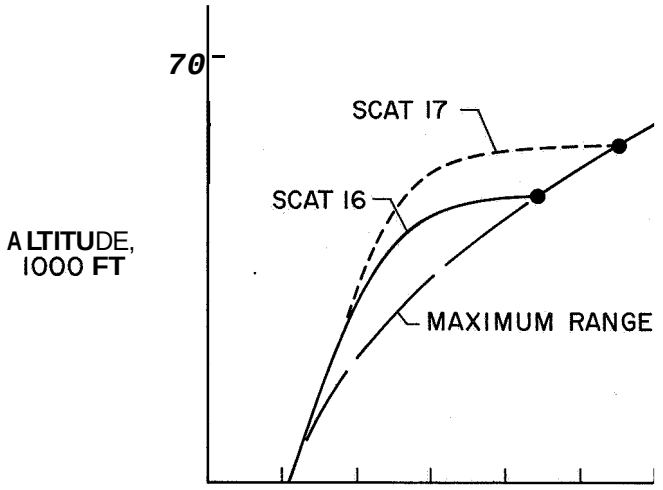

Figure 17

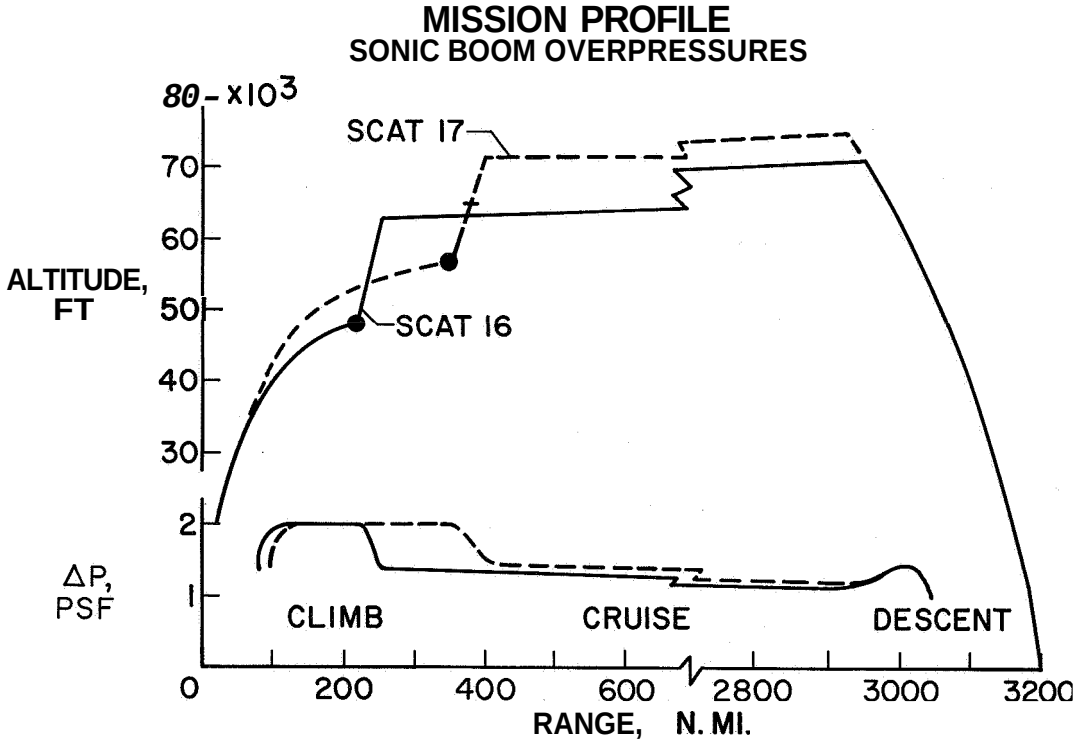

Figure 18

SCAT OPERATIONAL LIMITS

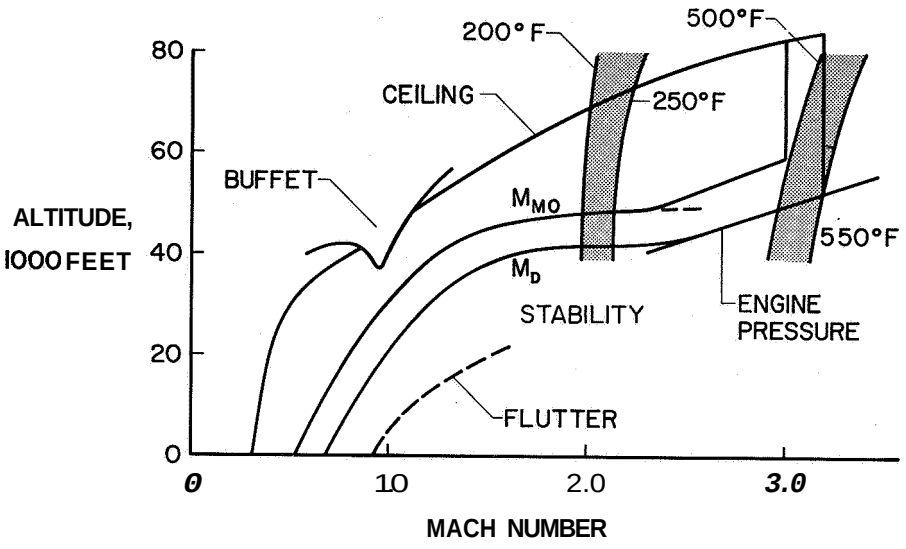

Figure 19

MATERIAL SELECTION

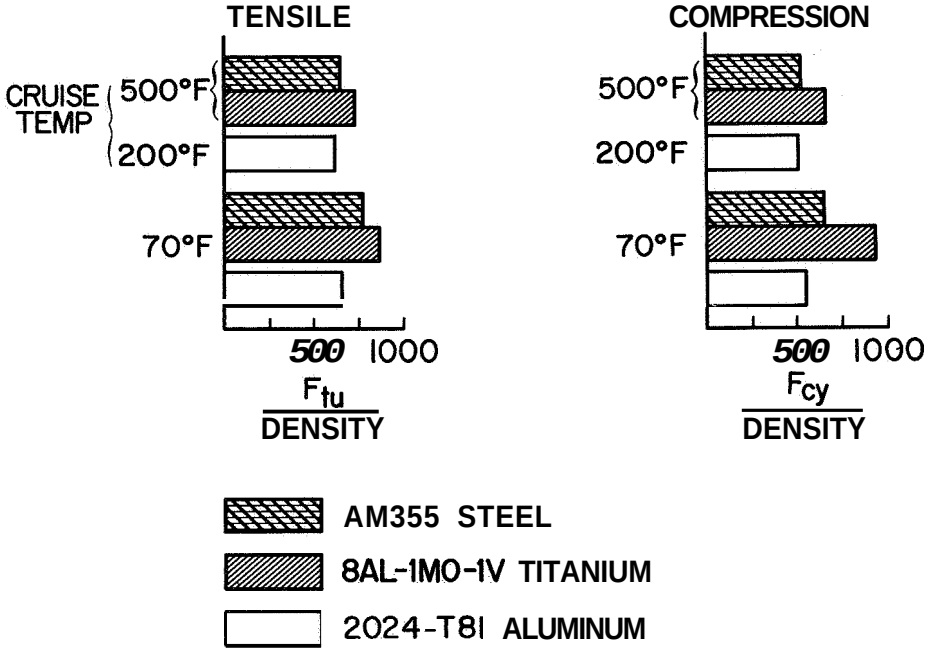

Figure 20

MATERIAL SELECTION

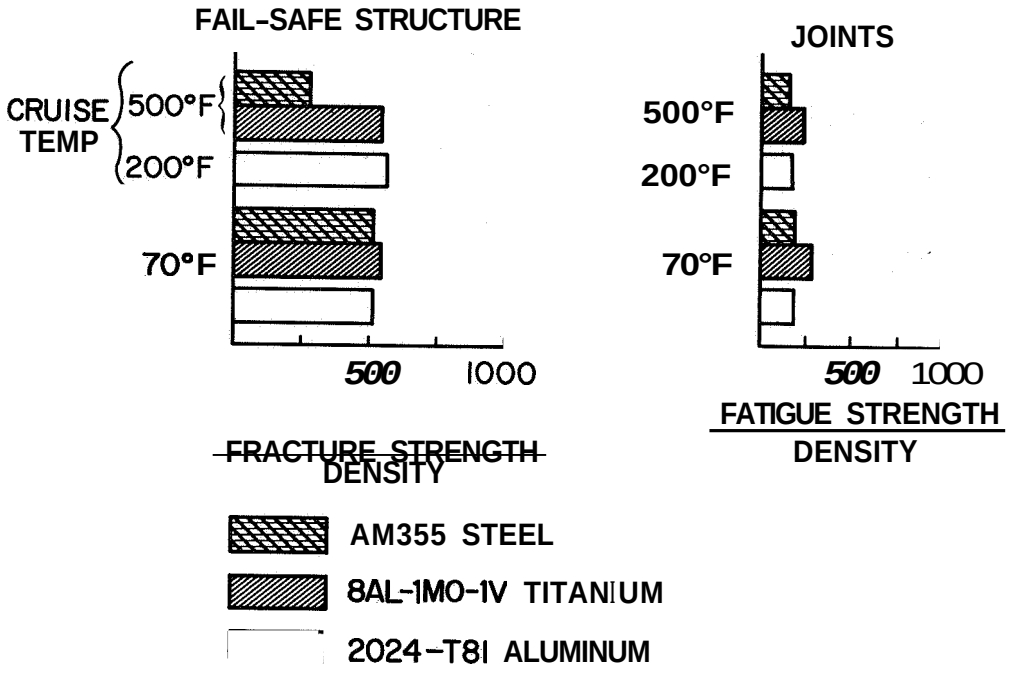

Figure 21

WING CONSTRUCTION
MACH 3 AIRPLANE

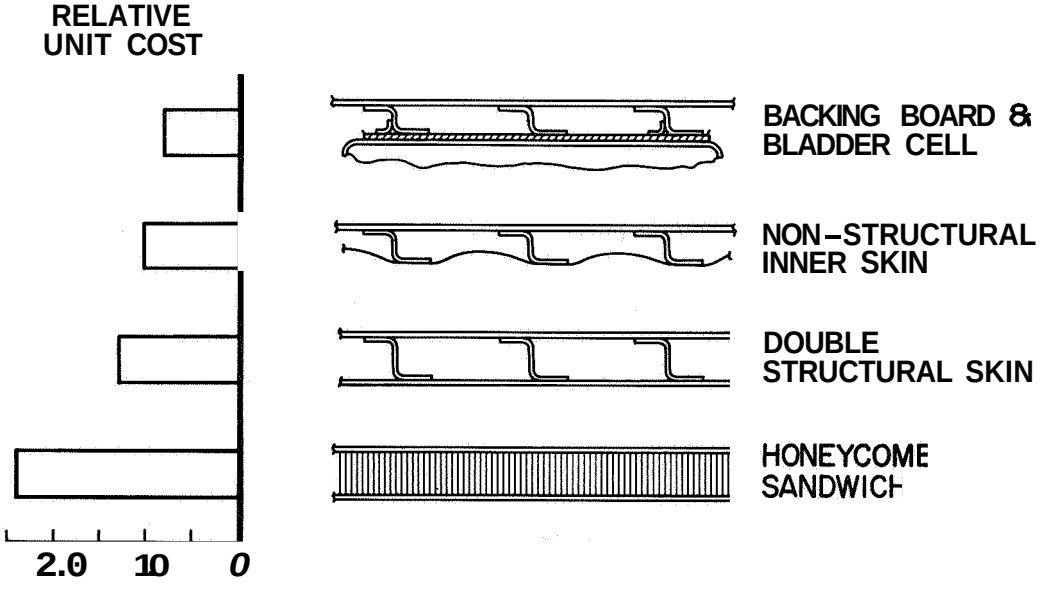

Figure 22

WEIGHT COMPARISON
SCAT 16 WING

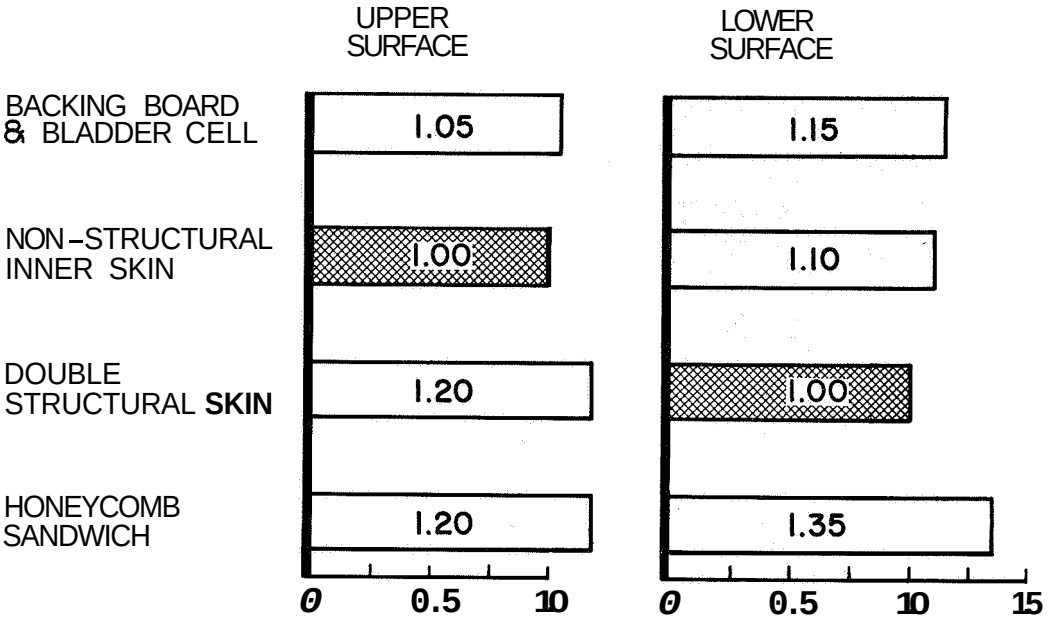

Figure 23

WEIGHT COMPARISON
SCAT 17 WING

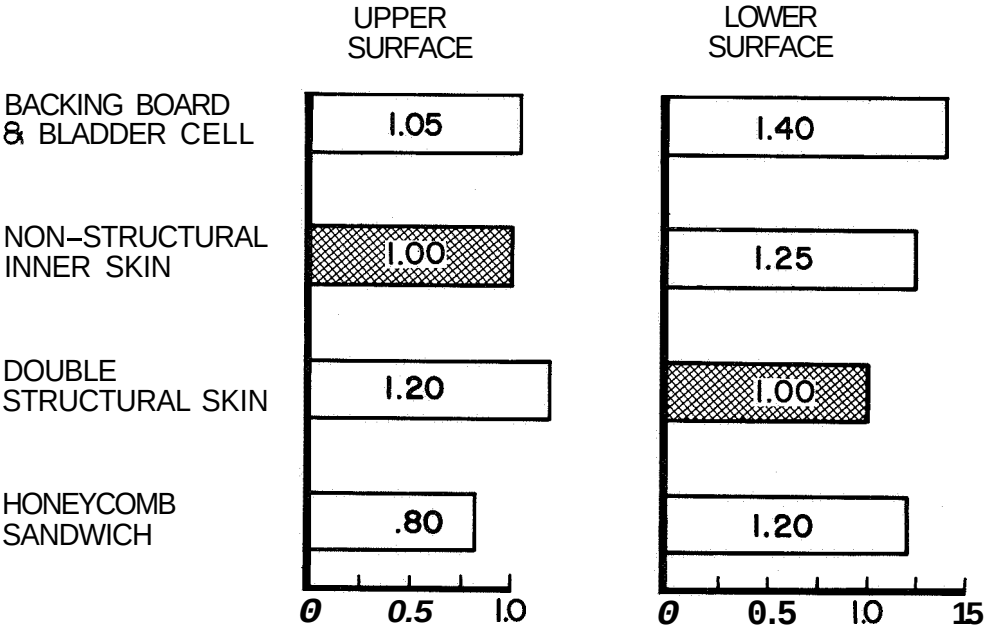

Figure 24

MACH NUMBER EFFECTS
SCAT 16AL STRUCTURAL WEIGHT

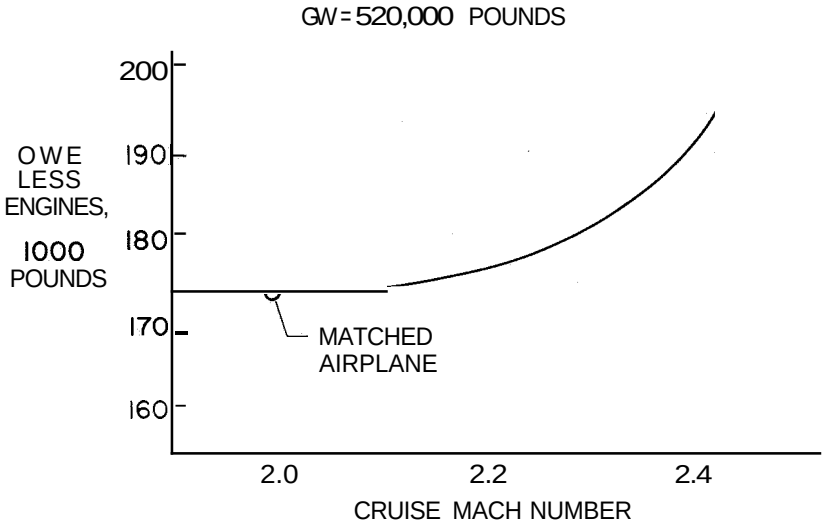

Figure 25

CRITICAL ENGINE DESIGN CONDITIONS

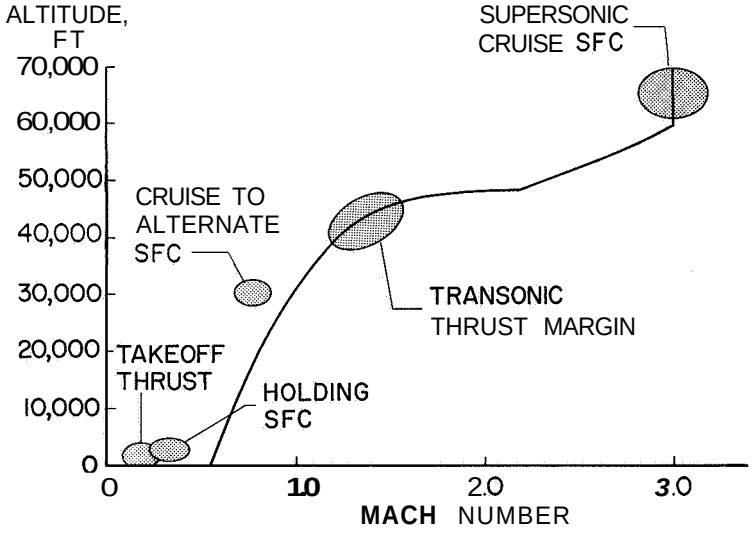

Figure 26

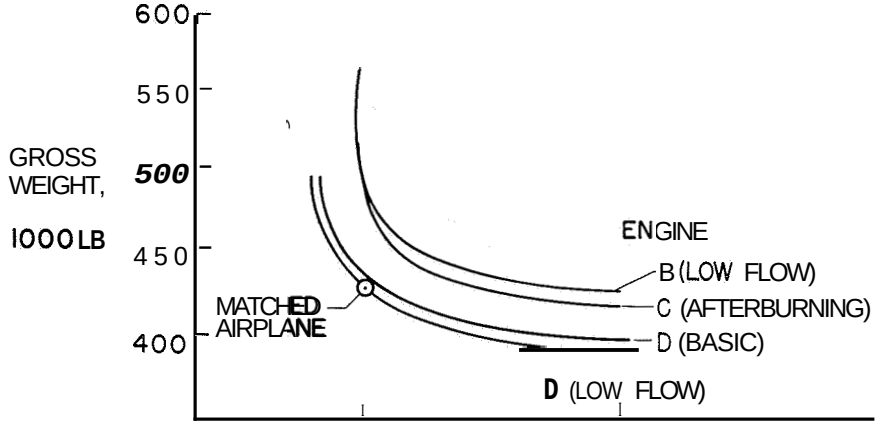

Figure 27

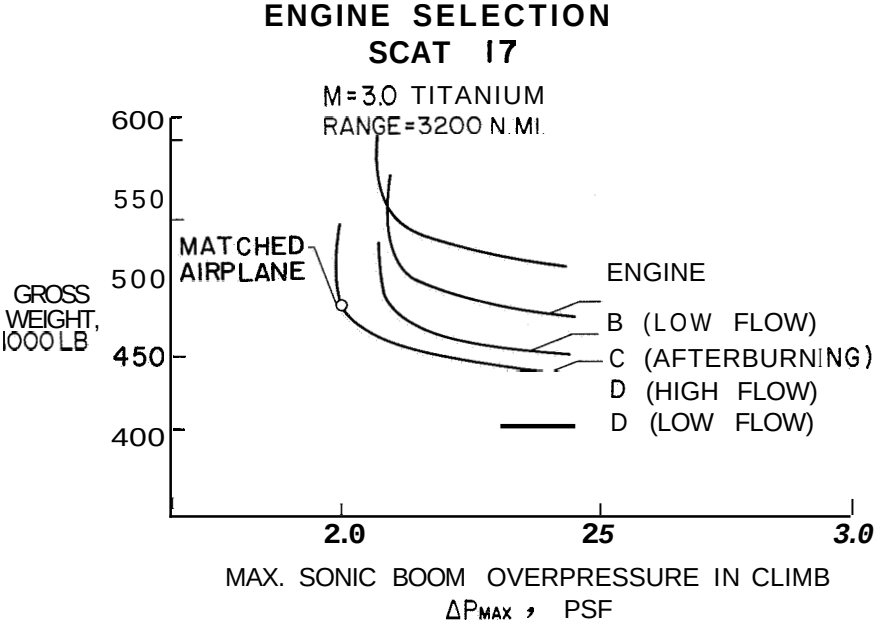

Figure *28*

AIRPLANE SIZE ANALYSIS
SCAT 16

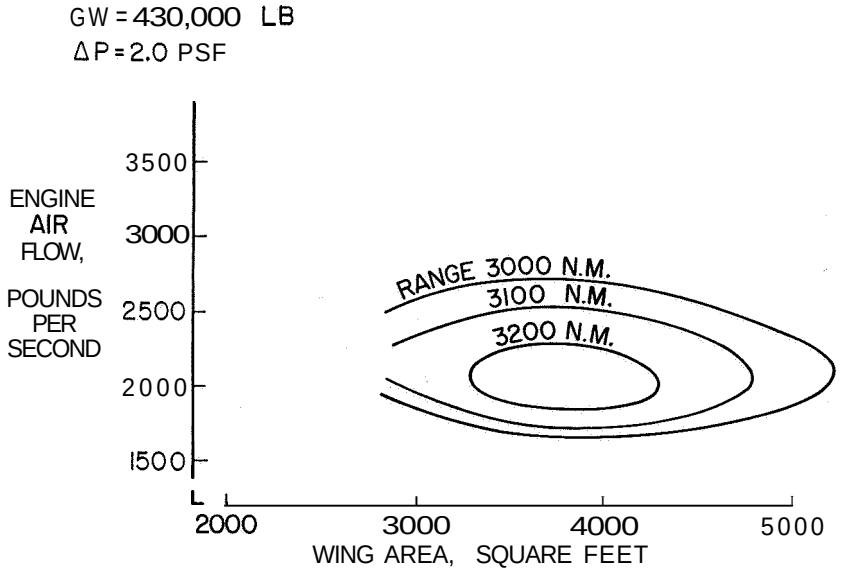

Figure 29

AIRPLANE SIZE ANALYSIS
SCAT 16

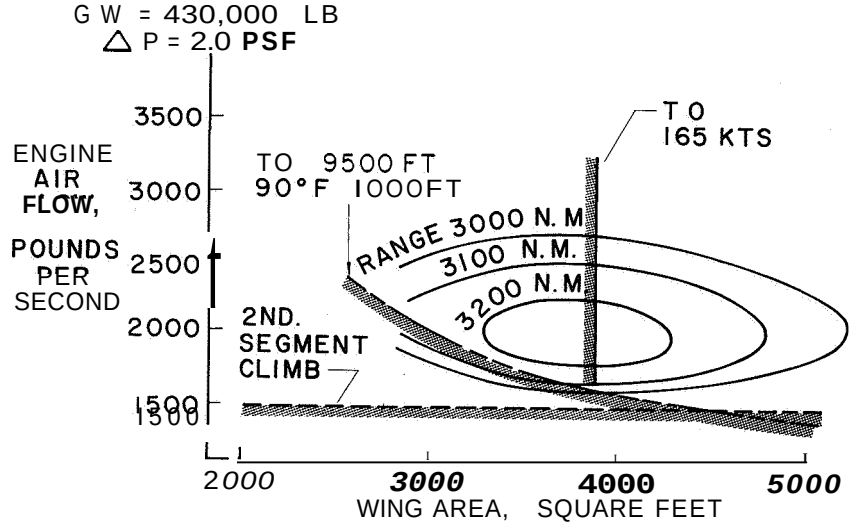

Figure 30

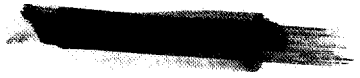

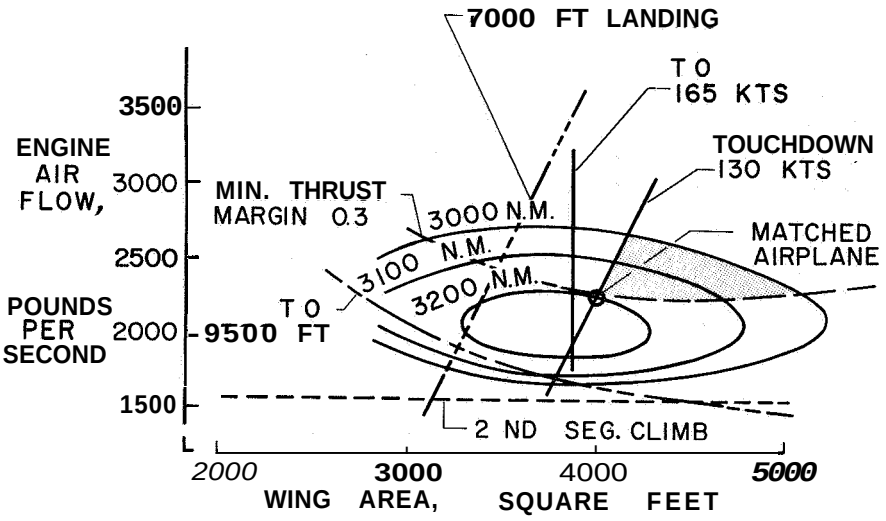

Figure 31

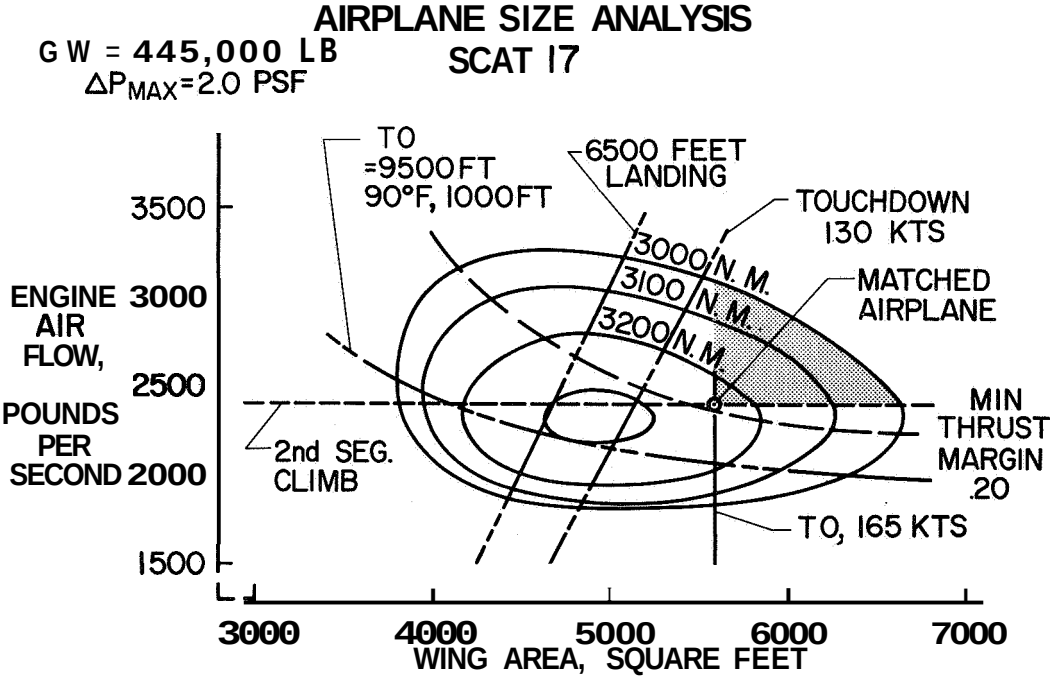

Figure 32

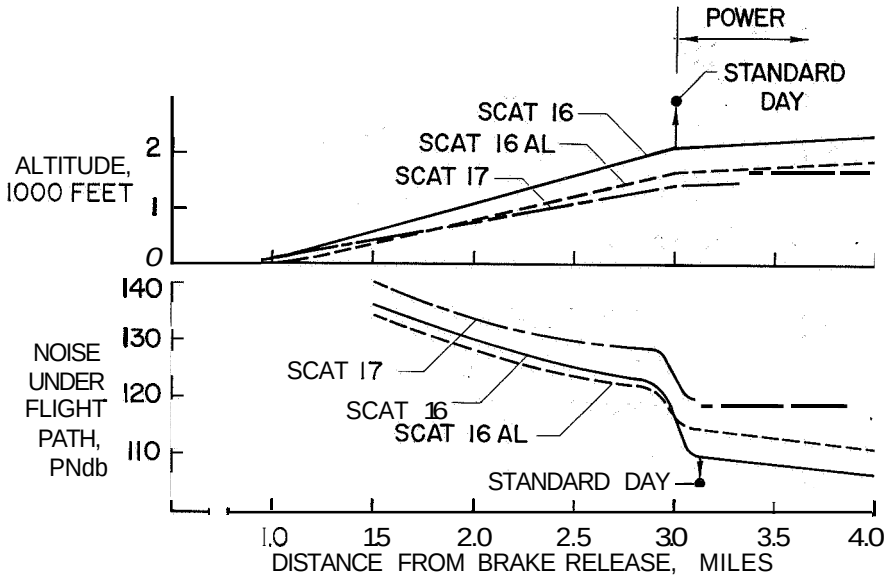

Figure 33

LANDING **NOISE**

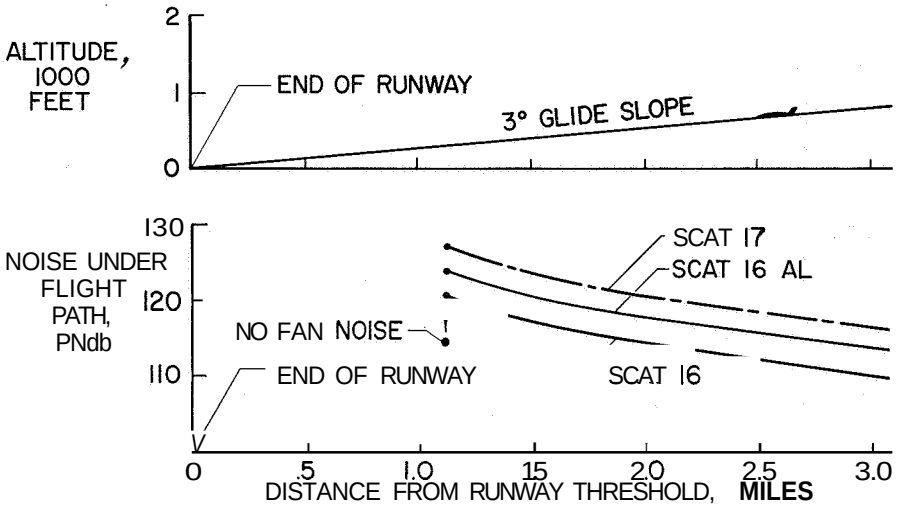

Figure 34

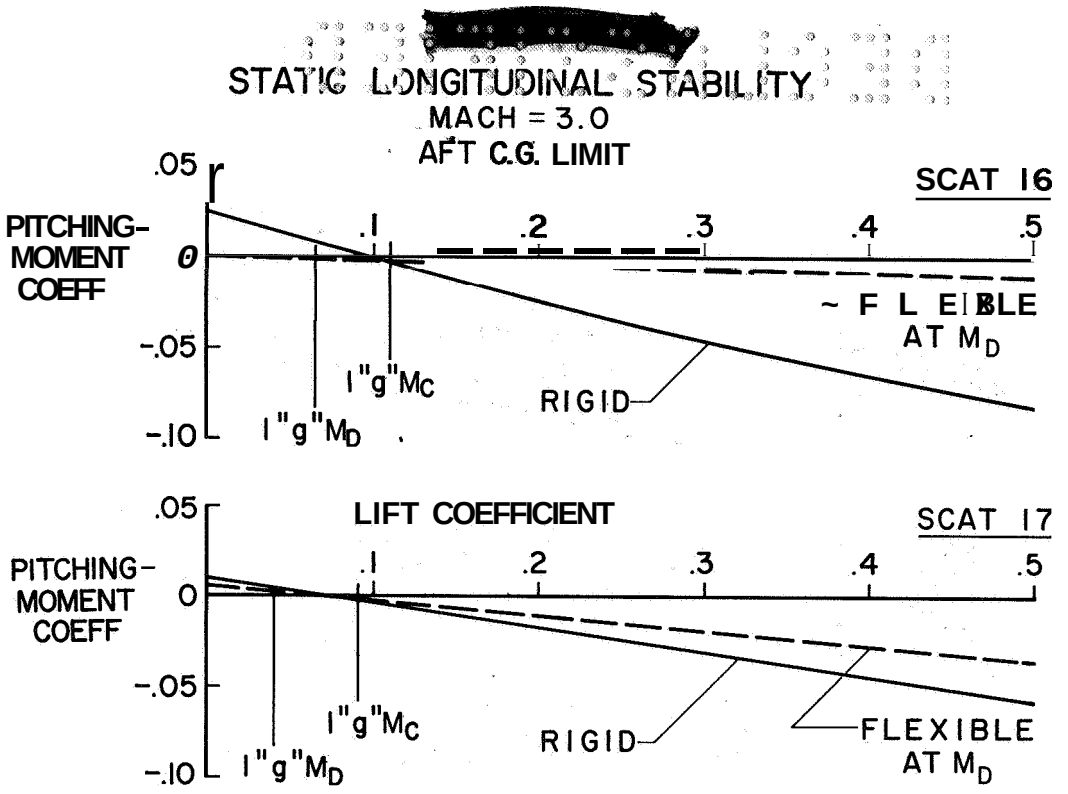

Figure 35

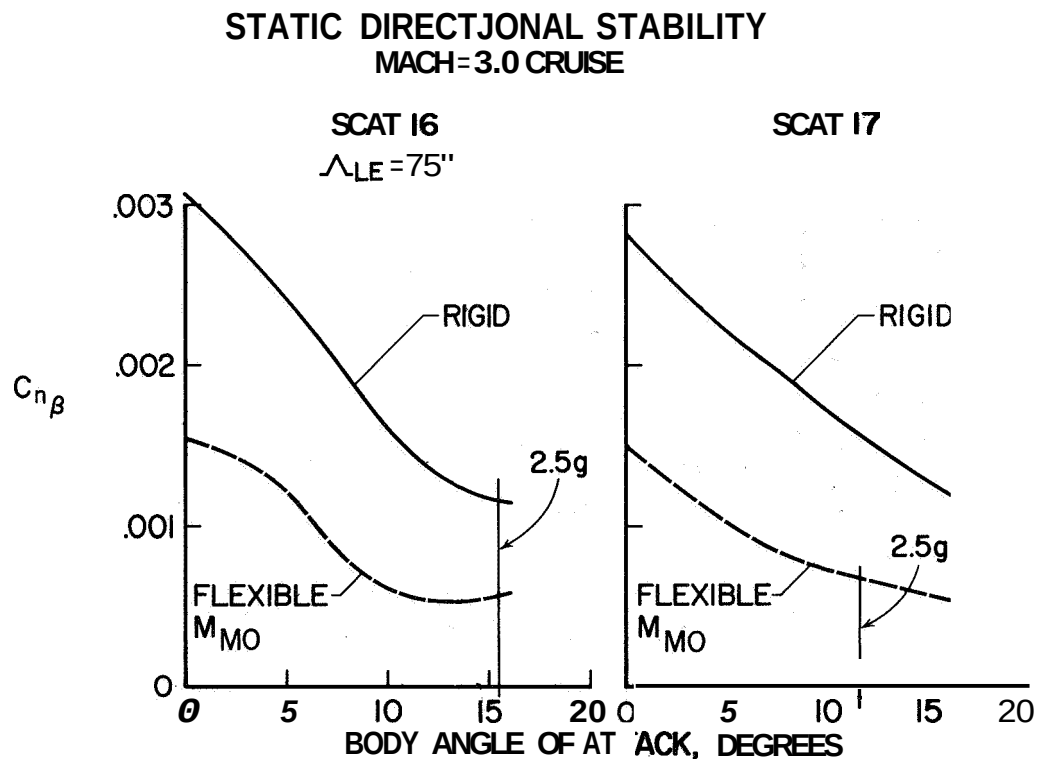

Figure 36

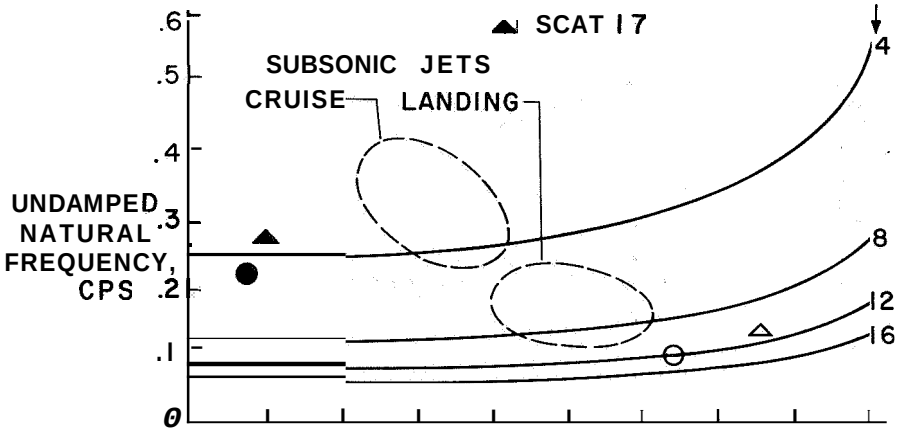

Figure 37

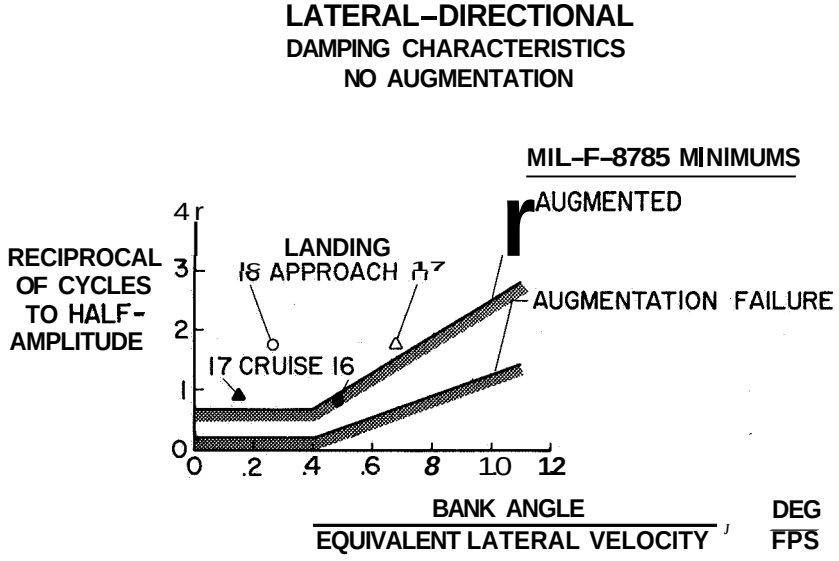

Figure 38

SPEED STABILITY IN APPROACH

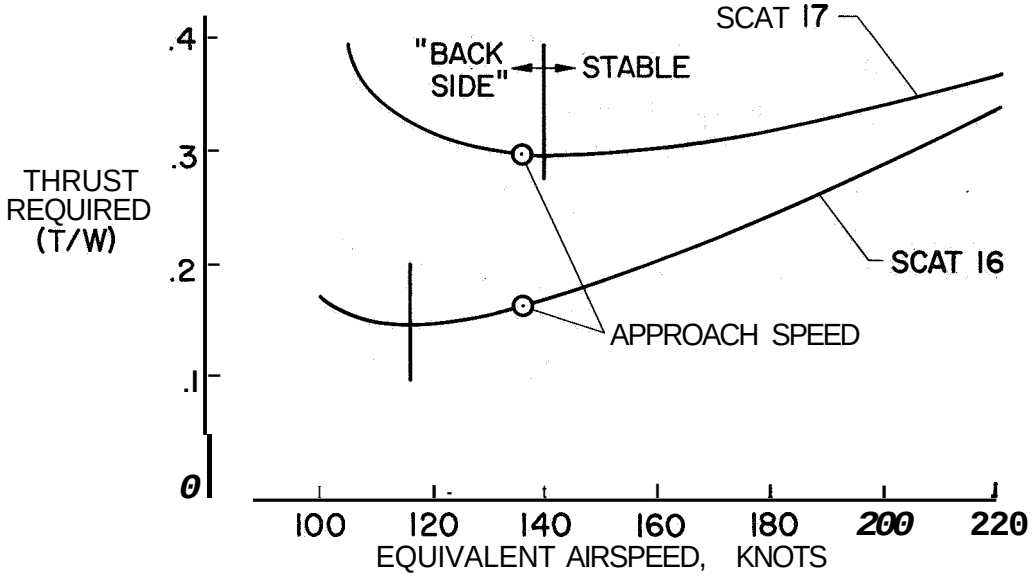

Figure 39

DESIGN EVOLUTION

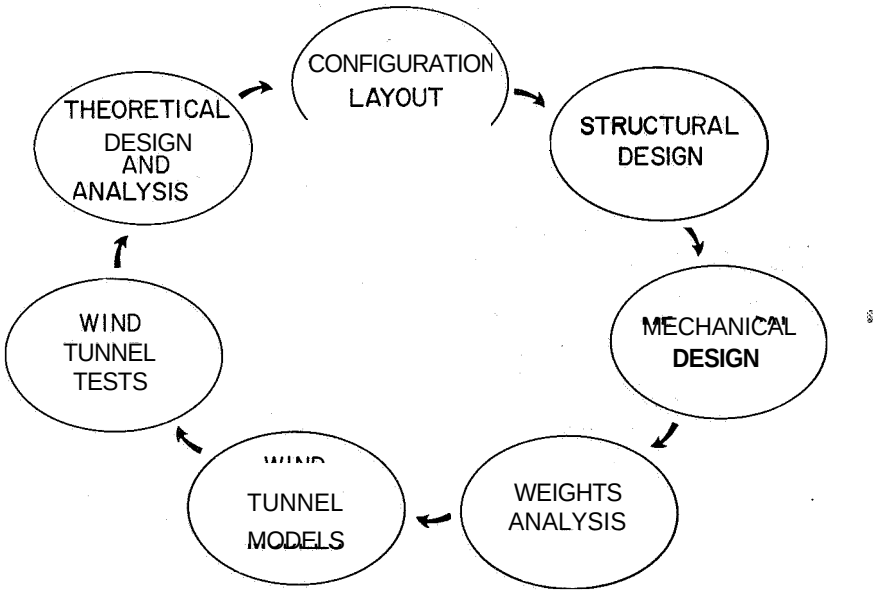

Figure 40

RELEASED

OPERATING COST COMPARISON

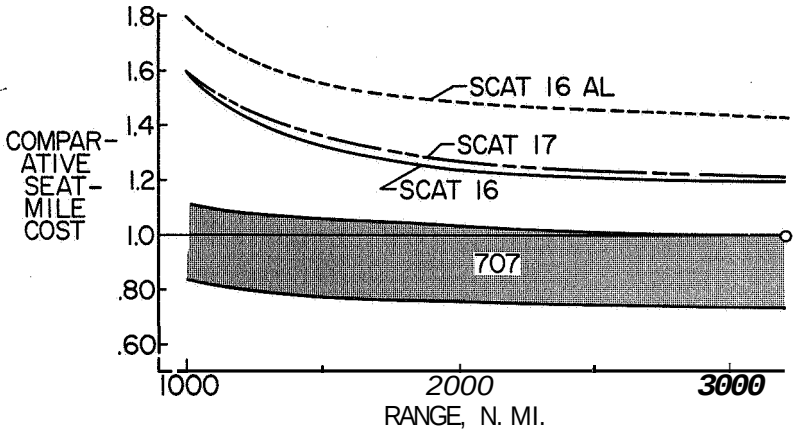

Figure 41

AERODYNAMIC TRADES

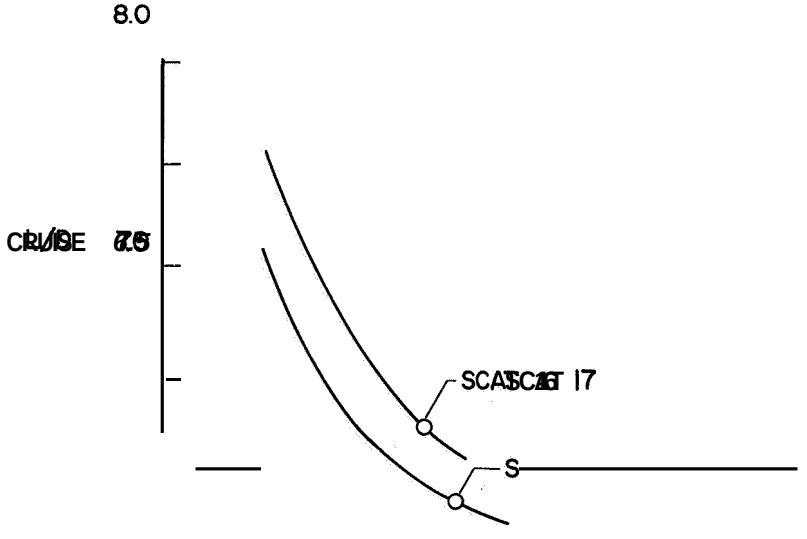

Figure 42

WEIGHT TRADES

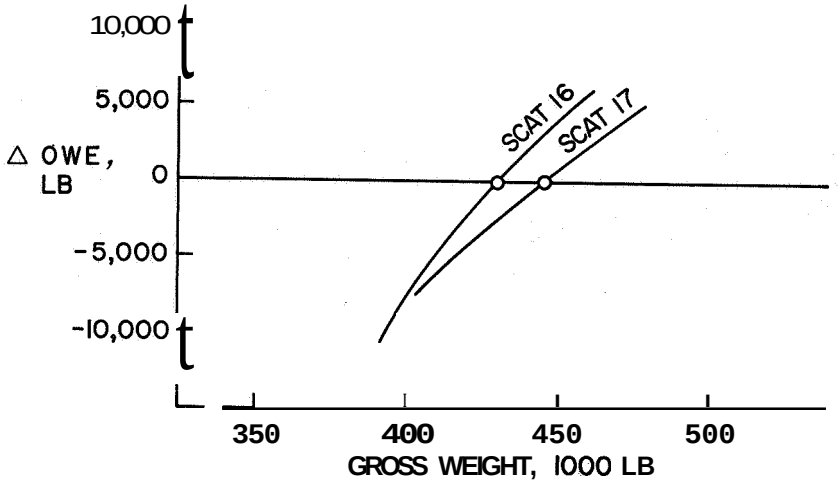

Figure 43

PROPULSION SYSTEM TRADES
ENGINE

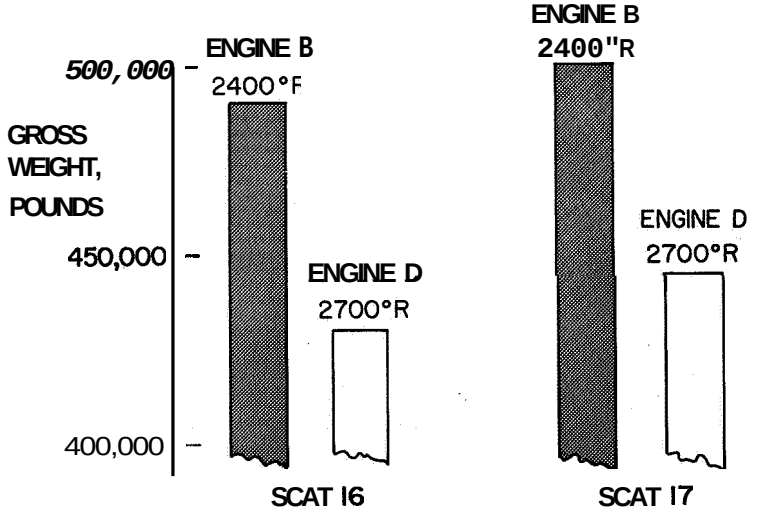

Figure 44

DECLASSIFIED

PROPULSION SYSTEM TRADES
INSTALLATION

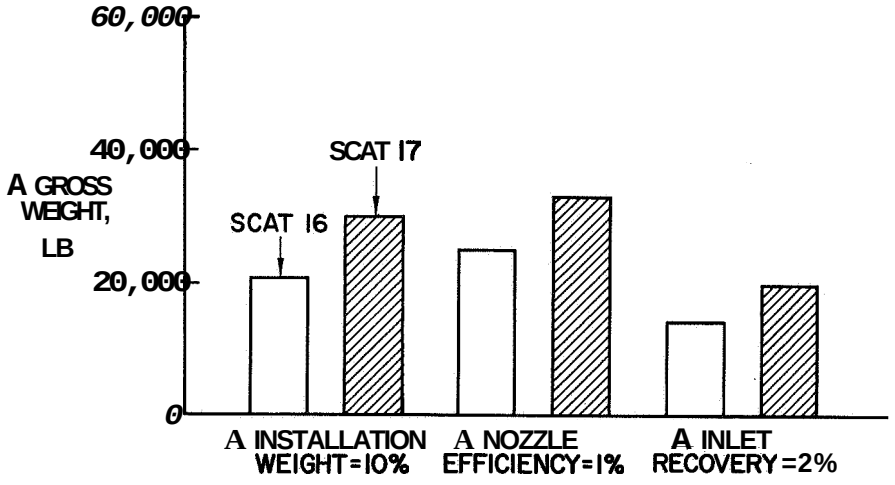

Figure 45

ECONOMIC TRADES

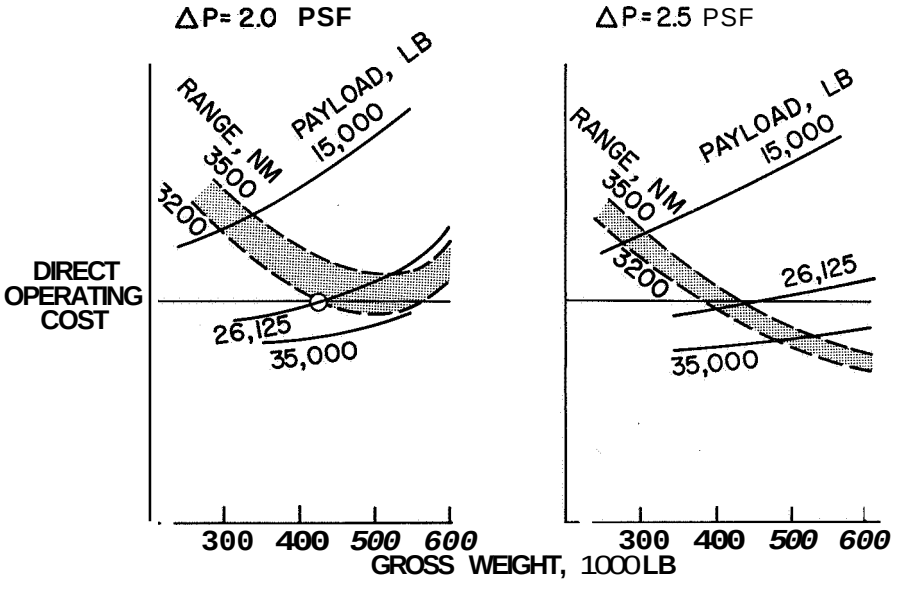

Figure 46

N67-31612 [redacted] ING PAGE BLANK NOT FILMED.

5. NASA SUMMARY AND ASSESSMENT OF FEASIBILITY-STUDY RESULTS

By John G. Lowry Langley

NASA Langley Research Center

SUMMARY

11947

The studies have indicated that through the use of an advanced engine technology and the use of an advanced material, titanium, either the variable-sweep approach or the fixed-wing approach can meet the required supersonic commercial air transport (SCAT) design objectives. Based on the same design objectives, an aluminum Mach 2.2 airplane did not have the same range, payload, or sonic-boom capability even with prohibitive increases in gross weight. Significant research will be required in the areas of aerodynamic performance, handling qualities, sonic boom, propulsion, and structural fabrication before the supersonic transport will be a success. conf. AUTHOR

5

INTRODUCTION

The supersonic commercial air transport feasibility studies were designed to supplement and complement related government and industry programs. The NASA program directed toward establishing a general level of supersonic transport efficiency studied many different SCAT concepts. Four of the more promising concepts evolved from this program were selected for the feasibility studies. Before discussing the results of these studies, it would be well to review the purpose of the feasibility studies and see the types of results that were desired.

The main objective of the SCAT feasibility studies was to have the contractor evaluate and compare the promising design concepts relative to all facets of a successful commercial design. It was not expected, nor desired, that the contractors arrive at a final design of a transport for the free-world airlines. As part of the evaluation and comparison, the contractors were to clarify the present technical state of the art for guidance of the national program and to define requirements for future NASA research. The studies were to be conducted in sufficient depth to assure an adequate degree of confidence in gross weight and payload-range characteristics.

An assessment of the overall study will be made to examine the feasibility of the various concepts, and the results of trade studies

[redacted]

52

Omega

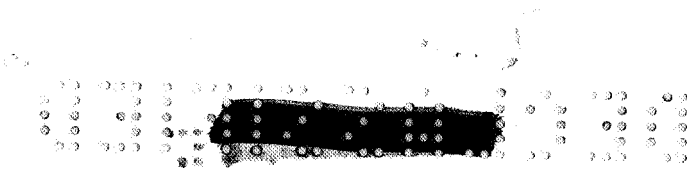

are discussed to assess the importance of variations in ground rules on the overall characteristics of a supersonic transport. The discussion is general in nature since a discussion of the details is presented in the contractors' summary reports.

CONCEPT FEASIBILITY

During the first 4 months of the contract effort, the contractor studied all four of the configurations furnished by the NASA, evaluating each with the four different engine types furnished with the data. After a review by the NASA, the contractors were instructed to focus their attention on SCAT 16 and SCAT 17 and use engines "B," "C," and "D" during the remaining part of the study effort. SCAT 4 and SCAT 15 were dropped from the study effort because there was not sufficient time to correct the deficiencies found in these concepts. At the time of the review, two aluminum SCAT designs were added to the study effort. Boeing was to study SCAT 16 and Lockheed was to study SCAT 17 with aluminum alloy as the basic structural material. The contractors were to choose the cruise Mach number which they felt would be compatible with the aluminum structure.

Before discussing the feasibility of the four configurations, it would appear desirable to compare the final configurations of SCAT 16 and SCAT 17. (See figs. 1 and 2.) There are two very noticeable differences in the final configurations for SCAT 16 from the original concept. (See fig. 1.) The first is the reduction in wing aspect ratio that was made to improve the structural weight characteristics. The second is that both contractors used a four-engine arrangement with two engines mounted below the wing and two above and to the rear of the wing instead of the three-engine arrangement of the original concept.

The contractors' final configurations of SCAT 17 (fig. 2) differ considerably from each other as well as from the original concept. Boeing, for example, used an aft-tail configuration whereas Lockheed used a canard configuration. The contractors changed the engine location both spanwise and vertically. Although it is not apparent from this figure, both contractors moved the engines up closer to the wing and Lockheed actually integrated the outboard engines with the wing structure, the engines being mounted on the wing-chord plane. Comparisons of the gross weights, payload-range characteristics, and other mission performance data for SCAT 16 and SCAT 17 were presented in paper no. 3 by R. Richard Heppe and Jim Hong and in paper no. 4 by Lloyd T. Goodmanson, William T. Hamilton, and Maynard L. Pennell.

Several of the more important factors that could determine the feasibility of the concepts are rated in a broad or gross manner in

table I. Figure 3 is presented so that the SCAT numbers can be associated with configuration concepts. The rating system used is shown at the bottom of table I, with ratings A, M, and P being used to delineate the difficulty of obtaining satisfactory characteristics for the particular item. The ratings are based on an NASA assessment of the contractors' results and show the strong and weak points of the various concepts. Even a quick glance at this table shows that there are no outstanding configurations. In comparing the configurations, it should be realized that there are different degrees of sophistication of design incorporated in the various SCAT configurations since SCAT 4 and SCAT 15 were studied for only 4 months. The ratings for all the configurations indicate that much additional research is needed to arrive at a satisfactory transport.

The poor ratings of SCAT 4 and SCAT 15 indicate the areas of deficiency found in the early part of the study which were responsible for their being dropped from the feasibility study. SCAT 4 had severe stability problems with no immediate solution apparent and SCAT 15 was plagued with very high wing weights resulting from the two overlapping wings and their attendant problems,

A comparison of SCAT 16 and SCAT 17 shows that although both are capable of performing the mission requirements, each has many problems that must be solved. As can be seen from the ratings, the seriousness of these problems varies between the two configurations. When the overall feasibility of the concepts is assessed, it appears that there is not much choice between SCAT 16 and SCAT 17 as supersonic transports. Of the two that were dropped, SCAT 4 and SCAT 15, it should be pointed out that either would be a very good configuration if the deficiencies could be corrected. Work is now underway to provide a means of alleviating the stability problems associated with SCAT 4 and a study is underway to arrive at a configuration of the SCAT 15 concept that has better structural characteristics. This work is discussed in paper no. 14 by A. Warner Robins and Richard T. Whitcomb.

TRADE STUDIES

Several trade studies were made by the contractors to determine the importance of some of the guideline restraints on the overall characteristics of a supersonic transport. A few of the more important ones will be discussed to point out the sensitive areas.

The contractors were given the choice of the materials they used for basic structure, except for the aluminum SCAT's, the only restraint being that the structure would be satisfactory for Mach 3.0 cruise. Figure 4 shows a structural-material comparison of the ratio of the operating weight empty to the operating weight empty for an aluminum structure

designed for room temperatures as a function of cruise Mach number. It is quite obvious that the use of titanium will result in an aircraft lighter than one using either aluminum or stainless steel. This figure was prepared from independent studies made by both Boeing and Lockheed and the results compare favorably with the SCAT configurations weighed for the various materials. It is quite obvious, of course, that aluminum would not be a satisfactory material for Mach 3.0 cruise. In fact, for Mach numbers of about 2.0, aluminum structure would result in a considerably heavier aircraft than an aluminum aircraft designed at room temperatures and much heavier than a titanium aircraft which would have material capabilities of operating at higher Mach numbers. Since low gross weight is necessary from a sonic-boom point of view, every effort should be made to use titanium as a structural material for a supersonic transport regardless of its cruise Mach number.

A comparison of the aluminum SCAT configurations studied by the two contractors with the corresponding titanium SCAT configuration designed for a Mach number of 3.0 is shown in table II. Table II(a) presents the results of the study by The Boeing Company to determine the characteristics of a Mach 2.0 aluminum SCAT 16 sized to fly the same mission as the Mach 3.0 SCAT 16. It is evident that the aluminum aircraft weighs more than the titanium airplane and does not meet the sonic-boom requirements. The sonic-boom overpressures are 2.23 lb/ft^2 in climb and 2.0 lb/ft^2 at start of cruise for the aluminum SCAT 16 compared with 2.0 lb/ft^2 and 1.5 lb/ft^2 for the titanium aircraft capable of operating at Mach 3.0.

Table II(b) shows a similar comparison for SCAT 17 prepared by the Lockheed-California Company. Here again the take-off gross weights are higher for the aluminum SCAT and the aircraft will not meet the sonic-boom restrictions, the sonic-boom overpressure being 1.8 lb/ft^2 at start of cruise instead of the specified 1.5 lb/ft^2. For these studies Lockheed used a cruising speed of M = 2.2. Thus, it would appear that an aluminum SCAT cruising at Mach numbers from 2.0 to 2.2 would not, with the engines used in these studies, meet all the mission requirements. If the aluminum SCAT had been powered with an advanced engine of engine "D" technology, the performance would have been better and would have compared more favorably with the titanium aircraft. However, it is not believed that this increase in engine performance would be sufficient to compensate for the greater structural weight of an aluminum SCAT and the beneficial effects on the airplane characteristics, including sonic boom, of flying at a Mach number of 3.0 instead of 2.0 or 2.2.

The very powerful effect of placing restrictions on the sonic-boom overpressures during transonic acceleration on airplane gross weight is shown in figure 5. In this figure are plotted the sonic-boom overpressures as a function of gross weight. The large band represents the

outer limits of the variation of gross weight with sonic-boom overpressure for the two SCAT configurations studied by the two contractors. It is interesting to note that there is only about a 60,000-pound difference in gross weight between the lightest and heaviest of the configurations studied by the contractors. The sensitivity of gross weight to sonic-boom overpressure for the best of these configurations at an overpressure of 2.0 indicates the importance of the selection of the design overpressure. If, for example, the design boom overpressure had been 2.1 instead of 2.0, a difference probably imperceptible to the general public, the *gross* weights would be from 20,000 to 40,000 pounds less than the weights based on an overpressure of 2.0 lb/ft^2. On the other hand, if the overpressure had been arbitrarily selected at 1.9 lb/sq ft, there would have been a 20,000- to 50,000-pound increase in gross weight and the heavier of the SCAT configurations would have been incapable of meeting the sonic-boom requirements and the 3,200-nautical-mile range. Since the sonic-boom problem is one of utmost importance to the design of the transport and can very well determine whether the aircraft will be capable of economically performing the design missions, extreme care should be exercised in picking the maximum overpressure during transonic acceleration to assure that undue restrictions are not placed on the design of the aircraft. These results indicate the extreme importance of continuing the studies to determine the intensity of sonic booms that will be acceptable to the public for commercial transport operation.

Figure 6, a comparison of the variation of take-off gross weight with the transonic sonic-boom overpressures for three of the four study engines, shows the importance of the sonic-boom-overpressure restriction on engine performance requirements. If engine "C" with afterburning had been used instead of engine "D" (low flow), a considerable increase in gross weight would have resulted. In fact, if engine "B" had been used, the aircraft would be incapable of meeting the sonic-boom requirement as set down in the "Guidelines." These results clearly show the need for an improved state-of-the-art engine of at least engine "D" performance to assure a satisfactory supersonic transport, particularly with the current sonic-boom restrictions.

For the SCAT studies the current FAA International Fuel Reserves were used, with an alternate airport distance of 250 nautical miles. Since fuel reserves are regulated from a safety point of view and are based, in part, on the current air traffic control system and weather minimums, variations in fuel reserves were studied to determine their importance on aircraft *gross* weight and/or range. Figure 7 shows the take-off *gross* weight as a function of range for a typical configuration with variations in fuel reserves of ±10,000 pounds from the SCAT values. Constant payload volume was assumed in determining these variations. The center curve is the variation of take-off gross weight

with range with the use of the SCAT fuel reserves. The lower curve shows the improvements in gross weight or range that would be obtained if fuel reserves could be reduced by 10,000 pounds and indicates the importance of improving the air traffic control system, and so forth, so that the reserves can be reduced without compromising the safety of commercial operations. If, for some reason, however, it were necessary to increase the fuel reserves, the aircraft would become very heavy or have decreased range.

Figure 8 has been prepared to show the effects of range and payload on the take-off gross weight of the airplane. For these results the fuselage was resized to accommodate the additional passengers for increases in payload and for fewer passengers in the case of decreased payload. The results in this figure are for an aircraft meeting the sonic-boom-overpressure restriction of 2.0 lb/ft^2 during transonic acceleration. The center curve again represents the variation of *gross* weight with range for a typical SCAT configuration with its payload of 26,125 pounds. Increases in range above the design value of 3,200 nautical miles result in very large increases in gross weight. In fact, a range of about 3,500 nautical miles would appear to be the maximum range for this configuration and would require increases in gross weight, of about 100,000 pounds. Increasing the payload to 35,000 pounds, the top curve, would also require large increases in gross weight at all ranges. With 35,000 pounds payload this particular SCAT would not meet the mission range requirement, since it has a maximum range of about 3,000 miles. The very rapid increase in gross weight with increase in range for take-off *gross* weights above 400,000 pounds is a result of the sonic-boom-overpressure limitation of 2.0 lb/ft^2 during acceleration and 1.5 lb/ft^2 during cruise. Another indication of the importance of sonic-boom restrictions is the fact that take-off gross weights of between 550,000 and 650,000 pounds appear to give the maximum range for this configuration regardless of its payload. As would be expected, there would be large decreases in take-off gross weight or large increases in range if the payload were reduced to values lower than 26,125 pounds as indicated by the large difference between the SCAT payload and a payload of 15,000 pounds. Because of the very pronounced effect that the sonic-boom restrictions have on the airplane's gross weight and range, it is evident that this picture would be considerably changed if the reductions in gross weight indicated by The Boeing Company for improved structures and advances in aerodynamic state of the art could be realized. Such reductions would lower the design point and would result in much better payload range characteristics because the adverse effects of sonic boom become less pronounced for gross weights less than 400,000 pounds. If, however, an advanced engine of "D" performance were not available, an airplane using current state-of-the-art engines, engine "B," for example, would have even more adverse characteristics than are shown in the figure.

In looking at the mission requirements for commercial transport aircraft, it appears that certain mission flexibilities may be required because of sonic-boom sensitive areas or operational procedures. Figure 9 has been prepared to show the variation in range for two flight profiles using the *gross* weight for the basic mission (3,200 nautical miles at a Mach number of 3.0). Mission A is a flight profile where the point of departure is in a sonic-boom sensitive area and the aircraft is required to fly subsonically for some distance prior to accelerating to supersonic speeds, in this case 800 nautical miles. Mission B is a subsonic mission at a Mach number of about 0.85. In the mixed subsonic-supersonic mission A, SCAT 16 has a range greater than for the normal mission and SCAT 17 has a range of about 3,200 nautical miles. This flight plan (mission A) could be used by SCAT 16, with its basic mission range of 3,200 nautical miles, for nonstop Paris-New York flights in winter with the headwinds since it would have a range of about 4,000 statute miles or close to the value that is needed for day-in and day-out operation. This plan would, of course, result in a block time about halfway between the supersonic time and the time for the current subsonic jets. Mission B is an indication of the subsonic aerodynamic performance of SCAT 16 and SCAT 17 and reflects the good subsonic performance of SCAT 16.

CONCLUSIONS

The conclusions reflect the very powerful influence of sonic boom on all phases of the study and indicate its importance as a design parameter for the supersonic transport.

Either the fixed-wing or the variable-sweep concept will meet the SCAT mission requirements with very little choice, for example, between SCAT 16 and SCAT 17. If mission flexibility is required, SCAT 16 appears to offer the better compromise; however, if structural simplicity and weight are of primary importance, SCAT 17 might offer the better compromise.

The results indicate that if SCAT is to be a competitive transport, advanced propulsion systems are required. This requirement means that the engine must have high inlet turbine temperatures and be an advance over the current state of the art with performance characteristics at least equal to those of engine "D."

The results also indicate that if the airplane is built with titanium as the basic structural material, there would be a significant reduction in *gross* weight over a stainless-steel airplane.

The results indicate that the aluminum SCAT configurations studied would not meet the mission requirements. The aluminum SCAT configurations with cruise speeds of Mach numbers from 2.0 to 2.2 would weigh more than the titanium Mach 3.0 aircraft; would, of course, fly slower; and would not meet the sonic-boom restrictions if it had a range of 3,200 nautical miles and carried the 26,125-pound payload.

The studies also emphasize that any substantial increase in fuel reserves, payload, or range will be very costly insofar as gross weight is concerned.

For the transport to have satisfactory characteristics, research in several areas is urgently needed. The aircraft needs to have better aerodynamic performance than was incorporated into these studies, and configurations need to be devised that can obtain the high aerodynamic performance while still maintaining low structural weight. Research is needed in the areas of stability and control to improve the flying qualities of the aircraft. Research and development work in the engine field is required to have available an engine of at least class "D" capability by the time the aircraft is ready to enter into service. Since titanium is by far the lighter material and offers the greatest potential, considerable work is needed to establish the level of confidence in titanium that now exists for aluminum. Since sonic boom is so important to the operational procedures of the aircraft and to its gross weight and performance, research is needed to see whether there are possible means of reducing the booms as well as research in the field of public acceptance to provide documented evidence from which the boom restrictions can be set at the highest acceptable level.

[redacted]

TABLE I

CONFIGURATION COMPARISON

	SCAT			
	4	15	16	17
AERODYNAMIC PERFORMANCE:				
SUBSONIC	M	A	G	M
TRANSONIC	M	M	M	M
SUPERSONIC	G	G	A	A
STABILITY AND CONTROL :				
LONGITUDINAL STABILITY	P	M	M	A
LATERAL STABILITY	P	M	M	M
CONTROL EFFECTIVENESS	M	M	A	A
STRUCTURAL WEIGHT	A	P	M	G
ENGINE INSTALLATION	M	A	M	A
COMMUNITY NOISE	M	M	M	M
SONIC BOOM	A	P	A	A

G - GOOD
A - ACCEPTABLE
M - MARGINAL
P - POOR

TABLE II

COMPARISON OF ALUMINUM AND TITANIUM AIRPLANES

(a) SCAT 16

	ALUMINUM	TITANIUM
TAKE-OFF GROSS WEIGHT, LB	520,000	430,000
RANGE, N. MI.	3,200	3,200
CRUISE SPEED	M = 2.0	M = 3.0
WING AREA, FT^2	4,750	4,000
ENGINES	F	D (LOW FLOW)
SONIC-BOOM OVERPRESSURE:		
IN CLIMB, LB/FT^2	2.23	2.00
AT START OF CRUISE, LB/FT^2	2.00	1.45

(b) SCAT 17

	ALUMINUM	TITANIUM
TAKE-OFF GROSS WEIGHT, LB	500,000	380,000
RANGE, N. MI,	3,200	3,200
CRUISE SPEED	M = 2.2	M = 3.0
WING AREA, FT^2	7,200	5,500
ENGINES	F	D
SONIC-BOOM OVERPRESSURE:		
IN CLIMB, LB/FT^2	2.0	2.0
AT START OF CRUISE, LB/FT^2	1.8	1.5

[redacted]

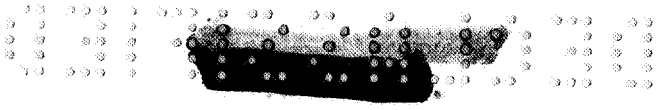

SCAT 16

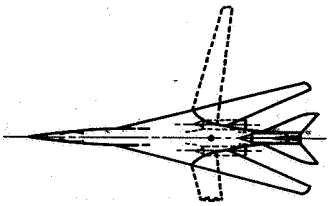

ORIGINAL CONCEPT

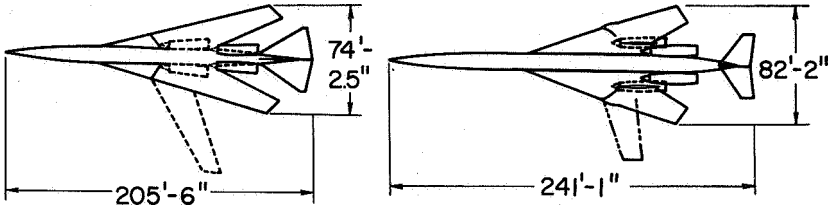

BOEING LOCKHEED

FINAL CONFIGURATIONS

Figure 1

SCAT 17

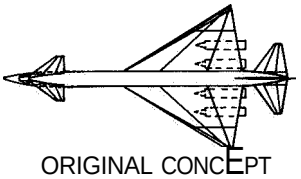

ORIGINAL CONCEPT

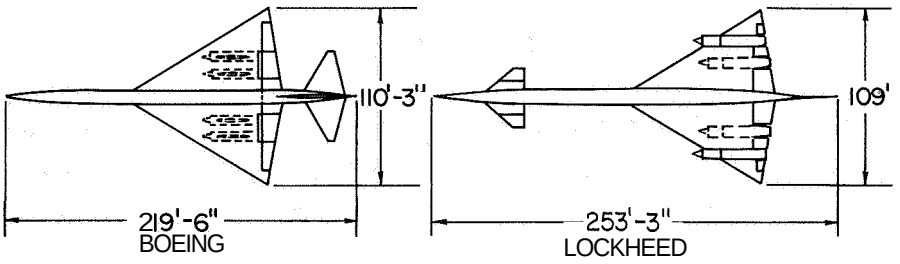

FINAL CONFIGURATIONS

Figure *2*

ORIGINAL STUDY CONCEPTS

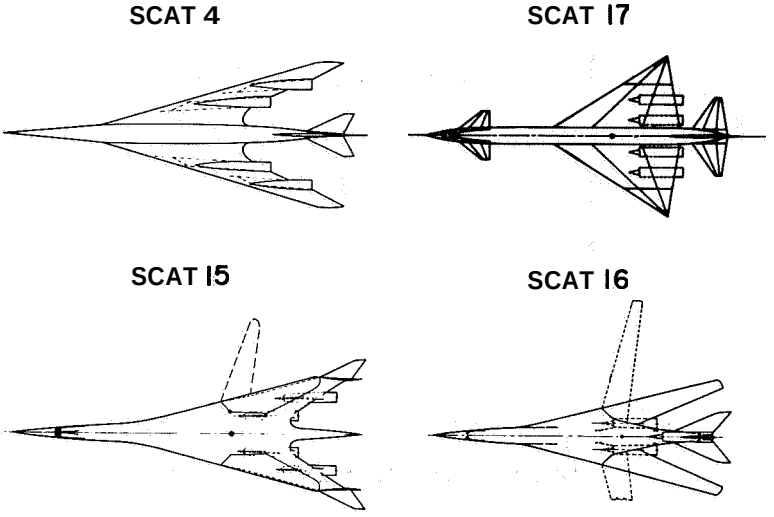

Figure 3

STRUCTURAL MATERIALS

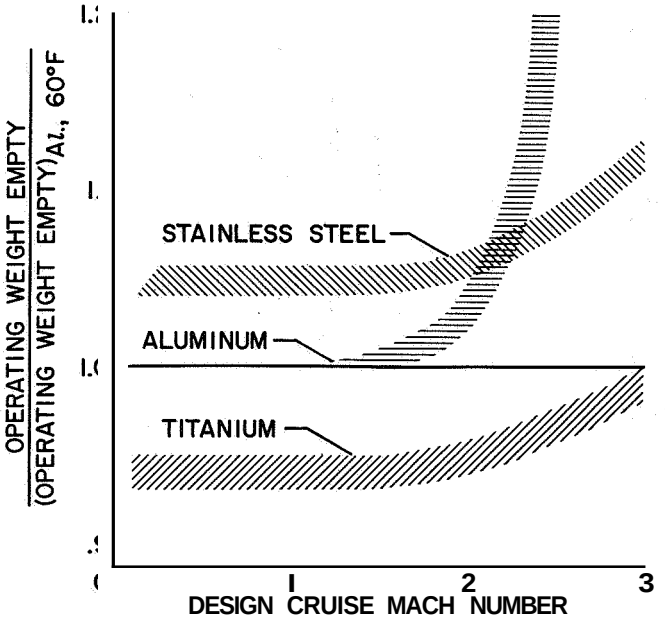

Figure 4

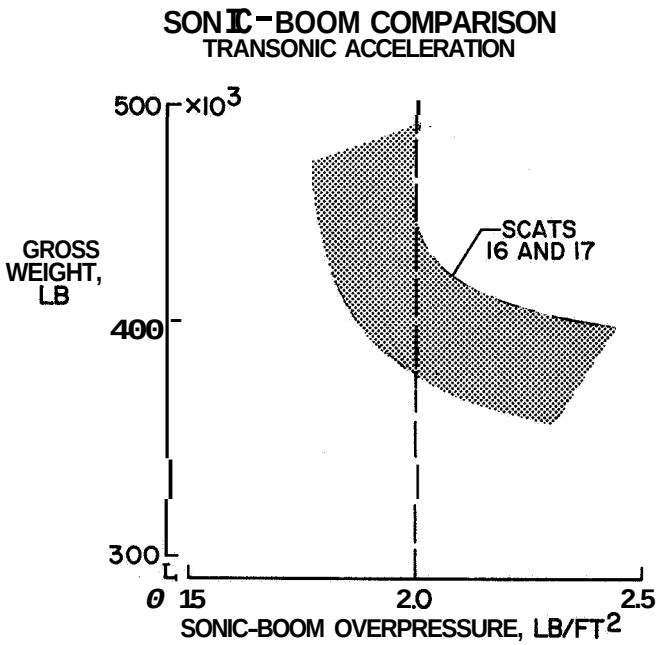

Figure 5

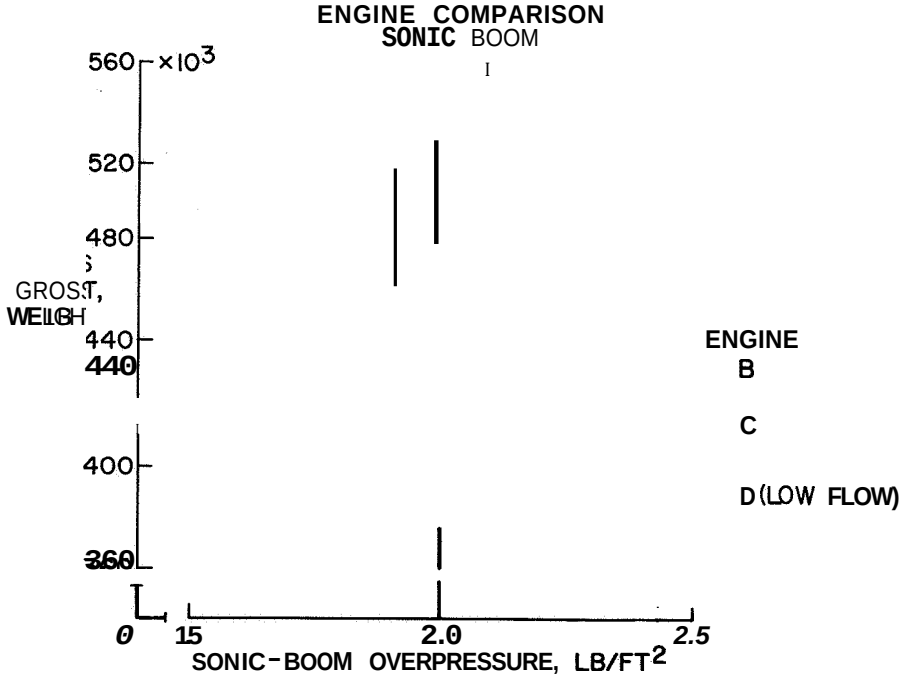

Figure 6

RANGE FOR VARIOUS FUEL RESERVES
CONSTANT PAYLOAD VOLUME

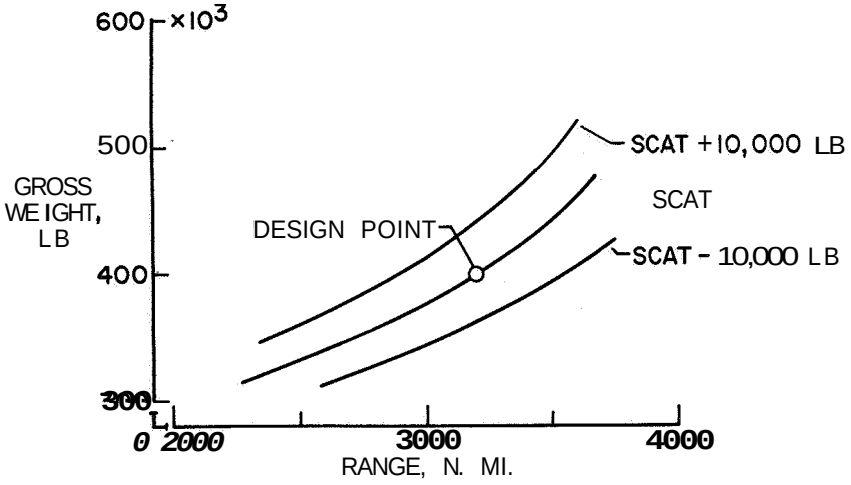

Figure 7

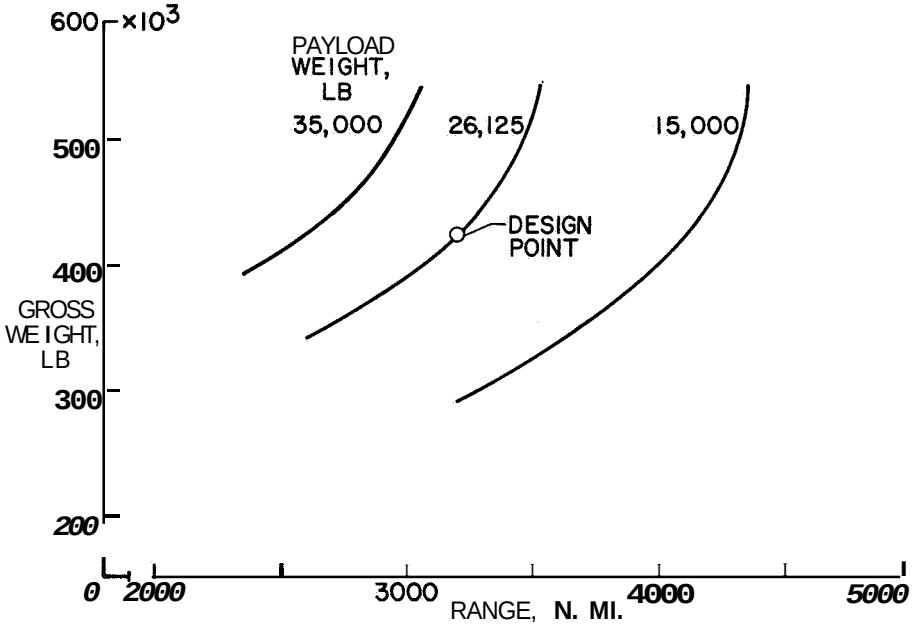

Figure 8

MISSION FLEXIBILITY
BASIC MISSION: M = 3.0; RANGE = 3,200 N. MI.

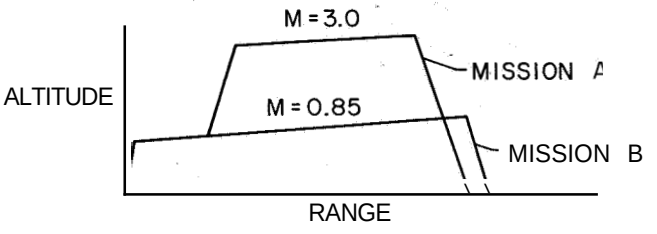

	RANGE, N. MI.	
	SCAT 16	SCAT 17
MISSION A (SUBSONIC FOR 800 N. MI.)	3,450	3,200
MISSION B	4,500	3,500

Figure 9

N67-31613

ANALYSIS AND CORRELATION OF AIRCRAFT WAVE DRAG

By Roy V. Harris, Jr.

NASA Langley Research Center

SUMMARY

Two approaches to the analysis and correlation of aircraft wave drag are discussed. The first approach is to compare the aircraft area distribution with the slender-body-theory optimum and the second approach employs the supersonic area rule to determine the equivalent-body area distribution.

Although the optimum-body wave-drag variations can be used to indicate the gross trends in aircraft wave drag with equivalent-body fineness ratio and the degree of afterbody closure, the relatively large amount of scatter in the correlating data, due to deviations in aircraft area distributions from the optimum, indicate that more precise computing techniques are required in order to estimate the aircraft wave-drag levels.

Several computer programs have been developed which apply the slender-body theory in combination with the supersonic area rule to the solution of aircraft wave drag. One such program, developed by The Boeing Company for use on the IBM 7090 electronic data processing system, has been studied at the Langley Research Center, and the results of this study indicate that, in addition to providing reasonably accurate supersonic wave-drag estimates, the computer program provides a useful tool which can be used in design studies and for configuration optimization.

INTRODUCTION

Since the rule was formulated, and verified experimentally, that the transonic wave drag of an aircraft is essentially the same as the wave drag of an equivalent body of revolution having the same cross-sectional-area distribution as the aircraft (ref. 1), attempts have been made to estimate aircraft wave drag by examining the equivalent-body area distributions. These attempts have led to two approaches for analyzing the equivalent-body, and hence the aircraft, wave drag. The first and simplest approach is to compare the aircraft area distribution with the slender-body-theory optimum. The second approach is more complex and employs the supersonic area rule (ref. 2) to

determine the equivalent-body area distributions. This paper discusses briefly the first approach, and then presents in more detail some recent developments in the application of the second approach to the analysis and correlation of wave drag.

SYMBOLS

A	cross-sectional area
$C_{D,WAVE}$	wave-drag coefficient
D	drag
2	length
M	Mach number
V	velocity
x,y,z	coordinates along X, Y, and Z axes
X,Y,Z	axis system of airplane
θ	azimuth angle
μ	Mach angle
ρ	density

Subscripts:

MAX	maximum
BASE	base

DISCUSSION

In the design of supersonic aircraft, the Sears-Haack (ref. 3) or Haack-Adams (ref. 4) optimum-body area distributions are often used as the basis for establishing the cross-sectional-area distribution of the aircraft. However, as can be seen in figure 1, attenpts to correlate aircraft wave drag with that of the optimum body indicate a considerable degree of scatter in the data. This figure shows the variation

of wave-drag coefficient based on maximum cross-sectional area with equivalent-body fineness ratio. The two curves show the optimum-body wave-drag variations. For the purposes of this paper; the optimum body is considered to be the body of revolution which, according to slender-body theory, has the minimum wave drag for a given length, volume, and base area. The upper curve is the wave-drag variation for the Sears-Haack optimum body which has 100-percent afterbody closure (ref. 3). The lower curve represents the optimum body which has a base area equal to 50 percent of the maximum area. The symbols indicate wave-drag coefficients determined by wind-tunnel tests of models of a wide variety of complete aircraft configurations. This comparison between aircraft wave drag and the theoretical optimum is made at the near-sonic Mach number of 1.2 because the slender-body theory does not consider the optimum-body wave-drag variations with Mach number. The Mach number effects, as presented subsequently, can be significant, particularly at the lower fineness ratios.

The deviations in the aircraft wave-drag levels from the optimum and the rather large amount of scatter in the data can be attributed to two effects. First, due to the techniques for simulating engine installations and the sting-mounting system used on the models from which these data were obtained, the various configurations have different amounts of afterbody closure ranging from about 60 to 90 percent. As can be seen by the difference in levels of the two optimum-body curves, the degree of afterbody closure can have a powerful effect on the equivalent-body wave drag. Second, as shown in the sketch of the area distribution of a typical wind-tunnel model (fig. 1), the aircraft area distributions are rather lumpy and depart considerably from the optimum. Although the optimum-body wave-drag variations can be used to indicate the gross trends in aircraft wave drag with variations in equivalent-body fineness ratio and the degree of afterbody closure, the large amount of scatter in the data due to deviations in the aircraft area distributions from the optimum indicates that more precise computing techniques are required in order to estimate the aircraft wave-drag level.

Reasonably good wave-drag estimates can be made near a Mach number of 1 if the slender-body theory is applied to the actual aircraft area distributions. This procedure can be extended to higher Mach numbers by using the supersonic area rule to determine the equivalent-body area distributions. A review of this procedure is given in figure 2.

Each equivalent body of revolution is determined by passing a series of parallel cutting planes through the configuration. The cutting planes are inclined with respect to the aircraft axis at the Mach angle μ. The area of the equivalent body at each station is the projection onto a plane normal to the aircraft axis of the area intercepted

by the cutting plane. It is evident that the series of parallel cutting planes can be oriented at various angles θ around the aircraft axis; and in order to determine the drag accurately, a family of equivalent bodies, each corresponding to a particular value of θ, must be considered. Thus, at each Mach number, a series of equivalent bodies of revolution are generated. The wave drag of each equivalent body is determined by the von Karman slender-body formula (ref. 5) which gives the drag as a function of the free-stream conditions and the equivalent-body area distribution. The wave drag of the aircraft at the given Mach number is then taken to be the integrated average of the equivalent-body wave drags.

For most practical applications, the complexity of this procedure requires that it be adapted to the high-speed electronic computer. As a result, several digital-computer programs have been developed which apply this theoretical approach to the solution of aircraft wave drag. One such program, developed by The Boeing Company for use on the IBM 7090 electronic data processing system, has been under study at the Langley Research Center and details of this program will be made available by the NASA. A simplified description of the program and some of the results of this study are shown in figures 3 to 6.

A major problem in adapting this procedure to machine computation is that of describing a rather complex aircraft to the computer in sufficient detail. The manner in which an aircraft is mathematically described to the computer for this program is illustrated in figure 3. The lower right portion of the figure shows a typical aircraft for which the supersonic wave drag is to be computed. The upper left portion of the figure shows the aircraft as it is described to the computer.

The locations of all the aircraft components are referred to an X-, Y-, Z-axis system with its origin at the nose of the fuselage. The fuselage is assumed to be sufficiently close to a body of revolution that it can be described in terms of its cross-sectional-area distribution. The variation in fuselage radius along the axis between stations is assumed to be linear.

The wing is described as a sequence of streamwise airfoils distributed along the span. The contour of the wing is assumed to be linear between successive ordinates. The horizontal and vertical tails are described in a manner similar to that of the wing.

The engine nacelles are located by specifying the x, y, and z ordinates of the nacelle center line at the inlet face, and are described in a manner similar to that of the fuselage by giving the radii at successive stations. The discontinuities caused by the inlet and exit faces are eliminated by assuming that infinitely long cylinders extend in both

directions from the inlet and the exit. The effects of inlet spillage on the wave drag can be included by properly contouring the cylindrical extension near the inlet face.

Once the aircraft description has been stored in the memory unit of the computer, the equivalent-body area distributions are determined by solving for the normal projection of the areas intercepted by the cutting planes.

In addition to the aircraft wave drag, which is evaluated by applying the method of Eminton and Lord (ref. 6) to the solution of the von Kármán integral (ref. 5), a check on the accuracy of the equivalent-body area distribution is provided. First, the exact volume of the wing of the mathematical model is computed, and then, independently, the volume is found by integrating the area distribution of the wing equivalent body. If a sufficient number of cutting planes have been used to define the wing equivalent body of revolution, then the two values of wing volume should be essentially the same.

In addition, the program lists the wave drags of the aircraft equivalent bodies at each Mach number, as well as selected equivalent-body area distributions. This additional information is particularly useful in tailoring a configuration for minimum wave drag since, in order to optimize a configuration at some supersonic Mach number, it is necessary to examine the series of equivalent bodies corresponding to the particular Mach number. It should be noted that the area distributions required in the computation of sonic-boom overpressures are provided.

In order to determine the accuracy of the wave-drag estimates obtained from this procedure, the drag was first computed for the optimum body of revolution; the results were then compared with experiment and the more precise characteristics theory. Figure 4 shows a comparison of the computed wave drag with experimental results for the optimum body having a base-to-maximum-area ratio of about 53 percent. The variations in wave drag with Mach number are shown for optimum-body fineness ratios of 7, 10, and 13. The data points were obtained in the Langley 8-foot transonic pressure tunnel, the Langley 4- by 4-foot supersonic pressure tunnel, and the Langley Unitary Plan wind tunnel by integrating the measured surface-pressure coefficients.

The characteristics theory, indicated by the solid line, shows excellent agreement with the experimental results. The slender-body theory, shown by the short-dash line, gives good agreement near a Mach number of 1. However, as the Mach number is increased, the slender-body theory overestimates the optimum-body wave drag. It should also be noted that the effects of Mach number are greater at the lower

fineness ratios than at the higher fineness ratios. This greater departure from slender-body theory should be expected as the bodies become less slender. The long-dash line shows the results obtained from the machine program which uses the slender-body theory in combination with the supersonic area rule.

As would be expected, the characteristics theory gives the best agreement with experimental results. However, when the slender-body theory is applied to the proper equivalent bodies, as in the machine program, the Mach number effects on the optimum-body wave drag are predicted with a fair degree of accuracy.

The most severe test of the theoretical approach used in this machine program lies in its application to the calculation of the drag of wings. Figure 5 shows a comparison of the machine-computed wave drag with experimental results for a series of semispan wings.

In the table at the right of figure 5 are shown sketches of the wings and the Mach numbers for which computations have been made. All the wings in the series had circular-arc airfoil sections. The first wing had a trapezoidal planform and a linear spanwise thickness distribution. The second wing had a complex planform with a linear spanwise thickness distribution. The third wing had a complex planform as well as a complex spanwise thickness distribution. The final wing had an arrow planform with a linear thickness distribution. The computations were made for Mach numbers ranging from about 1.4 to 2.2.

At the left of figure 5 is shown a plot of experimentally determined wave drag plotted against the computed values. The solid line is the locus of perfect agreement between theory and experiment. The experimental wave-drag coefficients were found by subtracting the equivalent flat-plate turbulent skin-friction drag coefficients from the measured total drag coefficients. As can be seen from the figure, the program tends to underestimate the wave drag of the semispan wings. This result for wings alone is not surprising, since a wing departs considerably from the equivalent body of revolution assumed by the theory.

A comparison of the machine-computed wave-drag coefficients with experimental results for complete airplane configurations is shown in figure 6. As indicated in the table, the comparison is made over the Mach number range from 1.4 to 3.2 for several of the SCAT configurations and a typical supersonic fighter. Again, the plot on the left shows, as a solid line, the locus of perfect agreement between the experimentally determined wave-drag coefficients and the machine-computed values. The experimental wave-drag coefficients were determined for each configuration by subtracting the equivalent flat-plate turbulent skin-friction drag and an estimated camber drag from the wind-tunnel results.

[redacted]

As can be seen from figure 6, this comparison indicates that the machine program, which uses slender-body theory in combination with the supersonic area rule, can produce good estimates of aircraft wave drag at supersonic speeds.

CONCLUDING REMARKS

In conclusion, it appears that although the optimum-body wave-drag variations can be used to indicate the gross trends in aircraft wave drag with equivalent-body fineness ratio and the degree of afterbody closure, the relatively large amount of scatter in the correlating data, due to deviations in aircraft area distributions from the optimum, indicates that more precise computing techniques are required in order to estimate the aircraft wave-drag levels.

Several computer programs have been developed which apply the slender-body theory in combination with the supersonic area rule to the solution of aircraft wave drag. One such program, developed by The Boeing Company for use on the IBM 7090 electronic data processing system, has been studied at the Langley Research Center, and the results of this study indicate that, in addition to providing reasonably accurate supersonic wave-drag estimates, the computer program provides a useful tool which can be used in design studies and for configuration optimization.

[redacted]

REFERENCES

1. Whitcomb, Richard T.: A Study of the Zero-Lift Drag-Rise Characteristics of Wing-Body Combinations Near the Speed of Sound. NACA Rep. 1273, 1956. (Supersedes NACA RM L52H08.)

2. Jones, Robert T.: Theory of Wing-Body Drag at Supersonic Speeds. NACA Rep. 1284, 1956.

3. Sears, William R.: On Projectiles of Minimum Wave Drag. Quarterly Appl. Math., vol. IV, no. 4, Jan. 1947, pp. 361-366.

4. Adams, Mac C.: Determination of Shapes of Boattail Bodies of Revolution for Minimum Wave Drag. NACA TN 2550, 1951.

5. von Kármán, Th.: The Problem of Resistance in Compressible Fluids. R. Accad. d'Italia, Cl. Sci. Fis., Mat. e Nat., vol. XIII, 1935, pp. 210-265.

6. Eminton, E., and Lord, W. T.: Note on the Numerical Evaluation of the Wave Drag of Smooth Slender Bodies Using Optimum Area Distributions for Minimum Wave Drag. Jour. R.A. S., vol. 60, no. 541, Jan. 1956, pp. 61-63.

COMPARISON OF AIRPLANE WAVE DRAG WITH SLENDER-BODY-THEORY OPTIMUM

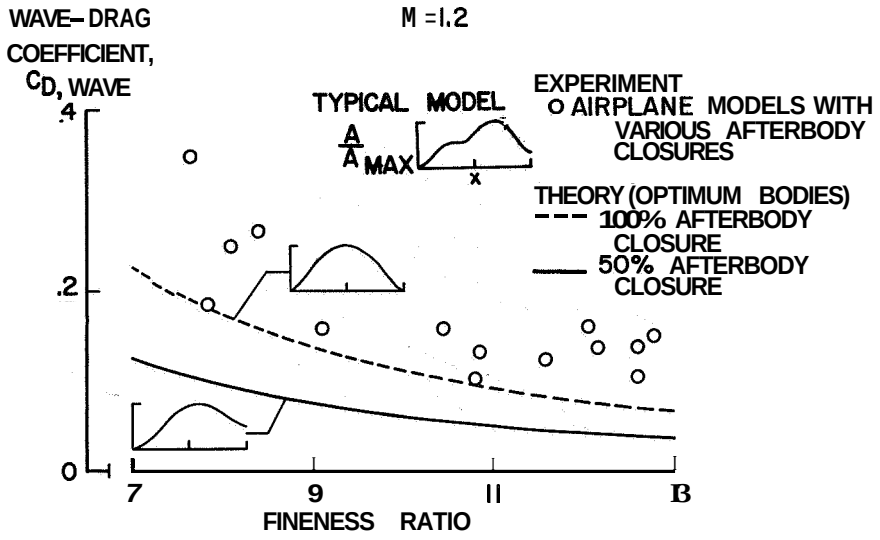

Figure 1

ILLUSTRATION OF WAVE-DRAG COMPUTING PROCEDURE

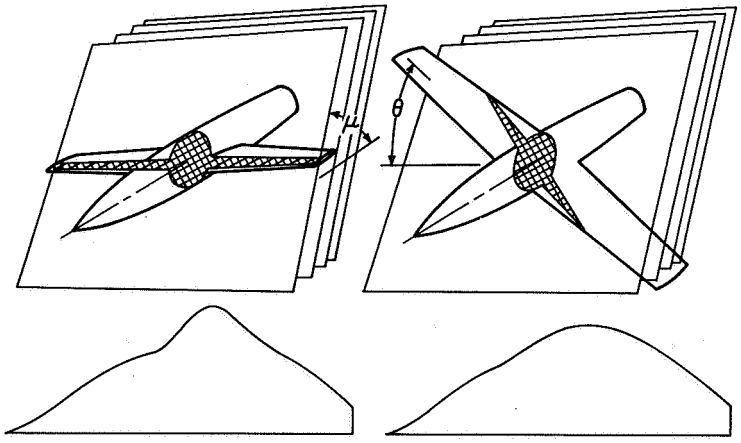

$$D(\theta) = -\frac{\rho V^2}{4\pi} \int_0^l \int_0^l A''(x_1)\, A''(x_2)\, \text{LOG} \left| x_1 - x_2 \right| dx_1 dx_2$$

$$D = \frac{1}{2\pi} \int_0^{2\pi} D(\theta)\, d\theta$$

Figure 2

MATHEMATICAL REPRESENTATION OF ILLUSTRATIVE AIRPLANE FOR MACHINE-COMPUTING PROCEDURE

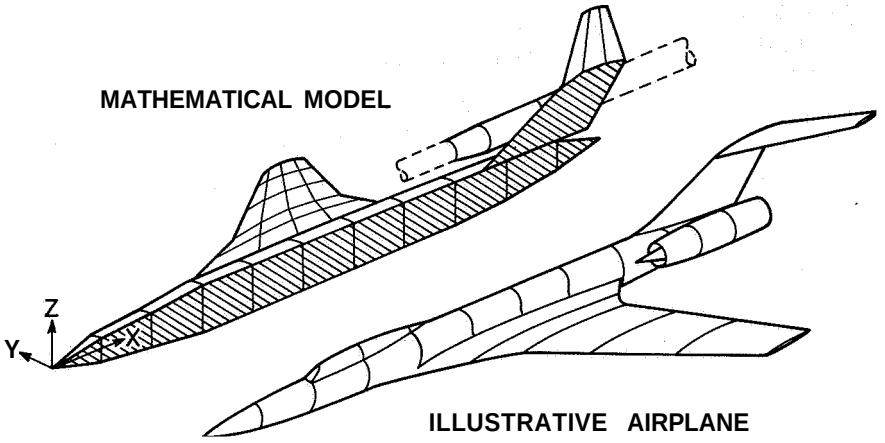

Figure 3

COMPARISON OF COMPUTED WAVE DRAG WITH EXPERIMENTAL RESULTS
OPTIMUM BODIES OF REVOLUTION

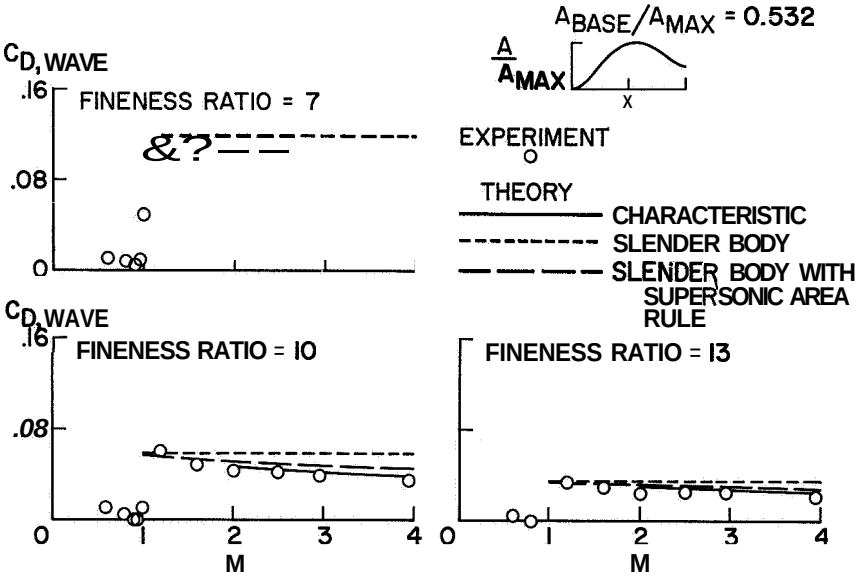

Figure 4

DECLASSIFIED

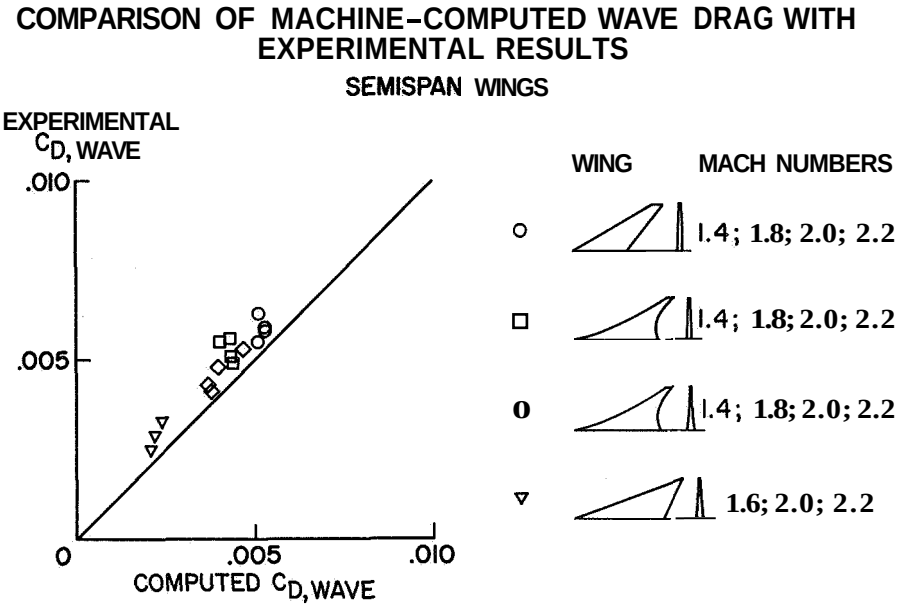

Figure 5

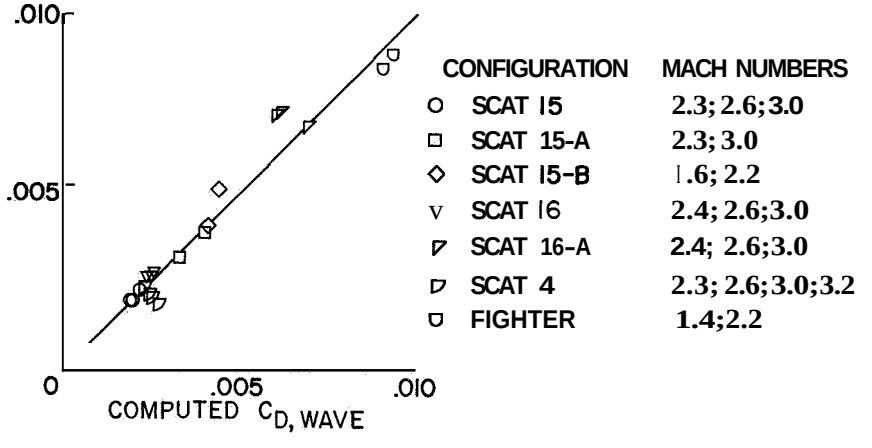

Figure 6

N67-31614

7. APPLICATION OF WING WARP AND AERODYNAMIC INTERFERENCE TO IMPROVE SUPERSONIC PERFORMANCE

By Francis E. McLean and Harry W. Carlson

NASA Langley Research Center

SUMMARY

A brief review is made of current information on highly swept warped-wing arrangements obtained from experiments with isolated wings, with wing-body configurations, and with complete configurations. The use of analytical methods for the solution of arbitrary planform problems is discussed.

INTRODUCTION

It is well known that linearized theory predicts high levels of supersonic performance for wings with leading edges which are swept behind the Mach cone - that is, subsonic leading edges. A prime ingredient of this performance potential is the theoretical premise that many wings of this class can be warped to produce lift more efficiently than wings with leading edges that lie ahead of the Mach cone. Several experimental investigations (refs. 1 to 3) have been conducted on wings which were warped, according to the specifications of theory, to provide these better lifting efficiencies. The results of these experiments were rather disappointing. Because of these disappointments, there is some feeling that the advantages of wing warp are questionable and that little is to be gained by the use of wings with subsonic leading edges. However, the fact that three of the NASA SCAT configurations make use of this type of wing is evidence of a continued interest in the design concept and is also evidence of the belief that research will find the key which will allow application of the concept to a practical airplane with improved supersonic performance.

The purpose of the present paper is to discuss some of the present information on highly swept warped-wing arrangements that has been obtained from tests of isolated wing and wing-body configurations, from tests of complete configurations, and from analytical methods.

7

p 165 - 176

SYMBOLS

c	local chord
C_m	pitching-moment coefficient
C_D	drag coefficient
$C_{D,o}$	zero-lift drag coefficient of symmetrical configuration
$\frac{\partial C_D}{\partial C_L^2}$	drag-due-to-lift factor (fig. 1)
C_L	lift coefficient
D	drag
L	lift
M	Mach number
R	Reynolds number
t	maximum thickness of airfoil section
Λ_{LE}	sweepback angle of wing leading edge

Subscripts:

DES	design
MAX	maximum
OPT	optimum
TRIM	trim value
THEORY	theoretical

[redacted]

RESULTS AND DISCUSSION

Design Considerations

At the outset, it would be in order to consider the design region of high lifting efficiencies as specified by theory (ref. 4) for the Mach 3.0 cruise condition of the supersonic transport. In figure 1 the theoretical drag-due-to-lift factors $\partial C_D/\partial C_L^2$ are shown as a function of leading-edge sweep angle for a Mach number of 3.0. The vertical line (long dash, short dash) at 70.5° separates the sweep-angle region into a supersonic-leading-edge condition and a subsonic-leading-edge condition as indicated in the figure. In the supersonic-leading-edge region (leading-edge sweepback less than 70.5°), theory indicates some minor drag-due-to-lift advantages from the use of highly notched arrow wings with wing warp, but, because of wave-drag disadvantages, this region is generally discounted as a suitable design region for this type of wing (ref. 4). For all practical purposes, then, the drag-due-to-lift factors for wings with supersonic leading edges can be represented by the constant value shown by the solid-line curve.

From figure 1 it can be seen that as the leading-edge sweepback is increased to clear the zero-lift drag peak (symbolized by the long dashed curve on the upper part of the fig.), the theoretical drag-due-to-lift values diverge into two bands. The upper band (shaded area) represents the drag-due-to-lift factors for flat lifting surfaces and is bounded by the curve for the delta wing (solid curve) and that for highly notched arrow wing (dashed curve) as indicated in the figure. The lower band (cross-hatched area), which is similarly bounded, represents the corresponding drag-due-to-lift factors if optimum wing warp is applied to the wing. It is apparent that an airplane designed in this subsonic leading-edge region must obtain some of the theoretical drag-due-to-lift potential predicted for optimum wing warp to exhibit high levels of supersonic performance.

In attempts to translate the drag-due-to-lift potential of warped wings that is shown in figure 1 into an increased lift-drag ratio, or efficiency, an important parameter has been found to be the design lift coefficient $C_{L,DES}$. Design lift coefficient $C_{L,DES}$ is the lift coefficient for which all the lift is obtained by wing warp. A wing with a high design lift Coefficient is extremely warped, whereas a design lift coefficient of zero designates a flat lifting surface with no warp. There is a certain design lift coefficient; that is, a certain degree of warp for which, theoretically, the highest possible lift-drag ratio is obtained. This design lift coefficient is called the optimum design lift coefficient $C_{L,OPT}$. A wing with either more or less warp will theoretically provide less lift-drag ratio.

[redacted]

For example, with the use of theoretical inputs from figure 1, figure 2 indicates the variation of theoretical lift-drag ratio with lift coefficient for three wings. The three wings have the same planform, are at the same Mach number of 3.0, and have the same assumed value of $C_{D,o}$ of 0.0060. The solid curve represents the flat wing with zero design lift coefficient $(C_{L,DES} = 0)$, a wing which depends on attitude for its lift. The short-dashed curve represents a wing which has a design lift coefficient equal to one-half the optimum $(C_{L,DES} = 0.5C_{L,OPT} = 0.062)$. This wing depends on both warp and attitude to reach the lift coefficient of peak efficiency. The long-dashed curve represents a wing which is warped for the optimum design lift coefficient $(C_{L,DES} = C_{L,OPT} = 0.124)$. At the design lift coefficient of this optimum wing, the highest possible theoretical lift-drag ratio is obtained for the assumed conditions. The point to be made from this figure is that not much is lost in theoretical lift-drag ratio if less than the optimum warp is used. A limited design lift coefficient, or degree of warp, can lead to reasonably good results as will be shown in subsequent figures.

Isolated-Wing and Wing-Body Tests

Experimental results, typical of those that have been obtained on thin wings with the relatively extreme warp associated with near-optimum design lift coefficients, are shown in figure 3. The comparisons in the figure are shown as the incremental increase in maximum lift-drag ratio of the warped wings over those of corresponding flat wings:

$$\Delta(L/D)_{MAX} = (L/D)_{MAX,WARPED} - (L/D)_{MAX,FLAT}$$

For the three configurations shown in the figure, which were near-optimum $(C_{L,DES} \approx C_{L,OPT})$ warped designs at Mach numbers 2.0, 2.5, and 3.0, the theoretically predicted increase in maximum lift-drag ratio over corresponding flat configurations was of the order 2.0 as represented by the solid curve. As can be seen from the symbols and dashed curve, which indicate the experimental results, these extremely warped surfaces were only slightly better than the flat wings.

Two reasons have been given for this lack of agreement between theory and experiment (ref. 5). First, the extremely warped optimum surface violates the linearized theory from which it is designed, and second, the induced transonic flow normal to the leading edges causes a breakdown in the careful balance between wing slope and pressure which has been designed into the wings.

As suggested by research on two-dimensional cambered airfoils, in the transonic flow regime better lifting efficiency may be obtained by using less than ideal camber combined with angle of attack. This compromise is essentially represented by a limiting condition such as $C_{L,DES} = 0.5C_{L,OPT}$ for the three-dimensional wing.

Some results obtained with this limitation on the magnitude of lift carried by the warped surface is shown in figure 4. The wings of the configurations shown in this figure were designed at Mach numbers 2.0, 2.2, and 2.6 to carry part of the lift by means of the angle of attack as mentioned previously. It can be seen by the symbols and dashed line, which indicate the experimental results, that the agreement with theory is much better with these wings than with the extremely warped optimum designs shown in figure 3, particularly at the low Mach numbers, It can be noted, however, by the solid diamond symbol at a Mach number of 2.6, that there is a strong nonlinear effect of thickness on the comparison of experiment with theory. Increasing the thickness ratio from 0.025 to 0.040 reduced the incremental lifting efficiency of the warped surface by more than 50 percent.

The design lift limitation illustrated in figure 4 appears to have an application in the design of thin, low-aspect-ratio configurations. It should be pointed out, however, that the restriction which has been employed ($C_{L,DES} = 0.5C_{L,OPT}$) is arbitrary and that the nature of the limitation would depend on the particular configuration.

Investigations such as those discussed in figures 2 to 4 have given an indication of the restrictions which appear to be necessary to get reasonable results from linear theory design of isolated wings. Research presently under way will hopefully lead to greater increases in the lifting efficiencies and some inputs into the thickness problem. Nevertheless, one might have to go contrary to these limitations, or restrictions, in the design of a complete airplane as indicated by the following discussion.

Complete Configuration Tests

In the design of SCAT 15 the wings had to be thick because of variable sweep, and longitudinal trim was a major problem. The flat version of the configuration had shown an inability to trim the moments due to the shift of aerodynamic center with Mach number. On the basis of available information, an extremely warped wing appeared to be necessary to provide the zero-lift pitching moment required for trim. Figure 5 indicates quite clearly that the warped surface, which was a basic linear-theory design, provided the desired trim characteristics.

In figure 5 the maximum trimmed lift-drag ratio of the SCAT 15 configuration at $M = 2.96$ is shown as a function of static margin $\partial C_m/\partial C_L$. It can be seen from the figure that the warped version of the configuration, $C_{L,DES} \approx C_{L,OPT}$, was trimmed near maximum lift-drag ratio over a wide range of static margins, whereas the flat version could not be trimmed to the required level of $\partial C_m/\partial C_L$ of -0.15. Possibly trim could have been obtained on the flat version with a larger tail but the loss in lift-drag ratio would have been substantial.

As pointed out in paper no. 4 by Lloyd T. Goodmanson and his colleagues, the SCAT 15 airplane had the highest aerodynamic performance level of any of the SCAT configurations. SCAT 15 was able to establish this relatively high performance level, in spite of high thickness ratio and extreme wing warp, because of favorable component interference effects. Other than the planform of the wing, the basic ingredients of these favorable interference effects were a positive lift produced by the nacelle arrangement under the wing and an efficient lift produced by outboard tails operating in an upwash field. (See ref. 6.) The results of these favorable interference effects are shown in figure 6.

In figure 6, variation of the ratio $C_D/C_{D,WING-BODY}$ with lift coefficient is shown for the SCAT 15 at $M = 2.96$. These curves show that when the nacelles were added under the wing-body, the drag coefficient at zero lift increased by about 14 percent. As a result of the favorable lift produced by the nacelles near a lift coefficient of about 0.1, however, the drag coefficient of the wing-body-nacelle arrangement is the same as that of the wing-body configuration. Furthermore, when the horizontal and vertical tails (represented by the shaded region) were added to make the complete configuration, the drag coefficient at zero lift was about 28 percent greater than that of the wing-body configuration. These results show that the combined favorable interference effects reduced the drag level of the complete configuration to that of the wing-body configuration at a lift coefficient of about 0.1. The effects illustrated can be interpreted to represent an increase in lifting efficiency due to the added components. Further research appears necessary to define more clearly the factors which contribute to these favorable interference effects in order that they may be efficiently applied to other configurations.

From the results shown in figures 5 and 6 for the SCAT 15, it can be concluded that desirable trim characteristics and supersonic efficiency may be obtained by making use of a warped wing, derived basically from linear theory, in combination with favorable component lift-interference effects. As reported in a previous paper (paper no. 4 by Goodmanson et al.), these aerodynamic advantages of the SCAT 15 could not overcome the structural penalties associated with the concept. There is reason to hope, however, that a wing planform and surface can

DECLASSIFIED

be found to employ the aerodynamic advantages without severe structural penalties and without the low-speed pitch-up problems found on highly swept arrow wings. Part of the present research effort is directed toward the use of arbitrary planform methods to find such a wing.

Analytical Methods

Digital computer programs which are available for the solution of arbitrary planform problems are outlined in figure 7. The programs will solve a variety of problems as indicated in the figure. Mr. Ralph Carmichael of the NASA Ames Research Center has formulated a more complete program for use in the design of an ogee wing planform for comparison with the SCAT 17.

Although linear theory has shortcomings, it has been useful in pointing out the design areas of high performance and, properly limited, provides warped surface shapes which can be worked with to obtain high lifting efficiency.

The programs indicated in figure 7 have been used to design delta and ogee configurations for comparison at a Mach number of 2.2. Because of the thin, low,-aspect-ratio wings which were considered for these configurations, a moderate degree of wing warp (approaching the limitation $C_{L,DES} = 0.5C_{L,OPT}$) was considered permissible and desirable. Figure 8 indicates the effect of wing warp on the performance of these two configurations at a Mach number of 2.2 and indicates the variation of lift-drag ratio with lift coefficient as predicted by theory and determined by experiment. It can be seen from the figure that wing warp improved the performance of both configurations and that there was reasonably good agreement between theory and experiment for both flat and warped versions of the configurations. It should be pointed out that the values of lift-drag ratio shown in figure 8 do not represent trimmed values. The trim considerations for the delta and ogee configurations are discussed in paper no. 12 by Robert T. Taylor et al.

CONCLUDING REMARKS

In summary, consideration of highly swept warped-wing arrangements indicates that, for thin wings, a moderate warped surface at angle of attack may be desirable. Wing warp offers favorable trim characteristics and in combination with component lift interference effects can lead to a high performance configuration. Analytical methods are being employed to find a configuration which can use these aerodynamic advantages without severe structural penalties.

REFERENCES

1. Carlson, Harry W.: Aerodynamic Characteristics at Mach Number 2.05 of a Series of Highly Swept Arrow Wings Employing Various Degrees of Twist and Camber. NASA TM X-332, 1960.

2. Hasson, Dennis F., Fichter, Ann B., and Wong, Norman: Aerodynamic Characteristics at Mach Numbers From 1.6 to 2.8 of 74° Swept Arrow Wings With and Without Camber and Twist. NASA TM X-8, 1959.

3. Hasson, Dennis F., and Wong, Norman: Aerodynamic Characteristics at Mach Numbers From 2.29 to 4.65 of 80° Swept Arrow Wings With and Without Camber and Twist. NASA TM X-175, 1960.

4. Brown, Clinton E., and McLean, Francis E.: The Problem of Obtaining High Lift-Drag Ratios at Supersonic Speeds. Jour. Aero. Sci., vol. 26, no. 5, May 1959, pp. 298-302.

5. Brown, Clinton E., McLean, F. E., and Klunker, E. B.: Theoretical and Experimental Studies of Cambered and Twisted Wings Optimized for Flight at Supersonic Speeds. Advances in Aero. Sci., vol. 3, Pergamon Press (New York), 1961, pp. 415-430.

6. Robins, A. Warner, Spearman, M. Leroy, and Harris, Roy V.: Aerodynamic Characteristics at Mach Numbers of 2.30, 2.60, and 2.96 of a Supersonic Transport Model With a Blended Wing-Body, Variable-Sweep Auxiliary Wing Panels, Outboard Tail Surfaces, and a Design Mach Number of 2.6. NASA TM X-815, 1963.

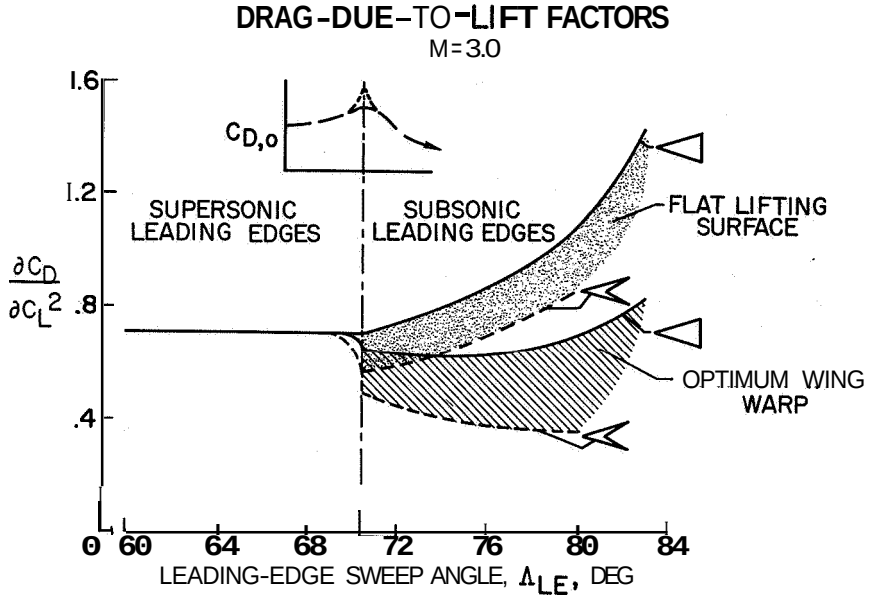

Figure 1

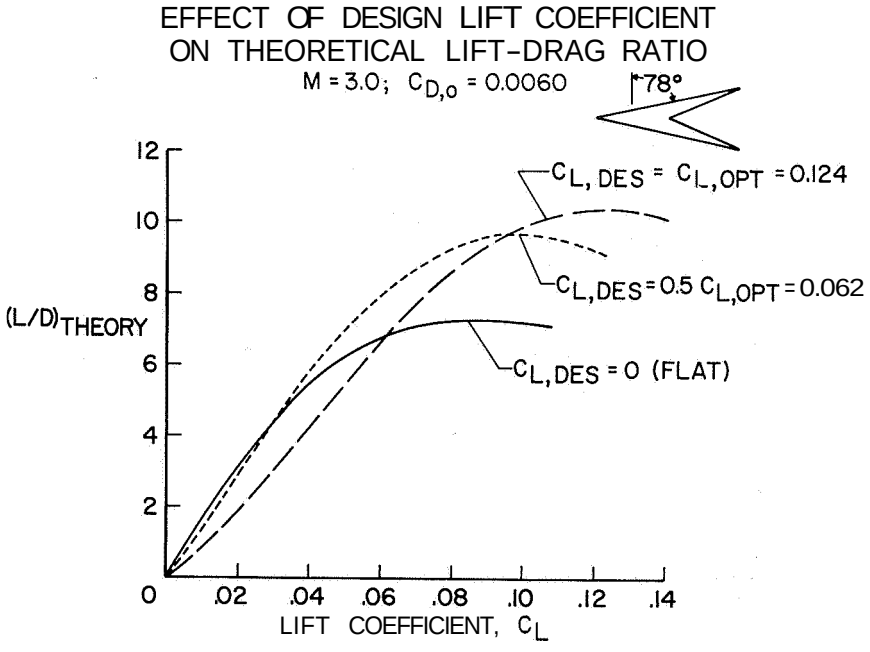

Figure 2

INCREASE IN MAXIMUM LIFT-DRAG RATIO DUE TO WING WARP

$C_{L,DES} \approx C_{L,OPT}$; $R \approx 4 \times 10^6$; CIRCULAR-ARC THICKNESS DISTRIBUTIONS, t/c = 0.025 TO 0.030

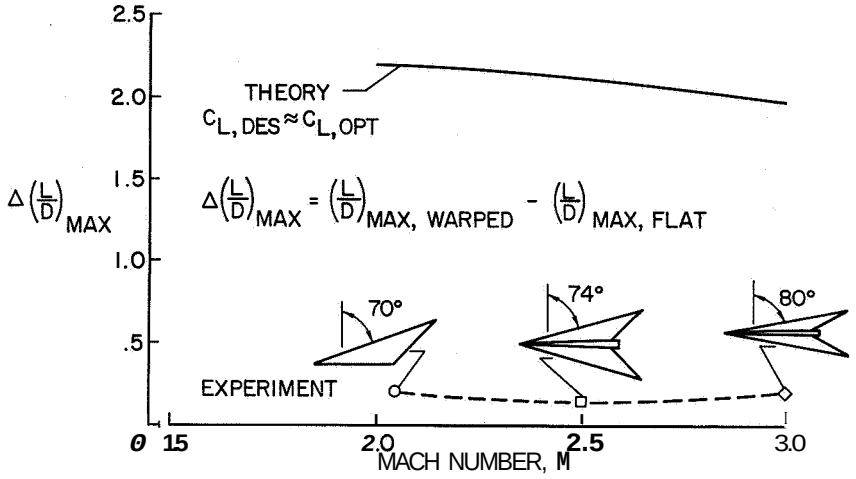

Figure 3

INCREASE IN MAXIMUM LIFT-DRAG RATIO DUE TO WING WARP

$C_{L,DES} \approx 0.5\, C_{L,OPT}$; $R \approx 4 \times 10^6$; CIRCULAR-ARC THICKNESS DISTRIBUTIONS, t/c = 0.025 TO 0.030

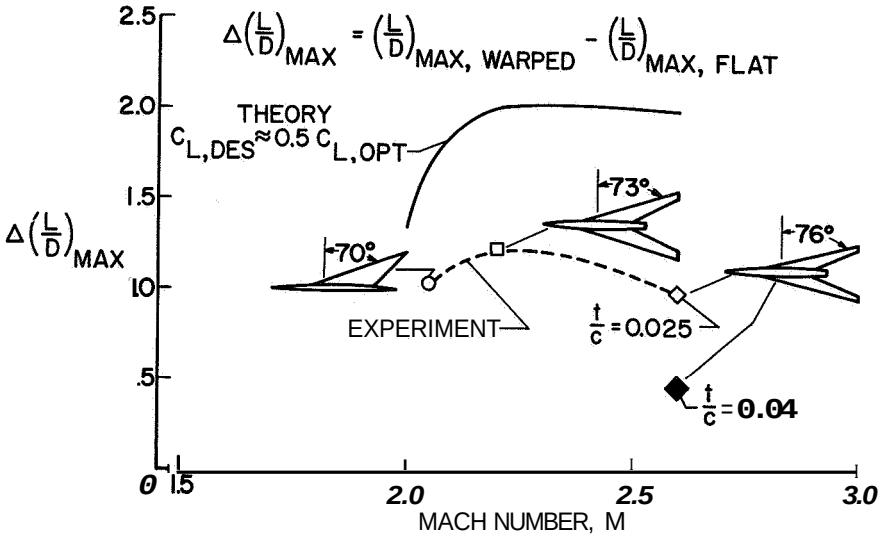

Figure 4

FAVORABLE TRIM CHARACTERISTICS DUE TO WING WARP

M = 2.96; R = 3.71×10^6; NACA 65 A-SERIES, t/c = 0.045 AT ROOT TO 0.035 AT TIP

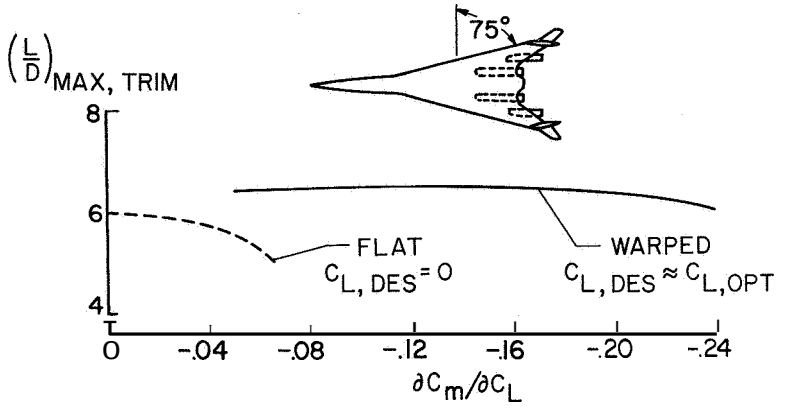

Figure 5

INTERFERENCE EFFECTS ON AIRPLANE CONFIGURATION **WITH** WARPED LIFTING SURFACES

M = 2.96; R = 3.71×10^6; $C_{L,DES} \approx C_{L,OPT}$

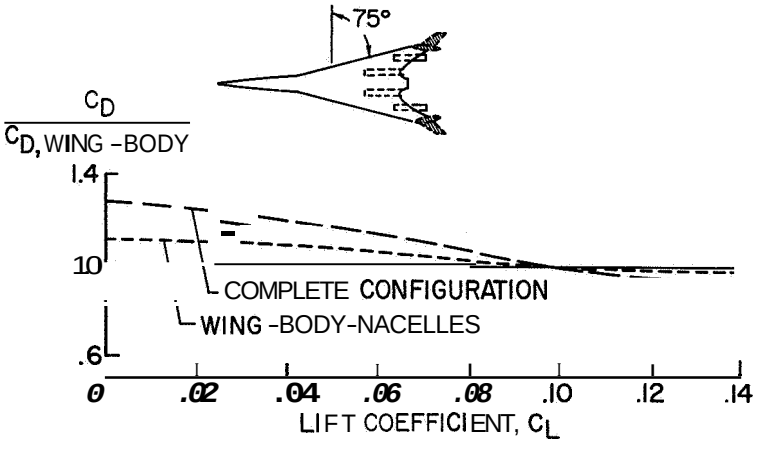

Figure 6

COMPUTER PROGRAMS AVAILABLE FOR SOLUTION OF ARBITRARY-PLANFORM PROBLEMS

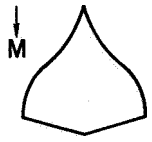

PROGRAM I		PROGRAM II	
1. GIVEN:	TOTAL LIFT	1. GIVEN:	LIFT DISTRIBUTION
SOLUTION:	OPTIMUM LIFT DISTRIBUTION OPTIMUM SURFACE SHAPE MINIMUM DRAG-DUE-TO-LIFT FACTOR	SOLUTION:	SURFACE SHAPE DRAG-DUE-TO-LIFT FACTOR
		2. GIVEN:	SURFACE SHAPE
		SOLUTION:	LIFT DISTRIBUTION DRAG-DUE-TO-LIFT FACTOR LIFT-CURVE SLOPE

GIVEN: COMBINATION OF SOLUTIONS FROM PROGRAMS I AND II
SOLUTION: OFF-DESIGN POLARS

Figure 7

EFFECT OF WING WARP ON PERFORMANCE OF DELTA AND OGEE CONFIGURATIONS

M=2.2; R=3×10^6; $C_{L,DES} \approx 0.5\, C_{L,OPT}$;
CIRCULAR-ARC THICKNESS DISTRIBUTIONS, t/c = 0.02 TO 0.03

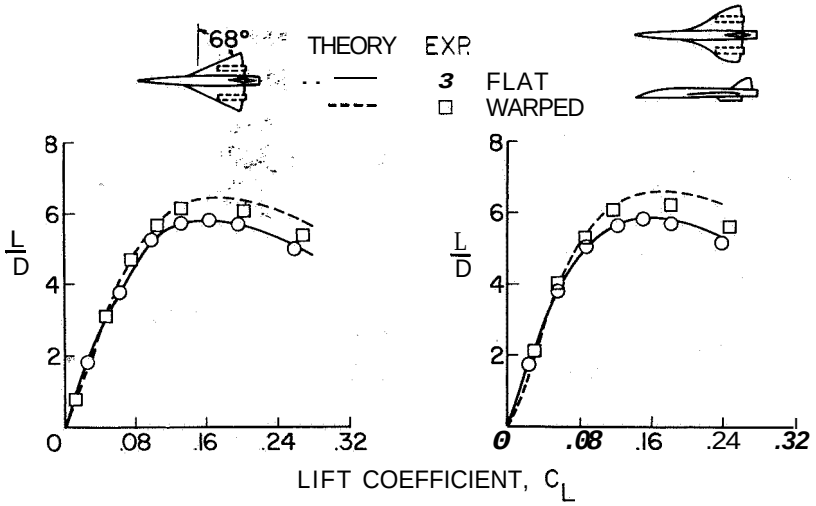

Figure 8

N67-31615

8. STUDIES OF SKIN FRICTION AT SUPERSONIC SPEEDS

By K. R. Czarnecki, Mary W. Jackson,
and William J. Monta

NASA Langley Research Center

SUMMARY

11950

A brief review has been made of the most significant results from recent research on turbulent boundary layers applicable to the supersonic transport. The review indicates that: High Reynolds number flat-plate boundary-layer skin friction with heat transfer will tend to agree with the predictions of the Sommer and Short T' method and those theories or methods which are in approximate agreement with this T' method. Three-dimensional boundary-layer flow probably will increase skin-friction drag over that expected from two-dimensional flat-plate theories or experiment. In general, local flow conditions and the proper correlating parameters will have to be used for the accurate prediction of drag due to surface roughness. conf. AUTHOR

INTRODUCTION

The successful design of a supersonic transport is critically dependent upon making a satisfactory estimate of the airplane drag. One of the major components of airplane drag is skin friction. Consequently, it becomes mandatory to have reliable methods for estimating skin-friction drag. Detailed examination of the available theories and experimental data, however, reveals many deficiencies and lack of proper verification. The purpose of this paper is to present and discuss some of the highlights from recent research being made on turbulent boundary layers to fill in some of the voids in the desired information. Specifically, a brief review will be made of the skin-friction level on smooth surfaces at high Reynolds numbers, the effects of some three-dimensional boundary-layer flows on skin friction, and the effects of surface roughness on the skin-friction drag.

8

SYMBOLS

C_D drag coefficient

[redacted]

$(C_{D,qk})_{av}$	roughness drag coefficient based on integrated pressure distributions, roughness height, and average dynamic pressure within boundary layer over roughness height
$(C_{D,qk})_{\infty}$	roughness drag coefficient based on integrated pressure distributions, roughness height, and free-stream dynamic pressure
C_F	average skin-friction drag coefficient based on wetted surface area and free-stream dynamic pressure
C_F^*	transformed average skin-friction coefficient
C_p	pressure coefficient
k	roughness height
δ^*	boundary-layer displacement thickness
k/δ^*	ratio of roughness height to boundary-layer displacement thickness
M_{∞}	free-stream Mach number
r	model radius measured normal to body axis
R_{FT}	free-stream Reynolds number per foot
R_x	Reynolds number based on free-stream conditions and distance to virtual origin or to body nose
R_x^*	transformed Reynolds number
x	distance from virtual origin or axial distance from body nose
Taw	adiabatic wall temperature
T_t	free-stream stagnation temperature
T_w	average model wall temperature
T_{∞}	free-stream static temperature
T_w/T_{∞}	temperature ratio
T'	reference temperature
a	angle of attack

[redacted]

[redacted]

RESULTS AND DISCUSSION

Skin Friction at High Reynolds Numbers

In a recent report by Peterson (ref. 1) a large amount of turbulent skin-friction data for smooth flat plates were correlated and compared with several methods of predicting the skin friction. The analysis shows that, by a small margin, the Sommer and Short T', or reference temperature, method may give the most reliable estimate of the value of skin friction. One of the major deficiencies existing in this correlation is the lack of reliable experimental skin-friction results at the high Reynolds numbers that will be encountered in flight by the supersonic transport. Figure 1, therefore, presents some flat-plate skin-friction results with Reynolds numbers up to about 150×10^6 recently obtained on the sidewall of the Langley 4- by 4-foot supersonic pressure tunnel by boundary-layer profile surveys and local skin-friction balances at Mach numbers of 1.61 and 2.20. The data were obtained within the constant Mach number rhombus of the test section at six or seven Reynolds numbers per foot at zero heat transfer. The data were reduced to coefficient form by a method utilizing both momentum surveys and local surface shear. (See ref. 1.) In the figure, the ordinate C_F is the average skin-friction coefficient, and R_x is the Reynolds number based on free-stream conditions and the distance to the virtual origin. Included in the figure are the curves determined by the Sommer and Short T' method and several of the other more reliable theories or empirical methods that can also handle heat transfer.

Inspection of the plots in figure 1 indicates that these high Reynolds number flat-plate skin-friction data are in good general agreement with the level of the Sommer and Short T' curve and the various other theories represented here, and that the variation of C_F with R_x at these high Reynolds numbers will tend to follow the predictions of these theories.

In figure 2 are presented some preliminary high Reynolds number skin-friction results obtained on an ogive-cylinder model by the usual technique of force balance minus nose- and base-pressure drag in the Langley 9- by 6-foot thermal structures tunnel at $M_\infty = 2.98$. These are three-dimensional boundary-layer flow data and are the only high Reynolds number results available which include the effects of heat transfer. The data were obtained with fixed transition at two stagnation temperature conditions and a model preheat condition to approximately zero heat transfer. The actual Reynolds number range was from about 36×10^6 to 200×10^6 and the wall-to-stream temperature ratio T_W/T_∞ varied

[redacted]

from 1.4 to 2.5. Because of the varying amounts of heat transfer involved, the experimental data are presented in terms of the coefficients C_F^* and R_x^* which are the transformed equivalent incompressible-flow zero-heat-transfer skin-friction coefficints and transformed Reynolds numbers, respectively. The data were reduced to this form by the Sommer and Short T' method. (See ref. 2.) For purposes of comparison, the standard Von Karman-Schoenherr incompressible-flow zero-heat-transfer skin-friction curve is included as a solid line.

Examination of the data in figure 2 indicates that the level of the experimental data is below the Von Karman-Schoenherr curve. The fact that the experimental results lie approximately 10 percent below the Von Karman-Schoenherr curve, whereas, for reasons to be illustrated shortly, the data were expected to lie somewhat above the reference curve, is ascribed to insufficiently accurate knowledge of either the model nose or base drag. This error in the experimental results will have little if any effect on the slope of the curve, and the slope of the experimental variation of C_F^* with R_x^* is in good agreement with the theoretical prediction. Consequently, the conclusion can be made that these experimental three-dimensional boundary-layer results at $M_\infty = 2.98$ with heat transfer (fig. 2) and the lower Mach number flat-plate zero-heat-transfer data (fig. 1) indicate that the Sommer and Short T' method and other methods giving similar results can be used to extrapolate low Reynolds number model data to the high Reynolds numbers and heat-transfer rates of the supersonic transport.

Skin Friction in Three-Dimensional Boundary Layer

Airplane skin friction has often been estimated on the basis of two-dimensional flat-plate theory or experiment. In the discussion of figure 2, however, mention was made that the skin-friction drag of the ogive cylinder was expected to be higher than that indicated for the body by flat-plate theory. Experimental evidence as to why this trend was expected is shown in figure 3. These data were obtained by the standard force-balance and nose-base-pressure technique (with fixed transition) on a minimum-drag type of body with a fineness ratio of 13 in a number of Langley facilities over a Mach number range from 0.60 to 3.95, a true Reynolds number range from 3×10^6 to 13×10^6, and at zero heat transfer. In order to simplify the comparisons, the data have been transformed to the incompressible-flow form by the Sommer and Short T' method as in figure 2 and are compared with the Von Karman-Schoenherr reference curve.

The results presented in figure 3 show that the drag of a three-dimensional axisymmetric body is always higher than that predicted by

the Sommer and Short T' method for a flat plate of equal wetted surface area. Similar drag increases were noted for other axisymmetric bodies in this particular investigation and on an ogive-cylinder model (in ref. 3). Furthermore, preliminary examination of wake surveys recently made behind flat and/or cambered and twisted sweptback wings has revealed the possibility of increased overall skin friction for the case in which small spanwise boundary-layer flow may exist on a three-dimensional body such as a wing. In view of all these indications it becomes apparent that it may be difficult, if not impossible, to achieve a skin-friction drag level on an airplane equal to that attainable on a flat plate of equal wetted area at identical free-stream conditions. Estimates of ast of these three-dimensional boundary-layer flow effects can be made, although not with the same order of accuracy as for the basic flat-plate skin friction.

Drag of Surface Roughness Elements

Roughness drag on the supersonic transport can be a problem and can lead to a decrease in performance. Considerable experimentation on the effects of surface roughness on supersonic turbulent skin friction has been accomplished. Some of the work of NASA on this subject has been reported in references 4 to 7. The present status of knowledge pertaining to the effects of surface roughness on turbulent skin friction at supersonic speeds is illustrated briefly in figures 4 to 7 relating to forward- and rearward-facing steps and surface waves, which represent the basic shapes from which most roughness shapes can be derived. In figure 4 is presented the drag coefficient for a two-dimensional forward-facing step roughness and in figure 5 is presented the drag coefficient for a two-dimensional rearward-facing step roughness, both as a function of the ratio of step height to boundary-layer displacement thickness k/δ^*. These data were obtained at a Mach number of 2.20 over a range of Reynolds number per foot at zero heat transfer by means of pressure distributions determined on a variable-height block mounted in the thick boundary layer on the sidewall of the Langley 4- by 4-foot supersonic pressure tunnel, and thus exclude changes in skin friction on streamwise surfaces ahead of and to the rear of the steps.

For the forward-facing step roughness (fig. 4) the drag coefficient was constant when it was based on the roughness height and the average dynamic pressure within the boundary layer over the height of the step (the undisturbed boundary layer) except when the step was immersed within the lowest 1 percent of the total boundary-layer thickness. Within this part of the boundary layer the flow becomes subsonic. Similar results were obtained at a Mach number of 1.61 except that the correlating drag coefficient value was higher, about 0.8, and indicated that an effect of Mach number is present.

For the rearward-facing step roughness (fig. 5), the drag coefficient was constant when based on the roughness height and the free-stream dynamic pressure, the relation again breaking down for the step immersed in the lowest 1 or 2 percent of the total boundary-layer thickness. Once more, decreasing the Mach number to 1.61 increased the correlating drag coefficient to 0.18 and again indicated an influence of the free-stream Mach number.

In figure 6 is depicted the pressure distribution (taken from ref. 6) over a sinusoidal-wave type of surface roughness. The wave was one of a number built into the cylindrical part of an ogive-cylinder model. The free-stream Mach number is 2.01; the R_{FT} range is from 1.25×10^6 to 7.08×10^6. The measured surface profile is shown, with a greatly exaggerated ordinate scale, in the lower part of the figure. The dashed line represents two-dimensional linearized-theory calculations using measured local flow conditions (experiment, smooth body) just outside the boundary layer and the measured surface profile.

The most salient feature of figure 6 is that at high values of R_{FT}, when the ratio of boundary-layer thickness to roughness height is least, it is possible to predict with good accuracy the pressure distribution and, hence, the wave drag of this type of roughness. As R_{FT} decreases, however, and the ratio of roughness height to boundary-layer thickness increases, there is an onset of flow separation within the recessed or trough parts of the roughness elements as evidenced by the decreases in C_p in this area, which results in a decreased drag and in more difficulty in predicting the drag.

It is apparent that the drag of all types of surface roughness is dependent upon local stream conditions, but that the controlling drag parameters will vary with the type of roughness. As shown in reference 7 and verified even more vividly by recent pressure tests of surface roughness in the transonic Mach number area, most of the surface roughness drag at supersonic speeds is wave drag with only small increases in boundary-layer momentum losses.

In the light of the knowledge derived from figures 4 to 6 in this series on surface roughness, it should be apparent from theoretical considerations that the effects of heat transfer on roughness drag generally will be small. This deduction is investigated by analysis of data such as those presented in figure 7. The data were obtained for two roughness configurations on an ogive-cylinder model in the previously mentioned Mach number 2.98 tests in the Langley 9- by 6-foot thermal structures tunnel. The ordinate C_D is the coefficient which represents the combined drag of the smooth-body skin friction plus surface

roughness based on wetted surface area and stream flow conditions. The abscissa is the average model-wall—free-stream temperature ratio.

From the relative constancy of the increment in drag between the smooth model and the roughness configurations over the temperature-ratio range, it is readily established that the data confirm the previously mentioned deduction that heat transfer will have relatively little effect on the increment in drag due to surface roughness.

In order to provide an interpretation of these roughness results as applied to a supersonic transport, figure 8 was prepared. Flight at 60,000 feet at $M_\infty = 2.20$ and a near 0° was assumed. The drag coefficients for a forward- and rearnard-facing step roughness are plotted as a function of step height. The coefficients are for 1 lineal foot of step roughness located on the wing of the supersonic transport having a reference wing area of 2,300 square feet. The drag coefficients are based on this wing area and free-stream dynamic pressure.

For the rearward-facing step roughness, the drag coefficient based on the airplane reference conditions increases linearly with step height in the range of k/δ^* for which the correlating drag coefficient in figure 5 was constant. The step drag is also independent of distance along the wing surface. Of course, for the very small heights, the drag contribution tends toward zero somewhat more rapidly, but the trend can hardly be distinguished.

For the forward-facing step roughness, the drag coefficient increases with height not only because of the increased frontal area but also because the average dynamic pressure increases on the front face. The drag coefficient, therefore, increases with step height at a faster rate than linearly. For this roughness, there is an effect of step location due to the variation with surface distance of the average dynamic pressure in the boundary layer over a given height.

As a further illustration, it is estimated that a thousand feet of each type of step roughness 0.050 inch high scattered over the wing will increase the airplane drag by nearly 4 percent. This drag contribution can be readily decreased by requiring smaller surface mismatch and lesser lengths of roughness. A surface waviness of height to length ratio of only $\frac{1}{2}$ of 1 percent, but covering the complete airplane wetted surface area between stringers and ribs, can increase airplane drag by 2 percent. This type of roughness drag may be somewhat more difficult to alleviate to acceptable values.

SUMMARY OF RESULTS

From this brief review of recent turbulent boundary-layer research applicable to the supersonic transport it may be summarized that:

High Reynolds number flat-plate boundary-layer skin friction with heat transfer will tend to agree with the predictions of the Sommer and Short T' method and those theories or methods which are in approximate agreement with this T' method.

Three-dimensional boundary-layer flow on the supersonic transport probably will increase skin-friction drag over that expected from two-dimensional. flat-plate theories or experiment.

In general, local flow conditions and the proper correlating parameters, which vary with roughness shape, will have to be used for the accurate prediction of drag due to surface roughness.

REFERENCES

1. Peterson, John B., Jr.: A Comparison of Experimental and Theoretical Results for the Compressible Turbulent-Boundary-Layer Skin Friction With Zero Pressure Gradient. NASA TN D-1795, 1963.

2. Sommer, Simon C., and Short, Barbara J.: Free-Flight Measurements of Turbulent-Boundary-Layer Skin Friction in the Presence of Severe Aerodynamic Heating at Mach Numbers From 2.8 to 7.0. NACA TN 3391, 1955.

3. Czarnecki, K. R., and Monta, William J.: Boundary-Layer Velocity Profiles and Skin Friction Due to Surface Roughness on an Ogive Cylinder at Mach Numbers of 1.61 and 2.01. NASA TN D-2048, 1963.

4. Czarnecki, K. R., Robinson, Ross B., and Hilton, John H., Jr.: Investigation of Distributed Surface Roughness on a Body of Revolution at a Mach Number of 1.61. NACA TN 3230, 1954.

5. Sevier, John R., Jr., and Czarnecki, K. R.: Investigation of Effects of Distributed Surface Roughness on a Turbulent Boundary Layer Over a Body of Revolution at a Mach Number of 2.01, NACA TN 4183, 1958.

6. Czarnecki, K. R., Sevier, John R., Jr., and Carmel, Melvin M.: Effects of Fabrication-Type Roughness on Turbulent Skin Friction at Supersonic Speeds. NACA TN 4299, 1958.

7. Czarnecki, K. R., and Monta, William J.: Pressure Distributions and Wave Drag Due to Two-Dimensional Fabrication-Type Surface Roughness on an Ogive Cylinder at Mach Numbers of 1.61 and 2.01. NASA TN D-835, 1961.

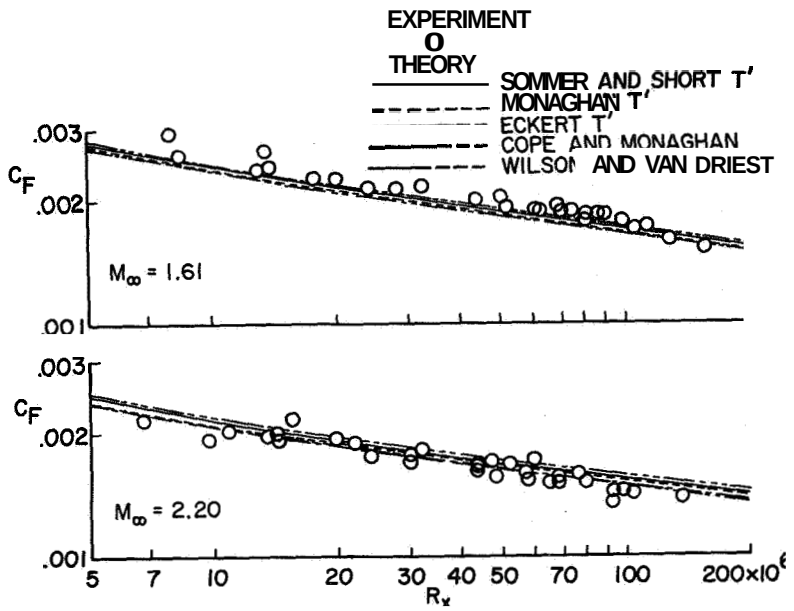

Figure 1

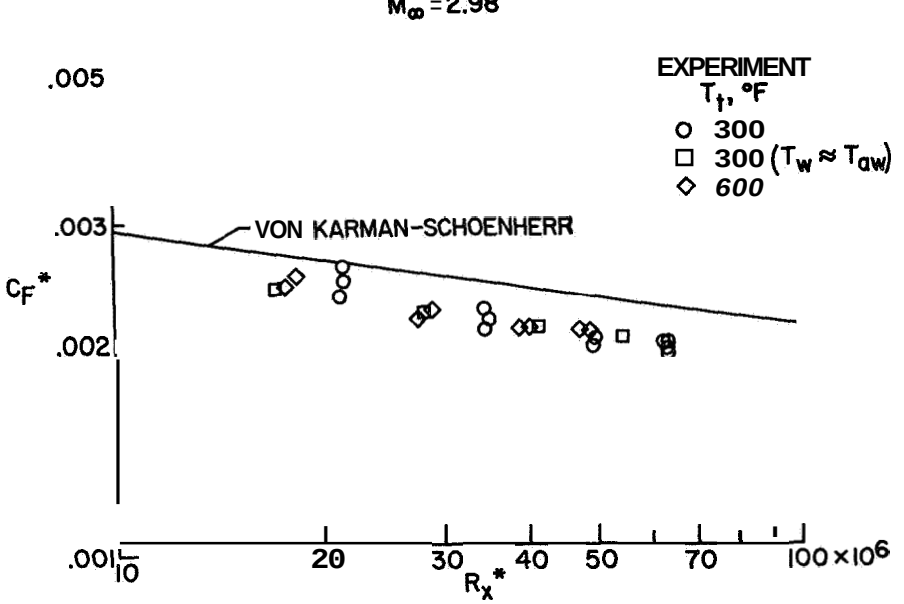

Figure 2

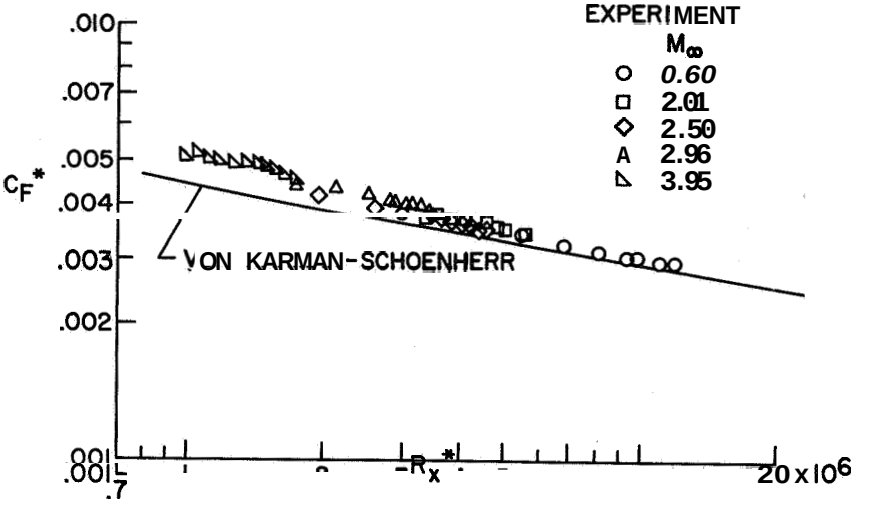

Figure 3

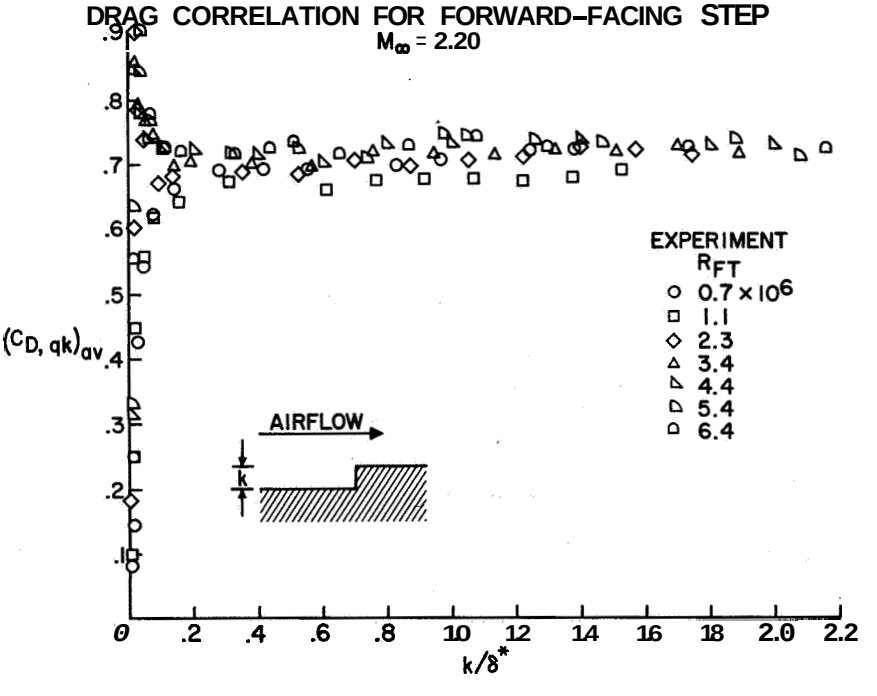

Figure 4

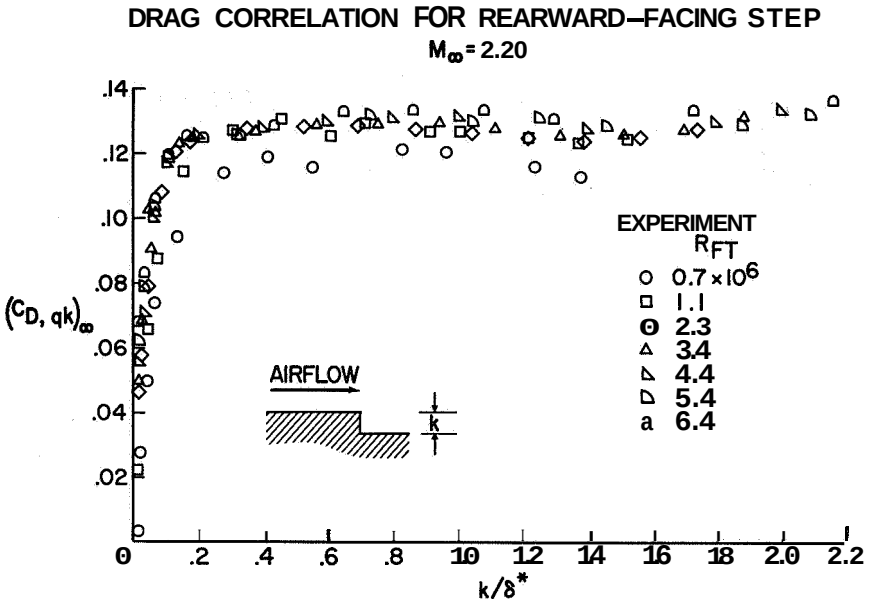

Figure 5

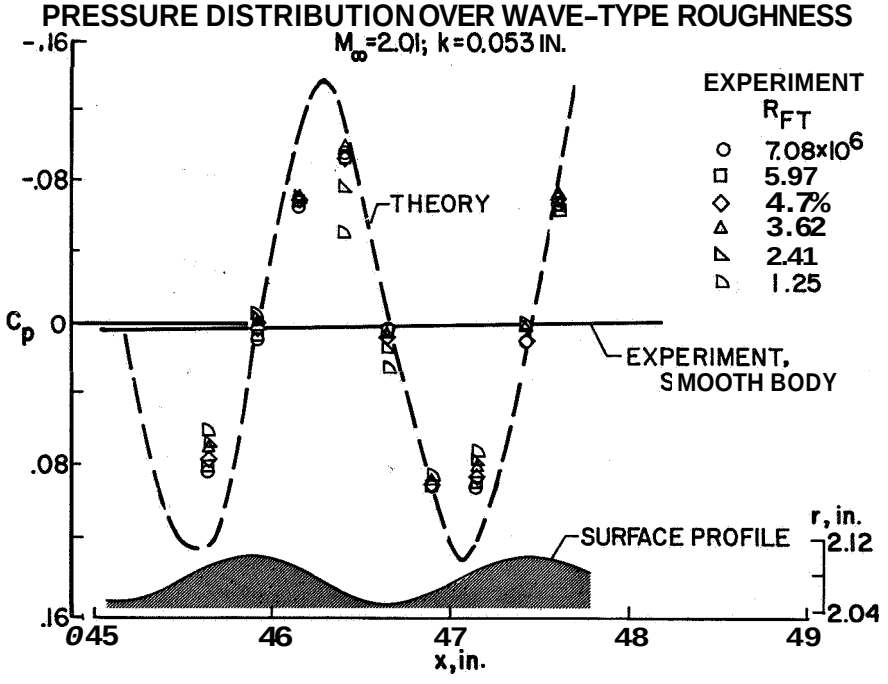

Figure 6

[redacted]

EFFECT OF HEAT-TRANSFER RATIO ON ROUGHNESS DRAG
$M_\infty = 2.98$; $R_x = 94 \times 10^6$

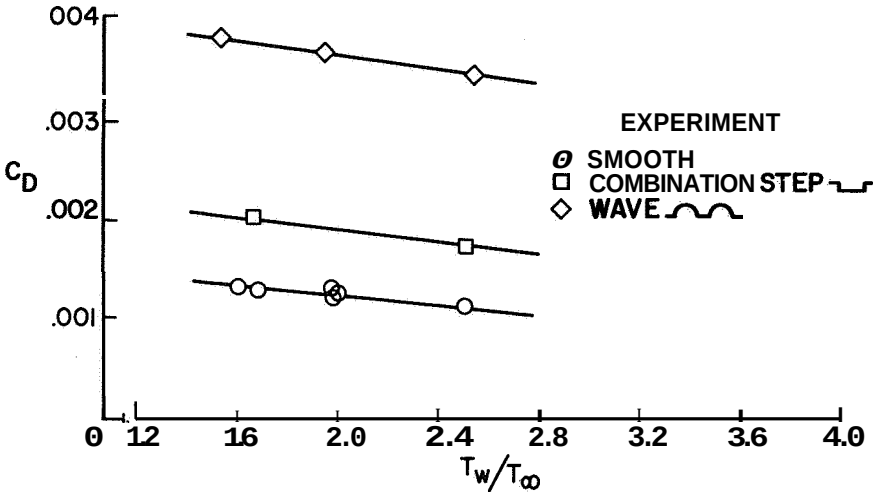

Figure 7

DRAG OF 1 FOOT OF ROUGHNESS ON SUPERSONIC TRANSPORT
$M_\infty = 2.20$; ALTITUDE, 60,000 FT; WING AREA, 2,300 SQ FT; $\alpha = 0°$

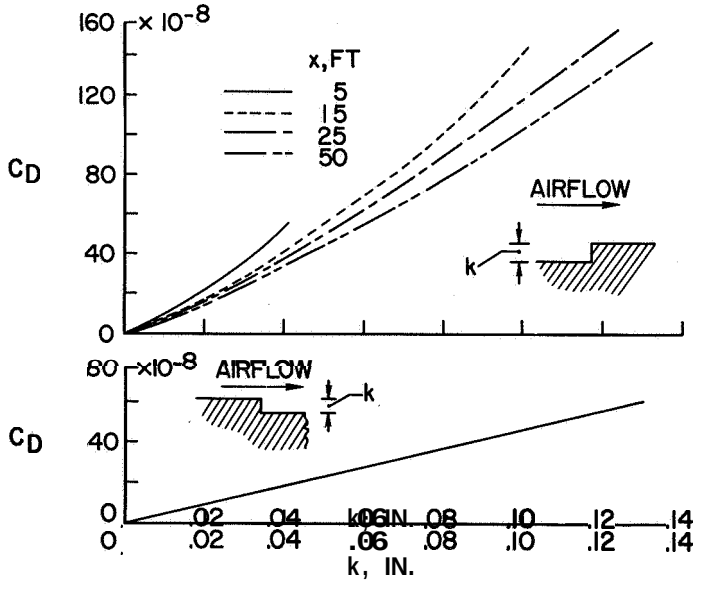

Figure. 8

[redacted]

N67-31616

PRECEDING PAGE BLANK NOT FILMED.

9. SOME FACTORS AFFECTING TURBULENT SKIN FRICTION AT SUPERSONIC SPEEDS

By Albert L. Braslow, John B. Peterson, Jr., and Donald I. McRee

NASA Langley Research Center

SUMMARY

Preliminary results are presented for two investigations of factors affecting turbulent skin friction at Mach 3: an investigation of the use of air injection into the turbulent boundary layer through rearward-facing inclined flush and step slots to reduce skin friction, and an investigation of the contribution to skin-friction drag of three-dimensional roughness trips used to fix boundary-layer transition.

SYMBOLS

C_D	model drag coefficient
$C_{D,INJECTION}$	total airplane cruise drag coefficient with air injection
$C_{D,NO\ INJECTION}$	total airplane cruise drag coefficient without air injection
$C_{D,F}$	skin-friction drag coefficient based on wing area
C_F	skin-friction drag coefficient based on wetted area
C_T	thrust coefficient
k	height of roughness
$\dot{m}$	mass rate of flow of injection air
$\dot{m}_\infty$	mass rate of flow of free-stream air, $\rho_\infty u_\infty S$
M	Mach number

R_k roughness Reynolds number, $\frac{u_k k}{\nu_k}$

R/FT free-stream Reynolds number per foot

S flat-plate reference area

u_k velocity at top of roughness

u_∞ free-stream velocity

w width of transition trip

x distance from leading edge

ν_k kinematic viscosity at top of roughness

ρ_∞ free-stream density

μ_∞ free-stream viscosity

Subscripts:

o without injection

$a = 0$ at zero angle of attack

th theory

AIR INJECTION

Introduction

The flow over the surfaces of the supersonic transport at supersonic cruise will be almost entirely turbulent. A large percentage of the total airplane drag will then be due to turbulent skin friction. It would be most desirable, of course, to find a means for obtaining extensive regions of laminar flow to reduce the skin-friction contribution to the total drag. Althoughthis has been a goal ever since Prandtl formulated the concept of the boundary layer, even today very little laminar flow is attained on airplanes in flight. Research on laminar flow, however, is still continuing. For example, the Nortbrop Corporation, under contract to the U.S. Air Force, is currently flight testing the

laminar-flow control of the X-21 airplane. Results of this program should provide considerable information on the practical aspects of using suction boundary-layer control at subsonic speeds. Research is also planned at Langley and at Northrop, under a combined USAF, FAA, and NASA contract, on laminar-flow control at supersonic speeds. Such effects as shock—boundary-layer interactions, wing sweep, noise, and vibrations on laminar-flow control will be investigated.

Since sufficient practical experience with laminar-flow control is not yet available at any speed and considerable fundamental research on its application at supersonic speeds is still required, laminar-flow control does not appear feasible for the first generation supersonic transport. Any possibility of reducing the level of the turbulent skin friction, therefore, should not be overlooked.

Previous research has shown that injection of air into the turbulent boundary layer through porous surfaces will significantly reduce the skin friction. The use of extensive porous surfaces on an airplane, of course, is not a very practical arrangement. In addition, such injection would result in a complete loss of all the momentum available in the injected air and a net drag increase rather than a decrease could occur. A preliminary investigation was made recently at a Mach number of 3 to determine whether injection through rearward inclined slots would reduce the skin friction and at the same time provide some recovery of the momentum of the injected air.

Discussion

Rearward-facing inclined flush slots and rearward-facing inclined step slots of various widths were tested near the leading edge of a flat-plate model. (See fig. 1.) Pertinent results for the most effective slot configuration so far tested are presented in figure 2 where flat-plate drag coefficient is plotted against a mass-flow parameter. The lower curve presents the variation of the measured C_D with rate of air injection through a 0.0085-inch rearward-facing inclined flush slot. This drag coefficient includes the reduction in skin friction as well as the momentum recovered from the injected air. The upper curve indicates the reduction in C_D that could be obtained if the same air were ejected overboard in the usual manner through a sonic nozzle. The fact that the drag is lower when the air is injected into the boundary layer indicates a reduction in skin friction.

A possible application of slot injection to one of the SCAT configurations is presented in figure 3. A four-engine SCAT 16 configuration at a Mach number of 3 and an altitude of 65,000 feet was selected. The

abscissa is the air injection flow in pounds per second through inclined slots on selected parts of the airplane where the air used is part of the inlet bleed air. It was estimated that the inlet bleed air at the assumed flight condition amounts to about 100 pounds per second. The ordinate is the ratio of the total airplane drag coefficient with injection over the indicated parts to the total drag coefficient without injection. The denominator includes the reduction in drag obtained from the expected thrust of all the inlet bleed air. Up to the first vertical line, it was assumed that part of the bleed air, as indicated on the abscissa, is injected through a slot near the leading edge of each of the four nacelles. The momentum recovered with the slots and the thrust lost from the decreased mass flow through the inlet bleed nozzles is included in the curve. The maxim injection flow rate over the nacelles of about 25 pounds per second is equivalent to a flow parameter of 1.00 · the maximum plotted in figure 2. At this injection flow rate, an overall reduction in drag of about 1.1 percent is indicated. If additional bleed air can also be injected over the vertical and horizontal tails up to the same maximum flow rate of 1.00, the net drag reduction is 2.3 percent. The same rate of injection over the aft part of the fuselage behind the passenger compartment increases the drag reduction to about 3 percent. If further research indicates that the skin friction will continue to decrease with increased flow rate (as fig. 2 indicates may be possible), further gains will be possible by injecting a greater amount of the available boundary-layer bleed air. In addition, perhaps other sources of air, such as part of the cabin cooling air, can be used for injection over other surfaces of the airplane. The feasibility of doing this depends upon many considerations, one of these being the weight increase required for any additional ducting. The point to be made, however, is that the total drag reductions that are indicated on this figure warrant further study of the use of air injection for reducing the turbulent skin friction.

BOUNDARY-LAYER TRIPS

Introduction

In paper no. 8 by K. R. Czarnecki, Mary W. Jackson, and William J. Monta, recent turbulent skin-friction data at high Reynolds numbers are presented to assist in the extrapolation of wind-tunnel model drag data to flight conditions. To obtain fully turbulent flow over the wind-tunnelmodels, it is almost always necessary to fix transition in the leading-edge regions of the various components. To do this, distributed roughness trips are most commonly used. The use of trips, however, requires a knowledge of their effect on the model drag. Ideally, the trip will cause an increase in drag due to the forward movement of transition only and will have no additional drag itself. If the trip is too

large, in either width or roughness height, it will add an additional amount of drag to the model. This drag increment is very difficult to estimate accurately, and the use of such trips should be avoided. In order to provide some information on the drag contribution of various three-dimensional boundary-layer trips, an experimental program is underway at Mach numbers of 3 and 4 on a flat-plate model.

Discussion

In figure 4, photomicrographs of typical boundary-layer trips are shown. An indication of the size of the trips can be obtained by noting the 1/4-inch length shown. The airflow is from left to right and the leading edge of the flat plate can be seen in each of the photographs. The left and center photographs show 1/4-inch-wide bands of carborundum grains - the left one beginning at the leading edge and the center one beginning 1/4 inch behind the leading edge. A narrow band of particles beginning 1/4 inch behind the leading edge is shown in the right photograph.

The drag results obtained with these three trips at a Mach number of 3 are presented in figure 5. The drag coefficient of the flat plate is plotted against the mean height of the carborundum grains in the trip. The drag coefficient was determined by a boundary-layer momentum survey $8\frac{1}{2}$ inches from the leading edge. The roughness height at which the trips at the 1/4-inch position equal a roughness Reynolds number of 600 is indicated. It is apparent that the trips at 1/4 inch do not affect transition when they are smaller than this height and do cause transition to move forward when they are larger. After the trip is high enough to cause transition, there is a range of sizes where the drag is constant; thus, there is probably no additional drag due to the trips themselves over this range. At larger sizes, the trip does cause additional drag as shown by the increase at the larger heights. The wide trip at the leading edge causes an additional drag which is larger than that associated with moving transition to the leading edge. This additional drag is most likely due to the fact that the roughness required to fix transition very near the leading edge actually protrudes through the boundary layer.

In order to determine whether the drag measured with the narrow band of distributed carborundum includes any trip drag, comparison was made with a trip consisting of a single row of evenly spaced spherical particles. The spherical particles (fig. 6) were placed at 1.9 inches from the leading edge, slightly ahead of natural transition, to allow the use of larger, more easily handled, particles. The photograph on the right is of a narrow band of distributed carborundum at the same position.

The single row of spherical particles is close to the ideal trip, since it contains the least number of particles to cause drag and the height of the particles can be accurately controlled.

Figure 7 shows the results of this comparison at Mach 3. The drag coefficient is once again plotted against roughness height. The narrow band of distributed roughness is represented by the triangles and the single row of glass beads by the circles. All the data presented are for roughness Reynolds numbers greater than 600. The curves show that a narrow band of distributed particles produces the same drag results as a single row of glass beads. The roughness height can be two to three times that required to fix transition before either the single row or narrow band of distributed roughness starts to contribute roughness drag. These results show that the use of a correctly sized narrow band of sparsely distributed roughness on wind-tunnel models will fix transition as desired and will not cause an additional trip drag.

An example of the application of this type of trip to a wind-tunnel model (fig. 8) is shown in figure 9. The configuration (fig. 8) was a clipped-tip delta-wing airplane model which was tested at $M = 1.61$. The model was tested with transition free and with three different sizes of carborundum grains in narrow trips, (See fig. 9.) The turbulent curve represents the model drag coefficient calculated with complete turbulent flow and with a wave drag coefficient of 0.0092. The gradual increase in drag with Reynolds number for the free-transition case indicates a slow forward movement in transition. As the roughness size is increased, the drag is equivalent to the value for transition at the trip at lower unit Reynolds numbers, as expected. In fact, the roughness Reynolds number for transition at the trip is approximately 600 in each case. The data points show that through a limited Reynolds number range, transition is fixed at the roughness without additional grit drag. At the higher Reynolds numbers, where the larger grit heights tested are considerably greater than the height required to fix transition, the grit begins to cause additional drag. This result clearly indicates that if the grit is sized to fix transition at a low Reynolds number, there is a limit to the range of Reynolds number through which tests should be made with only one grit size.

CONCLUDING REMARKS

The results of the tests on three-dimensional boundary-layer trips show that a narrow band of correctly sized sparsely distributed carborundum located behind the leading edge will fix transition without additional trip drag. The use of such trips, then, will allow an extrapolation of wind-tunnel drag to full-scale values with confidence. However, if a wide trip, a leading-edge location, or too large a roughness height

is used, excess trip drag will result which is difficult to estimate. The use of such trips, therefore, should be avoided. With regard to air injection into the turbulent boundary layer, the initial results on injection through rearward-facing inclined slots indicate that further study is warranted.

INJECTION CONFIGURATIONS

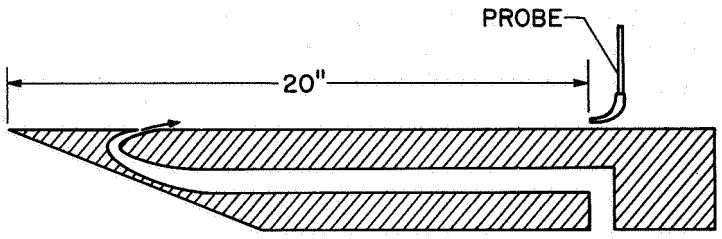

REARWARD-FACING INCLINED FLUSH SLOT

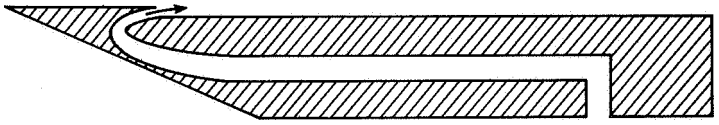

REARWARD-FACING INCLINED STEP SLOT

Figure 1

EFFECTIVENESS OF AIR INJECTION
M=3.0

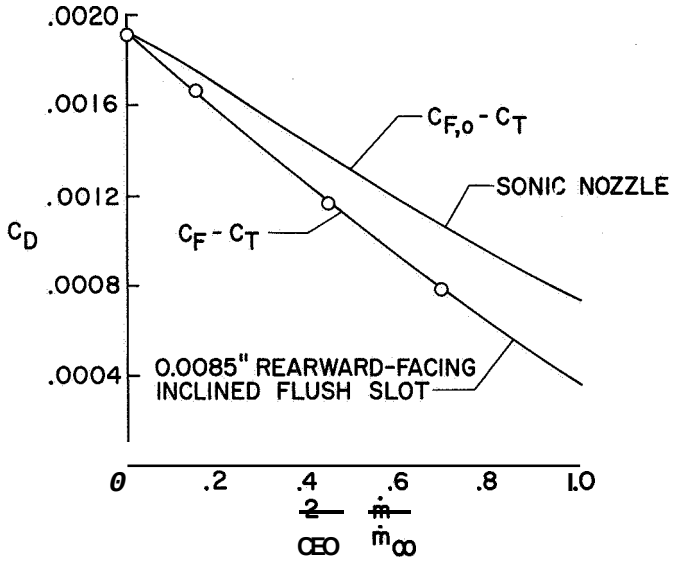

Figure 2

RECEIVED

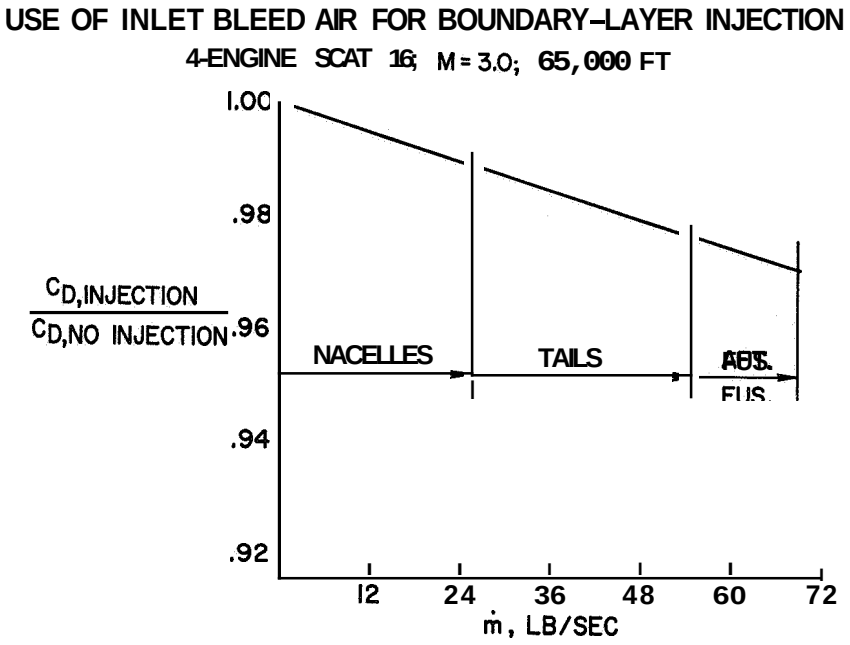

Figure 3

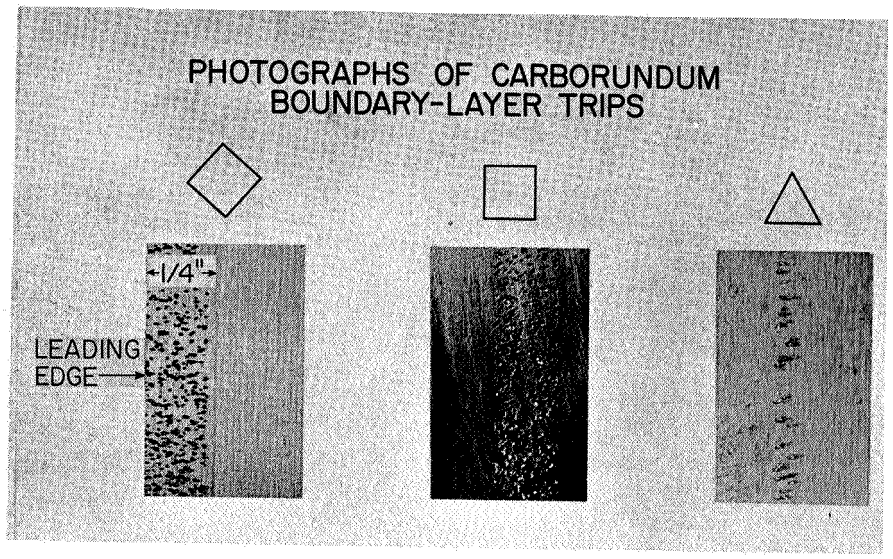

Figure 4 L-2104-4

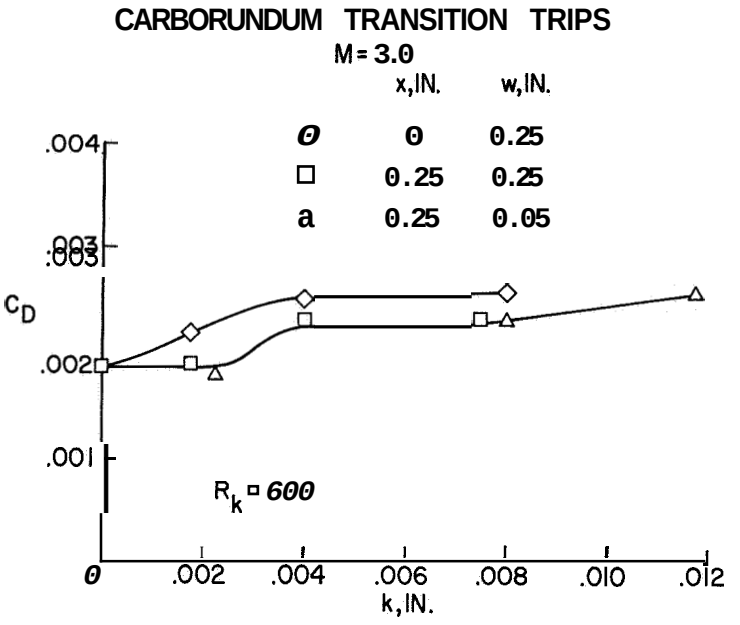

Figure 5

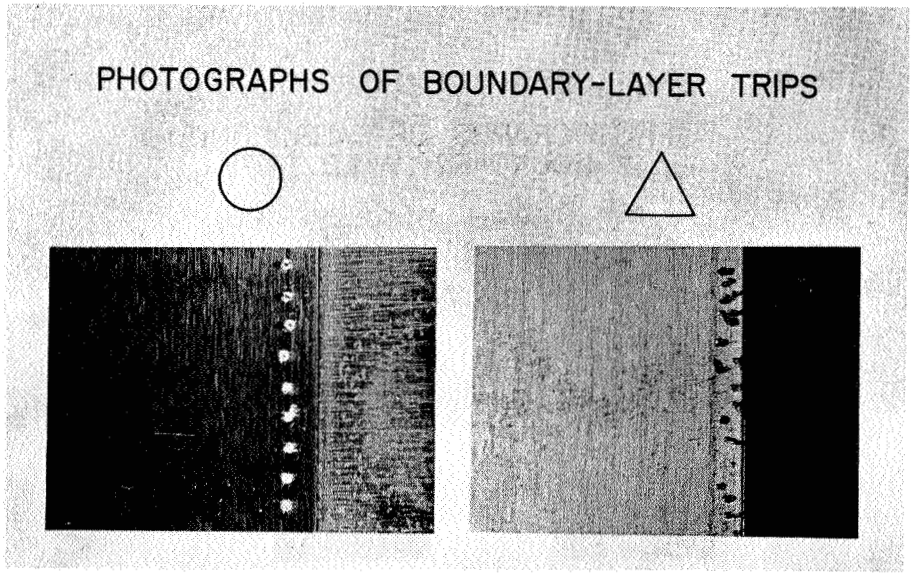

Figure 6 L-2104-6

COMPARISON BETWEEN SINGLE ROW AND DISTRIBUTED ROUGHNESS TRIPS

M = 3.0

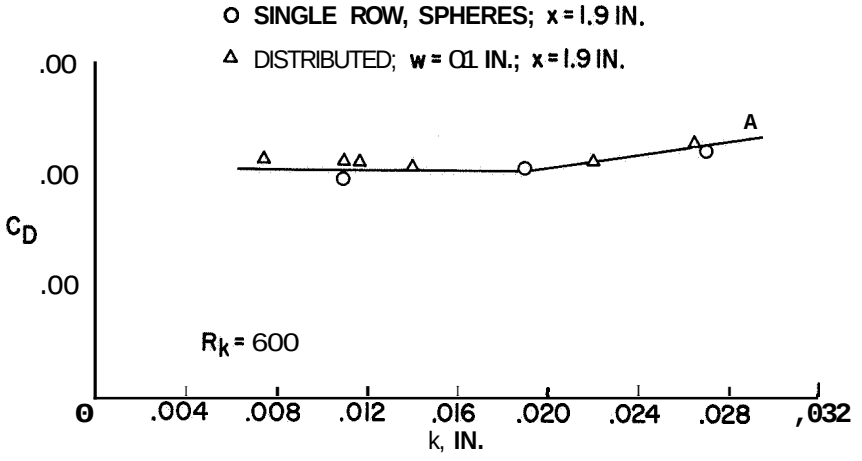

Figure 7

MODEL CONFIGURATION

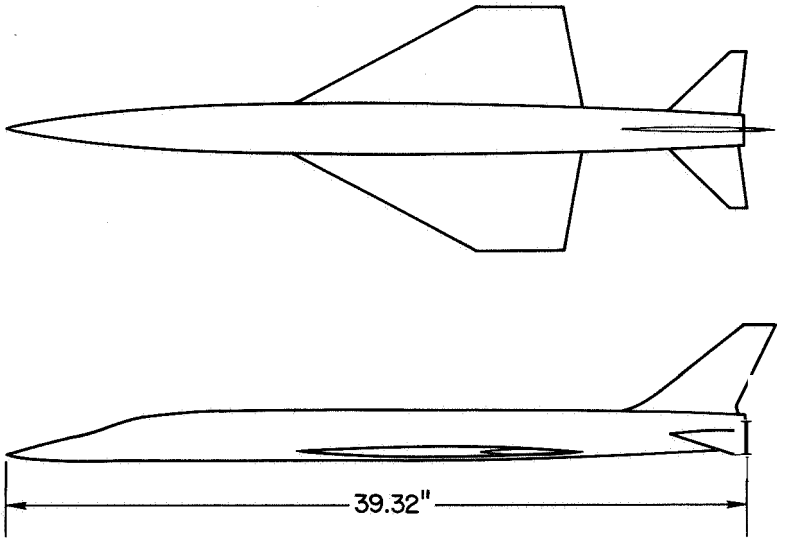

Figure 8

EFFECT OF BOUNDARY-LAYER TRIPS ON $C_{D,\alpha=0}$

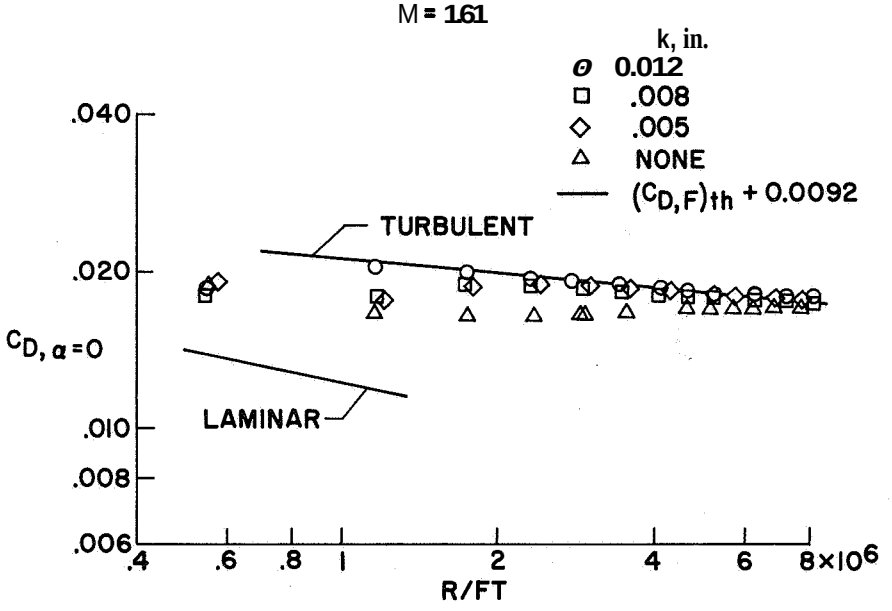

Figure 9

N67-31617

10. CONFIGURATION EFFECTS ON THE CHARACTERISTICS OF DELTA-WING SUPERSONIC TRANSPORTS

By Adrien E. Anderson

NASA-Ames Research Center

SUMMARY

11952

This paper discusses a number of items which are characteristic of or influence the characteristics of delta-wing supersonic transports. The topics discussed include: a comparison between the stability characteristics of the basic SCAT 17 configuration and configurations similar to the SCAT 17 designs proposed by the two feasibility study contractors; the lateral stability problem which arises when a design is compromised to achieve higher efficiency and directional stability; possible configuration and control utilization changes which can be made to improve efficiency; the effect of airfoil section and flap deflection on transonic efficiency; low-speed high-lift studies; and finally, aileron and spoiler characteristics obtained at high Mach numbers, The material presented is based on a portion of the studies made at the Ames Research Center in the course of evaluating the SCAT 17 configuration.

conf AUTHOR

INTRODUCTION

The primary emphasis in the SCAT 17 configuration is toward simplicity in design, and at the same time meeting the rigorous low-speed requirements and the high efficiency needed at supersonic speeds. The aft stabilizing tail was incorporated in the design to allow good longitudinal stability combined with adequate control at low speeds and to serve a dual function at higher speeds. Drooping the stabilizer to large anhedral angles permits some control over the natural rearward aerodynamic-center shift which occurs with increase in Mach number and allows improvement of the directional stability which tends to decrease with increase in Mach nuniber. In the feasibility study the two contractors submitted configurations which employ either the canard or the aft stabilizer, but not both. Thus, it is of interest to study the stability characteristics of the alternate concepts and compare them with the basic SCAT 17 configuration.

The development of high efficiency in the transonic and low-speed flight zones is as important as high efficiency at $M = 3$ because at

p 203-221 refs

transonic speeds, where the drag of the aircraft is high, high efficiency allows operation of the aircraft at lower drag levels, and less engine thrust is required for acceleration. At landing, high efficiency permits lower landing speeds. The importance of high efficiency has led to an extensive study of the effectiveness of leading-edge flaps as a means for improving the characteristics of the configuration.

The possibility of engine failure at high speeds places large demands on the aileron system, since aileron effectiveness has decreased considerably with Mach number. Thus, an investigation was made to determine the ability of wing spoilers to provide roll. control at supersonic speeds.

The material presented in this report is from studies made in the Unitary Plan wind tunnels and the 40- by 80-foot wind tunnel at the Ames Research Center.

NOTATION

a.c.	aerodynamic center, percent $\bar{c}$
b	wing span
b'	local span
c	wing chord
$\bar{c}$	wing mean aerodynamic chord
c.g.	airplane center of gravity
C	canard
C_L	lift coefficient
C_l	rolling-moment coefficient
C_{l_β}	dihedral parameter, $\frac{\partial C_L}{\partial \beta}$
C_n	yawing-moment coefficient
C_{n_β}	directional stability, $\frac{\partial C_n}{\partial \beta}$

[redacted]

D	drag
E	elevon
h	spoiler height above surface of wing
i	incidence angle
L	lift
L/D	lift-to-drag ratio
M	Mach number
t	thickness of wing section
t/c	wing thickness to chord ratio
α	angle of attack
β	angle of sideslip
Γ	dihedral angle
δ	deflection angle of control surface

Subscripts:

a	aileron
f	wing trailing-edge flap
max	maximum
n	wing leading-edge flap
S	stabilizer
T	wing tip
w	wing

DISCUSSION

Early in the feasibility studies the two study contractors took exception to the folding stabilizer of the basic **SCAT** 17 on the basis

[redacted]

that the jet blast impinging on the stabilizer in the down position might create stability problems as well as thermal and dynamic structural problems. Subsequently, the stability problem appears to be an insignificant one on the basis of large-scale wind-tunnel studies, and the structural situation appears to be one of whether you desire to pay the weight penalty of the heavier structure required to withstand the blast.

The study contractors suggested alternate designs which avoided the concept of the folding aft stabilizer. Thus, the thought arises as to the relative static stability characteristics of the three versions. In the NASA wind-tunnel tests, various studies were made to determine the aerodynamic contribution of a particular component of the basic configuration and in some cases substitute components. From these data it is possible to compare alternate configurations. This information is being presented to show the potentiality of various components and configurations and should not be construed as reflecting on the contractors' proposals, for no attempt was made to optimize the geometric relationship among the components in the alternate cases.

Figure 1 presents the variation of aerodynamic center a.c. in percent of the mean aerodynamic chord E with Mach number for the three configurations indicated in the silhouettes. In the case of the alternate configurations, the fuselage length and the location of the wing on the fuselage are identical to those of the basic configuration (center silhouette in fig. 1). At a Mach number of 0.9, as noted in the figure, the aft stabilizer dihedral angle is changed from 0° to -75° (down) on the basic SCAT 17. This change reduces the variation of aerodynamic center with Mach number. Had the stabilizer not been deflected, the movement of aerodynamic center would have been rearward, and at $M = 3$ would have been located at the value indicated by the "dot." The aerodynamic-center variation for the canard configuration without stabilizer is very similar to that of the basic configuration; however, the aerodynamic-center location is slightly forward. Removal of the canard produced a sizable rearward shift of the aerodynamic center and a larger variation of aerodynamic center with Mach number, as indicated by the top curve.

The large rearward aerodynamic-center shift produced by removing the canard indicates that the aerodynamic-center travel in the canard configuration might be reduced through the use of either a folding tip, a variable sweep, or a servo-controlled canard. The canard, if servo-controlled at subsonic speeds and adjustable at supersonic speeds, would allow a low-speed aerodynamic center which is almost equal to the cruise aerodynamic center, namely, 34 percent $\bar{c}$ versus 32.5 percent E. An abrupt change in aerodynamic center would occur at the Mach number where the canard is locked to the control system and some form of stability augmentation undoubtedly would be required. In the case of the

canard-off configuration, deflecting the stabilizer up would provide some aerodynamic-center control.

If the low-speed static margin is arbitrarily set at 2 percent (which is equivalent to around 18 inches on a 425,000-pound aircraft) and assuming no center-of-gravity change with Mach number, the static margin would be 9.0 percent at $M = 3$ for the basic configuration, 9 percent on the canard version, and around 15 percent on the canard-aft configuration. It should be borne in mind that this analysis assumes a rigid aircraft and that aeroelastic effects may alter these results.

The directional stability characteristics of the three configurations at $\alpha = 4^\circ$ is indicated in figure 2. The abrupt increase in C_{n_β} at $M = 0.9$ for the basic configuration results from deflecting the stabilizer. If the stabilizer is not deflected, the $M = 3$ stability level is lower as indicated by the "dot." This value is very close to that for the canard configuration. The directional stability of the canard configuration is less than that for the canard-off configuration because the canard produces a destabilizing effect by increasing the pressures on the up-wind side of the fuselage. These data are for zero canard deflection, but with the model set at cruise attitude ($\alpha = 4^\circ$). Thus, a further decrease in directional stability would be expected when the canard is deflected or the angle of attack is increased. In the canard configuration presented, the vertical tail is aft of the wing trailing edge and hence is more effective than if it were located directly over the wing.

The dihedral parameter is presented as a function of Mach number in figure 3. Positive stability is indicated by a negative value of C_{l_β}. The stability level decreases rapidly in the supersonic range and is lowest for the basic configuration. At $M = 3$, the value of C_{l_β} indicates a small amount of negative stability and, when compared with the "dot," shows that deflecting a surface could lead to a serious problem.

In the course of evaluating the basic SCAT 17 configuration, the use of deflected wing tips was investigated as a means of controlling the aerodynamic center. The strong negative dihedral effect of deflecting the wing tips is indicated in figure 4. The solid curve represents the case when both the stabilizer and the wing tips are undeflected. Deflecting the stabilizer at $M = 0.9$ reduces the stability somewhat; but when the wing tips are deflected from 0° at $M = 0.9$ to -60° at $M = 1.4$, an appreciable reduction in C_{l_β} occurs and a negative stability condition results. (The wind-tunnel studies indicated that the deflecting of the wing tip should be programed over the Mach number range from 0.9 to 1.4 to avoid abrupt variations in aerodynamic-center travel.) It would appear then that using wing-tip deflection to control

aerodynamic-center travel would be detrimental in the case of all three configurations shown in figure 3, since each has such low values of C_{l_β} at the higher Mach numbers.

In figure 5, the directional stability which could be achieved at M = 3 by deflecting the wing tips is presented and is found to be about twice that for the configuration with the wing tip and stabilizer at 0° and only half again as large as that for the configuration wherein the stabilizer had been deflected to a dihedral angle of -75°. Although the deflected wing tips increased C_{n_β}, their detrimental effect on C_{l_β} warranted the consideration of other configurations. The aerodynamic contribution of the alternate tail arrangements shown in figure 6 was determined in the course of the investigation. A side view of the low stabilizer deflected -75°, which is the reference configuration, is shown at the left. In the central figure is a high stabilizer, at zero dihedral, in combination with a small ventral fin which allows ground clearance. Note the relationship of the tail surfaces to the wing. The square end on the fuselage is the shape of the wind-tunnel model which was sting mounted. At the right is a high stabilizer deflected to a dihedral angle of 37.5° and a large ventral fin. The large ventral fin provided approximately one-half as much C_{n_β} with only one-tenth the C_{l_β} penalty of the deflected wing tips at M = 3. Positive deflection of the stabilizer to 37.5° provided approximately one-half as much C_{n_β} as deflecting the wing tips, but was beneficial in its effect on C_{l_P} and aerodynamic-center shift.

Figure 7 is included to indicate how deflecting the wing tips and the stabilizer affects aerodynamic-center travel on the basic SCAT 17. The smaller the variation in aerodynamic-center travel, the smaller will be the trim drag. The question is: How important is aerodynamic-center travel in affecting the trim drag of the basic configuration? Figure 8 presents the wind-tunnel model values of $(L/D)_{max}$, at a Reynolds number of 5×10^6, as a function of Mach number. The lower curves are for the three configurations in figure 7 when they are trimmed by deflecting the canard. The assumption is that there is a 2-percent static margin at M = 0.7 and that the center of gravity does not change with increase in Mach number. The trim curve for the configuration with the surfaces undeflected is quite far below the untrimmed curve. On the other hand, deflecting the stabilizer to a dihedral angle of -75° raises the curve appreciably, and deflecting the wing tips brought small gains in the low supersonic range, but a slight loss at M = 3.

Now there are other techniques for improving trim, two of which were investigated in the studies. One, shown in figure 9, was to incorporate wing incidence. The configuration considered here is the one

with the stabilizer deflected at -75°, the tips at 0°, and the canard is used for trim. It will be seen that an incidence of -1° (negative being trailing edge up) produces an appreciable increase in the trim $(L/D)_{max}$, whereas +1° caused a small loss at the higher Mach numbers.

Another possibility, shown in figure 10, is to develop maxim utilization of the control systems. The curve for trim with the canard alone is a repeat of the solid curve in figure 9. If trim is by elevon alone, the trim L/D drops greatly. However, when a combination of both the elevon and canard is used, it is possible to achieve an additional gain in $(L/D)_{max}$. In this case the elevon setting amounts to roughly 2° throughout the Mach number range.

Figure 11 presents a summary of what may be accomplished when the two concepts just described are applied in trimming the aircraft. The top curve is for the untrimmed configuration, whereas the bottom curve is for the configuration with the stabilizer deflected, but this time the wing is at -1° incidence and both the canard (C) and elevon (E) are used for optimum trim. This trimmed curve is much closer to the untrimmed curve and higher than the curve for the configuration where the wing tips were deflected (refer to fig. 8). Thus, it appears that high values of trim $(L/D)_{max}$ may be achieved without resorting to deflecting the wing tips.

In the SCAT 17 studies, the $(L/D)_{max}$ that was realized in the transonic speed range was rather disappointing. It was believed that the low L/D values might be due to the shape of the forward portion of the airfoil section of the wing. The data of figure 12 are presented to facilitate an understanding of the approach used to improve the L/D characteristics. The basic airfoil section of the wing was a 30 - 70 hexagon, 2 percent thick. The 30- and 70-percent points are indicated by the lines in the plan view and the 30-percent chord station by the arrow in the section view. Several years ago Menees of the Ames Research Center reported (ref. 1) that a delta planform wing incorporating the outboard 5 percent of the semispan of a wing having conical camber over the outboard 20 percent of the semispan had essentially the same efficiency as a wing with 20 percent of the semispan cambered. In SCAT 17, this concept was simplified - the outboard 5 percent of the local semispan was deflected down approximately 3.1° in the streamwise plane. The chord of this portion of the wing increases toward the tip. The wind-tunnel studies indicated that this type of leading edge would cause no penalty at M = 3 when left deflected. The increase, in $(L/D)_{max}$ over the plane wing for three transonic Mach numbers, indicated to the right in the figure, was less than achieved in Menees' investigation.

A flap with a constant chord equal to 10 percent of $\bar{c}$ was deflected to achieve further curvature of the leading edge. Gains in $(L/D)_{max}$ of around one unit were obtained at deflection angles of 12° to 15° at speeds below M = 1, but an insignificant gain was made at M = 1.2. The semispan of the flap was shortened to the 76-percent station to see whether the gain in $(L/D)_{max}$ would warrant the complexity of incorporating a flap at the wing tip. The increments in $(L/D)_{max}$ were around 2/3 those indicated in the figure.

The airfoil section used in the study made by Menees was an NACA 0003-63. Since his results indicated a gain in $(L/D)_{max}$ of 3, 2, and 1.3 units for M = 0.70, 0.95, and 1.20, respectively, it was felt that the thickness as well as the curvature of the leading edge was playing an important part in the results. Tests have been made recently with the leading edge modified as indicated in the bottom section of figure 12. In this case the camber line is that used by Menees and the top half of the airfoil section is an NACA 0002, which reaches maximum thickness at the 30-percent chord station. The lower surface has been faired straight back from the leading-edge radius to the 30-percent chord point. The gains in $(L/D)_{max}$ were not significant; in fact, at M = 3 there was a loss in $(L/D)_{max}$. These results are consequently considered to indicate that further study is required in this area.

The large-scale model used in the low-speed high-lift studies is presented in figure 13. In this model the airfoil section is an NACA 0003-03, which provides for a wing with a sharp leading edge, but with smooth curvature from the leading edge to the 30-percent chord station. Figure 14 gives an indication of the gains to be obtained by deflecting the leading-edge flap at M = 0.2 for the wing-body combination. In the plot of L/D as a function of C_L the undeflected flap condition is indicated by the solid curve, the 30° flap deflection by the dash-double dot curve, and the 45° flap deflection by the dash-dot curve. In this case, appreciable gains were made, and when the canard indicated in the figure was added to trim the vehicle, only small losses occurred. When only the portion of the flap out to the 76-percent semispan station was deflected, the peak of the L/D curve fell about midway between the 0° and 45° deflection curve. The optimum leading-edge flap angle will vary with the deflection of the trailing-edge flap. This information was taken from an investigation recently made by David G. Koenig of the Ames Research Center. This investigation also included information regarding midchord flaps and small wing planform variations.

Other work completed at Ames used the large-scale model to evaluate flap designs, effectiveness of various canard planforms, and canard flaps (refs. 2 and 3). The best way to sum up this work and indicate the present state of the art insofar as the achievements of reasonable

landing approach speeds is to use figure 15, which is from an IAS paper by J. L. Jones, et al. (ref. 4). Indicated in this figure is a comparison of the thrust-to-gross weight ratios and corresponding flight velocities to be expected with various nose and trailing-edge flap combinations. At the right is a canard configuration with no wing flap deflections and the center of gravity at the 18-percent chord station. This vehicle landing at a wing loading of 40 pounds per square foot and a static margin of 3 percent would have to approach at 212 knots or higher to avoid the range of speed instability which is the condition where an increase in thrust is required to maintain the flight path with decreasing speed. Deflecting the leading-edge flap 45° and the trailing-edge flap 10° (same static margin) reduces the speed to around 170 knots. The addition of the aft tail permits the trailing-edge flap angle to be increased to 20° and provides a more rearward center-of-gravity position, namely, 26 percent $\bar{c}$. The speed is then reduced to 145 knots. The fourth curve in the figure is for a larger canard which free floats. This allows a landing speed of 135 knots with the center of gravity at 30 percent $\bar{c}$.

Aileron effectiveness was found to decrease considerably at supersonic speeds and additional roll capability appeared necessary. Consideration was given to the use of wing spoilers and the results of the study are given in figure 16. On the right is a plan view of one wing panel. The aileron, designated as aileron A had a chord equal to 15 percent of the local chord, and extended to the 76-percent semispan station. Three sizes of spoilers located along the 80-percent-chord line and mounted perpendicular to the wing surface were tested. The spoiler designated as spoiler B extended to the 34-percent semispan station, while that designated spoiler C extended to the 76-percent station. In the left portion of the figure is a plot of rolling moment as a function of Mach number in the supersonic range.

Airplane roll is indicated for two differential aileron deflections, ±5° and ±10°. Aileron effectiveness at $M = 3$ is 0.00014 and is adequate to hold wings level to 5° of sideslip for deflections of ±5°. At lower Mach numbers, however, higher differential deflections would be required. Tests made to determine the effectiveness of various segments of the aileron indicated that the outboard three panels provide nearly all of the roll. Spoiler B was not too effective for a height-to-chord ratio of 0.03. A sizable gain was made at $M = 3$ by going to twice the height. The latter effectiveness was almost doubled by going to the full-span spoiler. More research is considered necessary in the area of aileron-spoiler effectiveness, because spoilers of this size, that is, over 6 feet high, at the inboard end essentially double the drag of the aircraft. Perhaps a combination of spoiler and aileron is the answer.

Additional material including engine-out and dynamic stability studies of a configuration similar to SCAT 17 will be found in references 5 through 8.

CONCLUDING REMARKS

The results presented herein on SCAT 17 indicate that:

1. The aerodynamic-center shift and the directional stability of the three types of configurations may be improved by deflecting surfaces, but there is the danger of getting into a dihedral-effect problem on all SCAT 17 configurations if the wing tips are deflected.

2. The trim drag may be improved by the use of negative wing incidence and judicious use of the canard and elevons so as to eliminate the need for deflecting the wing tips.

3. In the transonic and low-speed flight zones, improvements in L/D have been gained by the use of leading-edge flaps, and further improvements appear possible through the modification of the airfoil section, although additional studies are required.

4. An evaluation has been made of simple high-lift devices which, when combined with the aft stabilizer, permit landing speeds comparable to present-day jet-transport aircraft.

5. Aileron and spoiler studies indicate deficiencies which indicate a need for further study.

RESTRICTED

REFERENCES

1. Menees, Gene P.: Lift, Drag, and Pitching Moment of an Aspect-Ratio-2 Triangular Wing With Leading-Edge Flaps Designed to Simulate Conical Camber. NASA MEMO 10-5-58A, 1958.

2. Brady, James A., Page, V. Robert, and Koenig, David G. : Large-Scale Low-Speed Wind-Tunnel Tests of a Delta Winged Supersonic Transport Model With a Delta Canard Control Surface. NASA TM X-643, 1962.

3. Koenig, David G., Brady, James A., and Page, V. Robert: Large-Scale Wind-Tunnel Tests at Low Speed of a Delta Winged Supersonic Transport Model in the Presence of the Ground. NASA TM X-644, 1962.

4. Jones, J. Lloyd, Jr., Hunton, Lynn W., Gregory, Thomas J., and Nelms, Walter P., Jr.: A Critical Study of Delta-Wing Configurations for the Supersonic Transport Application. Paper No. 63-5, Inst. Aerospace Sci., Jan. 1963.

5. Fletcher, LeRoy S.: Static Stability Characteristics of a Delta Winged Configuration With a Canard Control and Nacelles at Mach Numbers From 0.25 to 3.50. NASA TM x-651, 1962.

6. Gnos, A. Vernon, and Kurkowski, Richard L.: Effect of Off-Design Inlet Mass Flow upon Static Stability of a Triangular Wing Configuration With a Canard Control and Pylon Mounted Nacelles for Mach Numbers From 0.65 to 3.50. NASA TM X-658, 1962.

7. Fletcher, LeRoy S.: Static Stability Characteristics of a Delta Winged Airplane Configuration With Nacelles, a Trapezoidal Canard, and a Drooped Tail at Mach Numbers From, 0.70 to 3.52. NASA TM X-780, 1963.

8. Fletcher, LeRoy S.: Dynamic Rotary Stability Derivatives of a Delta-Winged Configuration With a Canard Control and Nacelles at Mach Numbers From 0.25 to 3.50. NASA TM x-781, 1963.

CONFIGURATION EFFECT ON AERODYNAMIC CENTER

$C_L = 0°$

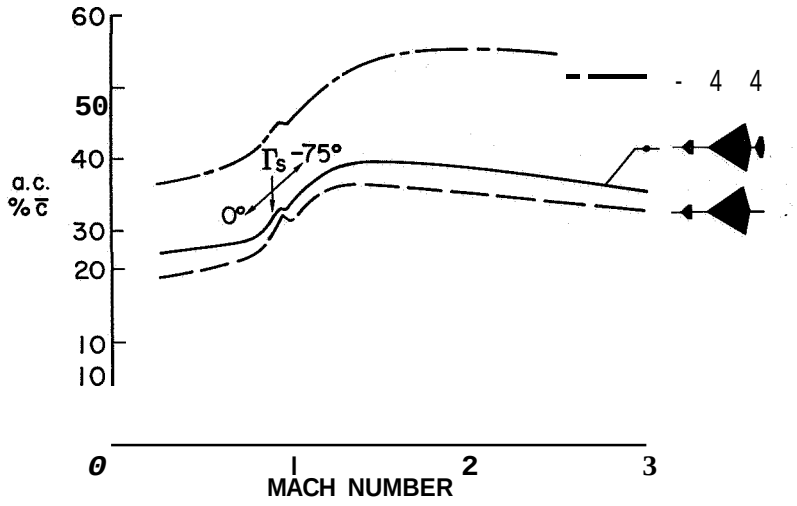

Figure 1

CONFIGURATION EFFECT ON DIRECTIONAL STABILITY

$\alpha = 4°$

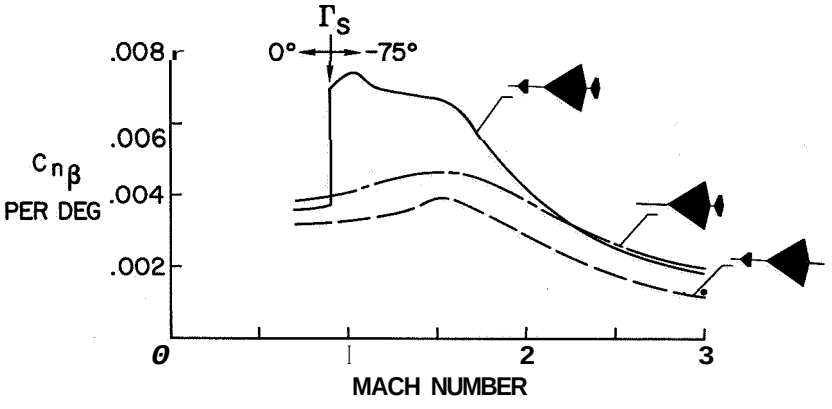

Figure 2

CONFIGURATION EFFECT ON DIHEDRAL PARAMETER

$a = 4°$

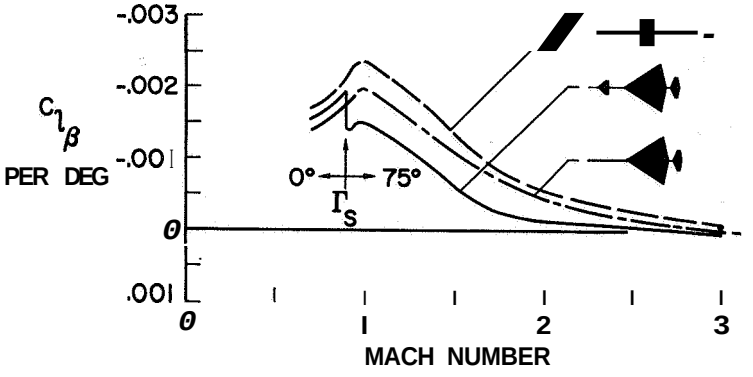

Figure 3

DIHEDRAL EFFECT, BASIC SCAT 17

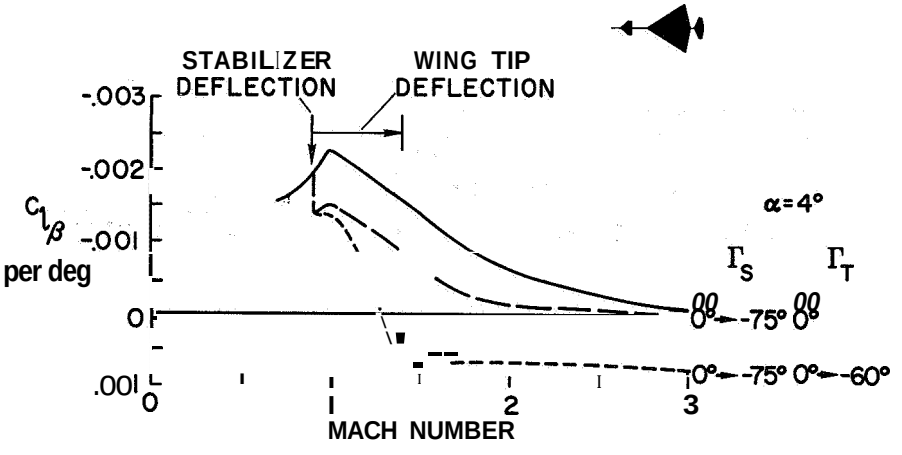

Figure 4

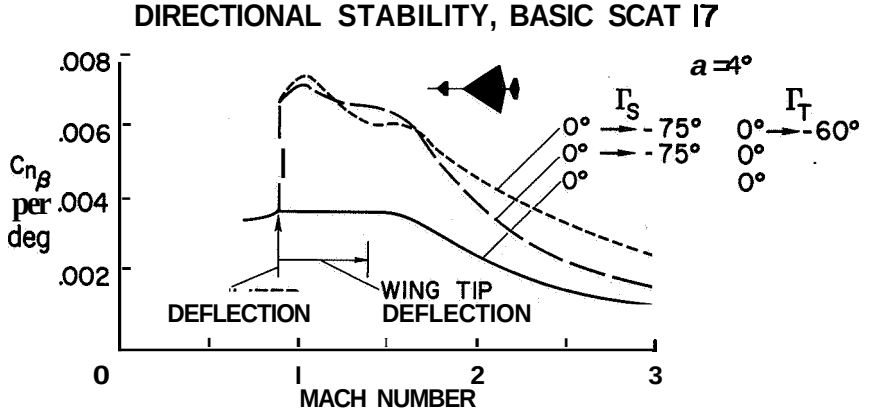

Figure 5

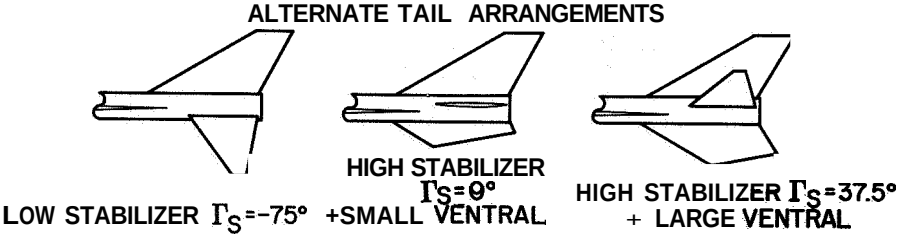

Figure 6

DECLASSIFIED

AERODYNAMIC-CENTER CONTROL, BASIC SCAT 17

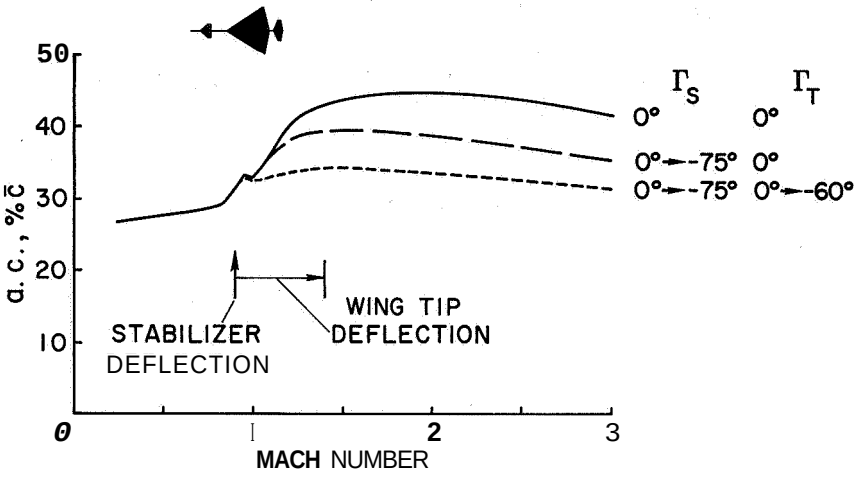

Figure 7

EFFECT OF SURFACE DEFLECTION ON L/D

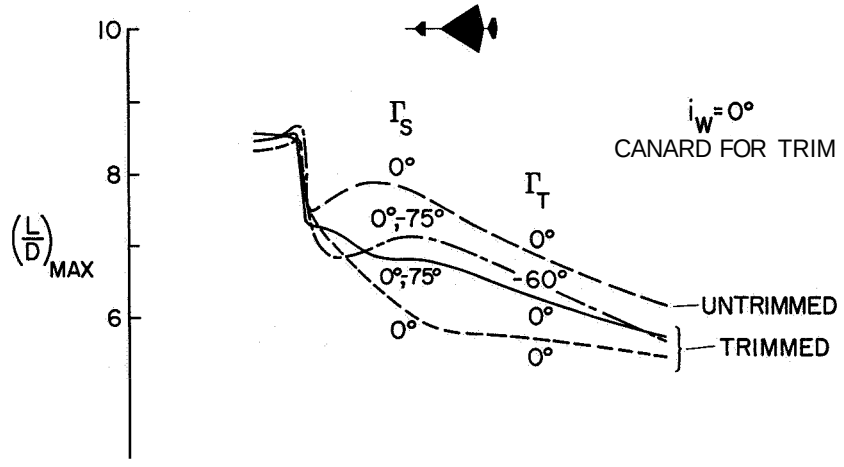

Figure 8

EFFECT OF WING INCIDENCE ON TRIM L/D

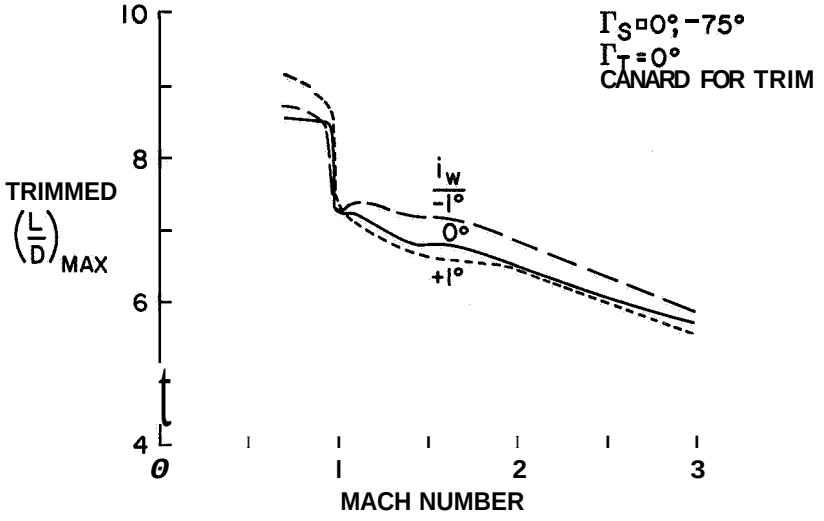

Figure 9

EFFECT OF CONTROL UTILIZATION ON TRIM L/D

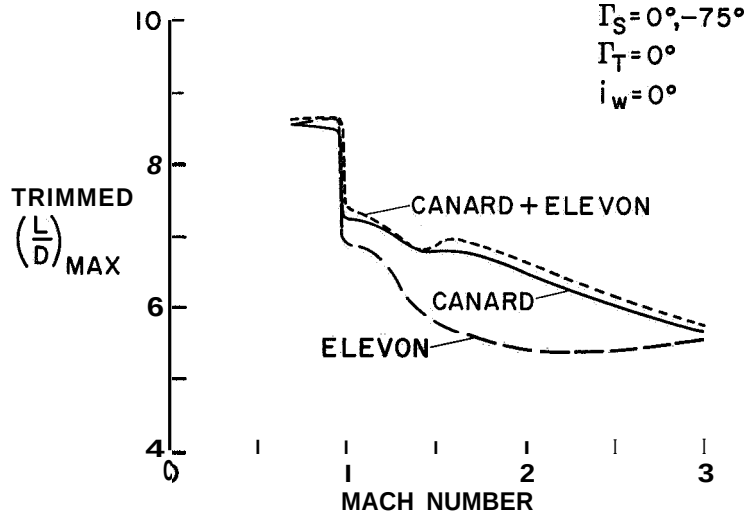

Figure 10

DECLASSIFIED

TR M L/D POSSIBLE WITHOUT DEFLECTING WING TIPS

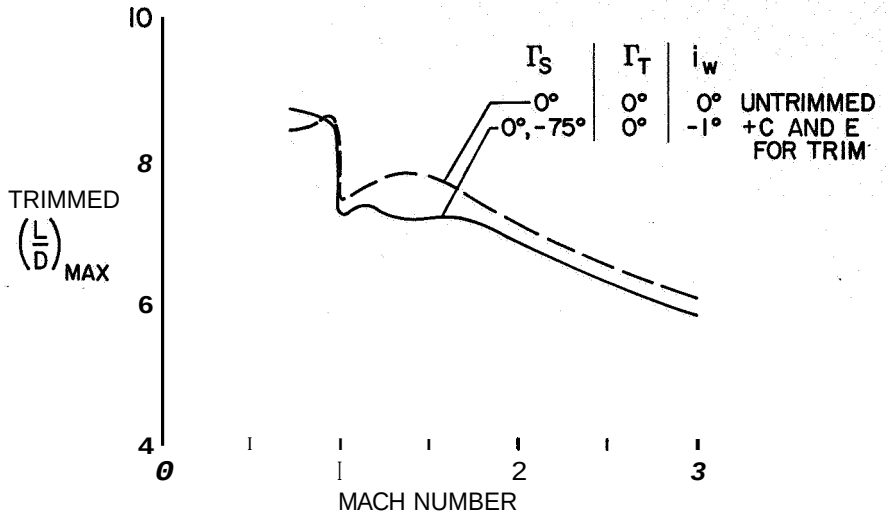

Figure 11

EFFECT OF AIRFOIL SECTION AND LEADING EDGE FLAP ON TRANSONIC L/D

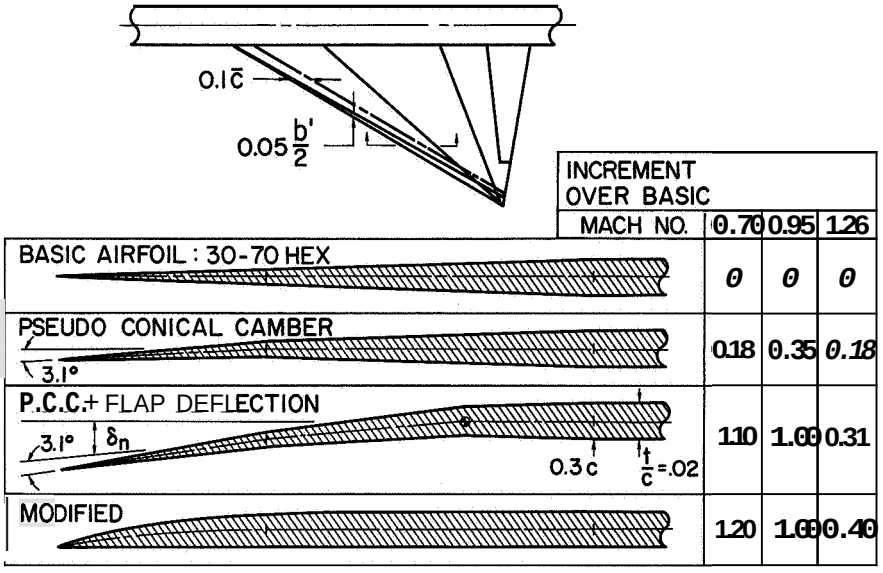

Figure 12

LARGE SCALE SCAT 17 MODEL USED IN HIGH LIFT STUDIES

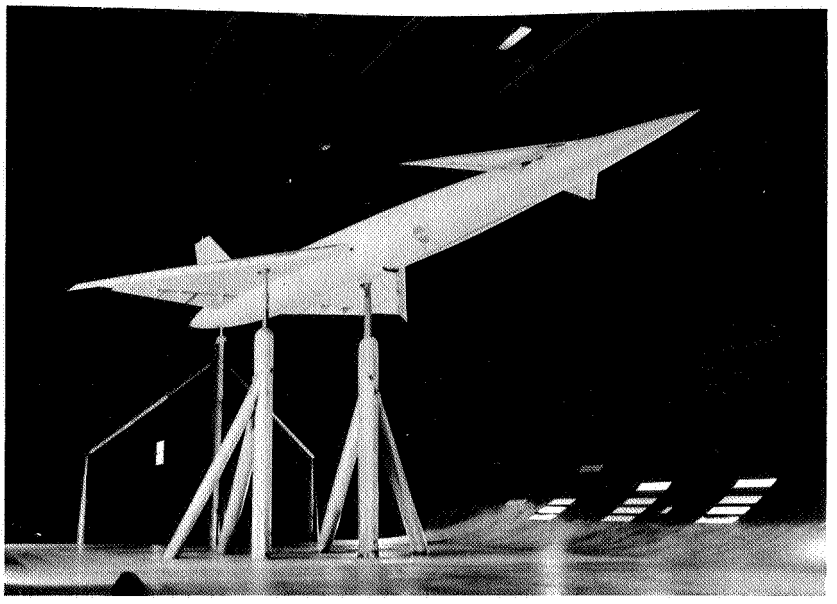

A-28218

Figure 13

EFFECT OF WING LEADING EDGE FLAP DEFLECTION

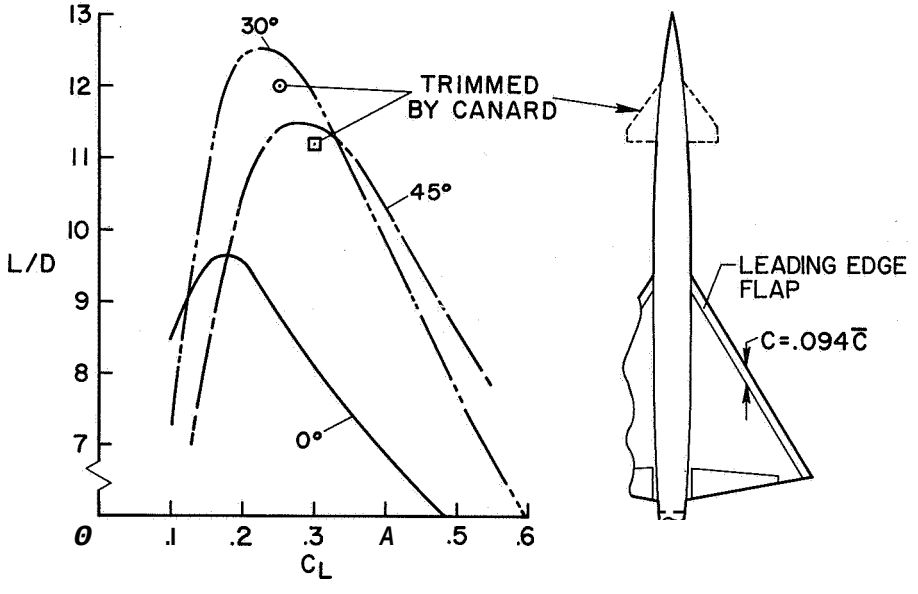

Figure 14

DECLASSIFIED

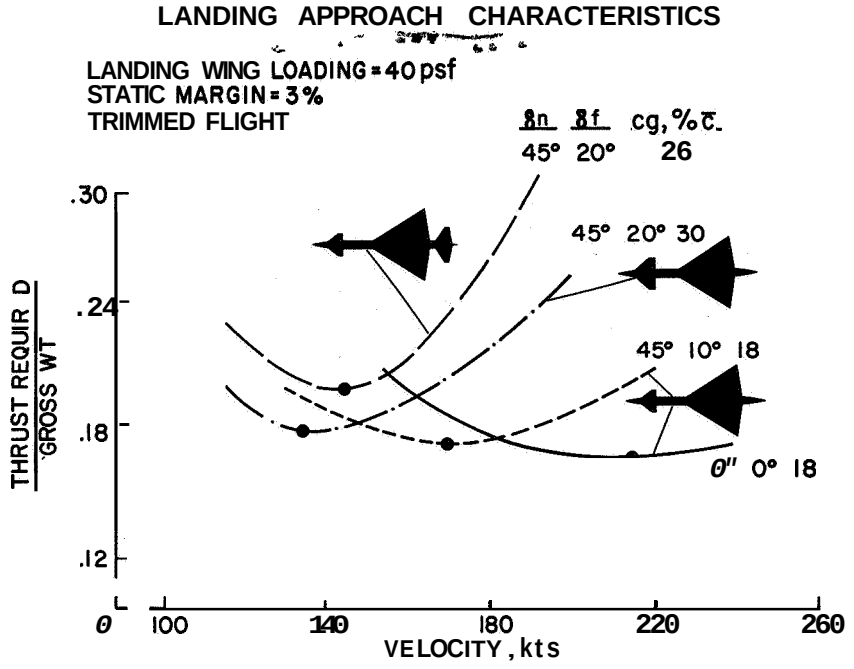

Figure 15

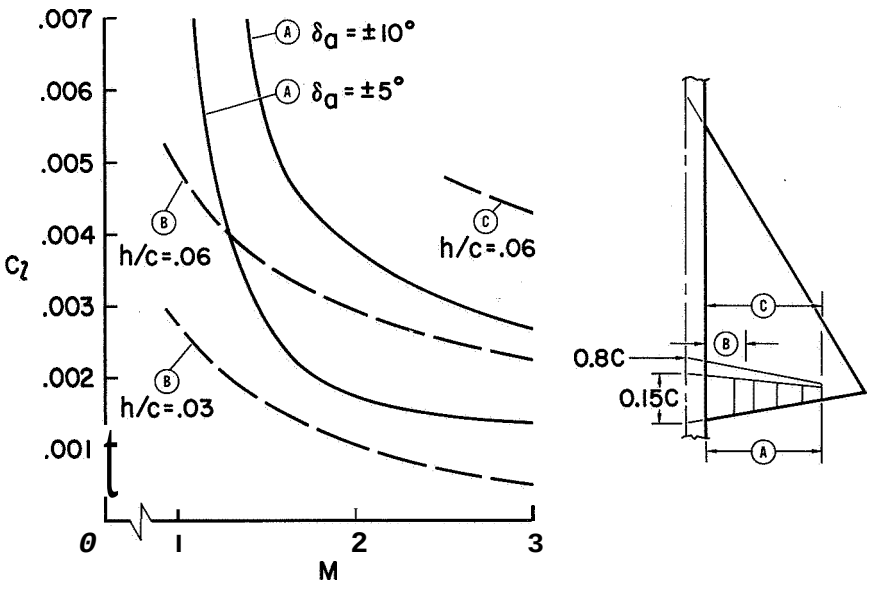

Figure 16

N67-31618

11

11. STABILITY AND HIGH-LIFT STUDIES APPLICABLE TO VARIABLE-SWEEP SUPERSONIC-TRANSPORT CONFIGURATIONS

By William J. Alford, Jr., Vernard E. Lockwood, Linwood W. McKinney
NASA Langley Research Center

and Richard K. Greif
NASA Ames Research Center

SUMMARY

11953

A consideration of the stability and high-lift characteristics applicable to variable-sweep supersonic transport configurations indicates that the more outboard pivot locations can be used to reduce the aerodynamic-center variation with wing sweep angle, and this reduction results in higher supersonic trimmed lift-drag ratios. Of the several configuration concepts considered, the smallest maximum lift-drag-ratio variation with stability level or center-of-gravity location was obtained with the auxiliary wing concept. The outboard pivot wings with fixed forward area have pitch instability problems at high lifts but these problems can be minimized by use of suitable forewing configurations and wing devices. The large spans provided by variable sweep allows the efficient attainment of high lift coefficients that provide very good take-off and landing characteristics. Representative lateral-directional stability and dynamic stability characteristics of several variable-sweep concepts are included to indicate the type of research information currently available. A bibliography of variable-sweep studies is also included.

Conf

AUTHOR

INTRODUCTION

The use of variable sweep offers potential not available to fixed wings and also poses several unique design problems. The purpose of this paper is to review several types of variable-sweep schemes and to discuss some advantages and disadvantages of two of these with reference to the longitudinal-stability – supersonic-perfomance trade-offs and the variation of longitudinal stability with lift, and to discuss the high lift characteristics attainable with the low sweep angles and large spans offered by variable sweep. The lateral-directional stability and dynamic stability characteristics of several variable-sweep concepts are also presented to indicate the type of research information available. An extensive bibliography of variable-sweep studies is included for reference.

[redacted]

p 223 - 255
refs

PRECEDING PAGE BLANK NOT FILMED.

COEFFICIENTS AND SYMBOLS

Unless noted otherwise, the coefficients are based on the geometric characteristics of the sweptback wings.

A	aspect ratio
b_f	span of flaps
b_w	span of wing
c	wing chord
$\bar{c}$	mean aerodynamic chord
C_L	lift coefficient
C_D	drag coefficient
$C_{D,o}$	drag coefficient at zero lift
C_m	pitching-moment coefficient
$(\Delta C_m)_{tail}$	tail pitching-moment-coefficient contribution, $(C_m)_{tail\ on} - (C_m)_{tail\ off}$
$\frac{\partial C_m}{\partial C_L}$	slope of pitching-moment curve through zero lift coefficient
$C_{m_q} + C_{m_{\dot{\alpha}}}$	damping-in-pitch parameter
$C_{n_r} - C_{n_{\dot{\beta}}}$	damping-in-yaw parameter
e	wing efficiency factor
$(L/D)_{max}$	maximum lift-drag ratio
M	Mach number
V	relative velocity
V_S	stalling speed

[redacted]

[redacted]

H_1 chord-plane horizontal-tail location

H_2 mid-high horizontal-tail location

H_3 high horizontal-tail location

α angle of attack

Λ_{FW} sweep angle of forewing

Λ_{LE} sweep angle of leading edge

δ_f flap deflection angle

δ_h horizontal-tail deflection

RESULTS AND DISCUSSION

Variable-Sweep Pivot Schemes

Several of the many possible variable-sweep wing-pivot schemes are shown in figure 1. Shown at the top left is the single inboard type which has good low-speed pitch characteristics in the low sweep position because of its straight leading edge and small fixed forewing area. It has, however, a large longitudinal stability variation with increasing sweep angle because of the large movable area and small forewing and, if the advantages of low sweep angles are to be maintained, would probably require wing translation to provide reasonable handling qualities and minimum trim drag. (See refs. 1 to 6.) The next scheme is the "virtual pivot," where the pivot does not physically lie on the wing surface. This arrangement should have excellent all-around aerodynamic characteristics but would also require wing translation with the associated mechanical complexity. (See refs. 7 and 8.) Shown at the bottom left of the figure is the double inboard pivot which provides both good pitching-moment characteristics throughout the lift range and minimum stability variations with sweep angle (ref. 9); however, its use would present some additional complexity and require a wide fuselage to be fully effective.

At the top right of figure 1 is shown the single outboard pivot scheme as utilized on the SCAT 16 concept. Previous investigations (refs. 1 and 2) have shown that this general arrangement can provide minimum longitudinal-stability change with wing sweep angle but that it has pitch problems at high lifts when the fixed forward area (shown as the hatched area) is required to have an extremely high sweep angle.

[redacted]

The auxiliary wing type as utilized by the SCAT 15 concept has a large longitudinal-stability change with wing sweep angle but maintains good supersonic performance levels because the trim drag associated with its wing-tip controls is low and relatively insensitive to stability level. (See refs. 10 and 11.) The final scheme shown is the "M" wing type with outboard pivot. Data recently obtained indicate a reasonably small longitudinal-stability variation with wing sweep with a potentiality for having reasonable pitching-moment variations with lift throughout the sweep range.

Longitudinal-Stability – Supersonic-Performance Trade-offs

For the SCAT 15 and SCAT 16 concepts, the variation of trimmed $(L/D)_{max}$ as a function of the longitudinal stability parameter $\frac{\partial C_m}{\partial C_L}$ for a Mach number of 2.96 is presented in figure 2. Inasmuch as a given level of longitudinal stability is associated with a particular center-of-gravity location, this figure presents, in essence, the variation of trimmed $(L/D)_{max}$ with center-of-gravity location. A comparison of the absolute levels of the lift-drag ratio is not pertinent to this discussion since this comparison has been covered in paper no. 2 of this compilation by Donald D. Baals. Of interest is the fact that for SCAT 15, which was trimmed with wing-tip tails operating in an upwash field, the highest trimmed lift-drag ratios were obtained with a center-of-gravity location giving a rather large stability level whereas SCAT 16, which was trimmed with a conventional aft tail operating in the wing-body downwash field, attained its maximum L/D at a considerably lower static margin, and exhibited a rather rapid decrease in L/D as the stability level was increased.

Before discussing the stability levels or center-of-gravity locations that are required for these configurations and the implications with regard to performance, it is well to consider briefly the effects of aeroelasticity since this property can appreciably affect the stability level. The effect of aeroelasticity on longitudinal stability and trim requirements is illustrated in figure 3 for a highly swept configuration at a Mach number of 3.0. For a given center-of-gravity location the longitudinal stability of the elastic aircraft is of course less than that of the rigid aircraft both with tail off and with tail on because of the increasing washout of the elastic wing with increasing lift. If the rigid aircraft is assumed to have an optimum aerodynamic shape for cruise at the design lift coefficient, the flexible aircraft will be optimum only if it is constructed in such a manner that when it is loaded to the design cruise condition, it will assume the same shape as the optimum rigid aircraft. The tail-off center of pressure, as well as the pitching moment of the elastic aircraft, will then be identical to

that of the rigid aircraft at the design condition regardless of the change in stability. Therefore, at the design C_L the tail load and incidence required to trim, and the resulting trimmed **L/D** will be unaffected by aeroelasticity. The results of figure 2 are therefore applicable to either flexible or rigid aircraft if the value used for $\frac{\partial C_m}{\partial C_L}$ is that of the equivalent rigid configuration. The aircraft stability is, however, affected by elasticity not only through the change in static margin but also through changes in other stability derivatives and must be considered in handling-qualities evaluations.

In order to determine the stability levels that are required for the SCAT 15 and SCAT 16 configurations, it is necessary to consider the variation of aerodynamic center with wing sweep angle and Mach number as presented in figure 4. For reference, center-of-gravity locations are assumed that vary with sweep angle because of the weight of the wing and its internal components. These center-of-gravity variations are for illustrative purposes only and do not necessarily correspond to those used by the contractors in their feasibility studies.

For SCAT 15, a center-of-gravity position A can be selected which provides a small amount of stability for low speed while producing nearly maximum available trimmed $(L/D)_{max}$ in supersonic cruise (see fig. 2) even though a large static margin exists at Mach 3.0. For SCAT 16, on the other hand, selection of a center-of-gravity position B which gives only a small trim-drag penalty in cruise requires a minimum sweep angle of 35° to 40° to achieve low-speed stability. (See fig. 4.) A lower minimum sweep angle would be desirable to improve the subsonic lift-drag ratio, pitch-up characteristics, performance of high-lift devices, and lateral-directional handling qualities. At a center-of-gravity position C which gives a reasonable level of static stability for low speeds at 16° of sweep, a noticeable penalty in trim drag must be paid in supersonic performance because of the large static margin. (See fig. 2.) This trim-drag penalty can be reduced somewhat (theoretically at least) by a more optimum design of wing warp.

Since the highest cruise **L/D** was obtained with center-of-gravity location B, it is of interest to find a means of obtaining low-speed stability at lower sweep angles for this more rearward center-of-gravity location. An illustration of what can be done by adjustment of the wing pivot location, the importance of which was pointed out in reference 1, is indicated in figure 5 where the variation of the longitudinal stability parameter $\frac{\partial C_m}{\partial C_L}$ with wing sweep angle is presented for SCAT 16 at low speed. The experimental points are from wind-tunnel tests made with the horizontal tail off. The calculated curves were obtained from a modified

lifting-line procedure for the wing alone. Because the calculation did not account for the fuselage contribution, the calculated curves have been arbitrarily shifted vertically to bring the results for $\Lambda_{LE} = 76^\circ$ into agreement with the experimental results. The calculation for pivot location 2, which corresponds to the experimental case, shows that the effect of sweep angle on the static margin can be predicted with fair accuracy. Calculations were also made for pivot locations 1 and 3, which lie on the locus of pivots and which provide identical planforms at maximum sweep and equal spans at minimum sweep. The open-wing position shown corresponds to pivot location 2. The results illustrate the large increase in stability at low sweep angles that can be gained by moving the pivot point outward. It is apparent, therefore, that with a more outboard pivot location a considerably lower minimum sweep angle can be utilized while retaining low-speed stability with the more rearward center-of-gravity location indicated by center-of-gravity location B, compatible with the desired supersonic performance. It should be pointed out that the original SCAT 16 design is characterized by an extremely high aspect ratio wing which makes it difficult to provide a pivot location and rotating wing-panel-geometry relationship compatible with the outboard pivot concept. It therefore appears desirable to reduce the aspect ratio and sacrifice some of the extremely high subsonic performance in order to provide the desired geometry.

Longitudinal Stability Characteristics

The variation of pitching-moment coefficient with lift coefficient for the SCAT 15 and SCAT 16 configurations are presented for low speeds in figures 6 and 7 and for transonic and supersonic speeds in figure 8. For low speed and low sweeps (fig. 6), both configurations exhibit varying degrees of instability at high lift; thus, each must be fitted with special devices to eliminate or minimize these undesirable trends. For the high-sweep case at low speeds (fig. 7), which is important for an emergency landing associated with stuck-back wings, the SCAT 16 type appears reasonably satisfactory whereas the auxiliary-wing type of SCAT 15 has undesirable characteristics that would also require additional devices. The effects of horizontal-tail deflection on the longitudinal stability characteristics are seen to be minor for both the low-sweep case (fig. 6) and the high-sweep case (fig. 7) and imply that major conclusions concerning the high-lift instabilities will not be appreciably affected by the horizontal-tail deflections required for trim. The subsequent figures will therefore present data for only one tail setting. At transonic speeds (fig. 8), the reverse is apparent in that the SCAT 16 type indicates an instability whereas the SCAT 15 type does not, at least for the lift coefficient range investigated. At $M = 3.0$ both types appear to be fairly satisfactory for the lift-coefficient

range shown, although there is some indication that *SCAT* 15 is approaching a statically unstable condition at the higher lift coefficients.

The cause of the high-lift instabilities which characterize these configurations at low sweep angles can generally be traced to the forewing where lift effectiveness increases with angle of attack and produces a strong vortex flow that induces high angularities on the outboard panels and causes them to stall or separate. The effects of forewing geometry on the-low-speed pitch characteristics of an outboard-pivot configuration are presented in figure 9. As would be expected, the degree of high-lift instability, or pitch-up, is reduced with reductions in forewing sweep angle and area for the tail-off configuration. The bottom graphs of figure 9 present the same forewing configurations with a low horizontal tail added. For the 75° forewing case, although an improvement is noted in longitudinal stability at high lift, the curve is still unacceptable. For the 70° forewing, however, a stable, although nonlinear, variation is obtained. If the forewing is deflected down about the hinge line indicated on the sketch, a very desirable variation is obtained. It should be noted that this configuration utilized engines mounted within the fuselage so that it was possible to employ a horizontal tail in a low location and thereby provide desirable pitch characteristics. For the SCAT 16 type configuration, however, there are conflicting requirements between the podded-engine location and horizontal-tail location which result in the tail being forced above the wing-chord plane in order to avoid hot gas efflux effects on the tail structure. The effects of horizontal-tail location on the low-speed tail pitch contributions of the SCAT 16 type configuration are presented in figure 10. For the mid-high tail location a negligible tail contribution results from placing the tail in the extreme downwash flow field caused by the strong vortex flow emanating from the body nose and fortified by that shed from the forewing. The data further show the well-known desirability of positioning the tail as low as possible. For the high location, the tail contribution is initially large but decreases rapidly with increasing angle of attack and then reverses as the tail moves into the aforementioned downwash field.

If it is assumed that a moderately high tail must be used for practical reasons, it is apparent that the achievement of a pitch-up–free configuration will require very careful tailoring of the detailed arrangement of the horizontal tail in combination with wing flow-control devices. Some selected results from such a detailed study at low speeds on a SCAT 16 type of configuration utilizing two nacelles side by side under each wing are presented in figure 11. The best horizontal-tail arrangement found which would remain clear of the jet blast was at a mid-high location with 30° anhedral. With a forewing of 73.5° sweep and an outer wing panel at 25° sweep, a definite instability at high

lift is evident. Addition of a leading-edge slat on the outer panel eliminated this instability with the exception of a minor break near maximum lift. The angle of attack at this point is above 18° and it is believed that even this minor instability could be eliminated with more careful tuning of the slat. An alternate arrangement of wing flow-control devices consisting of a notch in the outer panel leading edge combined with a 29° downward deflection of the forewing nose flap also produced fairly satisfactory pitch characteristics through the lift range. The contribution of the notch alone was about one-half the difference shown in figure 11 between the clean wing and the notch plus forewing deflection except for a slight pitch-up near maximum lift coefficient.

Recent M-Wing Variable-Sweep Investigation

Another type of variable-sweep pivot scheme that has been the subject of recent preliminary studies is the M-wing type with outboard pivot. The structural aspects of this type of configuration were not included in the feasibility studies and therefore the practical aspects have not as yet been evaluated. The low-speed longitudinal stability characteristics of such an M-wing configuration are presented in figure 12. This configuration employed a high horizontal-tail location. The static-margin variation with wing sweep angle is presented for both tail-off and tail-on conditions. For the tail-on case the static margin shifts about 17-percent c as the wing is swept from 34° to 74°. For the tail-off condition, at 34° sweep there are large variations in the pitching-moment coefficient with pitch-up occurring at $C_L \approx 0.5$ followed by a very stable break at $C_L \approx 1.0$. The initial pitch-up is presumed to be due to the stalling of the outer wing panel. Fixes on the outer wing panel, as shown earlier, should alleviate these undesirable trends. Since the tail-off curve breaks stable at the high lifts, a situation occurs that should be compatible with the use of a high tail which breaks unstable when it enters the wing downwash field. The addition of such a tail indicates that the desired pitch trends are mostly achieved and the use of outer wing panel fixes should provide even more linear curves.

High-Lift Characteristics

The configuration that has been used to obtain extensive high-lift data applicable to variable-sweep transports both at the Ames and the Langley Research Centers is shown in figure 13. The principal difference between this wing and conventional low-sweep wings is the addition of the forewing. High-lift devices investigated included a leading-edge slat and trailing-edge flaps of either the single slotted or double slotted types. It should be noted that this configuration has the horizontal tail below the chord line of the wing. Some selected results for a single slotted flap deflected 40° are presented in figure 14. The trimmed lift-coefficient characteristics shown in the upper

left graph are for a flap semispan of 98 percent of the wing semispan. Maximum trim lift coefficient values of 2.4 or higher based on the area of the 13.5° swept wing are seen attainable with this type of configuration. Increasing the wing sweep from 13.5° to 25° causes a loss in C_L of approximately 0.25 or about 12 percent at an angle of attack of 12°. The question of the lift that is available for landing in the case where the wings are stuck back is illustrated in the lower part of the graph. The comparison shows that no increase in lift at landing attitudes, $\alpha \geq 10°$, was obtained from deflection of these flaps at a wing sweep of 75° and indicated that careful flap design will be required to obtain a lift increment for the higher sweep angles.

The upper right part of figure 14 shows the effect of flap span on the high-lift characteristics. A reduction of flap span from $0.98b_w/2$ to $0.67b_w/2$ with the wings at 25° sweep reduced the lift coefficient by a value of 0.15 and resulted in a lift coefficient of 1.8 at an angle of attack of 12°. Consideration of ground effect should result in landing lift coefficients in excess of 2.0 even with the partial-span flap.

With regard to the pitch characteristics at high lift, the data for 25° of wing sweep with partial-span flaps are presented in the lower portion of figure 14. The data show that the pitching-moment-coefficient variation with lift coefficient is stable over most of the lift range and that the tail is capable of trimming the model over most of the lift range. It should be remembered, however, that this configuration has a relatively low horizontal tail which provides better variations of pitching moment with lift than other horizontal-tail locations. If it is found that the use of a higher tail location leads to insoluble pitch-up problems, some reduction of forewing area by use of a more inboard pivot location may be required although, as shown earlier, this would probably require the use of higher minimum sweep angles to restrict the aerodynamic-center variation with wing sweep angle.

The effect of high-lift devices on the drag characteristics of the configuration shown in figure 13 is presented in figure 15. The progressive improvement provided by more sophisticated devices is evident. It is also interesting to note that an envelope drag polar constructed by using the zero-lift drag coefficient and drag-due-to-lift factor of the basic wing is nearly tangent to each of the high-lift-device curves. This condition implies that high-lift devices can be designed which will retain the span efficiency of the basic wing. The resulting high lift-drag ratios will lead to low values of thrust required in the landing approach and will thereby reduce the problems of community noise. For reference, the lift coefficients corresponding to $1.3V_S$ and $(L/D)_{max}$ for the double slotted flap configuration are shown. Since $(L/D)_{max}$ occurs at a higher coefficient and therefore at a lower speed than the

assumed approach speed of $1.3V_S$, speed stability during the landing approach will be obtained with the efficient high-lift system shown.

Some results recently obtained at the Langley Research Center during a study to determine the effect of the addition of a forewing on the lift characteristics of an aspect-ratio-10 wing having a very efficient high-lift system are presented in figures 16 and 17. This wing-body arrangement utilized an unswept wing having leading-edge slats in combination with a double slotted flap as shown in figure 16. All coefficients are based on the area of the wing without the forewing. At zero angle of attack a 40° deflection of the flaps provided an increment in C_L of 2.0. At an angle of attack of 10° a maximum lift coefficient of approximately 3.1 was obtained. The addition of the forewing caused an increase in the slope of the lift curve and increased the maximum lift coefficient by about 0.1. The effect of the forewing on the drag characteristics was to cause an increase at low lifts and a small reduction at high lifts. (See fig. 17.) A comparison of the experimental data with the envelope drag polar constructed by using the basic-wing zero-lift drag and drag-due-to-lift factors again indicates that this high-lift system is very efficient.

Lateral-Directional Stability

The variation of the directional-stability parameter C_{n_β} and the effective dihedral parameter C_{l_β} with angle of attack for low speed and supersonic speeds are presented in figures 18 and 19, respectively, for both the SCAT 15 and 16 configurations. For the SCAT 16 configuration whose original body nose cross section was near circular but somewhat flat on the bottom, C_{n_β} was invariant with α up to about 10°, increased appreciably between 10° and 20°, and decreased sharply above 20°, for the $\Lambda_{LE} = 16°$ condition. Additional tests made with a fuselage nose section with a circular cross section caused C_{n_β} to decrease rapidly above $\alpha = 10°$. It is, therefore, apparent that fuselage cross section can have a large effect on the directional-stability variation with α especially when long fuselage forebodies are used. For the high-sweep case, C_{n_β} becomes exceedingly stable at the highest angles of attack. For SCAT 15, the low-sweep condition becomes unstable at an angle of attack of about 19° whereas the high-sweep case, although very nonlinear, generally becomes increasingly stable at the higher angles of attack. With regard to the effective dihedral parameter $-C_{l_\beta}$, the values for the SCAT 16 low-sweep wing are seen to reduce at the higher angles of attack whereas for the high-sweep case an increase is observed. The

[redacted]

reduction at high angles of attack for the low-sweep wing are associated with the stalling of the outer panel mentioned previously in connection with pitch-up problems and, when wing fixes are employed, the reduction in C_{l_β} would be expected to be considerably less. For SCAT 15 both sweeps have large levels at the higher angles of attack. For supersonic speed (fig. 19) both configurations have similar characteristics, C_{n_β} decreasing as M increases because of the reduction in vertical-tail side-force effectiveness, and become unstable at relatively low angles of attack. The level of effective dihedral also decreases with Mach number. It is beyond the scope of this paper to assess the effect of the rather high values of effective dihedral on handling qualities since this assessment would require extensive simulator studies.

Dynamic-Stability Derivatives

Knowledge of the dynamic stability derivatives is required in order to predict handling-qualities and stability augmentation requirements. Experimental measurement of these derivatives requires careful application of specialized techniques. Two different wind-tunnel techniques employing forced oscillation of the model have been employed at the NASA Ames and Langley Research Centers for measurement of the damping derivatives in pitch and yaw of models of a preliminary variable-sweep transport concept. Representative results at zero angle of attack are presented in figure 20 to illustrate the type of sweep and Mach number effects that might be expected for a variable-sweep transport. The data, regardless of wing-sweep position, are referred to the geometric characteristics of the wing in the 75° sweep position. The damping-in-pitch parameter $C_{m_q} + C_{m_{\dot{\alpha}}}$ was generally independent of wing sweep for sweep angles of 25°, 50°, and 75°. The data measured by the two techniques show reasonably good agreement throughout the Mach number range. The damping-in-yaw parameter $C_{n_r} - C_{n_{\dot{\beta}}}$ was also relatively independent of wing sweep 'but, in this case, the agreement between the two techniques was good only at supersonic speeds. The results indicate only minor effects of sweep, and Mach number effects reasonably compatible with the well-known variations in the lift effectiveness of the tail surfaces with Mach number. The complete results for the supersonic part of the Langley investigation are reported in reference 12.

CONCLUDING REMARKS

A consideration of the stability and high-lift characteristics applicable to variable-sweep supersonic transport configurations

[redacted]

indicates that the more outboard pivot locations can be used to reduce the aerodynamic-center variation with wing sweep angle and result in higher supersonic trimmed lift-drag ratios. Of the several configuration concepts considered, the smallest maxim lift-drag-ratio variation with stability level or center-of-gravity location was obtained with the auxiliary-wing concept. The outboard pivot wings with fixed forward area have pitch instability problems at high lifts but these problems can be minimized by use of suitable forewing configurations and wing devices. The large spans provided by variable sweep allow the efficient attainment of high lift coefficients that provide very good take-off and landing characteristics. Representative lateral-directional stability and dynamic stability characteristics of several variable-sweep concepts are included to indicate the type of research information currently available. A bibliography of variable-sweep studies is also included.

[redacted]

REFERENCES

1. Alford, William J., Jr., and Henderson, William P.: An Exploratory Investigation of the Low-Speed Aerodynamic Characteristics of Variable-Wing-Sweep Airplane Configurations. NASA TM X-142, 1959.

2. Alford, William J., Jr., Luoma, *Arvo* A., and Henderson, William P.: Wind-Tunnel Studies at Subsonic and Transonic Speeds of a Multiple-Mission Variable-Wing-Sweep Airplane Configuration. NASA TM X-206, 1959.

3. Spencer, Bernard, Jr.: Stability and Control Characteristics at Low Subsonic Speeds of an Airplane Configuration Having Two Types of Variable-Sweep Wings. NASA TM X-303, 1960.

4. Bielat, Ralph P., Robins, A. Warner, and Alford, William J., Jr.: The Transonic Aerodynamic Characteristics of Two Variable-Sweep Airplane Configurations Capable of Low-Level Supersonic Attack. NASA TM X-304, 1960.

5. Bielat, Ralph P., and Pierpont, P. Kenneth: Transonic Aerodynamic Characteristics of a Variable-Sweep Airplane Configuration Having a 12-Percent-Thick Wing and an Inboard Pivot Location. NASA TM X-429, 1960.

6. Hammond, Alexander D., and Polhamus, Edward C.: The Effects of Horizontal-Tail Position on the Longitudinal Aerodynamic Characteristics at Transonic Speeds of a Variable-Sweep Aircraft Having an Inboard Pivot. NASA TM x-612, 1961.

7. Kemp, William B., Jr., Becht, Robert E., and Few, Albert G., Jr.: Stability and Control Characteristics at Low Speed of a $\frac{1}{4}$-Scale Bell X-5 Airplane Model. Longitudinal Stability and Control. NACA RM L9K08, 1950.

8. Kemp, William B., Jr., and Becht, Robert E.: Stability and Control Characteristics at Low Speed of a $\frac{1}{4}$-Scale Bell X-5 Airplane Model. Lateral and Directional Stability and Control, NACA RM L50C17a, 1950.

9. Polhamus, Edward C., Alford, William J., Jr., and Foster, Gerald V.: Subsonic and Supersonic Aerodynamic Characteristics of an Airplane Configuration Utilizing Double-Pivot Variable-Sweep Wings. NASA TM X-743, 1962.

10. Driver, Cornelius, Spearman, M. Leroy, and Corlett, William A.: Aerodynamic Characteristics at Mach Numbers from 1.61 to 2.86 of a Supersonic Transport Model With a Blended Wing-Body, Variable-Sweep Auxiliary Wing Panels, Outboard Tail Surfaces, and a Design Mach Number of 2.2. NASA TM X-817, 1963.

11. Harris, Roy V., Jr., and Corlett, William A.: Longitudinal Aerodynamic Characteristics at Mach Numbers From 0.50 to 1.20 of a Supersonic Transport Model With a Blended Wing-Body, Variable-Sweep Auxiliary Wing Panels, and Outboard Tail Surfaces. NASA TM X-837, 1963.

12. Delaney, Bobby R., and Thompson, Wilson E.: Dynamic Stability Characteristics in Pitch and in Yaw for a Model of a Variable-Sweep Supersonic Transport Configuration at Mach Numbers of 2.40, 2.98, and 3.60. NASA TM X-761, 1963.

BIBLIOGRAPHY

Campbell, John P., and Drake, Hubert M.: Investigation of Stability and Control Characteristics of an Airplane Model With Skewed Wing in the Langley Free-Flight Tunnel. NACA TN 1208, 1947.

Donlan, Charles J., and Sleeman, William C., Jr.: Low-Speed Wind-Tunnel Investigation of the Longitudinal Stability Characteristics of a Model Equipped With a Variable-Sweep Wing. NACA RM L9B18, 1949.

Kemp, William B., Jr., Becht, Robert E., and Few, Albert G., Jr.: Stability and Control Characteristics at Low Speed of a $\frac{1}{4}$-Scale Bell X-5 Airplane Model. Longitudinal Stability and Control. NACA RM L9K08, 1950.

Kemp, William B., Jr., and Becht, Robert E.: Stability and Control Characteristics at Low Speed of a $\frac{1}{4}$-Scale Bell X-5 Airplane Model. Lateral and Directional Stability and Control. NACA RM L50C17a, 1950.

Silsby, Norman S., Morris, Garland J., and Kennedy, Robert M.: Longitudinal Characteristics at Mach Number of 1.24 of $\frac{1}{30}$-Scale Semispan Model of Bell X-5 Variable-Sweep Airplane With Wing Swept Back 60° From Tests by NACA Wing-Flow Method. NACA RM L50E02a, 1950.

Morris, Garland J., Kennedy, Robert M., and Silsby, Norman S.: The Effect of Sweepback on the Longitudinal Characteristics at a Mach Number of 1.24 of a $\frac{1}{30}$-Scale Semispan Model of the Bell X-5 Airplane From Tests by the NACA Wing-Flow Method. NACA RM L50I28, 1950.

Sawyer, Richard H., Kennedy, Robert M., and Morris, Garland J.: Longitudinal-Control Effectiveness and Downwash Characteristics at a Mach Number of 1.24 of a $\frac{1}{30}$-Scale Semispan Model of the Bell X-5 Airplane as Determined by the NACA Wing-Flow Method. NACA RM L50K15, 1951.

Kemp, William B., Jr., Becht, Robert E., and Few, Albert G., Jr.: Investigation of the Low-Speed Aerodynamic Characteristics of a Variable-Sweep Airplane Model With a Twisted and Cambered Wing. NACA RM L51K22, 1952.

Kemp, William B., Jr. : An Investigation of the Low-Speed Longitudinal Stability Characteristics of a Wept-Wing Airplane Model With Two Modifications to the Wing-Root Plan Form. NACA RM L52E07, 1952.

Becht, Robert E., and Byrnes, Andrew L., Jr.: Investigation of the Low-Speed Aerodynamic Characteristics of a Variable-Sweep Airplane Model With a Wing Having Partial-Span Cambered-Leading-Edge Modifications. NACA RM L52G08a, 1952.

Spreemann, Kenneth P., and Alford, William J., Jr.: Small-scale Transonic Investigation of the Effects of Twist and Camber on the Aerodynamic Characteristics of a 60°42' Sweptback Wing of Aspect Ratio 1.94. NACA RM L51I21, 1952.

Spreemann, Kenneth P., and Alford, William J., Jr.: Investigation of the Effects of Twist and Camber on the Aerodynamic Characteristics of a 50°38' Sweptback Wing of Aspect Ratio 2.98. Transonic-Bump Method. NACA RM L51C16, 1951.

Alford, William J., Jr., and Byrnes, Andrew L., Jr.: Small-scale Transonic Investigation of the Effects of Partial-Span Leading-Edge Camber on the Aerodynamic Characteristics of a 50°38' Sweptback Wing of Aspect Ratio 2.98. NACA RM L52D08a, 1952.

Kolnick, Joseph J., and Kennedy, Robert M: The Effects of Sweepback on Longitudinal Characteristics of a $\frac{1}{30}$-Scale Semispan Model of the Bell X-5 Airplane as Determined From NACA Wing-Flow Tests at Transonic Speeds. NACA RM L52I23, 1952.

Silsby, Norman S., and Morris, Garland J.: Longitudinal-Control Effectiveness and Downwash Characteristics at Transonic Speeds of a $\frac{1}{30}$-Scale Semispan Model of the Bell X-5 Airplane as Determined by the NACA Wing-Flow Method. NACA RM L52K12, 1953.

Bielat, Ralph P., and Campbell, George S.: A Transonic Wind-Tunnel Investigation of the Longitudinal Stability and Control Characteristics of a 0.09-Scale Model of the Bell X-5 Research Airplane and Comparison With Flight. NACA RM L53H18, 1953.

Donely, Philip, and Gillis, Clarence L.: Some Design Considerations Pertinent to the Rough-Air Behavior of Airplanes at Low Altitude. NACA RM L53J01b, 1953.

English, Roland D.: Some Effects of Aeroelasticity and Sweepback on the Rolling Effectiveness and Drag of a 1/11-Scale Model of the Bell X-5 Airplane Wing at Mach Numbers From 0.6 to 1.5. NACA RM L53I18b, 1953.

Becht, Robert E.: Stability Characteristics at Low Speed of a Variable-Sweep Airplane Model Having a Partially Cambered Wing With Several Chord-Extension Configurations. NACA RM L53L14, 1954.

Morris, Garland J., and Silsby, Norman S.: Distribution of Lift and Pitching Moment Between Wing and Fuselage and Effects of Wing Flexibility and Dive Brake on a 1/30-Scale Semispan Model of the Bell X-5 Airplane at Transonic Speeds as Determined by the NACA Wing-Flow Method. NACA RM L54A11, 1954.

Spearman, M. Leroy, and Foster, Gerald V.: Stability and Control Characteristics at a Mach Number of 2.01 of a Variable-Wing-Sweep Configuration With Outboard Wing Panels Swept Back 75°. NASA TM X-32, 1959.

Alford, William J., Jr., and Henderson, William P.: An Exploratory Investigation of the Low-Speed Aerodynamic Characteristics of Variable-Wing-Sweep Airplane Configurations. NASA TM X-142, 1959.

Alford, William J., Jr., Luoma, Arvo A., and Henderson, William P.: Wind-Tunnel Studies at Subsonic and Transonic Speeds of a Multiple-Mission Variable-Wing-Sweep Airplane Configuration. NASA TM x-206, 1959.

Spearman, M. Leroy, and Foster, Gerald V.: Effects of Various Modifications on the Supersonic Stability Characteristics of a Variable-Wing-Sweep Configuration at a Mach Number of 2.01. NASA TM x-260, 1960.

Foster, Gerald V.: Stability and Control Characteristics at Mach Numbers of 2.50, 3.00, and 3.71 of a Variable-Wing-Sweep Configuration With Outboard Wing Panels Swept Back 75°. NASA TM X-267, 1960.

Foster, Gerald V.: Effects of Spoiler-Slot-Deflector Control on the Aerodynamic Characteristics at a Mach Number of 2.01 of a Variable-Wing-Sweep Configuration With the Outer Wing Panels Swept Back 75°. NASA TM X-273, 1960.

Spencer, Bernard, Jr.: Stability and Control Characteristics at Low Subsonic Speeds of an Airplane Configuration Having Two Types of Variable-Sweep Wings. NASA TM X-303, 1960.

Foster, Gerald V., and Morris, Odell A.: Stability and Control Characteristics at a Mach Number of 1.97 of an Airplane Configuration Having Two Types of Variable-Sweep Wings. NASA TM X-323, 1960.

Bielat, Ralph P., Robins, A. Warner, and Alford, William J., Jr.: The Transonic Aerodynamic Characteristics of Two Variable-Sweep Airplane Configurations Capable of Low-Level Supersonic Attack. NASA TM X-304, 1960.

Spearman, M. Leroy, and Robinson, Ross B.: Stability and Control Characteristics at a Mach Number of 2.01 of a Variable-Sweep Airplane Configuration Capable of Low-Level Supersonic Attack - Outer Wing Swept 75°. NASA TM X-310, 1960.

Robinson, Ross B., and Howard, Paul W.: Stability and Control Characteristics at a Mach Number of 1.41 of a Variable-Sweep Airplane Configuration Capable of Low-Level Supersonic Attack - Outer Wing Swept 75° and 108°. NASA TM X-320, 1960.

Luoma, Arvo A., and Alford, William J., Jr.: Performance, Stability, and Control Characteristics at Transonic Speeds of Three V/STOL Airplane Configurations With Wings of Variable Sweep. NASA TM X-321, 1960.

Foster, Gerald V., and Morris, Odell A.: Aerodynamic Characteristics in Pitch at a Mach Number of 1.97 of Two Variable-Wing-Sweep V/STOL Configurations With Outboard Wing Panels Swept Back 75°. NASA TM x-322, 1960.

Foster, Gerald V., and Morris, Odell A.: Static Longitudinal and Lateral Aerodynamic Characteristics at a Mach Number of 2.20 of a Variable-Wing-Sweep STOL Configuration. NASA TM X-329, 1960.

Robinson, Ross B., and Spearman, M. Leroy: Stability and Control Characteristics at a Mach Number of 2.2 of a Variable-Sweep Airplane Configuration Capable of Low-Level Supersonic Attack - Outer Wing Swept 75°. NASA TM X-330, 1960.

Luoma, Arvo A.: Stability and Control Characteristics at Transonic Speeds of a Variable-Wing-Sweep Airplane Configuration With Wing Outboard Panels Swept 113.24° and 75°. NASA TM X-342, 1960.

Staff of the NASA: Compilation of Papers Summarizing Some Recent NASA Research on Manned Military Aircraft. NASA TM X-420, 1960.

Bielat, Ralph P., and Pierpont, P. Kenneth: Transonic Aerodynamic Characteristics of a Variable-Sweep Airplane Configuration Having a 12-Percent-Thick Wing and an Inboard Pivot Location. NASA TM X-429, 1960.

Trescot, Charles D., Jr., and Spencer, Bernard, Jr.: Effect of Reynolds Number on the Low-Speed Longitudinal Aerodynamic Characteristics of Two Variable-Wing-Sweep Airplane Configurations, NASA TM X-434, 1961.

Robinson, Ross B., and Howard, Paul W.: Stability and Control Characteristics at a Mach Number of 2.2 of a Variable-Sweep Airplane Configuration Having a 12-Percent-Thick Wing Swept 75° and an Inboard Pivot Location. NASA TM X-435, 1960.

Ward, Robert J.: Transonic Aerodynamic Characteristics at a Wing Sweep of 104° of a Variable-Sweep Airplane Configuration With an Over-and-Under Engine Installation. NASA TM X-444, 1961.

Cornette, Elden S.: Wind-Tunnel Investigation of the Wing Buffet Response of a Variable-Wing-Sweep Model at Subsonic and Transonic Speeds. NASA TM X-443, 1961.

Hayes, William C., Jr., and Thompson, Wilson E.: Wind-Tunnel Measurements at Subsonic and Transonic Speeds of the Rolling Stability Derivatives of a Variable-Sweep Airplane Configuration - Outer Wing Panels Swept 108°. NASA TM X-465, 1961.

Luoma, Arvo A.: Longitudinal Aerodynamic Characteristics at Transonic Speeds of Two V/STOL Airplane Configurations With Skewed and Variable-Sweep Wings. NASA TM X-527, 1961.

Morris, Odell A., and Foster, Gerald V.: Static Longitudinal and Lateral Aerodynamic Characteristics at a Mach Number of 2.20 of a V/STOL Airplane Configuration With a Variable-Sweep Wing and With a Skewed Wing Design. NASA TM X-521, 1961.

Spencer, Bernard, Jr.: A Simplified Method for Estimating Subsonic Lift-Curve Slope at Low Angles of Attack for Irregular Planform Wings. NASA TM X-525, 1961.

Henderson, William P., and Hammond, Alexander D.: Low-Speed Investigation of High-Lift and Lateral Control Devices on a Semispan Variable-Sweep Wing Having an Outboard Pivot Location. NASA TM X-542, 1961.

Bielat, Ralph P., and Robins, A. Warner: Stability and Control Characteristics at Transonic Speeds of Two Variable-Sweep Airplane Configurations Differing in Wing-Pivot Locations. NASA TM X-559, 1961.

Spearman, M. Leroy, and Robinson, Ross B.: Effects of Wing Sweep and Horizontal-Tail Position on the Aerodynamic Characteristics at a Mach Number of 2.2 of a Variable-Sweep Airplane Configuration Having an Inboard Wing Pivot. NASA TM X-585, 1961.

Vogler, Raymond D., and Turner, Thomas R.: Exploratory Low-Speed Wind-Tunnel Stability Investigation of a Supersonic Transport Configuration With Variable-Sweep Wings. NASA TM X-597, 1961.

Stonesifer, John C., and Goetz, Robert; C.: Transonic and Supersonic Flutter Trend Investigation of a Variable-Sweep Wing. NASA TM X-598, 1961.

Hayes, William C., Jr., Kemp, William B., Jr., and Thompson, Wilson E.: Wind-Tunnel Measurements and Estimated Values of the Rolling Stability Derivatives of a Variable-Sweep Airplane Configuration at Subsonic and Transonic Speeds. NASA TM X-600, 1961.

Hammond, Alexander D., and Polhamus, Edward C.: The Ef'fects of Horizontal-Tail Position on the Longitudinal Aerodynamic Characteristics at Transonic Speeds of a Variable-Sweep Aircraft Having an Inboard Pivot. NASA TM x-612, 1961.

Sleeman, William C., Jr., and Robins, A. Warner: Low-Speed Investigation of the Aerodynamic Characteristics of a Variable-Sweep Supersonic Transport Configuration Having a Blended Wing and Body. NASA TM x-619, 1962.

Ward, Robert J., and McKee, John W.: Low-Speed Aerodynamic Stability and Control Characteristics of a Cambered Fuselage, Variable-Sweep Supersonic Transport Configuration. NASA TM x-632, 1962.

Sleeman, William C., Jr.: Low-Speed Investigation of the Effects of Horizontal Tail Height and Extension of the Wing-Root Leading-Edge Sections on a Variable-Sweep Supersonic Transport Configuration. NASA TM x-681, 1962.

Bielat, Ralph P.: Effect of Model Modifications on the Transonic Drag Characteristics of a Variable-Wing-Sweep Airplane Configuration Having an Outboard Wing Pivot. NASA TM X-695, 1962.

Hillje, Ernest R., and Wiley, Harleth G.: Transonic Dynamic Stability Characteristics in Pitch and in Yaw for a Model of a Variable-Sweep Airplane Configuration Capable of Low-Level Supersonic Attack. NASA TM x-618, 1962.

Spencer, Bernard, Jr.: Low-Speed Longitudinal Aerodynamic Characteristics Associated With Variations in the Geometry of the Fixed Portion of a Variable-Wing-Sweep Airplane Configuration Having an Outboard Pivot. NASA TM x-625, 1962.

Luoma, Arvo A.: Longitudinal Aerodynamic Characteristics at Transonic Speeds of a V/STOL Airplane Configuration With a Fixed Delta Wing Having Auxiliary Variable-Sweep Outboard Panels. NASA TM x-661, 1961.

Land, Norman S., Wood, John H., and Foughner, Jerome T., Jr.: An Investigation of the Structural Characteristics of a Simplified Model of a Variable-Sweep Wing. NASA TM x-662, 1962.

Re, Richard J., and Cassetti, Marlowe D.: Transonic Longitudinal Aerodynamic Characteristics of a Model of a Tactical Fighter Airplane With a Fixed Delta Wing and Variable-Sweep Wing Panels. NASA TM X-674, 1962.

Capone, Francis J., and Lee, Edwin E., Jr.: Transonic Aerodynamic Characteristics of Three V/STOL Fighter Models With Variable-Sweep or Skewed Wings and Different Engine Installations. NASA TM X-706, 1962.

Vogler, Raymond D.: Low-Speed Wind-Tunnel Stability Investigation of a Supersonic Transport Model With Variable-Sweep Wings Equipped With High-Lift Devices. NASA TM x-728, 1962.

Ruhlin, Charles L., and Gurley, John R., Jr.: Transonic Flutter Investigation of Models of a Proposed Variable-Sweep Wing. NASA TM X-739, 1962.

Henderson, William P.: Low-Speed Longitudinal Stability Characteristics of a Supersonic Transport Configuration With Variable-Sweep Wings Employing a Double Inboard Pivot. NASA TM X-744, 1962.

Shaw, David S., and Henderson, William P.: Wind-Tunnel Investigation at Mach Numbers From 1.60 to 2.86 of the Static Aerodynamic Characteristics of a Supersonic Transport Configuration With Variable-Weep Wings Employing a Double Inboard Pivot. NASA TM X-745, 1962.

Foster, Gerald V.: Static Longitudinal and Lateral Aerodynamic Characteristics at a Mach Number of 2.20 of a Model of an 82° Delta-Wing Airplane Having Auxiliary Variable-Sweep Wing Panels. NASA TM X-707, 1963.

Spearman, M. Leroy: Static Longitudinal and Lateral Aerodynamic Characteristics at Mach Numbers of 1.41 and 2.20 of a Model of a Low-Aspect-Ratio 83.5° Delta-Wing Airplane Having Auxiliary Variable-Sweep Wing Panels. NASA TM x-708, 1963.

Spearman, M. Leroy: Longitudinal and Lateral Aerodynamic Character=istics at Mach Numbers From 0.60 to 2.20 of a Variable-Sweep Fighter Model With Wing Sweep Angles From 25° to 75°. NASA TM X-710, 1962.

Lockwood, Vernard E.: Low-Speed Longitudinal Aerodynamic Characteristics of an 83.5° Delta-Wing Airplane Model Having Auxiliary Variable-Sweep Wing Panels. NASA TM X-729, 1963.

Re, Richard J., and Simonson, Albert J.: Transonic Longitudinal Aerodynamic Characteristics of a Variable-Sweep Tactical-Fighter Model With Wing Sweeps of 25°, 65°, 85°, and 106°. NASA TM X-731, 1962.

Ruhlin, Charles L., and Gurley, John R., Jr.: Transonic Flutter Investigation of Models of a Proposed Variable-Sweep Wing. NASA TM X-739, 1962.

Polhamus, Edward C., Alford, William J., Jr., and Foster, Gerald V.: Subsonic and Supersonic Aerodynamic Characteristics of an Airplane Configuration Utilizing Double-Pivot Variable-Sweep Wings. NASA TM x-743, 1962.

Runckel, Jack F., Lee, Edwin E., Jr., and Simonson, Albert J.: Sting and Jet Interference Effects on the Afterbody Drag of a Twin-Engine Variable-Sweep Fighter Model at Transonic Speeds. NASA TM X-755, 1963.

Henderson, William P.: Low-Speed Aerodynamic Characteristics of a Double-Pivot Variable-Wing-Sweep Airplane Configuration Having Conventional and Outboard Horizontal Tail Surfaces. NASA TM X-773, 1963.

Spearman, M. Leroy, and Harris, Roy V., Jr.: The Longitudinal and Lateral Aerodynamic Characteristics at Mach Numbers of 1.41 and 2.20 of a Variable-Sweep Fighter Model With Wing Sweeps Varying From 25° to 75°. NASA TM X-759, 1963.

Alford, William J., Jr., Hammond, Alexander D., and Henderson, William William P.: Low-Speed Stability Characteristics of a Supersonic Transport Model With a Blended Wing-Body, Variable-Sweep Auxiliary Wing Panels, Outboard Tail Surfaces, and Simplified High-Lift Devices. NASA TM x-802, 1963.

Spearman, M. Leroy, Driver, Cornelius, and Robins, A. Warner: Aerodynamic Characteristics at Mach Numbers of 2.30, 2.96, and 3.50 of a Supersonic Transport Model With a Blended Wing-Body, Variable-Sweep Auxiliary Wing Panels, and Outboard Tail Surfaces. NASA TM x-803, 1963.

Spearman, M. Leroy, and Finch, Virginia M.: Static Longitudinal and Lateral Aerodynamic Characteristics at Mach Numbers of 2.36 and 2.86 of a Variable-Sweep Airplane configuration Having Vertical-Ramp Inlets. NASA TM X-835, 1963.

[redacted]

Baals, Donald D., and Polhamus, Edward C. : Variable Sweep Aircraft. Astronautics and Aerospace Eng., vol. 1, no. 5, June 1963, pp. 12–19.

[redacted]

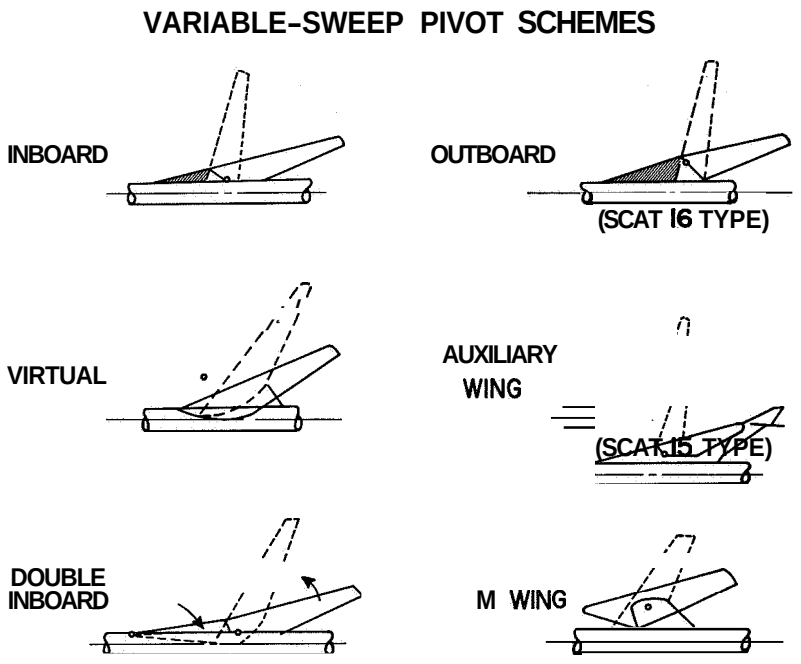

Figure 1

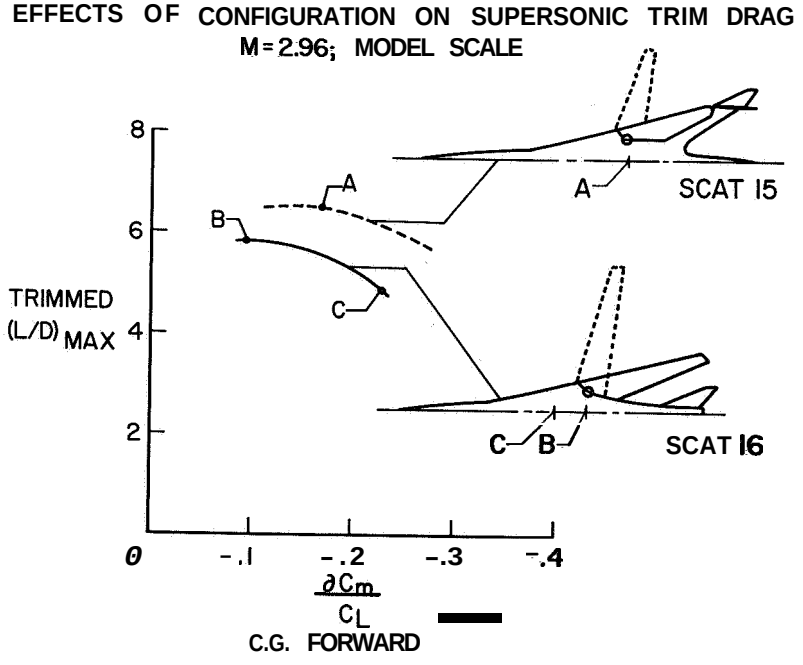

Figure 2

EFFECT OF AEROELASTICITY ON STABILITY AND TRIM
M□3.0

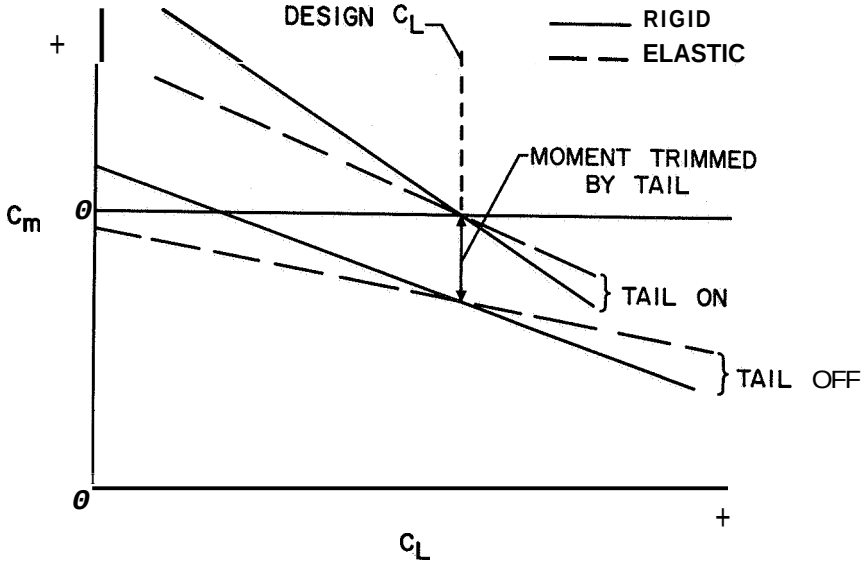

Figure 3

EFFECTS OF CONFIGURATION ON STABILITY VARIATIONS WITH WING SWEEP ANGLE AND MACH NUMBER

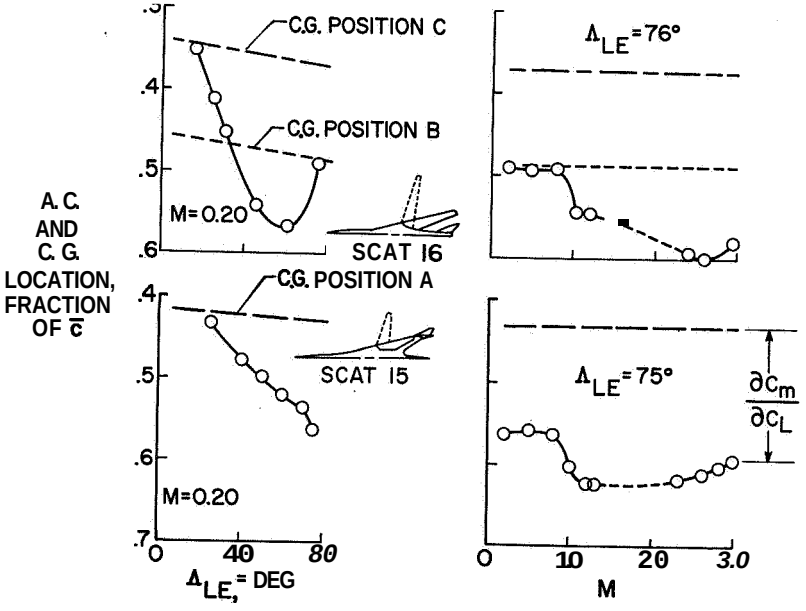

Figure 4

EFFECT OF PIVOT LOCATION ON STABILITY
VARIATION WITH SWEEP
M ≈ 0

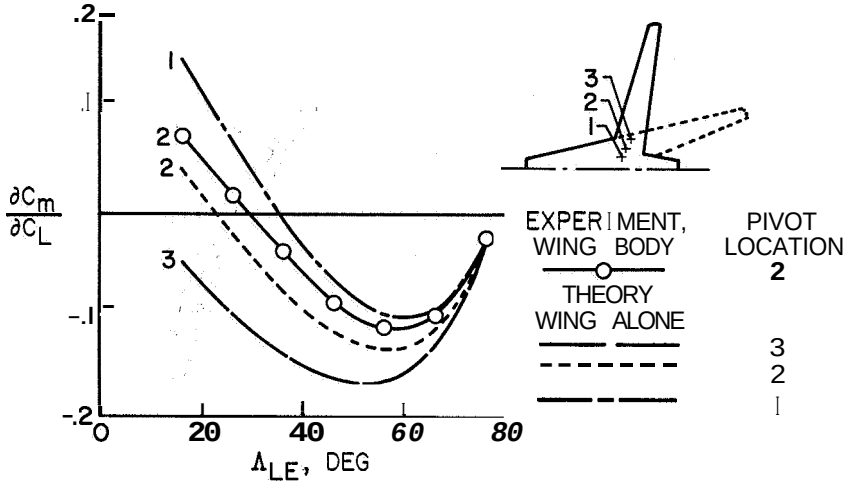

Figure 5

LOW-SPEED PITCH CHARACTERISTICS
LOW SWEEP

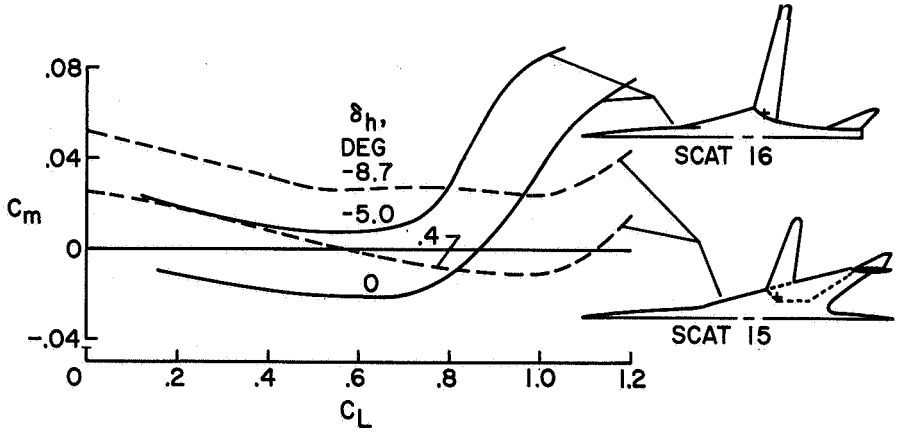

Figure 6

[redacted]

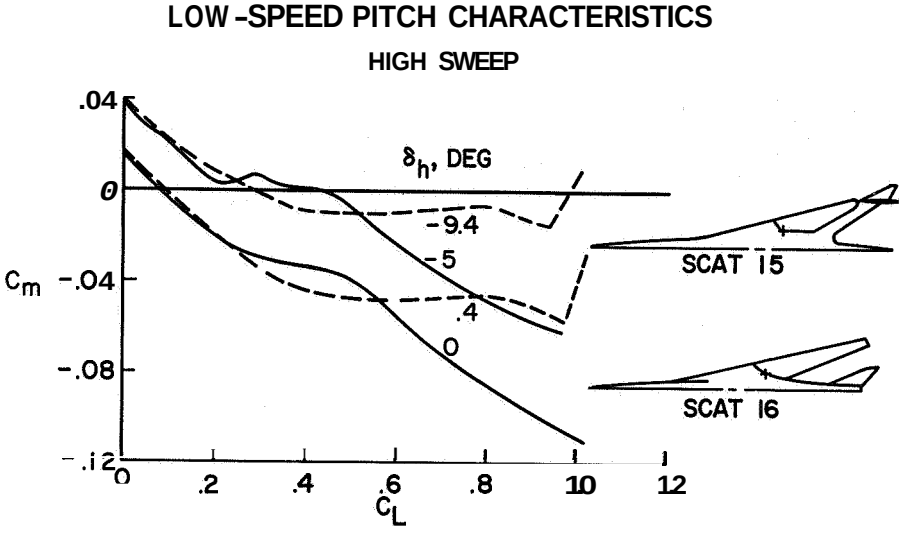

Figure 7

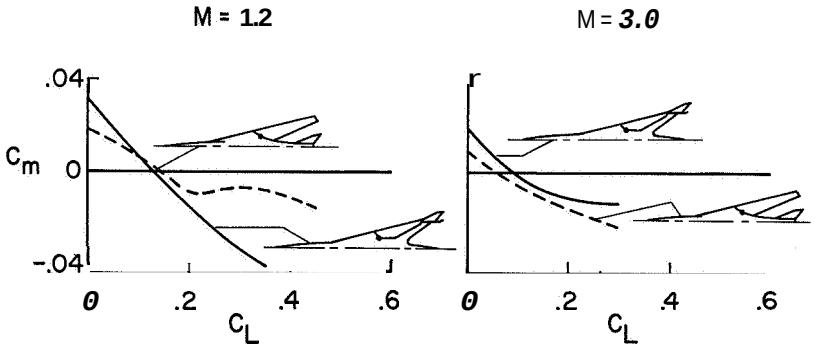

Figure 8

EFFECTS OF FOREWING GEOMETRY ON THE LOW-SPEED PITCH CHARACTERISTICS

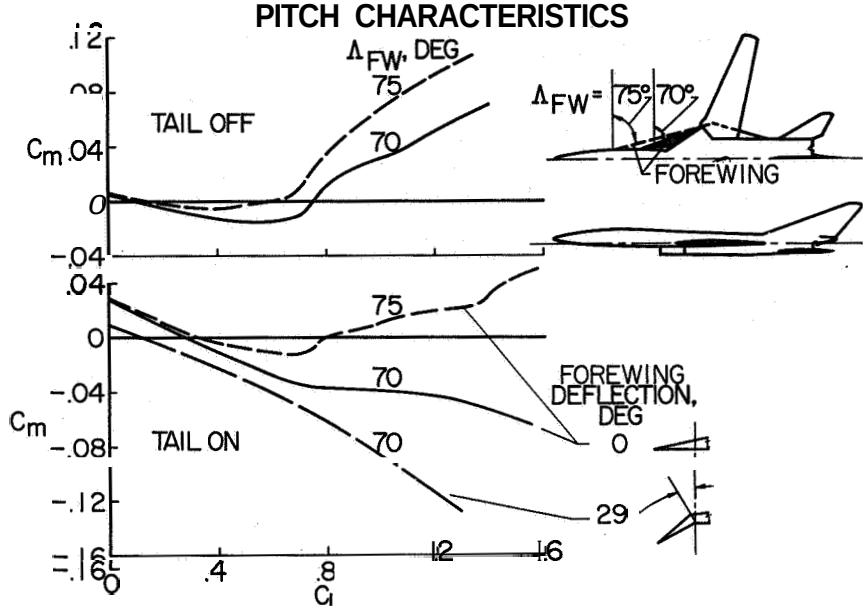

Figure 9

EFFECTS OF HORIZONTAL-TAIL LOCATION ON LOW-SPEED TAIL PITCH CONTRIBUTION

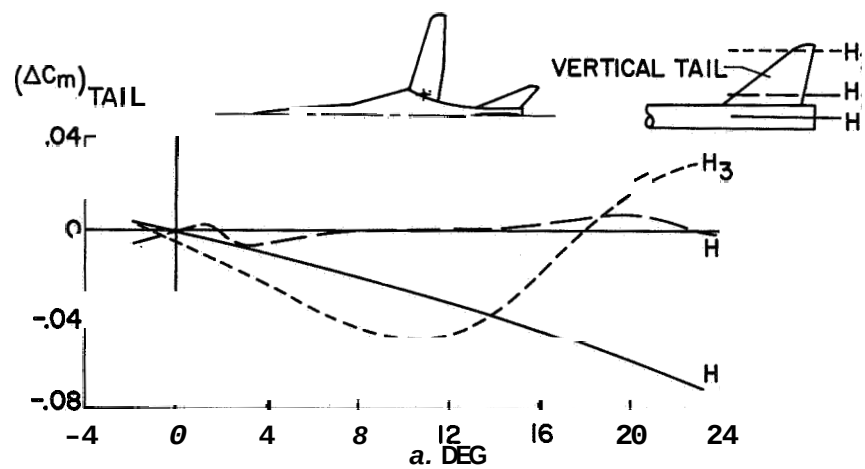

Figure 10

EFFECT OF WING DEVICES ON LOW-SPEED PITCH CHARACTERISTICS

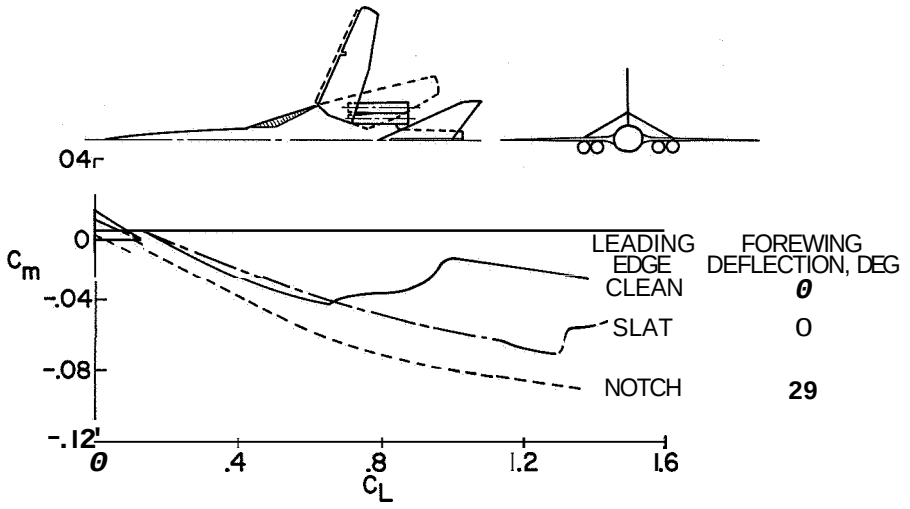

Figure 11

LOW-SPEED STABILITY CHARACTERISTICS OF M WING CONFIGURATION

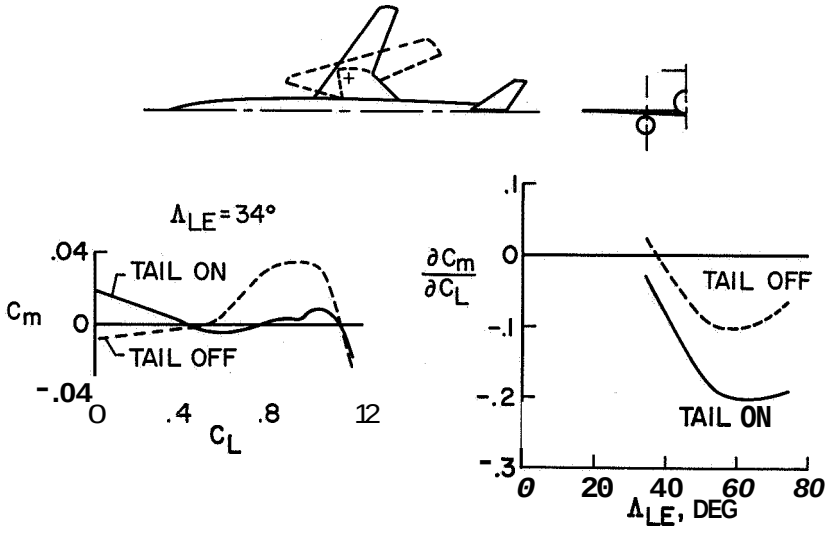

Figure 12

GEOMETRIC CHARACTERISTICS OF HIGH-LIFT MODEL

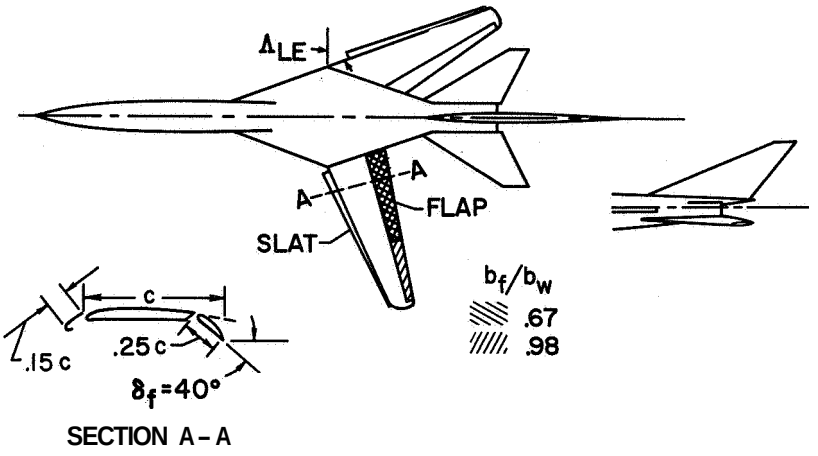

Figure 13

HIGH-LIFT CHARACTERISTICS

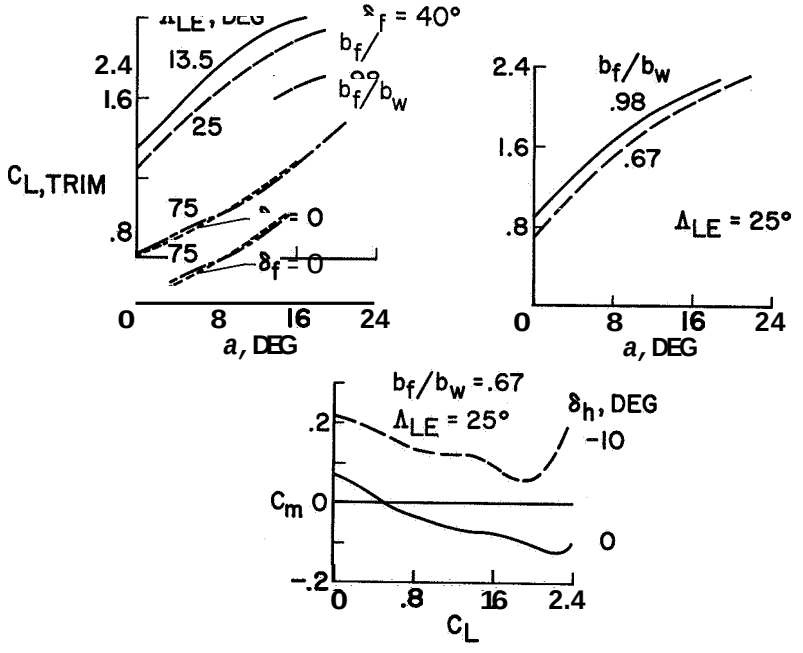

Figure 14

[redacted]

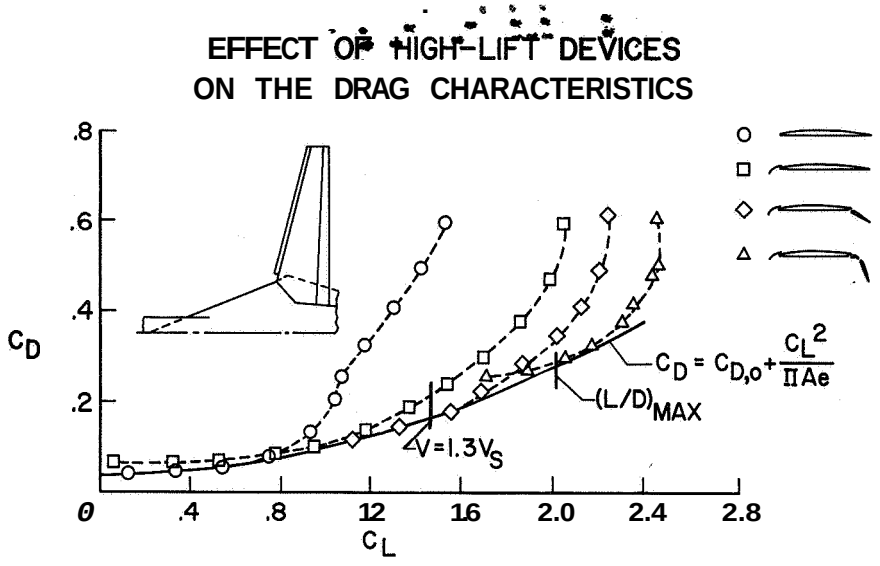

Figure 15

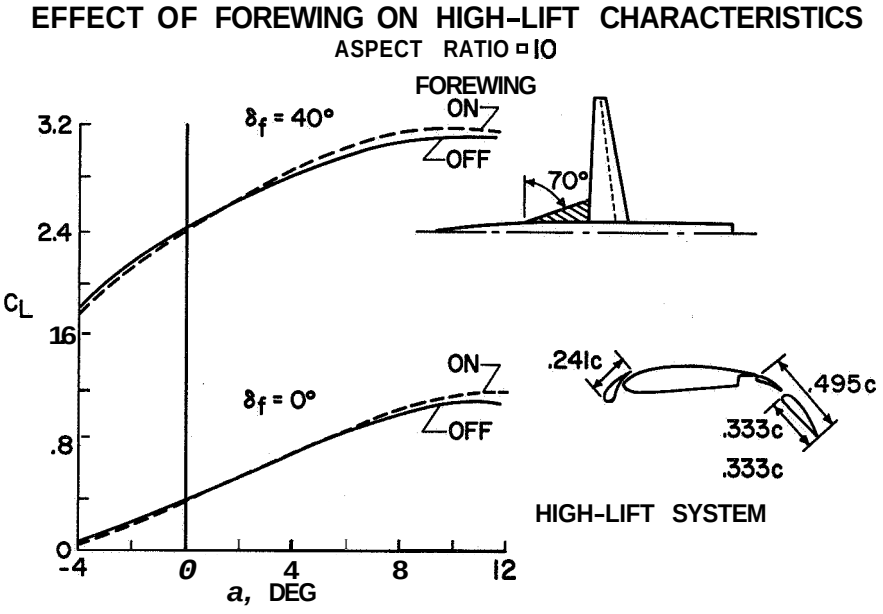

Figure 16

[redacted]

EFFECT OF FOREWING ON HIGH-LIFT CHARACTERISTICS

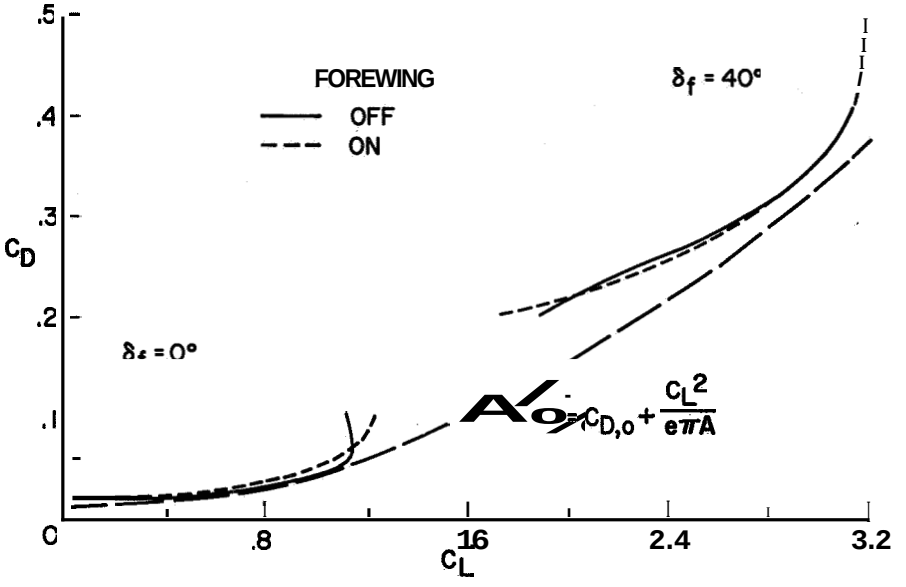

Figure 17

EFFECT OF CONFIGURATION ON LATERAL CHARACTERISTICS

M=0.2

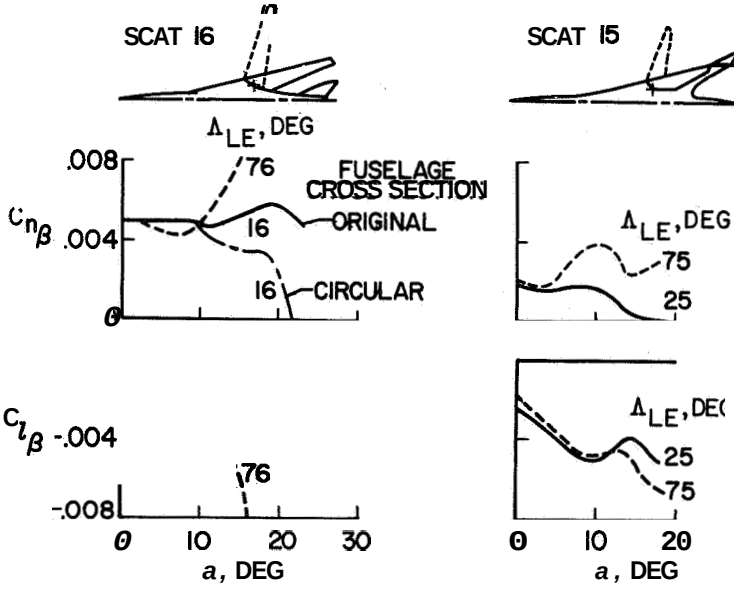

Figure 18

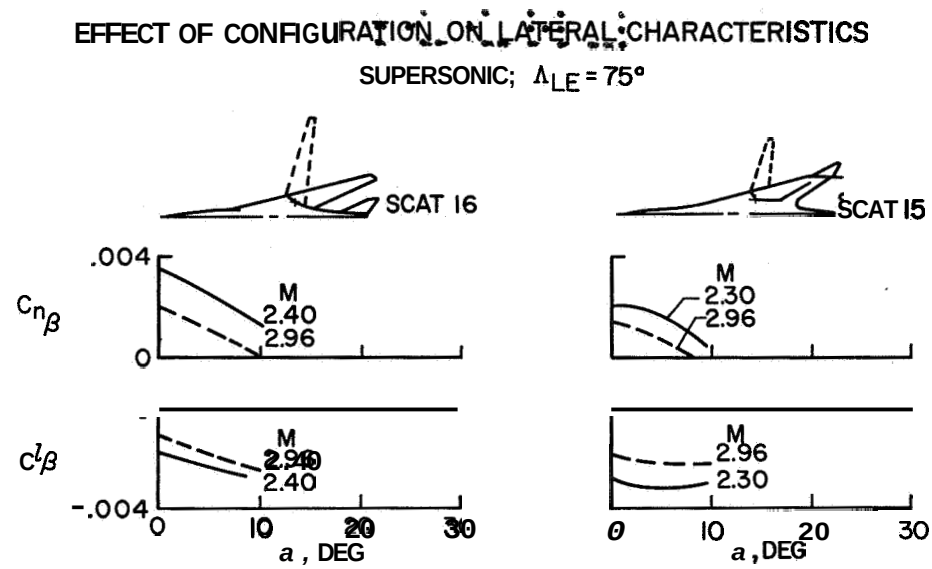

Figure 19

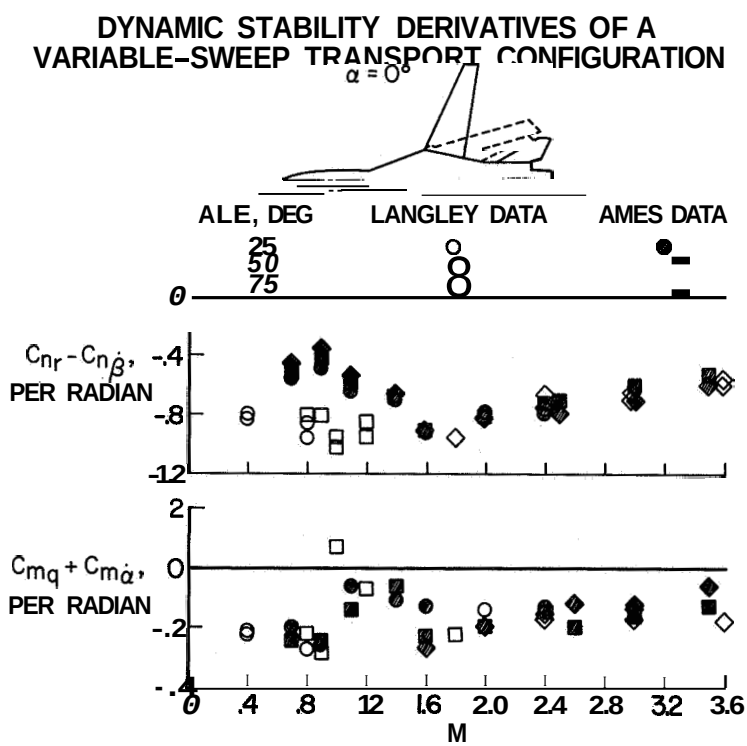

Figure 20

N67-31619

PRECEDING PAGE BLANK NOT FILMED.

12

12. NASA WING PLANFORM STUDIES

By Robert T. Taylor, William P. Henderson
NASA Langley Research Center

Raymond M. Hicks, and Edward J. Hopkins
NASA Ames Research Center

SUMMARY

Supersonic commercial air transport (SCAT) studies have shown the need for increased performance for wings with supersonic leading edges and the requirements for low-speed stability research on planforms with subsonic edges. Summarized are recent planform studies by the National Aeronautics and Space Administration which indicate wing warp to have a powerful effect on supersonic trimmed lift-drag ratio. Studies at low speed have shown that notched planforms tend to reduce the pitch-up tendency.

INTRODUCTION

Recent SCAT feasibility studies completed by The Boeing Company and Lockheed California Company have concentrated on the SCAT 16 variable-sweep-wing configuration and the SCAT 17 fixed-wing configuration.

SCAT 17 studies have shown that, although the planform chosen lends itself to lightweight construction, a need to increase the aerodynamic performance throughout the flight Mach number range exists. Other fixed-wing configurations incorporating some of the features of the SCAT 4 and SCAT 15 supersonic configurations are also of interest because of the high aerodynamic efficiency possible at the cruise condition. Low-speed stability problems, however, have been encountered with highly swept arrow wings.

The purpose of the present paper is to present the results of recent planform studies conducted by the NASA and to relate these studies to the problem of supersonic aircraft design. The first part of the paper then will concentrate on planform studies which indicate some possible gains in high-speed performance on the SCAT 17 type and on tailless configurations, and the last part will show the results of some Planform studies aimed at the low-speed stability problems of wings having subsonic leading edges at the Mach 3 design point.

SYMBOLS

A	aspect ratio
b	span
$C_{D,o}$	drag coefficient at zero lift
C_L	lift coefficient
C_m	pitching-moment coefficient
$C_{m,o}$	pitching-moment coefficient at zero lift
$\frac{\partial C_m}{\partial C_L}$	static margin
$\frac{L}{D}$	lift-drag ratio
$\left(\frac{L}{D}\right)_{MAX}$	maximum lift-drag ratio
$\left(\frac{L}{D}\right)_{TRIM}$	trimmed lift-drag ratio
M	Mach number
R	Reynolds number
t/c	thickness-chord ratio
Λ_{LE}	leading-edge sweepback angle, deg

DISCUSSION

The SCAT 17 wing is characterized by a planform having a near-delta shape and very thin airfoil sections. In order to assess changes in planform, several variations on this type of wing have been tested and are shown in figure 1. In the upper part of the figure are shown a delta wing, a wing with an ogee leading edge, and a trapezoidal wing. All these wings had the same span and had an aspect ratio of 1.55. All

the wings were tested on the same body and each had a circular-arc wing section with thickness-chord ratios of 3 percent at the fuselage and 2 percent near the tip.

In addition to the planar wings shown, wings employing twist and camber and designed for maximum lift-drag ratio at a Mach number of 2.20 were also tested in all these planforms. Wings in the lower part of the figure have an aspect ratio of 2.17 and are of modified trapezoidal, ogee, and delta planform. The wings had 30 - 70 hexagonal sections and all had a thickness-chord ratio of 2 percent.

The right-hand side of figure 2 shows a summary of the aerodynamic data obtained with the wings of aspect ratio 2.17; this summary is presented as $(L/D)_{MAX}$ and $C_{D,o}$ plotted against Mach number. Comparisons of the data for the wings of aspect ratio 2.17 and 1.55 are not valid because of differences in model fuselage and in model test conditions. The curves in the upper left of the figure show only minor differences in maximum lift-drag ratio for all three planforms throughout the test Mach number range, with a slight advantage in favor of the trapezoid of about 0.3 to 0.5 in $(L/D)_{MAX}$. For all practical purposes, the differences in maximum lift-drag ratio may have only a slight bearing on the selection of wing planform within the range of wings tested. In the right-hand portion of the figure note the larger differences in $C_{D,o}$ at all speeds, with values for the modified trapezoidal and delta wings appearing slightly higher. However, the differences in $C_{D,o}$ are offset to some degree by better drag-due-to-lift factors for these planforms and the maximum lift-drag ratio appears to be about the same for all planforms. These data showed a slight advantage in favor of the ogee planform, again about 0.3 to 0.5 in $(L/D)_{MAX}$. There appear again relatively small differences from which to select wing planform on a performance basis as indicated by these data.

Another parameter of interest is the shift in static margin with Mach number inasmuch as it may be a measure of trim drag throughout the speed range. Figure 3 shows static margin $\partial C_m/\partial C_L$ as a function of Mach number for the wings tested. A comparison of all wings, starting at about the same static margin, shows that changes from 4 percent to about 20 percent are evident as Mach number increases at both the aspect ratios. A slightly smaller shift in static margin is indicated for the ogee planform at the higher speeds. At M = 2.20 this advantage is about 2 percent for both aspect ratios. The effect of high static margin on trimmed lift-drag ratio may be sizable depending not only on tail arm but on pitching moment at zero lift as well. The warping of planforms such as those shown for maximum lift-drag ratio at some supersonic speed generally results in washout along the span. For wings with

highly swept leading edges then, a positive pitch is expected at zero lift; this pitch, when combined with a stable pitch variation, tends to reduce the drag due to trimming. Using the stability variations with Mach number shown in figure 3, figure 4 was prepared to show the favorable effect of wing warp on trimmed lift-drag ratio. Shown are trimmed lift-drag ratios as a function of static margin at full-scale Reynolds number and at Mach numbers of 0.97 and 2.20.

The data shown in figure 4 are applicable to a tailless configuration of aspect ratio 1.55. The planform and trailing-edge controls selected as illustrative are shown in the sketch at the top of the figure; however, similar curves may be shown for the other planforms. The vertical lines on the figure show the stability level consonant with each Mach number from figure 3.

At a Mach number of 0.97 the planar wing shows a decrement of about 3.0 in L/D due to trimming at the required stability level, whereas the warped wing trims with no control deflection at a static margin of 14 percent because of the higher positive C_m at zero lift. At M = 2.20 neither wing had sufficient $C_{m,o}$ to trim the potential L/D of the planform but the warped wing showed a value of L/D about 1.5 greater at trim with the required stability. The sensitivity of L/D to static margin is approximately the same for all these wings and it can be seen that the 2-percent advantage in static margin mentioned previously for the ogee wing will only amount to about 0.20 to 0.30 in L/D at the trim static margin.

As pointed out in paper no. 7 by Francis E. McLean and Harry W. Carlson, further warping of this wing for a higher design C_L may be expected to reduce the maximum value of L/D slightly. But, based on the results shown in figure 4, the higher $C_{m,o}$ associated with the higher design C_L may be expected to more than make up the slight loss in $(L/D)_{MAX}$ by providing a trimmed L/D which is much closer to the maximum value shown. According to this figure, the planform could be warped even more in an attempt to move the solid curve to the right while minimizing the reduction in the level of maximum L/D.

In addition to the data shown, lateral-directional data are available on all these planforms and, as might be expected, no radical differences appeared between wings as a result of the planform changes.

Now consider wings employing subsonic leading edges at the M = 3.0 cruise design point. As pointed out previously the wings thus far considered have been arrow planforms as on SCAT's 4 and 15; these wings have been characterized by a longitudinal instability known as pitch-up in the low-speed or landing flight regime.

Although it has been shown that placement of the horizontal tail below the wing-chord plane is effective in the elimination of pitch-up, many of the configurations developed for SCAT study preclude, for one reason or another, this tail placement. The problem then is confined to the development of wing planforms having high aerodynamic aspect ratio and low structural spans which are pitch-up free and to the placement of the horizontal tail in a suitable location consistent with overall good design.

The NASA has recently completed a preliminary investigation to study means by which pitch-up may be eliminated or, at least, helped by the judicious selection of planform and the careful matching of wing and horizontal-tail characteristics.

Some of the planforms tested are shown in figure 5. For the tests of this series of wings, the leading-edge sweepback was held constant at 75°. All the wings were tested in combination with a fuselage and employed flat-plate sections with rounded leading edges. Shown in the upper left-hand corner of the figure is a basic trapezoid, which is pitch-up free but shows limited cruise performance potential. Wings were tested with trailing edges cut away to increase aspect ratio; these wings are shown across the top of the figure. Leading edges were also notched or cut as shown in the left-hand column in the figure. In addition, several combinations were tried of leading-edge and trailing-edge notches as shown by the remaining planforms.

Some data which are typical of these tests are shown in figure 6. The wing planforms are those delineated by the aspect-ratio numbers with the sketches. Pitching-moment coefficient is plotted as a function of lift coefficient; these coefficients have been reduced by using the mean aerodynamic chord and the area of each wing, respectively. The static stability level at zero lift has been adjusted to 5 percent for all wings in order to judge nonlinearities more easily.

The curves in the upper left-hand plot in the figure are typical of those for the arrow wings and show pitch-up, as the basic trapezoid trailing edge is cut, at all the aspect ratios indicated. These data are typical of the curves obtained with the SCAT 4 configuration and were, to a large extent, responsible for the configuration being tabled at SCAT midterm.

The curves on the upper right-hand plot in the figure show data for variations in the leading-edge notch location from the basic trapezoid of 25 percent, 33 percent, and 40 percent of the semispan. Note that the planforms with the 25-percent and 33-percent leading-edge notch locations become more stable with increasing lift, whereas the planform with the 40-percent leading-edge notch location tends to less stability.

The lower plot is an attempt to show the sensitivity of the planform with the 33-percent leading-edge notch location to trailing-edge notch location. The trailing-edge notch is moved spanwise with ±50° trailing-edge sweep and a pronounced change in the shape of the pitch curve is evident.

Another wing, discussed in paper no. 14 by A. Warner Robins and Richard T. Whitcomb, is similar to the $A = 1.48$ wing but of higher aspect ratio and pitched down if chord-extensions were used on the outer panel.

Figure 7 shows a comparison of data at subsonic and supersonic speeds on similar, but not identical, planforms. These data are included to indicate the marked similarity between the subsonic and supersonic pitch curves and to indicate the type of data which are becoming available on arrow-type planforms as a function of speed. Further work of this sort will no doubt be accomplished in the future.

It appears from the test results shown that there are combinations of leading- and trailing-edge notch which provide acceptable longitudinal stability variations, at aspect ratios significantly higher than might be indicated by the Shortal-Maggin stability curve. Further tests are required, however, to validate the expected aerodynamic performance of the notched planforms at transonic and supersonic speeds.

CONCLUDING REMARKS

It has been shown that wing planform differences on thin sharp-edged wings appear to have small effects on the maximum lift-drag ratio at subsonic, transonic, and supersonic speeds. Planform differences were also shown to have a small effect on aerodynamic-center shift with a change in Mach number. Wing warp, on the other hand, was shown to have a powerful effect on trimmed lift-drag ratio of all planforms in the lower aspect-ratio series.

On wings with subsonic leading edges at a Mach number of 3.0, the notched wings appear to show promise of reducing the pitch-up tendency at low speed, although further testing is required to validate the expected aerodynamic performance at transonic and supersonic speeds.

[redacted]

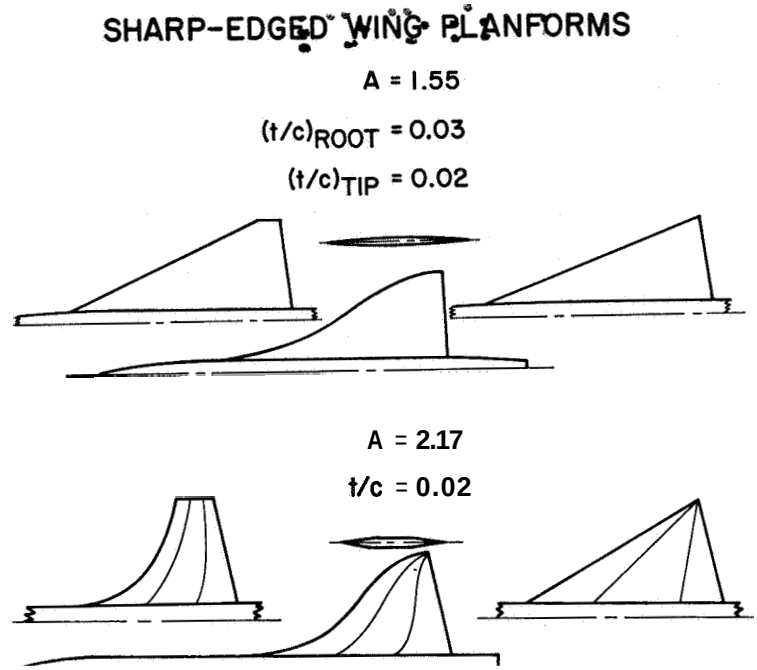

Figure 1

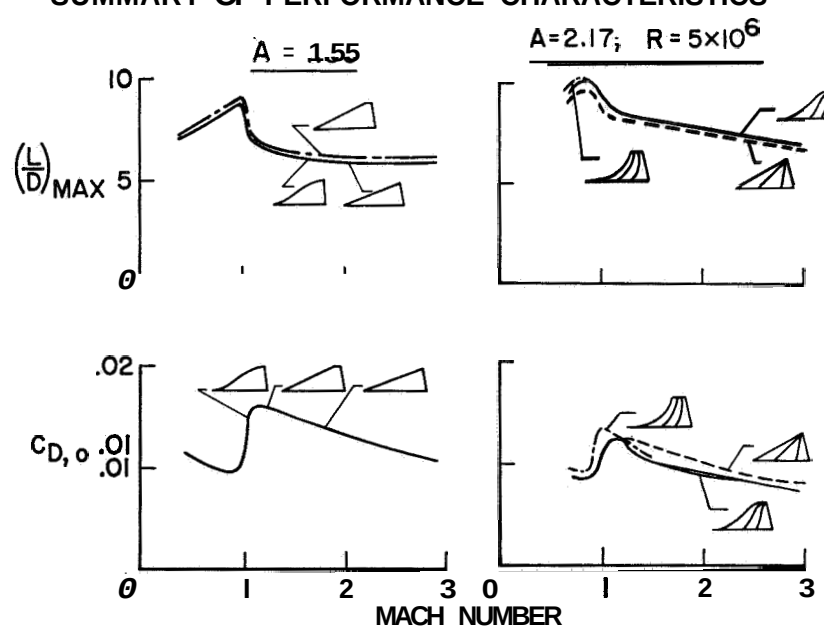

Figure 2

[redacted]

EFFECT OF MACH NUMBER ON STATIC MARGIN

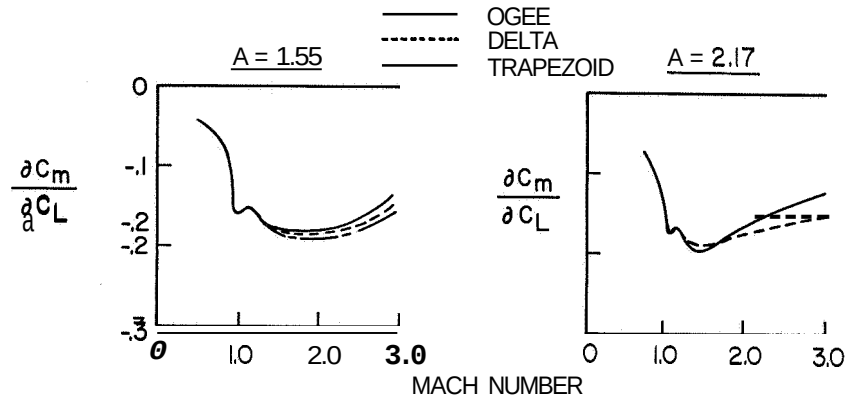

Figure 3

EFFECT OF WING WARP ON TRIMMED L/D
FULL-SCALE REYNOLDS NUMBER; A = 1.55

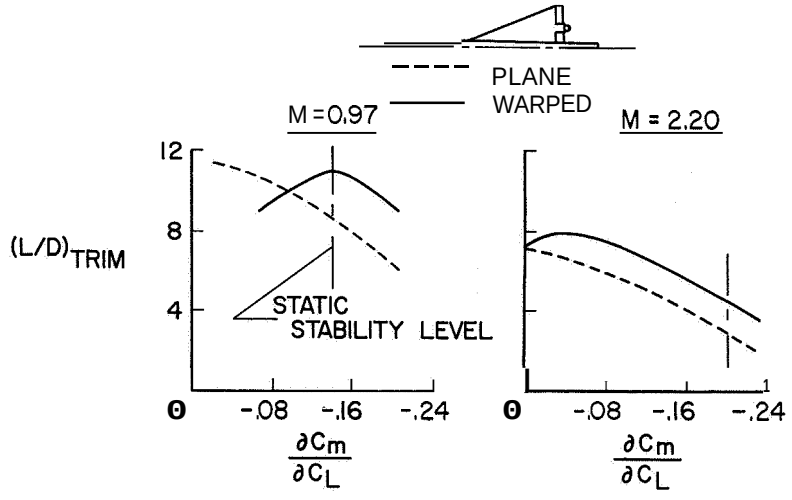

Figure 4

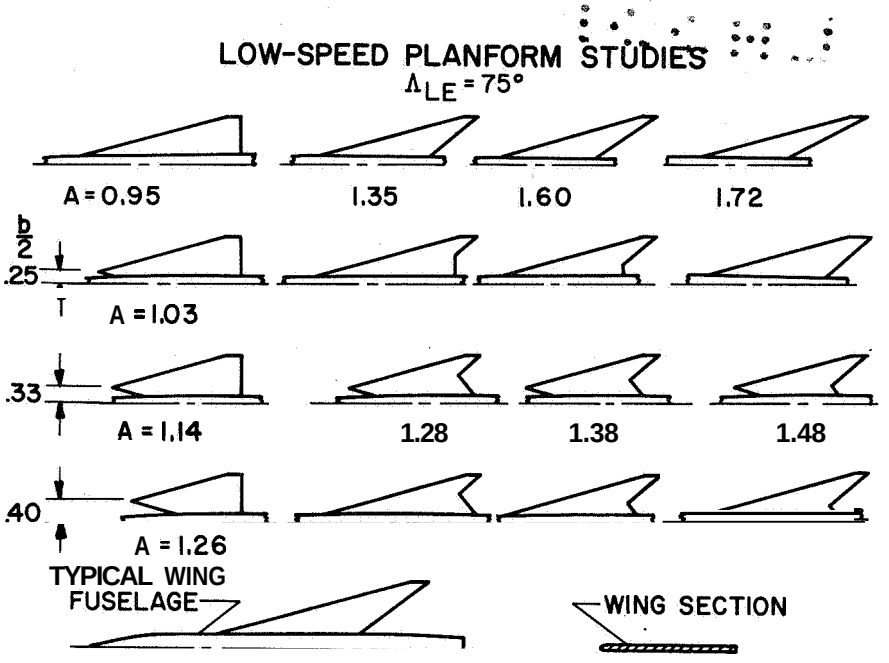

Figure 5

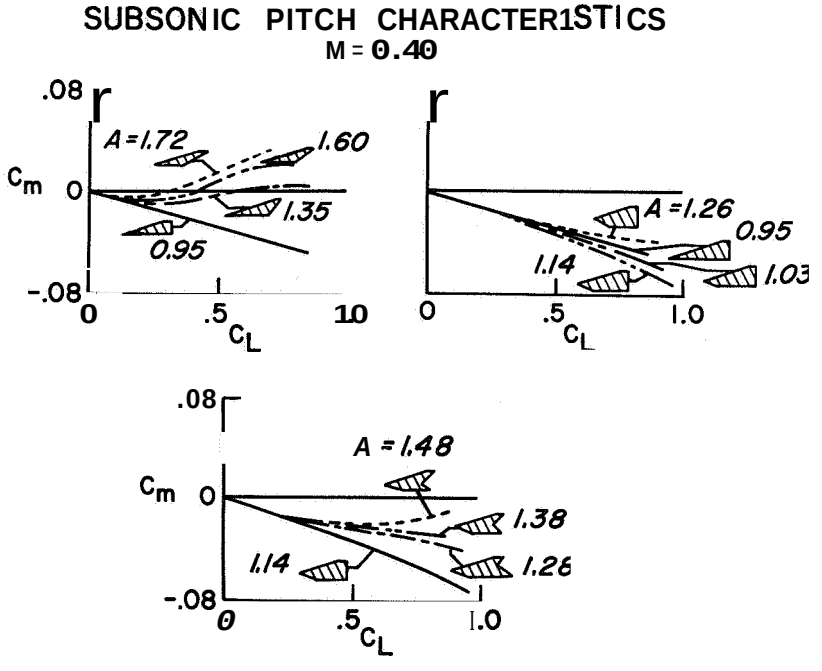

Figure 6

SUBSONIC AND SUPERSONIC PITCH COMPARISONS

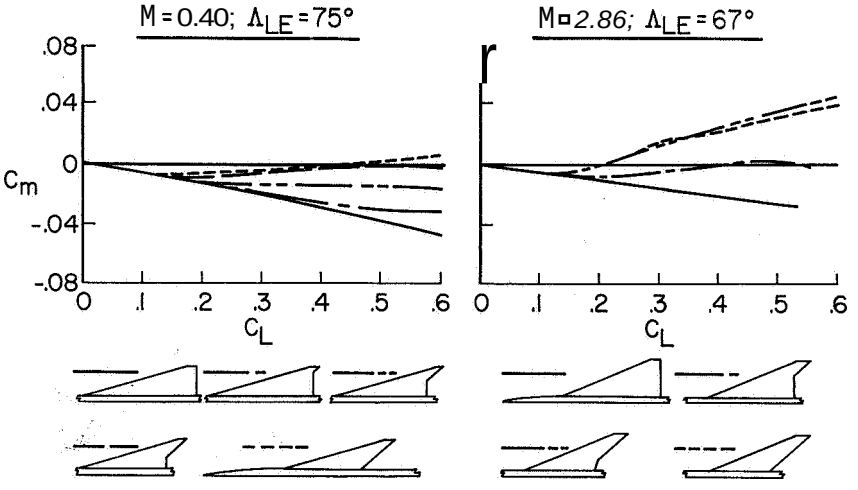

Figure 7

N67-31620

13. LATERAL-DIRECTIONAL STABILITY STUDIES AT SUPERSONIC SPEEDS

By M. Leroy Spearman

NASA Langley Research Center

13

SUMMARY

A substantial quantity of research information has been obtained on the stability characteristics of aircraft configurations at supersonic speeds. The investigations include the effects of variable wing sweep, wing modifications, vertical-tail modifications, and body-cross-section changes. Illustrative examples of the results are presented in order to point out some of the factors that affect the lateral-directional stability characteristics.

INTRODUCTION

SCAT feasibility studies have indicated some stability problem areas, such as pitch-up, low directional stability, and high effective dihedral. As a result, several wind-tunnel investigations have been undertaken in order to gain insight into these problems and to indicate some factors that may aid in providing solutions. Paper no. 11 by Alford, Lockwood, McKinney, and Greif, and paper no. 12 by Taylor, Henderson, Hicks, and Hopkins have considered the problem of pitch-up at subsonic speeds. The stability characteristics of delta-wing configurations are presented in the paper by Anderson (paper no. 10). The present paper will summarize some recent stability investigations conducted at supersonic speeds with the primary emphasis on the lateral-directional stability problems. The factors to be discussed include the effects of variable wing sweep, the effects of filling the notch of swept wings, the effects of outboard-vertical-tail shape, and the effects of body cross section.

SYMBOLS

C_L lift coefficient

C_{l_β} effective-dihedral parameter

$C_{l_{\beta C_L}}$ variation of effective-dihedral parameter with lift coefficient

C_{n_β} directional-stability parameter

$(\Delta C_{n_\beta})_{TAIL}$ tail contribution to directional-stability parameter

M Mach number

α angle of attack, deg

Λ_{LE} sweep angle of wing leading edge, deg

DISCUSSION

Variable-Sweep Aircraft

Since several transport configurations utilizing variable-sweep wings have been proposed, an investigation of a generalized variable-sweep model has been undertaken in which the effects of wing sweep have been studied systematically over a large Mach number range. The variable-sweep research model is presented in figure 1. The model was tested in combined pitch and sideslip for a range of wing sweep angles from 30° to 75° over a Mach number range from 1.4 to 3.5 with the vertical tail both on and off. Both a plane wing and a twisted wing were investigated. Three wing-tip controls having different hinge-line skew angles have also been investigated with various wing sweeps at M = 1.41 and 2.2, but none of these results are included in the present paper.

Wing sweep was found to have little effect on the directional stability characteristics, but, as might be expected, there are significant effects of sweep on the rolling-moment characteristics. The effects of wing sweep and Mach number on the variation of rolling moment due to sideslip with lift coefficient $\left(C_{l_{\beta C_L}}\right)$ are presented in figure 2. The coefficients are based on the geometry of the 75° wing. The results indicate a general increase in effective dihedral with increasing wing sweep and a general decrease with increasing Mach number.

The rolling moment provided by the wing is a function of the wing-panel lift-curve slope and thus would be expected to change with sweep angle and Mach number. Theoretically, the rolling moment due to sideslip would be negative for subsonic leading edges but would decrease and possibly change sign for supersonic leading edges. The tick marks

on the curves in figure 2 indicate the sonic-leading-edge points and show the relatively high negative values of rolling moment due to sideslip for wings swept behind the Mach lines and relatively low values for wings swept ahead of the Mach lines. In the case of the lowest sweep and the highest Mach number ($\Lambda_{LE} = 45^\circ$, $M = 3.5$), a small positive value was obtained. It is apparent that wings highly swept to provide subsonic leading edges for good lift-to-drag characteristics will inherently have high values of effective dihedral. Of course, the level of effective dihedral can be regulated to some extent by the contributions of the tail, wing geometric dihedral, and wing height. Another point to be noted is the fact that the variation of effective dihedral with Mach number can be regulated by varying the wing sweep provided that proper consideration is given to the effects of sweep on the other aerodynamic characteristics.

Fixed-Wing Modifications

One of the modifications proposed for highly swept fixed wings has been to reduce the notch ratio for the purpose of improving the pitching-moment linearity and also to improve the structural integrity. Accordingly, a systematic study has been made of the effects of various wing modifications, including variations in notch ratio. The wing-modification model is presented in figure 3. The basic model consisted of an ogive-cylinder body with a 62° swept wing. Various modifications to the wing provided for two full-span leading-edge extensions having sweep angles of 64° and 67° and three trailing-edge inserts that resulted in progressively filling the notch until a trapezoidal planform was obtained. Each of the trailing-edge inserts have been tested with each of the leading-edge extensions. In addition, two semispan leading-edge gloves having sweep angles of 67° and 71° were tested in conjunction with the basic 62° swept wing. Tests have been made of the model in combined pitch and sideslip with the vertical tail both on and off for Mach numbers of 1.6, 2.2, and 2.9.

The effects of progressively filling in the notch of the 62° swept wing until a trapezoidal wing is obtained are illustrated in figure 4. These results are all based on the geometry of the 62° swept wing as indicated by the shaded region; hence, a given value of C_L represents a constant weight condition but varying wing loadings. The sideslip characteristics indicate less deterioration of C_{n_p} with increasing C_L and generally lower values of effective dihedral for the filled-in wings. The improvement in C_{n_β} results from the fact that for a given lift the angle of attack is lower for the larger filled-in wings and the detrimental effects of the forebody lift on C_{n_p} are lessened.

The reduction in $-C_{l_\beta}$ is partly due to the reduction in wing-panel aspect ratio and the attendant decrease in panel lift-curve slope.

SCAT 15 Vertical-Tail Study

Previous investigations of the SCAT 15 model at supersonic speeds indicated relatively high values of effective dihedral and some deterioration of directional stability with increasing angle of attack. As a result, an investigation has been conducted to determine the effects of decreasing the vertical-tail area above the wing chord plane and increasing the area below the chord plane in the hope that the level of effective dihedral might be reduced while the directional stability was improved. The SCAT 15 model is represented in figure 5. The model was investigated with a series of equal-area vertical tails ranging from a tail having all its area above the wing chord plane to a tail having all its area below the wing chord plane. In addition, one test was made with the tails removed. The model was tested at combined angles of attack and sideslip for Mach numbers of 2.3, 2.6, 3, and 3.5.

The results for $M = 2.3$ (fig. 6) indicate that relocating the entire vertical-tail area from above the wing chord plane to below the wing chord plane does reduce the effective dihedral throughout the angle-of-attack range and provides an increase in directional stability at high angles of attack. The increment of effective dihedral provided by the vertical tails is relatively small compared with the basic level for the wing-body configuration, however, and it is doubtful whether the reduction in $-C_{l_\beta}$ obtained by placing the entire tail area below the wing would be worth the complications involved. The small effect of the vertical tail on C_{l_β} is characteristic of outboard-tail configurations and results from an interference effect such that the pressure field from the tail produces a rolling moment from the wing tip which is opposite to that provided by the tail.

Body-Cross-Section Study

Among other general studies made of factors affecting the lateral-directional stability characteristics has been the investigation of the effects of body cross section. The body-cross-section research model is presented in figure 7. The body cross sections shown extended over the entire body length and the wings were located at the midbody height. A 49° swept wing was investigated at Mach numbers of 1.4 and 2.2 and a 75° wing was investigated at $M = 2.5$, 3, 4, and 4.7. The model was tested

in combined pitch and sideslip with the vertical tail on and off. In addition, the model with triangular cross sections was also tested with the wing removed.

Lateral and directional stability characteristics are presented in figure 8 for the 49° swept configuration at $M = 2.2$ with a circular and a vertical elliptical body cross section. It is apparent that body cross section can have a significant effect on the sideslip derivatives in that not only are the variations of C_{n_β} and C_{l_β} with angle of attack considerably different for the wing-body configurations but the contributions of the vertical tail to C_{n_β} are affected as well. These differences are related to differences in the body cross flow for particular body shapes and, to some extent, might be affected by Reynolds number. However, results obtained for the triangular body shape indicated no effects of Reynolds number over a range from 1×10^6 to 4×10^6 per foot. Although these results are qualitative in nature, they serve as an indication that body-cross-section effects on the lateral stability characteristics should not be overlooked.

CONCLUDING REMARKS

A substantial quantity of research information has recently been obtained on the stability characteristics of aircraft configurations at supersonic speeds. The investigations include the effects of variable wing sweep, effects of wing modifications, effects of vertical-tail modifications, and effects of body cross section. Each of the investigations indicates important effects on the lateral-directional stability characteristics that should be considered in specific configuration design. Continuations of these investigations will include the effects of wing height and wing geometric dihedral for highly swept wings, additional studies of lateral control devices, and additional planform modifications.

VARIABLE-SWEEP MODEL

Λ_{LE} = 30°, 45°, 65°, AND 75"; M = 1.4, 2.3, 3, AND 3.5; VERTICAL TAIL ON AND OFF

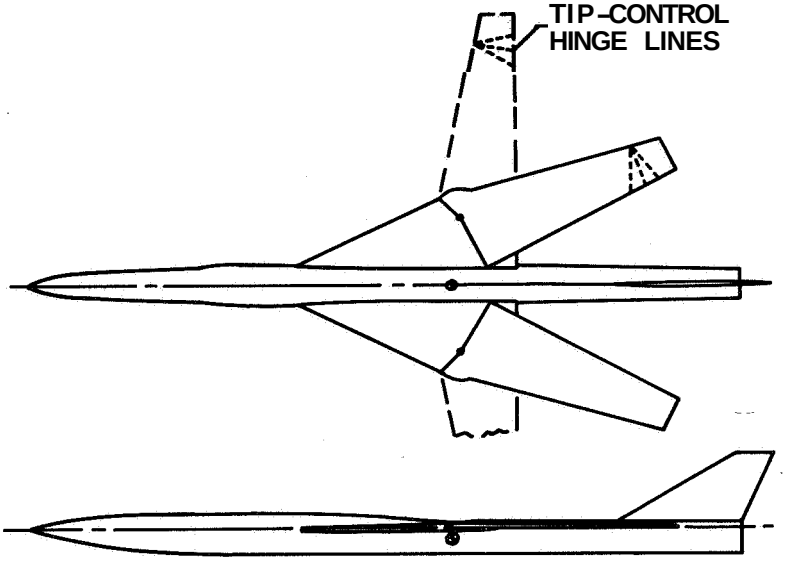

Figure 1

EFFECT OF SWEEP AND MACH NUMBER ON EFFECTIVE DIHEDRAL

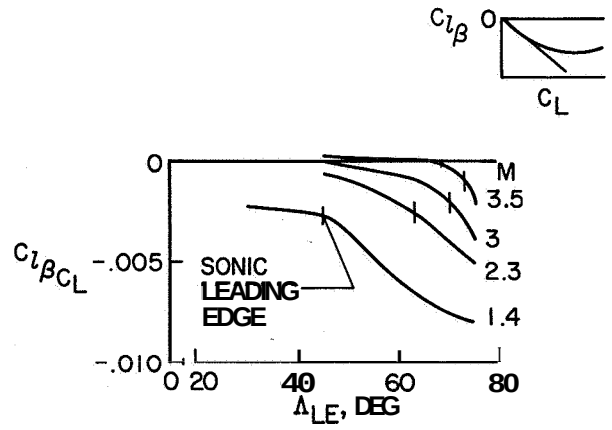

Figure 2

RESTRICTED

WING-MODIFICATION MODEL
M=1.6, 2.2, AND 2.9; VERTICAL TAIL ON AND OFF

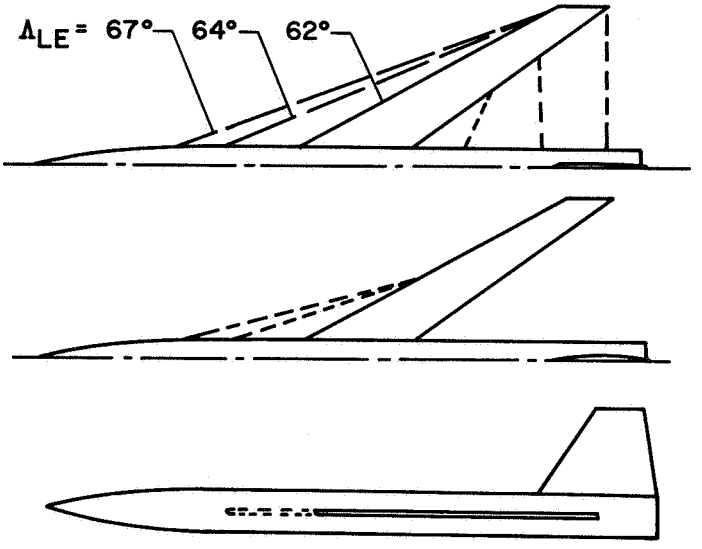

Figure 3

EFFECT OF WING MODIFICATION

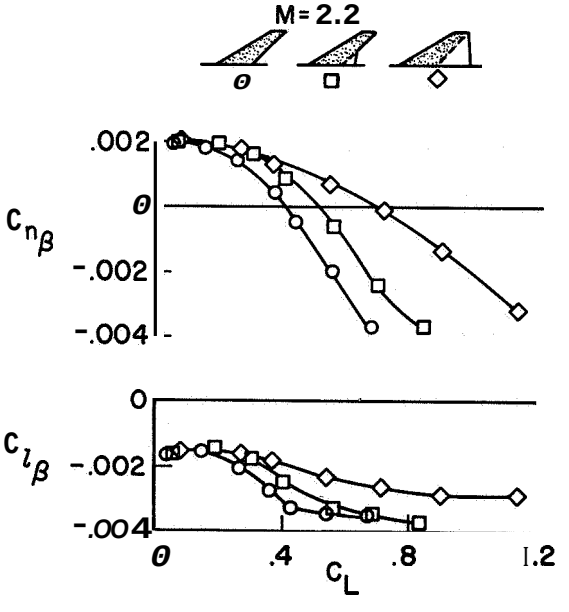

Figure 4

SCAT I5 VERTICAL-TAIL STUDY
M = 2.3, 2.6, 3, AND 3.5; VERTICAL TAIL ON AND OFF

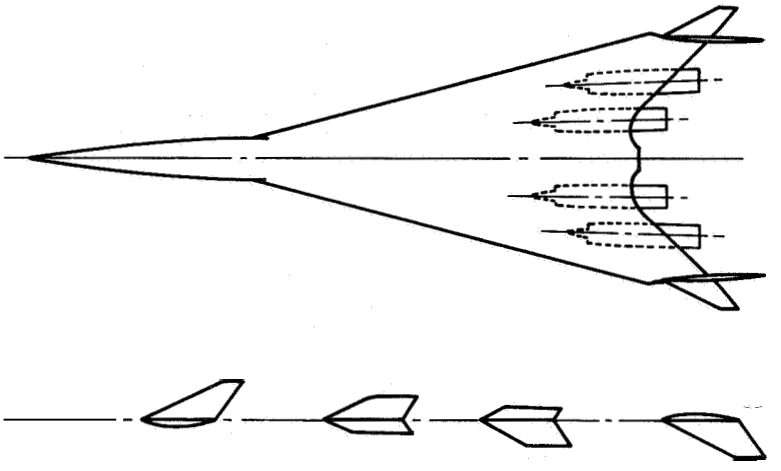

Figure 5

EFFECT OF TAIL VARIATIONS
SCAT 15; M = 2.3

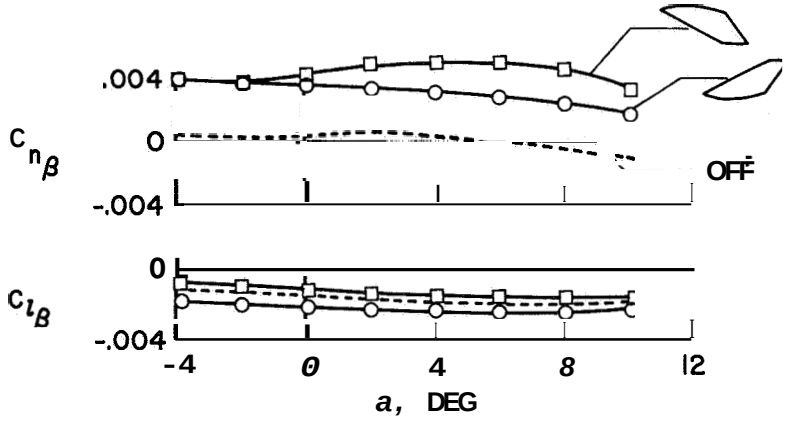

Figure 6

[redacted]

BODY–CROSS–SECTION MODEL

Λ_{LE} = 49° AT M = 1.4 AND 2.2 ;

Λ_{LE} = 75° AT M = 2.5, 3, 4, AND 4.7;

VERTICAL TAIL ON AND OFF; WING ON AND OFF

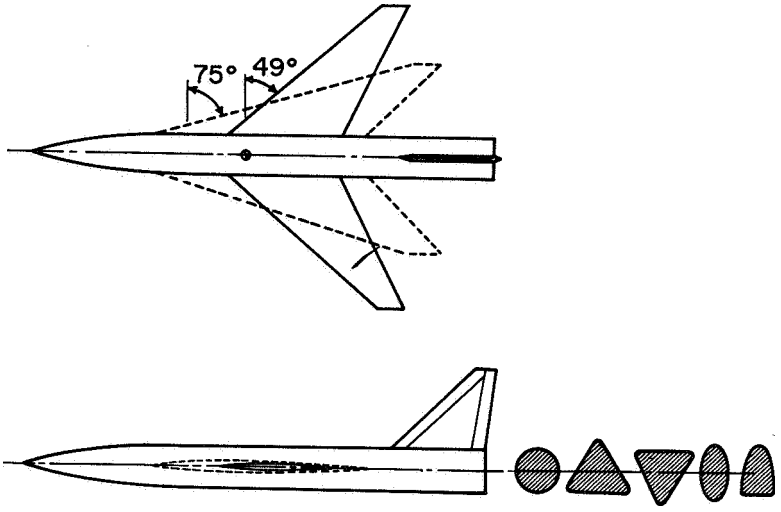

Figure 7

EFFECT OF BODY CROSS SECTION

Λ_{LE} = 49° ; M = 2.2

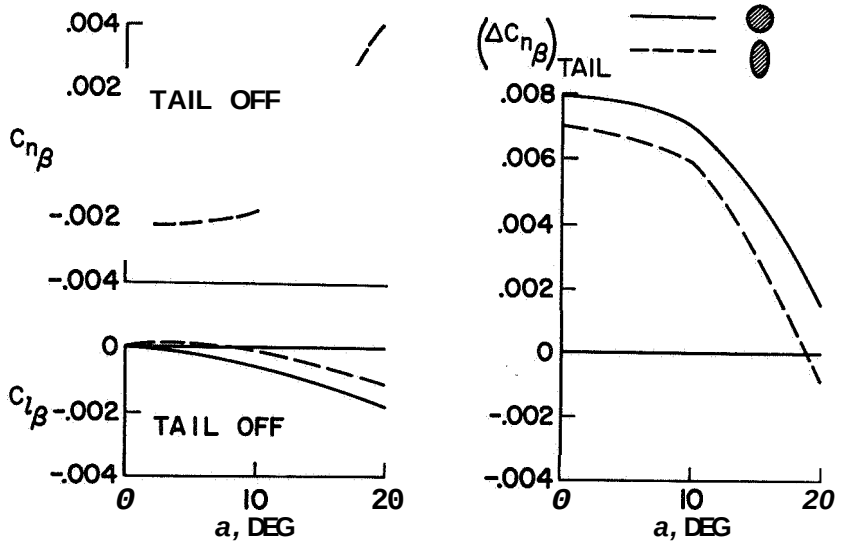

Figure 8

[redacted]

N67-31621

14. ADDITIONAL CONFIGURATION APPROACHES

By A. Warner Robins and Richard T. Whitcomb

NASA Langley Research Center

PRECEDING PAGE BLANK NOT FILMED.

SUMMARY

Some of the major problems encountered in the SCAT feasibility studies are reviewed and changes to improve the four basic SCAT configurations are discussed. Improvements in nearly all problem areas appear possible. Advanced versions of each of the four SCAT concepts are being investigated.

14

INTRODUCTION

The supersonic transport feasibility studies have replaced NASA's original qualitative assessment of the problems of each of the four SCAT concepts with a reasonably complete quantitative evaluation. With the provision of a better understanding of the relative importance of the problems of supersonic transport design, new approaches to existing concepts are suggested. Concepts represented are for SCAT's 17, 16, 15, and 4.

The purpose of this paper is to review some of these problems and to indicate the directions that the efforts of NASA are now taking toward making improved configurations of all four concepts.

SYMBOLS

A	aspect ratio
$A_{LE,MIN}$	aspect ratio of wing in minimum sweep position
$C_{D,W}$	wave-drag coefficient
c_{REF}	reference chord
L/D	lift-drag ratio

M	Mach number
	mass-flow ratio
x	longitudinal distance measured from wing apex
$\Delta a.c.$	aerodynamic-center shift, percent c_{REF}
Λ_{LE}	sweep angle at wing leading edge

Subscripts:

MAX	maxim
MIN	minimum

DISCUSSION

SCAT 17

Figure 1 shows a sketch of each of the final SCAT 17 configurations as developed by the two contractors. (See paper no. 3 by R. Richard Heppe and Jim Hong and paper no. 4 by Lloyd T. Goodmanson, William T. Hamilton, and Maynard L. Pennell.) The problems of these configurations include undesirably low lift-drag ratios in both low-speed and cruising flight and low-speed handling qualities that are inferior to those of present 3et transports. The two configurations do not share these problems equally.

A configuration indicative of the direction presently being taken by \$hose concerned with the SCAT 17 concept is shown in figures 2 and 3. Changes include the adoption of a wing planform having an increased effective aspect ratio and a complex leading edge, the inboard region being subsonic and the outboard region, supersonic. Increased wing volume and improved area progressions result. The new configuration reverts to the arrangement of the original configuration with both canard and aft tail. Figure 2 shows the aft tail folded down so as to increase directional stability and decrease longitudinal stability as required in cruising flight. The outboard wing leading edge is conically cambered and provides for leading-edge droop about a hinge line shown as the second line behind the leading edge. These changes were made with a view to improving low-speed lift-drag ratios and speed stability in approach, as well as low-speed handling qualities. In order to improve trim drag and to retain reasonably low drag due to lift at

the cruise point, several wing warp schemes are being studied. Additional work along these and, similar lines is planned.

SCAT 16

The contractors' final SCAT 16 configurations are sketched in figure 4. (See paper nos. 3 and 4.) Major problems, with magnitude varying between the two configurations, were as follows: jet impingement on empennage and aft-end structure, pitch-up, and undesirably low cruise lift-drag ratios. Changes which would result in significant improvements in each of these problem areas are incorporated in the configuration shown in figures 5 and 6. These changes include (1) shift to an inboard pivot with a small glove area, (2) notch-located nacelles in packaged pairs beneath the fixed underwing panel, and (3) increased wing area.

Selection of an inboard pivot arrangement substitutes the problem of large aerodynamic-center shifts for the pitch-up problems inherent in outboard pivot arrangements with large glove areas having high sweep. Ordinarily this pitch-up is solved by the installation of low horizontal tails but, in SCAT configurations, this solution generally tends to result in serious jet-impingement problems. Other means for solving the pitch-up have not as yet proved very satisfactory.

Figure 7 shows the difference in aerodynamic-center shift due to sweep between typical outboard and inboard pivot arrangements as well as the shift due to Mach number for both. (These curves are based on the forward-sweep reference chord and nonelastic wings.) The much larger aerodynamic-center shift with sweep for the inboard pivot practically precludes the use of a low minimum sweep; trim drags arising from attempts to trim out this entire shift would be prohibitive. This problem is the reason for the selection, at some loss in high-lift potential, of a forward-sweep restriction of 36° in the modified SCAT 16 (shown in fig. 5). Since the trim penalties are dependent on the increment between the aerodynamic-center curve and the curve of the center-of-gravity location, the variation in the center-of-gravity location due to the sweeping of the wings is also shown in figure 7. The increment remaining at the cruise Mach number, which includes both the aerodynamic-center shift due to sweep and to Mach number, is now seen to approach that which might be trimmed out without penalty through the use of wing warp as discussed in paper no. 7 by Francis E. McLean and Harry W. Carlson. Thus, the net result of the pivot-location change will be some reduction in high-lift capability, a reduction of trim drag in the midsweep (transonic) range, and a slight increase in the trim penalty at cruise; with pitch-up reduced to a type (classic swept-wing rather than glove-induced) which should permit solution without an accompanying jet-impingement problem.

The second change was in engine arrangement. In this area the problem was to provide a short, two-engine pack which could be located so as to provide for reasonably good aircraft balance as well as the desired buoyancy on the receding surfaces of the wings and fuselage afterbody. Furthermore, it was desired that all inlets be under the wings to provide better pressure recovery and common inlet control schemes. Figure 8 shows such a nacelle which utilizes, in addition to the precompression due to the wing, a 2.5° precompression from the splitter between the inlets. In paired inlets, such splitters are required so as to avoid unstart interference. In this arrangement, the splitter is wedged to provide the additional precompression. In comparison with two-engine packs without the additional precompression, this arrangement provides for reductions in inlet area, diffuser length, and wetted area. A better match of mass flow over the transonic and supersonic speed ranges is also provided.

The third change was in wing area. The achievement of high supersonic L/D levels lies to a great extent in obtaining low values of two ratios. The first is the ratio of wetted area to wing area and the second, the ratio of the 2/3 power of the total volume to the wing area. Earlier configurations of the SCAT 16 type had small wing areas and, in addition to high wing unit weights, had high values of these two ratios. Increasing the wing area would be beneficial in both respects and would reduce, as well, the high-lift-coefficient requirement at low speeds. Estimates of trimmed lift-drag ratio at the cruise point exceed by 0.6 the values for the original NASA SCAT 16 configurations.

In summary, the pitch-up and attendant problems of the outboard pivot arrangement have been replaced by the aerodynamic-center shift, problem of the inboard pivot arrangement, since such a trade is believed, at present, to provide a better overall result. Other considerations of the present approach appear promising. Design of wind-tunnel models of this configuration is therefore underway.

SCAT 15

The contractors' final versions of SCAT 15 are sketched in figure 9. Major problems were as follows: high structural weight of both the fixed and variable-sweep wing panels, the structural-mechanical problem of extensive wing overlap, and aeroelasticity. A modified configuration is shown in figures 10 and 11. Changes include (1) substantial reductions in the structural spans of both the fixed and variable-sweep panels, (2) increased absolute thickness of both panels, (3) decreased wing overlap with a full-depth pivot, and (4) higher maximum sweep with an attendant reduction in thickness ratio. The packaged engines provide for a structural box covering about one-half of the

fixed-wing semispan, and they are located to provide positive interference beneath the aft portion of the wing at cruise Mach number as in the original SCAT 15. The effects of these changes should be to reduce structural and aeroelastic problems substantially, at the expense of high aerodynamic performance at cruise. Additional work on this concept is contemplated.

SCAT 4

The final developments by the contractors of the SCAT 4 configurations are sketched in figure 12. Major problems were as follows: pitch-up, subsonic roll due to sideslip, speed stability in approach, and jet interference with the tail. Figures 13 and 14 show a revised version of SCAT 4 which incorporates an M wing discussed in paper no. 12 by Robert T. Taylor et al. Changes include (1) adoption of the M planform having an increased aspect ratio, (2) installation of a ventral fin, and (3) a substantial reduction in dihedral. The addition of the ventral fin should provide adequate directional stability at supersonic speeds; and all three of the changes listed should improve subsonic roll-due-to-sideslip characteristics.

Not included in the changes listed is the substitution of paired nacelles located lower, more inboard, and more forward than in the original arrangement. Reduction of jet interference on the tail should result.

The following discussion will deal with the effects of the principal modification - that of planform.

Tests at low speeds of M and related planforms have already been discussed in paper no. 12. With the exception of the leading-edge extension, the planform of the modified SCAT 4 is nearly identical to one shown in that paper. Additional data show a progressively improving pitching-moment curve with increasing leading-edge extension, with the more extreme extension (representing a Krüger flap, shown in fig. 13) exhibiting a gratifying pitch-down tendency. The same sort of improvement in the pitching-moment curve is seen in such data as are available for M wings in the transonic speed range.

Figure 15 compares the wave-drag coefficients of M and arrow wings having the same thickness ratio, aspect ratio, and leading-edge sweep. The values presented are theoretical because no comparative experimental M-wing data have been found beyond high transonic speeds since interest in the M wing has diminished with the advent of low horizontal tails. As might be expected from study of the inset area diagram, the M wing shows higher wave drag than the arrow wing at a Mach number of 1.0 but

lower values from high transonic speeds upward. The low Mach number of the crossover point of these drag-coefficient curves is characteristic of the comparative experimental data available. Thus, M wings offer definite promise from the wave-drag standpoint.

Figure 16 illustrates the interference fields of the nacelles, whether paired or in separate pods. With regard to wave drag, note that the nacelle compressions place buoyancy on the receding slopes of the wings as well as on the fuselage afterbody. Favorable interference, as noted in the discussion of the SCAT 4 and 15 concepts, should be realized.

With regard to lift interference for the M planform with an optimum loading, linear theory calls for an infinite slope of the chords containing the apexes and the trailing-edge notches. This slope is also called for in the root chord of arrow wings and is, by one means or another, faired out. Body camber in the case of arrow wings helps produce the interference required by theory and the moderate amounts practically permissible have, in fact, proven advantageous. For the M wing shown in figure 16, the nacelles should directly provide this lift interference so that some hope is held for approaching, more nearly, the values of the drag-due-to-lift factors indicated by theory. Tests at supersonic speeds of a family of flat and warped M wings are presently underway.

In summary, it would appear that the changes noted in the SCAT 4 presentation could provide a configuration with high cruise performance and satisfactory static stability characteristics throughout the speed range. Design of wind-tunnel models of a complete configuration based on this approach is underway.

CONCLUDING REMARK

The NASA is investigating advanced versions of all four basic SCAT concepts (SCAT's 17, 16, 15, and 4). Improvements appear possible in nearly all problem areas.

SCAT 17 CONFIGURATIONS

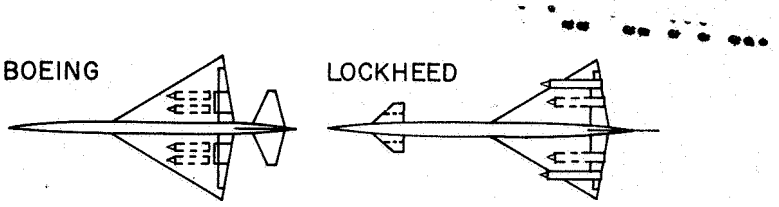

MAJOR PROBLEMS:

- o L/D AT LOW SPEED AND CRUISE
- ● LOW-SPEED HANDLING QUALITIES

Figure 1

MODIFIED SCAT 17 CONCEPT

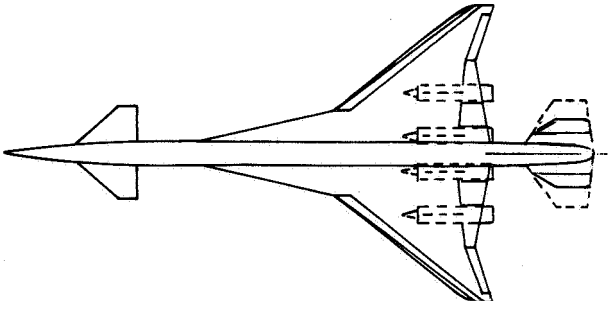

CHANGES:

- o PLANFORM
- o HORIZONTAL CONTROLS
- o WING LEADING EDGE

Figure 2

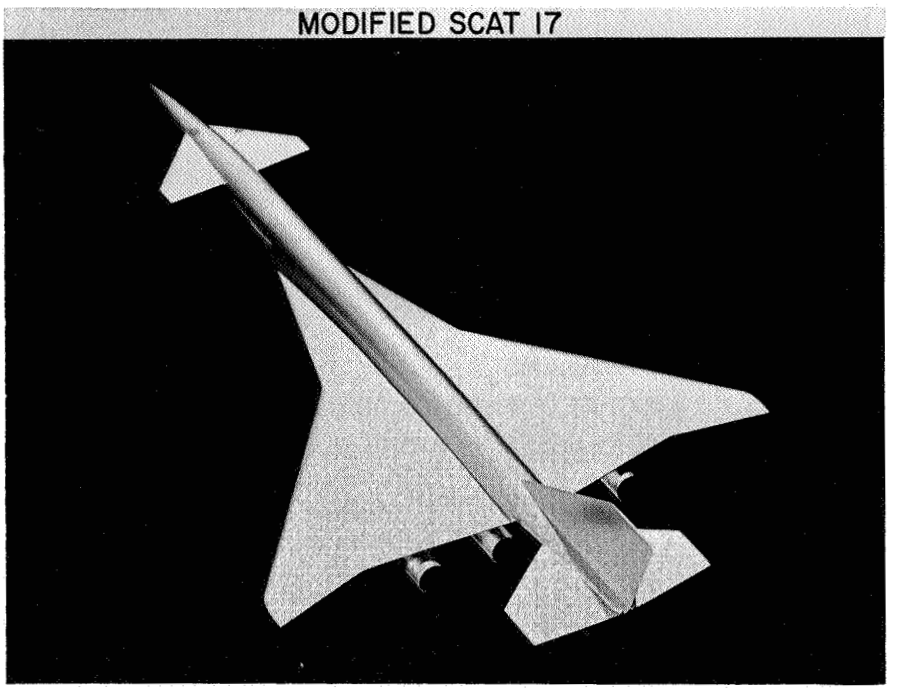

Figure 3 L-63-7734

SCAT 16 CONFIGURATIONS

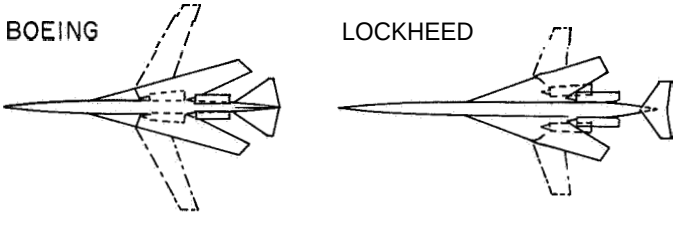

MAJOR PROBLEMS:

- JET INTERFERENCE WITH TAILS
- PITCH - UP
- CRUISE L/D

Figure 4

MODIFIED SCAT 16 CONCEPT

$(A)_{\Lambda_{LE,\ MIN}} = 7.0$

$\Lambda_{LE} = 36°$ TO $75°$

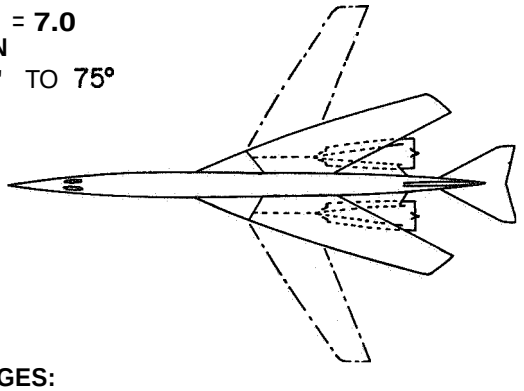

CHANGES:

- INBOARD PIVOT
- NACELLE ARRANGEMENT
- WING AREA INCREASED

Figure 5

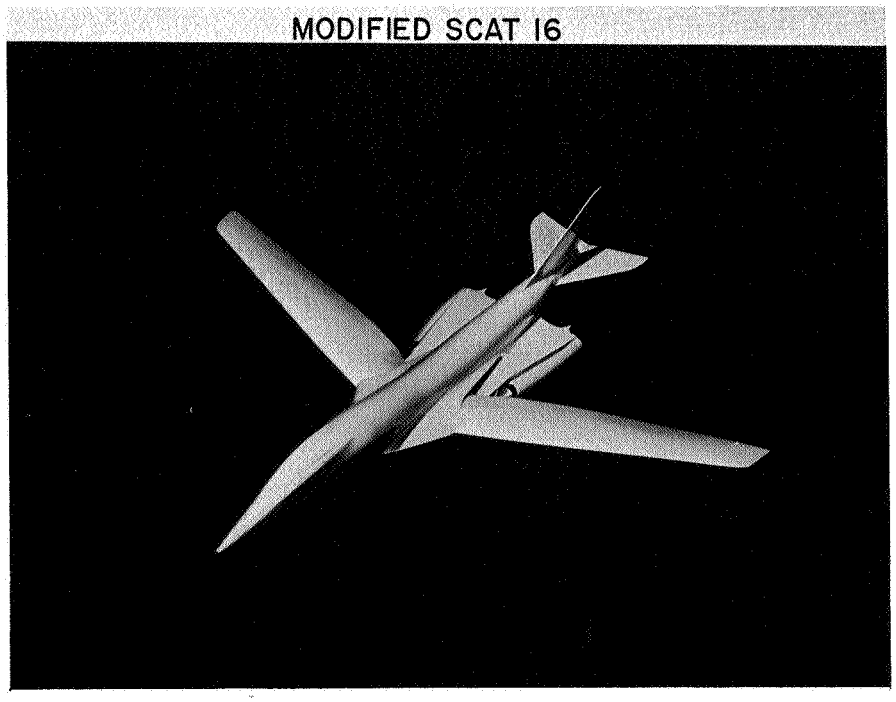

Figure 6

L-63-7735

LONGITUDINAL STABILITY CONSIDERATIONS OF SCAT 16 TYPE CONFIGURATIONS

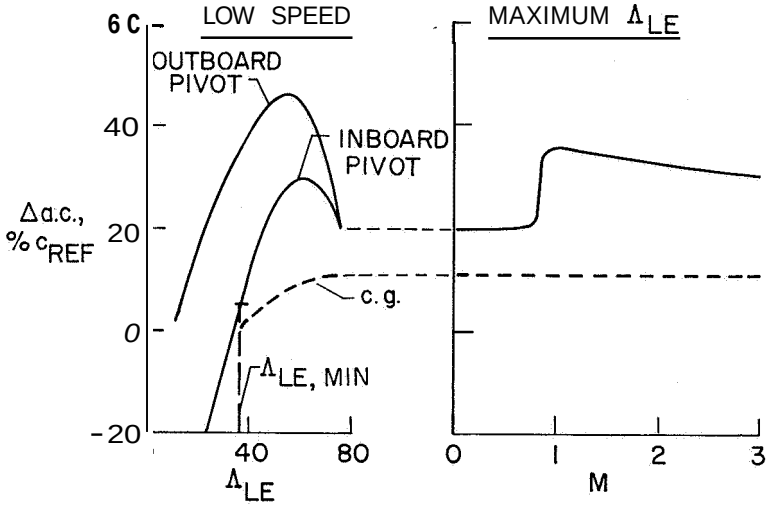

Figure 7

TWO-ENGINE NACELLE ARRANGEMENT

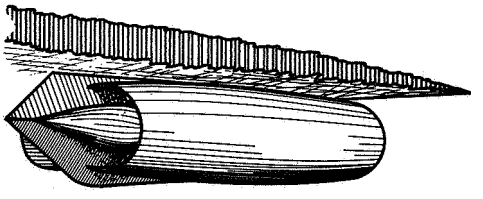

- SMALL INLET AREA
- SHORT DIFFUSER
- SMALL WETTED AREA
- GOOD VARIATION OF m/m_∞ WITH M

Figure 8

SCAT 15 CONFIGURATIONS

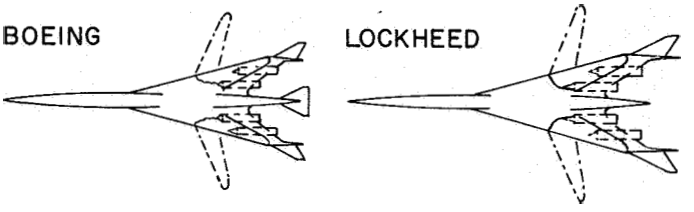

MAJOR PROBLEMS:

- HIGH STRUCTURAL WEIGHT OF WINGS
- WING OVERLAP
- AEROELASTICITY

Figure 9

MODIFIED SCAT 15 CONCEPT
$\Lambda_{LE,MIN} = 25°$; $\Lambda_{LE,MAX} = 78°$; A=6.36

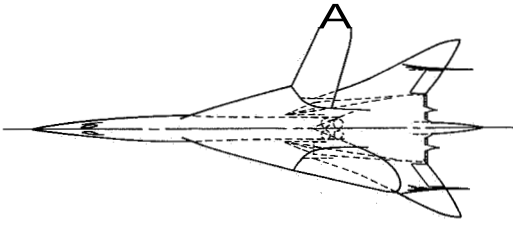

CHANGES:

- REDUCED STRUCTURAL SPANS
- INCREASED WING THICKNESS
- REDUCED OVERLAP - FULL-DEPTH PIVOT

Figure 10

MODIFIED SCAT 15

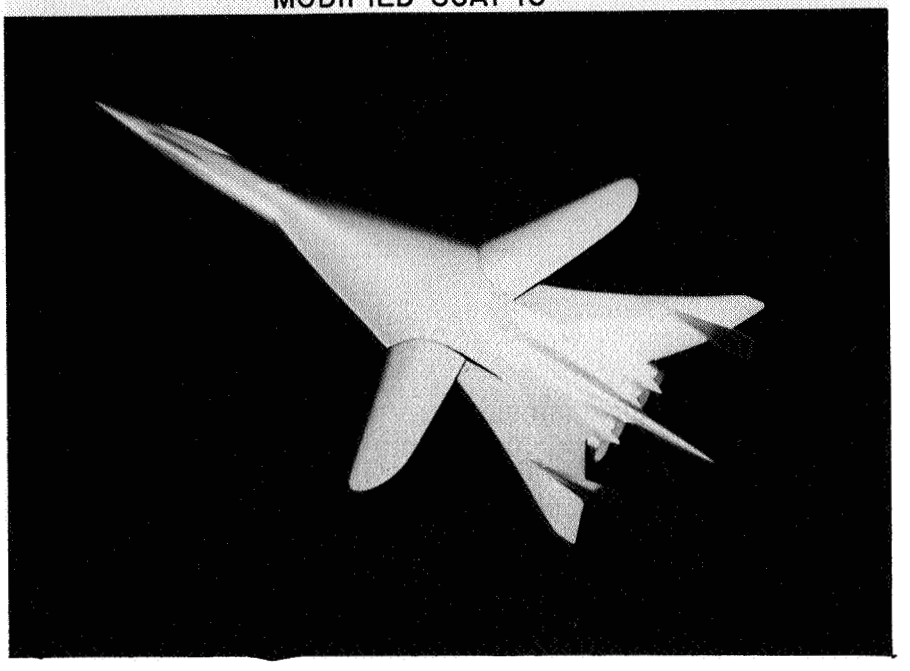

Figure 11

L-63-7737

SCAT 4 CONFIGURATIONS

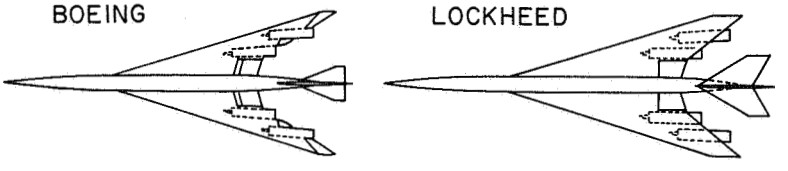

MAJOR PROBLEMS:

- PITCH-UP
- ROLL DUE TO SIDESLIP
- SPEED STABILITY IN APPROACH
- JET INTERFERENCE WITH TAIL

Figure 12

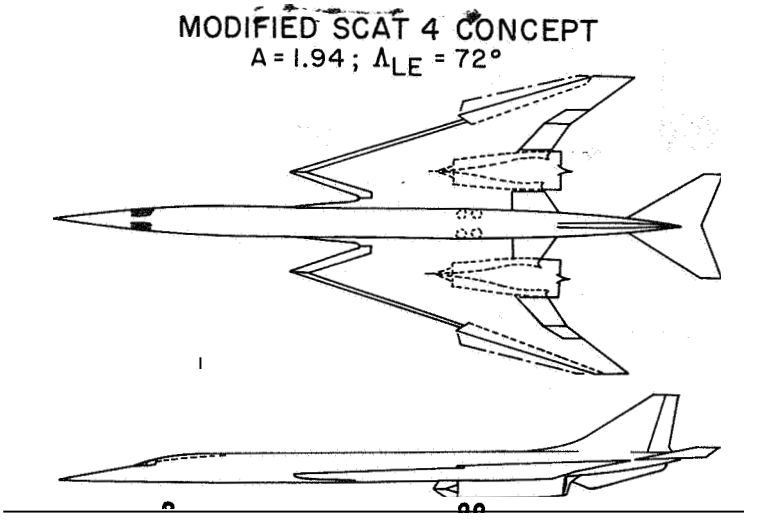

CHANGES :

- PLANFORM
- VENTRAL FIN
- DIHEDRAL

Figure 13

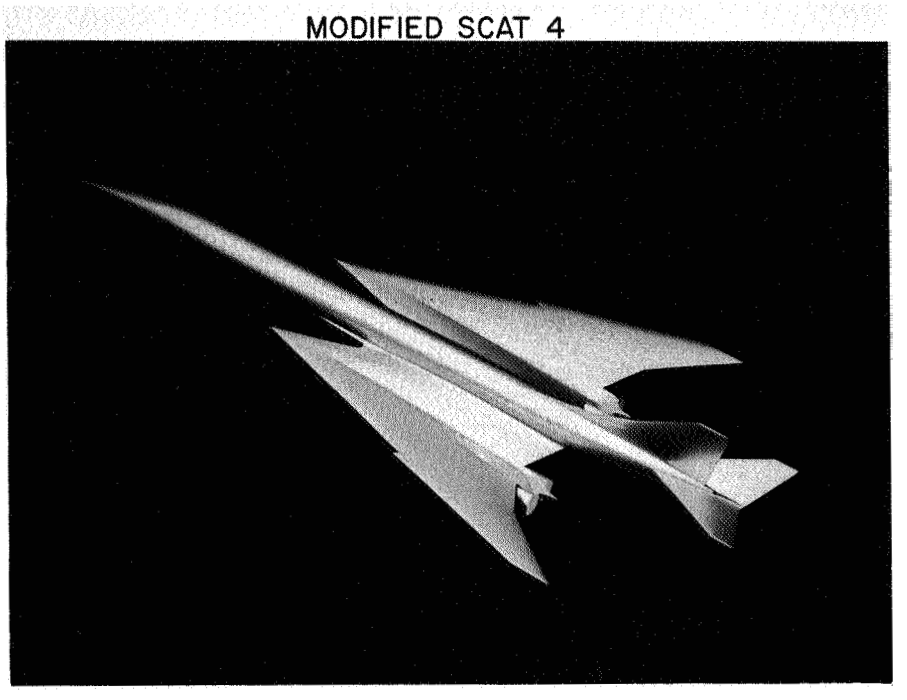

Figure 14 L-63-7736

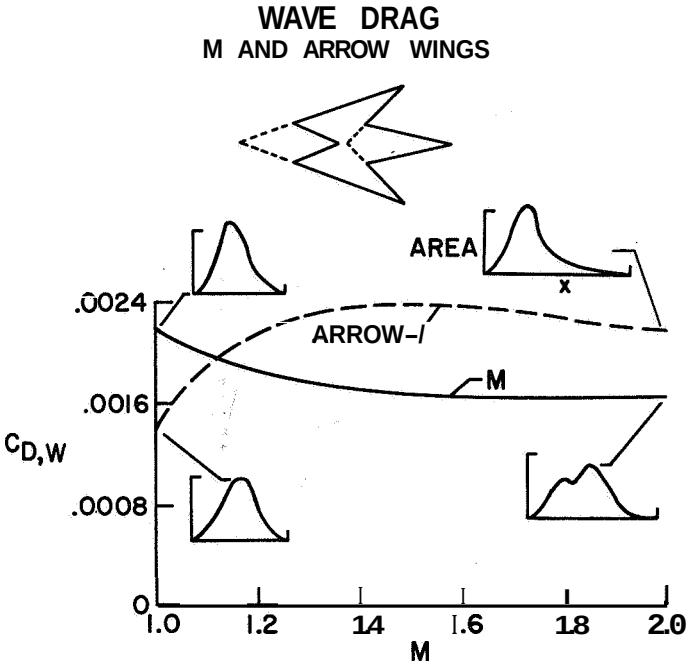

Figure 15

DRAG AND LIFT INTERFERENCE
NACELLES-WING-BODY

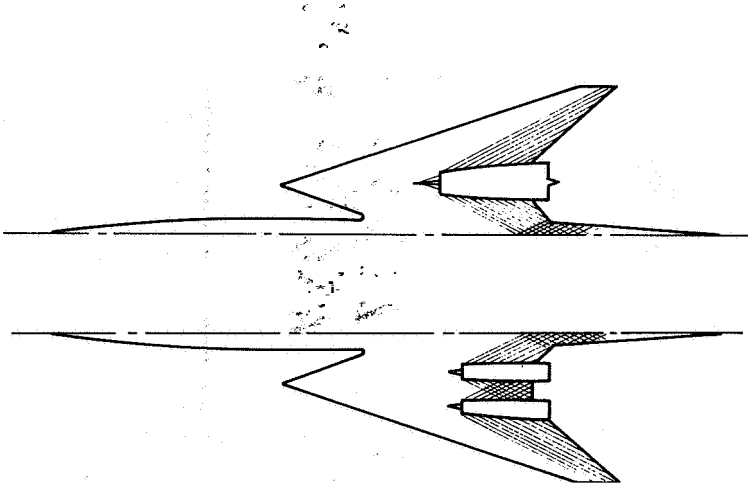

Figure 16

N67-31622

15. PROPULSION ASPECTS OF THE SUPERSONIC TRANSPORT

By James F. Dugan, Jr.
(NASA Lewis Research Center),

Arvid L. Keith, Jr., and Emanuel Boxer
NASA Langley Research Center

SUMMARY

The effectiveness of various advances in propulsion technology has been evaluated by using the ground rules of the NASA contracted SCAT feasibility studies. Increases in the operating turbine temperature beyond present-day values will permit substantial reductions in airplane gross weight. Unless significant advances beyond those anticipated are made in turbine cooling technology and in turbine materials, it is unlikely that additional gains will come from still higher turbine temperatures. Because efficiency of engine components is already high, it appears that the needed improvements will have to come from advances in lightweight engine construction and in variable-geometry technology.

Although the advanced turbojet engine and the advanced turbofan engine of the studies have shown substantial reductions in airplane gross weight compared with those of present state-of-the-art engines, the use of these engines results in a marginally acceptable supersonic transport. It is hoped that this particular result of the SCAT studies will stimulate those engaged in the propulsion effort to intensify their research and develop a very much improved propulsion system.

INTRODUCTION

The importance of propulsion to the success of a supersonic commercial transport can be appreciated when it is recognized that well over one-half of the take-off gross weight is comprised of the propulsion system and the fuel it will consume. In this paper consideration will be given to such problems as how good must the propulsion system be to result in an attractive take-off gross weight, and to what extent will improvements in the propulsion system decrease airplane gross weight. Basically, the means available to the propulsion engineer for developing a good system are few; he can try to improve component performance, integrate the components into a better package, and reduce weight.

SYMBOLS AND ABBREVIATIONS

$(L/D)_{max}$	maxim lift-drag ratio
M	Mach number
T_{max}	maximum augmentation temperature
T_{IT}	turbine inlet temperature
W_g	gross weight
$W_{g,REF}$	reference gross weight
ΔC_V	change in nozzle velocity coefficient
PR	pressure ratio
BPR	bypass ratio
SFC	specific fuel consumption
TJ	turbojet

DISCUSSION

In order to evaluate the significance of improvements in the propulsion system, it is necessary to consider both the airplane and the mission. Two airplane configurations were selected - one had a fixed wing and the other had a variable-sweep wing. Assumed aerodynamic characteristics of these configurations are shown in figure 1 as variation of $(L/D)_{max}$ with flight Mach number. Any postulated advances in propulsion will be evaluated by determining the effect on gross weight of one or the other of these two airplanes.

The selected mission, shown in the bottom half of the figure, is characterized by Mach 3 cruise, a 3,200 nautical-mile range, and reserve requirements as stated in the SCAT feasibility studies work statement.

Some of the propulsion-system requirements and problem areas .are pointed out in figure 2. When a specific engine is selected and

properly sized to fly the airplanes on the selected mission, engine thrust and airplane drag vary with flight Mach number as shown. The difference between the thrust and drag curves is the net force available for acceleration and climb to the initial Mach 3 cruise altitude. In sizing the engines, it is necessary to provide adequate acceleration margin in the transonic range where a limit on sonic-boom overpressure sets a lower limit on altitude. The engines must also be large enough to meet the restrictions on take-off distance, airport and nearby community noise, and second-segment climb.

When Mach 3 cruise is attained and engine thrust equals airplane drag, it is seen from figure 2 that the required thrust is very much less than the available thrust. This is also true for cruise to an alternate airport and holding prior to landing. These three steady-state conditions are very important, since the engine-airframe match at these conditions determines the amount of fuel consumed during cruise and the amount of fuel that is carried onboard as reserves. Thus, there is a basic requirement for high engine efficiency under part-power operating conditions.

The general character of the engine-airframe match at these three critical steady-state conditions is shown in figure 3 for a variable-sweep-wing airplane powered by either advanced turbojet or advanced turbofan engines.

For Mach 3 cruise, the required thrust is such that near-minimum specific fuel consumption is attained by both the turbofan and the turbojet engines. The turbojet minim specific fuel consumption is achieved with no augmentation, whereas the turbofan minimum specific fuel consumption is achieved with moderate augmentation.

In comparing the turbojet engine with the turbofan engine, it is generally true that the turbojet has lower specific fuel consumption during supersonic cruise, whereas the turbofan has lower specific fuel consumption during subsonic cruise. The relative merit of the two engine ty-pes is very dependent on the mixture of supersonic and subsonic portions of the cruise.

The effects of the major turbojet engine parameters on the gross weight of a fixed-wing airplane will be examined. It can be seen in figure 4 how airplane gross weight changes as the major parameters that characterize turbojet engines are varied: namely, turbine inlet temperature, compressor pressure ratio, engine weight, and the use of augmentation. For the range of turbine temperature considered, design compressor pressure ratio of the dry turbojet should be about 10.

The reduction in airplane gross weight that will result from being able to obtain lighter dry turbojets is shown in the right-hand plot in figure 4. A relative gross weight of 1.0 corresponds to a payload fraction of about 6 percent of the gross weight. If it is desired to raise the payload fraction to 8 percent of the gross weight, engines are needed that will result in a reduction of airplane gross weight of about 20 percent. For the dry turbojet, engine weight reductions of the order of 40 percent and turbine inlet temperatures of the order of 2,800° R are needed. Such an engine is not easily attainable, especially in view of the safety and reliability requirements and the desired goal of 2,000 hours time-between-overhaul. Since mid-1962, the engine companies have been engaged in a propulsion program in support of the supersonic transport. It is hoped that this program will answer two important questions: What level of turbine inlet temperature and how much reduction in engine weight can be achieved for the first U.S. supersonic transport?

In the upper left-hand plot of figure 4 is shown the reduction in airplane gross weight that results from using augmented turbojets rather than dry turbojets. If a higher climb path is required to meet the sonic-boom limitation, it will be even more advantageous to use augmentation. However, if a lower climb path proves to be acceptable, it is possible that a very lightweight, high-turbine-temperature dry turbojet will meet the requirements.

Before other means can be considered by which improvements in the propulsion system can lead to an improved supersonic transport, perhaps it would be worthwhile to consider some form of ideal engine. By determining the reduction in airplane gross weight that would result from the successful development of this ideal engine, the designer will have a yardstick against which he can measure the effectiveness of various practical means for improving the propulsion system.

To help define the ideal engine, overall propulsion efficiency is shown as a function of Mach number in figure 5. The lower two curves are for turbofan engines B and D of the SCAT feasibility studies as they operate during the acceleration and climb-to-cruise phase of flight; the engines are operating with full augmentation. Engine efficiencies read from the curve for the ideal engine are the highest values attainable by engine D at each Mach number. The optimum pressure-ratio curve represents the results of a parametric study at a constant turbine inlet temperature of 2,700° R in which the overall and fan pressure ratios were optimized at each flight Mach number to further increase engine efficiency; the optimum curve thus represents the envelope of many different engines. The open symbols are the supersonic cruise, subsonic cruise, and hold-at-landing efficiencies of engines B and D. The main conclusion to be drawn from this figure

DECLASSIFIED

is that there is considerable room for improvement in the propulsion efficiency during climb and acceleration.

The ideal engine chosen for consideration is one having variable mass flow through the use of variable geometry to allow it to operate during acceleration and climb at the propulsion efficiencies, shown by the long-dash curve, with the same thrust schedule and internal component efficiencies as those of engine D. To realize the full potential of this ideal engine, its inlet spillage and bypass drag are assumed to be zero.

The relative gross weight of the variable-sweep-wing airplane is shown in figure 6. The higher temperature turbofan, engine D, permits a gross-weight improvement of about 10 percent as compared with engine B. An additional reduction in gross weight of 18 percent is achieved by the ideal engine; this value is only 2 percent less than that for the optimum pressure-ratio engine. In absolute terms, this is a reduction of about 70,000 pounds for a 400,000-pound airplane. The improvement offered by the advanced technology engine D as compared with the present-day technology engine B represents a reduction in take-off gross weight of approximately one-third of that offered by the ideal turbofan. Similar results have been obtained for idealized and optimized turbojet engines. It should be emphasized that the techniques needed to build the ideal engine today are unknown, but perhaps some day when considerable advances in variable-geometry technology are realized the performance gains indicated may be approached.

It is natural to expect that the added complexity of variable geometry will increase the propulsion package weight. For the conditions just discussed the installed thrust-weight ratio of the ideal engine was assumed to be equal to that of engine D. The results of investigating the effects of increased power-plant weight on the relative take-off gross weight are shown in the right-hand plot in figure 6. It is noted that sizable reductions in gross weight are possible even with power-plant weight increases of as much as 50 percent.

The next problem to be considered is that of practical means for improving payload. It may be recalled that one feature of the ideal turbofan was that it had zero inlet spillage and bypass drag. In a practical engine, these drags exist over most of the flight Mach number range because it is not yet possible to build an engine that is capable of swallowing a full stream tube of air under all operating conditions. For the reference turbofan engine with an axisymmetric mixed compression inlet, the spillage drag is quite high during operation in the transonic speed range. One way of reducing this spillage drag is to build a turbofan with a different engine airflow schedule. This can be done by replacing the constant exhaust nozzle area of the

main gas stream with a variable-area nozzle. With such a nozzle, the engine airflow can be reduced at high flight Mach numbers. The revised engine airflow schedule results in less air being spilled during transonic operation. There are other effects - some good and some bad - so that it is necessary to evaluate the concept, which has come to be known as low flowing, by way of a mission study. In figure 7, the advantages of low flowing the reference turbofan engine are considered. The engine drag coefficients of the reference and low-flow turbofans are shown in the left-hand plot of the figure.

Below a Mach number of 2.5, the engine airflow schedule of the low-flow turbofan is the same as that for the standard-flow turbofan. Above Mach 2.5, engine airflow of the low-flow turbofan decreases until at Mach 3 it is 20 percent less than that for the standard-flow engine. Since the inlet is sized by the Mach 3 cruise conditions, the low-flow turbofan has a smaller and lighter inlet but also has more nacelle wave drag. Over most of the flight Mach number range, however, the low-flow turbofan has a lower engine drag coefficient than the standard-flow turbofan. This condition is due to the fact that the reduction in spillage drag more than compensates for the increase in wave drag. The net effect is shown in the bar graph on the right-hand side of the figure. By low flowing, the gross weight of the variable-sweep-wing airplane is reduced about 2 percent.

As was pointed out in figure 3, a shortcoming of the turbojet engine is its relatively poor SFC during subsonic flight. A way to improve this shortcoming is to equip the turbine with variable turbine stators. For subsonic flight at low levels of thrust, the fuel control and turbine stators can be adjusted simultaneously so as to result in lower SFC. In figure 8, the concept of using variable turbine stators to decrease the gross weight of the fixed-wing aircraft is considered. In the left-hand plot fixed and variable turbine-stator performances at a Mach number of 0.27 and an altitude of 1,500 feet are presented. At the low level of required thrust, the advantage is that the SFC for the variable turbine stators is reduced 8.5 percent. In the bar graph on the right-hand side of the figure, it can be seen that the use of variable turbine stators reduces the airplane gross weight by about 2 percent. This reduction results from the lower SFC attained in meeting the two reserve requirements for subsonic flight: cruise to an alternate airport and holding prior to landing.

In calculating engine performance, it is necessary to use some schedule of inlet pressure recovery with flight Mach number. The schedule utilized was that given in the work statement of the SCAT feasibility studies and is shown in the upper right-hand plot in figure 9. Since it is quite possible that inlets with higher performance can be built, the improved performance shown by the upper curve was

postulated. If engine B is mated with this higher performance inlet, the gross weight of the variable-sweep-wing airplane is reduced about 4 percent.

Comparable results are obtained if the nozzle velocity coefficient can be increased over the entire flight path by 1 percent. With this better nozzle performance, a reduction in gross weight of about 5 percent will result. It is realized that reaching out for such gains may result in complicated and weighty mechanisms. The importance of keeping component weight to a minimum can be seen in the lower right-hand plot of figure 9. If the gains in inlet and nozzle performance require overall power-plant weight increases of 4½ and 5½ percent, respectively, no gross-weight advantage can be realized. It should be pointed out that, if the inlet recovery schedule and nozzle performance assumed for the SCAT feasibility study are not realized, proportionate penalties in gross weight will accrue.

CONCLUDING REMARKS

The ground rules for the NASA contractors' feasibility studies have been used to evaluate the effectiveness of various advances in propulsion technology for the supersonic transport. This evaluation indicated that increases in operating turbine temperatures beyond the temperatures used in present-day transports will permit substantial reductions in airplane gross weight. However, without significant improvements in turbine cooling technology and in turbine materials, further gains from still higher turbine temperatures appear unlikely. Because efficiency of engine components is already high, it appears that the needed improvements will have to come from advances in light-weight engine construction and in variable-geometry technology.

Although the advanced turbojet engine and the advanced turbofan engine of the studies have shown substantial reductions in airplane gross weight compared with those of present state-of-the-art engines, the use of these engines results in a marginally acceptable supersonic transport. Additional research to develop a much improved propulsion system is therefore necessary.

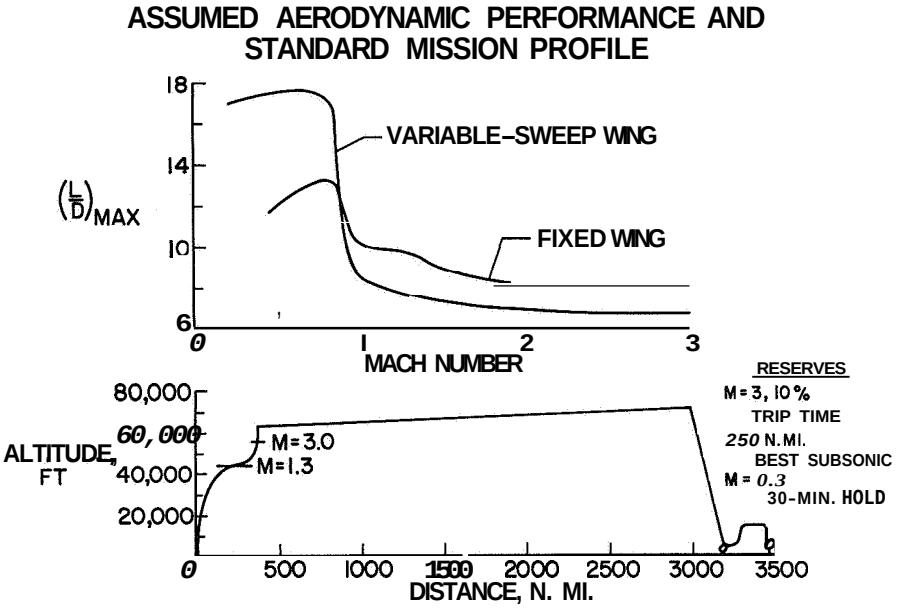

Figure 1

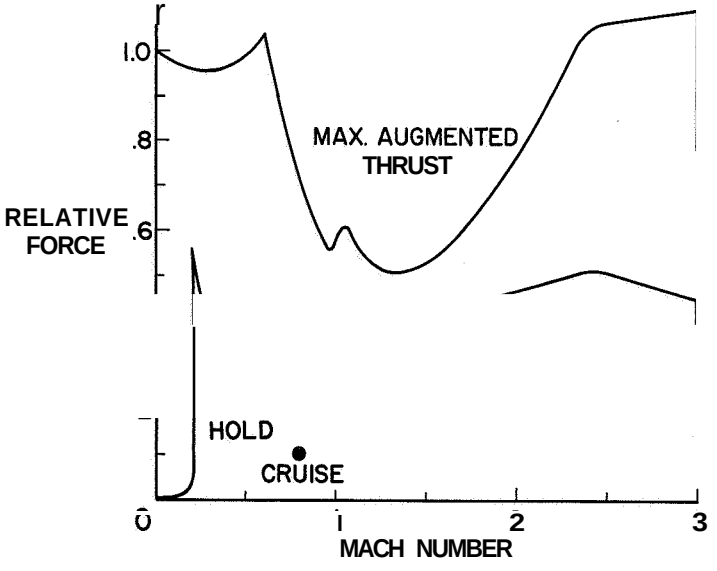

Figure 2

VARIATION OF SPECIFIC FUEL CONSUMPTION WITH THRUST
TYPICAL SCAT MISSION

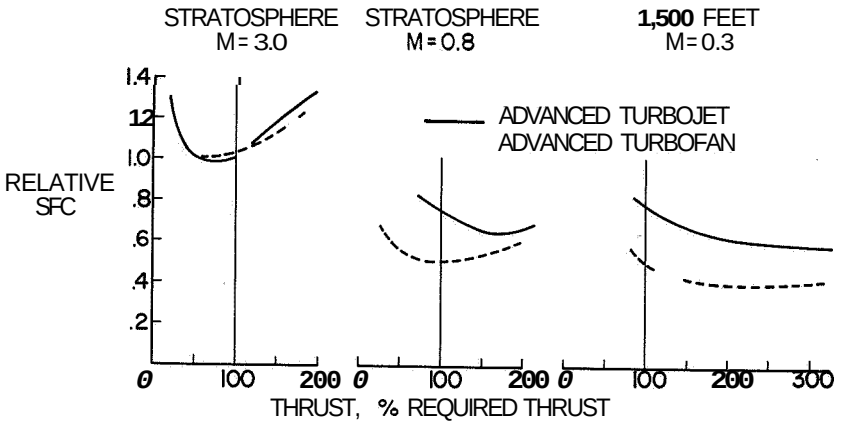

Figure 3

EFFECT OF TURBOJET-ENGINE-CYCLE VARIABLES ON GROSS WEIGHT

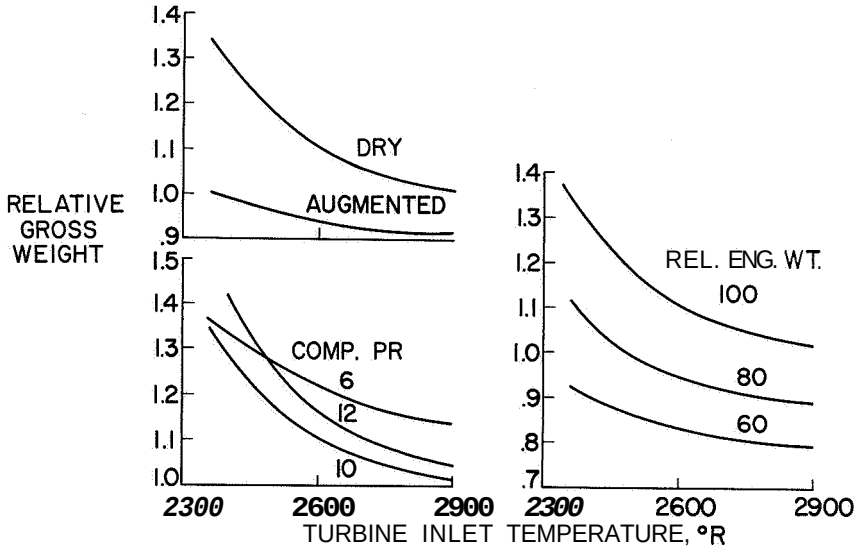

Figure 4

TURBOFAN ENGINE EFFICIENCY

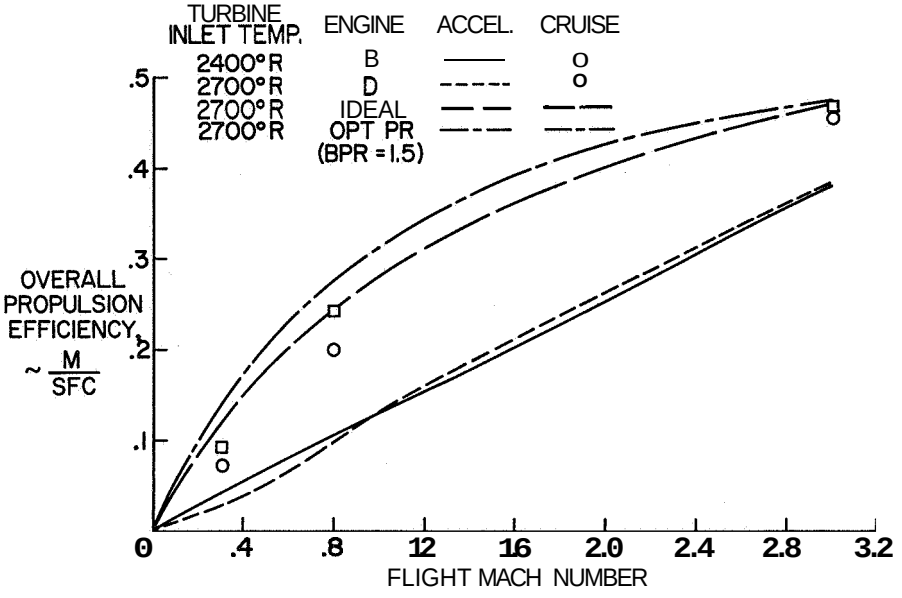

Figure 5

TURBOFAN-ENGINE-AIRPLANE OPTIMIZATION

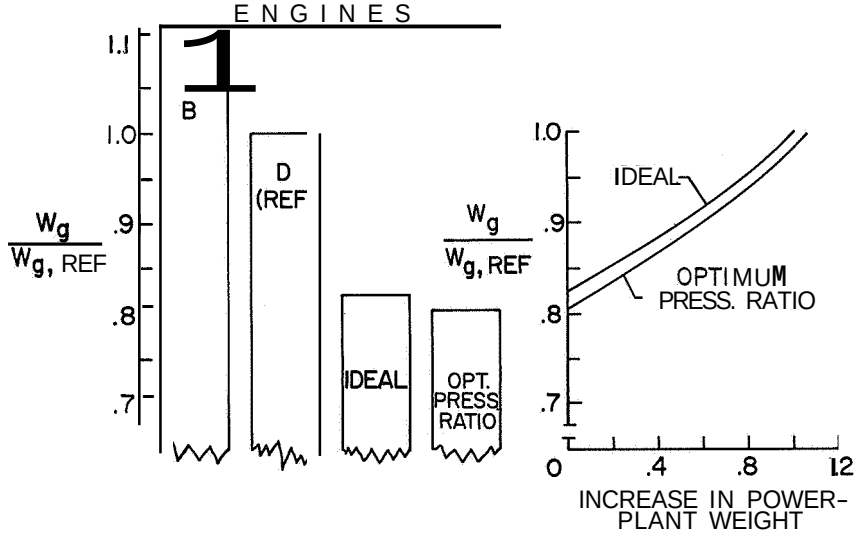

Figure 6

ADVANTAGE OF LOW FLOWING A TURBOFAN

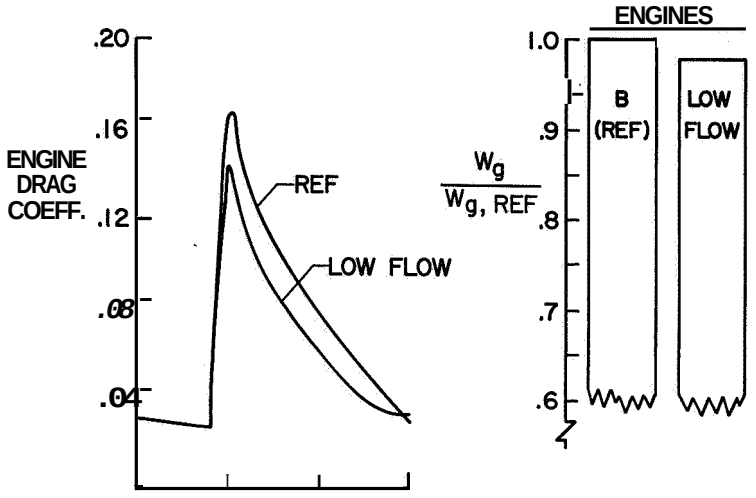

LOWER SFC FROM VARIABLE TURBINE {STATORS

AUG. TJ PR = 10 T_{IT} = 2760° R T_{MAX} = 3560° R

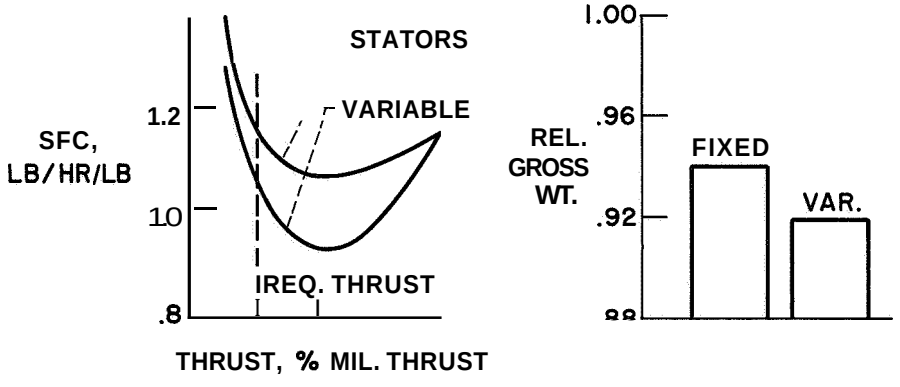

Figure 8

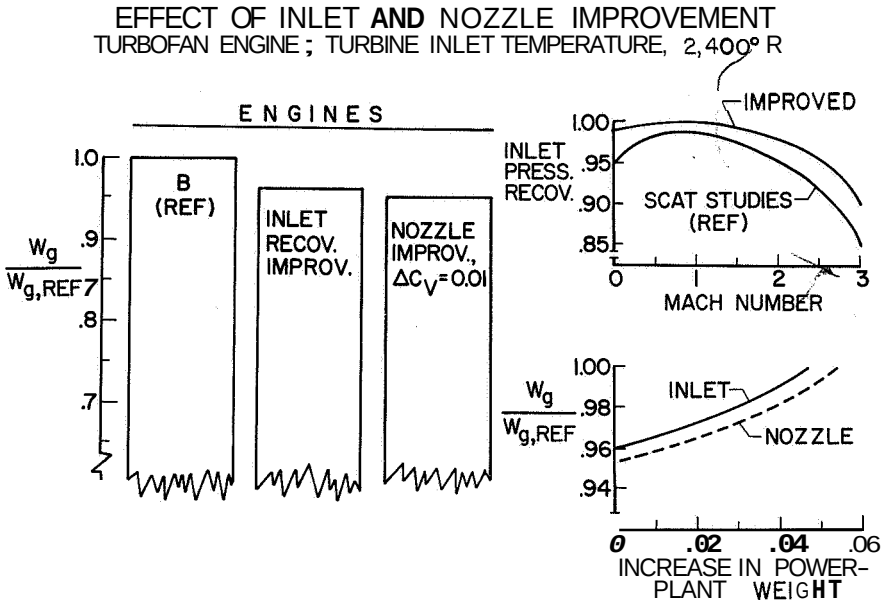
EFFECT OF INLET AND NOZZLE IMPROVEMENT
TURBOFAN ENGINE; TURBINE INLET TEMPERATURE, 2,400° R
ENGINES
B (REF)
INLET RECOV. IMPROV.
NOZZLE IMPROV., ΔCV=0.01
Wg / Wg,REF
1.0
.9
.8
.7
IMPROVED
INLET PRESS. RECOV.
1.00
.95
.90
.85
SCAT STUDIES (REF)
0
1
2
3
MACH NUMBER
Wg / Wg,REF
1.00
.98
.96
.94
INLET
NOZZLE
0
.02
.04
.06
INCREASE IN POWER-PLANT WEIGHT

Figure 9

N67-31023

16. STUDY OF AN AXISYMMETRIC SUPERSONIC-TRANSPORT INLET

By Norman E. Sorensen

NASA-Ames Research Center

SUMMARY

In support of the supersonic commercial air transport program, a 20-inch capture diameter axisymmetric mixed-compression inlet model has been designed and tested at the Ames Research Center. The main conclusions to be drawn from these preliminary tests are that the supersonic portion of the inlet performed as predicted, and the main loss in performance lies in the throat and subsonic diffuser. Since recoveries as high as 97 percent can be attained in the throat, it seems certain that with further development in the throat and subsonic diffuser and with more effort in determining better bleed configurations, an axisymmetric inlet with performance quite adequate for the supersonic transport will be developed.

INTRODUCTION

In support of the supersonic commercial air transport (SCAT) program, a 20-inch capture diameter axisymmetric mixed-compression inlet model has been designed and tested at Ames Research Center. A photograph of the model mounted in the wind tunnel is shown in figure 1. The inlet is suitable for application to a vehicle designed for a Mach number of 3.0 and is capable of performing at off-design Mach numbers by translating the centerbody. The length-diameter ratio of the inlet-engine-thrust reverser package is consistent with those tested on the SCAT configurations. The model, which is as large as practical, was tested in the wind tunnel at a Reynolds number per foot of about 2×10^6 corresponding to the Reynolds number per foot at an altitude of 65,000 feet and a Mach number of 3.0. The tests were conducted primarily to determine the internal performance and the bleed requirements of the inlet from Mach numbers of 0.6 to 3.0. Critical to the transonic performance of the propulsion system is the spillage drag. Since this drag does not yield well to theoretical analysis and little data are available, the spillage drag was experimentally determined at Mach numbers of 0.6 to 1.1. A number of bleed configurations were tested at a Mach number of 3.0 so that a suitable configuration could be chosen for tests at off-design Mach numbers. Limited data were obtained at flow angles up to 8°.

SYMBOLS

A_c	capture area
A_o	free-stream tube area
A_x	local duct area
C_{D_a}	additive drag coefficient
h	local height
H	local duct height
$m_{BL'D}$	bleed mass flow
m_{ENG}	engine mass flow
m_∞	free-stream mass flow
M_∞	free-stream Mach number
Pt_{ENG}	total pressure recovery at engine face
Pt_h	total pressure recovery in throat
p_{t_∞}	free-stream total pressure
R	inlet capture radius
Δx	incremental distance along center line
θ	centerbody conical half-angle

DESIGN

The aerodynamic design of an inlet naturally is a compromise of a number of requirements. One of the most important is the requirement of sufficiently low transonic spillage drag *so* that the thrust margin of the vehicle is large enough to accelerate through this critical Mach number range. Spillage drag is composed of cowl drag and additive drag

created by the spillage of excess airflow over the cowl lip at Mach numbers below the design. Both of these quantities can be kept low by keeping the cowl angle and the centerbody angle sufficiently low. Figure 2 shows such a design. An internal cowl angle of 0° was selected because a feasible internal design could be created with a 12.5° conical half-angle centerbody which produces reasonably low additive drag. The external cowl angle can then be as low as 2.5°. The internal contours were estimated for a free-stream Mach number of 3.0 beginning with this selected combination of angles and were then "tested" by a computer program employing the method of characteristics to describe the flow field. To determine a satisfactory set of contours, a goal must be set for the throat conditions and a limitation set on the pressure ratio across the shock-wave impingements to prevent boundary-layer separation. Uniform flow in the throat at a Mach number of 1.3 and a throat-pressure recovery above 95 percent were the goals; the pressure ratio across the first shock-wave impingement on the centerbody was less than 3 and across the impingement on the cowl was about 2. As final requirements, the design had to provide at least 40 percent of the capture mass flow at a Mach number of 1.0 to match the off-design flow demand of a typical turbofan engine, and the centerbody translation requirements had to be on the order of one-half the inlet diameter to avoid large weight penalties associated with long translation distances. The design shown is about as short as is thought practical largely because of the limit set on the pressure ratios across the shock-wave impingements. Once the supersonic design is determined, a satisfactory throat and: subsonic diffuser must be designed to fit the supersonic portion of the inlet. A throat which had boundary-layer bleed for a length of two throat heights was selected, and a 10° equivalent conical angle subsonic diffuser was selected as being reasonably short from the trade-off of weight with performance. Boundary-layer compensation was included in the throat and between the throat and the forward shock-wave impingements.

No high-performance inlet has as yet functioned properly without judiciously bleeding a portion of the boundary layer. It has not always been clearly understood where to bleed and how much to bleed. In this light the porous bleed configuration shown by the dotted areas was not necessarily the best but represented a fairly good compromise within present understanding.

SUPERSONIC RESULTS

Preliminary performance of the inlet at Mach numbers of 1.55 to 3.0 is presented in figure 3. The results shown and those to follow were obtained without the effects of the wing or fuselage. The bleed configuration was the one shown in figure 2. Eighty-six-percent pressure recovery was attained at the engine face with a rather high bleed

mass flow of 13 percent at a Mach number of 3.0. The recovery which increased at the lower Mach numbers and the bleed which decreased were results which were obtained with the same bleed exit settings as at a Mach number of 3.0. The recovery assumed in the SCAT feasibility studies is also shown. Even though the recovery indicated by the feasibility schedule is somewhat higher than the experimental recovery at off-design Mach numbers, this condition does not necessarily mean that the transport mission will suffer an appreciable penalty. It is usually more important to maintain as high a recovery as possible at the design Mach number and to sacrifice off-design recovery, if necessary, because the cruise time is so much longer than the acceleration time. Although the performance of the inlet was reasonably good, it is felt that better performance can be attained at a Mach number of 3.0 especially with regard to lowering the bleed requirements. The supersonic portion of the inlet performed as predicted by the computer program. The shock-wave impingements and the associated pressure rises correlate well with theory and the flow profiles in the throat indicate recovery as high as 97 percent at the end of the supersonic diffuser. A typical history of pitot-pressure profiles at a Mach number of 3.0 from the throat to the engine face is shown in figure 4. The pitot pressures are plotted as a function of the ratio of local height to local duct height. Comparison of the throat recovery, which averages about 95 percent, with the engine-face recovery, which averages 86 percent, indicates that the major losses occur in the region of the terminal shock wave and in the subsonic diffuser. The profile at the diffuser rake just downstream of the terminal shock train shows that a relatively large loss in recovery exists on the centerbody side of the duct. Turbulent mixing in the diffuser results in some increase in recovery in the region adjacent to the centerbody by the time the flow reached the engine face. However, as is usual, this increase is accompanied by a decrease in the recovery level in the balance of the duct. Although this condition is no doubt controlled to a considerable degree by the boundary-layer bleed, it is believed that the rather rapid divergence of the throat aggravates this flow distortion.

As part of the design requirements previously mentioned, the inlet must match the mass-flow demands of a typical turbofan engine. Figure 5 shows that the inlet does supply the mass flow when the inlet is sized to include the bleed mass flow at a Mach number of 3.0. Some of the inlet flow will have to be bypassed at most of the off-design Mach numbers as shown by the difference between the inlet flow and the engine (including bleed) requirements. The only point where the inlet may not supply enough air is near a Mach number of 1.6 where some reduction in bleed rate should be allowable without seriously harming the performance.

The rapid deterioration of inlet performance with increasing flow angle is a matter of critical concern with axisymmetric inlets. Figure 6 shows how the present inlet performance deteriorates above 2°.

Some results for Mach numbers of 2.5 and 3.0 are shown. Although only a single result is shown for a Mach number of 3.0, the trends for both Mach numbers are expected to be the same. A 12-percent loss of recovery and a 7-percent loss of mass flow at 5° are considered large penalties to pay for any sustained period of flight. It is, therefore, desirable that the inlet location on the vehicle be as insensitive to flow-angle changes as possible. Such a location could be in the flow field beneath the wing. Shown in the lower part of the figure is the variation with flow angle of centerbody translation distance required to keep the inlet flow "started." Rather large translation of the centerbody is required to keep the inlet "started"; hence, severe requirements are imposed on the inlet control system. In the event the control system was unable to produce the necessary translation, the internal shock-wave system would be expelled, large drag increases and severe flow oscillations thereby being produced. This condition means that not only should the inlets be located in flow fields relatively insensitive to vehicle attitude for performance reasons but also to provide some measure of protection from the effects of sudden external-flow disturbances.

From the foregoing discussion it seems reasonable to assume that modification of the throat and subsonic diffuser and careful attention to the bleed configuration should improve the supersonic results. However, before an improved model configuration is proposed, the transonic results should be examined.

TRANSONIC RESULTS

One of the main objectives of the transonic tests was to measure additive drag since it is so important to the vehicle acceleration as previously mentioned. The additive drag was determined by using momentum methods and is presented in figure 7. The additive drag is shown up to a Mach number of 1.1 for maximum pressure recovery, minimum additive drag, and an optimum computed for maximum thrust minus drag. The optimized results come about fromthe trade-off between additive drag and pressure recovery; that is, low additive drag is associated with a loss in thrust because of the accompanying reduction in pressure recovery. All of the results were obtained with the inlet at 0° to the free stream. The cowl drag is not included in the optimization since it is relatively small. The additive drag appears to peak at a value of 0.12 and a Mach number of 1.2 if the minimum transonic additive drag results are faired into the supersonic theoretical computed curve. The peak additive drag is somewhat lower than predicted but is still about 10 percent of the engine thrust. This more favorable result appears to be caused by the reduced pressure induced by the curvature of the exposed portion of the centerbody which can give a net additive thrust as indicated below a Mach number of 1.0. Other transonic performance

factors presented in figure 7 show that depending on the position of the centerbody, the pressure recovery can be changed radically. The more withdrawn positions of the centerbody are more favorable from a recovery and distortion standpoint but are very unfavorable to the additive drag. Total-pressure profiles at the engine face indicate that separation off the centerbody is the main cause for low recovery. If separation could be alleviated, a lower optimum drag would, of course, be indicated. At a Mach number of 1.0, it appears that about a 3-percent improvement in engine thrust can be attained if the recovery level can be raised to the maximum shown in the figure. It should be noted that the performance is sensitive to rather small centerbody translation changes, the wide range of performance shown being covered by a translation of about 10 percent of the inlet capture diameter. In addition, the inlet mass flow does not change appreciably over this range because the inlet throat area does not change with translation and the throat is choked or nearly choked for the data presented.

MODIFIED MODEL CONFIGURATION

The foregoing discussion suggests contour and bleed configuration changes that should result in improved performance in forthcoming tests. Since the supersonic portion of the inlet appears to perform as predicted, it is felt that the throat and subsonic diffuser performance can be improved with modified throat and subsonic diffuser contours which are initially less divergent. Figure 8 shows the tested diffuser contours compared with the modified contours. Modifications are made only on the centerbody and result in a throat area ratio profile which approaches a constant area throat and is considerably less divergent than the one tested. Since the modified subsonic diffuser is the same length as the one tested, it is necessary to curve the aft portion of the centerbody rapidly and, as a result, incur some loss in pressure recovery because of the sudden expansion. It is estimated, however, that the loss is only about 1 percent. Transonically, the new contours should alleviate the flow separation off the centerbody and improve the performance in this area.

Some need for bleed configuration changes is also suggested. The forward bleeds are effective and it appears that a scoop on the centerbody would be most effective because the low pressure in this area prevents porous bleed from removing more than about one-half percent of the inlet mass flow. On the cowl side, the forward bleed area does not need to be very wide to be effective. In the throat a concentrated bleed at the beginning of the throat will require less bleed than the broad area previously shown since the static pressure ahead of the terminal shock train is much lower than that behind. With the modifications suggested, it is estimated that not unrealistic performance goals at a Mach number

of 3.0 should be 86- to 90-percent pressure recovery with 6- to 10-percent bleed mass flow.

CONCLUDING REMARKS

The main conclusions to be drawn from these preliminary tests are that the supersonic portion of the inlet performed as predicted and the main loss in performance lies in the throat and subsonic diffuser. Since recoveries as high as 97 percent can be attained in the throat, it seems certain that with further development in the throat and subsonic diffuser and with more effort in determining better bleed configurations, an axisymmetric inlet with performance quite adequate for the supersonic transport will be developed.

The axisymmetric type of inlet is not the only type considered suitable for application to the supersonic commercial air transport. The two-dimensional type of inlet has demonstrated high performance capability and is therefore attractive for transport application. Design considerations similar to those discussed for the axisymmetric inlet have been applied to a two-dimensional design, and a large scale model is now being readied for tests.

AXISYMMETRIC INLET MODEL

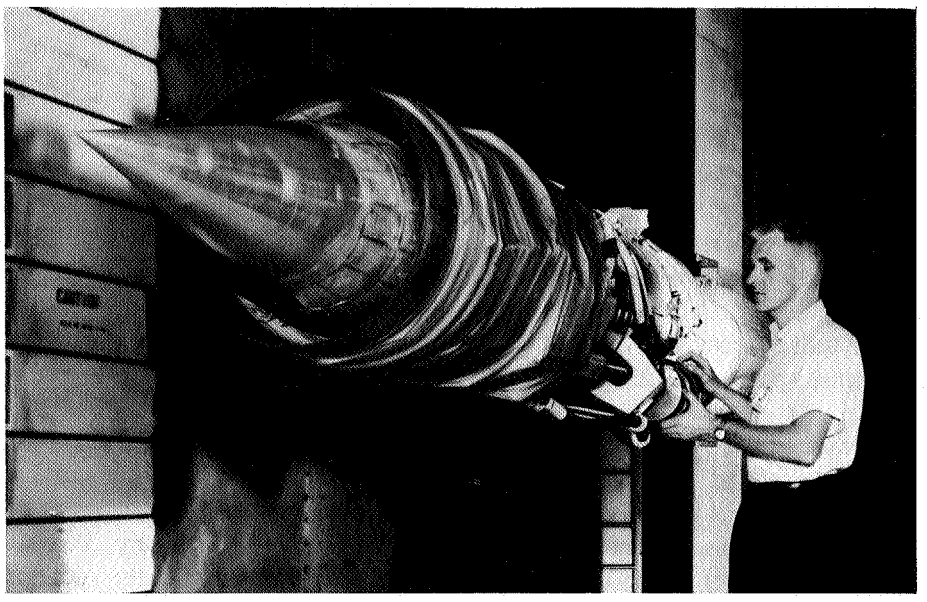

A-30906

Figure 1

AXISYMMETRIC INLET

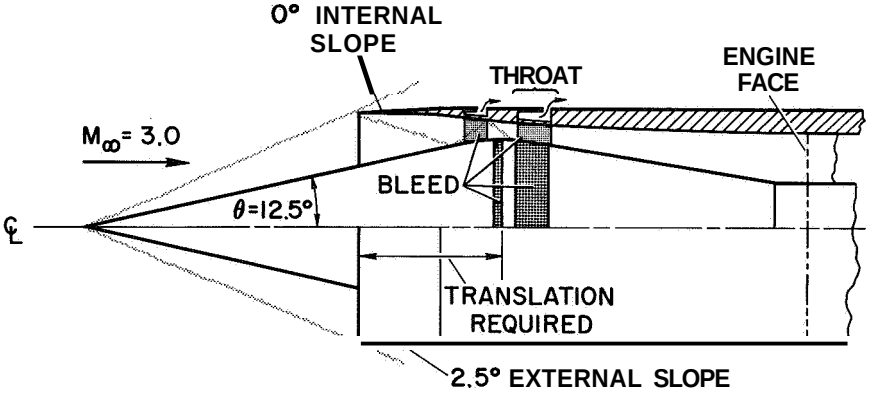

Figure 2.

SUPERSONIC PERFORMANCE

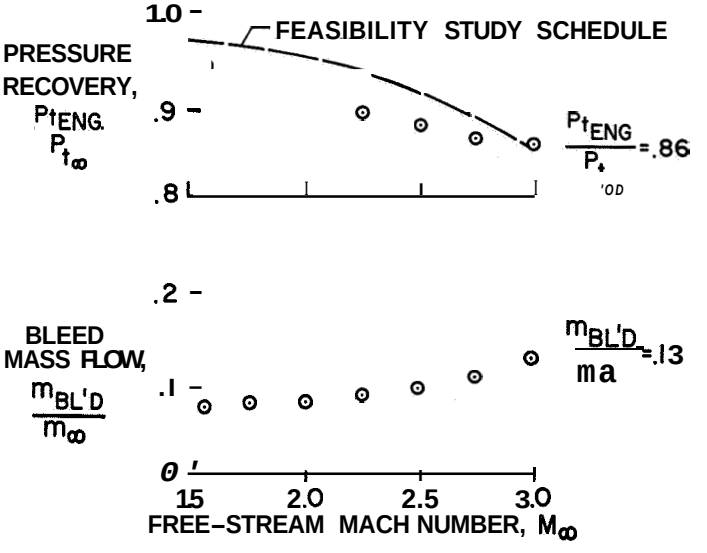

Figure 3

PITOT-PRESSURE PROFILES

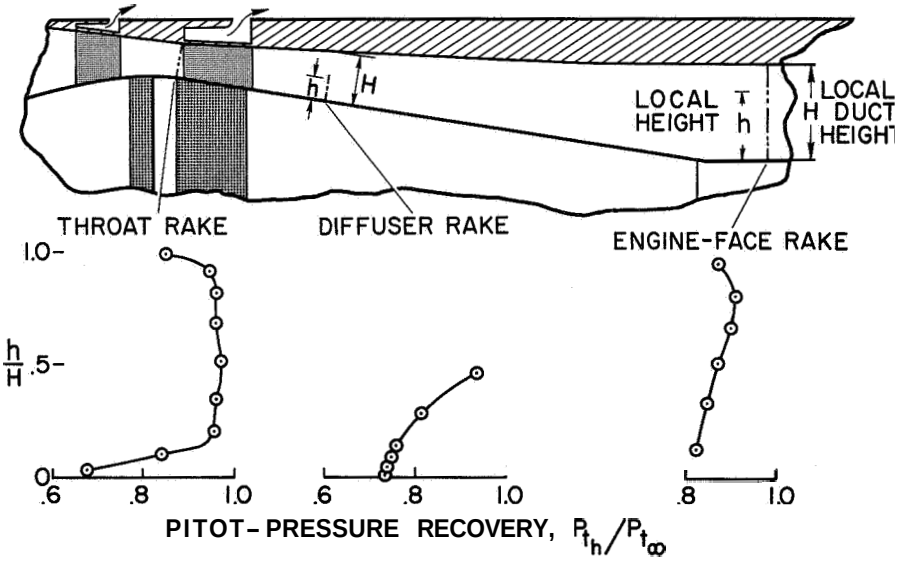

Figure 4

INLET-ENGINE MATCHING

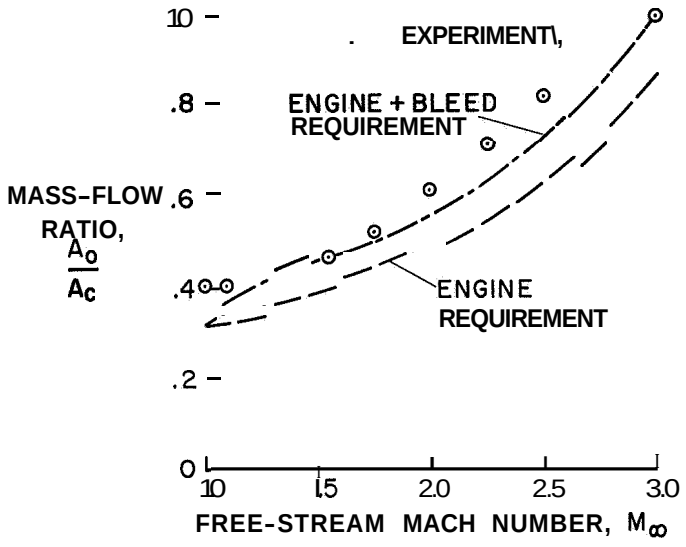

Figure 5

EFFECT OF INLET FLOW ANGLE

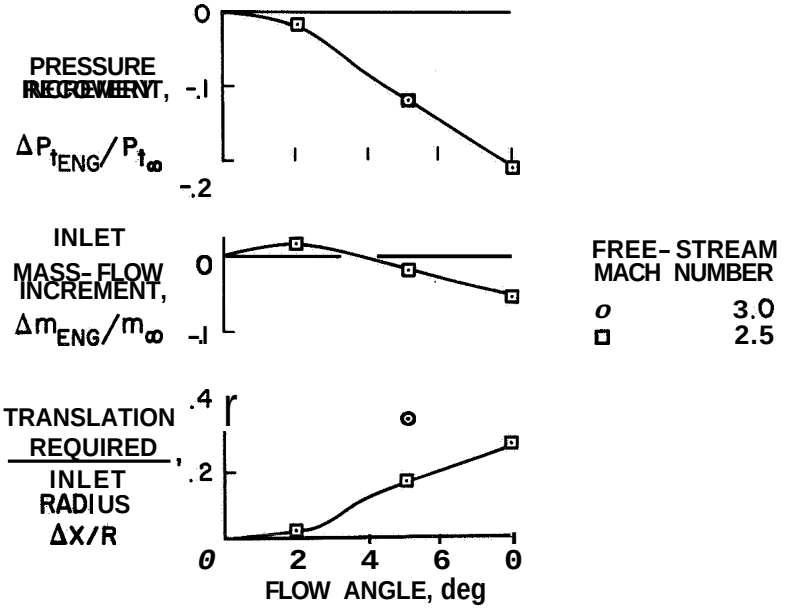

Figure 6

[redacted]

TRANSONIC PERFORMANCE

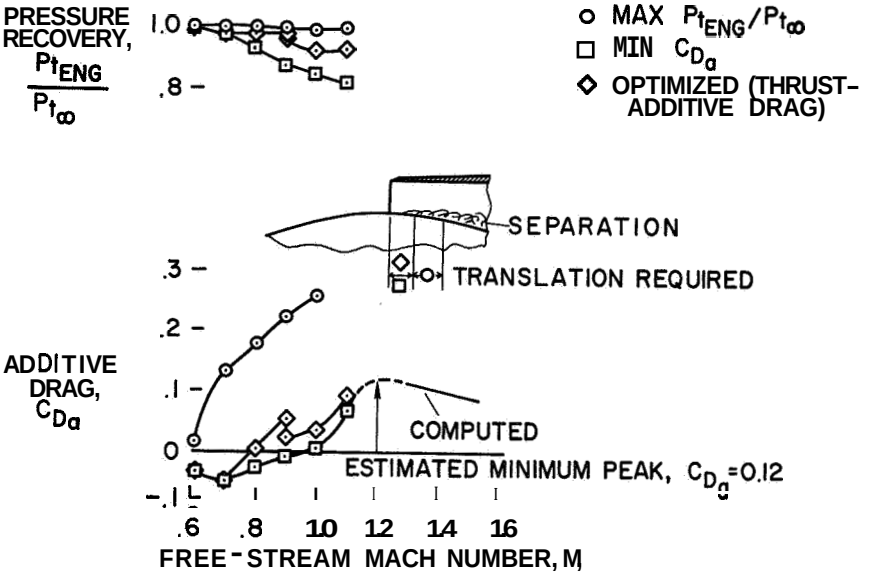

Figure 7

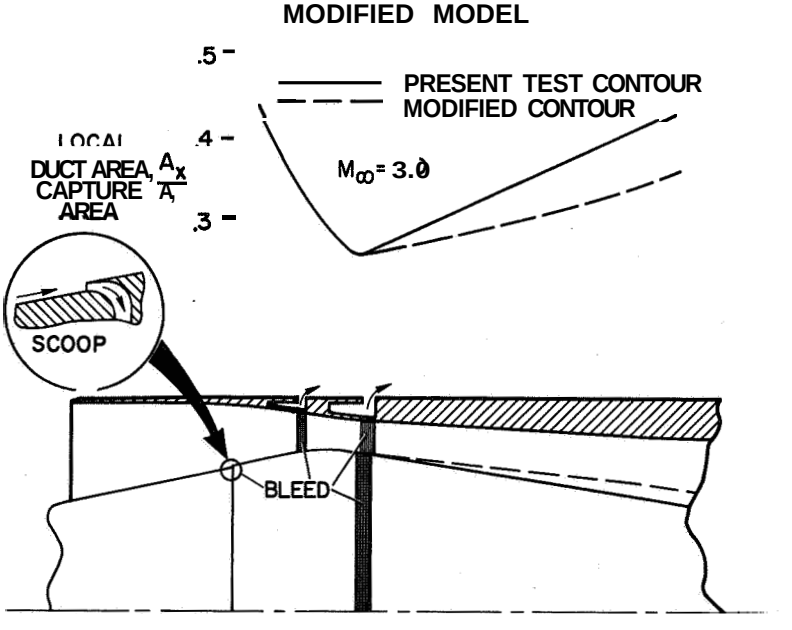

Figure 8

[redacted]

N67-31624

17. REVIEW OF NASA EXHAUST NOZZLE RESEARCH

By Jack F. Runckel

NASA Langley Research Center

SUMMARY

Exhaust nozzles proposed for the supersonic-transport propulsion system are examined in terms of performance, complexity, and special requirements imposed by the supersonic commerical air transport (SCAT) mission. Both nozzle internal performance and thrust-minus-drag performance are considered. Results from NASA investigations of the transonic performance of several representative types of exhaust nozzles applicable to the supersonic commercial air transport are presented.

INTRODUCTION

The jet exhaust nozzle of the supersonic transport must meet more severe operating requirements than nozzles used in the exhaust systems of current supersonic aircraft. It is the purpose of this paper to point out some of the problems of the SCAT jet-exit nozzle and the special features that must be incorporated in the exhaust system. The subject is very complex if dealt with in detail, and therefore only a simplified approach is presented here. Results from recent NASA investigations, primarily obtained in the transonic speed range, are presented to indicate the level of performance expected from various types of nozzles applicable to the supersonic transport.

17

SYMBOLS

A_e	nozzle exit area
A_N	nacelle cross-sectional area
A_t	nozzle throat area
ΔC_D	incremental drag coefficient of nozzles, $\frac{\text{Nozzle boattail drag}}{qS}$

PRECEDING PAGE BLANK NOT FILMED.

D total-nozzle-drag ratio, $\frac{\text{Nozzle drag}}{\text{Ideal primary thrust}}$

D_R secondary-air ram-drag ratio, $\frac{\text{Ram drag}}{\text{Ideal primary thrust}}$

D_β boattail drag ratio, $\frac{\text{Boattail drag}}{\text{Ideal primary thrust}}$

d_N nacelle diameter

F gross thrust ratio, $\frac{\text{Measured thrust}}{\text{Ideal primary thrust}}$

l nozzle external length

M Mach number

q dynamic pressure

S wing area, *3,500* sq ft

w_p primary nozzle weight flow

w_s secondary-air weight flow

$\left(\frac{w_s}{w_p}\right)_{corr}$ corrected secondary-weight-flow ratio

β boattail angle

η nozzle efficiency

$F - D$ thrust-minus-drag ratio

$F - D_R$ nozzle internal thrust efficiency

$F - D_\beta$ thrust-minus-boattail-drag ratio

$F - D_R - D_\beta$ nozzle propulsive performance

RESTRICTED

NOZZLE REQUIREMENTS

The nozzle must have the ability to provide high performance at all speeds up to a Mach number of 3. This includes not only the internal performance, or how efficiently the nozzle utilizes the energy in the exhaust gas to produce thrust, but also the effect of the drag on the nozzle external surfaces. The nozzle must be efficient not only for cruise at a Mach number of 3 but also during take-off, climb, and at subsonic cruise and loiter. The importance of nozzle efficiency is shown in paper no. 15 by Dugan, Keith, and Boxer where it is pointed out that a 1-percent change in nozzle gross thrust coefficient over the speed range resulted in a 5-percent change in airplane gross weight.

For many of the engine cycles under study, the nozzle system must have the capability of varying the throat sizes of either the engine or duct, or both, during augmented engine operation and for some engines during the cruise portion of the flight. The expansion surfaces may also have to be variable. The shape of the nozzle might have to change as shown in the top sketches of figure 1.

The choice of unmixed or mixed flows from the engine and duct (fig. 1) must be dealt with in nozzles for turbofan engines. For the unmixed-flow engine, consideration has to be given to the matching of static pressures between the engine and duct exits to prevent the flow from one throat from suppressing the gas flow from the other throat.

The nozzles must include provision for thrust reversal during both landing and in-flight operation to provide rapid descent. The lower half of the sketch in figure 1 of the mixed-flow turbofan indicates one possible type of thrust-reverser scheme utilizing cascade vanes to reverse the flow.

Cooling air must be provided during augmented engine operation to protect the nozzle surfaces from the very hot exhaust gases. Such secondary air may also be used to provide thrust increases in ejector nozzles and to improve off-design performance. (See refs. 1 and 2.) The use of inlet bypass air in an ejector nozzle as a trade-off for spillage drag at the lower speeds may also be considered. (See ref. 3.)

The mechanical actuation systems for accomplishing the necessary geometric variations of the nozzle components should be minimized to reduce the complexity. The aerodynamically adjustable types of nozzles meet this requirement. (See ref. 4.)

It would be desirable to design the nozzle to provide some noise attenuation during take-off and landing if this could be done without

decreasing the performance. However, the most successful noise-suppressor nozzle configurations have very complex geometric shapes or involve substantial increases in weight. Some indication of performance losses of typical noise-suppressor configurations are presented in reference 5.

The weight penalties for the aforementioned features should not be severe. An increase of 1 pound in nozzle weight can result in a 5-pound increase in the gross take-off weight of the airplane.

Consideration should be given to the location of the nozzle on the airplane in regard to the effect of the local flow field on the thrust and drag of the exhaust system (ref. 6) and the effect of the hot high-pressure jet on adjacent airplane surfaces (ref. 7). The effect of local interferences, such as wings, pylons, fuselage surfaces, tails, and adjacent engines, on nozzle performance and the jet interference effects on these components need evaluation in the final SCAT designs.

SCAT NOZZLE DESIGN STUDY

Internal Nozzle Geometry

In order that the design problems of supersonic-transport engine exits be illustrated, the basic nozzle requirements for a typical SCAT flight profile are presented. The duct-burning turbofan engine was selected for this study. The variation of pressure ratio and throat area with Mach number for both the primary-gas generator and the annular fan duct was used to expand isentropically the exhaust gas for each flow to ambient pressure at the flight altitudes, and the required exit areas were determined. Figure 2 shows the nozzle internal expansion ratios A_e/A_t which are required to produce maximum nozzle thrust at each Mach number. These nozzle area ratios are necessary to obtain optimum gross thrust regardless of the type of nozzle used. (See pp. 143 to 160 of ref. 8.)

The variation of expansion ratio shown for the duct (fig. 2) is that required for maximum augmentation with fuel burned in the fan duct. The expansion ratio for the duct stream with no augmentation would be somewhat less than that shown, and the fan annular throat would be further closed. The flows are unmixed at the throats of the engine and ducts, where, for example, the ratios of gas-stream total pressure to free-stream static pressure at a Mach number of 3 were 24 and 45, respectively. Because of this difference in the pressure levels, consideration has to be given to matching the static pressures between the

engine and duct throats to prevent flow from one throat from suppressing the gas flow from the other %&oat. *e.*,

Nozzle External Shape

If an engine-nacelle diameter of approximately 82 inches is assumed and the total nozzle-exit areas of both exhaust stream flows are related to the nacelle cross-sectional area, the variation shown in figure 3 results. The curves of the ratio of exit area to nacelle area indicate how the outside shape of the nozzle may have to vary with Mach number for a range of engine-power conditions. The nozzle system must have the capability of closing the outside shape on the nacelle exit to about 0.2 of the nacelle area and to open the exit area to 1.6 times the engine-nacelle size if a mechanically variable nozzle is used.

To determine the conical boattail angles on the outside nozzle surfaces corresponding to the area variations of figure 3, a nozzle length must be selected. For optimum performance, the length of an isentropic nozzle would be about 2 nacelle diameters. As a result, the nozzle would be about 14 feet long and would have low boattail angles throughout the Mach number range (maximum $\beta = 8^\circ$). These low angles are desirable, but the nozzle is too long and very heavy. If the nozzle is made half as long - that is, 1 nacelle diameter in length - the weight is reduced by about one-half at the expense of having higher boattail angles and drag and somewhat lower efficiency. The variation of boattail angle with Mach number for the short conical nozzle is shown in figure 4. The no-augmentation power-setting curve represents the upper limit in boattail-angle variation. At take-off, with partial augmentation, the boattail angle might be about 14°. During the acceleration period, the variation in boattail angle would follow the maximum power line up to a Mach number of 3 where a 6° flare would occur. At cruise some augmentation would be used, but the nozzle afterbody would be closed to a cylinder to minimize drag and the nozzle would then be somewhat underexpanded.

The variation of incremental airplane drag coefficient with Mach number due to drag of the long and short nozzles is presented in figure 5. These drag coefficients are based on the nozzle surface drag of four nacelles and on a wing area of 3,500 square feet. The data were obtained by using supersonic wave-drag theory (refs. 9 and 10) and interpolated experimental data (refs. 11 and 12) in the subsonic and transonic ranges. At a Mach number of 1.2 during acceleration (indicated by the circle in fig. 5), the drag of the short nozzles may be as much as 11 percent of the total airplane drag. This nozzle boattail drag represents 7 percent of the net thrust. The need for minimizing external drag is obvious, particularly in the transonic region, where the margin

of airplane thrust to drag is small. (See ref. 13.) It should be noted that drag forces exist on all types of nozzles in some form or another when a large variation of nozzle expansion ratio is required throughout the flight range. (See ref. 14.) From the preceding discussion it can be seen that the nozzle design may have to be a compromise involving internal performance, external drag, and nozzle weight.

RECENT NOZZLE INVESTIGATIONS BY NASA

Convergent-Divergent Nozzle

Some experimental data obtained with the convergent-divergent type of nozzle are shown in figure 6. This configuration represents a variable-geometry ejector, designed for a high-pressure-ratio turbojet engine, with the nozzle walls set for transonic operation. The ejector corresponds to the short-nozzle concept previously presented, except that it had contoured inner surfaces and a lower boattail angle in combination with a small base. The nozzle utilized secondary airflow for cooling and increasing the thrust through entrainment in the ejector. (See ref. 1.) The amount of corrected secondary airflow $\left(w_s/w_p\right)_{corr}$ was 7 percent of the flow passing through the primary nozzle. (See ref. 15 for definition of corrected secondary-weight-flow ratio.)

The performance or efficiency levels η as fractions of the ideal thrust of the primary nozzle are shown on the ordinate of figure 6 for the test Mach numbers. The curve labeled F represents the ejector-thrust ratio. This ratio is the measured thrust corresponding to the total momentum of both flows at the exit of the nozzle divided by the ideal thrust of the primary nozzle. To account for the secondary-air momentum, full ram drag of this air (divided by ideal primary thrust) has been subtracted out for the dashed curve labeled $F - D_R$. These data, then, represent the internal thrust efficiency of this nozzle.

The lowest curve (fig. 6) is the propulsive performance of the nozzle and includes, in addition, the drag of the nozzle external surfaces as a fraction of ideal primary thrust. This parameter $F - D_R - D_\beta$ accounts for everything except installation losses or benefits and forms the basis for comparison of different types of nozzles.

The data points shown at a Mach number of 3 (note broken scale) are for the ejector operating undereqanded with cylindrical outer surfaces and are based on data from reference 1. The results indicate that a shortened, contoured, ejector nozzle should have good performance throughout the Mach number range.

[redacted]

Blow-In-Do& Ejector Nozzle

The previous discussion has been concerned with the variable convergent-divergent types of jet-exit nozzles. Other types of nozzles which are not as complex mechanically and with which a reduction in weight is possible because of elimination of the divergent-shroud actuating mechanism will next be considered.

A type of nozzle that may be considered to be partially aerodynamically variable is known as the blow-in-door ejector nozzle. (See ref. 4.) The ejector consists of a fixed shroud with hinged trailing-edge flaps and hinged doors around the primary nozzle, as shown in the sketch of figure 7. The hinged portions of the nozzle open and close according to the pressure differential across them. At supersonic speeds the high engine pressures force the doors to close and the flaps to diverge, thereby approximating the convergent-divergent nozzle. At transonic and subsonic speeds, the jet is separated from the ejector walls and induces air through the blow-in-doors to alleviate overexpansion, and the trailing-edge flaps close inwardly.

Results from an investigation of a blow-in-door ejector nozzle are shown also in figure 7. For these tests the doors were fixed open and the trailing-edge flaps closed, as shown in the sketch. The net force of the blow-in-door air is included in the coefficients. Data are presented for a schedule of jet-pressure ratio with Mach number where the pressure ratio was 4 at a Mach number of 1.2. The ejector-thrust ratio F is the internal performance as previously presented. The thrust-minus-drag parameter (F - D) included only the' shroud and boattail drag for the region indicated in the sketch. Subsonically the thrust-minus-drag performance was actually higher than the internal performance because external forces in the thrust direction were obtained on the boattail and shroud in the indicated drag region. This occurred because of pressure recovery at the rear of the boattailed region. Some NASA investigations of blow-in-door ejectors are reported in references 15 and 16.

Plug Nozzles

The utilization of the aerodynamically adjustable nozzles can provide reductions in nozzle weight. The best known of this type is the isentropic plug nozzle for which the outer boundary of the exhaust stream continually adjusts to ambient pressure. There are, however, several problems associated with this type of nozzle for the supersonic transport. The excellent static performance of this nozzle suffers from detrimental effects of an external airstream. (See refs. 4, 14, and 17.) Some of the design problems found in applying the plug nozzle

[redacted]

to the SCAT mission are illustrated in figure 8. A mixed-flow exhaust is assumed and the nozzle is to be designed for a cruise Mach number of 3. The isentropic plug requires a steep turn at the throat, which results in a nozzle diameter greater than the basic nacelle diameter and in a steep boattail, both of which can have a sizable effect on drag (top left sketch).

Several methods of reducing the drag are illustrated by the other sketches. The nozzle shown in the top right-hand sketch is designed for a lower Mach number and has lower plug and boattail slopes. For the pressure ratios at a cruise Mach number of 3, the jet continues to expand beyond the nozzle-lip diameter (as indicated by the broken lines), and some penalty in performance occurs. The off-design performance at lower speeds should be better than the plug nozzle designed for a Mach number of 3. (See ref. 17.)

Another alternative is to provide some internal expansion as shown in the lower sketches. The use of conical plug surfaces has also been shown to provide good performance with a divergent shroud (lower left-hand sketch of fig. 8).

The nozzle shown in the lower right-hand sketch takes advantage of the underexpanded nozzle through the use of terminal fairings. These bodies, distributed around the exit, can be designed to take some thrust on their inner surfaces, and the fairings reduce the effective base area or boattail angle. With open spaces between the fairings, the overexpansion losses at lower speeds may also be alleviated. (See refs. 18 and 19.) There is an additional problem of varying the throat area for all these plug nozzles; and the proposed methods, such as flaps, collapsing and translating plugs, and translating shrouds, will require evaluation.

Plug Nozzle With Terminal Fairings

Some performance results obtained throughout the SCAT Mach number range on a plug nozzle with and without terminal fairings are presented in figure 9. (See also refs. 19 and 20.) The basic plug nozzle was designed for a pressure ratio of 10 corresponding to a Mach number of 1.8. The thrust-minus-drag performance of the basic plug is indicated by the solid line. The performance peaks at the design Mach number and drops off at the higher speeds (underexpanded nozzle) and at the lower speeds, around a Mach number of 1 (overexpanded nozzle); and, as typical for plug nozzles, the performance improves again at subsonic speeds. (See ref. 21.) Addition of the terminal fairings provided increased performance above the design Mach number and at transonic and subsonic speeds.

[redacted]

Concave-Base Plug Nozzle

Several types of plug nozzles have been designed and tested with various degrees of truncation of the plug. (See ref. 4.) A new concept of this type of nozzle has been under development at the Langley Research Center. This configuration is known as the concave-base plug nozzle, which eliminates the plug extension. (See ref. 22.) A sketch illustrating the principle of operation of the concave-base plug nozzle is shown in the upper portion of figure 10. The nozzle can be considered as having an aerodynamically variable plug since it has aerodynamically adjustable inner and outer jet boundaries and therefore eliminates a large portion of the plug weight. In operation, the base-recirculation principle develops a ring vortex which pressurizes the base. The throat area is varied with hinges on the plug surfaces; these surfaces can also be used to block the exhaust flow for cascade thrust reversal. The performance is highly dependent on lip geometry and jet pressure ratio.

Results are shown for the schedule of the jet pressure ratio previously used for most of the other nozzles. Even though the performance may be somewhat lower at transonic speeds than for the other nozzles, the reduction in weight makes it competitive. At higher pressure ratios and Mach numbers the performance is expected to improve.

SUMMARY OF NOZZLE PERFORMANCE

An attempt to summarize the state of the art of nozzle performance for the supersonic transport is presented in figure 11. Nozzle performance η is the thrust efficiency, including the secondary momentum drag of ejectors and the drag of the nozzle external surfaces. The predicted performance is indicated by a band which includes the various types of nozzles proposed for the supersonic transport, such as the variable convergent-divergent ejector, the blow-in-door ejector, the shrouded plug nozzle, and terminal-fairing configurations. The lowest nozzle efficiencies occur in the transonic speed range where nozzle overexpansion conditions or high drags on the nozzle external surfaces contribute to the losses. The spread in nozzle performance at a Mach number of 3, in addition to nozzle configuration differences, is a result of changing engine power from full augmentation to the cruise operating condition.

[redacted]

CONCLUDING REMARKS

The selection of an exhaust nozzle of the supersonic commercial air transport engine is still an area in which much further research is needed to determine the optimum configuration. Several promising types of nozzles appear to be competitive when compared on a thrust-minus-drag performance basis. These nozzles are the short variable convergent-divergent ejector, the blow-in-door ejector, the conical plug nozzle, and the plug nozzle with terminal fairings. In addition, other configurations offer interesting possibilities.

For the final nozzle evaluation, model investigations of complete supersonic-transport configurations will have to be conducted with a simulated propulsion-system exhaust. Performance of the installed exhaust nozzle must be obtained with the simulation of the external flow field that is expected to be encountered with the airplane. The model should include proper shaping of the aircraft and nacelles ahead of the nozzles, boundary layer and Reynolds numbers consistent with scaling practices, and local interferences, such as wings, pylons, fuselage surfaces, tails, and engine-cluster arrangements which can affect both the external and internal performance of the nozzle. The jet interference effects on drag, loads, dynamics, and temperatures of the airplane surfaces will also require evaluation.

DECLASSIFIED

REFERENCES

1. Stofan, Andrew J., and Mihaloew, James R.: Performance of a Variable Divergent-Shroud Ejector Nozzle Designed for Flight Mach Numbers up to 3.0. NASA TM X-255, 1961.

2. Beheim, Milton A.: Off-Design Performance of Divergent Ejectors. NACA RM E58G10a, 1958.

3. Hearth, Donald P., and Connors, James F.: A Performance Analysis of Methods for Handling Excess Inlet Flow at Supersonic Speeds. NACA TN 4270, 1958.

4. Migdal, David, and Horgan, John J.: Thrust Nozzles for Supersonic Transport Aircraft. Paper No. 63-AHGT-73, ASME, Mar. 1963.

5. Schmeer, James W., Salters, Leland B., Jr., and Cassetti, Marlowe D.: Transonic Performance Characteristics of Several Jet Noise Suppressors. NASA TN D-388, 1960.

6. Swihart, John M., Mercer, Charles E., and Norton, Harry T., Jr.: Effect of Afterbody-Ejector Configurations on the Performance at Transonic Speeds of a Pylon-Supported Nacelle Model Having a Hot-Jet Exhaust. NASA TN D-1399, 1962. (Supersedes NASA MEMO 1-4-59L, 1959.)

7. Swihart, John M., and Crabill, Norman L.: Steady Loads Due to Jet Interference on Wings, Tails, and Fuselages at Transonic Speeds. NACA RM L57D24b, 1957.

8. Talbot, J. E.: Aerodynamics of Power Plant Installations. Supersonic Engineering, J. T. Henshaw, ed., John Wiley & Sons, Inc., c.1962, pp. 143-160.

9. Fraenkel, L. E.: The Theoretical Wave Drag of Some Bodies of Revolution. R. & M. No. 2842, British A.R.C., 1955.

10. Jack, John R.: Theoretical Pressure Distributions and Wave Drags for Conical Boattails. NACA TN 2972, 1953.

11. Silhan, Frank V., and Cubbage, James M., Jr.: Drag of Conical and Circular-Arc Boattail Afterbodies at Mach Numbers From 0.6 to 1.3. NACA RM L56K22, 1957.

12. Cubbage, James M., Jr.: Jet Effects on the Drag of Conical Afterbodies for Mach Numbers of 0.6 to 1.28. NACA RM L57B21, 1957.

13. Nichols, Mark R. : Supersonic Transport Propulsion Requirements. Aerospace Eng., vol. 20, no. 9, Sept. 1961, pp. 12-13, 58-63.

14. Keenan, J. G. : Some Problems Associated With High Mach Number Air Breathing Powerplants. Interavia, vol. 18, no. 3, Mar. 1963, pp. 345-347.

15. Schmeer, James W., Mercer, Charles E., and Kirkham, Frank S.: Effect of Bypass Air on Performance of a Blow-in-Door Ejector Nozzle at Transonic Speeds. NASA TM x-896, 1963.

16. Kirkham, Frank S., and Schmeer, James W.: Performance Characteristics at Mach Numbers up to 1.29 of a Blow-in-Door Ejector Nozzle With Doors Fixed in Nl-Open Position. NASA TM x-830, 1963.

17. Valerino, Alfred S., Zappa, Robert F., and Abdalla, Kaleel L.: Effects of External Stream on the Performance of Isentropic Plug-Type Nozzles at Mach Numbers of 2.0, 1.8, and 1.5. NASA MEMO 2-17-59E, 1959.

18. Willis, Conrad M., and Mercer, Charles E.: Effect of Afterbody Terminal Fairings on the Performance of a Pylon-Mounted Turbojet-Nacelle Model. NASA TM X-215, 1960.

19. Willis, Conrad M., and Norton, Harry T., Jr.: Effect of Afterbody Terminal Fairings on the Performance of Plug-Type Exhaust Nozzles at Transonic Speeds. NASA TM x-762, 1963.

20. Norton, Harry T., Jr., and Swihart, John M.: Effect of Terminal Fairings on the Performance of a Plug-Type Exhaust Nozzle in Quiescent Air and at Mach Numbers of 1.62, 1.93, 2.55, and 3.05. NASA TM X-463, 1961.

21. Salmi, R. J., and Cortright, E. M., Jr.: Effects of External Stream Flow and Afterbody Variations on the Performance of a Plug Nozzle at High Subsonic Speeds. NACA RM E56F11a, 1956.

22. Mercer, Charles E., and Salters, Leland B., Jr.: Performance of a Plug Nozzle Having a Concave Central Base With and Without Terminal Fairings at Transonic Speeds. NASA TN D-1804, 1963.

SCAT EXHAUST-NOZZLE PROBLEMS

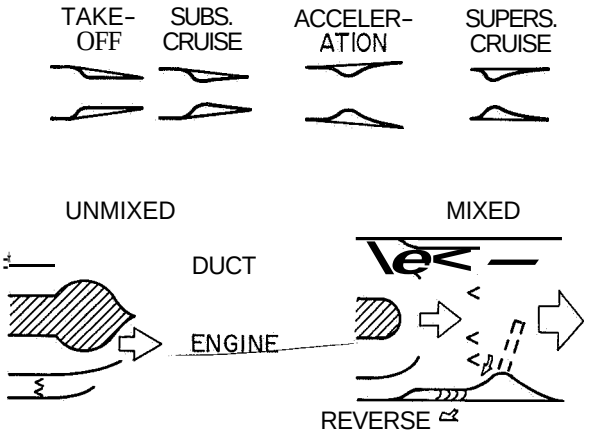

Figure 1

NOZZLE EXPANSION RATIOS FOR DUCT-BURNING TURBOFAN

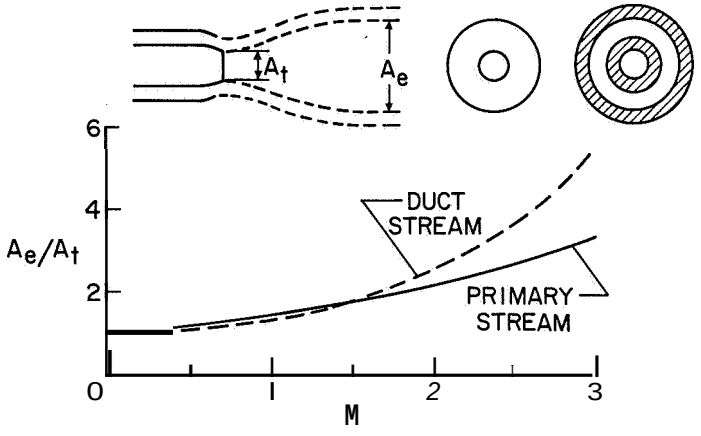

Figure 2

[redacted]

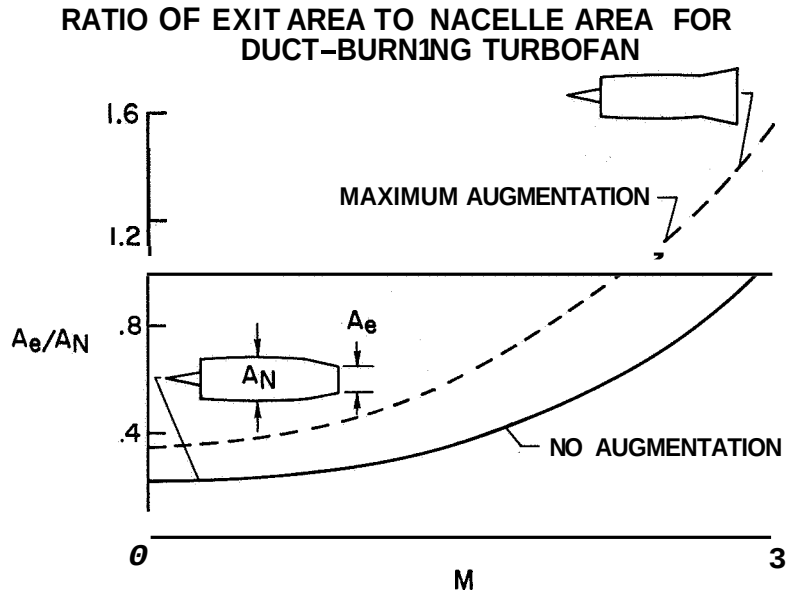

Figure 3

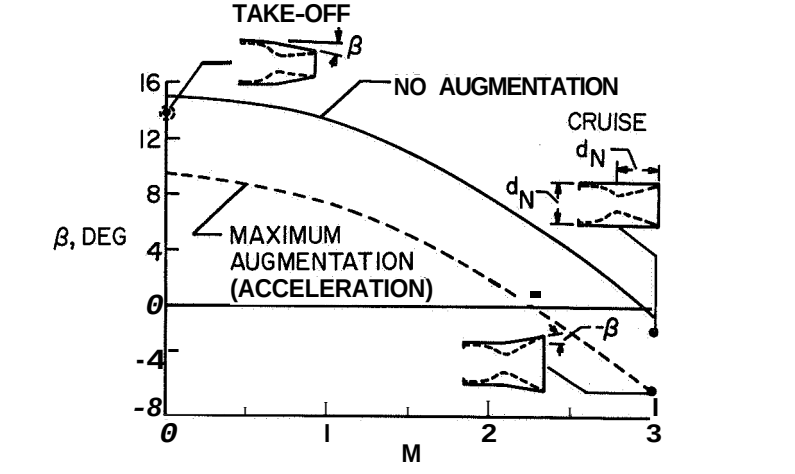

Figure 4

[redacted]

INCREMENTAL DRAG COEFFICIENTS OF FOUR NACELLE BOATTAILS
WING AREA = 3,500 FT^2

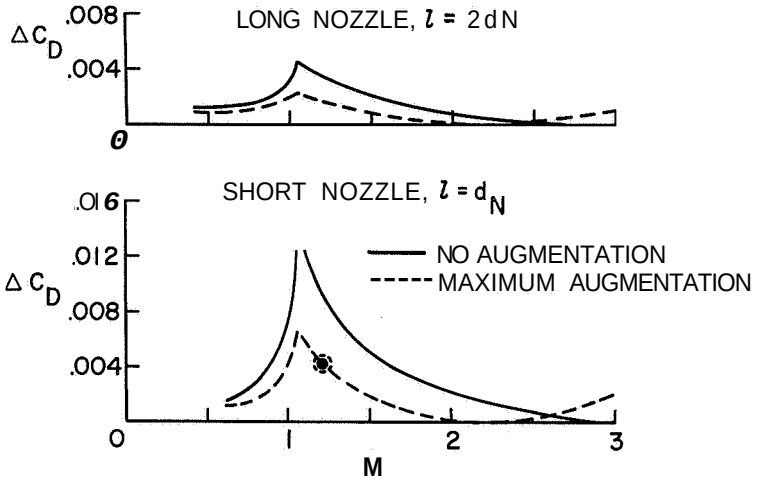

Figure 5

PERFORMANCE OF SHORTENED CONVERGENT-DIVERGENT NOZZLE

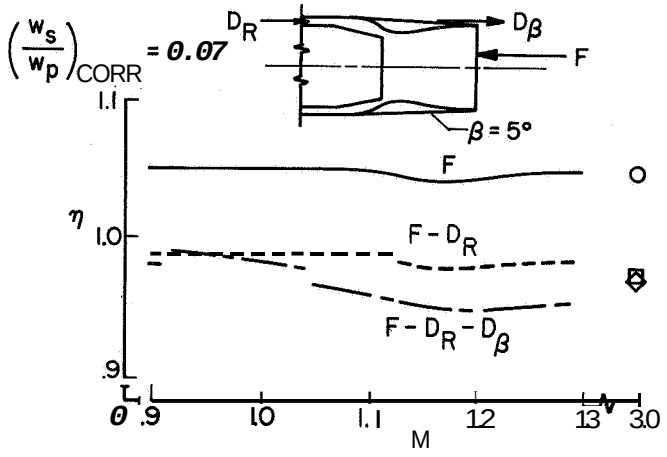

Figure 6

[redacted]

BLOW-IN-DOOR NOZZLE

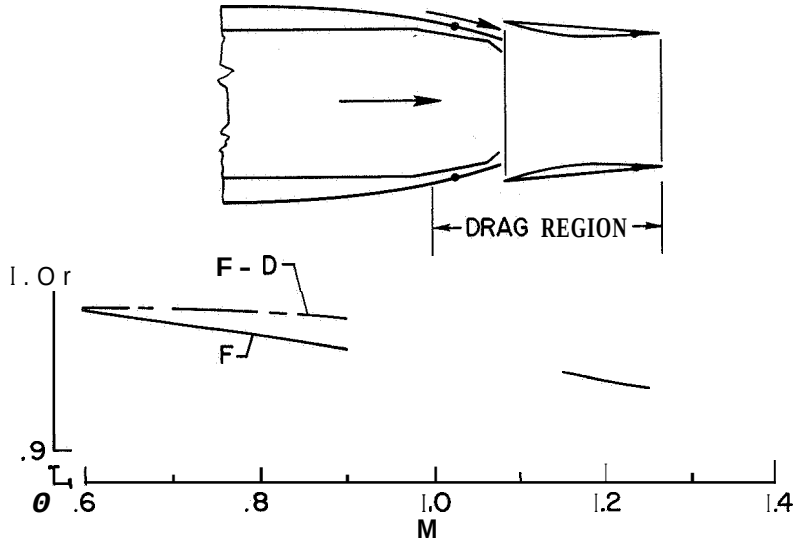

Figure 7

PLUG NOZZLES

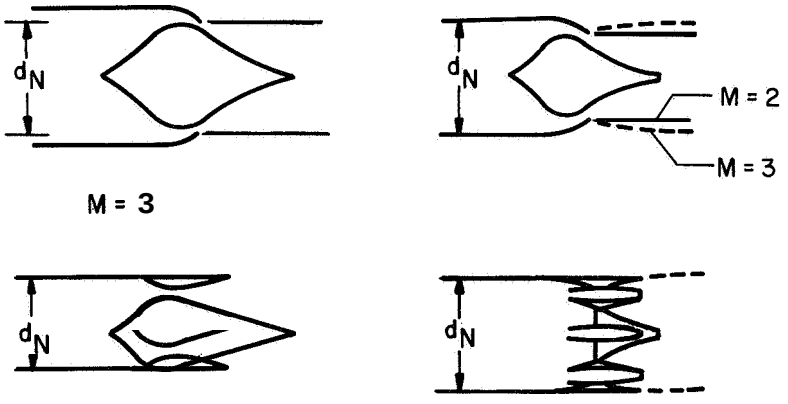

Figure 8

[redacted]

PLUG NOZZLE WITH AND WITHOUT TERMINAL FAIRINGS
M = 1.8 **DESIGN PLUG**

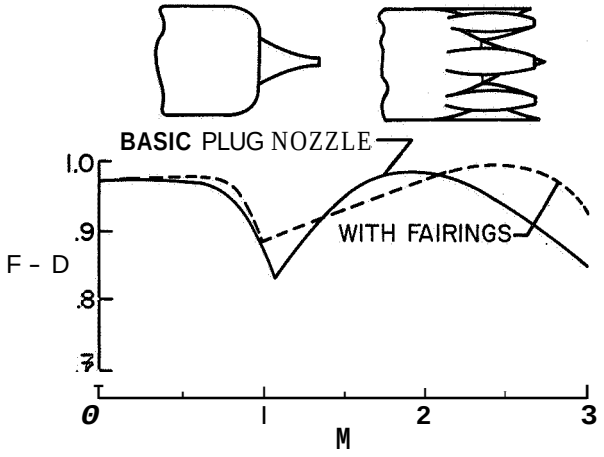

Figure 9

CONCAVE PLUG NOZZLE

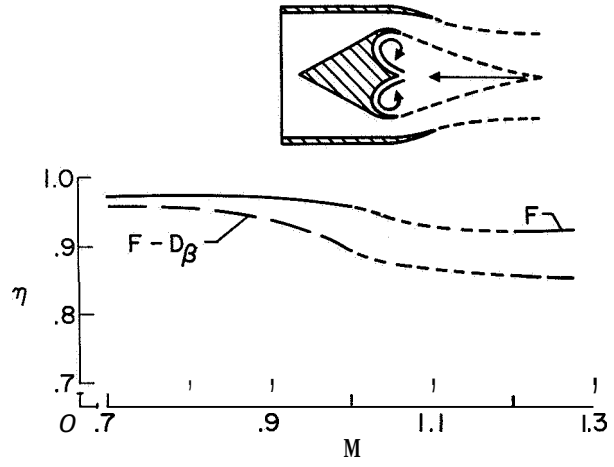

Figure 10

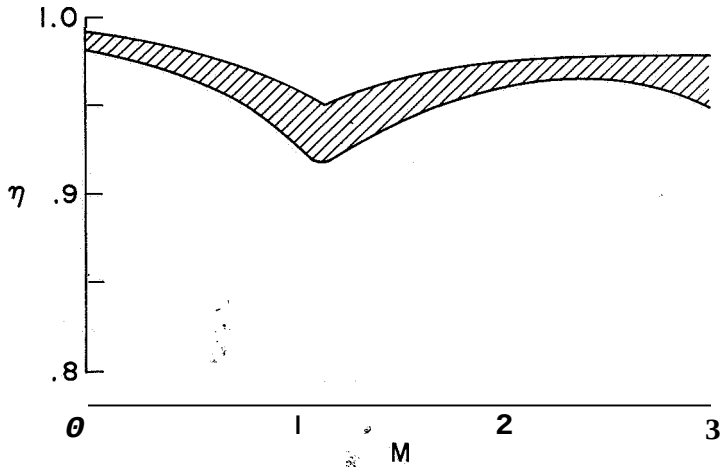

Figure 11

N67-31625

18. STRUCTURAL CONCEPTS AND MATERIALS SELECTION IN TEE FEASIBILITY STUDIES

By Richard A. Pride

NASA Langley Research Center

SUMMARY

Feasibility studies of the four SCAT configurations by two contractors have shown that 8Al-1Mo-1V duplex-annealed titanium alloy is the most efficient material for use in the primary structure. Skin-stringer type of construction was utilized in both wing and fuselage designs. Calculated thermal stresses were shown to result in an overall increase in structural weight of less than 2 percent, even though different methods were used to combine thermal stress with load stress for ultimate load conditions. Structural weights were 25 to 29 percent of the gross weight on all except a variable-sweep dual-wing configuration, which had a structural weight that was 37 percent of the gross weight.

INTRODUCTION

Paper no. 3 by R. Richard Heppe and Jim Hong and paper no. 4 by Lloyd T. Goodmanson, William T. Hamilton, and Maynard L. Pennell present the SCAT feasibility studies of the Lockheed-California Co. and The Boeing Co., respectively. These summary papers touch on the structural designs and materials used in the four Mach 3 configurations as well as in the two aluminum configurations that were added to the study. The present paper discusses in greater detail the material selection, some of the structural concepts and design allowables, the thermal stress problem, and the structural weight. The discussion primarily covers the Mach 3 configurations with some comparisons with the aluminum designs.

18

SYMBOLS

E	Young's modulus of elasticity, psi
g	acceleration due to gravity, ft/sec^2

T	temperature, °F
ΔT_{MAX}	maximum temperature difference between specified locations in structure, °F
W_S	structural weight of airplane, lb
W_{TO}	take-off *gross* weight of airplane, lb
E	strain
σ	stress, ksi

Subscripts:

Y	yield
Tu	tensile ultimate
LL	limit load
UL	ultimate load
TH	thermal
TH,L	thermal at limit load
TH,U	thermal at ultimate load

MATERIAL SELECTION

The Mach 3 cruise speed requirement in the initial studies resulted in structural temperatures high enough to remove aluminum alloys from consideration in the material selection process. Both stainless steels and titanium alloys were initially considered; however, the final choice of the 8 percent aluminum - 1 percent molybdenum - 1 percent vanadium (8Al-1Mo-1V) titanium alloy was made by both contractors.

Figures 1 and 2 show two of the many material-selection parameters used: tensile strength and stiffness. In figure 1 the tensile ultimate stress divided by the density is shown as a function of temperature for several materials. The top curve is the 8Al-1Mo-1V titanium alloy, the next curve is one of the better stainless steels (PH 14-8 Mo, [redacted] 1050 condition) and the bottom curve, shown as a band, includes several of the aluminum alloys which might be used at slower speeds and lower

temperatures. Included are X2020-T6, 2024-T81 and 2618-T61 aluminum alloys. The aluminum data are based on 10,000 hours of exposure to test temperature, the longest exposure data available, because aluminum-alloy strengths are reduced by exposure time. No such effect has been observed for the titanium or stainless steel, and the results shown in figure 1 are for short-time exposure. Two things should be noted. The higher strength of the titanium indicates that a tension member built from titanium would be about 10 percent lighter than one built from stainless steel over the entire temperature range shown. Also, the titanium tension member would be about 20 percent lighter than an aluminum tension member in its useful temperature range.

A similar comparison for stiffness is shown in figure 2 based on the modulus-density ratio. In this figure, there is not such a clear cut advantage in any one material since they all are grouped rather closely. Thus, for parts of the structure which must be designed for stiffness rather than strength, any of these materials would result in about the same weight. For elastic compression buckling of fuselage or wings, this modulus-density parameter becomes either the square root of the modulus or the cube root of the modulus divided by the density, and the order of weight saving would be aluminum first, titanium next, and steel last.

Additional material-selection factors were considered in the design studies. Such factors as fatigue life, compression yield strength, and weld strength modify the degree of weight saving experienced with titanium, but, in general, short-time-exposure material-selection parameters indicate that the 8Al-1Mo-1V titanium alloy is the best material for the SCAT configurations. Paper no. 19 by Herbert F. Hardrath and George J. Heimerl discusses NASA research programs concerning the effect of long-time exposure to temperature.

When a new material is recommended for commercial use, one of the questions raised is, "How reproducible is it?" Figure 3 shows the variation in tensile ultimate stress for the Ti-8Al-1Mo-1V alloy. This alloy is always used in the annealed condition. However, at least three different annealing processes are available and some of the data reported in various papers in this compilation were obtained from material in each of the three anneals. The simplest form is the single-anneal or mill-anneal process. In order to improve the crack propagation characteristics of the mill-annealed material, the triplex-anneal process was developed which involves three exposures in the heat-treating furnace. Subsequently, a duplex-anneal process was developed which gives essentially the same material characteristics as the triplex-anneal process but involves only two exposures in the furnace. The duplex-annealed material is that which is recommended today.

In the duplex-annealed condition, results of a compilation of tests at The Boeing Co., Lockheed-California Co., Langley Research Center, and Titanium Metals Corp. of America show about 15 percent scatter for eight different heats and about 6 percent scatter for different sheets within one heat. Strength of 1-inch-thick plate indicates the type of strength reduction associated with thicker material. Similar scatter can be seen for the mill-annealed and triplex-annealed materials. Note that in figure 3 the stress scale is expanded, by not starting at zero, to emphasize the effects. Comparative data for aluminum alloys show about 5 percent scatter between different sheets of one run and about 12 percent scatter between typical and minim properties. Establishing sound minimum design properties is one of the problems which needs continuing effort for the 8Al-1Mo-1V duplex-annealed titanium alloy.

Fabrication of structural test specimens from 8Al-1Mo-1V duplex-annealed titanium alloy under this SCAT contract and other related supersonic transport contracts indicates that there is no difficulty in working with the material. Additional experience is needed to establish optimum shop practices and to build a general level of confidence. Reasonable rates of machining integral skin-stringer panels from titanium plate have been accomplished. Stringers have also been brake-formed and joined to cover skins by resistance and fusion welding without serious degradation of the welded-area material strength.

STRUCTURAL CONCEPTS

A structural design approach has been followed for all SCAT configurations based on previous experience with subsonic commercial transport, modified locally where necessary to suit peculiar requirements such as wing pivots.

The basic structural concepts are shown in figure 4. Use of titanium favors skin-stringer construction in both wing and fuselage sections. If stainless steel were used, much more complex construction would be required to provide the local stiffening necessary to develop the high strength in compression and torsion. The structural weight of the design using steel would be at least 10 percent greater than that using titanium.

Fuel tank designs used include both integral and isolated internal tanks in both wing and fuselage sections. Fuselages are designed with sufficient area in the rings and crack-stopper straps where needed to prevent catastrophic crack growth. Minimum fuselage skin thickness is set at 0.028 to 0.032 inch for cabin pressure differentials of 10.5 to 11.9 psi. Both pressures meet specified requirements (ref. 1) but reflect slightly different attitudes on passenger comfort.

The structural designer for SCAT is faced with at least three problems which are of larger magnitude or are different from those encountered in previously designed transport aircraft. These problems include long-lifetime exposure to loads and elevated temperatures (discussed in paper no. 19), aeroelastic problems associated with the thin wings and long fuselages (discussed in paper no. 20 by Robert W. Boswinkle, Jr., and E. Carson Yates, Jr.), and thermal stress problems associated with the temperature gradients in the wing and fuselage panels (discussed in the following section).

THERMAL STRESS

Structural temperatures on the lower surface of the wing in the region of an integral fuel tank are shown in figure 5. The lower surface is a double-skin design with the inner skin forming the bottom of the fuel tank. The upper surface is single-skin Z-stringer construction with a radiation barrier attached to minimize heat transfer to the fuel. The temperature of the outer skin on the lower surface climbs very rapidly as the airplane attains supersonic speeds and quickly reaches equilibrium at about 450° F. The temperature of the inner skin rises very slowly since it is in contact with the fuel throughout the flight. The difference in temperature between these two skins results in thermal stresses because the skins are joined together through the Z-stringers. Temperatures shown are typical for this type of fuel tank. Large variations would be possible depending on the structural details.

A typical comparison of flight load stress and thermal stress for the lower surface of a wing in the region of an integral fuel tank is shown in figure 6. The short-dashed line represents the 1 g load stress history for both skins. The solid line represents the combined load and thermal stress history for the inner skin, and the long-dashed line represents the combined load and thermal stress history for the outer skin. Designing the inner skin thicker than the outer skin minimizes the additive effect of thermal stress in the inner skin, and results in compressive thermal stresses in the outer skin which are large enough to cancel out the tensile load stress near the end of the supersonic flight.

A similar situation exists in the fuselage temperature distribution, as shown in figure 7. The cutaway section is a portion of fuselage skin, supported by a longitudinal stringer and a circumferential ring. Calculated temperature histories are shown for four points. The solid lines designated A and B represent the temperature history of the skin and rings. The maximum difference in temperature between the skin and rings for this case is 340° F. This difference produces compression thermal stress circumferentially in the fuselage skin, which is

beneficial when combined with the pressurization stress. However, this temperature difference also produces tensile thermal stress in the rings, which may be detrimental to their role as crack stoppers. The dashed lines designated C and D represent the temperature history of the skin and inside flange of the stringer. The maximum temperature difference of 240° F produces longitudinal compression in the skin which may produce local buckling when combined with the fuselage bending-moment stresses.

Thermal stresses in the supersonic transport are of a magnitude that they can be combined with 1g load stresses by elastic superposition. But there is no uniformity of opinion as to how to combine thermal stress and load stress at limit or ultimate load. Two methods used by the contractors to assess the effect of thermal stress on structural weight are discussed. The first method is shown in figure 8; the details are worked out for a tension member, but similar relations would apply in compression.

A typical stress-strain curve for the material is shown in figure 8 with the yield stress and tensile ultimate stress designated by circles. The standard definition - that ultimate load must be 1.5 times the limit load - is maintained. Whether or not thermal stresses are present, the limit load stress must not exceed 67 percent of the ultimate load stress. Also, at limit load, the combination of thermal stress and limit load stress must not exceed the yield stress; that is, the combination shall produce no permanent set which would require repair, adversely affect the mechanical operation of components, or adversely affect the aerodynamic characteristics of the vehicle. The thermal stress is determined by combining a thermal strain with the limit load strain where the thermal strain is calculated from the temperature distribution in the structure. At ultimate load, the thermal stress plus 1.5 times the limit load stress is equal to the tensile ultimate stress of the material. Again, the thermal stress is based on combining the thermal strain with the ultimate load strain, which results in an alleviated thermal stress due to plasticity. The increment of thermal strain at limit load produces a large thermal stress; the same increment of thermal strain at ultimate load produces a much smaller thermal stress.

The thermal strain at ultimate load is based on the same temperature distribution as was present at limit load. The method may be deficient, therefore, because no "safety factor" is applied to the temperature distribution.

A more conservative method is shown in figure 9. The same stress-strain curve is shown as in figure 8 and the same definition - that thermal stress plus limit load stress must not exceed the yield stress - is applicable. However, the criterion at limit load is that limit load stress plus thermal stress must not exceed 67 percent of the tensile ultimate stress. Thermal stress is calculated elastically from the temperature distribution present at limit load conditions. At ultimate load,

both the limit load stress and the thermal stress are multiplied by the factor 1.5 before summing and equating to the tensile ultimate stress.

The FAA tentative standard for supersonic transport design (ref. 2) adopts a method similar to this second method (fig. 9) except that the thermal stress is multiplied by a factor of 1.25 instead of 1.5 before summing for the ultimate load.

A comparison between figures 8 and 9 shows a large difference in load stress available to carry the ultimate load on the portion of the structure considered. However, since thermal stresses are self-equilibrating within the structure, there will be other members in which the thermal stress will subtract from the load stress rather than add, with the resultant effect that more load stress can be carried in those members. Thus, a complete structural analysis is required to determine the impact of different thermal stress design criteria on the structural weight.

How much of a weight penalty associated with thermal stresses, then, did the contractors' studies show? Figure 10 shows the stiffened panel weights for one particular case of an 8Al-1Mo-1V titanium dry-bay wing lower surface. Wing panel weight is plotted as a function of panel end load. The curve for the room-temperature panel weight is shown for reference. Ascent thermal conditions appear to produce a 40-percent increase in panel weight. However, this is not the proper way to use these curves. At room temperature, any particular location in the wing will have a panel weight determined by the end load corresponding to the gross weight of the airplane at take-off and to subsonic aerodynamic loading. By the time the peak thermal condition is obtained, near the start of supersonic cruise, a considerable amount of fuel will have been consumed and the weight of the airplane reduced. Supersonic aerodynamic loading will apply and the panel end load will be reduced so that the panel weight will increase only slightly, if at all. In addition, many parts of the structure are not designed by thermal stress conditions; consequently, the studies showed less than a 2-percent increase in overall structural weight attributed to thermal stress.

STRUCTURAL WEIGHT

A comparison of structural weight breakdowns in terms of fraction of gross weight at take-off for the various SCAT configurations is shown in figure 11. Grouped together are the four titanium airplanes, the two aluminum airplanes, and the two subsonic transports. The numbers at the top of the bars are the SCAT numbers. Although the contractors did not

always agree on gross weight poundage, their structural fractions are very close and average values are therefore used in this presentation. It must be recognized that SCAT 4 and SCAT 15 did not receive as many refinement cycles in the feasibility study and therefore their weights are probably a little less well-defined. Also, since the aluminum SCAT airplanes were only brought into the study recently, they do not reflect as much refinement.

An interesting item is the weight of the SCAT 15 wing, about two times heavier than any other wing. This heaviness is due to the double-wing feature for variable sweep and is the main reason for the gross weight being unacceptable (having a weight fraction of 0.37). However, the weight fractions of the other components in the SCAT 15 structure are not very different from the same components in the other SCAT airplanes. The titanium SCAT airplanes, with the exception of SCAT 15, have structural weight fractions ranging from 0.25 to 0.29 - values which are not too different from those for the subsonic Boeing 707-320B or the Electra airplane with weight fractions of about 0.24. This small difference, however, amounts to about 50 percent of the payload weight for the SCAT airplanes.

Structural weight fractions for the aluminum airplanes also are in the same range - about 0.28 - probably by coincidence since both aluminum SCAT airplanes had less efficient strength-weight materials and less efficient propulsion systems. Actually, one version of the aluminum SCAT did not make the range requirement and the other did not make the sonic-boom overpressure requirement.

CONCLUDING REMARKS

Both contractors have used skin-stringer type of construction in their Structural concepts for the feasibility studies of the four SCAT configurations. Both selected 8Al-1Mo-1V duplex-annealed titanium alloy as the primary structural material for use in the Mach 3 configurations. Differences in design techniques for thermal stress may require closer specification by a contracting agency, but these differences do not have serious consequences on ultimate loads for the supersonic transport. Thermal stresses were shown to inflict a structural weight penalty of less than 2 percent on wing and fuselage panels. Structural weights were 25 to 29 percent of the take-off *gross* weight for all but SCAT 15 which had a structural weight that was 37 percent of the *gross* weight. This weight fraction of 0.37 was generally unacceptable. Structural weight fractions of aluminum SCAT airplanes were about 0.28 but the aluminum designs did not meet the range or sonic-boom requirements for SCAT. The titanium airframe appears to be

RELEASED

the most efficient way to carry the design payload supersonically over the design range within the sonic-boom overpressure restrictions.

REFERENCES

1. Anon.: Airplane Airworthiness; Transport Categories. Civil Air Regulations Part 4b, Rules Service Co. (Washington, D.C.), Jan. 7, 1963.

2. Anon.: Tentative Airworthiness Objectives and Standards for Supersonic Transport Design Proposals. Flight Standards Service, FAA, Aug. 15, 1963.

MATERIAL SELECTION
TENSILE STRENGTH

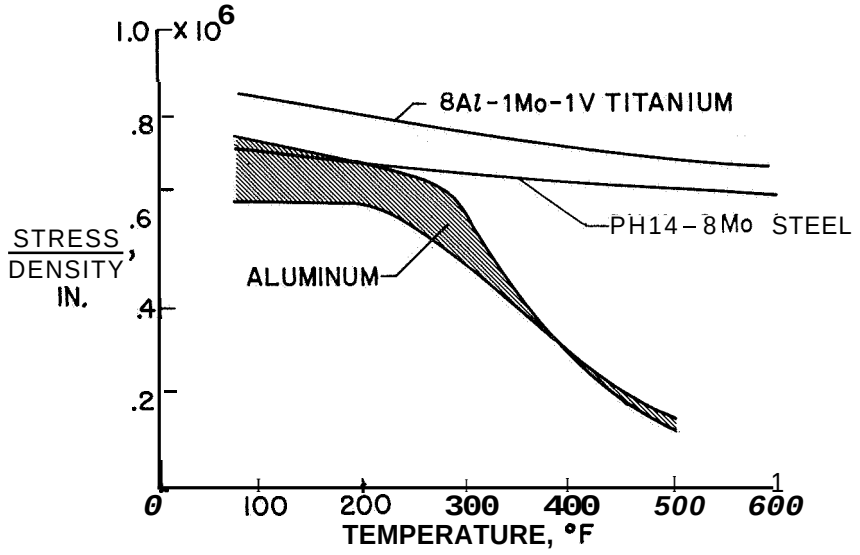

Figure 1

MATERIAL SELECTION
STIFFNESS

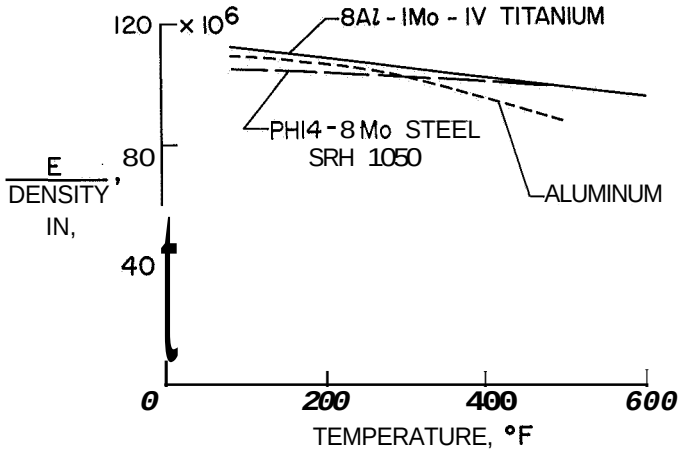

Figure 2

VARIATION OF TENSILE STRENGTH
Ti - 8At - 1Mo - 1V (ANNEALED)

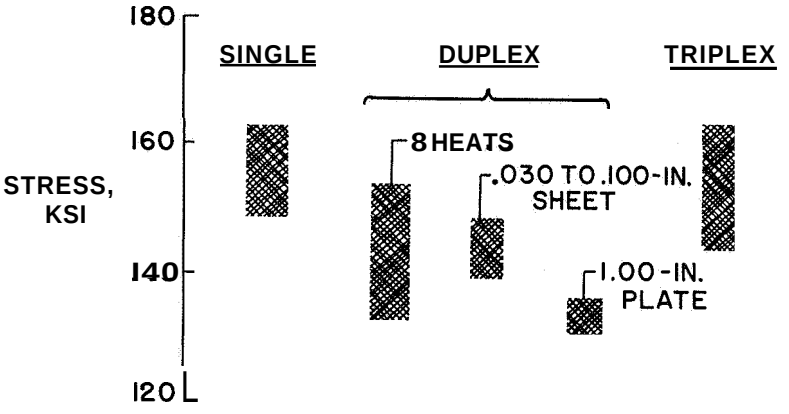

Figure 3

BASIC STRUCTURAL CONCEPTS

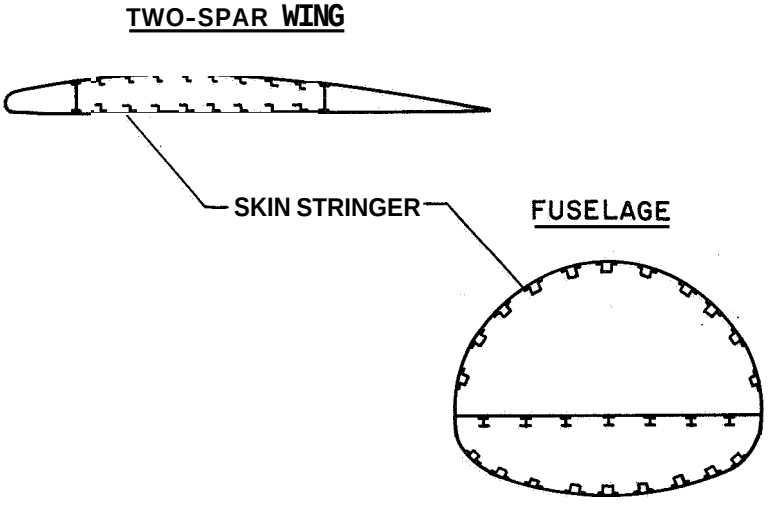

Figure 4

STRUCTURAL TEMPERATURE
WING LOWER SURFACE; INTEGRAL FUEL TANK

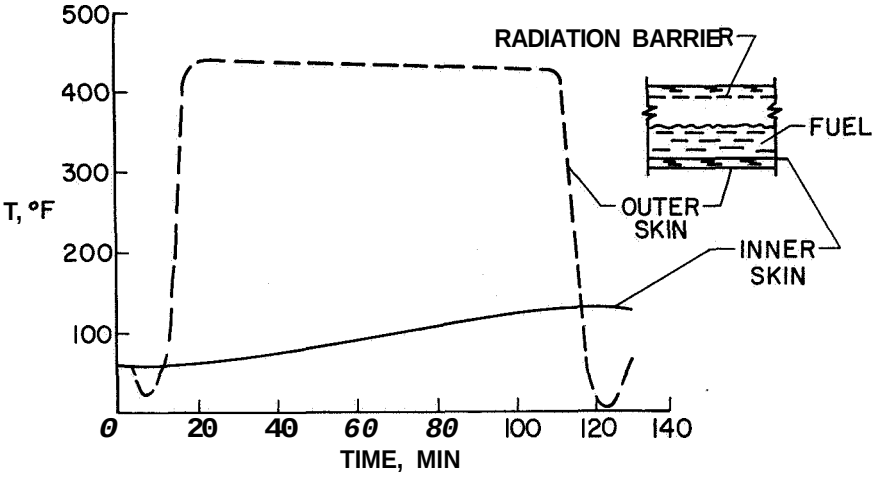

Figure 5

FLIGHT STRESS PROFILE
WING LOWER SURFACE

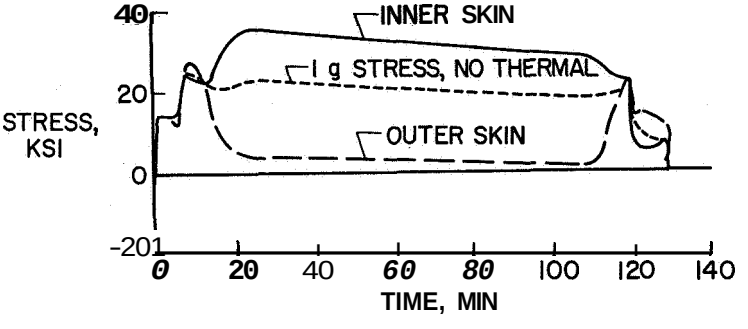

Figure 6

DECLASSIFIED

STRUCTURAL TEMPERATURE
FUSELAGE CABIN AREA

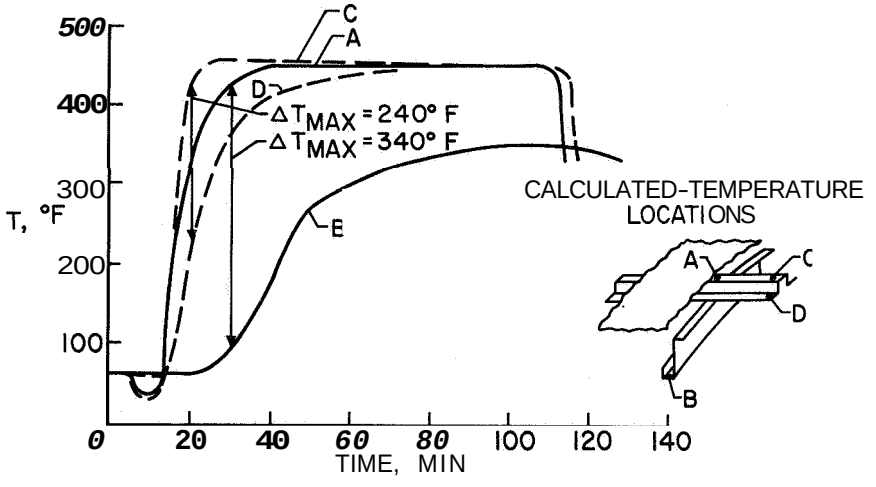

Figure 7

COMBINED THERMAL **AND** LOAD STRESS
TENSION MEMBER, METHOD I

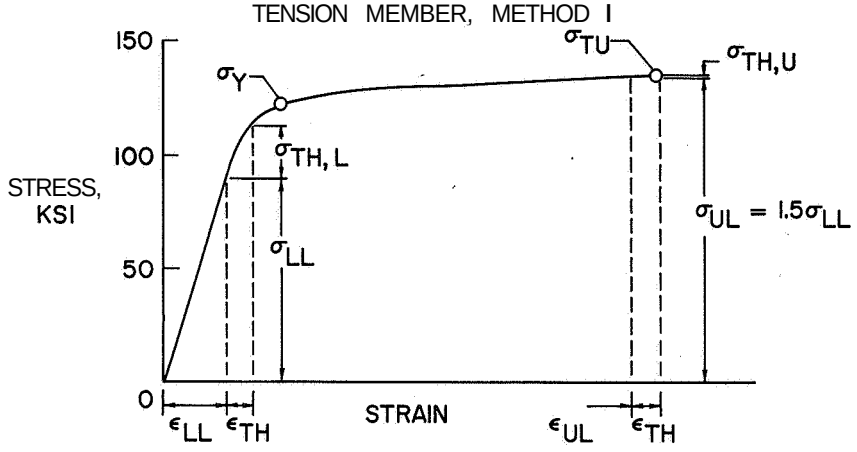

LIMIT: $\sigma_{LL} \leq 0.67\sigma_{UL}$

$\sigma_{TH,L} + \sigma_{LL} \leq \sigma_Y$ $\quad \sigma_{TH,L} = f(\epsilon_{TH}, \epsilon_{LL})$

ULTIMATE: $\sigma_{TH,U} + 1.5\sigma_{LL} = \sigma_{TU}$ $\quad \sigma_{TH,U} = f(\epsilon_{TH}, \epsilon_{UL})$

Figure 8

COMBINED THERMAL AND LOAD STRESS
TENSION MEMBER, METHOD *2*

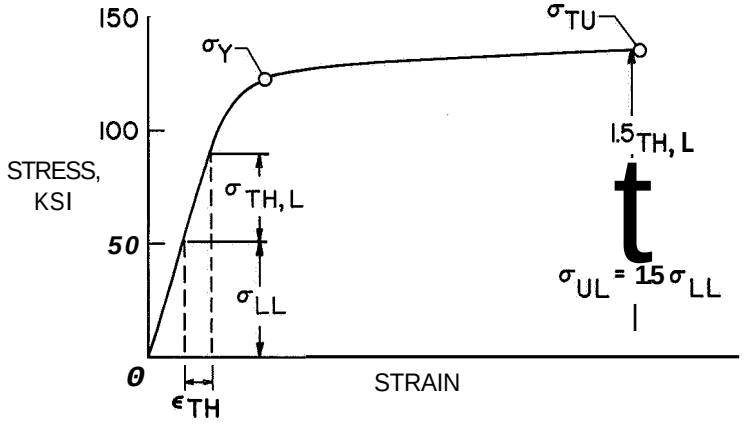

LIMIT: $\sigma_{TH,L} + \sigma_{LL} \leq 0.67\sigma_{TU}$

$\sigma_{TH,L} - \sigma_{LL} \leq \sigma_Y$

ULTIMATE: $1.5\sigma_{TH,L} + 1.5\sigma_{LL} = \sigma_{TU}$

Figure 9

DECLASSIFIED

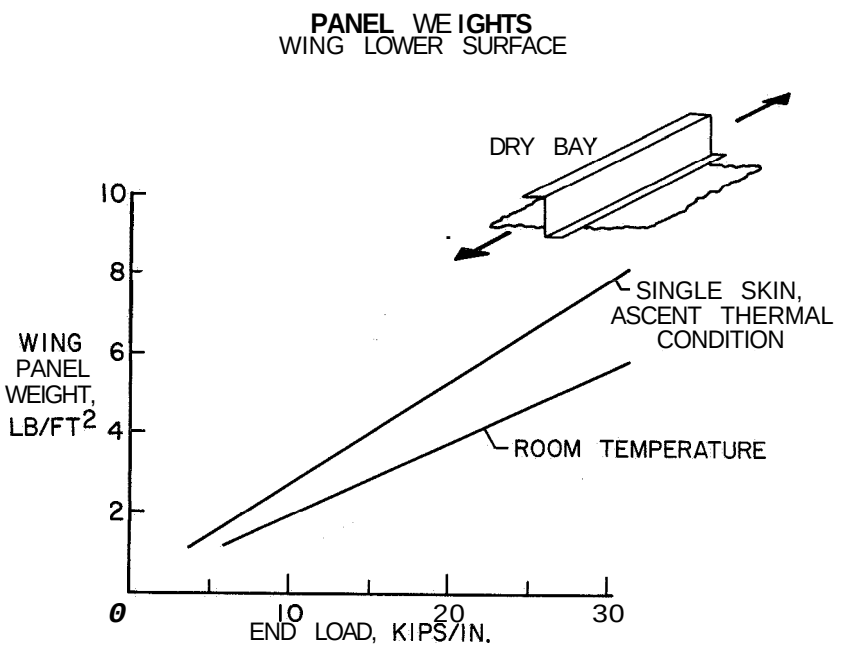

Figure 10

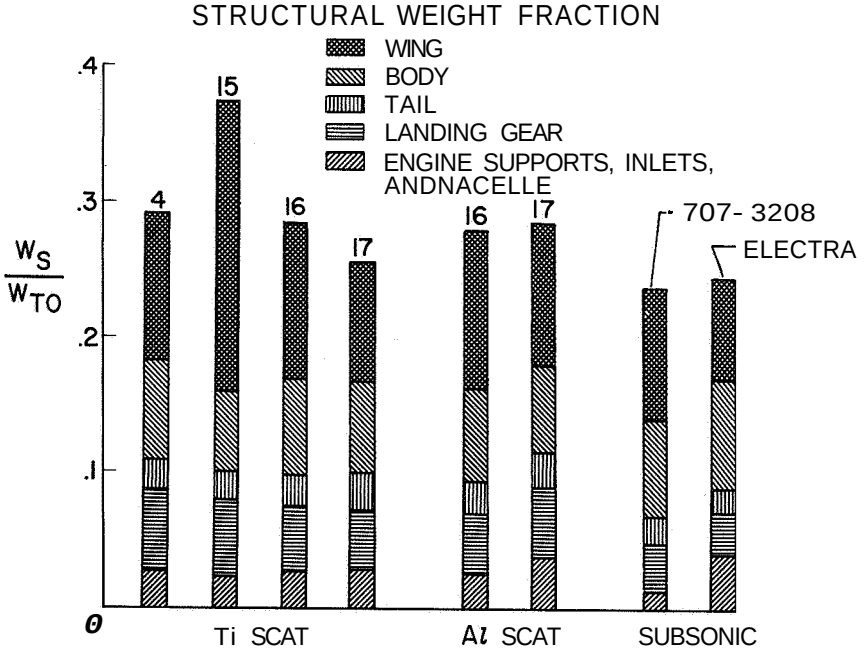

Figure 11

N67-31626

19. NASA RESEARCH ON MATERIALS APPLICABLE TO SUPERSONIC TRANSPORTS

By Herbert F. Hardrath and George J. Heimerl

NASA Langley Research Center

SUMMARY

The National Aeronautics and Space Administration has conducted tests to determine the mechanical properties of materials suitable for use in a supersonic transport over the temperature range of interest and after prolonged exposure to temperature. On the basis of studies on fatigue behavior, rate of fatigue crack propagation, residual static strength, and resistance to deterioration of properties due to prolonged exposure to temperature, no serious materials problems are anticipated However, stress corrosion is found to be a potentially serious problem in titanium alloys in a hot salt environment and in stainless steels in an ambient environment. The Ti-8Al-1Mo-1V alloy is found to be generally superior to other contending materials in all respects studied except for salt stress corrosion in which respect it was poorer than all others. Further research is recommended on stress corrosion; on the combined effects of fatigue, thermal exposure, and creep; and on the development of structural configurations and fabrication procedures suitable for the supersonic transport.

INTRODUCTION

The design of a successful supersonic-transport structure is in large part contingent upon the proper selection of material and in the use of proper allowable stress levels. Current airplanes may utilize established materials at stress levels that experience has proven will produce efficient and reliable structures. Such background information does not exist for materials of interest to the designers of a supersonic transport.

This paper presents some of the results of several studies into the behavior of various materials that were candidates for use in the structure of a supersonic transport at the time the studies began. The results of earlier studies for screening purposes are not included because these data and the conclusions drawn from them have been published in reference 1. Most of the work described herein was done at

PRECEDING PAGE BLANK NOT FILMED.

the Langley Research Center but some information from contracted studies and from the Lewis Research Center are also included.

The earlier screening studies treated a wide variety of sheet materials subjected to quick tests at temperatures higher than those that will be encountered in the vehicle to exaggerate the temperature effect. The present series deals with a few selected materials tested in more nearly realistic ways at realistic temperatures and includes the effects of long-time exposures. It is believed that these results will be helpful in making final selections of materials and in choosing the allowable stress levels to be used in design. This discussion is limited to materials suitable for use in the skin of a vehicle capable of traveling at a Mach number of 3.

SYMBOLS AND ABBREVIATIONS

K_T	stress concentration factor
N	number of cycles to failure
N_O	number of cycles to failure of unexposed specimens
R	ratio of minimum stress to maximum stress
S	stress
S_m	mean stress
S_{TU}	tensile ultimate strength
S_{1g}	stress for 1 g loading at take-off gross weight
A	aged
CR	cold rolled
CRT	cold rolled and tempered
DA	double aged
El	elongation in 2-inch gage length
GAG	ground-air-ground

DECLASSIFIED

HT heat treated

MA mill annealed

NS notch strength

TA triplex annealed

STATEMENT OF PROBLEMS

In order to focus attention on the specific questions to be discussed, it is of interest to review the operating environment for major portions of the structure. Figure 1 represents a time history of stress for typical flight at a given station on the wing of the airplane. Obviously, this time history will change significantly depending upon the specific airplane configuration, the station within the airplane, the particular flight, dynamic response characteristics, and so forth. However, the general features will usually be similar to those shown. The stress values are normalized with respect to the nominal stress present for level undisturbed flight at take-off gross weight and the time axis is not to scale.

The features of interest to the structural designer are as follows:

1. Most of the significant stress cycles occur during the climb portion of the flight while the airplane is at ambient temperature.

2. Few dynamic stress cycles are encountered during cruise because gust activity is reduced at high altitudes.

3. The exposure to elevated temperatures up to about 550° F may be as long as 90 minutes per flight.

4. The change in temperature can produce thermal stresses of significant magnitude depending on detail designs. These stresses are not shown in figure 1.

5. Dynamic loads encountered during descent are less severe because the airplane has lost substantial weight because of the burning of the fuel.

6. At stations outboard of the landing gear, a rather significant ground-air-ground cycle is introduced.

7. With the exception of the length of exposure to elevated temperatures, the fatigue damage accrued during a given flight is to a first approximation independent of flight length.

Some of the engineering questions that must be answered to provide a structure capable of surviving the loadings shown for useful lives of the order of 36,000 hours are as follows. First of all, the basic material properties must be established over the temperature range of interest. In the NASA studies the notch and tensile strengths, basic fatigue behavior, rates of fatigue crack propagation, and residual static strength of sheets containing cracks were obtained. Of the various studies made of creep properties, it appears that overall creep will not be a significant problem if the structure is built of any of the leading titanium alloys, stainless steels, or superalloys. Having established these properties over the temperature range of interest, one must know how some of these properties might be affected by the prolonged exposure to elevated temperatures. The Langley Research Center has studied notch and tensile strengths, fatigue behavior, the rather perplexing salt stress corrosion, and to some extent strain-rate sensitivity. The last of these properties was studied to only a limited extent with no significant effects found, so it is not discussed further. Some work has been started on methods of welding the materials of interest and on studying the effects of fabrication procedures on the strength of structural components.

RESULTS OF RESEARCH IN INDIVIDUAL PROBLEM AREAS

In the following sections, each of these problem areas is discussed in turn with sample data presented to indicate the conclusions reached in each investigation. Generally, no insurmountable problems have been discovered and the Ti-8Al-1Mo-1V alloy appears to be one of the best available on the basis of the results given here. Salt stress corrosion has been found to be one of the areas of concern and one on which additional study is recommended.

Materials

Most of the various investigations were carried out on each of the following sheet materials:

	Condition
Titanium alloys:	
Ti-4Al-3Mo-1V	Aged
Ti-6Al-4V	Annealed

RESTRICTED

	Condition
Ti-8Al-1Mo-1V	Mill annealed
Ti-8Al-1Mo-1V	Triplex annealed
Stainless steels:	
AM 350	Double aged
AM 350	Cold rolled (20%) and tempered
PH15-7Mo	TH 1050
PH14-8Mo	SRH 950
AISI 301	Cold rolled (50%)
AM 367	Cold rolled (20%) and tempered
Superalloy:	
René 41	B

Only a few tests have been conducted on the superalloy, René 41, which may be useful in the construction of leading edges and nacelle structures.

Notch and Tensile Strengths

Most information on these properties was obtained in connection with studies of the effects of long exposure to elevated temperatures. Since no startling results were obtained, these properties are discussed in a subsequent section.

Fatigue Behavior

Most of our study of fatigue behavior of materials of interest in the design of a supersonic transport was devoted to Ti-8Al-1Mo-1V and to AM 350 stainless steel. The titanium alloy was studied in the mill-annealed and in the triplex-annealed conditions and the AM 350, in the cold-rolled-and-tempered condition. A major part of this research was conducted under NASA contract at Battelle Memorial Institute and at Lance Vought Corporation.

A summary of some of the data on the titanium alloy is shown in figure 2. The bar graphs indicate the fatigue strength at a life of about a million cycles for each of several configurations tested at three temperatures (room (80° F), 550° F, and 800° F), as indicated by the shading. All tests were conducted on sheet specimens subjected to axial loads producing a mean stress of 25 ksi.

The fatigue strength of unnotched specimens was not adversely affected by the elevated temperatures; in fact, a slight increase in strength was noted. The mill-annealed material behaved as well as the triplex-annealed material in unnotched specimens. Fusion welding of the mill-annealed material produced only a moderate reduction in strength. A specimen having an unloaded square of material spot-welded to one face had a fatigue strength about the same as that for a specimen with an open hole with a stress concentration factor of 2.5. A spot-welded double butt-strap joint had fatigue properties not too different from those of edge-notched specimens with a theoretical stress concentration factor of 4. This latter configuration is identical to the configuration Langley has come to regard as representative of the overall quality of construction achieved in current aluminum-alloy structures. The effect of temperature is minor in all cases where it was studied as a parameter.

The same general comments apply to similar results of tests on AM 350 stainless steel which are presented in figure 3. The mean stress for this material was 40 ksi.

These limited results do not, of course, provide all the information needed to design a structure from a fatigue point of view. However, they do indicate that notch sensitivities are reasonable and that welds and spot-welds produce strength reductions not too different from those of stress raisers representative for current structures. Obviously, considerable testing will be required to prove the adequacy of specific design details.

Information is still needed on the possible interaction of creep and fatigue, especially around fasteners and other points of stress concentration. A current series of tests are being conducted at the Lockheed Aircraft Corporation under an FAA-NASA-DOD sponsored contract and other tests are being conducted at Langley.

Fatigue Crack Propagation

The rate of fatigue crack propagation is a most significant consideration in assessing the fail-safe characteristics of a structure. Figure 4 presents a sample of data obtained in axial-load fatigue tests of 8-inch-wide-sheet specimens tested at $R = 0$ (zero to tension loading). The rate of crack propagation is a reasonably straight-line function of crack length when both are plotted on a log scale. The results presented are for room-temperature tests with a mean stress of 25 ksi for titanium alloys and 40 ksi for steels. The most desirable material would be the one having the lowest rate of crack propagation. Of the titanium alloys, the Ti-8Al-1Mo-1V alloy in the triplex-annealed condition is superior. Two stainless steels, AM 350 CRT and AISI 301,

appear superior to the Ti-8Al-1Mo-1V alloy, but the rate of propagation in both materials increases by a large factor at elevated temperatures.

For reference, the rates of propagation for two aluminum alloys, 2024-T3 and 7075-T6, are also plotted in figure 4. The data shown are for a mean stress of 15 ksi. At these stress levels, the aluminum-alloy curves are somewhat steeper, indicating a faster increase in rate of crack propagation as a function of crack length. The 7075-T6 material also experiences crack growth rates higher than those for the other materials shown.

The effect of temperature was studied at -110° F and at 550° F, with only moderate effects on the results, except that AISI 301 and AM 350 CRT experienced a marked increase in rate of crack propagation at 550° F. This preliminary study indicates that rates of fatigue crack propagation at the stress levels considered are not too different from the behavior of current aluminum alloys at a corresponding stress level. The effects of temperature are moderate except for AISI 301 and AM 350 CRT. The Ti-8Al-1Mo-1V alloy stressed at 25 ksi appears to be the best choice from among the materials tested.

Residual Static Strength

Another important consideration with regard to fail-safe characteristics is the residual static strength of a part containing a fatigue crack or other damage. Langley conducted static tests on the same set of specimens used to study rates of fatigue crack propagation. A sample of the results is shown in figure 5. The solid bar graphs show the residual strength of specimens containing 1-inch cracks as compared with the original static tensile strength of the material. The strengths are divided by density to compare structural efficiencies. The data were obtained for nine materials at each of three temperatures.

In general, the strength of these materials exhibited moderate sensitivity to cracks. Exceptions are AM 350 (DA) and PH15-7Mo, both of which had low strength and failed by shattering at the lowest temperature and AISI 301 which deteriorated seriously at elevated temperature. The titanium alloys are generally superior on a strength-density basis, Ti-8Al-1Mo-1V in the triplex-annealed condition being the overall leader. The triplex-anneal process improved the residual static strength of this latter alloy at room and subzero temperature. In several materials tested at elevated temperature, cracks produced little or no reduction in residual static strength beyond that of reducing the cross-sectional area. The superalloy René 41 does not compare favorably here. It is, of course, affected very little by temperature.

The data presented in figure 5 are for 1-inch cracks only, but the general ranking of materials would be quite similar if strengths for other crack lengths had been compared. In most cases the reduction in static strength caused by cracks is moderate and, in general, is considerably less than that for current. aluminum alloys. Several materials experience no loss of static strength except that produced by loss of area. Again, triplex-annealed Ti-8Al-1Mo-1V is the best overall choice of the materials evaluated.

Notch and Tensile Strength After Exposure to Temperature

The Langley Research Center is conducting a study of the effects of prolonged exposure to elevated temperatures on static tensile and notch strength properties. Specimens are exposed without stress at 550° F for various periods of time and then tested at room temperature and at -110° F. The notched specimens were 1 inch wide and contained 60° V notches with root radii <0.001 inch (ASTM ty-pe). Table I presents a summary of the results obtained to date. Exposure times up to 14,000 hours have shown no significant effect on static tensile or on notch strengths. In a few cases, elongations at failure have shown rather large percentage changes, but most of the materials in question have rather low elongations (4 to 8 percent) initially, so the absolute changes are not much greater than the accuracy of measurement.

Some of the studies at the Lewis Research Center indicated stability problems with the two precipitation hardening stainless Steels, PH13-8Mo and PH14-8Mo, and with AM 367. Special heat treatments of AM 367 have improved the stability characteristics but at the expense of a serious decrease in corrosion resistance.

Unstressed exposure to elevated temperatures for as long as 14,000 hours produced no significant effect on static strength properties at' 80° F and -110° F. Consequently, the materials studied at Langley appear to be reasonably stable for the exposures obtained at the present time.

Fatigue Behavior After Exposure to Temperature

In another study, fatigue test specimens are being exposed to 550° F for prolonged times without stress. Figure 6 presents the results of tests on Ti-8Al-1Mo-1V in the mill-annealed condition. Four configurations of specimens were tested: unnotched, edge-notched ($K_T = 4$), fusion welded, and a double butt-strap spot-welded joint. Complete S-N curves were derived from axial-load tests of unexposed specimens, but exposed specimens were tested at a single stress level

chosen to produce failure in approximately 10^5 cycles. The mean stress in all cases was 25 ksi and all tests were at room temperature. The data presented are normalized with respect to the life of unexposed specimens and are plotted against exposure time in hours. Each point is the geometric mean of five test results.

These data for Ti-8Al-1Mo-1V display almost the extreme variations noted in this series of tests which included seven other materials. A factor of about two or less on life is noted at each data point except the one for unnotched specimens exposed for 9,000 hours which had a life 10 times as long as the original. There is some doubt that the highest point is valid because two of the tests produced lives much more nearly equal to the original life; thus, this point may be associated with the small statistical sample used.

The tests will continue until exposure times reach about 30,000 hours. Unfortunately, this test series cannot be accelerated; therefore, the final data are not available at the present time.

The data available at this date show no cause for alarm over deterioration of fatigue properties with exposure. This general conclusion is supported by supplementary information obtained at Battelle where notched specimens of AM 350 were tested in fatigue after exposure to 550° F under 40 ksi stress for 3,000 hours with no significant effect of this exposure on fatigue behavior.

Salt Stress Corrosion

The final investigation that is to be discussed in detail is a study of salt stress corrosion at elevated temperature, a recognized problem area for titanium alloys. Figure 7 presents a summary of results of salt-stress-corrosion studies conducted at Langley. The specimens tested are indicated by the small sketch. Strips of sheet about 1/4 inch wide and 4 inches long were bent through a specified angle near each end so that when two such strips were spot-welded at the ends the center portions were subjected to a constant bending moment. The bending stresses involved were either 50 ksi or 100 ksi. The specimens were dipped in concentrated salt solutions to form a substantial crust over the entire specimen. The coated specimens were stored in ovens at 550° F for various times. Upon removal from the oven, the specimens were cleaned and subjected to axial compression loads as indicated in the sketch. The reduction or shortening in the overall length of the specimen prior to failure of one of the legs was noted. This value is normalized relative to the value obtained in unexposed specimens and plotted against the exposure time in hours. If severe stress-corrosion cracking occurs, the shortening at fracture is reduced and the relative shortening may approach zero. Metallographic examinations have shown that the depth

and number of stress-corrosion cracks in the specimens correlates well with the relative shortening parameter plotted in figure 7.

The alloy Ti-4Al-3Mo-1V is virtually unaffected by salt stress corrosion but Ti-8Al-1Mo-1V (MA) is affected very severely in only 2,000 hours of exposure and Ti-6Al-4V, in 4,000 hours. No specimens have failed in the furnace in as many as 7,000 hours.

The same tests have been conducted on the stainless steels with no effect noted when the compression test was conducted immediately upon removal from the oven. However, several specimens of AM 350 (DA) have failed in about 2 months after removal from the oven. Also one specimen of AM 350 (DA) failed after several months exposure to the Langley outdoor atmosphere without salt and without artificial heat.

It is difficult to assess the importance of the salt-stress-corrosion problem. Certainly the test condition is too severe but not so severe as to suggest that no problem exists. If moisture, and thus soluble contaminants, can reach the inside of the structure or lodge in crevices on the outside, salts will tend to collect over a period of time in service. Tests elsewhere in fast-moving air have indicated that the attack is less severe under these circumstances. However, the insides of structures will not have such ventilation. It was disappointing to find Ti-8Al-1Mo-1V most susceptible to this attack when this material appears to be one of the most suitable of the materials based on other considerations. The problem deserves more study with emphasis on a more realistic representation of conditions to be encountered in service. Some information on the combined effects of corrosion and fatigue is desirable. Langley is planning tests to provide some data and other data will be supplied under FAA-NASA-DOD sponsored contracts.

The problem of stress corrosion may be quite serious for steels in view of the fact that failures occurred without salt or heat.

The final solution to the stress-corrosion problem may require some form of corrosion inhibitor and probably very careful inspection.

CONCLUSIONS AND RECOMMENDATIONS FOR FUTURE RESEARCH

Recent investigations at Langley on the properties of titanium and stainless-steel sheet materials suitable for a supersonic transport indicate that:

1. The fatigue problem appears not to be a formidable barrier at the stress levels considered.

[redacted]

2. Fail-safe considerations involving rates of fatigue crack propagation and residual static strength appear more promising for the better titanium and stainless-steel materials tested than is true for current aluminum alloys.

3. Prolonged exposure to 550° F has not been found to degrade static and fatigue properties significantly at least in the first 10,000 to 14,000 hours.

4. Stress corrosion may be a problem with titanium alloys in *dry* salt at elevated temperatures and in some of the stainless steels at normal temperatures.

5. Of the contending materials, Ti-8Al-1Mo-1V alloy appears superior from all viewpoints considered except stress corrosion in salt.

6. Further study is recommended to evaluate the combined effects of dynamic loadings, thermal exposure, and creep.

7. Further study is also needed to assess the severity of the hot salt-stress-corrosion problem for supersonic-transport applications.

8. Studies are needed to develop practical, efficient, and reliable structures for supersonic transports built of titanium alloy.

REFERENCE

1. Raring, Richard H., Freeman, J. W., Schultz, J. W., and Voorhees, H. R.: Progress Report of the NASA Special Committee on Materials Research for Supersonic Transports. NASA TN D-1798, 1963.

[redacted]

TABU I

EFFECT OF EXPOSURE AT 550° F

Material	Condition	Exposure time, hr	Test temperature, °F	Percent change		
				S_{TU}	NS	El
Titanium alloys						
Ti-6Al-4V	A	14×10^3	-110	0	0	0
			80	0	0	15
Ti-8Al-1Mo-1V	A	10	-110	0	0	---
			80	0	0	-10
Ti-4Al-3Mo-1V	HT	7	-110	--	0	10
			80	0	0	25
Stainless steels						
PH15-7Mo	HT	7×10^3	-110	--	-5	---
			80	0	5	25
AM 350	CRT	7	-110	0	0	10
			80	0	0	5
AISI 301	CR	4	-110	10	5	0
			80	10	5	-5

DECLASSIFIED

SCHEDULE OF LOADS AND TEMPERATURES FOR SUPERSONIC TRANSPORT FLIGHT

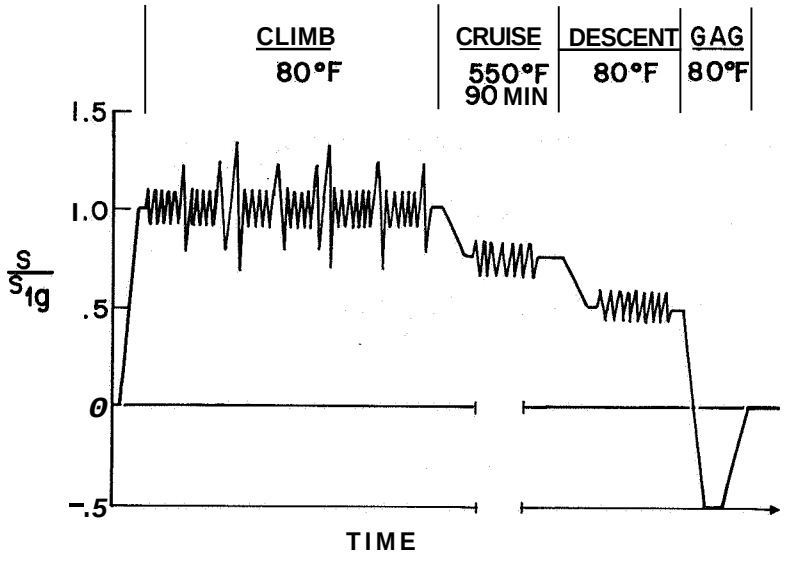

Figure 1

FATIGUE STRENGTH AT N=10^6 CYCLES

Ti-8Al-1Mo-1V; S_m = 25 KSI

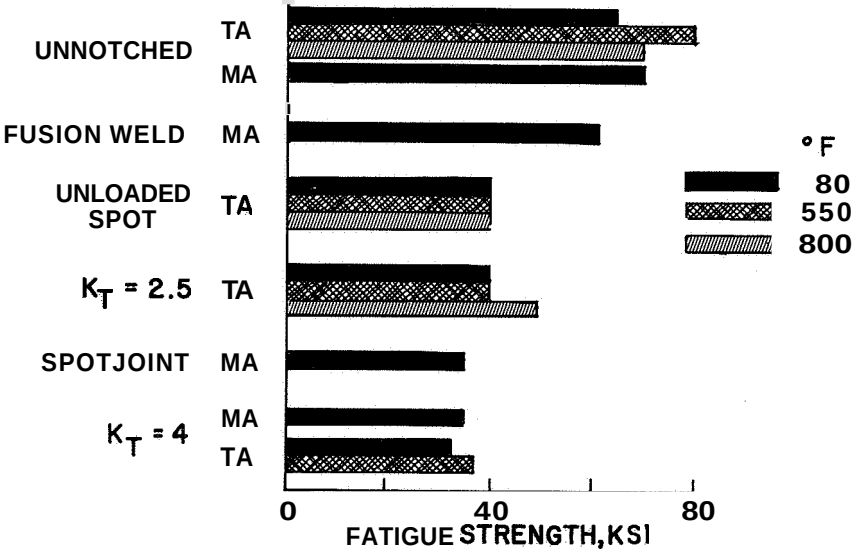

Figure 2

[redacted]

FATIGUE STRENGTH AT $N=10^6$ CYCLES
AM 350 CRT; S_m = 40 KSI

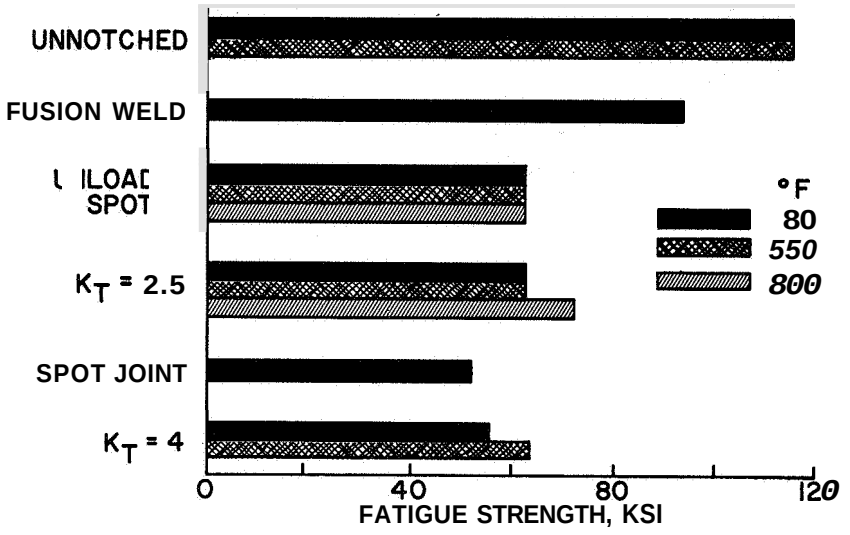

Figure 3

FATIGUE CRACK PROPAGATION IN CENTRALLY NOTCHED TITANIUM, STEEL, AND ALUMINUM SHEET SPECIMENS
8-INCH WIDTH; R=0; 80° F

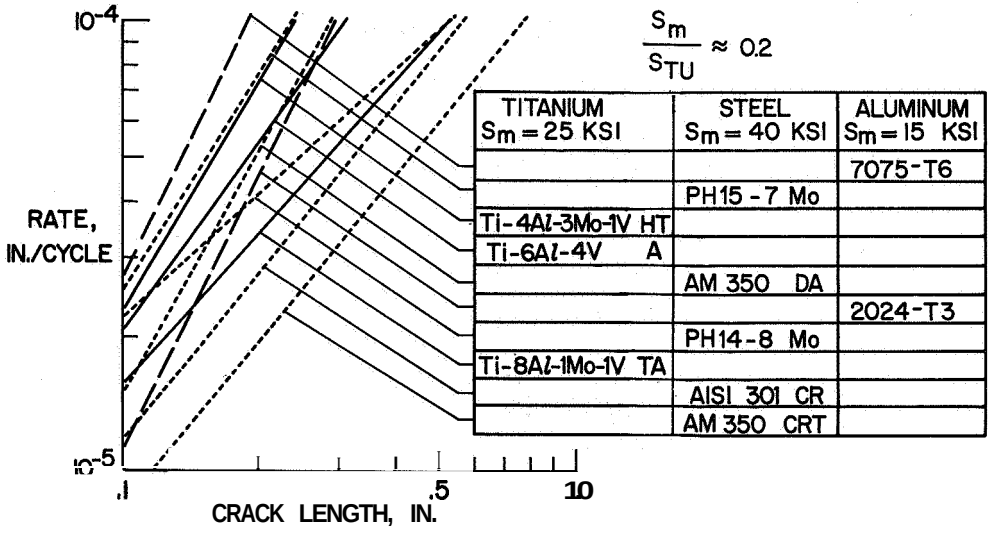

TITANIUM S_m = 25 KSI	STEEL S_m = 40 KSI	ALUMINUM S_m = 15 KSI
		7075-T6
	PH15-7 Mo	
Ti-4Al-3Mo-1V HT		
Ti-6Al-4V A		
	AM 350 DA	
		2024-T3
	PH14-8 Mo	
Ti-8Al-1Mo-1V TA		
	AISI 301 CR	
	AM 350 CRT	

Figure 4

[redacted]

[redacted]

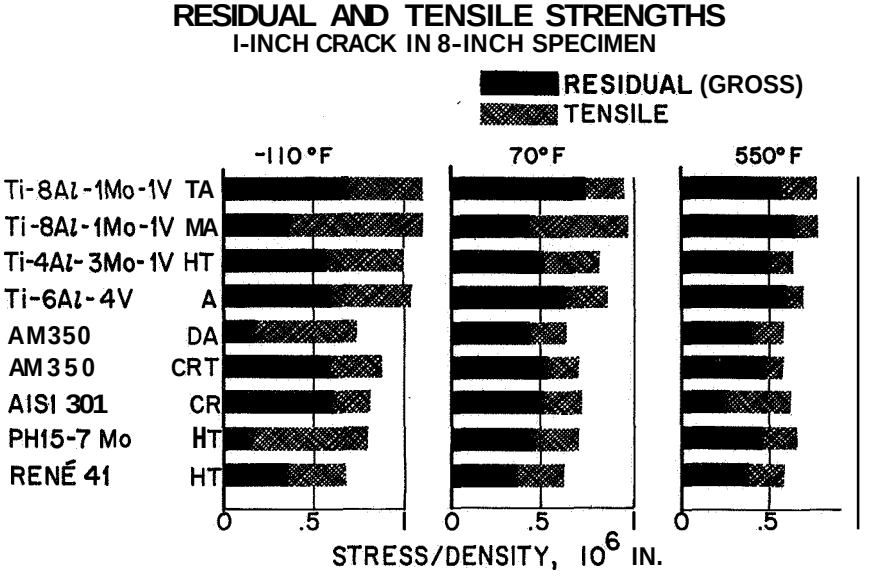

Figure 5

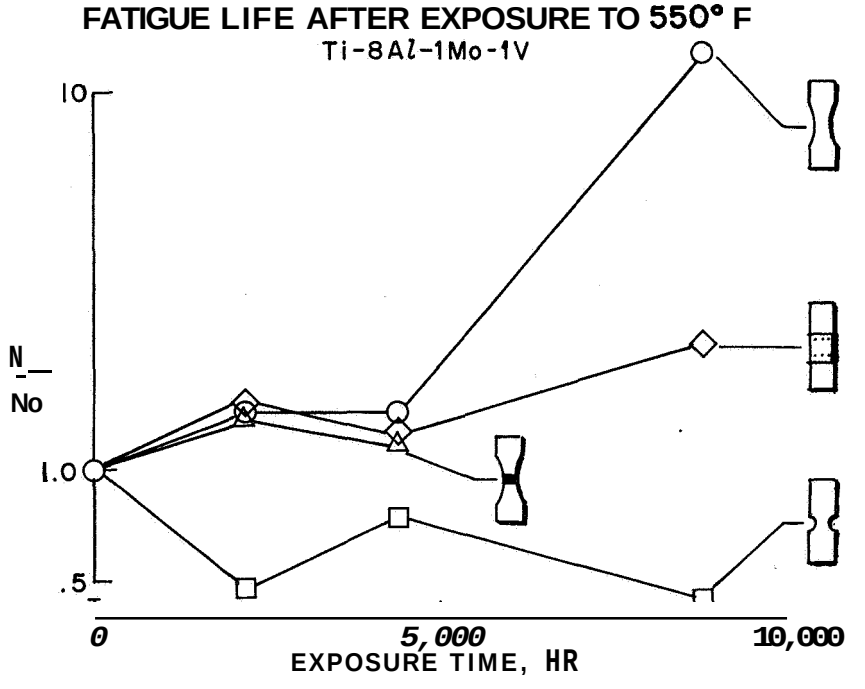

Figure 6

SALT STRESS CORROSION AT 550" F

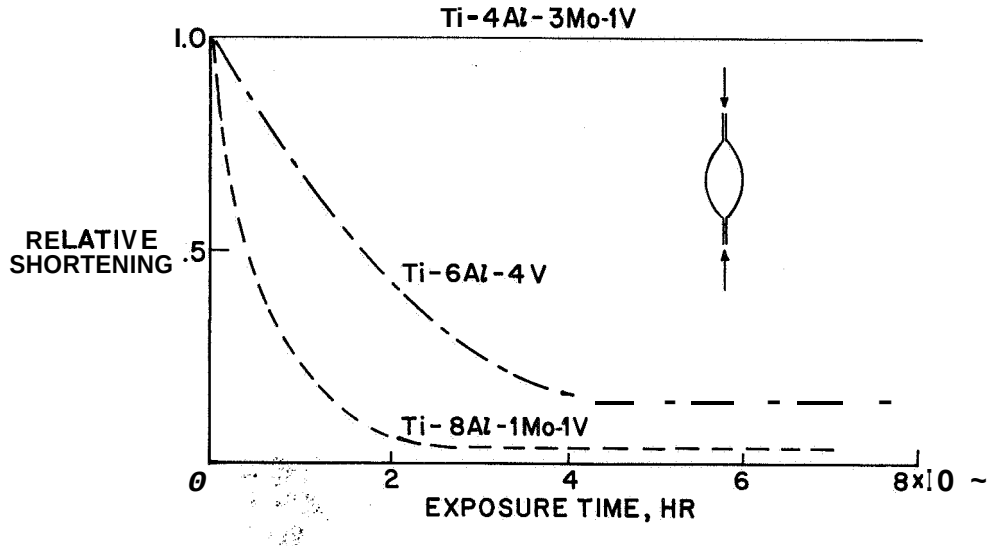

Figure 7

N67-31627

20. AEROELASTIC CONSIDERATIONS

By Robert W. Boswinkle, Jr., and E. Carson Yates, Jr.

NASA Langley Research Center

SUMMARY

Problem areas which involve combinations of aerodynamic, elastic, and inertial forces are considered in relation to the design of the supersonic transport. Some problems of ground loads, buffet, flutter, panel flutter, gust loads, and a consideration of aeroelastic effects on stability and control are discussed. Aeroelastic-dynamic considerations will be very important in the design and flight-test phases of the supersonic transport; however, in general, the techniques for handling the problems which will arise appear to be reasonably adequate.

INTRODUCTION

Many problem areas in the design of the supersonic transport will involve combinations of aerodynamic, elastic, and inertial forces. A few of these problem areas, which are illustrated in figure 1, are discussed herein. The parameters are altitude and Mach number. The flight region would be above the design dive flight condition boundary. Flutter of lifting surfaces, gust response, panel flutter, and buffet will probably be critical near transonic speeds. The effects of aeroelasticity on stability and control will probably be greatest at the high supersonic Mach numbers where the dynamic pressure is greatest; although, problems may be encountered elsewhere.

A goal of the design is to have the instabilities, the excessive loads, and other undesirable conditions represented by the problem areas fall a sufficient distance below or above the flight region. The area of ground loads is shown at the low-speed end of the Mach number scale.

Two major factors which complicate the solutions to most of these aeroelastic problems are:

(1) The low stiffnesses which result from thin lifting surfaces and a slender fuselage

(2) The wide range of operating conditions involving variations in Mach number, altitude, aerodynamic heating, weight, and possibly aircraft configuration.

CONFIDENTIAL

SYMBOLS

a	length of skin panel in stream direction
b	width of skin panel perpendicular to stream direction
E	Young's modulus
M	Mach number
q	dynamic pressure
t	thickness of skin panel
$\beta = \sqrt{M^2 - 1}$	
ALE	leading-edge sweep angle
σ_{cr}	wind-off buckling stress
σ_x	compressive midplane stress in direction of flow

AEROELASTIC PROBLEM AREAS

Following brief comment on two of the areas shown in figure 1, ground loads and buffet, the other areas are discussed in more detail.

Ground Loads

In regard to ground loads, the problems associated with taxiing, take-off, and landing for the supersonic transport are not expected to be greatly different from those of the current, large, high-performance aircraft. However, current design practices may be affected by the anticipated long fuselages, new gear configurations, and high nose-up landing attitudes (ref. 1). In addition, as in current aircraft, an important aspect of the airframe design will be the loads generated by runway and taxiway roughness, These may even be the critical loads for some designs (paper no. 3 by R. Richard Heppe and Jim Hong). In general, the analytical techniques for handling ground loads are believed to be reasonably adequate.

CONFIDENTIAL

Buffet

Buffet may be defined as structural response to randomly fluctuating aerodynamic forces caused by separation of the flow (ref. 2). Since flow separation must be minimized to maintain low drag, buffet would not be expected to present major difficulties over much of the flight region. However, one part of the flight region where buffet may be troublesome is at transonic speeds. Flow separation becomes a greater problem at transonic speeds because of shock boundary-layer interactions and possibly because relatively high angles of attack may be required as a result of high-altitude flight at transonic speeds to reduce sonic-boom overpressures. Few buffet problems are amenable to analytic study; however, buffet indications often have been obtained as a byproduct of wind-tunnel force-test studies on models. In addition, some buffet studies have been made by using elastically scaled models.

Flutter

Flutter is a self-induced oscillation of a structure which can lead to catastrophic failures. A flutter boundary for a variable-sweep wing is shown in terms of altitude and Mach number in figure 2. The boundaries, shown by the three solid curves for sweep angles of 20°, 45°, and 65°, were based on the scaled model flutter studies of reference 3. (See also ref. 4.) The dashed extension for the 65° sweep curve is extrapolated to indicate the typical trend. An example design-dive-speed boundary for the supersonic transport is also shown. This figure may be used to make several points:

(1) In order to insure freedom from flutter, the civil air regulations require that the flutter boundary be at an equivalent speed at least 20 percent higher than the design dive speed (ref. 5).

(2) Sweepback as indicated in figure 2 increases the flutter margin, and early sweepback might be used for variable-sweep wings to provide the required flutter margin at transonic Mach numbers.

(3) For most supersonic aircraft, the minimum flutter margin occurs at transonic speeds with increasing flutter margins occurring in the low supersonic range. However, the characteristic rise in the flutter boundary at the higher Mach numbers may cause some designs to become critical again at Mach numbers as high as 3.

(4) Over this wide operating range, different components of the aircraft may become flutter-critical at different Mach numbers, and the

flutter boundary for the complete aircraft must be considered rather than that of only the wing component as illustrated here.

The following general procedure for treating flutter has been evolved over the years and appears applicable to the supersonic transport:

(1) Inputs, based on experience and existing data, during initial design to avoid conditions which appear unfavorable from the standpoint of flutter

(2) Use of analyses and model experiments to study flutter of components, with the initial simplified approaches being superseded by more complex methods as the design progresses

(3) Use of analyses and model experiments for the complete airplane

(4) Verification of full-size aircraft structural properties as components become available followed by ground vibration tests of the complete aircraft

(5) Flight flutter tests

The flutter analyses, referred to in items 2 and 3, may be discussed with the aid of figure 3. Many analytical methods are available for representing the various forces involved in flutter. Usually the most difficult of these forces to represent is the aerodynamic force. Some of the methods used at different Mach numbers for representing the aerodynamic force are illustrated; however, the actual range of applicability depends on the configuration. Shown as applicable are the kernel-function method (refs. 6 and 7) at subsonic speeds, various aerodynamic-influence-coefficient methods (refs. 8 to 10) at supersonic speeds, and the relatively simple but nonlinear piston theory (refs. 11 to 13) at the higher supersonic speeds.

It should be noted that none of these theories may be applicable over a relatively wide band at transonic speeds which is often the critical region. This difficulty has led to the development of approximate methods. Many of the approximate methods have as their basis the steady-state flow, which may be obtained either from theory or experiment. One such scheme is the so-called modified-strip method (refs. 14 to 17). For a 45° swept wing at subsonic speeds, the modified-strip-analysis results, shown with a solid line, yielded excellent agreement with the theoretical kernel-function results shown by the dashed line. Results of the modified-strip analysis are in good agreement with experimental data throughout the transonic speed range.

CLASSIFIED

Approximate aerodynamic theories are often used throughout the Mach number range in the place of more rigorous theory to save computing time and to provide a more flexible analysis; however, the use of approximate theory requires discretion and caution.

Figure 4 illustrates a system for mounting complete flutter models in wind tunnels. (This system has application to item 3 in the preceding listing.) One of the problems in experimental transonic studies of complete models has been deficiencies in the various mounting systems proposed. The system illustrated, which was developed recently at the NASA Langley Research Center (ref. 18), appears to avoid most of the deficiencies. It consists of a cable in the vertical plane and one in the horizontal plane; both cables are attached to the tunnel walls and are passed around pulleys in the model. The mount permits the model to be tested with minimum restraint on its free-flight motions. Three different aircraft configurations have been investigated at transonic speeds with this mount system.

It may be remarked that flutter studies of complete models at supersonic speeds have not often been necessary because of the large flutter margins which usually exist in the low supersonic range; however, if, as previously discussed, a second critical flutter region exists at the maximum Mach number, a supersonic study of a complete model may be required.

A few comments that may be made in regard to the flutter characteristics of specific configurations are as follows:

(1) The solution of delta-wing flutter problems requires careful adjustments of local mass and stiffness in order to avoid unnecessary weight. Few other generalities for delta wings can be made.

(2) For a variable-sweep wing, the pivot does not present any particular difficulty in making a flutter analysis, and on the basis of several design studies, it appears that a pivot designed to have enough strength to accommodate the loads may be considered almost rigid from the standpoint of flutter.

(3) For wings with engines attached, the flutter speed may vary considerably with engine location (refs. 19 and 20); since engine location affects other structural quantities such as sonic fatigue, it may be necessary to involve the flutter characteristics in trade-off studies.

Panel Flutter

Panel flutter is a self-excited oscillation of external skin panels in which the deformation of the skin surfaces generates aerodynamic forces which sustain the oscillations. Thus, the response of a panel to acoustic or mechanical forces is excluded from consideration in this discussion of panel flutter.

The following is a list of some factors which affect panel flutter:

Flow	Panel	
Dynamic pressure	Aspect ratio	Edge restraint
Mach number	Thickness	Elastic modulus
Boundary layer	Curvature	Cavity size
Orientation	Construction	Cavity pressure
	Midplane stress	

Since the number of factors is large, panel flutter is a difficult problem to handle. The phenomenon may manifest itself as either fatigue or as sudden disintegration of the skin. It usually occurs only at supersonic speeds on panels with low design loads which have minimum skin gage and large spacings between stiffeners.

In the last decade, panel flutter has caused many problems which required considerable time and expense to correct. Examples of airplanes involved are the A3J, X-15, and the F-101. The difficulties with these airplanes generated considerable experimental research, which generally correlated poorly with theory. The experiments also gave rise to panel-flutter criteria which were not reliable. Theoretical- and experimental-prediction methods are still somewhat deficient and larger design margins of safety are recommended than for lifting-surface flutter; however, the situation appears to be improving. The improvements are coming about through a better understanding of the importance of adequate representation in analyses of such items as the edge conditions and through an awareness of the extreme care with which any experiments must be conducted.

An example of recent research (ref. 21; see also, refs. 22 and 23) is shown in figure 5 where the frequently used panel-flutter parameter is plotted against a parameter which is proportional to the compressive midplane stress in the flow direction. One of the major effects of temperature on panel flutter occurs through the production of midplane stress. The effect of increasing compressive midplane stress is to reduce the dynamic pressure at which flutter occurs for unbuckled panels. For higher values of midplane stress, the panel is buckled and the dynamic pressure for flutter increases with increases in midplane

stress. The minimum value of dynamic pressure is a critical value for panel design and is the subject of current analytical and experimental studies.

The recommended design procedure for avoiding panel flutter is as follows:

(1) Identify, on the basis of experience, which panels are least safe.

(2) Estimate, from available experimental and theoretical data, the flutter margins of the identified panels.

(3) For panels indicated to be critical, either make specific experimental and theoretical studies to verify the indications or change the design.

(4) Verify freedom from flutter during flight tests.

Gust Loads

The gust response of an aircraft may be computed by combining two quantities: The turbulence input from the atmosphere and the transfer function of the aircraft. Figure 6 shows a sample power spectrum of atmospheric turbulence in a thunderstorm at 40,000 feet (ref. 24). Curves for other atmospheric conditions tend to be parallel to this one. This curve shows relative power as a function of the wave length of the turbulence with the wave length increasing to the left. The solid line represents measurements made recently to a wave length of 14,000 feet. The shape of the dashed line is theoretical.

Shown above the abcissa are the wave lengths which correspond to the short-period stability mode for present subsonic jet transports and for the supersonic transport. Figure 6 may be used to illustrate the following comments:

(1) The wave lengths of atmospheric turbulence which are most important to the response tend to be longer for the supersonic transport than for the present subsonic jets.

(2) The available atmospheric measurements, of which this is a sample, indicate that the relative power of the turbulence input is higher for the longer wave lengths so that the airplane response would be expected to be greater for the supersonic transport than for the present subsonic jets for flight in the same atmospheric conditions. Whether or not the supersonic transport will actually experience a more

severe response history will depend also on such factors as the frequency of encountering turbulence in the flight regime of interest and the success of avoiding turbulent regions.

(3) Various deficiencies exist in the description of the atmospheric turbulence; the most important are power-spectral descriptions for the longer wave lengths (to confirm the degree to which the curve bends over), power-spectral descriptions for clear-air turbulence at altitudes above 5,000 feet, and measurements of the frequency of encounter for various vertical velocities at the higher altitudes.

As previously noted, the supersonic transport will probably have the greatest gust problem at transonic speeds; however, there has not yet been adequate experimental confirmation that the transfer function at transonic speeds for proposed supersonic-transport configurations can be calculated satisfactorily. The problem is being studied at Langley.

Figure 7 illustrates the importance of including structural flexibility in the gust analyses (ref. 25). The configuration is a large, flexible, swept-wing airplane. The vertical acceleration of the airplane center of gravity is shown on the left, and wing bending strain is shown on the right as functions of the frequency of the sinusoidal gust input. The data points shown by the circles were obtained from flight tests. The solid lines are theoretical predictions for the flexible airplane. The dashed lines are predictions which assume that the airplane is rigid. The conclusions drawn from figure 7 are:

(1) Although the inclusion of airplane flexibility did not greatly affect the maximum acceleration at the center of gravity, large effects of flexibility were shown for the wing bending strain.

(2) The theoretical methods yielded adequate results.

Aeroelastic Effects on Stability and Control

A wide spectrum of problems are classified as aeroelastic effects on stability and control (see refs. 26 to 28). Aeroelasticity affects:

(1) The static-stability quantities such as lift-curve slope, center of pressure, and aerodynamic center; some of these factors have been studied in connection with supersonic transport configurations in paper no. 11 by William. J. Alford, Jr., Vernard E. Lockwood, Linwood W. McKinney, and Richard K. Greif, and in the midterm SCAT review.

(2) The dynamic-stability quantities such as the frequency and damping of aircraft oscillations (see ref. 29)

(3) The effectiveness and reversal characteristics of various controls (e.g., refs. 28 and 29) as influenced by the flexibility of the wings, fuselage, stabilizer, and fin

(4) Various other items such as the performance, particularly at off-design conditions, due to changes in trim drag and the transient response due to engine failure.

One of the aeroelastic effects on the dynamic stability of a delta-wing canard configuration (ref. 29) is illustrated in figure 8. The relative damping for the first three elastic modes of the fuselage and the relative damping in the short-period stability mode are shown. The abscissa is the square root of the relative structural stiffness of the fuselage. Figure 8 shows that as the fuselage stiffness decreases, the aerodynamic damping in the short-period stability mode decreases, and, actually, for low stiffnesses, is shown to become unstable. An instability is also indicated at low fuselage stiffness for one of the elastic modes.

The methods of analysis used to study aeroelastic stability and control effects are generally well known. Steady-state aerodynamic loadings can be calculated from proven lifting-surface theories. The usual procedure has been to compute static aeroelastic corrections to wind-tunnel data obtained with rigid models. Recently, however, for at least one airplane, static stability wind-tunnel data are being obtained with an elastically scaled model.

When oscillatory aerodynamic loadings are required, they are usually obtained from aerodynamic methods used in flutter analyses. The stability augmentation system should, of course, be considered in the dynamic analysis (ref. 30). In fact, the blending of dynamic stability into the flutter area has led in some cases to the use of a single analysis for both problem areas.

CONCLUDING REMARKS

Aeroelastic-dynamic considerations will be very important in the design and flight-test phases of the supersonic transport; however, in general, the techniques for handling the problems which will arise appear to be reasonably adequate.

REFERENCES

1. Anon.: Tentative Airworthiness Objectives and Standards for Supersonic Transport Design Proposals. Flight Standards Service, FAA, Aug. 15, 1963.

2. Garrick, I. E., and Rainey, A Gerald: Remarks on the State-of-the-Art of Buffet-Loads Prediction. Presented to Structures and Materials Panel of AGARD (Paris, France), July 3-6, 1962.

3. Ruhlin, Charles L., and Gurley, John R., Jr.: Transonic Flutter Investigation of Models of a Proposed Variable-Sweep Wing. NASA TM X-739, 1962.

4. Stonesifer, John C., and Goetz, Robert C.: Transonic and Supersonic Flutter Trend Investigation of a Variable-Sweep Wing. NASA TM X-598, 1961.

5. Anon.: Airplane Airworthiness; Transport Categories. Civil Air Regulations Part 4b, Rules Service Co. (Washington, D.C.), Jan. 7, 1963.

6. Watkins, Charles E., Runyan, Harry L., and Woolston, Donald S.: On the Kernel Function of the Integral Equation Relating the Lift and Downwash Distributions of Oscillating Finite Wings in Subsonic Flow. NACA Rep. 1234, 1955. (Supersedes NACA TN 3131.)

7. Watkins, Charles E., Woolston, Donald S., and Cunningham, Herbert J.: A Systematic Kernel Function Procedure for Determining Aerodynamic Forces on Oscillating or Steady Finite Wings at Subsonic Speeds. NASA TR R-48, 1959.

8. Pines, Samuel, Dugundji, John, and Neuringer, Joseph: Aerodynamic Flutter Derivatives for a Flexible Wing With Supersonic and Subsonic Edges. Jour. Aero. Sci., vol. 22, no. 10, Oct. 1955, pp. 693-700.

9. Li, Ta: Aerodynamic Influence Coefficients for an Oscillating Finite Thin Wing in Supersonic Flow. Jour. Aero. Sci., vol. 23, no. 7, July 1956, pp. 613-622.

10. Zartarian, Garabed, and Hsu, Pao-Tan: Theoretical Studies on the Prediction of Unsteady Supersonic Airloads on Elastic Wings. WADC Tech. Rep. 56-97, Pts. I and 11, U.S. Air Force.
Part I. Investigations on the Use of Oscillatory Supersonic Aerodynamic Influence Coefficients. ASTIA Doc. No. AD 110591, Dec. 1955.
Part 2. Rules for Application of Oscillatory Supersonic Aerodynamic Influence Coefficients. ASTIA Doc. No. AD 110592, Feb. 1956.

11. Lighthill, M. J.: Oscillating Airfoils at High Mach Number. Jour. Aero. Sci., vol. 20, no. 6, June 1953, pp. 402-406.

12. Ashley, Holt, and Zartarian, Garabed: Piston Theory - A New Aerodynamic Tool for the Aeroelastician. Jour. Aero. Sei., vol. 23, no. 12, Dec. 1956, pp. 1109-1118.

13. Chawla, Jagannath P.: Aeroelastic Instability at High Mach Number. Jour. Aero. Sci., vol. 25, no. 4, Apr. 1958, pp. 246-258.

14. Yates, E. Carson, Jr.: Calculation of Flutter Characteristics for Finite-Span Swept or Unswept Wings at Subsonic and Supersonic Speeds by a Modified Strip Analysis. NACA RM L57L10, 1958.

15. Yates, E. Carson, Jr.: Use of Experimental Steady-Flow Aerodynamic Parameters in the Calculation of Flutter Characteristics for Finite-Span Swept or Unswept Wings at Subsonic, Transonic, and Supersonic Speeds. NASA TM X-183, 1960.

16. Yates, E. Carson, Jr.: Subsonic and Supersonic Flutter Analysis of a Highly Tapered Swept-Wing Planform, Including Effects of Density Variation and Finite Wing Thickness, and Comparison With Experiments. NASA TM X-764, 1963.

17. Yates, E. Carson, Jr., and Bennett, Robert M.: Use of Aerodynamic Parameters From Nonlinear Theory in Modified-Strip-Analysis Flutter Calculations for Finite-Span Wings at Supersonic Speeds. NASA TN D-1824, 1963.

18. Reed, Wilmer H., III, and Abbott, Frank T., Jr.: A New "Free-Flight" Mount System for High-speed Wind-Tunnel Flutter Models. NASA paper presented to the Symposium on Aeroelastic and Dynamic Modeling Technology (Dayton, Ohio), Sept. 23-25, 1963.

19. Walberg, Gerald D.: Transonic Flutter Tests of a Highly Swept Arrow Wing With and Without Simulated Trailing-Edge-Mounted Engine Masses. NASA TN D-1023, 1962.

20. Anon.: Commercial Supersonic Transport Flutter Studies. NAA Rep. No. 63-646 (Contract No. AF 33(657)-8514), North American Aviation, Inc., July 30, 1963.

21. Guy, Lawrence D., and Dixon, Sidney C.: A Critical Review of Experiment and Theory for Flutter of Aerodynamically Heated Panels. Symposium on Dynamics of Manned Lifting Planetary Entry. S. M. Scala, A. C. Harrison, and M. Rogers, eds., John Wiley & Sons, Inc., c.1963, pp. 568-595.

22. Stocker, James E.: A Comprehensive Review of Theoretical and Experimental Panel Flutter Investigations. Rep. No. NA61H-444, North American Aviation, Inc., Sept. 15, 1961.

23. Anon.: Commercial Supersonic Transport Panel Flutter Studies. NAA Rep. No. 63-952 (Contract No. AF 33(657)-8515), North American Aviation, Inc., Aug. 23, 1963.

24. Rhyne, Richard H., and Steiner, Roy: Turbulence and Precipitation Problems Associated With Operation of Supersonic Transports. NASA paper presented to Fourth Conference on Applied Meteorology (Hampton, Va.), Sept. 10-14, 1962.

25. Houbolt, John C., Steiner, Roy, and Pratt, Kermit G.: Flight Data and Considerations of the Dynamic Response of Airplanes to Atmospheric Turbulence. Presented to Structures and Materials Panel and to Flight Mechanics Panel of AGARD (Paris, France), July 3-13, 1962.

26. Taylor, A. S.: The Present Status of Aircraft Stability Problems in the Aeroelastic Domain. Tech Note No. Aero.2538, British R.A.E., Dec. 1957.

27. J. B. Rea Co., Inc.: Aeroelasticity in Stability and Control. WADC Tech. Rep. 55-173, U.S. Air Force, Mar. 1957.

28. Anon.: B-70 Technology Applicable to the Supersonic Transport. Rep. NA-62-601, North American Aviation, Inc., June 1, 1962.

29. Runyan, H. L., Pratt, K. G., and Bennett, F. V.: Effects of Aeroelasticity on the Stability and Control Characteristics of Airplanes. Presented to AGARD Specialists Meeting on Stability and Control (Brussels, Belgium), Apr. 10-14, 1961.

30. McRuer, D. T., Benun, D., and Click, G. E.: The Influence of Servomechanisms on the Flutter of Servocontrolled Aircraft. AF Tech. Rep. No. 6287, Wright Air Dev. Center, U.S. Air Force, Mar. 1954.

DECLASSIFIED

AEROELASTIC PROBLEM AREAS

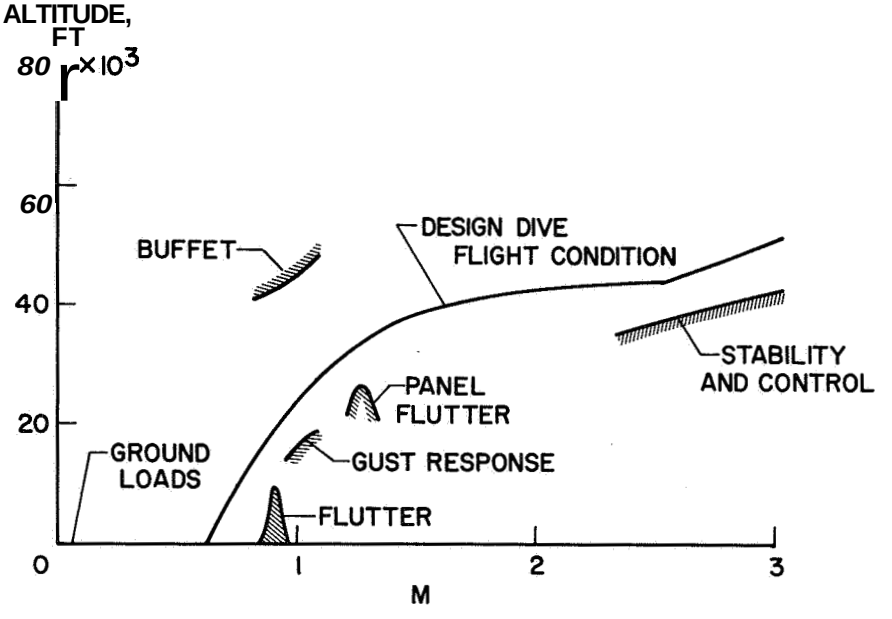

Figure 1

FLUTTER BOUNDARY

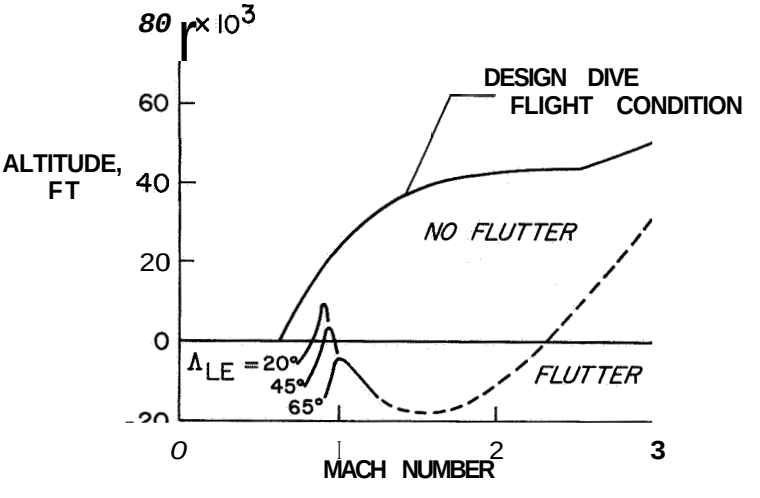

Figure 2

COMPARISON OF FLUTTER ANALYSIS AND EXPERIMENT
FOR SWEPT WING

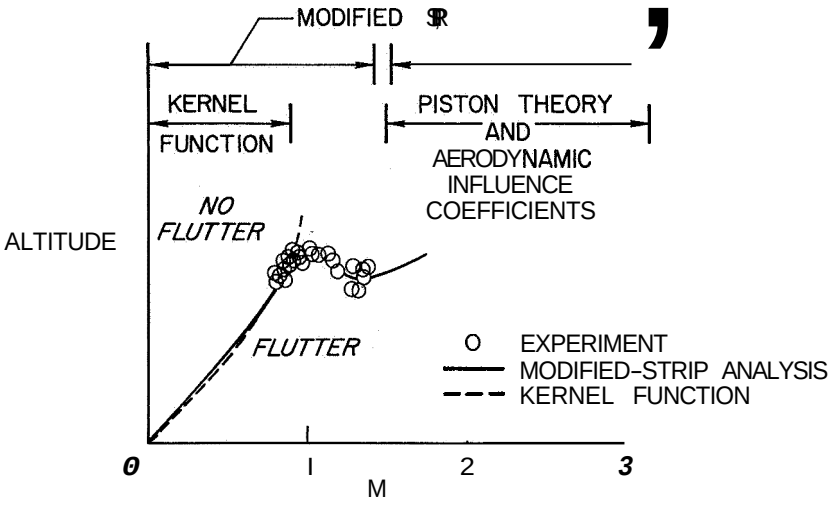

Figure 3

TWO-CABLE MOUNT

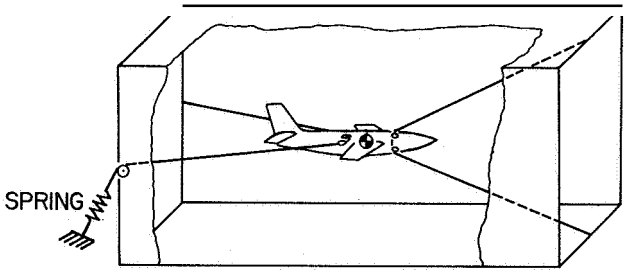

Figure 4

[redacted]

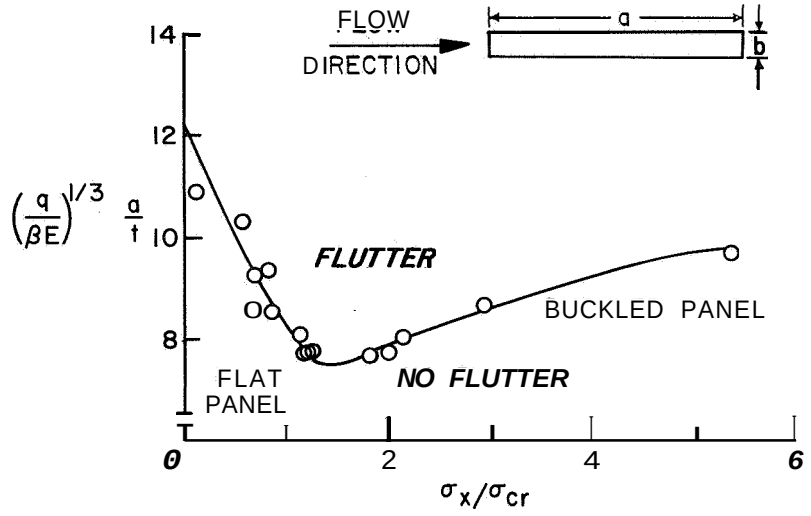

Figure 5

SAMPLE SPECTRUM OF TURBULENCE FOR THUNDERSTORM

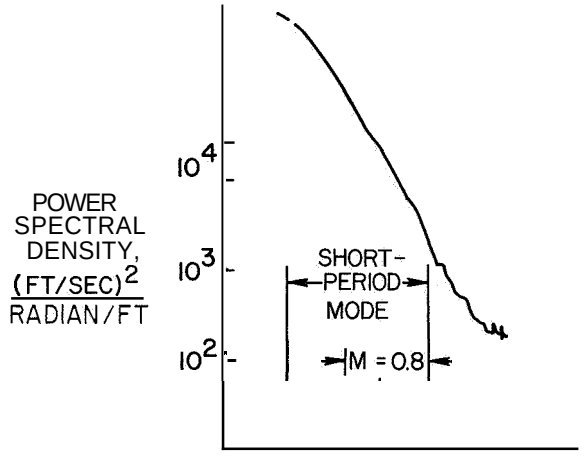

Figure 6

[redacted]

SUBSONIC RESPONSE OF LARGE SWEPT-WING AIRPLANE

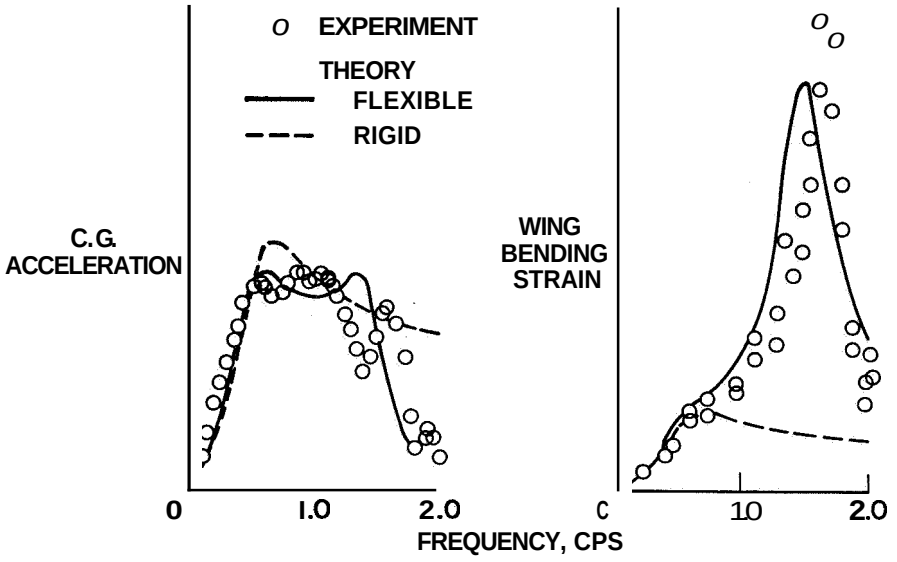

Figure 7

EFFECT OF FUSELAGE STIFFNESS ON DAMPING FOR DELTA-WING CANARD

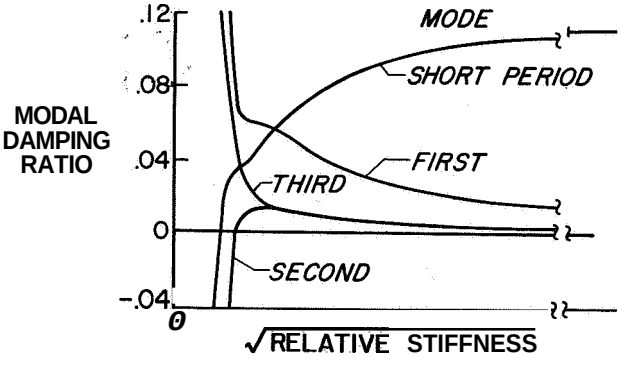

Figure 8

N67-31628

21. CONFIGURATION EFFECTS ON SONIC BOOM

By Harry W. Carlson

NASA, Langley Research Center

SUMMARY

An outline of current theoretical methods for sonic-boom estimation is presented and the correlation of this theory with experimental data is illustrated. Sonic-boom lower bound concepts are used in examining the dependence of sonic boom on configuration variables and in pointing out design considerations tending to minimize the problem.

INTRODUCTION

One of the most important problems to be faced in the development of a supersonic transport is that posed by the sonic boom. Feasibility studies have shown that sonic-boom considerations alone may dictate allowable minimum altitudes along most of the flight path and have indicated that in many cases the airframe sizing and engine selection depend directly on the sonic-boom characteristics.

It is the purpose of this paper to outline current theoretical estimation methods, to illustrate the correlation of this theory with experimental data, and to examine the dependence of sonic-boom overpressures on configuration variables pointing out, in general, design considerations tending to minimize the problem.

SYMBOLS

A	cross-sectional area of airplane or model determined by supersonic area-rule concepts
$A(t)$	nondimensionalized cross-sectional area A/l^2 at nondimensionalized station $t = \frac{x}{l}$
$A_E(t), A_E$	effective nondimensionalized cross-sectional area due to a combination of volume and lift effects, $A(t) + B(t)$

[redacted]

A_b cross-sectional area at base of airplane or model

B equivalent cross-sectional area due to lift at airplane or model station given by the equation

$$B = \frac{\beta}{2q} \int_0^x F_L' \, dx$$

$B(t)$ nondimensionalized equivalent cross-sectional area due to lift B/l^2 at nondimensionalized station $t = \frac{x}{2}$

$C_{D,o}$ drag coefficient at zero lift

C_L lift coefficient

F_L' lifting force per unit length along airplane or model longitudinal axis

$F(\tau)$ effective area distribution function given by the equation

$$F(\tau) = \frac{1}{2\pi} \int_0^\tau \frac{A_E''(t)}{\sqrt{\tau - t}} \, dt$$

h airplane flight altitude or lateral distance from model to measuring probe

K_r reflection factor

l length of airplane or model equivalent body

M Mach number

n,r integers

p reference pressure

Δp incremental pressure due to flow field of airplane or model

q dynamic pressure

S wing planform area

[redacted]

t nondimensionalized distance measured along longitudinal axis from airplane or model nose, x/l

W airplane weight

$\beta = \sqrt{M^2 - 1}$

γ ratio of specific heats for air

τ dummy variable of integration measured in same direction and using same units as t

T_o value of τ giving the largest positive value of the integral, $\int_0^{\tau} F(\tau)d\tau$

x distance measured along longitudinal axis from airplane or model nose

μ Mach angle, $\sin^{-1}\frac{1}{M}$

Subscript:

MAX maximum

A prime ' is used to indicate a first derivative and a double prime '', a second derivative with respect to distance.

DISCUSSION

The nature of the airplane shock field which is responsible for the sonic-boom phenomena is illustrated in the schematic sketch of figure 1. At supersonic speeds the airplane-generated flow field is concentrated within a bow shock front and a tail shock front fanning out from the airplane to reach the ground and there to be reflected upward. Near the airplane the pressure signature is quite complex containing pulses from the airplane nose, wing-fuselage juncture, engines, tail surfaces, and other airplane components. As the distance from the airplane increases, the separate pulses merge and only a nose and tail shock remain. The resultant N-wave signifies the attainment of the so-called far-field conditions. At ground level the incident and reflected

signatures are coincident and an amplification of the pressure rise occurs. On a hard level surface a doubling of the pressures takes place. For other surfaces this reflection factor may be somewhat less than 2.0. It is this pair of pressure jumps traveling with the airplane and passing over the ground that is sensed by the observer.

An outline of the theoretical method used in estimating the intensity of the far-field bow-shock pressure rise directly below an airplane in level supersonic flight is shown in figure 2. The method illustrated in the figure, in a form suitable for a numerical solution using electronic computing machines, has been derived from the work of references 1 and 2, the main differences stemming from changes in terminology and in the expression of lift effects in terms of equivalent cross-sectional area. The following equation relates overpressure to the geometry of the airplane and the flight conditions:

$$\frac{\left(\frac{\Delta p}{p}\right)_{MAX}\left(\frac{h}{l}\right)^{3/4}}{K_r \beta^{1/4}} = \frac{1.19\gamma}{\sqrt{\gamma+1}}\sqrt{\int_0^{T_o} F(\tau)\,d\tau} \qquad (1)$$

The right-hand side of equation (1) depends only on the geometry of the airplane and is evaluated by taking into consideration a distribution of nondimensionalized airplane area $A(t)$ formed by supersonic-area-rule cutting planes and a distribution of nondimensionalized equivalent area due to lift $B(t)$ evaluated through an integration of the lifting force per unit length along the airplane longitudinal axis. Since the pressure field directly below the airplane is of primary concern, only one set of cutting planes having an angle μ with respect to the horizontal is used. The many sets necessary in drag evaluation are not pertinent. Improved accuracy results when the area distributions include the increases in cross-sectional area due to boundary layer and engine exhaust effects. Configuration sonic-boom characteristics are directly dependent on an effective area distribution curve $A_E(t)$ formed by a direct addition of actual area and equivalent area due to lift. The $A_E(t)$ curve may be approximated by a series of parabolic arcs having a first derivative composed of connected straight-line segments and a second derivative composed of a step or pulse function. The integral involved in the $F(\tau)$ function can be evaluated quite easily when $A_E''(t)$ is a constant; by superposition, a complete F curve may be built up corresponding to the $A_E''(t)$ pulse distribution. An integration of the $F(\tau)$ function to the point T_o (cross-hatched area in fig. 2) is then used in evaluating the right-hand side of

equation **(1).** The degree of approximation of the $A_E(t)$ curve can be improved by increasing the number of pulses used. A machine computing procedure using this technique is described in the appendix.

When the computational procedure is carried out for a series of values of lift coefficient, the results may be conveniently plotted in the parametric form used in figure *3* to illustrate the correlation of theoretical estimates with measured wind-tunnel overpressures for a bomber model (ref. *3).* **An** overpressure parameter derived from theory has been plotted as a function of a lift (or airplane weight) parameter. The area distribution used in the theory includes the estimated cross-sectional area under the displacement thickness of the laminar boundary layer assumed to exist on the small model. In figure *3,* the variation of the measured pressure-rise parameter with lift coefficient closely follows the theoretical estimate. As a matter of interest, theoretical curves are shown for volume effects alone **or** lift effects alone. A notable feature of the data shown here is that through a favorable combination of area and lift distributions the resultant overpressure becomes less than that associated with lift alone. The uniform atmosphere results shown here may be applied in making estimates of ground overpressures in the real atmosphere provided that proper account is taken of the pressure and temperature variation between the airplane and the ground. This may be accomplished by replacing the ambient pressure p by an appropriate reference pressure. A rigorous treatment of atmospheric effects has been made in reference 4. A reference pressure based on the method of reference 4 has been used in the correlation of estimated ground overpressure with flight-test results for the bomber (ref. 5) shown in figure 4.

A reflection factor of 2.0 corresponding to that measured for the *dry* lake bed over which flight tests were conducted has been used in the estimates. Estimates based on tunnel data are made with differences in area distributions due to estimated differences in the model and airplane boundary layer being considered. Both the theory and the tunnel estimates are shown as a band to account for variations in airplane weight and Mach number at a given altitude. The flight data points represent an average pressure for the 6 or 7 ground track microphones in use during a single overpass. The agreement of measured and estimated overpressures is reasonably good, there being a slight tendency toward underestimation.

The theory of references 1 and 2 as further developed in references 6 and 7 has made possible the definition of a lower bound of sonic-boom overpressure. Figure 5 illustrates some of these lower bound concepts. As shown previously, sonic-boom strength depends on an effective area distribution combining both volume and lift components. An example of an effective-area-distribution curve for an arrow-wing

transport configuration is shown at the right of the figure. The sonic-boom overpressure is primarily dependent on the value of the effective cross-sectional area at the base of the airplane which in turn is directly dependent on the airplane base area (including boundary-layer and engine exhaust effects) and the flight lift coefficient. The overpressure also depends on the shape of the effective-area curve. A theoretical study (ref. 6) has shown that the shape of the area curve yielding a minimum sonic boom is represented by a function in which the area is proportional to the square root of the distance except in the immediate neighborhood of the airplane nose, as illustrated by the dashed line. Thus, it is possible to define a relationship for a lower bound of attainable sonic-boom overpressure that may be shown on the plot of overpressure parameter as a function of lift parameter at the left of figure 5. The area below the curve represents unattainable values of sonic-boom overpressures. This lower limit of attainable overpressures depends only on the airplane length, weight, and base area (including boundary-layer and engine exhaust effects) and on the flight conditions.

This lower bound concept not only sets limits on attainable overpressures but also suggests design methods of approaching these limiting values. Theoretically for a selected flight condition (a design point), it should be possible to redesign a configuration to approach the sonic-boom minimization requirements. In the example shown, the modification consisted of a tailoring of the fuselage area distribution as shown by the dashed line. In this example, the design point represents the transonic acceleration portion of the flight for a 300,000-pound airplane ($M = 1.4$, $h = 35{,}000$ ft). The overpressure characteristics of the original and modified configuration are shown on the left of figure 5. The maximum theoretical reduction in boom strength (about 25 percent) occurs at the design point and benefits fall off rapidly on either side of that point. Whether any substantial portion of these benefits could be achieved in practice and whether the compromises with other airplane design considerations would be profitable is yet to be demonstrated.

Some experimental data believed to be applicable in connection with these concepts are shown in figure 6. Measured and theoretical overpressures in parametric form have been plotted against a lift parameter for two wing-body models. The model with the wing in the rear location theoretically approaches the lower bound even though it was not designed strictly in accordance with the concepts previously discussed. The experimental data however show only a part of the theoretical gains. Some of this discrepancy may be due to unknown boundary-layer and separated flow effects on the small models.

Of fundamental importance in any evaluation of configuration changes aimed at sonic-boom reduction is the resultant change in airplane drag. Figure 7 shows theoretical sonic-boom characteristics and corresponding values of zero-lift wave drag for an arrow-wing transport configuration and two modifications. .The original configuration has reasonably good sonic-boom characteristics and large reductions in overpressures should not be expected. Drag calculations were made by using the machine computing procedure discussed in paper no. 6 by Roy V. Harris, Jr. The modifications consisted only of changes in fuselage area distribution. The second configuration which was modified to approach the sonic-boom lower bound for a design point of $M = 3$ at an altitude of 60,000 feet for a 300,000-pound airplane required a greatly enlarged forward fuselage with a resultant total airplane volume increase of 60 percent. This increase in volume resulted in an extremely large zero-lift drag penalty and also showed up as an increase in overpressure for zero lift. The large drag penalty associated with the attainment of near lower bound sonic-boom values is not the contradiction it might outwardly appear to be. The explanation lies in the fact that the drag is dependent on the shock strength of the flow field to all sides of the airplane, not just below, as in the case of the boom. Although the lower bound configuration results in reduced ground overpressures, it probably results in an increased shock strength in the remainder of the airplane flow field particularly above the airplane. The third configuration represents a compromise design having no volume change, in which an attempt was made to produce a smooth effective-area-distribution curve (similar to that of the area distribution for a minimum-wave-drag body of revolution) at the design point of $M = 3$ at an altitude of 60,000 feet. The decrease in overpressure which was not as pronounced as that for the other modification extended over the whole range of lift coefficients and only a small drag penalty was shown. There are, of course, so many other factors involved (including the important matter of airplane balance) which have not been studied that it is not possible at this time to draw any conclusions regarding the feasibility of these sonic-boom minimization concepts.

In order to provide an illustration of configuration effects on sonic-boom characteristics, an interesting comparison for two transport configuration models is shown in figure 8. Both theoretical and experimental wind-tunnel data are shown and are compared with a lower bound curve for which the base area A_b is a minimum which includes only the area of the model sting support. Cross-sectional areas used in the theory include the area within the estimated displacement thickness of a laminar boundary layer. The lower overpressures for the arrow-wing design may be attributed to the reduced base area and to smooth area and lift distribution curves. In order to assess these configuration effects in terms of changes in Ap, estimated ground overpressures for these configurations sized to accommodate 125 passengers (take-off

weight of 400,000 pounds) are shown in figure 9 and are compared with a lower bound for which A_b included only the estimated engine exhaust stream tube area less inlet capture area. A reflection factor of 1.9 was assumed. The reference pressure was taken as the standard atmosphere pressure at mid-altitude which for a standard atmosphere is a reasonable approximation to the results of reference 4. (Mid-altitude is the altitude halfway between the ground and the airplane.) A weight of 360,000 pounds at a Mach number of 1.4 was chosen to represent the critical climb portion of the flight, whereas a weight of 300,000 pounds at a Mach number of 3 was chosen to represent the cruise portion. For an assumed overpressure limit of 2.0 lb/sq ft in climb at M = 1.4, the arrow-wing configuration could fly at an altitude of about 48,000 feet whereas the canard configuration would be restricted to altitudes above 57,000 feet. For a representative cruise altitude of 70,000 feet the canard design would have an overpressure of about 1.6 lb/sq ft as compared with 1.4 lb/sq ft for the arrow-wing design. In view of the many compromises involved it is believed that a practical sonic-boom optimized airplane would not be able to achieve the corresponding lower bound value of 1.15 lb/sq ft and that attainable minimum overpressures are likely to be nearer to the 1.4 lb/sq ft level. Any change in airplane weight would, of course, critically affect this comparison, the overpressure being roughly proportional to the square root of the weight.

CONCLUDING REMARKS

Experimental data from wind-tunnel and flight tests have indicated that existing theory can provide reasonably accurate estimates of sonic-boom overpressure for the steady-state condition. Additional developments of the theory have made possible the definition of a lower bound of sonic-boom overpressure which depends only on airplane length, weight, and base area (including boundary-layer and engine exhaust effects) and on the flight conditions. The lower bound concept also suggests airplane design methods that theoretically allow lower bound overpressure values to be achieved. However, it has been indicated that compromises with other design considerations will prevent anything more than a limited approach to lower bound overpressures.

DECLASSIFIED

APPENDIX

A NUMERICAL EVALUATION OF SONIC-BOOM THEORY FOR USE ON HIGH-SPEED ELECTRONIC COMPUTING MACHINES

The effective nondimensionalized cross-sectional area discussed previously and illustrated in figure 2 may be expressed as:

$$A_E(t) = \frac{A}{l^2} + \frac{\beta}{2} C_L \frac{S}{l^2}\left[\frac{\int_0^x F_L' \, dx}{\int_0^l F_L' \, dx}\right]$$

$$A_E(t) = A(t) + \frac{\beta}{2} C_L \frac{S}{l^2}\left[\frac{B(t)}{B(1)}\right] \qquad (A1)$$

If it is assumed that local lifting pressures are directly proportional to the total lift coefficient, the quantity in brackets in the above equation is a constant for any airplane station. The inputs to the program are thus a tabulation of $A(t)$ and the ratio $B(t)/B(1)$ as a function of equally spaced nondimensionalized airplane stations. Equation (A1) then allows an evaluation and tabulation of the effective area distribution $A_E(t)$ for selected values of the lift parameter $\frac{\beta}{2} C_L \frac{S}{l^2}$. A series of parabolas fitted to these points so that the resultant curve has no discontinuities in slope may be expressed as:

$$A_{E,1}(t) = \frac{A_{E,1}}{\Delta t^2} t^2 \qquad (0 < t < \Delta t)$$

$$A_{E,2}(t) = A_{E,1} + \left(A'_{E,1}\right)t + \frac{\left(A_{E,2} - A_{E,1}\right) - \left(A'_{E,1}\right)\Delta t}{\Delta t^2} t^2 \qquad (\Delta t < t < 2\Delta t)$$

[redacted]

$$A_{E,3}(t) = A_{E,2} + \left(A'_{E,2}\right)t + \frac{\left(A_{E,3} - A_{E,2}\right) - \left(A'_{E,2}\right)\Delta t}{\Delta t^2} t^2$$

$$(mt < t < 3\Delta t)$$

$$A_{E,n}(t) = A_{E,n-1} + \left(A'_{E,n-1}\right)t + \frac{\left(A_{E,n} - A_{E,n-1}\right) - \left(A'_{E,n-1}\right)\Delta t}{\Delta t^2} t^2$$

$$((n - 1)\Delta t < t < n\Delta t)$$

The second derivative then is

$$A''_{E,1}(t) = \frac{2}{\Delta t^2} A_{E,1} \qquad (0 < t < At)$$

$$A''_{E,2}(t) = \frac{2}{\Delta t^2}\left(A_{E,2} - A_{E,1}\right) - 2A''_{E,1} \qquad (At < t < 2\Delta t)$$

$$A''_{E,3}(t) = \frac{2}{\Delta t^2}\left(A_{E,3} - A_{E,2}\right) - 2\left(A''_{E,1} + A''_{E,2}\right) \qquad (2\Delta t < t < 3\Delta t)$$

$$A''_{E,n}(t) = \frac{2}{\Delta t^2}\left(A_{E,n} - A_{E,n-1}\right) - 2\sum_{r=1}^{r=n-1} A''_{E,r} \qquad \left((n - 1)\Delta t < t < n\Delta t\right)$$

(A2)

The $F(\tau)$ function then becomes

$$F(\tau) = \frac{1}{\pi} A''_{E,1}\sqrt{\tau} \qquad (0 < \tau < At)$$

[redacted]

DECLASSIFIED

$$F(\tau) = \frac{1}{\pi}\left[A''_{E,1}\sqrt{\tau} + \left(A''_{E,2} - A''_{E,1}\right)\sqrt{\tau - \Delta t}\right] \qquad (\Delta t < \tau < 2\Delta t)$$

$$F(\tau) = \frac{1}{\pi}\left[A''_{E,1}\sqrt{\tau} + \left(A''_{E,2} - A''_{E,1}\right)\sqrt{\tau - \Delta t} + \left(A''_{E,3} - A''_{E,2}\right)\sqrt{\tau - 2\Delta t}\right]$$

$$(2\Delta t < \tau < 3\Delta t)$$

$$F(\tau) = \frac{1}{\pi}\sum_{r=1}^{r=n}\left(A''_{E,r} - A''_{E,r-1}\right)\sqrt{\tau - (r-1)\Delta t} \qquad ((n-1)\Delta t < \tau < n\Delta t)$$

and the integral of the $F(\tau)$ function may be written as

$$\int_0^{\tau=\Delta t} F(\tau)d\tau = \frac{2}{3\pi} A''_{E,1}(\Delta t)^{3/2}$$

$$\int_0^{\tau=2\Delta t} F(\tau)d\tau = \frac{2}{3\pi}\left[A''_{E,1}(2\Delta t)^{3/2} + \left(A''_{E,2} - A''_{E,1}\right)(\Delta t)^{3/2}\right]$$

$$\int_0^{\tau=3\Delta t} F(\tau)d\tau = \frac{2}{3\pi}\left[A''_{E,1}(3\Delta t)^{3/2} + \left(A''_{E,2} - A''_{E,1}\right)(2\Delta t)^{3/2} + \left(A''_{E,3} - A''_{E,2}\right)(\Delta t)^{3/2}\right]$$

$$\int_0^{\tau=n\Delta t} F(\tau)d\tau = \frac{2}{3\pi}\sum_{r=1}^{r=n}\left(A''_{E,r} - A''_{E,r-1}\right)\left[(n - r + 1)\Delta t\right]^{3/2}$$

Because of the deviations introduced by the curve-fitting technique used, it has been found that improved accuracy results when the integral expression is averaged and is rewritten as

[redacted]

$$\int_0^{\tau=n\Delta t} F(\tau)d\tau = \frac{1}{3\pi}\sum_{r=1}^{r=n}\left(A''_{E,r} - A''_{E,r-1}\right)\left[(n - r + 1)\Delta t\right]^{3/2}$$

$$+ \frac{1}{3\pi}\sum_{r=1}^{r=n-1}\left(A''_{E,r} - A''_{E,r-1}\right)\left[(n - r + 1)\Delta t\right]^{3/2} \quad (A3)$$

The overpressure is then found by selecting the maximum value of equation (A3) and substituting in the following equation:

$$\frac{\left(\frac{\Delta p}{p}\right)_{MAX}\left(\frac{h}{l}\right)^{3/4}}{K_r\beta^{1/4}} = \frac{1.19\gamma}{\sqrt{\gamma + 1}}\sqrt{\left[\int_0^{\tau=n\Delta t} F(\tau)d\tau\right]_{MAX}} \quad (A4)$$

The computational program may be summarized as follows. The inputs are a tabulation of nondimensionalized area $A(t)$ and the integrated lift distribution ratio $B(t)/B(1)$ as a function of equally spaced nondimensionalized airplane stations. Equation (A1) then allows the determination of a table of effective cross-sectional areas for preselected values of the lift parameter $\frac{\beta}{2} C_L \frac{S}{l^2}$. The second derivative step function is then generated by using equation (A2). Tabulated values of $A''_E(t)$ are used in evaluating the integral of equation (A3), the maximum value of this integral being selected and used in equation (A4) in evaluating the configuration sonic-boom characteristics. For airplane configurations employing camber the loading distribution at zero lift may be taken into account by using a modified area distribution. In this case $\frac{A}{l^2}$ is replaced by $\frac{A}{l^2} + \frac{1}{2ql^2}\int_0^x F'_L\,dx$ where F'_L is the lifting force per unit length at zero lift.

[redacted]

REFERENCES

1. Whitham, G. B.: The Behaviour of Supersonic Flow Past a Body of Revolution, Far From the Axis. . Proc. Roy. Soc. (London), ser. A, vol. 201, no. 1064, Mar. 7, 1950, pp. 89-109.

2. Walkden, F.: The Shock Pattern of a Wing-Body Combination, Far From the Flight Path. Aero. Quarterly, vol. IX, pt. 2, May 1958, pp. 164-194.

3. Carlson, Harry W.: Wind-Tunnel Measurements of the Sonic-Boom Characteristics of a Supersonic Bomber Model and a Correlation With Flight-Test Ground Measurements. NASA TM X-700, 1962.

4. Friedman, Manfred P., Kane, Edward J., and Sigalla, Armand: Effects of Atmosphere and Aircraft Motion on the Location and Intensity of a Sonic Boom. AIAA Jour., vol. 1, no. 6, June 1963, pp. 1327-1335.

5. Hubbard, Harvey H., Maglieri, Domenic J., Huckel, Vera, and Hilton, David A. : Ground Measurements of Sonic-Boom Pressures for the Altitude Range of 10,000 to 75,000 Feet. NASA TM X-633, 1962.

6. Jones, L. B.: Lower Bounds for Sonic Bangs. Jour. R.A.S. (Tech. Notes), vol. 65, no. 606, June 1961, pp. 433-436.

7. Carlson, Harry W.: The Lower Bound of Attainable Sonic-Boom Overpressure and Design Methods of Approaching This Limit. NASA TN D-1494, 1962.

AIRPLANE SHOCK FIELD

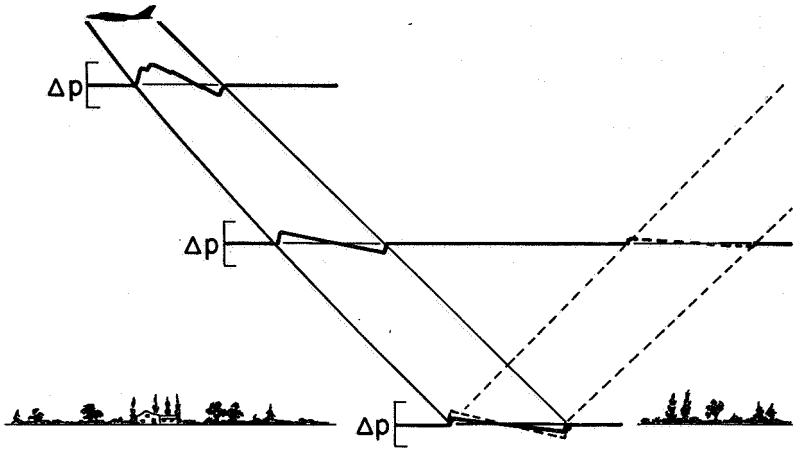

Figure 1

THEORETICAL ESTIMATION METHOD

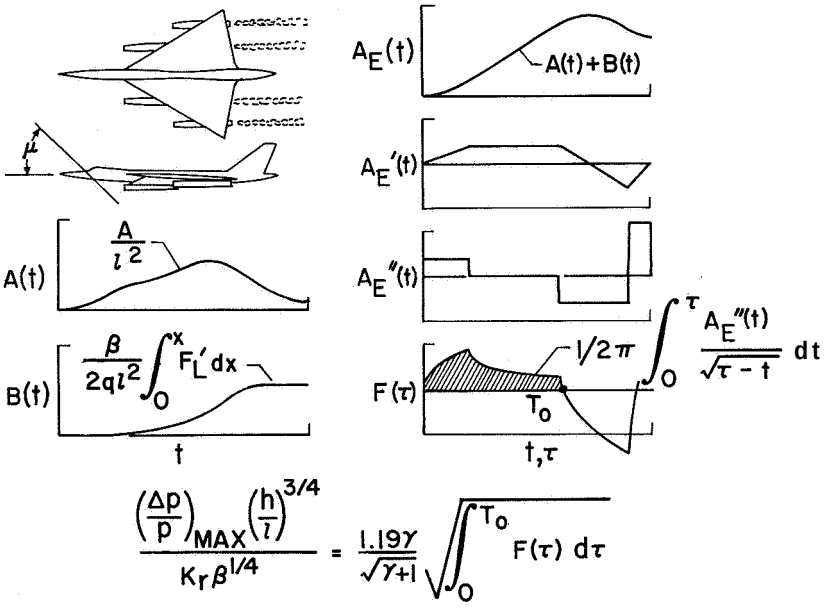

Figure 2

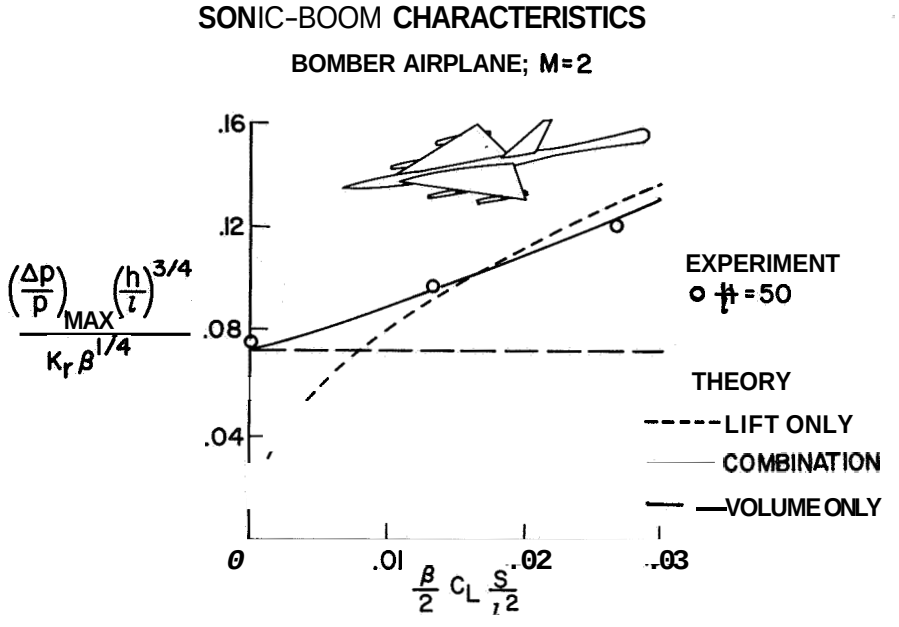

Figure 3

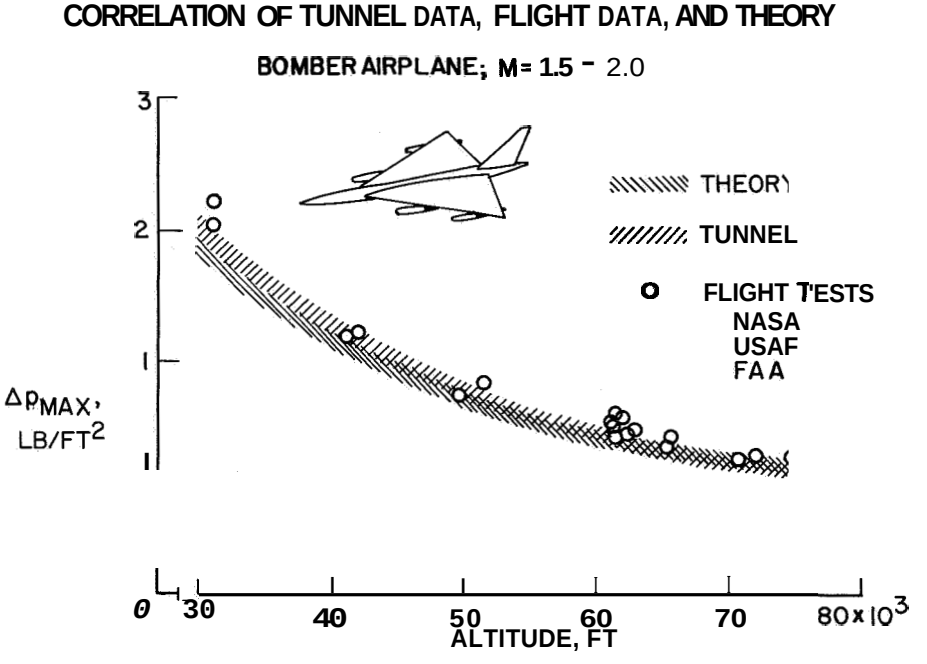

Figure 4

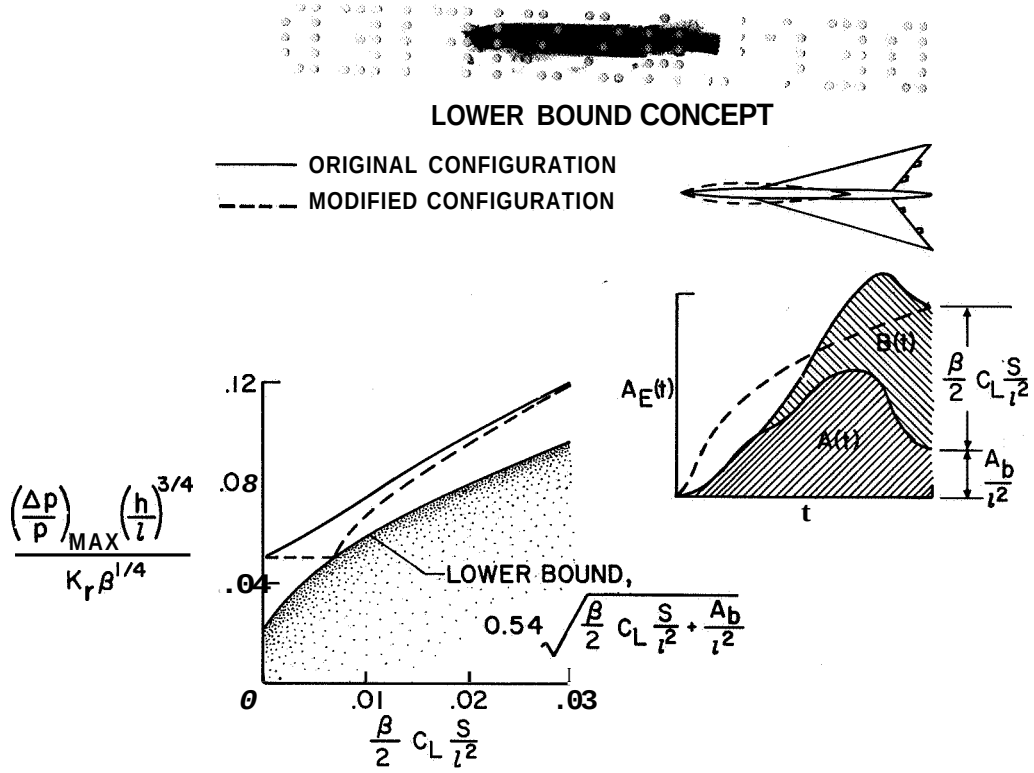

Figure 5

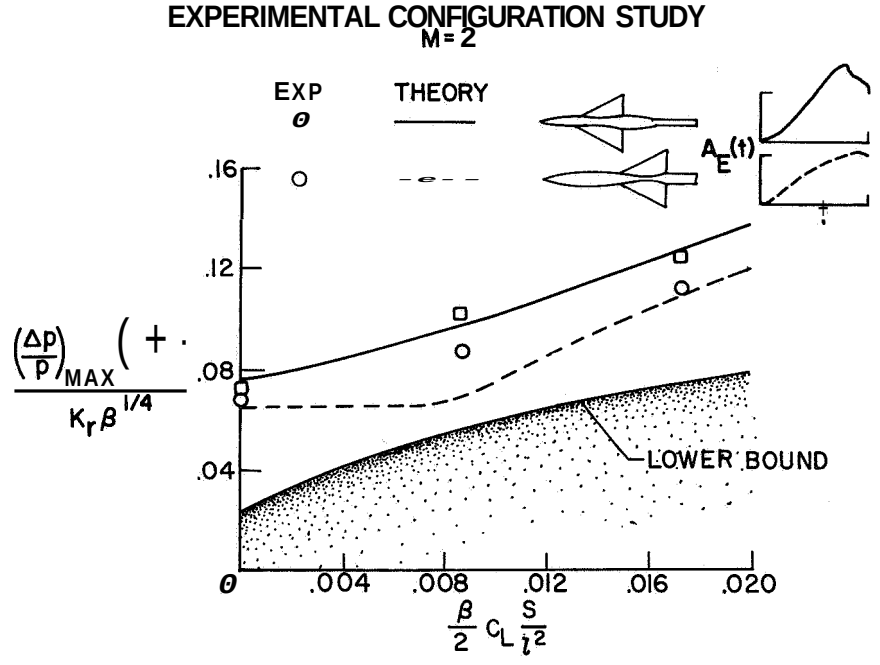

Figure 6

[redacted]

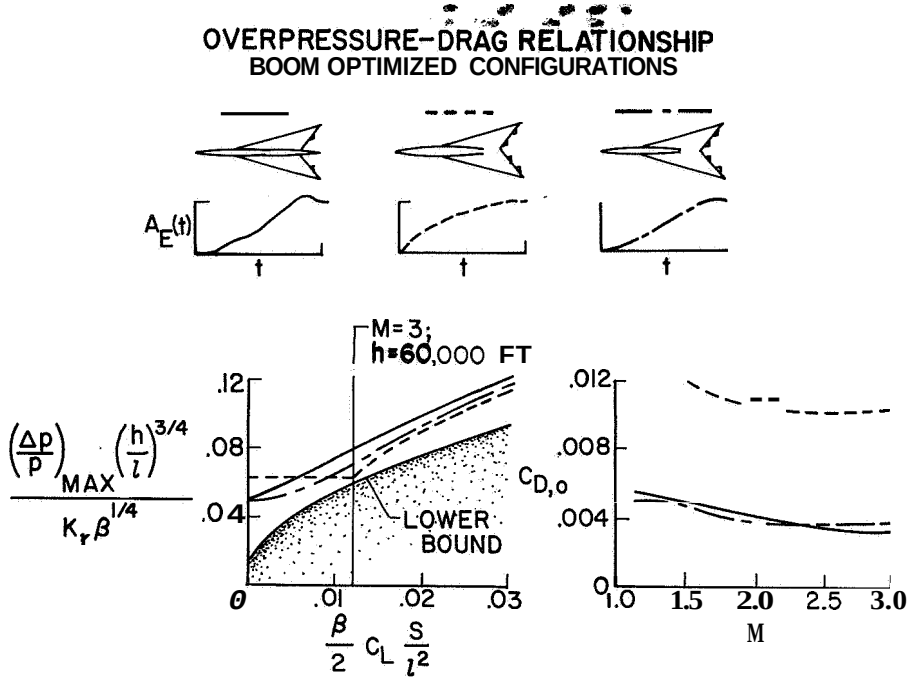

Figure 7

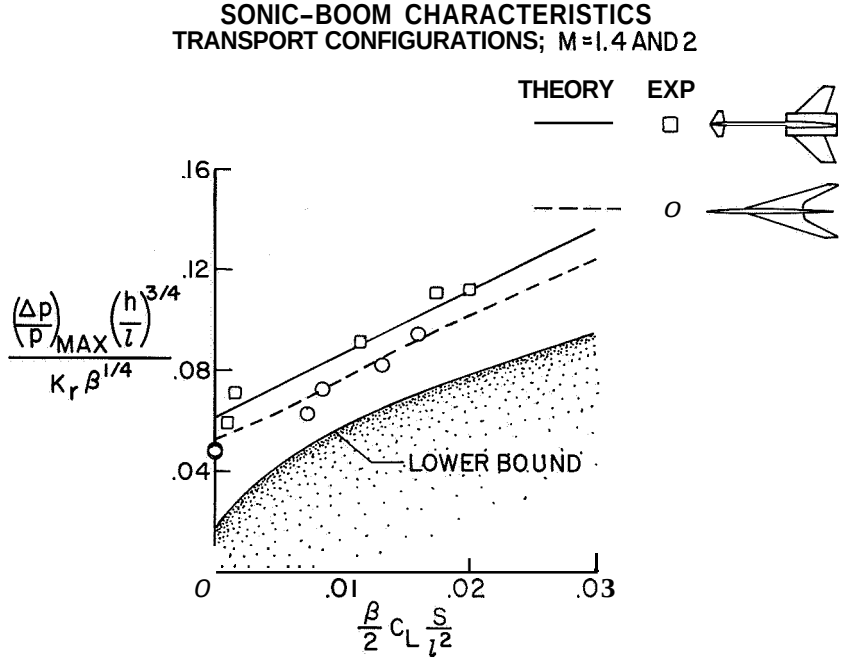

Figure 8

[redacted]

CONFIDENTIAL

ESTIMATED GROUND OVERPRESSURES
TRANSPORT CONFIGURATIONS

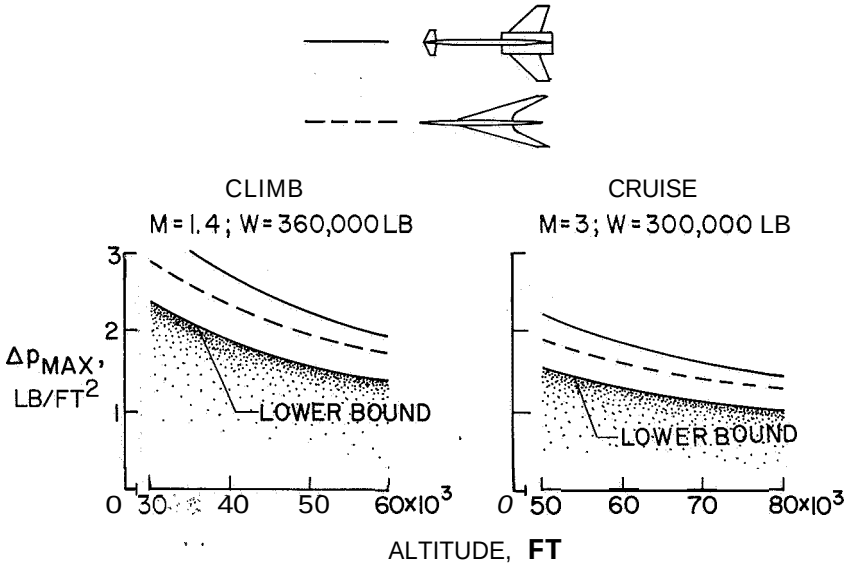

Figure 9

N67-31629

22. FACTORS AFFECTING COMMUNITY ACCEPTANCE OF THE SONIC BOOM

By Harvey H. Hubbard and Domenic J. Maglieri

NASA Langley Research Center

SUMMARY

Discussions are given of ground overpressure exposures for current military operations and how these exposures are affected by the atmosphere and by aircraft maneuvers. Brief remarks are included about various operations for which some response information has been obtained. Indications are that building response is a very important factor in influencing public reaction. Based on these data, some estimates are given regarding the frequency and nature of damage incidents resulting from sonic-boom exposures.

INTRODUCTION

One of the important questions relating to the operation of the supersonic transport is whether or not its sonic booms will be acceptable over inhabited areas. This question has led to the joint collection of pertinent data by the National Aeronautics and Space Administration, the United States Air Force, and the Federal Aviation Agency during several supersonic-flight research programs. Although these studies have not produced the final answers, they have markedly broadened knowledge of the subject both with regard to the overpressure patterns to which communities are exposed and with regard to the complex manner in which the communities react to these exposures. It is the purpose of this paper to summarize available information on both aspects of the problem.

Figure 1 illustrates schematically a cross-country flight. Altitude is indicated on the vertical scale and distance, on the horizontal scale; several other items of interest are also noted. The first discussion relates to the sonic-boom overpressure values that have recently been experienced and how they may have been affected by atmospheric phenomena and by the operation of the aircraft, including maneuvers. The second topic, which constitutes the main portion of the paper, relates to community reaction induced by sonic boom.

Atmospheric Effects

One of the effects of the atmosphere on the propagation of sonic-boom waveforms can be illustrated with figure 2. Shown schematically in this figure is a theoretical curve of overpressure Ap as a function of airplane altitude; the shaded region extending above and below the theoretical curve indicates the normal spread of measured data. Also shown in the figure are three sample sonic-boom pressure waveforms that are representative of many that have been measured. (See refs. **1** and 2.) It can be seen that these waveforms differ widely with regard to detailed shape, and thus the associated overpressure values as defined in the figure will also vary. Such differences as these, which follow an orderly statistical pattern, are believed to result from the effects of sound-speed gradients associated with atmospheric turbulence in the lower layers of the atmosphere.

There is a similar effect due to large-scale temperature and wind gradients which takes the form of overpressure buildups or changes in the ground pressure distributions. The basic nature of such an effect, namely, that of a sound-speed inversion, is demonstrated in figure 3.

This figure illustrates schematically the shapes of the shock fronts for propagation in two different atmospheric conditions. The standard atmospheric condition for zero wind is illustrated in the left-hand sketch. Waves propagating to the ground in the presence of a standard sound-speed gradient have a slight curvature due to the increasing value of sound speed in the lower levels of the atmosphere. The case of a sound-$peed inversion due either to temperature or wind effects results in a different wave-pattern diagram, as indicated in the sketch on the right. In this case, the extremities of the wave propagate faster than the middle portion with the result that the ray paths tend to be squeezed together, thus causing a local increase in the shock-wave pressure. This phenomenon is presently under study by Dr. Manfred **P.** Friedman at the Massachusetts Institute of Technology, according to the method of reference 3. His initial results suggest that a sound-speed inversion at a relatively low altitude can have a marked detrimental effect on the pressure patterns. If a similar sound-speed inversion exists at relatively high altitudes, the effect is negligible since the disturbances at high altitudes are compensated for by the wave as it propagates. At the lower altitudes, the mechanism for such an adjustment does not have time to act effectively. One of the implications here is that weather forecasting for sonic-boom purposes will more than likely be required only at the lower altitudes.

The Superboom Phenomena

Certain maneuvers of an aircraft in which longitudinal, lateral, or normal accelerations occur can result in so-called "superbooms." (See ref. 4.) This latter phenomenon can be illustrated with the aid of figure 4 which shows the shock-wave ground-intersection patterns for two flight conditions of an aircraft. For simplicity, a homogeneous atmosphere is assumed, and only the bow shock wave is considered. In the left diagram is indicated the ground pattern for an aircraft in steady flight. It can be seen that the ray paths, represented by the straight lines, are generally parallel to each other, and the ground pattern, represented by the heavy curved line, is essentially hyperbolic in shape. On the other hand, the pattern on the right is for an aircraft experiencing a lateral acceleration. It can be seen that the ray paths are no longer parallel. In some regions they tend to converge and in others, to diverge. Likewise, the shock-wave ground-intersection pattern is no longer symmetrical and may contain some irregularities and cusp formations in which the pressures are higher than those for the steady-flight condition. Such pressure buildups are referred to as superbooms. The case for lateral acceleration is shown only for convenience. Similar results would be obtained for flight conditions involving normal or longitudinal accelerations. One important consideration is the shape of these superboom areas on the ground. These areas are shown in figure 5 for some common flight maneuvers.

In the upper part of the figure is illustrated a level, or linear, acceleration. Linear acceleration is a common maneuver which must be executed during every flight to supersonic speeds. As indicated in the sketch by the stippled areas, superbooms occur over relatively small expanses of the ground. Dimensions are such that total superboom area is approximately 1 square mile. The pressure buildups in these stippled areas are believed to be a function of the rate of acceleration of the aircraft but, for a practical operating range, are approximately 2 times the corresponding steady-flight values. Also of possible concern in the operation of the supersonic transport are such maneuvers as horizontal turns and push-overs, as might occur during changes in course and airplane attitude. In the latter instances the ground patterns of pressure buildups are different in shape, as indicated in figure 5, and, because of the higher accelerations involved, the buildup factors may tend to be higher and the areas smaller than for the case of linear acceleration.

Summary of Recent Sonic-Boom Overpressure Experience

Before some of the effects induced by sonic boom are discussed, it will be helpful to become familiar with current sonic-boom exposures as indicated in figure 6. The ground overpressures due to routine training

operations involving two types of service aircraft are shown as a function of aircraft altitude. (See ref. 2.) It should be noted that such operations are limited to altitudes above 30,000 feet but have been carried on over many metropolitan areas in the United States. The stippled region relates to fighter aircraft for steady-flight operations, and it can be seen that, depending on the altitude of the operation, the associated overpressure range varies from less than 0.3 lb/sq ft to about 1.8 lb/sq ft. The crosshatched region relates to B-58 operations. It can be seen that the overpressure range associated with these operations varies from about 1.3 lb/sq ft to nearly 3 lb/sq ft, again depending on the altitude. The hatched region is not well defined but has been estimated, based on fragmentary experimental data, to encompass the superboom overpressure range associated with training maneuvers of both fighter and bomber aircraft.

Estimated values of overpressure for the supersonic transport are within the range of current experience for fighter and bomber aircraft. Three differences are, however, anticipated between the service type of operations and the supersonic-transport operations. One of these differences is that the transport operations will be of much longer duration; that is, they will sweep over more area, the frequency of exposure will eventually be greater, and, furthermore, the associated wavelength will be about 2.0 times as long as for the B-58 and about 4.0 times as long as for the fighter-aircraft wavelengths that are indicated in the figure.

A recording of the pressure time history of thunder is illustrated in figure 6 for comparison. The peak pressures involved are approximately 0.5 lb/sq ft for lightning discharges located at distances of about 1 mile from the observer. It is believed, of course, that higher overpressures would be associated with closer strikes, Although sonic booms are often judged to sound like thunder, it is obvious that the pressure time history of thunder consists of many peaks within a rather short time interval and, hence, is markedly different from the pressure time histories of the sonic booms.

Wave shape and wavelength may be significant influences in response, although they have not as yet been evaluated.

COMMUNITY RESPONSE *TO* SONIC BOOMS

Results of Judgment Studies

It is very difficult to devise an experiment of a subjective nature that will give all the desired answers. Some of these answers will only come as a result of simulated or actual supersonic-transport operations. During the past few years, however, several attempts have

been made in conjunction with physical measurements to collect subjective data. The following table is a list of the available studies during which some subjective observations were obtained. (See refs. 2 and 5 to 9.)

Study	Number of flights	Number of observers	Range of overpressure, lb/sq ft
A	1	4,000,000	Up to 1.6
B	33	10	0.3 to 2.1
C	64	2,600,000	0.3 to 2.9
D	12	10	0.6 to 3.1
E	13	10	0.4 to 6.8
F	63	10	0.5 to 7.4
G	25	50	2.0 to 100

It can be seen that observations have been made for relatively large numbers of flights and for observers ranging from small groups to entire populations of large cities; also, a wide range of overpressure values was involved in these studies. It is interesting to note that for study A there was very little, if any, recorded reaction to the portion represented in the table. There were numerous complaints, however, associated with another portion of the mission for which the pressures were considerably higher. It is a matter of record that some scheduled supersonic flights prompted complaints and claims of damage even though the flights were never accomplished.

Where small groups were involved, judgments were solicited regarding acceptability. There were, of course, inherent differences of opinion of the observers, and the test conditions differed in many respects. The so-called acceptable range of overpressures varied from about 0.9 lb/sq ft to about 1.9 lb/sq ft. This range is significant since it includes the overpressure range estimated for the operation of the supersonic transport.

The fact that scatter exists in these and other judgment data is not surprising since it is believed that several different factors can affect these judgments. Some of these factors relate to the physical characteristics of the pressure wave, such as its overpressure magnitude, its wavelength, and its detailed Shape. Other factors which are believed to be significant, based on sociological considerations, are

the time of day of the observed boom, the type of operation causing it, the type of community in which the observer lives, the observer's personal environment, and the frequency of supersonic flights.

Summary of Reported Effects

In one instance there was actually an opportunity to interview representative segments of the population of a large metropolitan area in order to get a direct sampling of reaction to sonic booms. The results of these interview studies are summarized in figure 7. People representing about 1,100 homes were interviewed to determine their reactions to 64 known sonic booms over a period of several months. Of the 1,100 interviewed, about 90 percent indicated an awareness of the sonic booms to the extent that they discussed various effects. For instance, the most commonly mentioned effect was the vibration of building structures. About 40 percent of those interviewed indicated some concern over possible detrimental effects of such vibrations. Those who said they actually went to the trouble to file a formal complaint were 5 in number and thus constituted roughly 0.5 percent of the total. The types of incidents reported as a basis for such formal complaints from over 3,000 cases in Air Force files have been broken dom into several categories and are plotted in figure 8 in the form of bar graphs to indicate frequency of occurrence.

For instance, plaster cracks were reported most frequently and, in fact, were mentioned in 43 percent of the complaints registered. Other damage, such as cracks in window glass, walls, tile, and so forth, was reported to have occurred less frequently. It is believed significant that a large percentage of the complaint reports mentioned some type of damage, whereas only about 7 percent mentioned miscellaneous effects, including annoyance only. The implication is that the ability of the sonic boom to cause buildings to vibrate is very significant since it is readily observable; it is suggestive that damage can occur, and such damage is, of course, of concern to the general public.

Because of the obvious significance of building vibration, a test was made in which the sonic-boom-induced stresses in several components of a flat-roofed frame building were measured. In figure 9, as an example of the type of data obtained, rafter stresses σ are plotted as a function of sonic-boom overpressure Δp for a range from about 0.3 to 3 lb/sq ft. The measured stresses did not exceed 20 lb/sq in. and were noted to be of the same order of magnitude as those associated with such everyday occurrences as door closing. Door slamming would result in values corresponding to the highest measured values of the figure. The sonic-boom-induced stress values were also noted to be relatively low compared with the design stresses of the building. The implication

is that if a building was well designed and in good repair, no damage would be anticipated because of the relatively small loads induced by sonic booms.

Probability of Damage

On the basis of the results of architectural and engineering surveys in areas where sonic-boom damage was reported and of the knowledge of the exposure patterns and the population densities of the areas involved, there is a strong suggestion that the probability of damage is related to population density. The data of figure 10 have been determined on the assumption that the average occupancy rate is five persons per building. Plotted on the vertical scale is the accumulative probability of damage occurrences per million buildings shown as a function of the overpressure on the horizontal scale. The data are presented in the form of shaded bars. The four lower bars represent routine training type of operations, whereas the two upper bars represent isolated accidental-damage incidents. The calculated probability curve is adjusted to a best fit of available data. Several features of this curve are worthy of mention. The number of damage incidents, of course, decreases as the overpressure value decreases, but even at very low pressures there still seems to be the possibility of damage occurrences. One explanation for this is that the investigators were lenient in their judgments against the complainants. In other words, some of the damage incidents which were judged valid may in fact not have been valid. There is always the possibility of other contributing factors in any damage occurrence. These are, for instance, weathering effects, vibration due to road traffic, degradation of building materials, settling of the building, poor workmanship, and so forth. All these factors can contribute to the same type of damage attributed to sonic booms, and hence the job of honestly evaluating claims is a difficult one. Consequently, it is believed that the numbers quoted in figure 10 are conservative; that is, they are no doubt higher than the actual number of damage incidents. It is obvious that additional studies are needed for the purpose of better defining the values of the lower portion of the curve and particularly for repeated exposures over a period of time.

Even though there is reason to suspect the absolute value of the numbers quoted in figure 10, the trends indicated may be very significant. For instance, the number of damage incidents is essentially proportional to the overpressure in the overpressure range of greatest interest. This fact would suggest that even a sizable increase in overpressure should not result in an unusually large increase in the damage occurrences.

CONCLUDING REMARKS

There are still some differences of opinion regarding acceptable sonic-boom exposure. Experience with military aircraft has been in the range of overpressures of interest but has not otherwise been definitive enough for making a quantitative evaluation of the problem. Recent experience has been very useful qualitatively and indicates that a major factor in shaping attitudes toward sonic booms is the matter of building vibrations. Only occasionally does building vibration due to sonic booms result in damage, and ensuing damage is, in turn, limited in extent. There does not, however, seem to be any assurance of completely eliminating damage, and hence this damage problem will be a continuing one.

[redacted]

REFERENCES

1. Maglieri, Domenic J., and Parrott, Tony L.: Atmospheric Effects on Sonic-Boom Pressure Signatures.. Sound, vol. 2, no. 4, July-Aug. 1963, pp. 11-14.

2. Hubbard, Harvey H., Maglieri, Domenic J., Huckel, Vera, and Hilton, David A.: Ground Measurements of Sonic-Boom Pressures for the Altitude Range of 10,000 to 75,000 Feet. NASA TM X-633, 1962.

3. Friedman, Manfred P., Kane, Edward J., and Sigalla, Armand: Effects of Atmosphere and Aircraft Motion on the Location and Intensity of a Sonic Boom. AIAA Jour., vol. 1, no. 6, June 1963, pp. 1327-1335.

4. Maglieri, Domenic J., and Lansing, Donald L.: Sonic Booms From Aircraft in Maneuvers. Sound, vol. 2, no. 2, Mar.-Apr. 1963, pp. 39-42.

5. Maglieri, Domenic J., and Carlson, Harry W.: The Shock-Wave Noise Problem of Supersonic Aircraft in Steady Flight. NASA MEMO 3-4-59L, 1959.

6. Maglieri, Domenic J., Hubbard, Harvey H., and Lansing, Donald L.: Ground Measurements of the Shock-Wave Noise From Airplanes in Level Flight at Mach Numbers to 1.4 and at Altitudes to 45,000 Feet. NASA TN D-48, 1959.

7. Lina, Lindsay J., and Maglieri, Domenic J.: Ground Measurements of Airplane Shock-Wave Noise at Mach Numbers to 2.0 and at Altitudes to 60,000 Feet. NASA TN D-235, 1960.

8. Power, J. K.: Sonic Boom & Community Relations. [Preprint] 683B, Soc. Automotive Eng., Apr. 1963.

9. Maglieri, Domenic J., Huckel, Vera, and Parrott, Tony L.: Ground Measurements of Shock-Wave Pressure for Fighter Airplanes Flying at Very Low Altitudes and Comments on Associated Response Phenomena. NASA TM X-611, 1961.

[redacted]

OPERATING CONSIDERATIONS

SONIC BOOM

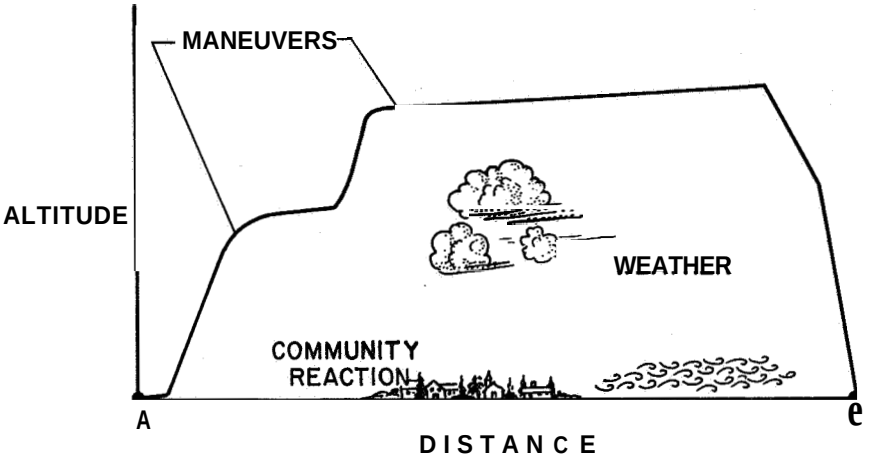

Figure 1

METEOROLOGICAL EFFECTS

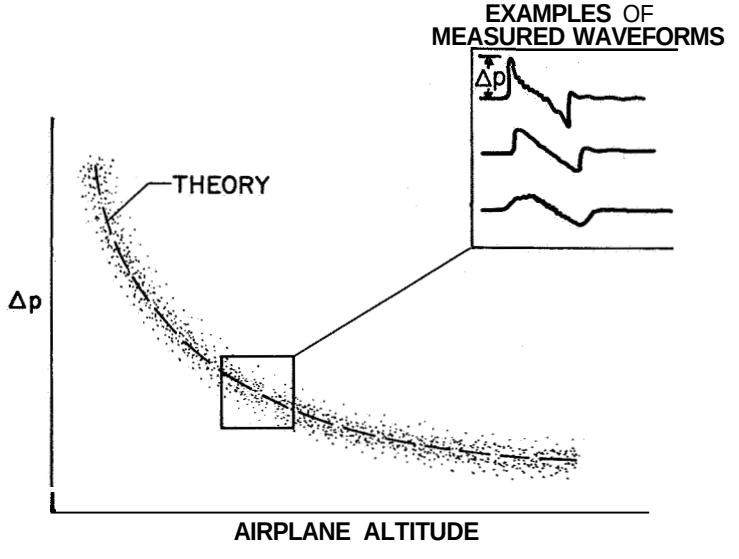

Figure 2

[redacted]

EFFECT 0F SOUND–SPEED GRADIENT

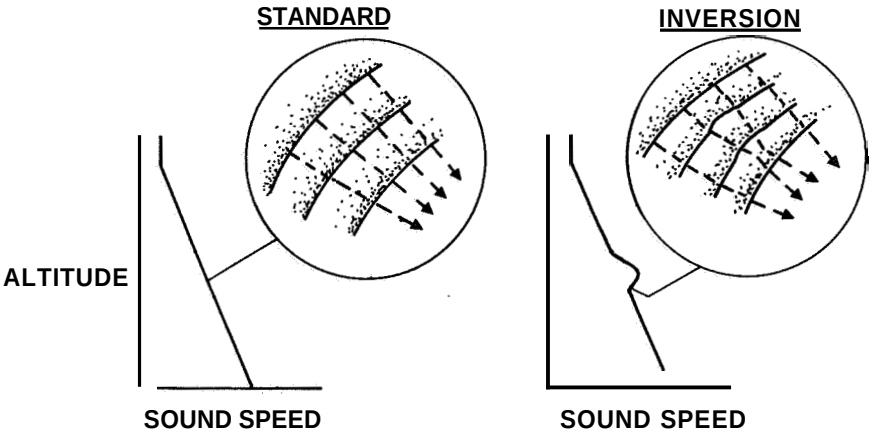

Figure 3

GROUND PRESSURE PATTERNS

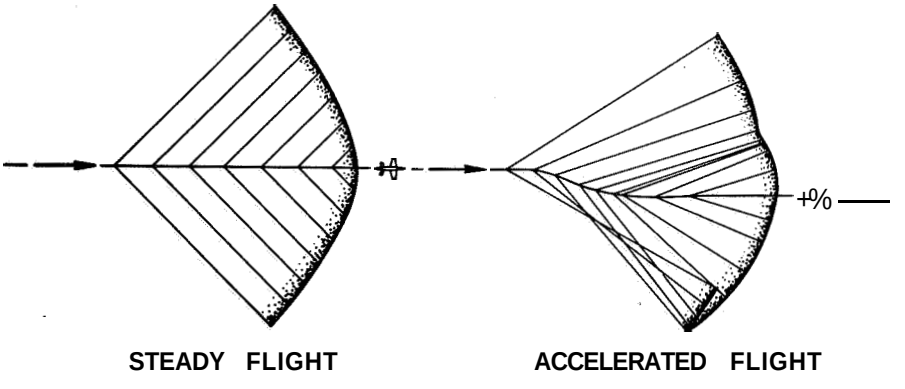

Figure 4

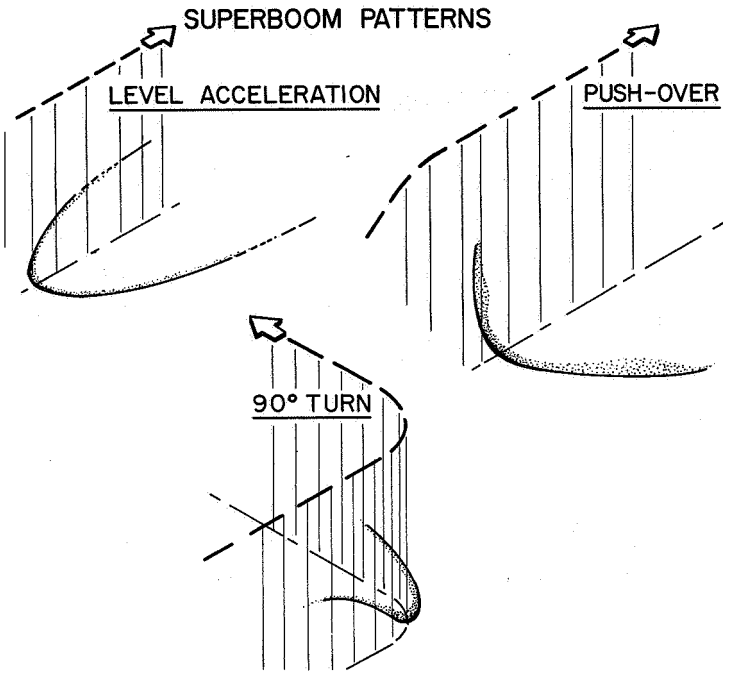

Figure 5

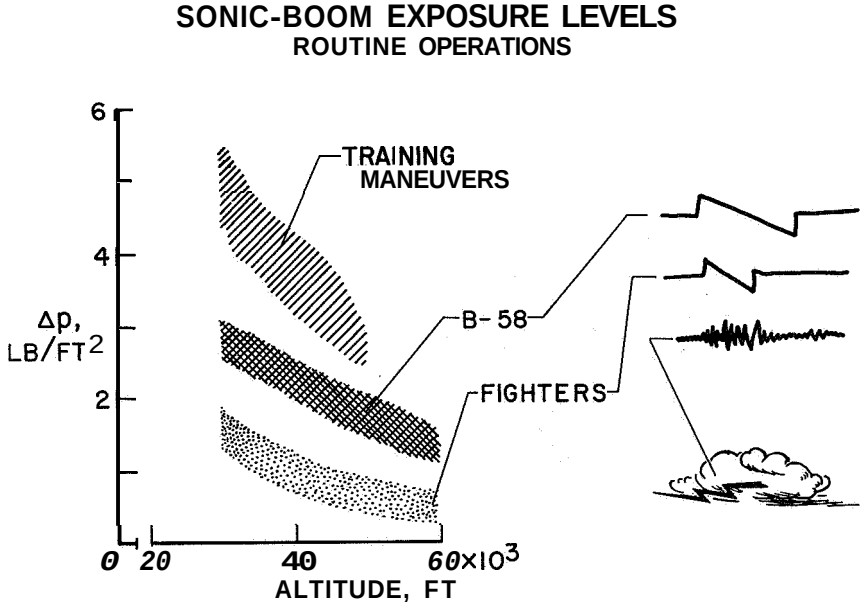

Figure 6

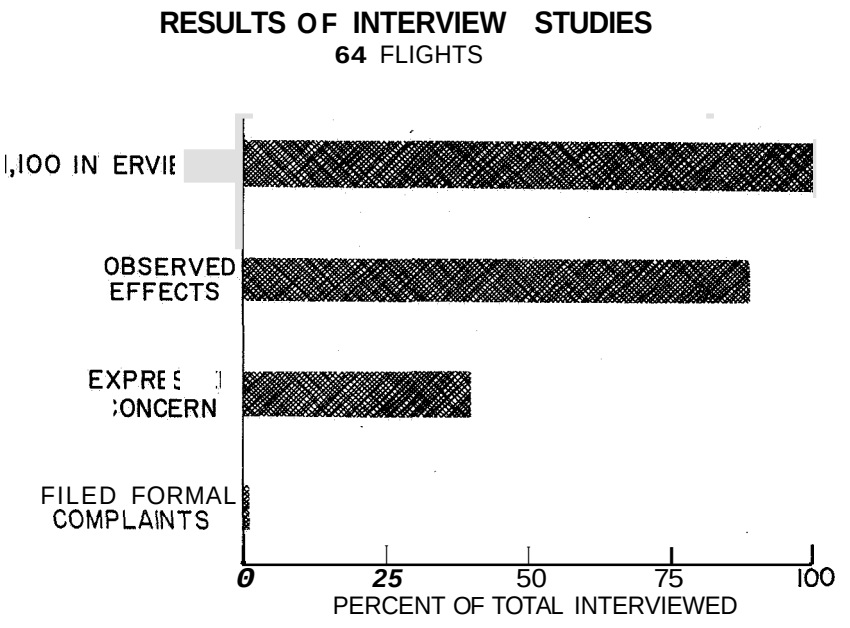

Figure 7

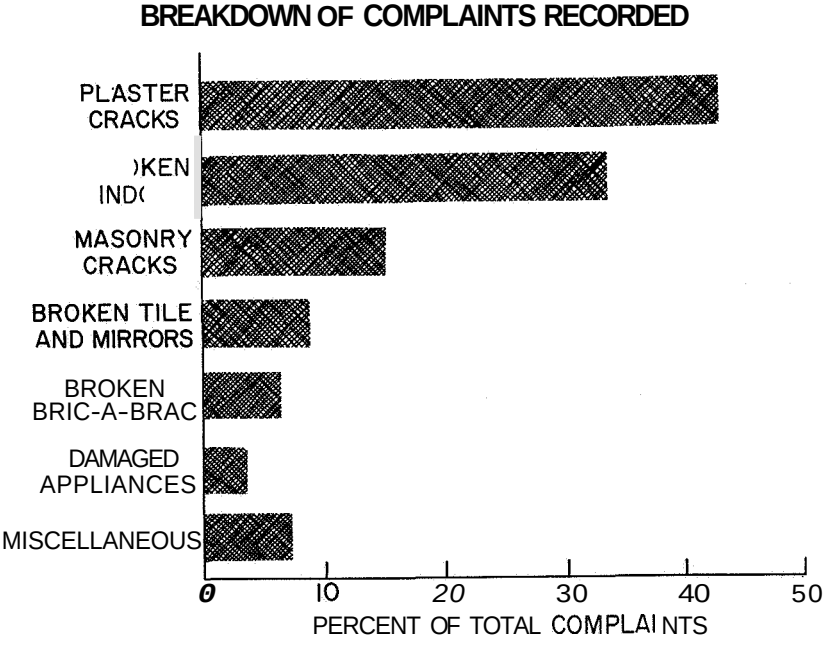

Figure 8

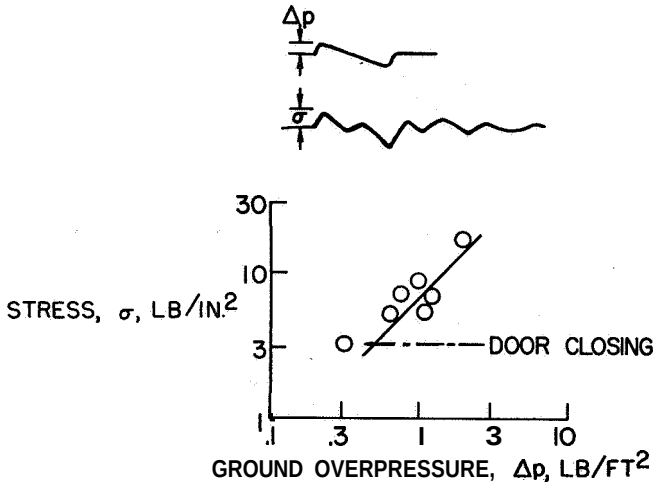

Figure 9

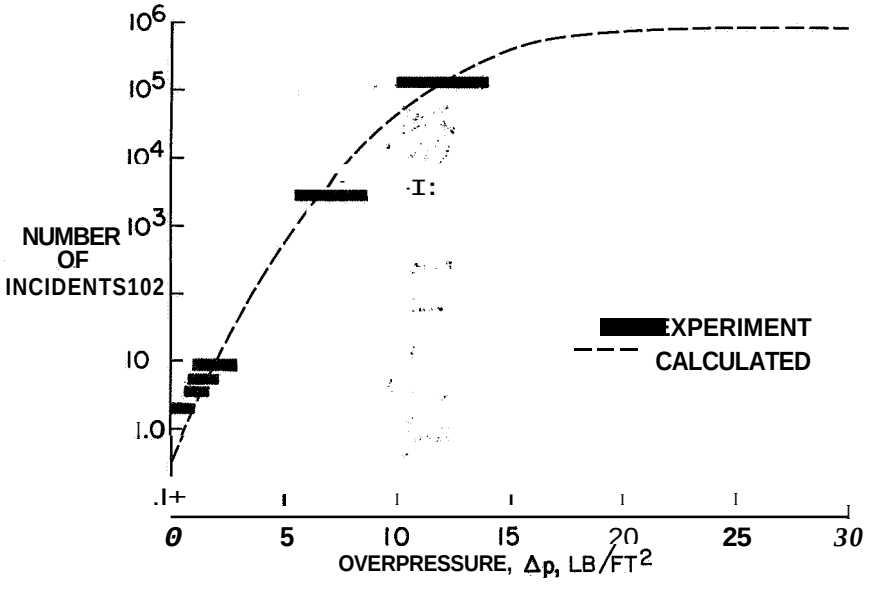

Figure 10

N67-31630

23. ENGINE AND BOUNDARY-LAYER NOISE CONSIDERATIONS

By Jimmy M. Cawthorn and Domenic J. Maglieri

NASA Langley Research Center

SUMMARY

The main findings of the contractor studies are summarized with regard to noise problems during the take-off, initial climb, and landing approach. Data are presented in the form of perceived noise levels, and comparisons are made with a current subsonic transport of comparable range. Airport noise levels are estimated to be higher than those for the current aircraft, whereas the climbout and landing-approach noise levels can be of the same order of magnitude or lower, depending on the aircraft configuration and the operating procedures used. Brief mention is also made of the noise-induced structural-response problem during take-off and cruise.

INTRODUCTION

Since the supersonic transport will be integrated into existing air traffic systems, it is required that its acoustic characteristics be compatible with those of current aircraft. This is particularly desirable for take-off and landing operations during which power-plant noise is an important consideration. Noise in the community due to the power plants is, of course, a function of the type of power plant used and the manner in which it is operated and also, as will be shown in the paper, the configuration of the aircraft in which it is installed.

The objectives of this paper can be discussed with the aid of figure 1. Noise considerations during the take-off run, the initial climbout from the airport, and the landing approach will be discussed. Some mention will also be made of the structural response problems of the airframe due to noise excitation by the power plants and by the aerodynamic flows. An attempt is made to include the main findings of the contractors during their feasibility studies.

TYPES OF ENGINE CYCLES

First let us consider the significance of the type of engine cycle chosen. Noise level data for advanced turbojet (engine C) and turbofan

engines (engine D) are given in table 1 for both augmented and unaugmented thrust conditions. The basic engine noise data presented are taken from the Boeing studies and have been normalized to a thrust of 45,000 pounds. Also shown for comparison are similar data for a current turbofan at 17,000-pound thrust. Listed in the second column are the maximum sound pressure levels estimated at a distance of 1,000 feet. It can be seen that the lower overall noise levels are associated with the turbofan type of power plant. It can also be noted, however, that even the advanced turbofan engine cycles have associated with them higher overall noise levels than do the current turbofan engines. These higher levels for both proposed engines are due to the fact that they will be larger and have higher exhaust velocities because of their greater thrust requirements.

Estimated exhaust noise spectra for the engines of table 1 are shown in figure 2. The range of sound pressure levels estimated for the advanced turbojet and turbofan engines is indicated by the two shaded regions. The noise levels associated with the lower extremity of each shaded region correspond to the unaugmented operating condition, whereas those associated with the upper extremity of each band correspond to full augmentation. It can be seen that these levels are higher at all frequencies than those for the current turbofan engine, as illustrated by the dashed curve.

When the perceived noise level procedure (ref. 1) is applied to the spectra of figure 2, the perceived noise level values listed in the last column of table 1 are obtained. Since the shape of the spectra is not markedly different, the perceived noise levels exhibit the same rank order as the sound pressure levels. It is therefore obvious from the data of table 1 and figure 2 that on the basis of minimum noise generated, it would be desirable to use a turbofan engine cycle rather than a turbojet.

TAKE-OFF AND INITIAL CLIMBOUT

The manner in which the airport noise situation is affected can be illustrated by the plan view sketch of figure 3, in which are plotted constant perceived noise level contours of 110 decibels for a current fan-powered subsonic, 2,500-mile-range, intercontinental jet and for a proposed supersonic transport. The origin represents the start of take-off roll. The horizontal scale is, then, the distance parallel to the runway, and the vertical scale is the distance perpendicular to the runway. The solid line represents the perceived noise level contour of 110 decibels for the subsonic airplane without power cutback. The unbounded shaded area represents the range of estimated perceived noise level contours of 110 decibels for SCAT 16 with no power cutback, which

came from the two contractor studies. The width of the shading is due to differences in the aircraft configuration involved as well as to the different assumptions which go into making these estimates. It can be seen that the estimated perceived noise level contour of 110 decibels for the supersonic airplane extends laterally to a greater distance than that for the current airplane and would extend further in the direction of the runway unless a power cutback were initiated. Current procedures employ a power cutback which shortens the pattern in the direction of the runway, as indicated by the dashed line. This sane power cutback procedure is judged feasible for the supersonic transport and, as suggested by the bounded shaded region, would further shorten the contour in the direction of the runway.

The effect of such a power cutback in the initial climb is further illustrated in figure 4, which contains a summary of the data produced by the two contractors for SCAT 16 and SCAT 17 and a comparison with similar data for a current fan-powered '2,500-mile-range aircraft. Shown in the top sketch are the altitude-distance profiles, and in the lower sketch are shown the variations of perceived noise levels as a function of distance from brake release. It can be seen that both of the supersonic aircraft take off in a shorter distance and climb initially at a greater angle, and, as a result, they attain a higher altitude over the community than the subsonic aircraft does. It can be seen that SCAT 16 attains a more rapid initial climb angle and a resulting higher altitude in the initial climbout than does SCAT 17 because of its inherently better low-speed aerodynamic characteristics. The differences in the performance of the two aircraft also show up in the resulting noise exposures as illustrated in the lower sketch of the figure. The solid line again represents the noise levels of a current subsonic aircraft and the hatched areas represent the ranges of estimates by the two contractors for SCAT 16 and 17, hot-day operation being assumed. It can be seen that the SCAT 16 noise levels are generally lower than those of SCAT 17. The data of the figure seem to indicate, however, that either configuration might have noise levels comparable to or lower than those of the current airplane when operated as in the top sketch of the figure.

In summary of these two plots, it can be seen that the noise levels for the supersonic aircraft will be higher within the confines of the airport and the immediate surrounding areas. At greater distances there is an indication, however, that either configuration might have noise levels comparable to or lower than those of the current airplane, depending on the operational procedures used.

The state of development of the configurations studied has not progressed to the point where the optimum take-off and climbout procedures have been determined. It should be noted, however, that the supersonic transport aircraft has inherent operational flexibility that would

permit a power cutback, as illustrated, or some other altitude-distance profile that might be more attractive.

LANDING APPROACH

The noise during landing approach can be discussed with the aid of figure 5 and involves the geometry of the engine installation and the aircraft operating characteristics. Shown in the figure are perceived noise levels as a function of distance from touchdown for SCAT 16, SCAT 17 (based on the contractor studies), and a comparable current fan-powered subsonic aircraft. A 3° glide slope has been assumed in all cases. The solid line represents the perceived noise levels on landing-approach for the current subsonic airplane. The upper bounds of each of the shaded areas represent the landing-approach noise levels for SCAT 16 and SCAT 17, hot-day operations with no inlet noise suppression being assumed. It can be seen that the SCAT 16 noise levels are lower than those of SCAT 17 as a result of its better low-speed aerodynamics which permit it to approach at lower engine power settings. However, the SCAT 16 noise levels at best only approach those that are currently experienced on the subsonic aircraft.

The extent of the shading which is shown for the two SCAT configurations indicates the variation in perceived noise levels that have been estimated for varying amounts of inlet noise suppression. These estimates of the perceived noise levels for inlet noise suppression based on contractors' past experience varied from 6 to 12 decibels. The point to be made is that some inlet noise suppression will be required to bring the landing noise levels of the SCAT configurations below those of the current subsonic aircraft.

"he significance of geometry is suggested in figure 6, in which are shown schematic diagrams of a subsonic and a supersonic engine installation. The shading represents the extent of the inlet surface area.

For current subsonic airplanes it is generally agreed that the inlet noise during landing approach is more objectionable than the exhaust noise, and thus accounts for most of the registered complaints. As suggested by the shading of the upper sketch, there is only a limited area for application of noise reduction procedures. In the case of the supersonic transport, however, the situation may be considerably different since there is a greater working area. In addition, there is the possibility of deliberately choking the flow, and in this regard a concerted effort is being made in NASA research studies to evaluate inlet noise reductions by means of variable inlet geometry with particular application to the landing-approach condition and associated operating problems.

[redacted]

It is obvious from the data of these two figures that the landing-approach noise problem should be considered as a major design goal. It is believed possible to reduce the landing-approach noise levels through further improvements in the low-speed aerodynamics and through suitable inlet noise-suppression procedures.

STRUCTURAL RESPONSE TO NOISE

The noise-induced structural-response problems of the supersonic transport which are important from the standpoint of maintaining acceptable cabin noise levels and minimizing sonic fatigue can be discussed with the aid of figure 7. The shaded areas of the airplane plan view sketch at the top of the figure represent regions where noise loads may be a design consideration. At the bottom of the figure are sample flow noise and engine noise input spectra estimated for the proposed operating conditions of the airplane. The flow noise loading will exist for nearly the entire duration of the flight. The curve of the left diagram is based on recent NASA free-flight measurements at the appropriate Mach numbers and Reynolds numbers. (See ref. 2.) For some local flow separation, surface roughness, or shock-wave — interaction conditions, the levels would be higher as indicated by the shading. For these latter conditions the estimated spectral content (shaded area of fig. 7) which is based on results of recent contract wind-tunnel studies by the Douglas Aircraft Company is similar to that given by the solid line.

The noise from the engines is believed to be significant for only a short period during each mission, and only the structure in the vicinity and to the rear of the engines, as indicated by the cross-hatching in the sketch, will be affected. It can be seen that the estimated spectra peak at lower frequencies and reach higher sound pressure levels than the flow noise spectra. (See ref. 3.)

Some brief comments with regard to structural design are suggested by the data of the figure. Although the acoustic loads are more severe than those for current aircraft, the design of structures to withstand these loads is not a brand new problem since similar environments have been encountered in other current operational vehicles. It is believed that engine noise structural response experience to date is directly applicable; however, the flow noise problem has not been satisfactorily defined, particularly for long-term exposures at elevated temperatures. Both the flow noise inputs and associated structural responses are currently being studied in NASA research programs.

[redacted]

CONCLUDING REMARKS

The results presented in the paper are based on proposed engine and airplane configurations, and it should be emphasized that no noise data were furnished to the contractors. Because of their present state of development, it is only possible to indicate broad ranges of noise predictions. The higher thrust engine proposed for the supersonic transport will result in relatively higher noise levels in the airport confines and in the areas immediately adjacent to the airport. Because of its predicted operational flexibility, however, the climbout and landing-approach community noise levels may be lower than those of current aircraft of similar range. The most urgent research problems relate to optimizing low-speed aerodynamic characteristics of the aircraft, minimizing inlet noise, and defining the flow noise-induced structural-response problem.

REFERENCES

1. Bolt Beranek and Newman, Inc.: Studies of Noise Characteristics of the Boeing 707-120 Jet Airliner and of Large Conventional Propeller-Driven Airliners. Prepared for The Port of New York Authority, Oct. 1958.

2. Hilton, David A., Bracalente, Emedio M., and Hubbard, Harvey H.: In-Flight Aerodynamic Noise Measurements on a Scout Launch Vehicle. NASA TN D-1818, 1963.

3. Trapp, W. J., and Forney, D. M., Jr., eds.: WADC - University of Minnesota Conference on Acoustical Fatigue. WADC Tech. Rep. 59-676, U.S. Air Force, Mar. 1961.

[redacted]

TABLE I

NOISE FROM VARIOUS ENGINES

DISTANCE = 1,000 FT

ENGINE	THRUST, LB	SOUND PRESSURE LEVEL, db	PERCEIVED NOISE LEVEL, db
PROPOSED			
TURBOJET, AUGMENTED	45,000	129	136
TURBOJET	45,000	125	133
TURBOFAN, AUGMENTED	45,000	124	130
TURBOFAN	45,000	114	123
TURBOFAN	17,000	104	115

[redacted]

[redacted]

NOISE PROBLEM AREAS DUE TO POWER PLANT AND AIRFLOW

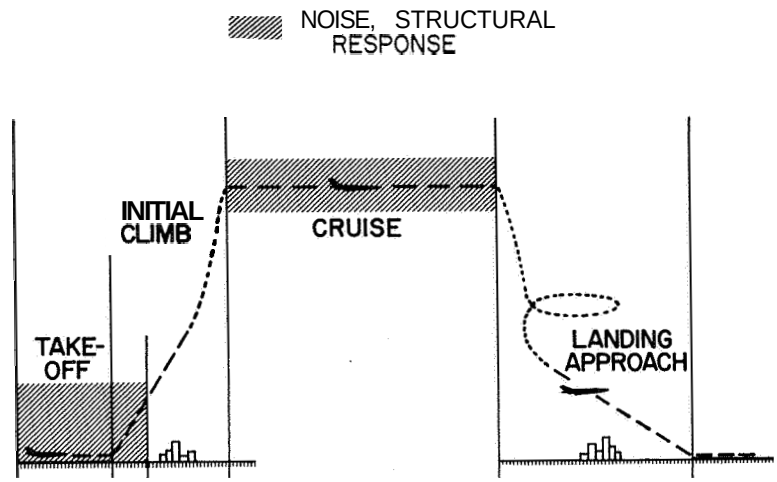

Figure 1

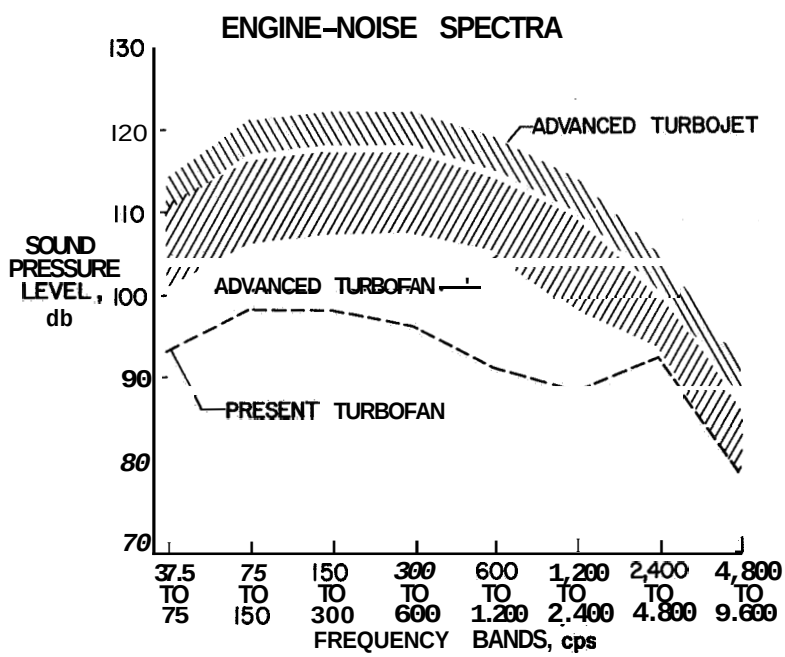

Figure 2

[redacted]

[redacted]

NOISE-LEVEL CONTOURS FOR TAKE-OFF

PERCEIVED NOISE LEVEL, 110 db

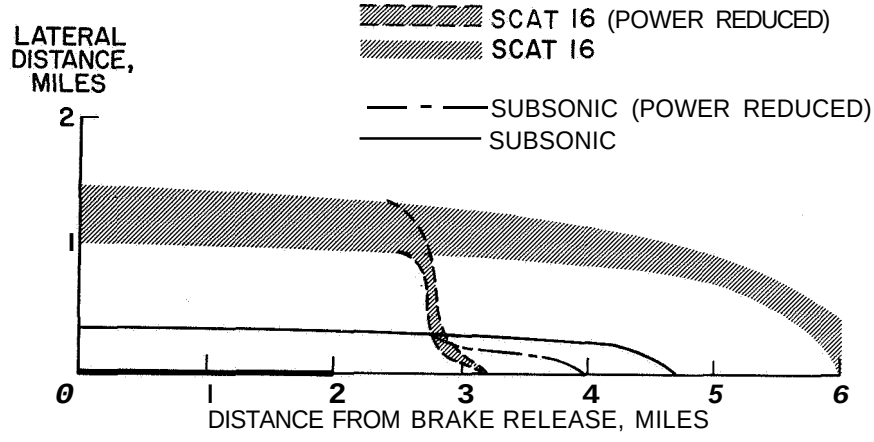

Figure 3

NOISE DURING CLIMBOUT

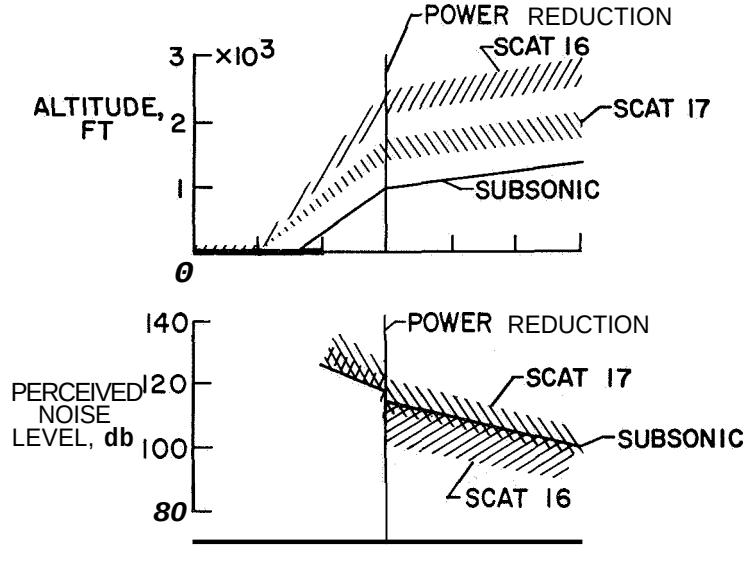

Figure 4

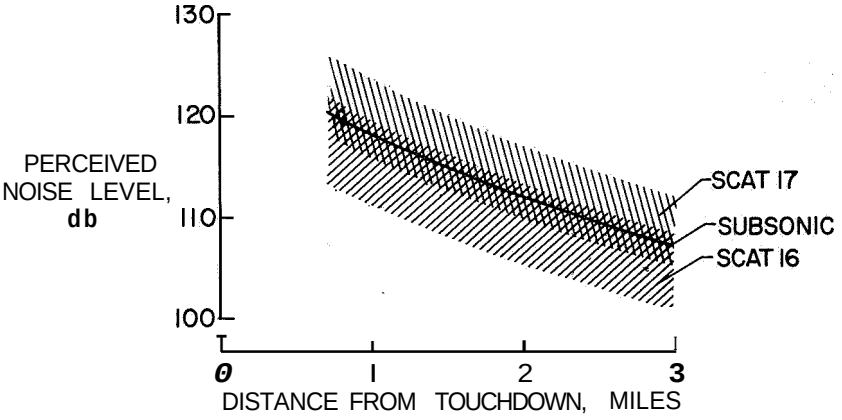

Figure 5

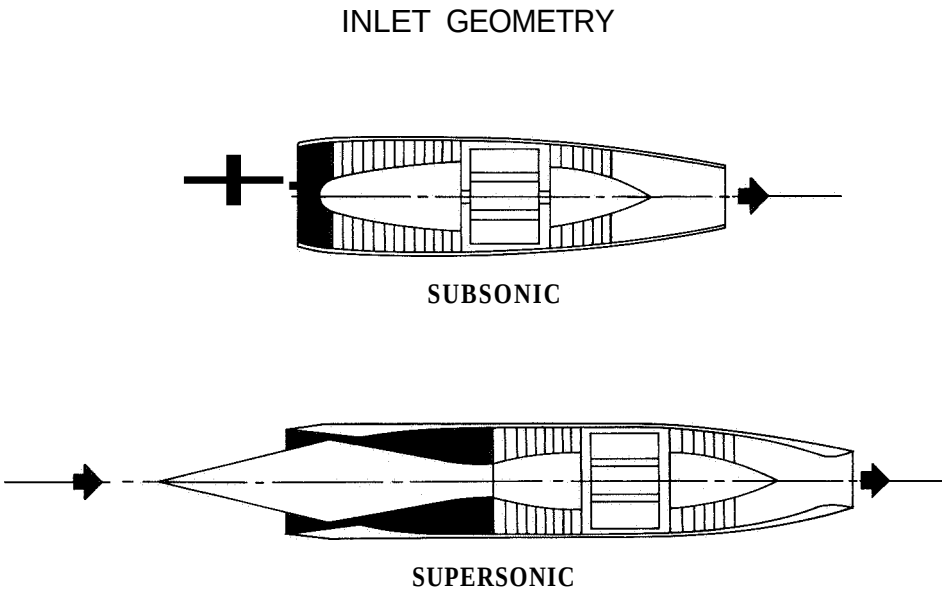

Figure 6

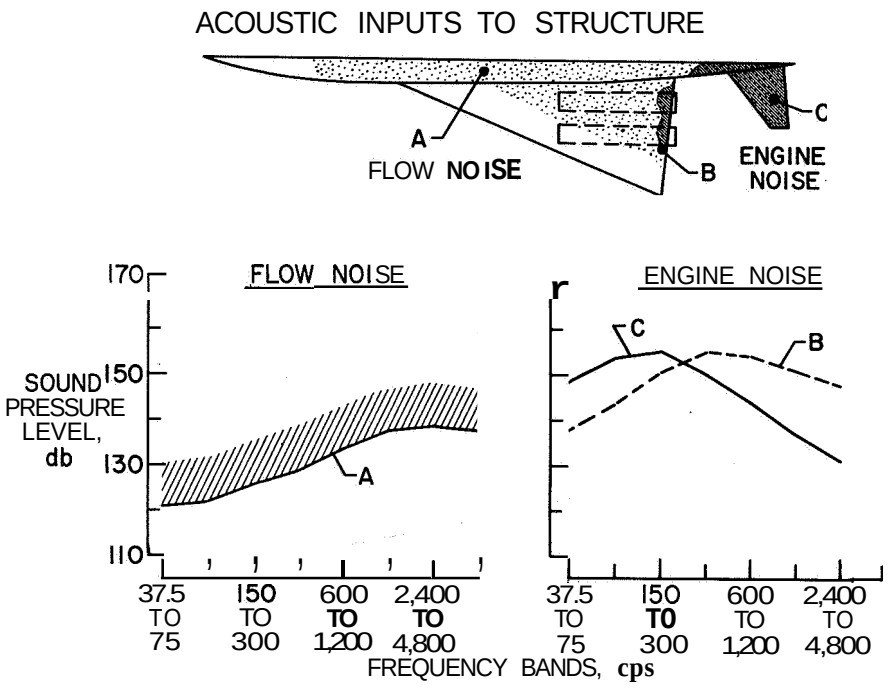
ACOUSTIC INPUTS TO STRUCTURE
A
FLOW NOISE
B
C
ENGINE NOISE
FLOW NOISE
ENGINE NOISE
170
150
130
110
SOUND PRESSURE LEVEL, db
A
B
C
37.5 TO 75
150 TO 300
600 TO 1,200
2,400 TO 4,800
FREQUENCY BANDS, cps

Figure 7

PRECEDING PAGE BLANK e A FILMED

DECLASSIFIED

N67-31631

24. OPERATIONAL FACTORS IN RELATION TO SUPERSONIC-TRANSPORT FUEL REQUIREMENTS

By Joseph W. Wetmore and Joseph W. Stickle

NASA, Langley Research Center

SUMMARY

An analysis of the interaction of operational environment and aircraft characteristics of the supersonic transport (SST) in the area of fuel requirements has been made. The increment in design range or fuel-carrying capability above that of the basic trip distance is considered in relation to the effects of wind, temperature, anticipated flight-level assignment, and payload load factor.

Reserve fuel requirements are discussed and a statistical approach is used in determining en route and holding reserves. It is indicated that protection equivalent to that provided for subsonic jets by current reserve requirements is obtained for the supersonic transport with less than the present Civil Air Regulation (CAR) en route and holding requirements.

INTRODUCTION

A complete understanding of all the factors which will affect the operations of the SST can only be gained from service experience with the actual airplane in its own operational environment. Nevertheless, it is necessary at an early stage to anticipate and account for these operational factors to the fullest extent possible where they may have an important bearing on the design and ultimate capabilities of the airplane. The purpose of this paper is to examine the interaction of operational environment and aircraft characteristics of the SST in the very important area of fuel requirements.

With the use of statistical approaches, two aspects of fuel requirements are analyzed. First, the design range or destination fuel will be considered in relation to the effects of wind, temperature, anticipated flight-level assignments, and payload load factors. The other area of consideration is fuel reserves in which en route reserves, accounting for various uncertainty factors, as well as fuel for holding and diversion to alternate airports are discussed. Fuel allowances for en route engine failure are related to the reserve needs for the more normal operational variations.

[redacted]

DESIGN RANGE

The design fuel-carrying capability of the supersonic transport should provide a rational margin to allow for likely variations of those factors which a dispatcher normally accounts for in planning destination fuel. Destination fuel is considered to be that fuel required to fly to and land at the destination. In the following discussion, the statistical effects of these factors on destination fuel requirements are presented in terms of variations in standard atmosphere and still-air range relative to the basic trip distance of the aircraft, here taken to be from New York to Paris or 3,160 nautical miles.

Atmospheric Effects

One of the primary factors to be accounted for in determining destination fuel is the expected atmospheric conditions en route, that is, winds and temperatures. The statistical characteristics of the east-west effective wind component and effective temperature difference from international standards (refs. 1 and 2) are shown for the winter season, December through February, and the summer season, June through August, in table I. In the case of wind, the effective means and standard deviations are shown separately for climb and descent and for cruise. The temperature variations from standard are averages for the critical climb-and-accelerate range of altitudes and are assumed to apply to the whole flight since the effects of temperature are most important in the climb-and-accelerate stage. The mean winds and variability are considerably greater in the winter, particularly at cruise altitudes, than in the summer. The summer mean temperatures are higher, as would be expected, but the standard deviation is somewhat less than in the winter.

The increment of still-air range required to account for the effect of wind is, of course, the product of the average wind during the flight and the flight time. Primary consideration is given to westbound flights to account for the adverse effects of prevailing head winds.

The effects of temperature on incremental range required were calculated specifically for the variable-sweep supersonic-commercial-air-transport SCAT 16 configuration with turbofan engine B of the feasibility studies, sized to yield representative climb-and-accelerate performance. However, similar effects were indicated by limited calculations for the fixed-delta SCAT 17 configuration powered for equivalent basic performance. In general, each degree of temperature

[redacted]

variation above standard required between 6 and 7 nautical miles of additional range.

Both the wind and temperature variations have approximately Gaussian, or normal, distributions. Since the effects of wind and temperature on incremental range required are nearly linear throughout the range of conditions of interest, the corresponding distributions of incremental range required are also normal. Therefore, the combined effects of temperature and wind were incorporated in the probabilities of requiring given range increments by the usual methods applicable to normal frequency distributions.

A comparison is given in figure 1 of winter and summer conditions for the combined effects of wind and temperature on the probability that the increment in standard-day no-wind range required to achieve the westbound trip with full payload will equal or exceed given values. These results indicate that a greater range increment is required for winter than for summer conditions. For example, to compensate for possible adverse wind and temperature conditions for all but 1 percent of winter flights, the airplane should have a design-range capability about 244 nautical miles greater than the basic trip distance. For summer conditions the range increment for the same probability level would be 200 nautical miles. The winter condition is therefore assumed in the following discussion of the effects of other factors. The 1-percent probability level will also be used in evaluating these effects, but only for purposes of illustration. It is not within the purpose of this analysis to suggest the probability level that should ultimately be selected for design.

Effect of Flight-Level Assignment

Thus far it has been assumed that the airplane would always cruise at optimum altitude. It is quite likely, however, that the supersonic transports, as for present trans-Atlantic jets, at times will be assigned flight levels other than optimum altitude to provide adequate separation from either high-flying military aircraft or from other supersonic transports. Figure 2 illustrates the effect on the incremental range required of flying at altitudes other than optimum for a typical supersonic transport. Here again, incremental range is a representation of the added fuel required in terms of the increased range it would provide under standard-temperature still-air optimum-altitude conditions. It is shown that for small deviations from optimum, the effects of off-design altitude are about the same, whether the flight altitude is above or below optimum level. However, for larger deviations, flying above optimum altitude entails a somewhat greater penalty than flying below optimum altitude. A preliminary

[redacted]

estimate has indicated that all the one-direction supersonic-transport traffic of the same type could be accommodated at three levels, separated, as at present, by 4,000-foot increments. Thus, all flights in one direction could cruise within 4,000 feet of optimum altitude which, as indicated in the figure, would give a penalty of about 65 and 80 nautical miles in range increment required, for below- and above-optimum altitude conditions, respectively.

It was assumed that for all westbound flights one level would be required for one-third of the time, two levels, for one-third of the time, and three levels, for the remaining third of the time. In other words, one-half of all flights would be made at optimum altitude and the remaining flights, 4,000 feet above or below optimum.

A probability curve of incremental range required, incorporating the effects of this distribution of discrete-altitude assignments, together with winter wind and temperature effects, was computed and is shown in figure 3. A corresponding curve for all flights at optimum altitude is given for comparison. Again, with the 1-percent probability level, the results indicate that if three cruise flight levels are required for westbound supersonic-transport traffic, the increment in design range over the basic trip distance should be about 288 nautical miles or about 44 nautical miles greater than if all flights could cruise at optimum altitude.

Effect of Payload Load Factor

In the preceding discussion of the factors of weather and flight-level assignments, the objective of carrying full payload for a large percentage of flights was assumed. However, a 100-percent load factor, for passenger payload at least, is not a practical goal because of the variability of demand for accommodations. Therefore, unless the assumption can be made that variability in passenger payload can be compensated by providing excess cargo capacity in the airplane and standby cargo, the load factor will be substantially less than 100 percent. Allowing for a reduced average load factor and a suitable variation about this average would tend to reduce the design-range increment required to limit to a reasonable frequency the need for denying requested accommodations. Average passenger load factor for the supersonic transport has been variously estimated between 55 and 70 percent of capacity.

The effect of load factor on the range increment required is illustrated by assuming a normal distribution of load factor about a mean value of 60 percent with a standard deviation of 12 percent (20-percent standard deviation of demand). It is further assumed that

the design or capacity payload is 7 percent of design take-off gross weight. The effects on range capability of the variations of take-off weight resulting from this varying payload were computed and combined statistically with the effects of winter wind and temperature conditions and variation in flight-level assignments discussed previously.

The overall effect of these factors on the probability of requiring incremental range capability is shown in figure 4. For comparison, the probability curve from figure 3 for the corresponding 100-percent-mean-load-factor case is given. The results indicate that allowing for the assumed variability in load factor considerably reduces the incremental range required to provide a given probability of meeting the demand for seats. For the 60-percent mean load factor, a design range increment of approximately 160 nautical miles should be sufficient for all but 1 percent of the winter westbound flights, whereas, if the goal were to be the 100-percent mean load factor of mixed passengers and cargo payload, range increments of 288 nautical miles would be needed at the same probability level.

FUEL RESERVE REQUIREMENTS

En Route Factors

There are a number of factors which introduce some uncertainty in the determination of en route or destination fuel. These factors, together with estimated standard deviations from their predicted values and the corresponding variabilities calculated for en route fuel requirements, are listed in table II. The standard deviation of incremental fuel requirement due to each factor is shown as a percent of the predicted destination fuel requirement. It is indicated that the effect of variations between forecast and actual wind velocity is relatively small for the supersonic transport, whereas, for the subsonic jet, uncertainty in accounting for wind effects has been indicated to be the primary factor in en route reserve requirements. The primary factor, in the case of the supersonic transport, is shown to be variability in specific fuel consumption.

The estimate of 4-percent standard deviation in specific fuel consumption for each engine is a third greater than values that have been used for subsonic jet engines; this estimate allows for the possibility of more variability with the more complex supersonic engines. With four engines, the overall standard deviation in specific fuel consumption, hence, in fuel consumed, reduces to 2 percent. The next most important factor is indicated to be drag variation. This variation is assumed to have a standard deviation of 1.5 percent among different airplanes

of the same design and is based on observations of speed variations for subsonic transports. The effects of each of the other factors are 0.5 percent, or less, in standard deviation of fuel required. The combined effects of the listed factors give a standard deviation in destination fuel required of 2.55 percent. When these factors are applied to a subsonic transport for comparison, the standard deviation in destination fuel is 4.05 percent.

Combined En Route and Holding Requirement

It is apparent that protection in the form of reserve fuel, referred to as en route reserve, will be required to allow for those occasions in which the foregoing variability of fuel consumption results in burning more fuel than the planned destination fuel. On other flights, however, this added fuel would not be used and would be available for holding at the destination. It would appear logical, therefore, to consider these two reserve requirements together, with the ultimate objective of limiting to a reasonable frequency the need for diversion to an alternate airport because of fuel limited holding time. To this end, holding-time statistics for subsonic jet transports have been obtained from an airline source for the New York International Airport. These data indicated that 23 percent of the arriving flights during 1962 were delayed for clearance by Air Traffic Control for an average of 10 minutes. Inasmuch as the frequency distribution of these delays was not available, it was assumed that they would be described by the positive half of a Gaussian, or normal, distribution which would give the 10-minute mean delay. Accordingly, the frequency distributions of fuel consumption corresponding to these holding times were calculated for a delta and a variable-sweep supersonic transport and combined with the en route reserve statistics to give the probability curves shown in figure 5.

These curves indicate the probabilities of exhausting given amounts of combined reserve fuel. The reserve fuel ΔW_F is shown divided by the destination fuel $W_{D.F}$. Further delay would then require either proceeding to the alternate airport or consuming alternate reserve fuel. In order to obtain a realistic probability level, hence, the reserve fuel which should be provided for the supersonic airplanes, a similar analysis to that described was made for a subsonic jet transport and the probability curve for this case is also shown. The CAR en route plus holding fuel was then determined for the subsonic transport and is indicated by the vertical line. The intersection of this line with the probability curve for the subsonic transport indicates the probability level of equaling or exceeding the CAR reserve which is assumed to be acceptable. The reserve fuel required to give the same probability of exhausting en route and holding reserves is shown to be about 10 percent for the variable-sweep supersonic transport and about 11 percent for the

delta-wing supersonic transport. The combined en route reserve (10 percent of trip time) and holding reserve (30 minutes at 1,500 feet), as specified for subsonic turbine transports in CAR 41,* were computed for both aircraft and faund to be 13 percent and 14 percent of destination fuel for the variable-sweep and delta wings, respectively, or about 3 percent of the destination fuel greater than the values determined by the statistical. procedure utilized in this paper.

Two-Engine Failure

The possibility of two-engine failure, even though remote, requires that the airplane carry sufficient fuel on board to proceed, with two engines stopped, from any point en route to a suitable airport. If the fuel required in this case were to exceed the planned destination fuel by more than the amount provided by the en route, holding, and diversion reserves, the reserve fuel allowance would be, in effect, determined by this contingency.

It was found that the two-engine range potential of both the variable-sweep and delta configurations is better at subsonic speeds than at supersonic speeds. The range remaining at various points along the route after two-engine failure was computed for both configurations for a Mach number of 0.80 and the corresponding optimum altitudes. It was assumed that fuel for diversion to an alternate airport 250 nautical miles distant would be available in addition to en route and holding reserve fuel determined by the procedure of the preceding section entitled "Combined En Route and Holding Requirement."

The range remaining after two-engine failure is plotted against distances from the origin airport at which failure occurred in figure 6 for the two configurations. It is assumed that at landing, fuel burnout of destination and reserve fuel is complete. The two 45° lines (dashed) represent the distance for either returning to the origin or proceeding to the destination. The lower boundary indicates the distance to the nearest adequate alternate airport along the route from New York to Paris. Inasmuch as neither the variable-sweep nor the delta-wing transport falls below the alternate boundary, the reserve fuel allowance provided is sufficient to meet this requirement. It should also be noted that, except for this small portion near the midpoint of the flight, the variable-sweep transport could either return to the origin or proceed to the destination.

---

* Anon.: Certification and Operations Rules for Certificated Route Air Carriers Engaging in Overseas and Foreign Air Transportation and Air Transportation Within Hawaii and Alaska. Civil Air Regulations Part 41, Rules Service Co. (Washington, D.C.), May 6, 1963.

CONCLUSIONS

In conclusion, this analysis of operational factors in relation to fuel requirements for the supersonic transport has indicated the probabilities of requiring additional design-range capability above the basic trip distance to allow for the effects of atmospheric variations, flight-level assignments, and payload load factors. It is shown, for example, that with all the factors considered and the assumptions used, an addition of about 160 nautical miles to the basic trip distance. from New York to Paris would be sufficient to permit acceptance of all payload offered except for 1 percent of the flights.

In the area of fuel reserves, it was found that 10 percent of the destination fuel for the variable-sweep supersonic transport and 11 percent for the delta-wing supersonic transport would provide equivalent protection to that given subsonic jet transport operations by the combined civil air regulations (CAR) en route and holding requirements. These reserves for the supersonic transport represent a savings equivalent to about 3 percent of the destination fuel over those calculated by using CAR en route and holding requirements.

It was also found that these reserves, in combination with a planned alternate airport 250 nautical miles distant, would provide ample fuel to proceed at subsonic speeds to an adequate airport in the event of a two-engine failure anywhere en route from New York to Paris.

REFERENCES

1. Crutcher, Harold L.: Climatology of the Upper Air as Related to the Design and Operation of Supersonic Aircraft. Weather Bur., U.S. Dept. Commerce, Mar. 1963.

2. Tolefson, H. B.: Atmospheric Temperature Observations to 100,000 Feet for Several Climatological Regions of the Northern Hemisphere. NACA TN 4169, 1957.

DECLASSIFIED

TABLE I.- VARIATION OF ATMOSPHERIC CONDITIONS FROM STANDARD

Season	Flight phase	Mean wind, knots (a)	Standard deviation, knots	Mean temperature, °F (b)	Standard deviation, °F
Winter	Climb and descent	37 W	522	-4.1	510.2
	Cruise	33 W	±18		
Summer	Climb and descent	26 W	±19	+5.9	±7.6
	Cruise	2 W	±8		

TABLE II.- EN ROUTE RESERVE FUEL FACTORS

Factor	Standard deviation	Standard deviation in fuel required, percent of planned destination fuel
Wind	10 knots	0.46
Temperature	4° F	.50
Drag	1.5 percent	1.33
Specific fuel consumption	4 percent (each engine)	2.00
Fuel-gage error	0.5 percent	.50
Navigation errors	58 nautical miles (lateral)	.06
Weather avoidance	58 nautical miles (lateral)	.06
Air traffic control	58 nautical miles (lateral)	.06
Altimetry error	100 ft at 65,000 ft	.10
Combined standard deviation of destination fuel = 2.55 percent		

EFFECT OF WIND AND TEMPERATURE ON
INCREMENTAL DESIGN-RANGE REQUIREMENTS

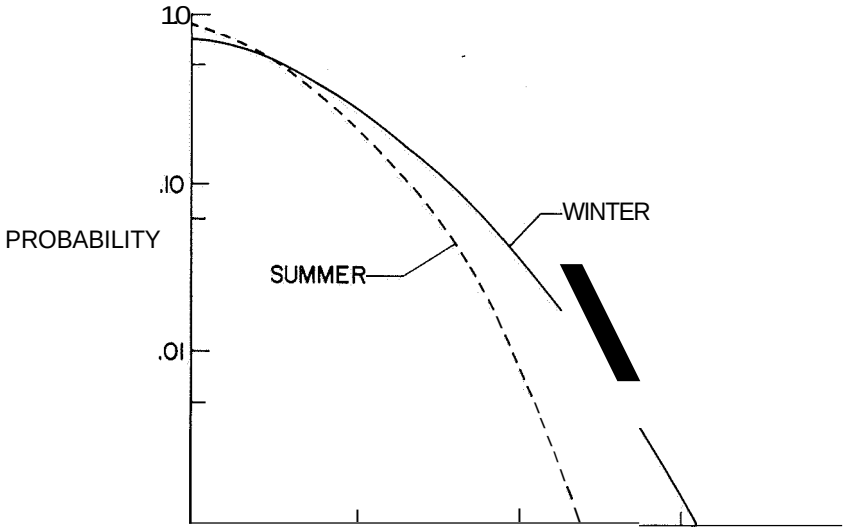

Figure 1

EFFECT OF OFF-DESIGN ALTITUDE ASSIGNMENT ON
DESIGN-RANGE INCREMENT REQUIRED
BASIC RANGE = 3,160 N. MI.

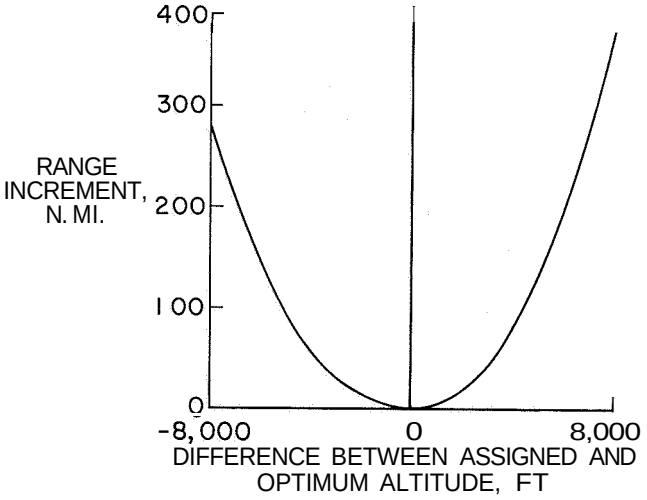

Figure 2

[redacted]

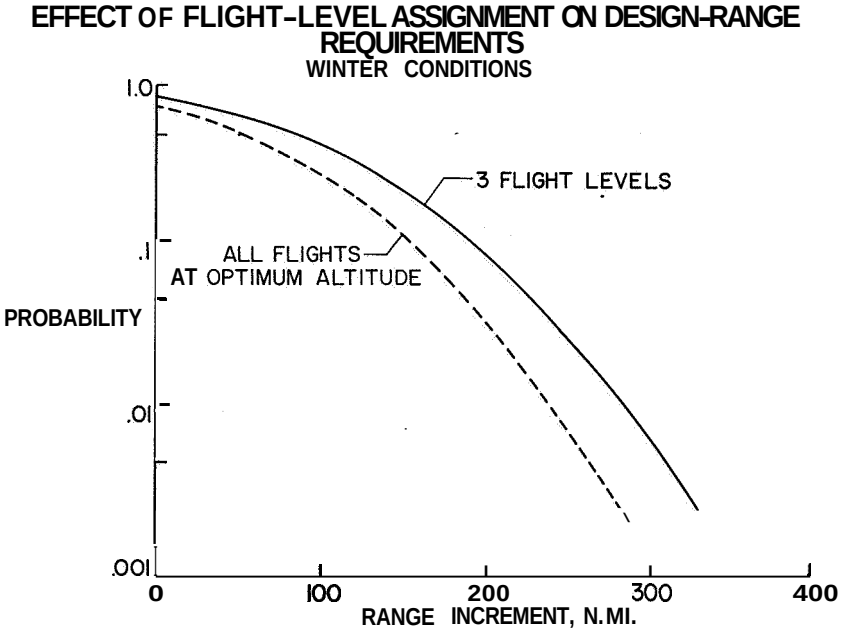

Figure 3

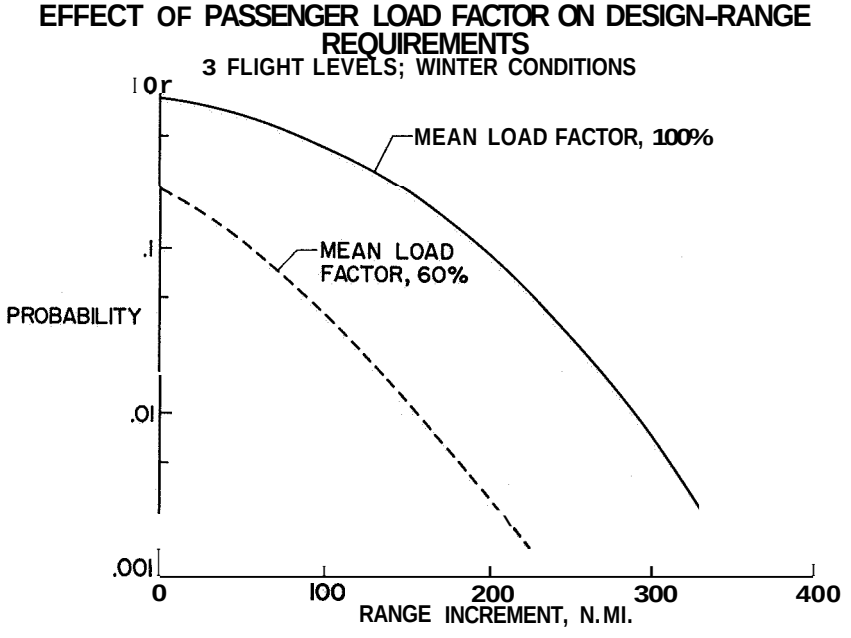

Figure 4

[redacted]

DECLASSIFIED

PROBABILITY OF RESERVE FUEL REQUIREMENT
EN ROUTE AND HOLDING FUEL

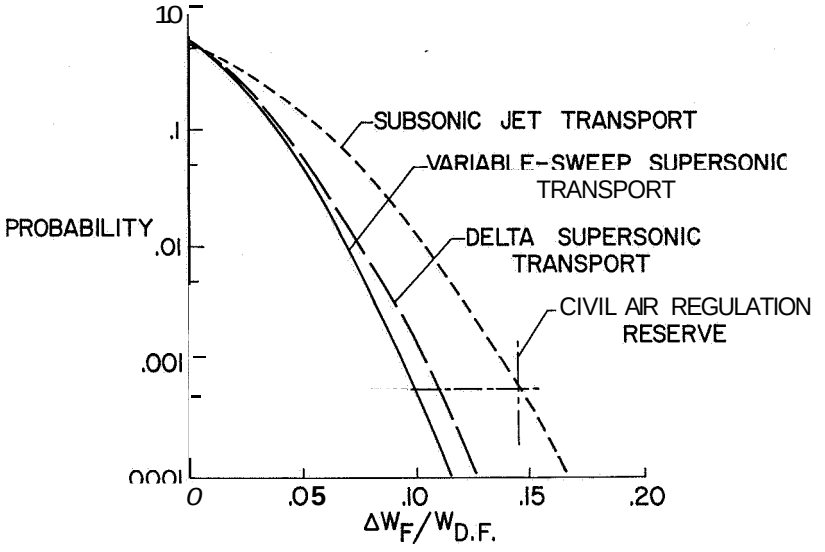

Figure 5

SUBSONIC RANGE REMAINING AFTER TWO-ENGINE LOSS

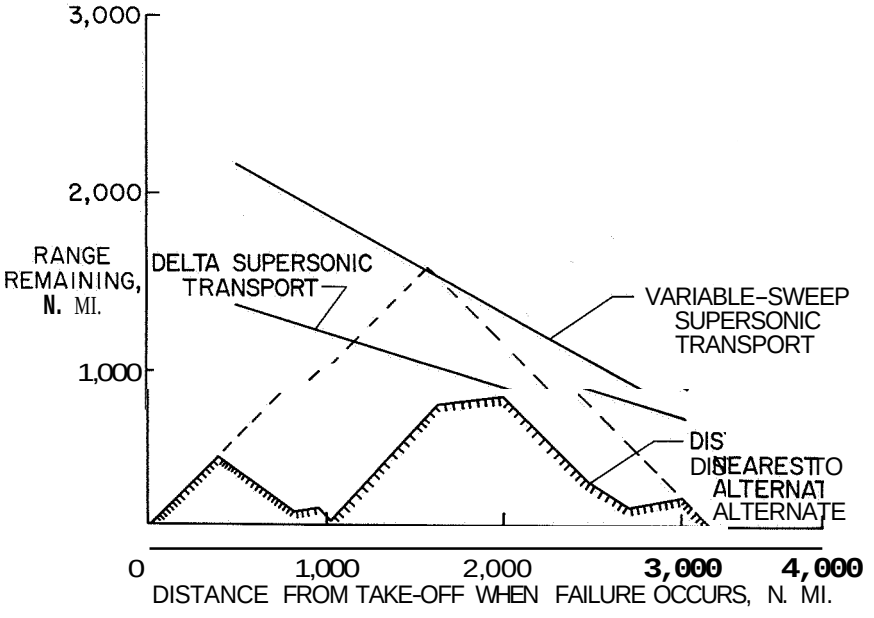

Figure 6

RELEASED

N67-31632

25. CONSIDERATION OF SOME AIRWORTHINESS REQUIREMENTS FOR SUPERSONIC TRANSPORTS

By Thomas L. Coleman Jr.

NASA Langley Research Center

SUMMARY

Some airworthiness requirements for supersonic transports in the areas of structural design criteria, performance, and handling qualities are discussed. Several areas are indicated wherein present Civil Air Regulations are not directly applicable to the supersonic transport. For some areas, it appears that the requirements can be adapted to supersonic-transport configurations by only minor modifications or extensions. For other areas, it appears that basic concepts on which the requirements are based will require reexamination.

INTRODUCTION

That supersonic transports be sufficiently airworthy to maintain, or improve, current levels of safety *is* a matter of concern to airline operators, manufacturers, Government regulatory agencies, and the NASA. Although NASA is not charged with the responsibility of specifying airworthiness requirements, it does have a role in anticipating airworthiness problems, conducting research to find solutions, and in disseminating research results to the aviation community.

Airworthiness is interwoven with the aerodynamic and propulsion characteristics, the operational environment, and the manner that the airplane is flown. Research in the airworthiness area is a continuing effort involving the accumulation **and** extrapolation of fundamental knowledge and operational experience to new configurations and anticipated operating conditions. In some cases, this research has stayed ahead of the problems but, in other cases, has fallen behind.

NASA research, the supersonic-tsansport feasibility studies, and discussions with various aviation groups have given an insight into some airworthiness aspects **of** supersonic transports. In this paper, the information from these sources are discussed to indicate the state of the art in several airworthiness areas. The paper will highlight a few airworthiness items which, if the thesis of maintaining current levels

25

of safety is accepted, could have a bearing on the merits of the configurations and the operating procedures.

The discussion will touch on three broad areas of airworthiness: (1) structural design criteria, (2) performance, and (3) handling qualities. Each of the three areas will be more specifically covered in subsequent sections.

SYMBOLS

V_A	maneuvering speed
V_B	rough-air speed
V_C	cruise speed
V_D	dive speed
M	Mach number
C_L	lift coefficient
$(C_L)_{MAX}$	maximum lift coefficient
$(C_L)_{OPERAT}$	operational lift coefficient
a	angle of attack
$(C_L)_{USEABLE}$	useable lift coefficient
ΔV	airspeed error
V_{ACTUAL}	actual airspeed
V_{TARGET}	target airspeed
F	thrust
W	weight
$C_{1/2}$	cycles to damp to one-half amplitude

RELEASED

DISCUSSION

Structural Design Criteria

Structural design speeds.- The strength requirements and operational airspeed limits for transport airplanes are tied directly to a set of structural design speeds. Figure 1 illustrates a set of these speeds in terms of the variation of Mach number with altitude for a supersonic transport. The curves labeled maximum lift, buffet, engine blowout, maximum temperature, airframe and engine strength, and flutter are boundaries imposed on the airplane by aerodynamic, propulsion, and structural characteristics.

The flight region is bounded on the low-speed side by the maneuvering speed V_A and the rough-air speed V_B. These are the speeds at which the airplane can develop full load factor or withstand the maximum gust velocity without stalling or overstressing the structure. The high-speed side of the flight region is bounded by the design cruise speed V_C, which is the maximum speed for normal flight operations. The speed spread between V_C and the design dive speed V_D is a margin provided to insure structural integrity in the event of overspeeds caused by such factors as: airplane upset in turbulence, traverses of wind and temperature gradients, and inadvertent speed exceedances of V_C by the pilot.

Several problem areas appear to exist in adapting current Civil Air Regulations and concepts to specifying the structural design speeds to supersonic transports and these areas are:

(1) The procedure of basing the maneuvering speed V_A on a maximum lift coefficient may not be feasible for low-aspect-ratio configurations since, as will be discussed subsequently, the maximum lift occurs at such high angles of attack as to be operationally impractical. A possible approach is to base the speed on an attitude limit of the airplane.

(2) The concept of the rough-air speed V_B may not be applicable to the supersonic transport because:

(a) At subsonic speeds, slowing down from V_C to V_B, traversing rough air, and then regaining speed will be unattractive from the fuel-requirement standpoint.

(b) At supersonic speeds, the airplane response characteristics are such that no appreciable reduction in gust loads can be obtained unless speed is reduced to subsonic values. In addition, it is doubtful whether the turbulence can be detected sufficiently in advance to permit slowing down prior to traversing the turbulence.

Consequently, it is thought that the rough-air speed and slowdown concepts may not be applicable to supersonic transports. This condition would imply that the supersonic transport may have to be designed for the maximum gust velocity at a speed higher than V_B, possibly at the design cruise speed V_C.

(3) In regard to the design cruise speed V_C, it is thought that the current practice of permitting the manufacturer to select the speed will be as applicable to the supersonic transport as it is for present transports.

(4) The present requirement for determining the minimum speed margins between V_C and V_D may not be adequate for the supersonic transport. This apparent inadequacy is due primarily to the much higher thrust-weight ratio anticipated for the supersonic transports than for present transports. The higher thrust-weight ratio increases the possibility of inadvertent overspeeds following transition from climbing flight to level flight, or from level flight to descending flight. Overspeeding is an operational problem on present transports (ref. 1) and is likely to be one with supersonic transports unless attention is given to this potential problem area.

Limit loads.- It is likely that the supersonic transport will be designed, as are present transports, for limit loads resulting from maximum expected in-flight and ground loads. In this section, three sources of loads - vertical velocity at landing impact, gust loads, and maneuvers - will be discussed.

Vertical velocity: Present Civil Air Regulations (ref. 2) require that transports be designed for a limit vertical velocity, or sinking speed, of 10 feet per second at touchdown. There is some question as to the applicability of this value to the supersonic transports. As shown in figure 2, this question stems from the evidence that the vertical velocities of current turbojet transports are significantly higher than those experienced by piston transports. (See ref. 1.) For example, 1 landing in 100 exceeds a vertical velocity of about 2.5 feet per second for piston transports and about 5 feet per second for turbojet transports. As a point of interest, an extrapolation of the turbojet curve indicates that a vertical velocity in excess of about 6 feet per second would be expected in the estimated 2,000 landings made each day by the U.S. turbojet fleet.

Simulator studies aimed at determining the causes of the increased vertical velocities have been conducted by NASA (ref. *3)* and, also, are being conducted under a contract sponsored by the Federal Aviation Agency. So far, however, the reasons for the increased vertical velocities of the turbojets over the piston transports have not been determined. It

is thought, though, to be due in large part to the turbojets having a more sluggish response to pilot control inputs during the flare maneuver. (See ref. 1.) Studies have indicated that the flare-response characteristics of supersonic-transport configurations may be decreased from that for present turbojets. In this event, it may be that the supersonic transports will experience higher vertical velocities than present transports. If this is true, the question arises as to whether the 10-feet-per-second design value is adequate for the supersonic transport. This question cannot be simply answered but, rather, it must be considered from the viewpoint of maintaining a minimum level of safety. In this regard, the answer will depend, to a large extent, on the basis (number of flights, flight hours, flight miles, or a fleet concept) used to define the level of safety.

Gust loads: In view of the new configurations, increased operating speeds, and altitudes of the supersonic transport, it is well to consider the implications of these changes relative to gust loads. The plot on the left of figure 3 summarizes information on the average percent time that rough air has been experienced by subsonic airplanes at the various altitudes (ref. 4). The portion of this curve below 40,000 feet is based, to a large extent, on data collected during transport operations. Above 40,000 feet, the curve is based on military operations and special flight investigations. As shown, the amount of rough air decreases rapidly with increasing altitude, but is still present about 2 percent of the time at altitudes between 60,000 and 75,000 feet. Although not shown here, the intensity of the turbulence also decreases with increasing altitude. Additional data on the turbulence environment are being obtained by the NASA and by the U.S. Air Force from measurements made during routine operational flights and also from special investigations.

Studies considering the turbulence environment together with the supersonic-transport flight profiles and response characteristics have indicated that the transonic flight region (fig. 3) is likely to result in the most critical gust loadings. Also, the studies indicate that the low-altitude turbulence environment associated with subsonic flight is likely to be a more prolific source of repeated gust loads than the turbulence environment at high altitude associated with supersonic flight. The high supersonic flight region is not expected to be critical from the loads standpoint. Because of the high speeds and the likelihood of decreased damping of airplane motions at the cruise altitudes, the small amount of turbulence at high altitude is thought likely to be more of a problem as regards airplane control and stability than as regards loads.

The plot on the right in figure 3 shows the present Civil Air Regulations design gust velocities applicable to the design cruise speed V_C and the design rough-air speed V_B. Gust velocities are presently

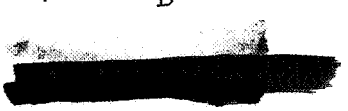

specified up to an altitude of 50,000 feet. Data are available, however, on which to base the selection of design gust velocities up to altitudes of 75,000 feet.

As previously mentioned, there is some question regarding the applicability of the slowdown and rough-air speed concept to the supersonic transport. Thus, although available data do not indicate that the design gust velocities need to be altered for the supersonic transport, there is a need to re-assess the speeds at which they are to be applied. Factors which should be considered in this re-assessment are: (1) feasibility of accomplishing effective and practical slowdown, (2) effect of weather radar and flight planning on turbulence avoidance, and (3) maneuverability of airplane for avoiding detected turbulence.

Gust loads are currently calculated by using two complementary methods: (1) discrete gust and (2) continuous turbulence. The discrete-gust method has been used to set the level of loading and the continuous method, to detect unusual response characteristics of the airplane for use in modifying the load level derived from the discrete method. Although progress has been made in developing the continuous turbulence method (ref. 5), it is doubtful that it will be sufficiently developed in time to permit its employment on an absolute basis to the supersonic transport. Consequently, it appears that the present practice of calculating gust loads by using the two methods on a complementary basis will have to be applied to the supersonic transport design.

Maneuver loads: As is the case with present transports, the supersonic transport will experience maneuver loads during operational passenger-carrying flights and during pilot and airplane training and check flights. For use in fatigue analyses, it is thought that, at present, the best estimate of the maneuver loads can be obtained by assuming that the supersonic-transport maneuver experience will be similar to that for current turbojet transports. Information on turbojet maneuvers experienced is being obtained by NASA and some data have been published in references 1 and 6. Maneuvers performed during pilot and airplane training and check flights constitute a major source of the overall maneuver experience for turbojet transports. (See ref. 6.) It is anticipated that training and check flights also will be a major source of maneuver loads for supersonic transports. Based on a crude assessment of the many factors which may influence the amount of check flying required, it is estimated that on the order of 4 percent of the total flight time for the supersonic transport will be spent in pilot training or airplane check flights. Further, it is estimated that about one-fourth of the training and check flying will be at supersonic speeds.

Inasmuch as limit maneuver load factors in combination with thermal stresses at supersonic speeds are apt to be a critical design condition,

careful attention to the limit-maneuver-load-factor requirements at supersonic speeds is warranted. In the absence of operational data applicable to supersonic transports, the specification of the supersonic maneuver load factors will have to be done primarily on the basis of engineering judgment based on extrapolating experience gained from present transports to the new configurations and operational requirements. Available data from turbojet transports (ref. 1, for example) indicate that these airplanes are occasionally subjected to maneuvers as large or larger than the limit values of -1g and -2.5g. Further, these maneuvers appear to be induced by a variety of causes such as recovery from loss of control, improper operation of autopilot, and collision avoidance. Consideration of available maneuver data in conjunction with anticipated supersonic-transport operational requirement has not indicated that the present design maneuver load factors of -1g and +2.5g should be changed for either subsonic or supersonic flight.

Ultimate loads.- Present Civil Air Regulations (ref. 2) require that the airplane structure be designed to support ultimate loads equal to 1.5 times the limit loads. The specification of ultimate load design requirements for the supersonic transport is complicated by the necessity of considering thermal effects on the structural material. There are three major effects which require consideration: (1) short-term degradation of the material properties, (2) long-term effects of the thermal history on the material, and (3) thermal stresses which are highly dependent on the flight profile. The first two effects can be accounted for by using degraded material properties and do not appear to be a major problem. In the case of thermal stresses, however, it is not clear which of several possible approaches is the most rational. There are two major aspects of the thermal stresses which need to be resolved. These are: (1) what factor of safety should be used? and (2) how should the thermal stresses for the high-speed portion of the V-n envelope be treated?

As was discussed in paper no. 18 of this compilation by Richard A. Pride, two different approaches were used in the feasibility studies to account for the thermal stresses in computing ultimate loads. In one approach, a factor of safety of 1.5 was applied to the combined thermal and mechanical stresses. In the other approach, ultimate loads were determined without directly considering a factor of safety for the thermal stresses. It would appear that this latter approach, in effect, assumes that either the thermal stresses are precisely known or that the safety factor applied to the mechanical stresses also can adequately cover any unknowns associated with the thermal stresses. At this time, it is not clear which thermal factor of safety would be the most rational. It would appear, however, that the thermal stresses may be known to a higher degree than are the mechanical stresses and, consequently, the factor of safety could be less than 1.5. On the other hand, there will be

some error in determining the thermal stresses and, consequently, a factor greater than 1.0 would appear to be required.

As the normal flight profile will not encompass speeds higher than the design cruise speed V_C, it appears that thermal stresses for the high-speed portion of the V-n envelope based on transient overspeed or emergency conditions must be considered. This approach was used in the feasibility studies.

Fatigue loads.- The major load sources to be considered in deriving fatigue loading spectra for the supersonic transport are:

(1) Ground-air-ground cycles
(2) Thermal stress cycles
(3) Maneuver loads
(4) Gust loads
(5) Pressurization cycles
(6) Landing impact
(7) Taxi load
(8) Sonic-induced loads

Except for the addition of the thermal stress cycles, the spectra involve the load sources which have been considered for present transports. Because of the increased concentration of the airplane weight inboard on the supersonic transports, the ground-air-ground cycle may be of more relative importance in their fatigue life than on present transports. Calculations have indicated that the thermal stress cycles which the structure will experience on each flight will be an important source of fatigue damage. Because of the strong dependence of the thermal stress cycles on the detailed mission profile, possibly more consideration will need to be given to deriving the fatigue loading spectra based on mission analyses than has been required in the past.

Performance

From the overall viewpoint, the performance requirements for supersonic transports would not appear to be greatly different from those for present transports. In applying current requirements and insuring that minimum performance margins are attained in practice, however, there are several areas which will require further consideration. Two of these areas are discussed in the following sections.

Performance reference.- Many of the current low-speed performance margins and operating speeds are tied directly to a stall speed. Because a clearly defined stall speed may not exist for some supersonic-transport

RESTRICTED

configurations, the present concept of relating performance to a stall speed may require modification.

To illustrate this point, figure 4 shows two plots of lift coefficient C_L against angle of attack a for two configurations. The curve on the left is representative of a subsonic turbojet transport having an aspect ratio of about 7. The other curve is representative of a supersonic-transport configuration having an aspect ratio of about 2. For the high-aspect-ratio configuration, the lift-coefficient curve reaches a maximum value $(C_L)_{MAX}$ at a particular angle of attack. A fairly definite stall speed also is associated with this maximum lift coefficient. Present low-speed performance requirements use this stall speed as a reference for specifying operational speeds so that the operational lift coefficient will be sufficiently below $(C_L)_{MAX}$ to provide adequate maneuverability.

In the case of the low-aspect-ratio configuration, the lift-coefficient curve does not have a distinct $(C_L)_{MAX}$ nor does a definite stall speed exist within practical angles of attack. Consequently, the concept of basing performance requirements on a stall speed is not applicable to the low-aspect-ratio configurations.

One procedure used in the feasibility studies to assess the performance of the low-aspect-ratio configurations involved:

(1) Selection of the lift coefficient at which it was desired that the airplane operate.

(2) Examination of the aerodynamic and control characteristics of the airplane to insure that the airplane was capable of producing a useable lift coefficient sufficiently high to provide maneuverability comparable to that inherent in present requirements. The angle of attack corresponding to the useable lift coefficient would, in effect, be a maximum operational limit. Above this limit, the flying qualities would likely deteriorate.

Another, and possibly more fundamental, approach would be to divorce completely the performance specification from a reference speed. In this approach, the manufacturer would be permitted to select the operational speeds, but would be asked to meet minimum maneuverability requirements associated with the particular flight condition. At this time, however, it is doubtful whether sufficient data are available on which to make a rational determination of the minimum maneuverability requirements. Nevertheless, the possible merits of the approach are thought to warrant further consideration.

Climb gradient.- Present Civil Air Regulations specify minimum climb gradients for various segments of flight and for engine-out conditions. These gradients have evolved from past operating experience with transports. In view of the novel configurations being considered for supersonic transports, it appears that the implications of the new configurations on the climb gradients may need to be examined.

Figure 5 illustrates one aspect of the effect of configuration on the climb gradient for the second-segment flight condition. The upper plot shows two drag or thrust-required curves as a function of airspeed. The lower curve is for an aspect-ratio-7 subsonic turbojet transport, and the upper curve is for an aspect-ratio-2 supersonic transport configuration. As only the shapes of the curves are pertinent to this discussion, the curves have been shifted closer together along both the drag and airspeed axis for convenience of presentation.

During the climb-out, the pilot will be attempting to fly at a particular speed, referred to as "V_{TARGET}." At this speed, the airplanes are required to have sufficient thrust with one engine out to provide a minimum climb gradient - 3 percent for this case.

In practice, the actual airspeed achieved by the pilot will miss the target speed by some amount ΔV with the result that the actual airspeeds achieved form a distribution about the target speed. The available climb gradient is (for each configuration) proportional to the difference between the engine-out thrust and drag curves and decreases as the actual speed falls below the target speed.

The lower plot in figure 5 shows the remaining climb gradients for both configurations as a function of the airspeed error ΔV. The results indicate that a given negative airspeed error causes a significantly larger reduction in climb gradient for the low-aspect-ratio configuration than for the high-aspect-ratio configuration. Other factors such as deviations of weight and thrust from nominal values also have a more deleterious effect on the climb gradient for the low-aspect-ratio configuration than for the high-aspect-ratio configuration. From this comparison, it appears that the configuration may have a significant effect on the actual level of performance achieved in service. For other flight segments, the order of the results may be reversed from those shown in the figure. Nevertheless, it would appear that the configuration effects may be sufficiently large to warrant consideration in the specification of performance margins. A more detailed discussion of the effect of configuration on climb performance is given in reference 7.

Handling Qualities

The handling qualities which appear to be desirable for the supersonic transport are not thought to be very different from those desired for present transports. The major problems appear to be in obtaining configurations with characteristics which are inherently conducive to good handling qualities. Consequently, it appears that considerable stability augmentation will be required to provide satisfactory handling qualities as is discussed in several other papers in this compilation (papers no. 3, 4, 26, and 27). Three aspects of handling qualities which will require special consideration are subsequently discussed.

Speed stability.- Although the subject of speed stability during approach is discussed in several papers (papers no. 3, 4, 26, and 27), it is briefly discussed here from the standpoint of airworthiness. Figure 6 shows thrust required curves for four supersonic-transport configurations during the approach condition. The portion of the curves to the left of the vertical lines is the familiar "back-side" of the power curve and that to the right is the region of speed stability. As shown by the symbols, the approach speeds for three of the configurations are on the back side of the curves. Although some military airplanes operate on the back side, current transports operate in the region of speed stability during approach. The question, then, is whether operations on the back side of the power curve during approach can be tolerated in transport operations. If not, shifting the drag curves to a more favorable position by use of drag brakes may be one method of improving the approach characteristics. (See ref. 8.)

Some pilots are of the opinion that operations on the back side would be acceptable for transport operations, provided the rate of change of thrust required with airspeed is not too large. It is felt, however, that additional simulator studies and flight tests will be required before a final answer is obtained.

Ground handling.- The handling qualities of the supersonic transport during the take-off roll and during execution of the rotation maneuver may be adversely affected by the airplane response characteristics to runway roughness. Figure 7 shows the variation of the root-mean-square acceleration of the pilots' compartment with speed for a turbojet and supersonic transport configuration. These results are taken from reference 9 and are based on a simplified analysis considering rigid-body pitch and vertical translation and linearized landing-gear characteristics. The level of runway roughness was comparable to that of a good commercial runway.

The results in figure 7 indicate that over most of the speed range, the response of the supersonic transport is much higher than that for the turbojet transport. Turbojet pilots have complained that present response

levels sometimes cause discomfort, affect control of the airplane during the take-off run, and interfere with the precise execution of the rotation maneuver. Consequently, it would appear that the higher indicated response level for the supersonic transport may not be acceptable. Thus, the response characteristics of the supersonic transport to runway roughness may be more of a problem than it is for present transports. Detailed study of the response of configurations to specific runway roughness profiles will be required to assess this problem area further.

Stability augmentation.- It is anticipated that the supersonic transport will require increased use of stability-augmentation devices to provide acceptable handling qualities during low-speed operations and during cruise flight. At this time, the effects which the increased use of stability-augmentation systems may have on airworthiness requirements are not fully known. Unless a very high degree of reliability of the augmentation systems can be assured, however, it would appear that the requirements will need to cover both the failed and unfailed systems. In this regard, the amount and reliability of the augmentation systems could have a bearing on the selection of speed placards and on some load requirements.

Vertical-tail loads appear to be one of the areas where special attention must be given to the case of a failed lateral-stability augmentation system. In this connection, figure 8 indicates the effect of period and damping on the vertical tail due to turbulence. The ordinate values are the ratio of the root-mean-square sideslip angle at the vertical tail to the root-mean-square gust input angle. The abscissa is the reciprocal of the number of cycles to damp the lateral motion to half amplitude. The results, except for the supersonic transport, were taken from reference 10 and were calculated on the assumption that the predominant parameters are the period and the damping of the airplane. The cross-hatched area in the figure represents the range of results obtained for several supersonic transports by using estimates of the period and damping of the lateral mode for the unaugmented airplane. The results indicate that, for the unaugmented case, the vertical-tail loads for the supersonic transport may be amplified to a greater extent than for present turbojet airplanes. It may be expected, therefore, that the case of failed lateral-stability augmentation may constitute one of the critical design conditions for the vertical tail.

CONCLUDING REMARKS

A review of several aspects of airworthiness for supersonic transports has indicated some areas wherein present Civil Air Regulations are not directly applicable. In some cases, it appears that the requirements can be adapted to supersonic-transport configurations by only minor

DECLASSIFIED

modifications or extensions. In other cases, basic concepts will require re-examination. It should be recognized that the Federal Aviation Agency is cognizant of the airworthiness problems discussed herein and has circulated tentative supersonic transport airworthiness objectives. (See ref. 11.)

REFERENCES

1. Staff of Langley Airworthiness Branch: Operational Experiences of Turbine-Powered Commercial Transport Airplanes. NASA TN D-1392, 1962.

2. Anon.: Airplane Airworthiness; Transport Categories. Civil Air Regulations Part 4b, Rules Service Co. (Washington, D.C.), Jan. 7, 1963.

3. Bray, Richard S.: Piloted Simulator Studies Pertaining to the Low-Speed Longitudinal Handling Qualities of a Supersonic Transport Airplane. Paper presented at AIAA Meeting (Columbus, Ohio), Aug. 26-28, 1963.

4. Coleman, Thomas L., and Stickle, Joseph W.: Turbulence Environment for Supersonic Transports. Proceedings Symposium on Supersonic Transports. Soc. Exp. Test Pilots, Sept. 1961, pp. 144-160.

5. Houbolt, John C., Steiner, Roy, and Pratt, Kermit G.: Flight Data and Considerations of the Dynamic Response of Airplanes to Atmospheric Turbulence. Presented to the Structures and Materials Panel and to Flight Mechanics Panel of AGARD (Paris, France), July 3-13, 1962.

6. Hunter, Paul A., and Coleman, Thomas L.: Operational Experiences of Jet Transports. SAE Trans., vol. 71, 1963, pp. 34-40, 61.

7. Chaplin, J. C.: Safety and Airworthiness Aspects. Supersonic Engineering, J. T. Henshaw, ed., John Wiley & Sons, Inc., c.1962, pp. 18-38.

8. Greene, L. P., and Bonner, E.: Performance Requirements for Supersonic Transports. [Preprint] 674B, Soc. Automotive Eng., Apr. 1963.

9. Silsby, Norman S.: An Analytical Study of Effects of Some Airplane and Landing-Gear Factors on the Response to Runway Roughness With Application to Supersonic Transports. NASA TN D-1492, 1962.

10. Funk, Jack, and Cooney, T. V.: Some Effects of Yaw Damping on Airplane Motions and Vertical-Tail Loads in Turbulent Air. NASA MEMO 2-17-59L, 1959.

11. Anon.: Tentative Airworthiness Objectives and Standards for Supersonic Transport Design Proposals. Flight Standards Service, FAA, Aug. 15, 1963.

STRUCTURAL DESIGN SPEEDS

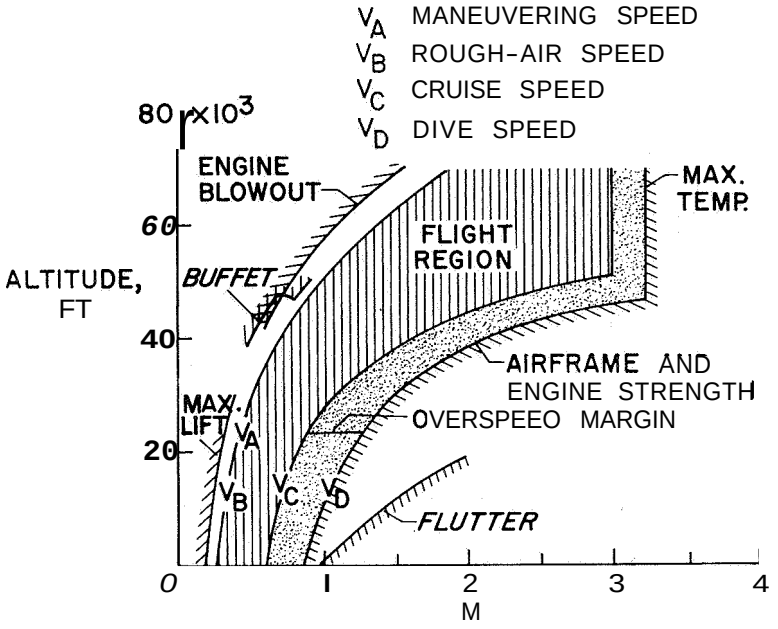

Figure **1**

DESIGN SINKING SPEED

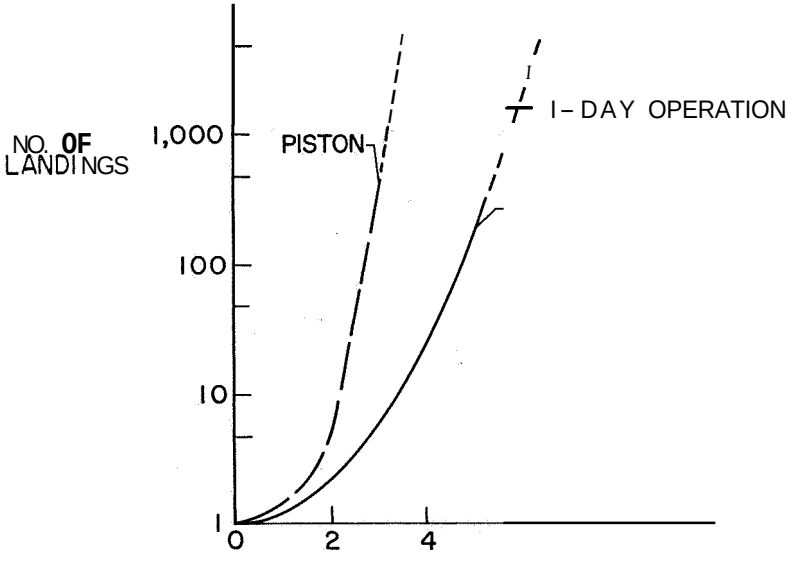

Figure *2*

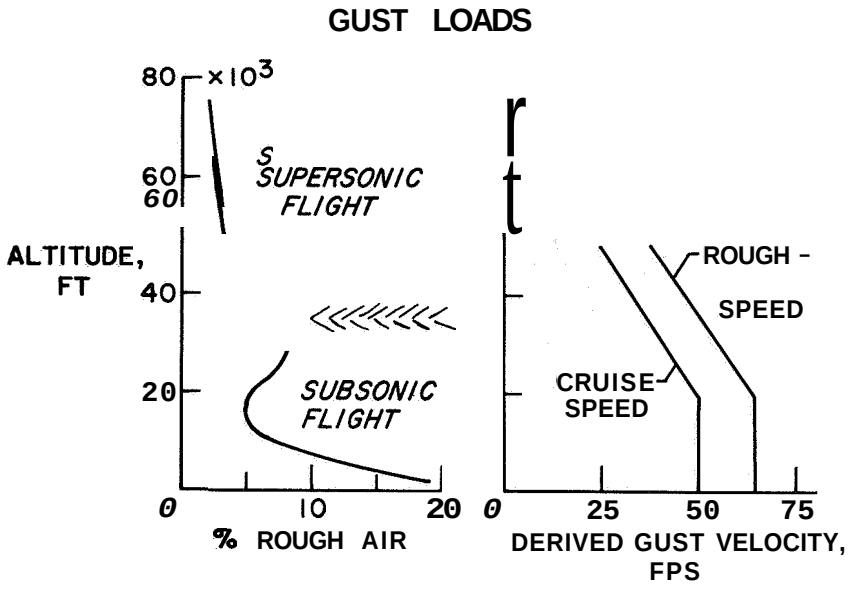

Figure 3

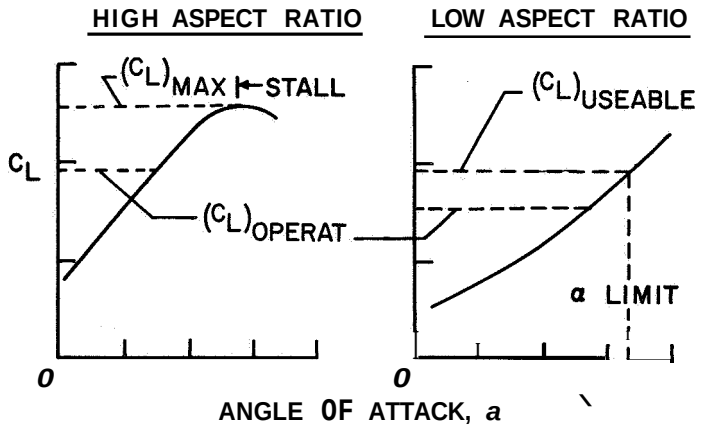

Figure 4

[redacted]

RELEASED

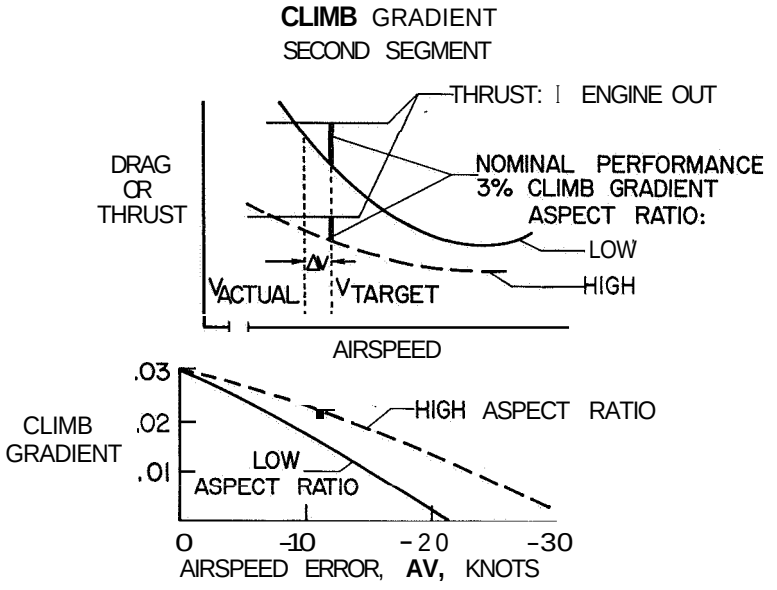

Figure 5

SPEED STABILITY DURING APPROACH

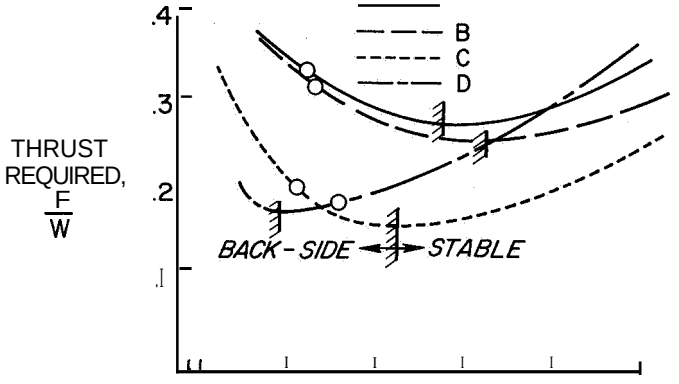

Figure 6

CONFIDENTIAL

PILOT COMPARTMENT RESPONSE
TO RUNWAY ROUGHNESS

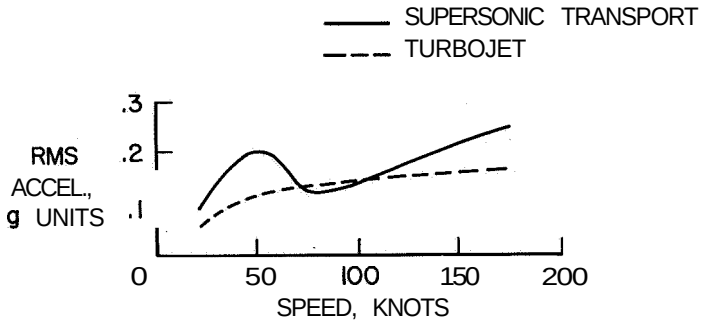

Figure 7

EFFECT OF DAMPING ON VERTICAL-TAIL LOADS

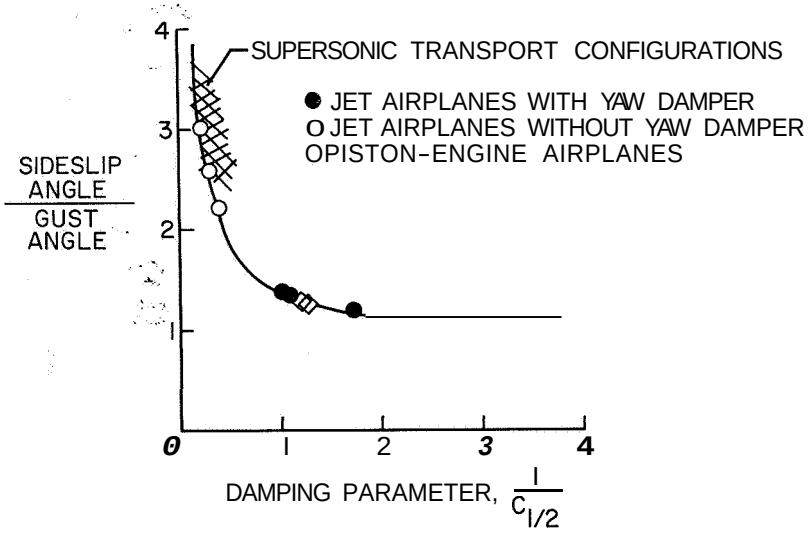

Figure 8

[redacted] N67-31633

26. DEVELOPMENT OF SATISFACTORY HANDLING QUALITIES

FOR A SUPERSONIC-TRANSPORT CONFIGURATION

THROUGH SIMULATOR STUDIES

By Maurice D. White, Alan E. Faye, Jr.,
and George E. Cooper Jr. NASA

NASA Ames Research Center

SUMMARY

Piloted simulator studies have been conducted of an early supersonic-transport configuration to provide advanced indications of possible handling-qualities problems. These studies have shown that the configurations being considered for the supersonic transport result in some handling-qualities problems that are novel for a transport class of airplane. Careful tailoring of the design may be required to achieve satisfactory handling qualities.

INTRODUCTION

A number of different types of configurations are being considered for the supersonic transport. In order to obtain prompt indications of the possible handling-qualities problems, simulator studies were made of early versions of the various concepts. In this paper results will be reported for a simulator study of a supersonic-transport configuration that had a variable-sweep wing. The program was conducted by using the aerodynamic and inertial characteristics of a specific design; however, the basic similarity of many of the aerodynamic and inertial characteristics of the test configuration to those of other supersonic-transport concepts suggests that some of the problems discussed may be of concern for the other supersonic-transport concepts. Two views of the test configuration are shown in figure 1. Although the general proportions of the test configuration are similar to those of variable-sweep designs that have evolved more recently, the aerodynamic characteristics are generally sensitive to design details. Thus, results for the test configuration are not necessarily directly applicable to the newer versions; they are of more value for demonstrating the classes of problems and the design trade-offs that must be considered in tailoring the design for good handling qualities.

[redacted]

p 457 - 469

SYMBOLS

$\bar{c}$	mean aerodynamic chord referred to swept-wing configuration
C_{m_q}	pitch damping derivative
C_{n_r}	yaw damping derivative
$\partial C_m/\partial C_L$	longitudinal static margin
$C_{n_{\beta_o}}$	static-directional-stability derivative at zero angle of attack
M	Mach number
N_r'	effective value of yaw-damping derivative, body axes
N_β'	effective value of static-directional-stability derivative, body axes
ζ	damping ratio of short-period longitudinal oscillation
ζ_d	damping ratio of Dutch roll lateral-directional oscillation
ω_d	frequency of Dutch roll lateral-directional oscillation
$\frac{\lvert\varphi\rvert}{\lvert\beta\rvert}$	ratio of bank angle to sideslip angle in control-fixed lateral-directional oscillations
$\left(\frac{\omega_\varphi}{\omega_d}\right)^2$	parameter used to define aileron-yaw effect (ref. 1)

TESTS

The flight profile and weight variation that were used for the simulator study are shown in figure 2. The flight profile was an idealized one, but there were no features in it that would compromise the conclusions drawn from the study. The Mach number scale is divided into three ranges: 0 to 3.0, representing the climb and acceleration to Mach 3.0 at an altitude of 60,000 feet, followed by a further climb at constant Mach number to an altitude of 70,000 feet; cruise at a constant altitude of 70,000 feet and Mach number of 3.0 during which the fuel expenditure (and corresponding decrease in weight) results in some stability parameter changes; and, finally, a deceleration at constant altitude, which would be followed by a descent at constant dynamic pressure. Flight conditions at Mach numbers below 2.3 in the descent were not studied after

it was determined that handling qualities consistently improved as the descent progressed. Also, the landing-approach characteristics were not considered in this program; however, the landing-approach handling qualities of a more advanced variable-sweep configuration, the SCAT 16, are discussed in paper no. 27 by Walter E. McNeill and Robert C. Innis. The wing-sweep schedule provided for continuous variation of sweep angle with Mach number to provide essentially maximum lift-drag ratio at each Mach number.

The simulation was conducted under instrument flight conditions with six-degree-of-freedom equations of motion on a simulator that had motion in roll, pitch, yaw, and side translation (fig. 3); these motions were adjusted to represent those of a pilot compartment located about 90 feet ahead of the center of gravity.

In the tests, the handling qualities were examined at each of a number of discrete points along the mission, identified by the test points in figure 2. At each point the airplane was balanced and the pilot performed maneuvers appropriate to transport operation, such as turns, precise control of altitude, and so forth.

The pilot rating scale shown in table I was used in rating the configurations. A rating of $3\frac{1}{2}$ would define the boundary between satisfactory conditions and conditions that are only acceptable for emergency conditions, and a rating of $6\frac{1}{2}$ would mark the lower limit of acceptability in an emergency, the emergency in the present instance being assumed to be a stability-augmenter failure. The philosophy underlying the study was that the aerodynamic characteristics of the airplane should never result in ratings poorer than $6\frac{1}{2}$, and that artificial stability augmentation could be relied on to improve the rating to better than $3\frac{1}{2}$.

RESULTS

Before entering into a detailed discussion of the results it would be desirable to review the background for one assumption that had a very powerful effect on the results obtained. Preliminary evaluation of the rigid-airplane aerodynamics for the test configuration indicated that if a constant center-of-gravity position were assumed that would provide longitudinal stability at low speeds, the high-speed trim-drag penalties would be prohibitive. This is the well-known effect of aerodynamic-center shift between subsonic and supersonic speeds which has been a matter of concern for all supersonic-transport configurations. Other papers in this compilation indicate the large level of effort

that is being applied to the development of detail modifications to reduce the aerodynamic-center shifts. These efforts, in combination with beneficial. aeroelastic effects, should provide solutions that do not involve in-flight adjustment of center-of-gravity position. However, in the absence of a well-defined aerodynamic solution, it was decided at the time of the simulation tests that center-of-gravity adjustment by fuel transfer could be assumed.

In figure 4(a), the center-of-gravity movement that was used to provide a constant static margin of 5 percent is shown as a percentage of the swept-wing mean aerodynamic chord. The maximum physical movement associated with this curve is 17.7 feet, a very large distance which would, of course, severely tax any fuel-transfer-system design that might be considered for achieving this center-of-gravity movement. In fact, it is unlikely that a final. design would be accepted that incorporated fuel-transfer requirements of this magnitude. However, center-of-gravity adjustments of smaller magnitude could conceivably be incorporated in a final design, and the present results, even though they are of exaggerated magnitude, remain of interest in that they define problem areas and trade-offs that need consideration.

The most important effects of the assumption regarding center-of-gravity movement are shown in figure 4(b). Here is shown a comparison of the static-directional-stability derivative $C_{n_{\beta_O}}$ as it would vary with Mach number if the center of gravity were held fixed and as it varied with the assumed center-of-gravity travel. It is apparent that a considerable loss in directional stability occurred at high Mach numbers as a consequence of the assumed center-of-gravity travel, and this loss had a significant effect on the results obtained. The implications of this result will be discussed further.

Figure 5 shows some of the results that were obtained in the tests. Plotted against Mach number are the pilot ratings and several stability parameters that indicate the nature of the handling-qualities problems that were encountered. Plotted against a Mach number scale that corresponds to that of figure 2 are:

(1) Pilot rating

(2) The Dutch roll damping ratio ζ_d, which is a measure of the control-fixed damping of the lateral-directional oscillations. (Desirable values for this parameter are equal to or greater than the range 0.4 to 0.7.)

(3) The pitch damping ratio ζ, which is a measure of the damping of the control-fixed short-period longitudinal oscillation. (Desirable values for this parameter are also equal to or greater than the range 0.4 to 0.7.)

(4) The roll-yaw ratio $\frac{|\varphi|}{|\beta|}$, which is a measure of control-fixed cross-coupling effects in lateral-directional oscillations. (Minimum values for this quantity are desired.)

(5) The aileron-yaw-effect parameter $\left(\frac{\omega_\varphi}{\omega_d}\right)^2$, which describes the cross-coupling effect introduced in aileron-control maneuvers. (Desirable values for this parameter are in the region of 1.0.)

Consider first the variation of pilot rating for the basic airplane; the spread in the data covers the scatter of data from five participating test pilots. As shown in figure 5, the airplane was slightly unsatisfactory at the lowest test airspeeds, and as the Mach number increased through the climb and acceleration, the airplane handling qualities became progressively worse until at a Mach number of 3.0 and an altitude of 70,000 feet the airplane was virtually unflyable. With decréasing weight (and correspondingly decreasing angle of attack) through the cruise, the characteristics improved somewhat, and there was a very slight further improvement during the deceleration at constant altitude prior to descent. The pilots' comments identified the initial degradation in pilot rating with Mach number at subsonic speeds with the decrease in Dutch roll damping. The reduced level of Dutch roll damping attained at sonic speeds persisted at all supersonic speeds and should, without further repetition, be inferred to be a factor in the problems encountered at higher speeds. As Mach number increased through the transonic range, the emphasis of the pilot complaints shifted to lateral-directional cross-coupling effects, both in control-fixed oscillations $\frac{|\varphi|}{|\beta|}$ and aileron control maneuvers $\left(\frac{\omega_\varphi}{\omega_d}\right)^2$. Further increase in Mach number to 1.6 indicated more serious complaints about lateral-directional characteristics; in addition, the reduced longitudinal damping contributed to difficulties in holding altitude precisely in turns or in leveling off after climbs. Further continuation along the climb to cruising speeds and altitudes resulted in marked deterioration of lateral-directional coupling parameters and of pitch damping, which reflected the poorer ratings assigned by the pilots.

The handling-qualities problems identified in these operations have been the subject of studies which have led to the development of numerical criteria for satisfactory conditions. Boundaries derived fromthese studies for two of the factors are shown in figure 5. The boundary in figure 5(d) was derived from reference 2, and the boundary in figure 5(e) was derived from reference 1. These boundaries represent a $6\frac{1}{2}$, pilot rating; they were, however, developed from fighter-airplane studies and primarily with consideration of the landing-approach condition. The agreement shown, then, in the crossover of these boundaries

and the area where the pilot rating crossed the $6\frac{1}{2}$ level provides encouraging indication that these criteria may be applied more generally.

A variety of stability augmentation arrangements was examined in an effort to achieve a practicable solution. As shown in figure 6, a fairly reasonable arrangement that provided pilot ratings at or below $6\frac{1}{2}$ throughout the mission was to increase the size of the vertical tail by 50 percent and increase pitch damping by 4 times. The directional stability recovered by this increase in tail size was about the same as that lost through center-of-gravity movement. A change in horizontal-control gearing to provide a 75-percent reduction in sensitivity or power at high Mach numbers was also required, but this change should probably not be considered as stability augmentation.

With an additional increase in pitch-damping derivative C_{m_q} to 11 times the basic value and the yaw-damping derivative C_{n_r} to 10 times the basic values, pilot ratings of the order of $3\frac{1}{2}$ were achieved at the critical condition of $M = 3.0$. Although this set of values was not evaluated throughout the Mach number range, it seems reasonable to deduce from the trends of the data that the improvements provided by this augmentation would hold throughout the mission. Substantiating a point made in the "Introduction," it will be noted that a delta-wing—canard model previously studied on the simulator in Mach 3 flight required similar amounts of augmentation. (See ref. 3.)

It will be noted that dihedral effect, which is usually considered a primary factor in cross-coupling problems, was not reduced as one of the augmentation changes. In fact, an attempt to reduce dihedral effect at supersonic speeds resulted in a more adverse rating. The explanation for this effect lies in the fact that, for the marginal directional stability that existed at high Mach numbers, most of the apparent lateral-directional stability was contributed by the dihedral effect. Reduction of this contribution with lowered dihedral effect affected the lateral-directional static stability more adversely than it improved roll-yaw coupling. It is pertinent in connection with these results to recall the assumption regarding center-of-gravity movement discussed previously, which resulted in greatly reduced directional stability at high Mach numbers. The character and magnitude of the contributions of dihedral effects that were just indicated would be greatly affected by that assumption.

Another point of interest developed by the studies is indicated in figure 7. Contrary to the usual expectation, the Dutch roll damping

ratio, which is an important measure of lateral-directional damping, was actually reduced with the 50-percent increase in vertical-tail area. This result is, of course, due to the relative contributions of the increased tail size to the directional damping and to the static directional stability, which are indicated to a first order in the lower part of the figure. As noted, the percentage change in N_{β}' (an important static-stability or frequency term) is much greater than the percentage change in N_{r}' (an important damping term); hence, the reduction in damping ratio previously noted.

These data demonstrate why it may prove difficult to provide required levels of yaw damping by simple increase in tail size, Simultaneous changes in static directional stability would increase the frequency of directional oscillations to undesirably high levels; in the current operations, pilots noted that the period of $3\frac{1}{2}$ seconds that occurred with the 50-percent increase in tail size did not seem a reasonable value for the long, relatively limber fuselage that would probably characterize the supersonic transport. This result would indicate a possible requirement for achieving damping by artificial means, even if the use of increased tail size could have been tolerated otherwise. Here again the basic assumption regarding the effect of center-of-gravity position on directional stability would have a significant effect on some rather important conclusions.

CONCLUDING REMARKS

11968

In conclusion, it appears from simulation studies of an early supersonic-transport design that coping with the problems of Longitudinal aerodynamic-center shift with Mach number can present difficulties other than the well-known trim-drag effects. The sensitivity of the directional stability to longitudinal center-of-gravity position is one of a number of factors that result in relatively novel lateral-directional handling-qualities problems which may require careful tailoring of the design. In cruising flight, augmentation of aerodynamic damping appears to be a requirement for both the variable-sweep and the delta-wing—canard configurations.

AUTHOR

REFERENCES

1. Vomaske, Richard F., Sadoff, Melvin, and Drinkwater, Fred J., III: The Effect of Lateral-Directional Control Coupling on Pilot Control of an Airplane as Determined in Plight and in a Fixed-Base Flight Simulator. NASA TN D-1141, 1961.

2. Anon.: Flying Qualities of Piloted Airplanes. Military Specification MIL-F-8785(ASG), Sept. 1, 1954; Amendment-2, Oct. 17, 1955.

3. White, Maurice D., Vomaske, Richard F., McNeill, Walter E., and Cooper, George E.: A Preliminary Study of Handling-Qualities Requirements of Supersonic Transports in High-speed Cruising Flight Using Piloted Simulators. NASA TN D-1888, 1963.

TABLE I

PILOT OPINION RATING SYSTEM

	ADJECTIVE RATING	NUMERICAL RATING	DESCRIPTION	PRIMARY MISSION ACCOMPLISHED	LANDED
NORMAL OPERATION	SATISFACTORY	1	EXCELLENT, INCLUDES OPTIMUM	YES	YES
		2	GOOD, PLEASANT TO FLY	YES	YES
		3	SATISFACTORY, BUT WITH SOME MILDLY UNPLEASANT CHARACTERISTICS	YES	YES
EMERGENCY OPERATION	UNSATISFACTORY	4	ACCEPTABLE, BUT WITH UNPLEASANT CHARACTERISTICS		
		5	UNACCEPTABLE FOR NORMAL OPERATION		
		6	ACCEPTABLE FOR EMERGENCY CONDITION ONLY[1]		
NO OPERATION	UNACCEPTABLE	7	UNACCEPTABLE EVEN FOR EMERGENCY CONDITION[1]		DOUBTFUL
		8	UNACCEPTABLE – DANGEROUS		
		9	UNACCEPTABLE–UNCONTROLLABLE		

[1]FAILURE OF A STABILITY AUGMENTER

TEST CONFIGURATION

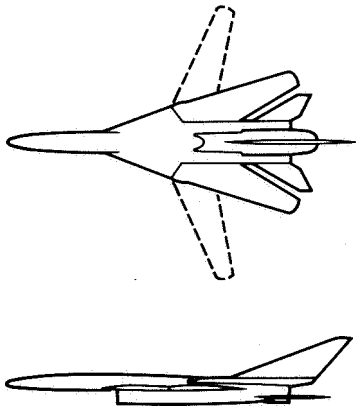

Figure 1

SIMULATOR TEST CONDITIONS

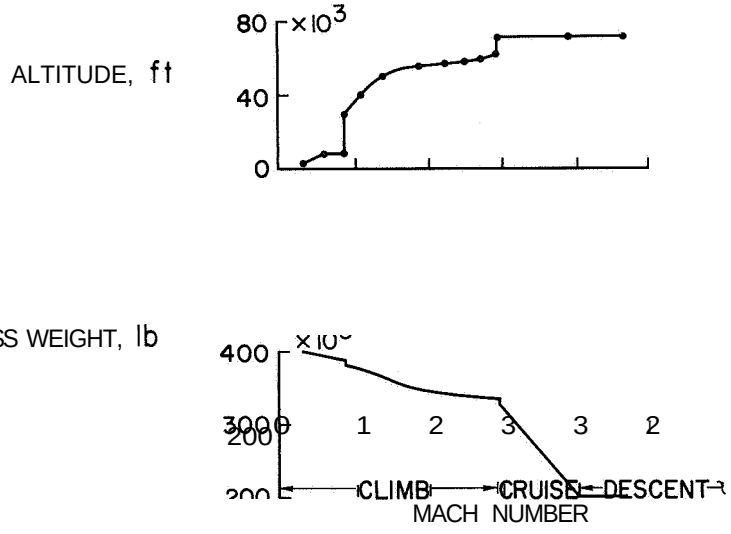

Figure 2

MOTION SIMULATOR

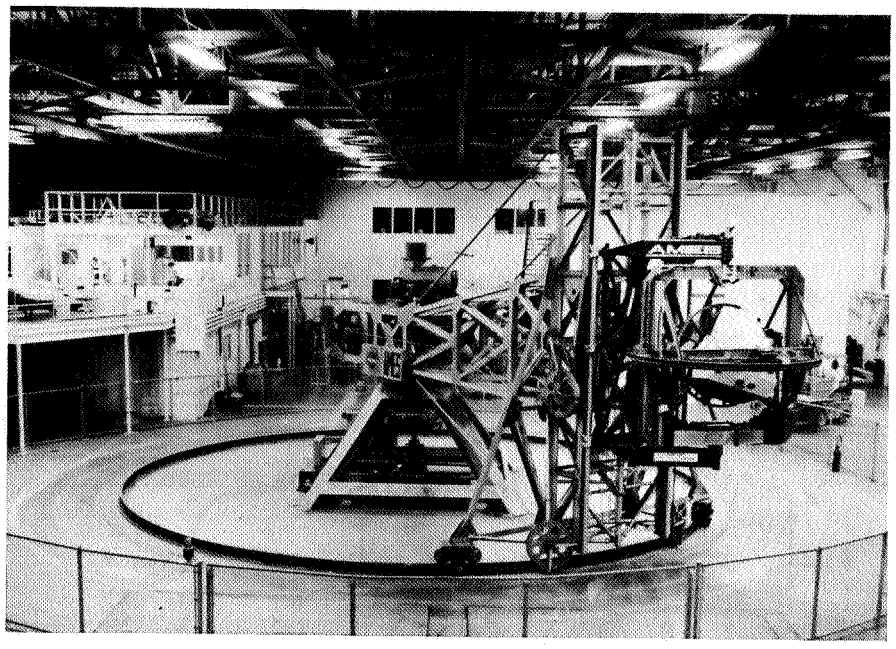

A-29190

Figure 3

CENTER-OF-GRAVITY EFFECTS

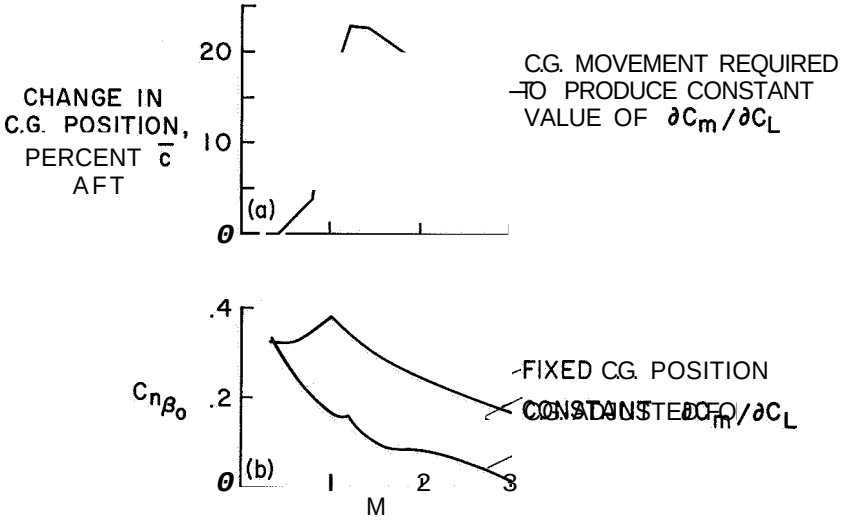

Figure 4

VARIATIONS OF SELECTED HANDLING QUALITIES PARAMETERS

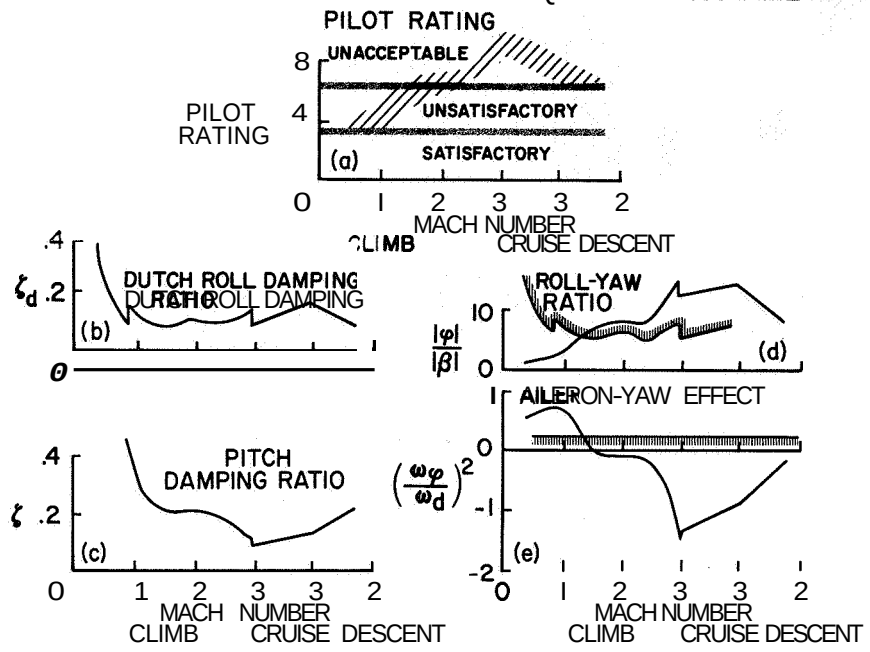

Figure 5

STABILITY AUGMENTATION REQUIREMENTS

AUGMENTATION

1. INCREASE VERTICAL TAIL SIZE 50%
2. INCREASE PITCH DAMPING 4 TIMES
3. a) INCREASE PITCH DAMPING 11 TIMES
   b) INCREASE YAW DAMPING 10 TIMES

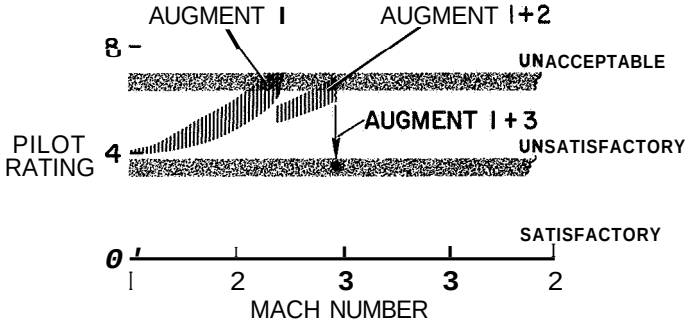

Figure 6

[redacted]

EFFECT OF TAIL SIZE ON DAMPING RATIO

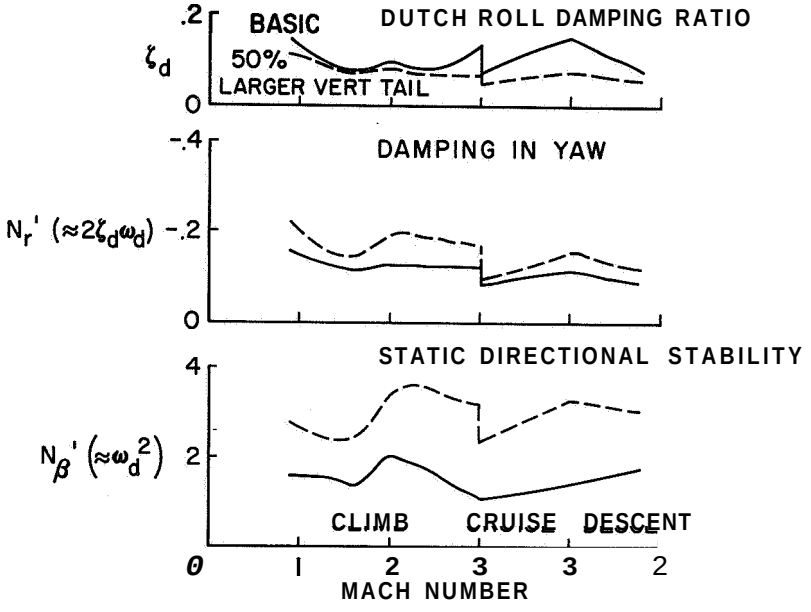

Figure 7

PRECEDING PAGE BLANK NOT FILMED.

[redacted]

N67-31634

27. A SIMULATOR STUDY OF THE LATERAL DIRECTIONAL HANDLING QUALITIES OF TWO SCAT CONFIGURATIONS IN THE LANDING APPROACH

By Walter E. McNeill and Robert C. Innis

NASA-Ames Research Center

SUMMARY

A piloted simulator study of the lateral directional handling qualities of one SCAT 16 and two SCAT 17 configurations showed that the SCAT 16 and one SCAT 17 would have acceptable handling qualities in an emergency condition without stability augmentation. The SCAT 16 exhibited almost satisfactory behavior without augmentation. It was found that these SCAT 16 and 17 configurations could be improved to a satisfactory level, as far as lateral directional stability is concerned, by ordinary means of stability augmentation.

INTRODUCTION

As in the case of many large, slender airplane configurations, the present supersonic transport designs, or SCAT configurations, are expected to have undesirable handling qualities which will require some form of artificial stability augmentation in the lateral directional modes of motion. It is the purpose of this paper to present and discuss some preliminary results of a piloted simulator study which indicate the types and amounts of lateral. directional augmentation desirable for two SCAT configurations, the SCAT 16 and the SCAT 17. In this study, only the landing-approach condition was investigated.

SYMBOLS

b	wing span, ft
$\frac{1}{C_{1/2}}$	reciprocal of cycles required for lateral oscillation to damp to half amplitude

[redacted]

P	period, sec
p	rolling velocity, radians/sec
q	dynamic pressure, lb/sq ft
r	yawing velocity, radians/sec
S	wing reference area, sq ft
V	true airspeed, ft/sec
α	angle of attack, deg
β	sideslip angle, deg
ϕ	bank angle, deg
$\frac{\lvert\phi\rvert}{\lvert\beta\rvert}$	ratio of bank-angle amplitude to sideslip-angle amplitude in the lateral oscillatory mode
δ_a	aileron deflection, radians
δ_r	rudder deflection, radians

$$C_l = \frac{\text{Rolling moment}}{qSb}$$

$$C_n = \frac{\text{Yawing moment}}{qSb}$$

$$C_{l_\beta} = \frac{\partial C_l}{\partial \beta}$$

$$C_{l_{\delta_r}} = \frac{\partial C_l}{\partial \delta_r}$$

$$C_{l_p} = \frac{\partial C_l}{\partial \left(\frac{pb}{2V}\right)}$$

$$C_{l_r} = \frac{\partial C_l}{\partial\left(\frac{rb}{2V}\right)}$$

$$C_{n_\beta} = \frac{\partial C_n}{\partial \beta}$$

$$C_{n_{\delta_a}} = \frac{\partial C_n}{\partial \delta_a}$$

$$C_{n_p} = \frac{\partial C_n}{\partial\left(\frac{pb}{2V}\right)}$$

$$C_{n_r} = \frac{\partial C_n}{\partial\left(\frac{rb}{2V}\right)}$$

TESTS

Configurations Investigated

The plan views and major size parameters of the SCAT configurations studied on the simulator are presented in table I. Three designs for which pertinent information was available are considered as they existed at the time of the midterm review. It should be noted that there are some differences between the basic configurations shown here and the final versions evolved by the contractors. The results of this study, therefore, should be interpreted in a general fashion as indications of probable augmentation requirements.

The SCAT 16 is shown in table I with the wings in the forward position at 30° of sweep; the landing weight was 242,500 pounds; the approach airspeed was 138 knots; the trim angle of attack for the approach was 4.2°.

The other configuration shown in table I is the SCAT 17. The information presented pertains to two versions of the SCAT 17 which differed rather significantly and thus were felt to deserve separate attention in the study. These are shown labeled 17-A and 17-B. The SCAT 17-A configuration had a canard surface for primary pitch control and an aft horizontal tail for trim; the SCAT 17-B had a canard for trim and elevons for pitch control, but no horizontal tail. These two versions had landing

weights of 253,300 pounds and 210,000 pounds and approach speeds of 132 knots and 145 knots. The approach angles of attack of 12° and 7° for the SCAT 17-A and the SCAT 17-B, respectively, should be noted; the difference was due primarily to the difference in approach speeds.

Piloted Simulator

The simulator used in this study consisted of a fixed, transport-type cockpit containing the essential pilot controls, instruments, and external visual display for performing ILS landing approaches to touchdown with minimum visibility. A photograph of the cockpit is presented in figure 1. The standard flight and engine instruments are shown, as well as the view of the runway and approach lights projected on a screer 12 feet from the pilot. Throttles for control of engine thrust also were available. The visual motion cues were provided by a landing simulator which employs closed-circuit television for transmission of the visual image. The motions and the instrument readings were generated from six-degree-of-freedom equations of motion by using a general-purpose analog computer. Applications of the simulator and more detailed descriptions thereof are available in references 1, 2, and 3.

Evaluation Tasks

"he evaluating pilots were two NASA research pilots and two company test pilots experienced in flying large commercial jet aircraft.

The pilots first familiarized themselves with the general handling qualities of a particular basic SCAT design at the given approach speed and assessed the longitudinal dynamics. In all cases, the longitudinal behavior proved to be satisfactory. The lateral directional characteristics of that configuration were then rated according to the widely used Cooper rating scale (ref. 4) after a number of specified tasks were performed. These tasks, which are often required in air transport operation during the instrument approach and the subsequent landing, are as follows.

First were lateral or Dutch roll oscillations with controls fixed; second were ILS approaches and landings in still air, mild to moderate rough air, and in steady crosswinds requiring removal of drift or crab angle immediately prior to touchdown; and third were offsets which called for corrective sidestep turns to line up with the runway immediately following transition from ILS to visual flight. The remaining task was that of correcting, with flight controls only, for failure of an outboard engine during a go-around from an aborted landing.

Stability Augmentation

The pilot ratings and comments obtained during the previously mentioned maneuvers were used as criteria for adding stability augmentation. In general, the procedure was to vary, one by one, the stability derivatives which the pilot believed offered the best improvement in lateral directionalbehavior, and then to arrive at a combination of augmented derivatives which should produce an overall rating of satisfactory. The resulting augmented configuration was then assessed on the bases of the tasks just described to verify the satisfactory behavior.

In order to include practical effects of limited augmenter authority and aerodynamic cross coupling, variation of the derivatives was in most cases accomplished through the roll- and yaw-control surfaces.

RESULTS AND DISCUSSION

Basic Configurations

All the SCAT configurations were found to require some form of stability augmentation to provide satisfactory handling qualities for normal operation in the landing approach. Before consideration is given to the augmentation, however, it would be well to look at the principal factors which the evaluating pilots felt to be objectionable in the basic configurations. These are summarized for each design in table II. The reader is reminded that the configurations studied represent interim designs that existed at the time of the midterm review.

First, the SCAT 16 was characterized by large adverse sideslip during turn entries and a difficulty in controlling heading accurately. Directional stability C_{n_β} and yaw due to rolling C_{n_p} were immediate candidates for augmentation. Low C_{n_β} would account for the poor heading control and would also accentuate any effect of C_{n_p} (which had a negative sign in this case) in producing adverse sideslip. While these characteristics were objectionable in the midterm configuration, they are not necessarily ty-pical of the variable-sweep concept. In spite of these qualities, the SCAT 16 was considered marginally satisfactory.

The SCAT 17-A exhibited low damping of the lateral directional or Dutch roll oscillation, which was easily excited in turn entries and in rough air. Other objectional qualities were high dihedral effect and low roll damping, which contributed to the unsatisfactory Dutch roll characteristics and which proved bothersome in removing the crab angle during a crosswind landing and in rough air. Adverse sideslip in turn

entries, which undoubtedly was accentuated by the highly inclined roll axis at 12° angle of attack, also was noted. This configuration was rated generally unsatisfactory to unacceptable for normal operation.

The SCAT 17-B was troubled by a high ratio of bank to sideslip in the Dutch roll oscillation (though the damping was not objectionable); however, the principal problem which made this configuration unacceptable even for an emergency condition without augmentation was an easily excited second lateral oscillatory mode. During such ordinary tasks as an ILS approach, this mode apparently contributed to a continual roll oscillation which the pilots had difficulty distinguishing from unacceptable Dutch roll behavior. Pulse-type aileron control appeared to subdue the oscillation, but extremely close attention to bank attitude was required. Use of rudder control resulted only in making the problem more difficult. In addition, the pilots complained of excessive dihedral effect and excessive favorable, or "proverse", aileron yaw, both of which probably contributed to the roll-control problem discussed previously.

Desired Augmentation

The degrees of augmentation found desirable for the various derivatives of the SCAT configurations studied are shown in figure 2. The amounts of augmentation of the static derivatives which determine dihedral effect C_{l_β}, directional stability C_{n_β}, and aileron yaw $C_{n_{\delta_a}}$ are presented. The variations indicated are in terms of the basic or unaugmented value. For each case, both a nominal and an actual variation from the basic ratio of 1.0 are given. The nominal variations are those which would be obtained with pure derivative changes or with no cross coupling; the actual variations represent the net effects (through aerodynamic cross coupling) on rolling-moment derivatives due to rudder augmentation (changing C_{n_β} can also change C_{l_β}) and on yawing-moment derivatives due to aileron augmentation. All variations indicated in figure 2 except for $C_{n_{\delta_a}}$ were obtained through the control surfaces; $C_{n_{\delta_a}}$ was varied as a pure derivative change to allow some freedom in tailoring $C_{n_{\delta_a}}$ by design of the roll-control surfaces. The augmenter authority in both roll and yaw was one-third of the total control travel. This authority appeared to be more than adequate for all normal maneuvers.

Inspection of figure 2 reveals some differences and some similarities in the desired augmentation which one might expect from what was learned about the basic configurations. Both the SCAT 17-A and 17-B required a sizable decrease in dihedral effect C_{l_β} - to about 30 to

50 percent of the basic value. All the pilots indicated that the SCAT 16, because of the heading-control problems mentioned previously, required about twice the directional stability C_{n_β} of the basic configuration. To decrease adverse sideslip in turn entries and to aid in controlling sideslip, and hence roll, in the event of asymmetric engine failure, the SCAT 17-A also required about twice the basic C_{n_β}. The SCAT 17-B, however, was made satisfactory without changing C_{n_β}, probably because of, first, the overshadowing improvement in the overall lateral oscillatory behavior brought about by the other augmentation and, second, the fact that no adverse yaw or sideslip problem existed in the basic airplane. Indeed, the SCAT 17-B required about a 73-percent decrease in proverse aileron yaw $C_{n_{\delta_a}}$ to be considered satisfactory.

Figure 3 shows the corresponding augmentation desired for the rotary or damping derivatives. All variations indicated were accomplished through actuation of the control surfaces, except for C_{l_r}. Consider first the roll damping C_{l_p}. As one might expect, the relatively high aspect ratio SCAT 16 required no augmentation of roll damping. The SCAT 17, however, was found to benefit from the addition of a roll damper which provided an additional 100 to 150 percent of basic roll damping. This increased damping was especially advantageous in rough air and in all rolling maneuvers, so long as sufficient aileron-control power also was available.

Both the SCAT 16 and the SCAT 17-A benefited from C_{n_p} augmentation sufficient to result in a value of the derivative of equal magnitude but of opposite sign (that is, changed from negative to positive). This was found to aid significantly in the apparent adverse yaw problems of the basic configurations. Since the value of. C_{n_p} for the SCAT 17-B was already positive in sign, no change was made in that derivative.

The Dutch roll behavior of the SCAT 16 and the SCAT 17-A were improved by yaw dampers which increased C_{n_r} to three times the basic value. As will be shown later, this amount of yaw damping in the SCAT 16 did not bring about a large improvement in the Dutch roll damping. In fact, the pilots complained of having to hold excessive rudder control into steady turns with the yaw damping indicated. Of course, stability augmentation designers are well aware of this problem and suitable wash-out networks are usually the answer. As indicated, the SCAT 17-B was improved sufficiently without a yaw damper.

As shown in the last graph of figure 3, a nominal variation of roll due to yawing C_{l_r} to a value of zero was found to be helpful to the

SCAT 17-A in suppression of roll following asymmetric engine failure. Because of the simultaneous change in C_{n_r}, however, the net decrease in C_{l_r} was very small. Variation of C_{l_r} was not investigated further in the other two airplanes.

One item of a fundamental, though interesting, nature is shown in figures 2 and 3; that is, the precise variation desired in a given derivative is not always obtained when augmenting through the control surfaces, For example, if one is attempting to augment at the same time C_{l_p} and C_{n_p}, aerodynamic cross coupling can come into play and modify the desired changes in both derivatives. The required augmenter gains can, of course, be readily computed, and proper compensation introduced, but reliable results depend on accurate knowledge of the values of $C_{n_{\delta_a}}$ and $C_{l_{\delta_r}}$.

Lateral Oscillatory Characteristics

The improvements in the lateral oscillatory or Dutch roll characteristics of the augmented SCAT configurations over those of the unaugmented configurations are shown in figure 4. The characteristics are indicated in terms of the damping parameter $\frac{1}{C_{1/2}}$ and the bank-to-sideslip ratio $\frac{|\phi|}{|\beta|}$. The scale change on the abscissa should be noted. The basic characteristics are indicated by the black symbols and the corresponding behavior with augmentation sufficient to produce an overall pilot rating of satisfactory is indicated by the light symbols. The numbers to the left of the symbols are the periods in seconds. The boundary indicates the degree of damping found by pilots in a flight study with a variable-stability airplane (ref. 5) to be satisfactory for normal operation in the landing approach. To indicate current behavior, the Boeing 707-320 without a yaw damper has a value of $\frac{1}{C_{1/2}}$ of 0.54 and a value of $\frac{|\phi|}{|\beta|}$ of 1.57 with a period of 8.2 seconds.

Figure 4 indicates that various degrees of change were achieved in the Dutch roll behavior. As mentioned earlier, the improvement for the SCAT 16 configuration was slight. Without any augmentation at all, the Dutch roll characteristics of the SCAT 16 were rated satisfactory by two pilots.

For the SCAT 17-A, a dramatic improvement in damping and about a 50-percent reduction in bank-to-sideslip ratio were brought about by the combined effects of the several augmented derivatives. Not all the augmentation was aimed directly toward the Dutch roll behavior, but the large increase in damping shown did result. The increase in period should also be noted; no complaints were made about this.

The two lateral oscillatory modes of the SCAT 17-B in the unaugmented condition are shown in figure 4. They are not greatly different in period and have comparable bank-to-sideslip ratios. In the augmented case, only one oscillatory mode remains and the other splits into the usual aperiodic spiral and rolling modes. The Dutch roll damping of the augmented SCAT 17-B, while not as high as for either of the unaugmented modes, is still respectable and the reduction in bank-to-sideslip ratio and elimination of the coupling problems associated with the two oscillatory modes resulted in satisfactory lateral directional handling qualities.

Some remaining mildly objectionable characteristics were noted: For the SCAT 16, the additional yaw damping required excessive rudder into steady turns and some difficulty holding a heading was still reported; for the SCAT 17-A, rudder control required in turns was still considered excessive and even further reduction in dihedral effect was considered desirable.

CONCLUDING REMARKS

It has been shown through use of a piloted simulator that the SCAT 16 and one version of the SCAT 17 should have acceptable handling qualities in an emergency condition without stability augmentation and that the SCAT 16 studied actually should border on satisfactory behavior without augmentation. It has also been shown that all the SCAT configurations investigated on the simulator can be improved to a satisfactory level, as far as lateral directional handling qualities are concerned, by ordinary means of stability augmentation. Unquestionably, some of the improvement in handling qualtities effected in this study could be achieved by careful design of the airplane (and estimation of the critical stability derivatives, especially those which are sensitive to high-lift configuration), thus reducing the requirements placed on the augmentation equipment.

REFERENCES

1. White, M. D., Sadoff, M., Bray, R. S., and Cooper, G. E.: Assessment of Critical Problem Areas of the Supersonic Transport by Means of Piloted Simulators. Paper No. 62-20, Inst. Aerospace Sci., Jan. 1962.

2. Bray, Richard S.: Piloted Simulator Studies Pertaining to the Low-Speed Longitudinal Handling Qualities of a Supersonic Transport Airplane. NASA paper presented at AIAA Meeting (Columbus, Ohio), Aug. 26-28, 1963.

3. McNeill, Walter E.: A Piloted Simulator Study of the Loss of Altitude by a Jet Transport in a Go-Around From an Instrument-Landing Approach. NASA TN D-2060, 1963.

4. Cooper, George E.: Understanding and Interpreting Pilot Opinion. Aero. Eng. Rev., vol. 16, no. 3, Mar. 1957, pp. 47-51, 56.

5. McNeill, Walter E., and Vomaske, Richard F.: A Flight Investigation To Determine the Lateral Oscillatory Damping Acceptable for an Airplane in the Landing Approach. NASA MEMO 12-10-58A, 1959.

[redacted]

DECLASSIFIED

TABLE I.- SCAT CONFIGURATIONS STUDIED

SCAT 16	
Span, ft	154
Wing area, sq ft	2,540
Landing weight, lb	242,500
Approach velocity, knots	138
α, deg	4.2
SCAT 17	
SCAT 17-A	
Span, ft	105
Wing area, sq ft	5,100
Landing weight, lb	253,300
Approach velocity, knots	132
α, deg	12
SCAT 17-B	
Span, ft	106
Wing area, sq ft	5,200
Landing weight, lb	210,000
Approach velocity, knots	145
α, deg	7

TABLE 11.- MAJOR OBJECTIONABLE CHARACTERISTICS

SCAT 16
Large adverse sideslip in turn entries Difficult to maintain heading
SCAT 17
SCAT 17-A
Low Dutch roll damping High dihedral effect Low roll damping Adverse sideslip in turn entries
SCAT 17-B
High Dutch roll bank-to-sideslip ratio Second lateral oscillatory mode High dihedral effect High proverse aileron yaw

SIMULATOR INSTRUMENTS AND VISUAL DISPLAY

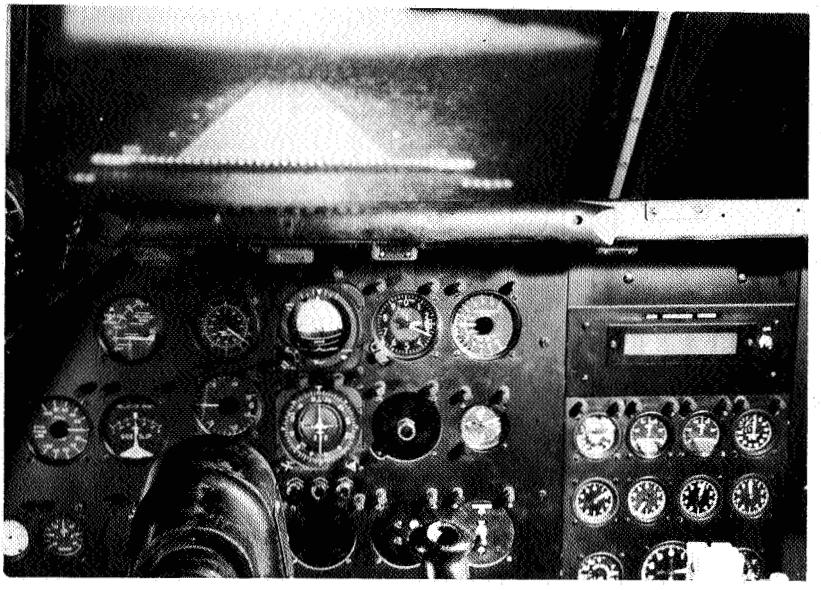

A-31061

Figure 1

DESIRED SCAT AUGMENTATION
STATIC DERIVATIVES

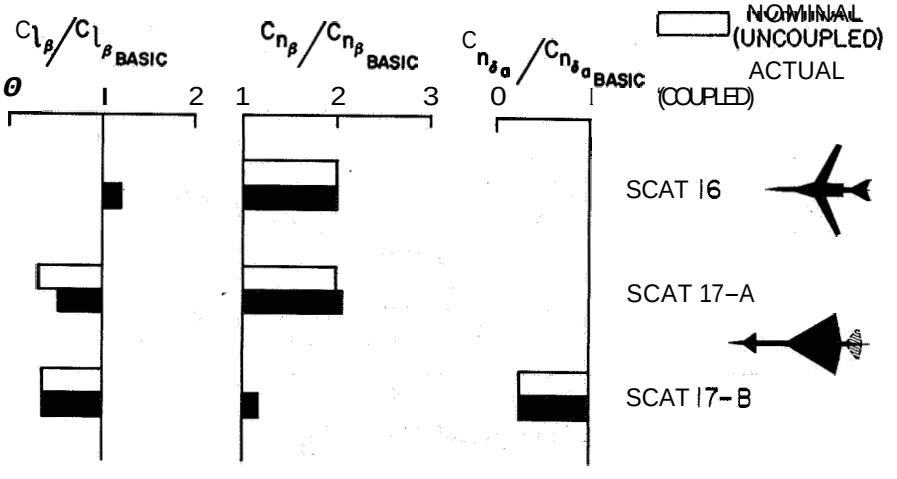

Figure 2

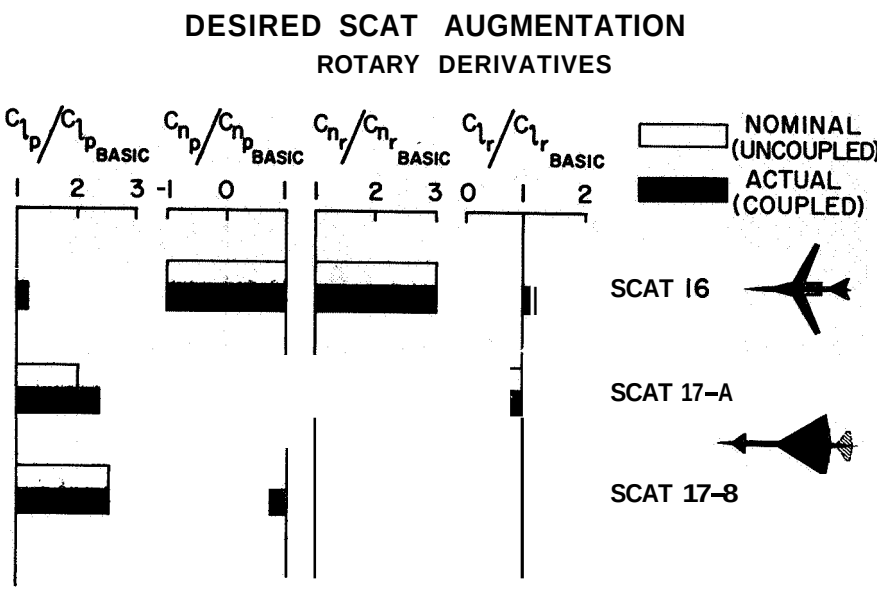
DESIRED SCAT AUGMENTATION
ROTARY DERIVATIVES
$C_{l_p}/C_{l_{p_{BASIC}}}$
$C_{n_p}/C_{n_{p_{BASIC}}}$
$C_{n_r}/C_{n_{r_{BASIC}}}$
$C_{l_r}/C_{l_{r_{BASIC}}}$
1 2 3
-1 0 1
1 2 3
0 1 2
NOMINAL (UNCOUPLED)
ACTUAL (COUPLED)
SCAT 16
SCAT 17-A
SCAT 17-8

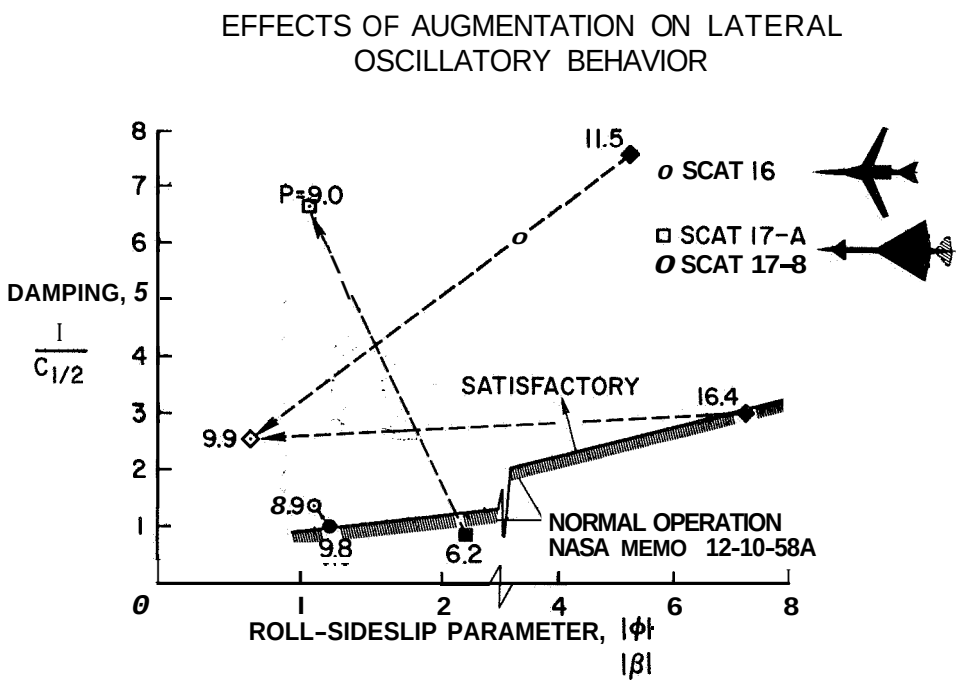
EFFECTS OF AUGMENTATION ON LATERAL OSCILLATORY BEHAVIOR
DAMPING, $\frac{1}{C_{1/2}}$
ROLL-SIDESLIP PARAMETER, $\frac{|\phi|}{|\beta|}$
11.5
P=9.0
o SCAT 16
□ SCAT 17-A
O SCAT 17-8
9.9
SATISFACTORY
16.4
8.9
9.8
6.2
NORMAL OPERATION
NASA MEMO 12-10-58A
0 1 2 4 6 8
1 2 3 4 5 6 7 8

Figure 4

[redacted]

28. PILOTING PROBLEMS ASSOCIATED WITH THE SUPERSONIC-TRANSPORT MISSION PROFILE

N67-31635

By Glen W. Stinnett, Alan E. Fayé, Jr., and Emmett D. Fry Jr.

NASA-Ames Research Center

SUMMARY

A simulator study was conducted of the piloting problems associated with the supersonic-transport mission profile. Several problem areas not common to present transport operations were examined and solutions for these problems are suggested.

INTRODUCTION

During the simulator study described by White, Fayé, and Cooper in paper no. 26, it was convenient to examine the handling qualities of the supersonic transport (SST) at discrete flight conditions along the mission profile, where altitude and Mach number were held constant for each flight condition. In actual operation, however, the pilot is confronted with the task of continuous flight along the profile where altitude and/or Mach number are continuously changing. The purpose of this paper is to discuss, from a pilot's point of view, potential problem areas arising from the many adjustments which must be made to follow such a profile.

Eight pilots participated in this program which utilized the same moving-base simulator and airplane configuration described in paper no. 26. The piloting problems were studied under instrument flight conditions, in smooth air, with the basic airplane characteristics augmented to provide satisfactory handling qualities.

The flight profile (fig. 1) used in this study should be examined in order to become familiar with the potential problem areas. This figure shows altitude plotted against time and depicts the climb, cruise, and descent portions of the mission. Across the top, Mach number is shown as it varies through the climb phase, being held constant at 0.9 for a short time and at 3.0 for the last portion of climb and the establishment of cruise. The time scale is broken and the normal- and emergency-descent time histories begin from a new zero reference time. This profile was chosen, not as an optimum, but as a representative type for the purpose of studying piloting problems associated with SST operations.

28

[redacted]

pp 485-494
0 refs

Tracing a typical run, the first task is to establish a climb schedule, avoiding sonic speeds at low altitudes. Then, above the altitude requiring subsonic speed, the task is to accelerate as rapidly as possible to cruise Mach number while climbing sufficiently to keep the sonic-boom ground overpressure below 2 pounds per square foot. The next task is to climb to cruise altitude and level off while maintaining cruise speed. During the cruise portion of the mission, the task is simply to maintain speed and altitude. During the normal descent, a constant equivalent airspeed of 310 knots is maintained. The task in an emergency descent is to reach, as quickly as possible, a safe altitude where 100 percent oxygen will sustain life.

In the simulator flying of this profile a number of piloting problems were disclosed. These are

(1) Conventional display deficiencies

(2) Overshoot at top of climb

(3) Speed control during cruise

(4) Emergency descent

Proceeding sequentially along the profile, the initial establishment of the subsonic climb presented no particular problems although the acceleration and climb performance of the SST in this area is very high and appeared to be quite similar to fighter-airplane performance. In fact, if duct burning proves to be uneconomical in this region, or if noise-abatement considerations preclude full-throttle operation, part-throttle performance is more than adequate for the subsonic acceleration.

CONVENTIONAL DISPLAY DEFICIENCIES

The first problem encountered concerns the deficiencies of conventional instrument displays. Specifically, two kinds of information are involved - precise pitch attitude and Mach number error. Figure 2 shows the area on the climb profile where this problem is most serious. In this figure, altitude is shown as a function of Mach number M. The solid line is the reference profile, and the dashed line is a line of constant-longitudinal-acceleration A_X capability. Note here the portion of the climb around Mach number 1.4. In this area longitudinal acceleration is at a minimum, rate of climb is quite low, and any departure from the reference profile to the high side results in a

further reduction of acceleration. Departure to the low side, of course, results in increased ground overpressure. Of incidental interest in this connection was the value for net longitudinal acceleration of 0.4 ft/sec^2, which was found to be the minimum necessary to provide for drag increase in maneuvering during profile tracking.

Figure 3 shows profile tracking performance when conventional instruments were used. The oscillations apparent here seem to be the result of two factors. First, pitch-attitude changes, required for flight-path corrections, are so small (on the order of 1/2°) that they are barely perceptible on the attitude indicator. Second, no single parameter remains constant during this portion of the climb where the ground-overpressure boundary determines the relationship between Mach number and altitude. In other words, the pilot has no good instrument to use as a primary reference for pitch-attitude control.

Incidentally, this lack of adequate pitch-attitude information is not peculiar to ground-base simulation. Practice SST climb profiles are being flown from the NASA Flight Research Center in a North American Vigilante to an altitude of 50,000 feet and a Mach number of 1.7. There, similar difficulties are being reported, even when operating in visual flight conditions.

One solution that was found to be acceptable consisted of displaying Mach number error directly to the pilot by use of an indicator located within and at the left edge of the attitude indicator as shown in figure 4. This pointer, which moves vertically, was used to display the Mach number error. Full-scale deflection of the pointer equaled a Mach number error of 0.1 or, in other words, each dot represented a Mach number error of 0.05. This signal was generated by using as inputs the actual Mach number, the actual altitude, and the profile Mach number appropriate to the actual altitude. Correction for Mach number error was made using an instantaneous rate-of-climb indicator for slight pitch-attitude adjustments. This provided better scaling as a pitch reference than did the attitude indicator, and the use of these two indicators - the Mach number error and the instantaneous rate of climb - resulted in improved profile tracking as can be seen in figure 5. This figure shows a comparison of the tracking seen previously in figure 3 with a conventional display and the tracking with the improved display where Mach number error was held to much lower values. Whether these instruments could be implemented for actual aircraft use as nicely as for simulator use is another question. It would seem, however, that some such improvement in pitch attitude and climb-schedule-error displays is in order for the SST.

OVERSHOOT AT TOP OF CLIMB

The next problem area is that of altitude and speed overshoot at the top of the climb. In figure 6, which shows longitudinal acceleration along the climb profile used, it can be seen that, following the

rather sluggish performance in the middle portion of the climb where power is marginal, acceleration increases as Mach number increases, and the SST really gets a "second wind" as it approaches a Mach number of 3. If this power is converted to vertical momentum at a constant Mach number of 3, rate of climb becomes quite high. Rate of climb with full throttle would increase from 4,000 feet per minute at 59,000 feet to 20,000 feet per minute at 70,000 feet. This results in a need for timely throttle adjustment. An example of this is illustrated in figure 7 which is a time history showing the last portion of the climb. The upper portion of this figure shows altitude and the middle portion shows both thrust-weight ratio T/W at full throttle and that being used. These parameters are plotted against time. The insert at the bottom of the figure shows tracking performance relative to the reference profile with altitude plotted against Mach number. Here, throttle was reduced from 100-percent thrust to cruise power (or 42-percent thrust) as the vehicle passed 62,000 feet. The vertical momentum at this point was sufficient to achieve the last 8,000 feet of altitude. This is an area, then, which requires close pilot attention, and even a minor or routine distraction could cause a considerable overshoot, as illustrated by figure 8 which shows an overshoot resulting from inadequate throttle adjustment. It can be seen here that throttle reduction was begun at the proper point, but the adjustment was made too slowly, simply because of a scan-pattern interruption. It is interesting to note also that, although the overshoot in altitude was about 7,000 feet, the overshoot in Mach number was only about 0.1. No conclusions can be drawn concerning the relative likelihood of overspeeding to overshooting in altitude, however, because on this simulation speed-control cues were considerably better than normal-acceleration cues. Also, the pilots were briefed to be particularly careful not to exceed a Mach number of 3.2. Although not pictured here, normal acceleration varied between zero and 2g during this run. What can be seen from this is that timely throttle adjustment at the top of the climb is quite critical.

SPEED CONTROL DURING CRUISE

Regarding the third problem area shown, speed control during cruise, the same thrust-speed instability responsible for the high longitudinal acceleration during the last portion of the climb is present in the cruise condition, resulting in a need for continuous throttle adjustment to maintain a constant Mach number. Figure 9 is a short time history of pilot performance in this area. It can be seen that Mach number control was fairly good, but frequent throttle adjustments were necessary. This is not a difficult task, but it does demand constant attention and undoubtedly wastes some fuel. These last two

problem areas both suggest a need for some type of speed-sensitive fuel-control unit.

EMERGENCY DESCENTS

Normal descents were made using a constant equivalent velocity of 310 knots and no particular problems were noted. Emergency descents were briefly examined where attempts were made to reduce altitude as quickly as possible, constrained only by an airspeed limit of 500 knots equivalent, and vertical acceleration values of 2g and -1g. The goal was to descend in less than 2 minutes from a cruise condition at an altitude of 70,000 feet and a Mach number of 3 to an altitude of 40,000 feet, roughly the maximum safe altitude for sustained breathing with 100 percent oxygen. This goal was achieved through the use of a drag-producing device, such as speed brakes, a drag parachute, or thrust reversers, equivalent on the vehicle simulated to an incremental drag coefficient of 0.025. Oscillations were encountered as a result of the rapid initial attitude change made to commence the descent. These oscillations persisted through 40,000 feet but did not result in exceeding the airspeed limit or the vertical-acceleration values specified.

SUMMARY OF RESULTS

Referring again to the list of problems discussed:

First, conventional instrument displays appear to present inadequate pitch-attitude information at the higher speeds. The addition of velocity-error information and an instantaneous rate-of-climb indicator resulted in improved performance.

Second, overshoot problems at the top of the climb require very timely throttle adjustment because of the large excess of thrust available at full throttle.

Third, an unstable thrust-speed relationship at cruise caused a need for continuous throttle adjustment and suggests a need for some type of speed-sensitive fuel-control unit.

Fourth, in order to achieve an emergency-type descent from cruise conditions at an altitude of 70,000 feet to 40,000 feet in 2 minutes, an incremental drag coefficient of 0.025 was found necessary.

TYPICAL SIMULATED SST MISSION PROFILE

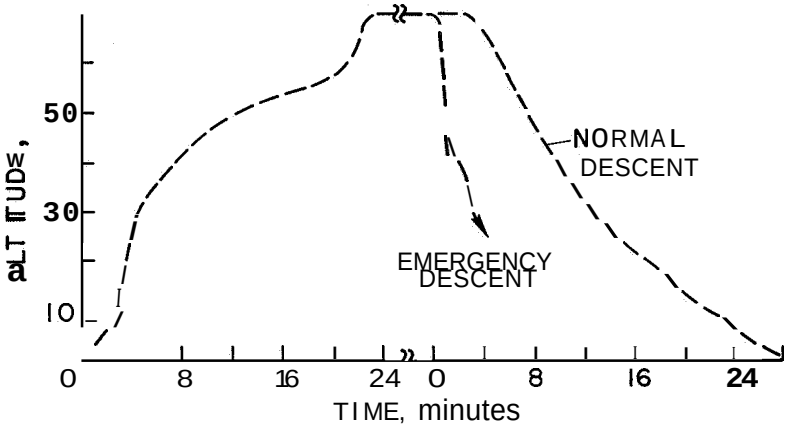

Figure 1

SST CLIMB PROFILE
LONGITUDINAL ACCELERATION BOUNDARY

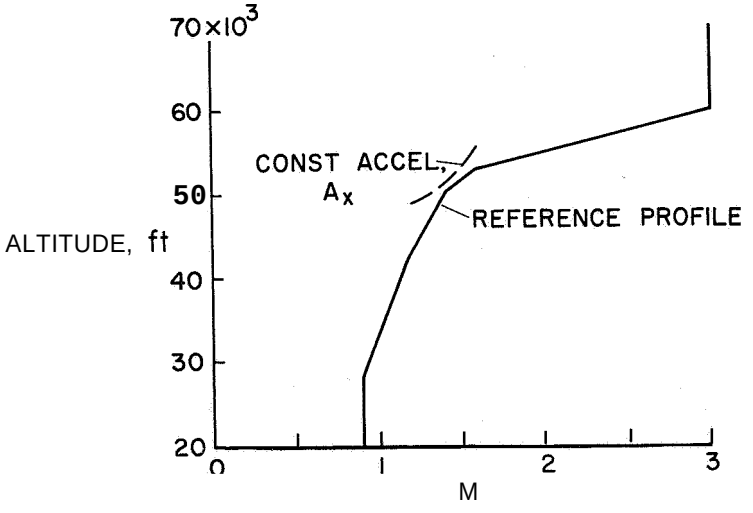

Figure 2

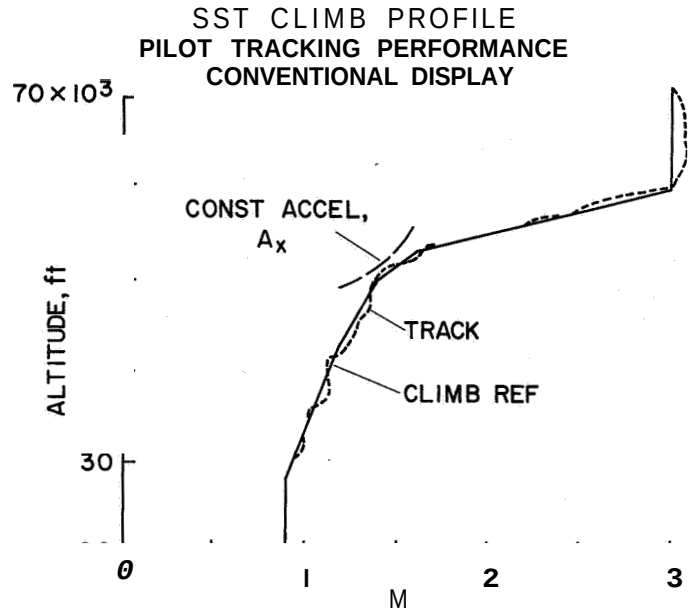

Figure 3

ATTITUDE INDICATOR WITH SPEED ERROR INDEX

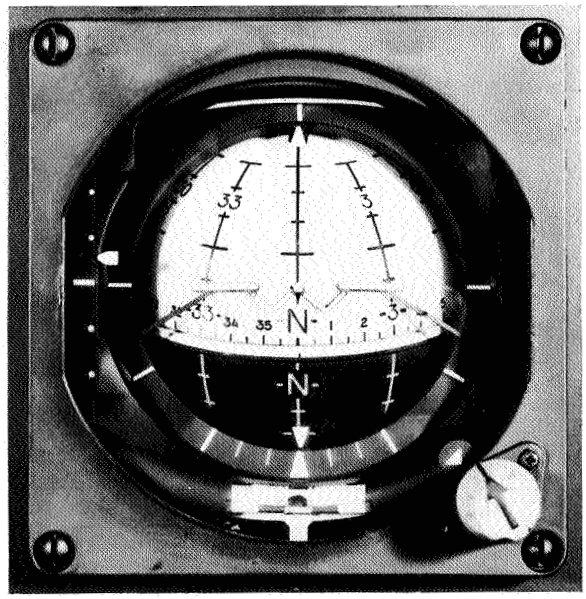

A-31302

Figure 4

SST CLIMB PROFILE
PILOT TRACKING PERFORMANCE

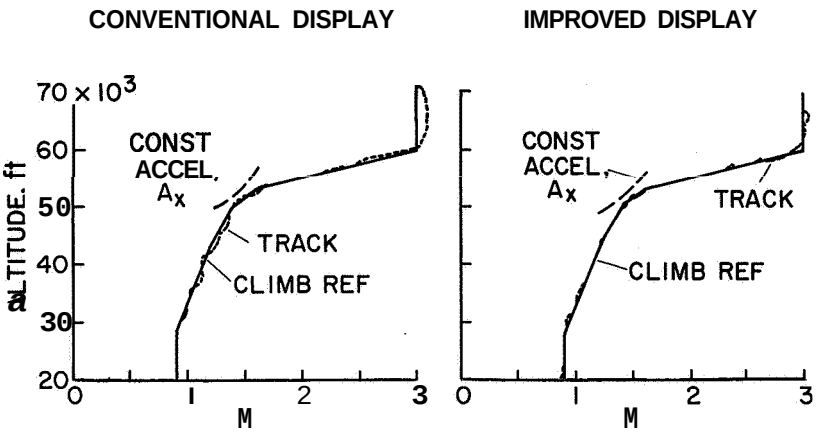

Figure 5

LONGITUDINAL ACCELERATION ALONG CLIMB PROFILE
UTILIZED FOR SIMULATOR PROGRAM

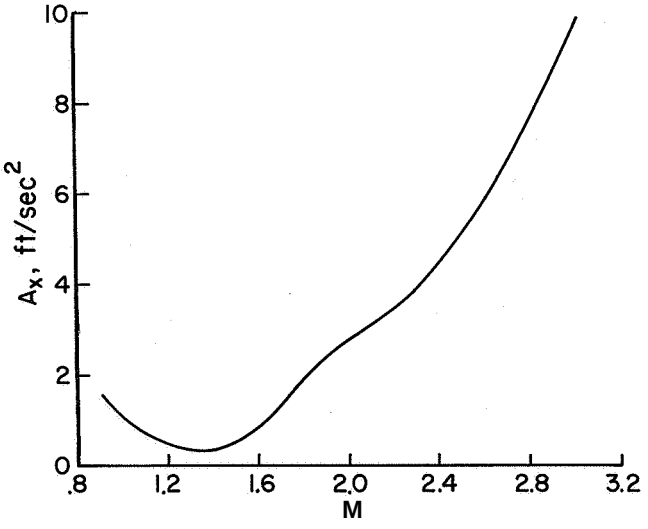

Figure 6

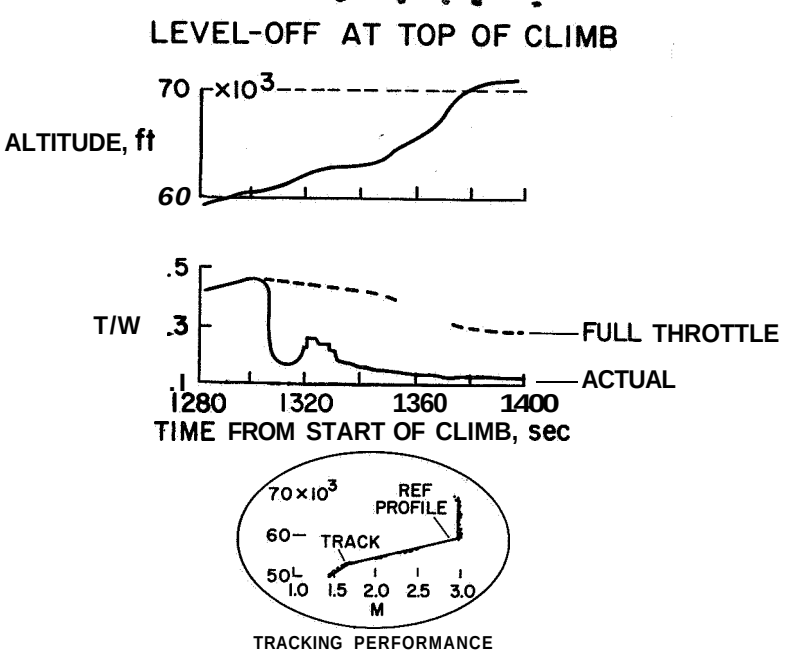

Figure 7

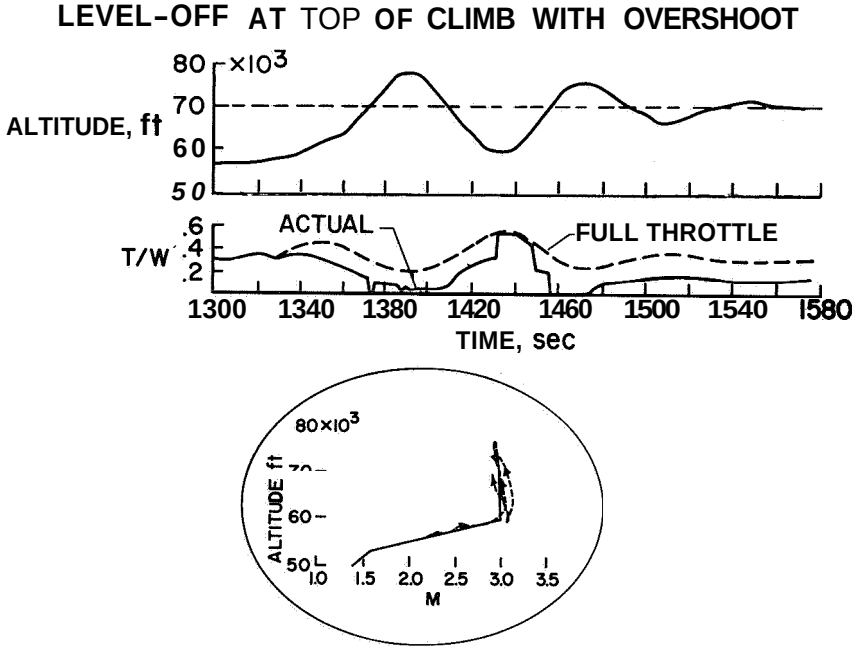

Figure 8

TIME HISTORY OF CRUISE THROTTLE ADJUSTMENTS

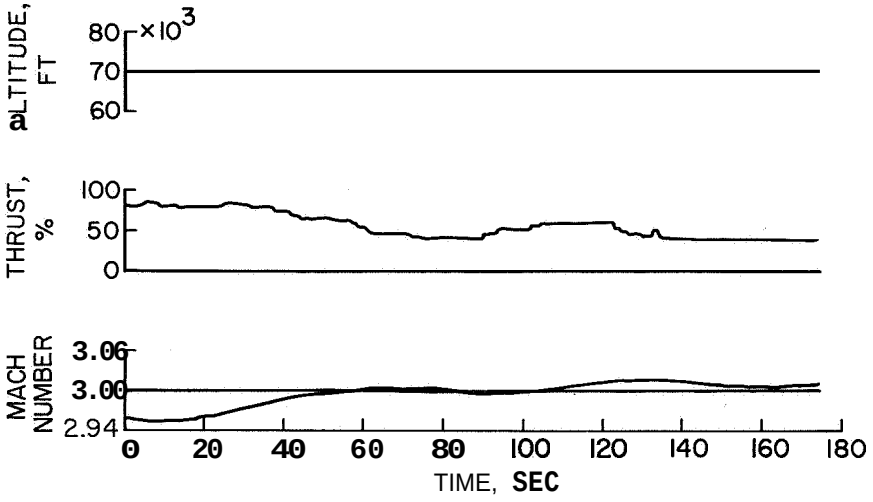

Figure 9

29. GENERAL SUMMARY AND ASSESSMENT

By Mark R. Nichols

NASA Langley Research Center

The present conference has reviewed in-house and contract work being conducted by the National Aeronautics and Space Administration in support of the national supersonic transport program. The purpose of this paper is to provide a condensed summary of the results presented together with an assessment of supersonic transport capabilities and of further research needs.

RECENT NASA RESEARCH CONTRIBUTIONS

NASA research on the special problems of supersonic-cruise airplanes began in connection with the B-58 and B-70 programs. A number of significant contributions of direct interest for the supersonic commercial air transport (SCAT) have been made since this time and are listed as follows:

Airframe and engine configuration concepts: As emphasized in the initial papers, a basic part of the NASA program has been the evolution of advanced airframe and engine configuration concepts and the submittal of these concepts to the industry for study from the viewpoint of the practical airplane designer. This activity is quite different from the traditional NASA research effort but has been considered necessary in this case because many of the special problems of the supersonic transport are directly dependent on the overall airplane configuration and on the compromises that the designer must make to arrive at a practical airplane.

Performance aerodynamics: A large amount of research has been accomplished recently in the field of performance aerodynamics. For example, a method for calculating and optimizing the pressure drag has been evolved, validated, and adapted for machine computing. As mentioned in preceding papers, an advanced machine computing program developed by and obtained through courtesy of The Boeing Company will be made available to the industry by NASA.

Additional research on boundary layers has resulted in verification of the applicability of the T' method of extrapolating the turbulent skin friction of smooth surfaces from model-scale Reynolds number to full-scale supersonic-transport Reynolds numbers. It is hoped that these new data will settle the long-standing controversy on this subject.

The drag contributions of a variety of additional types of surface roughness also have been correlated and quantitized.

Studies of the use of wing warp for reducing the drag due to lift and trim have been continued with successful results. Overall improvements in lift-drag ratio of about 1.0 have been obtained for wing planforms of interest for the supersonic transport. In addition, special calculation methods have been evolved for handling arbitrary planforms such as cranked, ogee, and M wings.

Finally, a much better understanding has been obtained of the nature of both drag and lift interference effects at supersonic Mach numbers. This understanding has led to the capability of using these interference effects to obtain overall configuration improvements. SCAT 15 provides an outstanding example along this line inasmuch as addition of the engine nacelles to the basic wing-body combination was accomplished with no loss in cruise lift-drag ratio.

Stability and control: NASA stability and control research has defined methods for minimizing the aerodynamic-center shift and pitch-up of variable-sweep-wing configurations, has demonstrated the feasibility of high-lift systems for both the variable-sweep-wing and the SCAT 17 type, fixed-wing configurations, and has evolved highly swept wing planforms which are regarded as promising successors to the SCAT 4 concept. In addition, the lateral-directional and control problems of a number of candidate and general research configurations have been explored, and extensive simulation research has been conducted to help define problems and requirements in the areas of handling qualities and flight operations.

Propulsion: In the area of propulsion, studies conducted in 1959 and 1960 provided an early definition of the basic requirements for the supersonic-transport engine. Promising engine cycles were subsequently evolved in a joint program with Federal Aviation Agency (FAA), U.S. Air Force (USAF), and industry. Major air-inlet problems have been explored, and promising jet-exit concepts have been both evolved and studied experimentally. This latter item is regarded as particularly important inasmuch as a 1-percent loss in nozzle efficiency in $M = 3$ cruise is equivalent to a 4- to 5-percent increase in specific fuel consumption. Hence, jet-exit research is being given attention in the current SCAT program comparable to that devoted to reduction of aircraft drag.

Materials: In the area of materials, a preliminary screening of structural materials of interest for the Mach 3 class of supersonic transport was accomplished by a special NASA committee composed of representatives of the airframe companies, alloy producers, and interested government agencies. In a follow-on program, the mechanical properties of the more promising candidate materials are being determined after

prolonged exposure to M = 3 temperatures. At the present time, some of the materials already have passed the 14,000-hour mark. Initial results also have been obtained in research on other important areas such as the susceptibility of the materials to salt stress corrosion and the determination of practical methods of fabrication.

Sonic boom: Because of its dominant effect on the overall feasibility of the airplane, a great deal of research has been devoted to the sonic boom. In this research, basic sonic-boom theory was verified, measurements of intensity were obtained, and exploratory studies of public acceptance were conducted in a joint program with the FAA and USAF. Calculation methods and wind-tunnel techniques also have been developed by NASA for studying configuration effects. Because of their first-order influence on configuration geometry and aircraft weight, it is anticipated that these methods and techniques will take their place along with classical drag-estimation methods as primary tools of the designer, Finally, this total effort has led to the establishment of approximate lower bounds of sonic-boom intensity from the configuration-effects viewpoint.

BROAD CONCLUSIONS OF CONTRACT STUDIES OF SCAT CONFIGURATIONS

The purpose of the contracts let with The Boeing Company and Lockheed California Company was fourfold: To obtain the input of the industry in the areas in which it is uniquely qualified; to determine the feasibility of the four concepts studied as candidate concepts for the U.S. supersonic transport; to establish the technological state of the art for the guidance of the national program; and to uncover problem areas needing further research attention by NASA. This section of the paper summarizes the broad conclusions of these contract studies.

First, airplanes developed from the SCAT 16 and 17 configuration concepts appear to meet essentially all of the specified mission requirements. They are competitive with regard to overall performance in this mission but are larger and heavier than corresponding subsonic jets.

Airplanes based on the initial SCAT 4 and 15 configuration concepts are ruled out unless solutions can be found to their stability or weight problems. The fact that they were dropped from further consideration by the contractors after midterm review of the contracts does not mean that hope is abandoned for these concepts, but rather that they were considered noncompetitive with their stability and weight problems outstanding.

Solutions to these problems were not foreseen in time to permit proper study by the contractors during the remaining period of the contracts.

Variable sweep provides improvements in mission versatility, low-speed handling qualities, and community noise.

Delta-type wings provide low structural weight and near-linear pitching-moment characteristics for most operating conditions.

The sonic boom has become a dominant factor in design with effects on the gross weight and range comparable to lift-drag ratio, specific fuel consumption, and structural weight. It is clear that great care must be exercised both in specifying the sonic-boom requirements and in configuring the airplane so as to obtain a minimum sonic-boom "form factor."

New and advanced engines are required for the airplane. An associated major research and development effort will be required in the areas of air inlets, jet exits, and propulsion system controls.

Major reductions in gross weight and sonic-boom intensity comparable to the gains obtained by the use of advanced engines are obtainable by the use of titanium as the basic structural material and also by substantial reduction of the fuel reserves such as might become feasible following improvements in air traffic control and landing systems. It appears mandatory that these avenues of improvement be exploited.

Within the ground rules of the study, $M = 3$ airplanes with advanced engines and titanium structures have lower gross weights and lower levels of sonic boom than lower-speed aluminum airplanes. The lower-speed airplane probably would have been more nearly competitive if more advanced engines had been permitted in the study. However, the use of highly advanced engine technology was considered to be inconsistent with the assumption of an aluminum structure.

Finally, the overall implication of the results of the studies is that highly advanced airframe and engine configurations are needed to meet the objectives of the national program.

ASSESSMENT OF SCAT CAPABILITIES

On the basis of the NASA research results and the results of the SCAT feasibility studies by Boeing and Lockheed, it is possible to arrive at an assessment of the state of the art. It is useful in such an assessment to begin with a look at the Breguet range equation:

$$\text{Range} = \underbrace{\left(\frac{V}{SFC}\ \frac{L}{D}\right)}_{\substack{\text{Flight}\\ \text{efficiency}}} \log_e \left(\frac{1}{1 - \frac{W_{FUEL}}{W_{INITIAL}}}\right)$$

(Symbols used are defined in the appendix at the end of this paper.) As indicated by the grouping of terms, the two basic factors affecting aircraft range are the flight efficiency (range factor) and the fuel-to-initial weight ratio or, in the case of a complete mission, the fuel-to-gross weight ratio. The state of the art with regard to these two factors will be reviewed briefly.

The flight efficiency expressed in the form $\frac{M(L/D)}{SFC}$ is plotted in figure 1 as a function of Mach number for representative U.S. subsonic jet transports and for supersonic airplane designs developed from the four SCAT configuration concepts by the NASA SCAT feasibility study contractors. Each of the supersonic airplanes was assumed to be powered by the highly advanced D-type turbofan engines, and its engines and wing area were sized to satisfy the mission rules spelled out in the SCAT feasibility study work statement.

At supersonic speeds, the SCAT 16 and 17 airplanes in their present form provide approximately equal flight efficiencies. The level of these efficiencies is significantly lower than those for the SCAT 4 and 15 class of airplanes which featured highly advanced aerodynamics but were found to be impractical for other reasons. The present SCAT 16 and 17 airplanes provide only about three-quarters of the cruise flight efficiencies of the best present subsonic jets. Hence, it is regarded as extremely important that research be continued to attain a higher level of supersonic cruise efficiency for practical configurations. The flight efficiencies of the SCAT 4 and 15 class of configurations are considered to establish a realistic goal for this upgrading of the state of the art.

At subsonic speeds, the SCAT 16 type of airplane characteristically exhibits marked superiority over the SCAT 17 type and provides flight efficiencies approaching those of the present subsonic jets. This good subsonic efficiency is of advantage in subsonic cruise and hold operation but may or may not be a determining factor in overall configuration selection, depending on the degree of mission flexibility demanded of the airplane.

In figure 2 the disposable-load ratio, which is the ratio of the weight of the usable fuel plus payload to the take-off gross weight, is plotted as a function of airplane gross weight. The disposable-load ratio is a significant parameter inasmuch as it defines the upper limit

of the fuel-carrying capability of the airplane and recognizes, to some extent, the fuel-payload trade. The disposable-load gross weight characteristics of a number of U.S. subsonic jet transports and of the SCAT 16 and 17 airplanes (as determined by Boeing and Lockheed) are shown by the circular, square, and diamond symbols, respectively.

For the subsonic jets, the points plotted include nearly all the Boeing, Douglas, and Convair series and represent a consistent family of carefully optimized designs beginning with small ranges and payloads at the lower left of the figure and extending to large payloads and very long ranges at the upper right. The Boeing 707-120 airplane is identified because it has approximately 3,200-nautical-mile range capability with the 26,125-pound payload. In other words, it meets all of the performance requirements of the NASA SCAT mission with the exception of cruise speed.

The SCAT 16 and 17 airplanes require a disposable-load ratio of 0.02 to 0.05 greater than that for the 707-120 for the design SCAT mission. This difference is caused by the flight efficiency of the SCAT airplanes being lower than that for the 707-120 both in cruise (as shown in fig. 1) and in off-design flight so that more fuel is needed. The requirement for a higher disposable-load ratio plus the inherent weight penalties of the supersonic airplane associated with greater overall slenderness, higher-thrust engines, more complex inlets and exits, and so forth, results in the SCAT 16 and 17 airplanes being 130,000 to 200,000 pounds heavier than the 707-120. The present objective of NASA advanced-concepts research is to evolve designs which will provide major reductions in this penalty through improvements in aerodynamics, propulsion, and structural weight.

The lines plotted in the vicinity of the points for the SCAT 16 show estimates of the way in which the disposable-load ratio attainable with this configuration with a payload of 26,125 pounds varies over a range of design gross weights. Two acceleration sonic-boom limits are considered: 2.5 and 2.0 lb/sq ft. At *gross* weights in excess of the plotted points, the slope of the curve for Δp_{MAX} = 2.5 lb/sq ft is low compared with the trend curve through the family of subsonic jets. Thus, it is indicated that with even a modest boom limitation the gross weight of the supersonic airplane is much more sensitive to changes in payload and range than is the case for its subsonic counterpart.

With a boom limit of 2.0 lb/sq ft, the slope of the trend curve is further reduced and the curve actually hooks down at *gross* weights exceeding about 480,000 pounds. This hooking is caused by the necessity for increasing the acceleration altitude progressively as the gross weight is increased in order to maintain a constant level of sonic-boom overpressure. Each increase in altitude requires increases in both engine size and wing size so that eventually the operating weight empty

begins to increase at a faster rate than the gross weight. The net result is that, in contrast to the subsonic case, it is no longer possible to increase range-payload performance by merely further increasing the gross weight. At this point further performance gains can be obtained only through basic improvements in flight efficiency, reductions in the sonic-boom "form factor," or reductions in the operating weight empty.

From the preceding discussion, it is clear that the sonic boom has introduced another factor into the design process and that this factor has effects on gross weight and range fully comparable to the flight-efficiency and weight-ratio terms of the Breguet equation. This situation means that once more, as in the case of jet noise, a compromise must be made between the desire of the designer and operator to develop the most economical airplane and the desire of the public to be subjected to a minimum amount of noise. The situation is complicated by the fact that the level of sonic boom acceptable to the public cannot be pinned down exactly at the present time. A great deal of additional thought and study will have to be devoted in the near future to the question, "What should the specified sonic-boom requirement be?" if unnecessary design penalties are to be avoided.

The state of the art with regard to mission performance is presented in figure 3 in which the gross weight and the payload-to-gross weight ratio are plotted as a function of design range. The mission requirements considered are those specified in the NASA SCAT feasibility study work statement and include a 26,125-pound payload and appropriate operating restrictions. The cruise Mach number is 3; the maximum allowable sonic-boom overpressure is 2.0 lb/sq ft; and the airplane is assumed to have titanium structures and the D-type turbofan engines incorporated. It should be recalled that the D engine is highly advanced and is approaching the limit of present development capabilities. The band of values shown covers the spread between the minimum-weight configurations determined by the two contractors in their NASA SCAT studies.

At a 3,200-nautical-mile design range, the state-of-the-art minimum gross weights as defined in figure 3 range from 380,000 to 430,000 pounds with a corresponding spread of payload-to-gross weight ratios from 6.9 to 6.1 percent. When the range is increased to 4,000 statute miles (3,475 n. mi.), a value of current interest, the required gross weights increase by increments of 40,000 to 80,000 pounds.

Figures 4 and 5 present the results of extensive computer studies conducted by NASA, utilizing a complete mission optimization process, to establish the importance of the major design trades for SCAT's 16 and 17. The values shown generally are in good agreement with values reported to date by the contractors.

The following qualifications should be made regarding the data presented in figures 4 and 5 to permit proper interpretation:

(1) To correspond with the results presented by the contractors, the sonic-boom calculations of the upper left plots were made with the reference-pressure term in the Whitham equation defined as $\sqrt{p_{alt} \times p_{sl}}$ instead of the mean-altitude pressure which now appears to give somewhat better correlation between measurements and theory.

(2) In the plots at the upper right, the range or weight increments caused by changes in passenger-type payload take into account changes in fuselage and accommodation weights and changes in the fuselage drag in addition to the change in the payload weight itself.

(3) In the plots at the lower right, the engine and structure weight increments were assumed to be reflected directly without growth factors in changes in the operating weight empty.

The results of these trade studies have been used to determine a projection of the present state of the art (fig. 6) because of the belief that modest or significant improvements can be made in a number of areas during the airplane development process. As a starting point, it was assumed that the correct weights for the SCAT 16 and 17 airplanes are each the average of the values reported by the contractors. The particular improvements listed are considered to be individually attainable. (The reductions in engine and structure weight are assumed to be reflected in equal changes in the operating weight empty.)

As shown in figure 6, if all of these gains can be achieved simultaneously, it appears that a 4,000-statute-mile range can be attained with the standard payload of 26,125 pounds with a gross weight in the neighborhood of 360,000 pounds. Further, if the payload is increased to 35,000 pounds, the predicted gross weight for the sane range increases only to about 430,000 pounds. These values represent very substantial improvements over the current capabilities and provide a much more attractive airplane. The main questions are: How soon can such improvements be realized? and Can they all be realized in one design?

NASA RESEARCH PROGRAM

The NASA **SCAT** research reported at this conference is being continued with the objective of solving outstanding specific problems and bringing about a general upgrading of aircraft capabilities. The overall program includes extensive research in the following areas:

(1) Advanced configuration concepts such as the improved versions of the present configurations illustrated in figure 7

(2) Basic and configuration aerodynamics

(3) Propulsion (engine cycles, air inlets, jet exits)

(4) Sonic boom and noise

(5) Materials and their fabrication problems

(6) Fabricated and fail-safe structures

(7) Handling-qualities problems

(8) Operating and airworthiness problems

It is hoped that this research **will** make major contributions to the first U.S. supersonic transport.

APPENDIX

SYMBOLS

V	velocity
SFC	specific fuel consumption
L/D	lift-drag ratio
W	weight
M	Mach number
Δp_{MAX}	sonic-boom overpressure at sea level
p_{alt}	ambient pressure at altitude
p_{sl}	ambient pressure at sea level

Subscripts:

ENG	engine
STRUCT	structural

STATE OF THE ART – FLIGHT EFFICIENCY
D ENGINES, NASA MISSION RULES

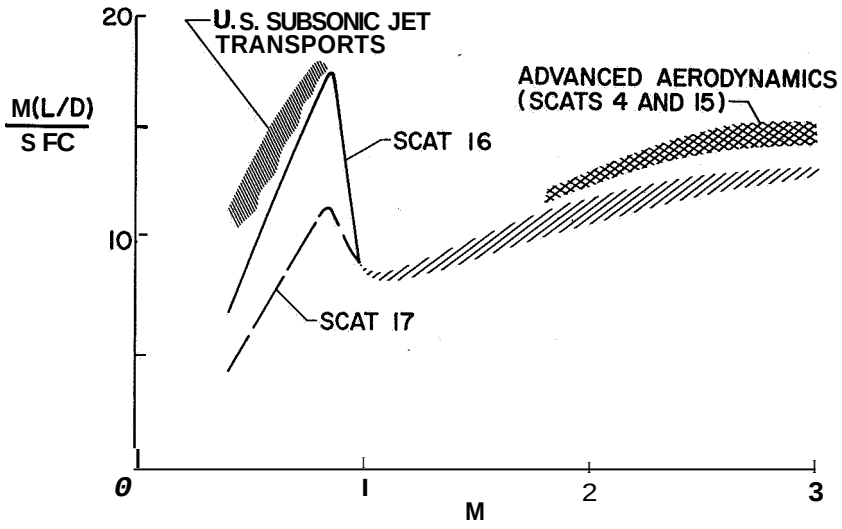

Figure 1

STATE OF THE ART – DISPOSABLE LOAD

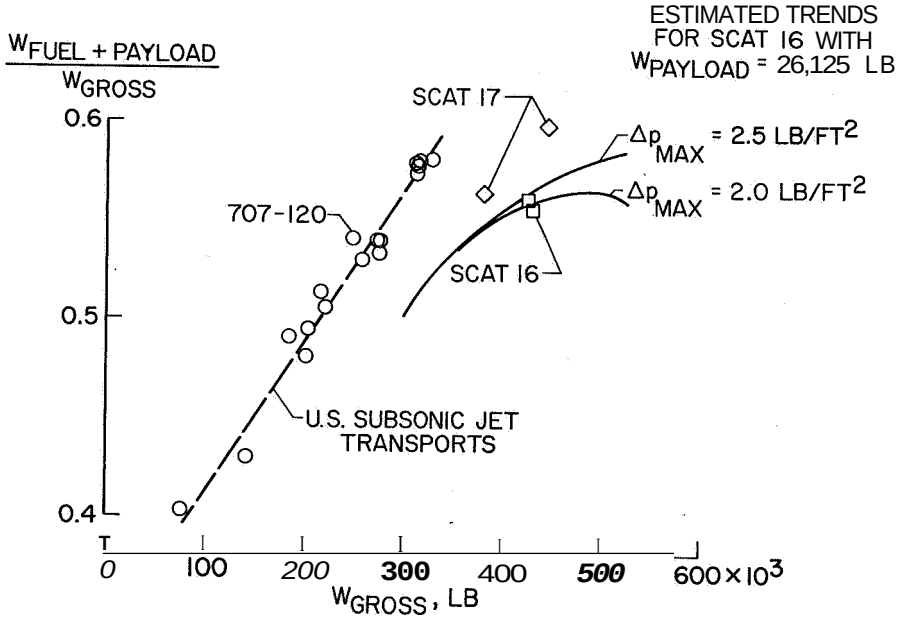

Figure 2

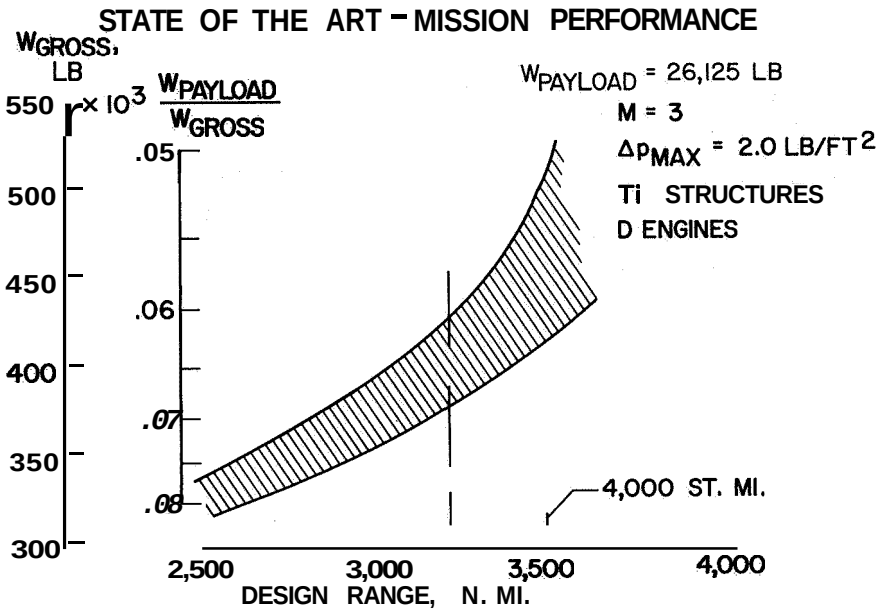

Figure 3

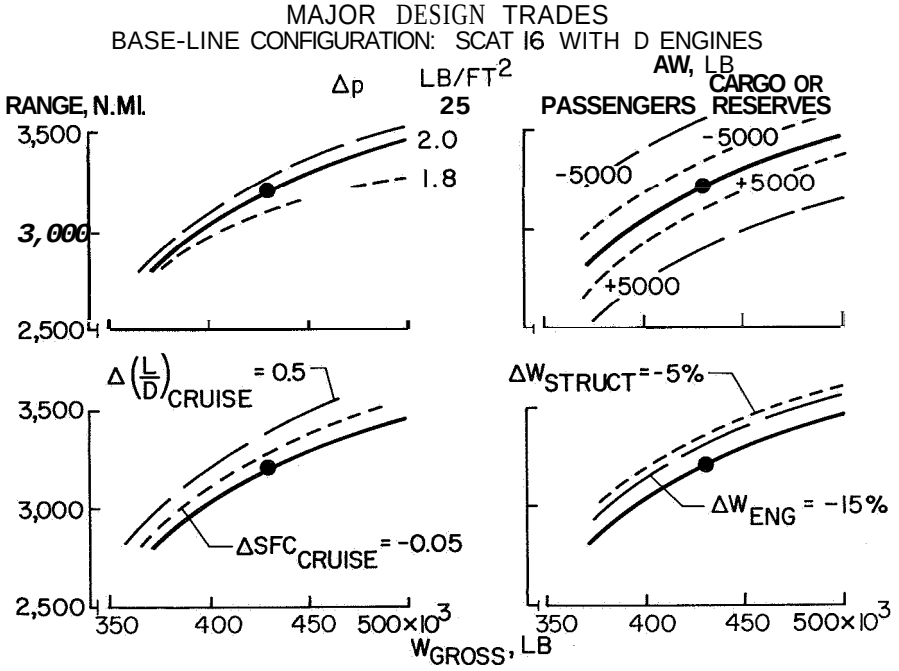

Figure 4

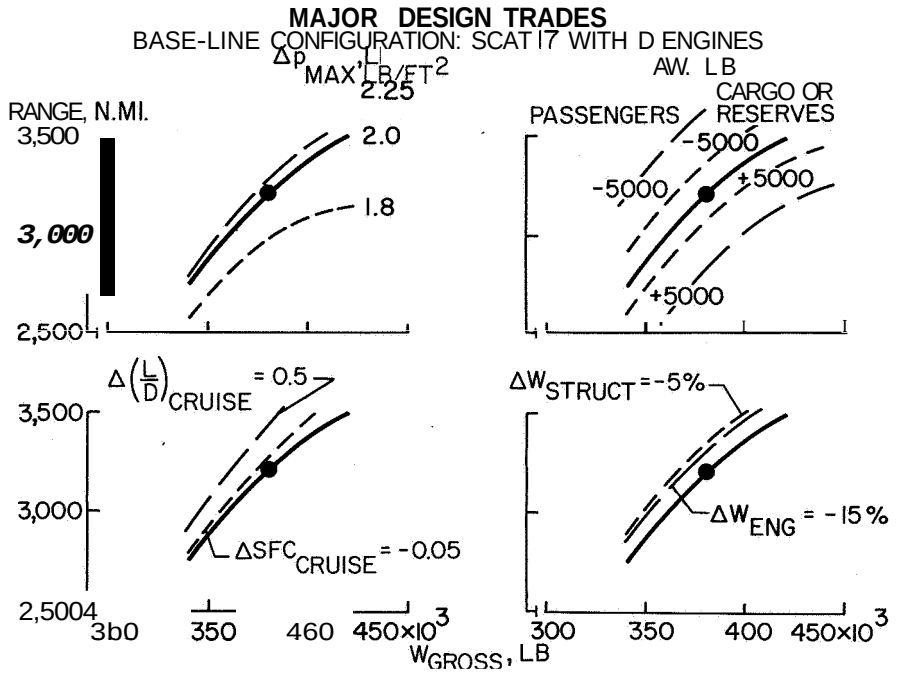

Figure 5

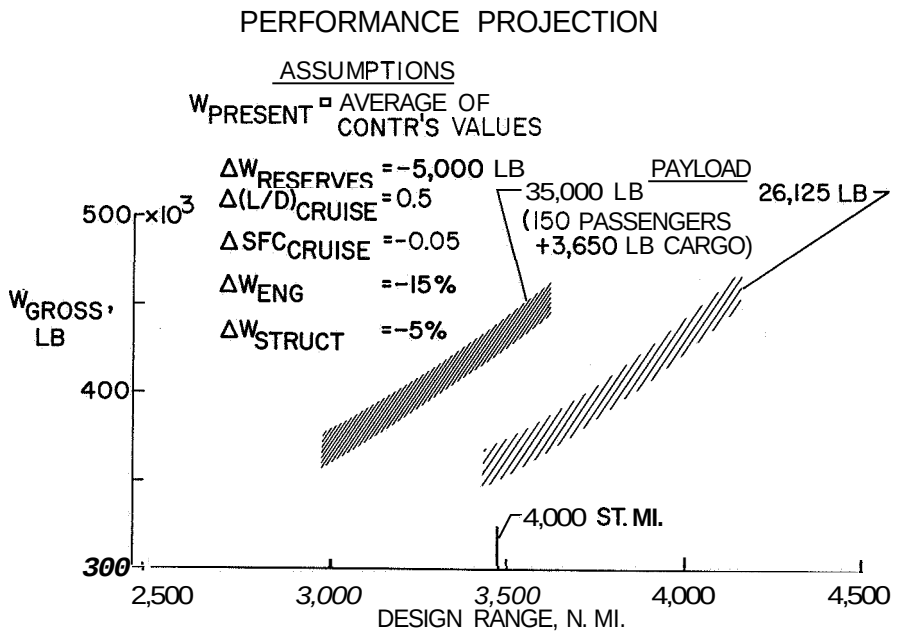

Figure 6

ADVANCED CONFIGURATION CONCEPTS

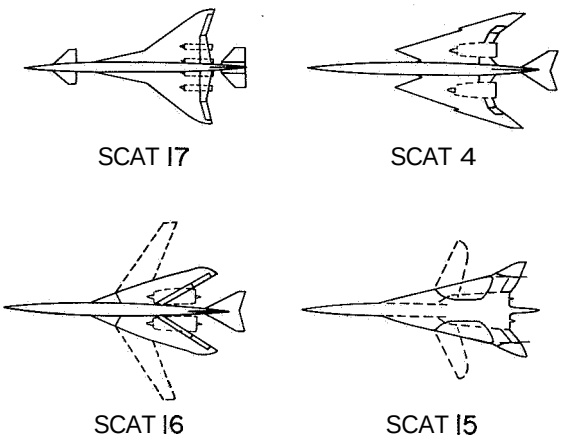

Figure 7

NASA-Langley, 1963